



A possible role for CD26/DPPIV enzyme activity in the regulation of psoriatic pruritus



Eriko Komiya^{a,b}, Ryo Hatano^a, Haruna Otsuka^a, Takumi Itoh^{a,c}, Hiroto Yamazaki^a, Taketo Yamada^{d,e}, Nam H. Dang^f, Mitsutoshi Tominaga^b, Yasushi Suga^g, Utako Kimura^g, Kenji Takamori^{b,g}, Chikao Morimoto^a, Kei Ohnuma^{a,*}

^a Department of Therapy Development and Innovation for Immune Disorders and Cancers, Graduate School of Medicine, Juntendo University, 2-1-1 Hongo, Bunkyo-ku, Tokyo 113-8421, Japan

^b Institute for Environmental and Gender Specific Medicine, Juntendo University Graduate School of Medicine, 2-1-1 Tomioka, Urayasu, Chiba 279-0021, Japan

^c Graduate School of Health and Sports Science, Juntendo University, 1-1 Hiragakakuendai, Inzai, Chiba 270-1695, Japan

^d Department of Pathology, Keio University School of Medicine, 35 Shinanomachi, Shinjuku-ku, Tokyo 160-8582, Japan

^e Department of Pathology Saitama Medical University, 38 Morohongo, Moroyama-cho, Iruma-gun, Saitama 350-0459, Japan

^f Division of Hematology/Oncology, University of Florida, 1600 SW Archer Road- Box 100278, Room MSB M410A, Gainesville, FL 32610, USA

^g Department of Dermatology, Juntendo University Urayasu Hospital, 2-1-1 Tomioka, Urayasu, Chiba 279-0021, Japan

ARTICLE INFO

Article history:

Received 6 October 2016

Received in revised form 22 February 2017

Accepted 8 March 2017

Keywords:

CD26/DPPIV

Substance P

Pruritus

Psoriasis

ABSTRACT

Background: Psoriasis (PSO) is one of the most common chronic inflammatory skin diseases, and pruritus affects approximately 60–90% of patients with PSO. However, the pathogenesis of pruritus in PSO remains unclear. Dipeptidyl peptidase IV (DPPIV) enzyme activity is involved in the regulation of peptide hormones, chemokines and neurotransmitters.

Objectives: Our aim is to evaluate for a potential association between DPPIV and an increased risk of pruritus, and to identify possible underlying treatment targets in affected patients.

Methods: Utilizing clinical serum samples of PSO patients and *in vivo* experimental pruritus models, we evaluated for a potential association between DPPIV and an increased risk for pruritus, and attempted to identify possible underlying treatment targets in pruritus of PSO.

Results: We first showed that levels of DPPIV enzyme activity in sera of patients with PSO were significantly increased compared to those of healthy controls. We next evaluated levels of substance-P (SP), which is a neurotransmitter for pruritus and a substrate for DPPIV enzyme. Truncated form SP cleaved by DPPIV was significantly increased in sera of PSO. In an *in vivo* pruritus model induced by SP, scratching was decreased by treatment with a DPPIV inhibitor. Moreover, DPPIV-knockout mice showed attenuation of scratching induced by SP. Finally, scratching was decreased following the administration of a DPPIV inhibitor in an imiquimod-induced PSO model. On the other hand, scratching induced by imiquimod was increased in DPPIV overexpressing-mice.

Conclusions: These results suggest that inhibition of DPPIV enzyme activity regulates pruritus in PSO.

© 2017 Japanese Society for Investigative Dermatology. Published by Elsevier Ireland Ltd. All rights reserved.

1. Introduction

Psoriasis (PSO) is one of the most common inflammatory skin diseases, and is found in approximately 1–3% of the world general population [1]. For a long time, PSO had been considered as a non-pruritic dermatitis. However, more recently, a number of studies have demonstrated that approximately 60–90% of patients with PSO suffer from pruritus [1–6]. Although psoriatic patients consider pruritus as the most bothersome subjective sensation [5,7], effective therapy for pruritus in PSO has not been established.

Abbreviations: CD26KO, CD26/DPPIV knockout; DPPIV, dipeptidyl peptidase IV; DPPIV-Tg, CD26/DPPIV transgenic; i.d., intradermal; IMQ, imiquimod; i.p., intraperitoneal; NK-1R, neuropeptide-1 receptor; PSO, psoriasis; rsCD26(DPPIV+), recombinant soluble CD26 protein containing DPPIV enzyme activity; rsCD26 (DPPIV-), recombinant soluble CD26 with deficient DPPIV enzyme activity; sCD26, soluble CD26; sDPPIV, soluble DPPIV enzyme activity; SP, substance P.

* Corresponding author.

E-mail address: kohnuma@juntendo.ac.jp (K. Ohnuma).

CD26 is a 110 kDa surface glycoprotein with dipeptidyl peptidase IV (DPPIV, EC 3.4.14.5) activity as a serine protease that cleaves dipeptides from the N-terminus of peptides at the penultimate position [8–10]. CD26 is also associated with T cell signal transduction processes as a costimulatory molecule, as well as being a marker of T cell activation [11,12]. We have previously reported that CD26-mediated costimulatory activity is exerted via its DPPIV enzyme activity [13]. More recently, we have shown that serum soluble CD26 (sCD26) and DPPIV enzyme activity (sDPPIV) are inversely correlated with disease activity in patients with systemic lupus erythematosus [14]. In addition, sCD26 and sDPPIV are involved in the pathogenesis of various cancers including colorectal cancer, hepatocellular carcinoma, prostate cancer and malignant mesothelioma [15–19]. Other investigators have reported that CD26/DPPIV was upregulated in psoriatic skin and that DPPIV inhibitor ameliorated psoriasis [20–23], although the biological role of CD26/DPPIV in PSO has not yet been elucidated. Meanwhile, DPPIV enzyme activity has been widely studied in metabolic and endocrine disorders, and DPPIV inhibitors have been developed as a new class of anti-diabetic drugs which act by inhibiting DPPIV, the enzyme that inactivates incretin hormone [24–26]. The potentially important role played by CD26/DPPIV in the clinical setting has led to rising interest in serum sCD26 level and sDPPIV enzyme activity in various human conditions over the past decade.

Substance P (SP) is a neuropeptide involved in afferent neuronal signal transduction [27,28]. Activation of sensory neurons in the skin causes the release of SP [29,30]. Once released, SP binds to neurokinin receptors including neurokinin-1 receptor (NK-1R) found on keratinocytes and cutaneous nerve endings, resulting in the release of additional itch mediators [29,31]. Substance P therefore appears to act to induce itch. It has been reported that the number of SP-containing nerves in the perivascular areas of pruritic psoriatic skin was increased and that expression of SP receptor in epidermis from pruritic psoriatic subjects was upregulated [3,32]. On the other hand, SP consists of 11 amino acids residues and contains the DPPIV-target sequence at its N-terminal position [33]. Previous report utilizing DPPIV deficient rat showed that circulating SP was metabolized by DPPIV enzyme [34]. However, it is not clear whether degradation of SP by DPPIV enzyme affects pruritus in patients with PSO.

In the present study, utilizing clinical serum samples of PSO patients and *in vivo* experimental pruritus models, we evaluated for a potential association between DPPIV and an increased risk for SP-induced pruritus, and attempted to identify possible underlying treatment targets in pruritus of PSO. We showed that levels of DPPIV enzyme activity in sera of patients with PSO were significantly increased compared to those of healthy controls. Moreover, truncated form SP cleaved by DPPIV was significantly increased in sera of PSO. In an *in vivo* pruritus model induced by full-length SP, scratching was decreased by treatment with a DPPIV inhibitor. Moreover, scratching was increased following injection of truncated form SP. Furthermore, DPPIV-knockout (CD26KO) mice showed attenuation of scratching induced by SP. Finally, scratching was decreased following the administration of a DPPIV inhibitor in an imiquimod (IMQ)-induced PSO model. On the other hand, scratching induced by IMQ was increased in DPPIV over-expressing transgenic (DPPIV-Tg) mice. These results suggest that inhibition of DPPIV enzyme activity regulates pruritus in PSO.

2. Materials and methods

2.1. Patients and serum collections and storage

The base cohort consisted of all PSO patients regularly seen and treated at the Juntendo Urayasu Hospital between May 2013 and

October 2014. Peripheral blood samples were collected from 48 PSO patients and 18 healthy adult volunteers, using BD Vacutainer blood collection tube SSTII (BD, Franklin Lakes, NJ). Serum was obtained from 5 mL whole blood by centrifugation at 1500 × g at 4 °C for 10 min, and stored at –80 °C in 500 μL aliquots. Human study protocols were approved by the Ethics Committees at the Juntendo Urayasu Hospital (Authorization Number 2013074). Informed consent was obtained from all patients. All studies on human subjects were conducted according to the principles set out in the Declaration of Helsinki.

2.2. Reagents and recombinant proteins

Recombinant full-length SP(1–11) and the DPPIV inhibitor sitagliptin were purchased from Peptide Institute (Osaka, Japan) and Sigma-Aldrich (St Louis, MO), respectively. Truncated SP(5–11) pyroglutamyl peptide was purchased from Eurofins Genomics (Ebersberg, Germany). IMQ (5% Beselna Cream) and control Absorptive cream were purchased from Mochida Pharmaceutical (Tokyo, Japan) and Nikko (Gifu, Japan), respectively. Recombinant sCD26 protein containing DPPIV enzyme activity (rsCD26(DPPIV+)) and mutant rsCD26 with deficient DPPIV enzyme activity (rsCD26(DPPIV–)) were produced according to the method described previously [13].

2.3. Animals

C57BL/6 mice were purchased from CLEA Japan (Tokyo, Japan). CD26^{–/–} mice developed from C57BL/6 mice were kindly gifted from the laboratory of Dr. Takeshi Watanabe at Kyusyu University (Fukuoka, Japan) [35]. DPPIV-Tg mice developed from C57BL/6 mice were kindly provided from the laboratory of Dr. Chien-Te K. Tseng at University of Texas Medical Branch (Texas) [36]. These mice were bred in-house and used at 8–11 weeks of age. They were kept under controlled temperature (23–25 °C) and light (on time 8:00 A.M.–8:00 P.M.) conditions. Food and water were freely available. All experiments on animals were approved by animal ethics committee in Juntendo University (Authorization Numbers 270242 and 280038).

2.4. sCD26 concentration and DPPIV enzyme activity assay procedure

For measurement of sCD26 concentration and DPPIV enzyme activity in human samples, serum samples were removed from the –80 °C freezer and quickly thawed in a water bath at 37 °C. All samples were centrifuged 3000 × g for 5 min to discard debris, and were then assayed in duplicate. An in-house sandwich ELISA for sCD26 and sDPPIV enzyme was established in our laboratory [14,37]. For evaluation of SP concentrations in human samples, the serum levels of SP and its fragments were evaluated utilizing two distinct ELISA kits, one detects SP(1–11), (2–11) and (3–11) (Substance P ELISA kit, Abcam, Cambridge, MA), and the other, SP(4–11) and (5–11) as well as SP(1–11), (2–11) and (3–11) (Substance P (Human, Rat, Mouse)-EIA kit, Phoenix Pharmaceuticals, Burlingame, CA). For measurement of DPPIV enzyme activity in murine samples, peripheral blood was harvested from tail vein at the indicated periods. After the blood samples were centrifuged to isolate sera, levels of DPPIV activity were measured utilizing DPPIV-Glo Protease Assay (Promega, Fitchburg, WI). For blood glucose analysis in murine sera, mice were put into an acrylic cage for 1 hr for acclimation and for food deprivation, followed by i.p. injection of 30 mM of sitagliptin or saline. Peripheral blood samples were harvested from tail vein, and the blood glucose concentrations were measured utilizing animal glucometer LAB Gluco (ForaCare Inc. CA) at the indicated periods.

Table 1
Demographic characteristics of cohorts.

Variable	Patients with PSO (n = 48)	Healthy Control (n = 18)
Age, years, mean \pm SD (range)	49.9 \pm 14.9 (19–88)	45.1 \pm 10.3 (25–65)
Male/Female, n (ratio)	41/7 (5.9)	15/3 (5.0)
BMI, kg/m ² , mean \pm SD (range)	26.9 \pm 2.0 (19.3–42.3)	24.6 \pm 1.5 (18.4–32.0)
PASI score, points, mean \pm SD (range)	12.2 \pm 12.0 (0.0–60.0)	N/A
Itch VAS, mm, mean \pm SD (range)	29.4 \pm 31.0 (0–100)	N/A
Use of Biologics ^a , n (%)	13 (27.1%)	N/A
Use of Immunosuppressant ^b , n (%)	2 (4.0%)	N/A

BMI, body mass index; n, number; N/A, not applicable; SD, standard deviation; PASI, psoriasis area and severity index at blood collection; PSO, psoriasis; VAS, visual analogue scale at blood collection.

^a Biologics includes anti-TNF α , anti-IL-12/23p40 and anti-IL-17A monoclonal antibody therapy.

^b Immunosuppressant includes oral prednisolone and methotrexate.

2.5. In vitro digestion assay for SP and amino acid sequence analysis

Recombinant full-length SP(1–11) was incubated with rsCD26 (DPPIV+) or rsCD26(DPPIV-) at a molecular ratio of 100:1. For DPPIV inhibition experiments, 5 nmol of sitagliptin was added to the recombinant full-length SP(1–11) and rsCD26(DPPIV+) at a molecular ratio of 100:1. After incubation at 37 °C for 4 h, aliquots were transferred to PVDF membrane and subjected to N-terminal amino acid sequencing as determined by the Edman method (Toray Research Center Inc., Tokyo, Japan).

2.6. Itch murine models

For SP-induced itch murine model, mice hairs were clipped over the rostral part of the back one day before experiment. Under isoflurane anesthesia, mice received i.d. injection of full-length SP (1–11), truncated SP(5–11) or control solvent at the indicated doses, and then subjected to scratching behavior evaluation. For IMQ-induced psoriatic itch murine model, mice received a daily dose of 30 mg of IMQ or control vehicle cream on the shaved back for 5 days. On the 6th day, mice were subjected to scratching behavior evaluation as described below. On the 7th day, after macrophotographs of mice were taken, mice were sacrificed, and the skin specimens were harvested for histopathology examination.

2.7. Measurement of scratching behavior and locomotor activity

Before behavioral recording, mice (4 animals per observation) were put into an acrylic cage (19.5 \times 24 \times 35 cm) for at least one hour for acclimation. Subsequently, the frequency of scratch behavior of the rostral back was analyzed by the SCLABA®-Real system (NOVERTEC, Kobe, Japan) for the indicated time intervals, with observers being kept out of the experimental room. For evaluation of locomotor activities, mice were put into an acryl cage by the same method as in the scratching behavior evaluation, and were evaluated with the use of the SCLABA®-Real tracking software. Locomotor activities were measured and expressed as the total horizontal moving distance of mice during itch behavioral experiments.

2.8. Tissue histopathology

Skins from the upper back of treated mice were fixed in 10% formalin, embedded in paraffin, sectioned, mounted on slides, and stained with hematoxylin and eosin (H&E) to determine pathology. Images were captured with an Olympus digital camera DP21 attached to an Olympus BX43 microscope using CellSens software (OLYMPUS, Tokyo, Japan). Slides were evaluated by a pathologist blinded to experimental groups.

2.9. Statistics

All experiments were performed in triplicates and repeated at least 3 times. Data were expressed as mean values \pm SEM (standard error of the mean), and were analyzed by two-tailed Student's *t*-test for two group comparison or by ANOVA test for multiple comparison testing followed by the Tukey-Kramer *post-hoc* test. *P* values <0.05 were considered statistically significant. Calculations were performed and graphed using GraphPad Prism 6 (GraphPad Software Inc., La Jolla, CA).

3. Results

3.1. Serum levels of sCD26 and sDPPIV enzyme are increased in patients with PSO

To determine whether sCD26 and sDPPIV enzyme play a role in PSO, we first evaluated levels of sCD26 and sDPPIV enzyme activity in sera of patients with PSO. For this purpose, peripheral blood samples were collected from healthy adult volunteers and PSO patients (regularly seen and treated at the Juntendo Urayasu Hospital). Of the 48 patients, mean (years \pm S.D.) age was 49.9 (\pm 16.9), male/female was 41/7. No patients with diabetes mellitus,

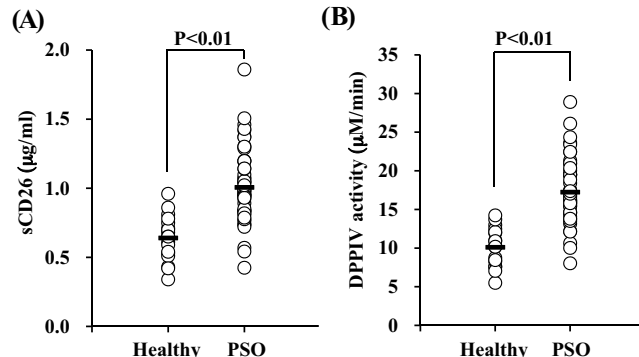


Fig. 1. Serum levels of sCD26 and DPPIV enzyme activity in patients with PSO. (A) Levels of sCD26 were measured in sera of PSO patients (n = 48) or healthy adult volunteers (n = 18). Levels of sCD26 in PSO patients were significantly increased as compared with healthy controls (1.02 ± 0.28 v.s. 0.64 ± 0.16 μ g/ml; $P < 0.01$ by two-tailed Student's *t*-test). Each dot indicates individual value. The horizontal lines in the middle of scattergrams indicate each mean value. sCD26 concentration was measured using our in-house capture method as described in Materials and Methods. (B) Levels of sDPPIV enzyme activity were measured in sera of PSO patients (n = 48) or healthy adult volunteers (n = 18). Levels of sDPPIV enzyme activity in PSO patients were significantly increased as compared to healthy controls (17.38 ± 4.18 v.s. 10.17 ± 2.47 μ M/min; $P < 0.01$ by two-tailed Student's *t*-test). Each dot indicates individual value. DPPIV enzyme activity was measured using our in-house capture method as described in Materials and Methods.

hepatic or renal dysfunction were included in PSO cohort to exclude the possible influence of these conditions on serum levels of DPPIV enzyme activity [12,24]. Of the 18 healthy adult volunteers, mean (years \pm S.D.) age was 45.1 (\pm 10.3), male/female was 15/3. All healthy adult volunteers had no history of cancers and chronic diseases including diabetes mellitus, hepatic diseases, allergic diseases, HIV infection, PSO and atopic dermatitis. There was no significant difference in body mass index between PSO and control cohorts ($26.9 \pm 2.0 \text{ kg/m}^2$ v.s. $24.6 \pm 1.5 \text{ kg/m}^2$, $p = 0.287$ by two-tailed Student's *t*-test). Other demographic characteristics of the patients are summarized in Table 1.

As shown in Fig. 1A, serum sCD26 concentration of PSO patients was significantly higher than that of healthy adults ($1.02 \pm 0.28 \mu\text{g/ml}$ v.s. $0.64 \pm 0.16 \mu\text{g/ml}$). Moreover, it has been reported that DPPIV enzymatic activity was correlated with the concentration of sCD26 in normal human sera [37,38]. We therefore evaluated for potential correlation between DPPIV

enzymatic activity and sCD26 level in the serum samples described above. For this purpose, we performed our in-house capture assay method using anti-human CD26 mAb as a capture antibody for detecting DPPIV enzyme activity specific to sCD26 [37]. Since commercially available DPPIV enzyme assay kits measure DPPIV activity in whole serum, but not in captured sCD26 molecules from the samples, it is possible that DPPIV-like peptidase activity other than that possessed by the captured sCD26 molecules was measured, leading to an overestimate of the DPPIV activity in the samples [39]. As shown in Fig. 1B, serum levels of sDPPIV enzyme activity were also significantly higher in patients with PSO compared with healthy adult controls ($17.38 \pm 4.18 \mu\text{M/min}$ v.s. $10.17 \pm 2.47 \mu\text{M/min}$). These data suggest that DPPIV enzyme activity is increased in sera of patients with PSO, which is linked to a concomitant increase in sCD26 in the same patient population. These observations also suggest that DPPIV enzyme plays a role in the pathogenesis of PSO.

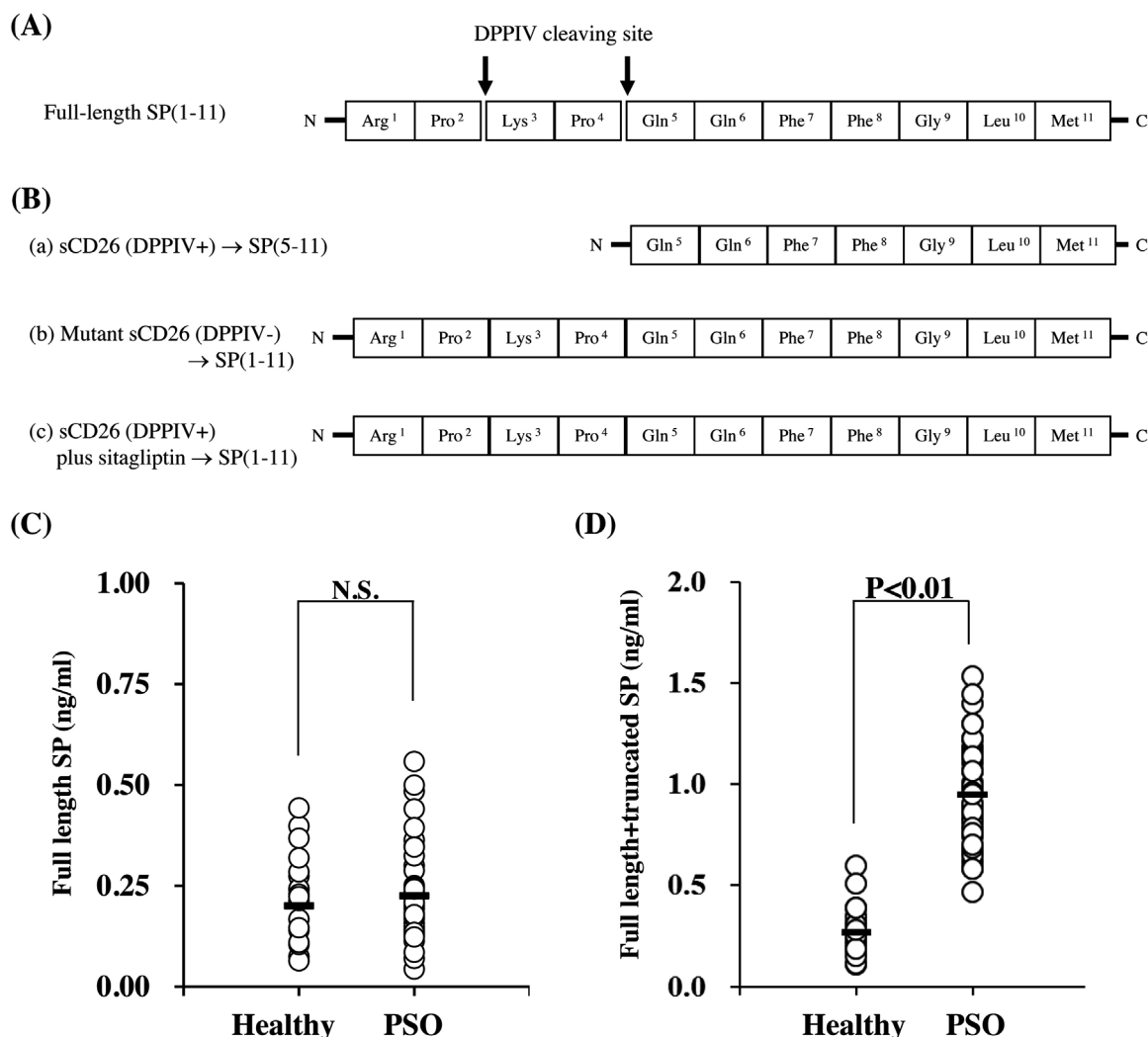


Fig. 2. *In vitro* digestion assay of substance P (SP) and serum levels of full length and truncated SP in patients with PSO. **(A)** Schematic diagram of amino acid sequence of full-length SP(1-11). Arrows indicate two DPPIV cleavage sites. **(B)** The recombinant full-length SP(1-11) was incubated with rsCD26(DPPIV+) (panel a) or rsCD26(DPPIV-) (panel b). For DPPIV inhibition experiment, sitagliptin was added to recombinant full-length SP(1-11) and rsCD26(DPPIV+) (panel c). After incubation at 37 °C for 4 h, aliquots were transferred to PVDF membrane and subjected to N-terminal amino acid sequencing as determined by the Edman method. The results of amino acid sequencing were shown in each right panel. **(C)** The levels of SP(1-11), (2-11), and (3-11) were measured in sera of PSO patients ($n = 48$) or healthy adult volunteers ($n = 18$). There was no significant difference in the serum levels of SP(1-11), (2-11), and (3-11) between PSO patients and healthy controls (0.23 ± 0.11 v.s. $0.22 \pm 0.11 \text{ ng/ml}$; $p = 0.95$ by two-tailed Student's *t*-test). Each dot indicates individual value. The horizontal lines in the middle of scattergrams indicate each mean value. **(D)** The levels of SP(4-11) and (5-11), including SP(1-11), (2-11) and (3-11) concentrations, were measured in sera of PSO patients ($n = 48$) or healthy adult volunteers ($n = 18$). The serum levels of SP(4-11) and (5-11), including SP(1-11), (2-11) and (3-11) in PSO were significantly increased as compared to healthy controls (0.95 ± 0.25 v.s. $0.28 \pm 0.13 \text{ ng/ml}$; $P < 0.01$ by two-tailed Student's *t*-test). Each dot indicates individual value. The horizontal lines in the middle of scattergrams indicate each mean value.

3.2. Truncated form of SP cleaved by DPPIV enzyme is increased in sera of PSO patients

It is well-known that many patients with PSO have pruritus that is generally refractory to therapy. Among various mediators of pruritus investigated in inflammatory skin diseases, SP is one of key molecules in an itch sensory nerve. While SP consists of 11 amino acids residues with dual DPPIV cleavage sites at its N-terminal position (Fig. 2A), it is unclear whether truncation of SP by DPPIV enzyme plays a role in pruritus in inflammatory skin lesions. To determine whether DPPIV enzyme cleaves full-length SP(1–11), we performed *in vitro* digestion experiments utilizing rsCD26 protein. For this purpose, recombinant full-length SP(1–11) was incubated with rsCD26 protein containing DPPIV enzyme activity (rsCD26(DPPIV+)), and an amino acid sequence analysis was performed to determine the amino acid sequence of incubated SP. Our findings indicated that rsCD26(DPPIV+) digested recombinant full-length SP(1–11), resulting in a truncated form of SP(5–11) (Fig. 2B–(a)), while rsCD26(DPPIV–) exhibited no digestive activity on SP(1–11) (Fig. 2B–(b)). On the other hand, digestion of recombinant full-length SP(1–11) by rsCD26(DPPIV+) was inhibited by the presence of the DPPIV enzyme inhibitor sitagliptin (Fig. 2B–(c)). These data indicate that native sCD26 containing DPPIV enzyme activity in sera degrades full-length SP(1–11), leading to the formation of SP(5–11).

To expand on these *in vitro* findings, we next analyzed the serum concentrations of full-length and truncated SP in patients with PSO. For this purpose, we utilized two different ELISA kits, one detects SP(1–11), (2–11) and (3–11), and the other, SP(4–11) and (5–11) as well as SP(1–11), (2–11) and (3–11). As shown in Fig. 2C, levels of SP(1–11), (2–11) and (3–11) in sera of PSO were similar to those in healthy controls (0.23 ± 0.11 ng/ml v.s. 0.22 ± 0.11 μ g/ml). On the other hand, serum levels of SP (4–11) and (5–11) were significantly increased in patients with PSO compared with healthy controls (0.95 ± 0.25 ng/ml v.s. 0.28 ± 0.13 μ g/ml) (Fig. 2D). Taken together with the above data, our observations suggest that levels of SP degraded by DPPIV were increased in sera of patients with PSO, and that the increase in DPPIV activity appears to play an important role in PSO by truncation of SP.

3.3. DPPIV inhibitor suppresses SP-induced pruritus

We next utilized *in vivo* models to determine whether DPPIV activity regulates pruritus induced by SP. For this purpose, we established an itchy mouse model by intradermal injection (i.d.) of full-length SP(1–11) and quantified scratching behavior in mice to determine an itchy symptom. As shown in Fig. 3A, mice treated with SP i.d. demonstrated increased scratching behavior in a dose-dependent manner of SP. Utilizing this itch model, we evaluated the effect of the DPPIV inhibitor sitagliptin on pruritus. Since we could not formally exclude the possibility that the DPPIV inhibitor induced hypoglycemia and decreased activity in treated mice, resulting in reduced scratching behavior, we measured the blood glucose levels in mice receiving sitagliptin. As shown in Fig. 3B, suppression of DPPIV enzyme activity in mice sera was clearly observed from 5 to 30 min after intraperitoneal injection (i.p.) of sitagliptin at doses of 30 mM. Meanwhile, blood glucose levels in mice treated with 30 mM of sitagliptin were similar to those in mice treated with control saline (Fig. 3C). These data suggest that *in vivo* DPPIV inhibition is observed in mice treated by i.p. sitagliptin, while mice receiving this regimen of sitagliptin did not develop hypoglycemia which might have an effect on locomotor activity. We therefore administered 30 mM of i.p. sitagliptin to SP-induced itchy model mice, and measured the frequency of scratching behavior for 1 h. Under these experimental conditions, scratching behavior in SP(1–11) i.d. mice was significantly

decreased in mice treated with sitagliptin (115.9 ± 49.1 v.s. 13.6 ± 9.4 times/hr) (Fig. 3D). On the other hand, sitagliptin had no effect on the scratching behavior of mice treated with i.d. of control solvent (3.3 ± 3.5 v.s. 9.3 ± 9.5 times/h) (Fig. 3D). Meanwhile, there were no significant differences in movement length among all cohorts, indicating that the decreased scratching behavior did not result from decreased mouse activity (Fig. 3E). To further confirm that suppression of DPPIV enzyme activity decreased SP-induced pruritus, we used CD26KO mice to evaluate scratching behavior induced by SP(1–11). As shown in Fig. 3F, SP-induced scratching behavior was significantly attenuated in CD26KO mice compared with that observed in C57BL/6 wild type mice (36.5 ± 28.3 v.s. 97.0 ± 50.9 times/h). Meanwhile, there were no significant differences in movement length between CD26KO and wild type mice, indicating that the decreased scratching behavior did not result from decreased mouse activity (Fig. 3G). To show effects of truncated form of SP(5–11) on pruritus, an itch mouse model experiment was conducted utilizing i.d. injection of recombinant SP(5–11) peptide. As shown in Fig. 3H, mice treated with SP(5–11) i.d. demonstrated significant increase in scratching behavior (158.5 ± 29.3 times/h), compared with mice receiving control solvent (12.7 ± 9.5 times/h) or mice receiving full-length SP (1–11) (104.5 ± 30.7 times/h). Meanwhile, there were no significant differences in movement length among SP(1–11), SP(5–11)-treated and control mice, indicating that the increased scratching behavior did not result from increased mouse activity (Fig. 3I). Taken together, our data suggest that SP-induced itch sensation is attenuated by inhibition of the DPPIV activity.

3.4. DPPIV inhibitor suppresses IMQ-induced psoriatic itch

To further determine that DPPIV inhibition affects pruritus, we evaluated scratching behavior utilizing an IMQ-induced psoriatic itch model [40,41]. For this purpose, mice were treated with IMQ cream or control absorptive cream at a daily dose of 30 mg on the rostral part of the back for 5 consecutive days. As shown in Fig. 4A, mice treated with control absorptive cream showed no sign of psoriatic features (panel a), while IMQ-treated mice exhibited psoriasis-like skin including erythema, scaling and thickness (panel b). Histopathology of skin specimens obtained from IMQ-treated mice showed hyperkeratosis, acanthosis and infiltration of inflammatory cells which were compatible to those found in psoriatic skin (panel e of Fig. 4A). On the other hand, histopathology of skin specimens from control cream-treated mice showed none of these pathologic findings (panel d of Fig. 4A). We next analyzed the serum concentrations of full-length and truncated SP in IMQ-treated mice. As shown in Fig. 4B, levels of SP(1–11), (2–11) and (3–11) in sera of IMQ-treated mice were similar to those in control cream-treated mice (0.32 ± 0.06 ng/ml v.s. 0.39 ± 0.01 μ g/ml). On the other hand, serum levels of SP (4–11) and (5–11) were significantly increased in IMQ-treated mice compared with control cream-treated mice (0.63 ± 0.09 ng/ml v.s. 0.32 ± 0.08 μ g/ml) (Fig. 4C). Moreover, scratching behavior was significantly increased in IMQ-treated mice than control cream-treated mice (118.7 ± 47.2 v.s. 26.7 ± 20.9 times/hr) (Fig. 4D). These data indicate that IMQ induces psoriatic itchy skin lesions in mice associated with an increase in the truncation of SP. Utilizing this psoriatic itch model, we analyzed the frequencies of itch scratching behaviors with DPPIV inhibitor administration. As shown in Fig. 4D, IMQ-treated mice receiving sitagliptin showed significant decrease of scratching behavior compared with IMQ-treated mice receiving control solvent (31.0 ± 16.0 v.s. 118.7 ± 47.2 times/hr). Meanwhile, there was no change in scratching behavior between control cream-treated mice receiving sitagliptin or control saline (30.8 ± 17.8 v.s. 26.7 ± 20.9 times/hr), with baseline levels of scratching behavior in both cohorts. Moreover, there were no

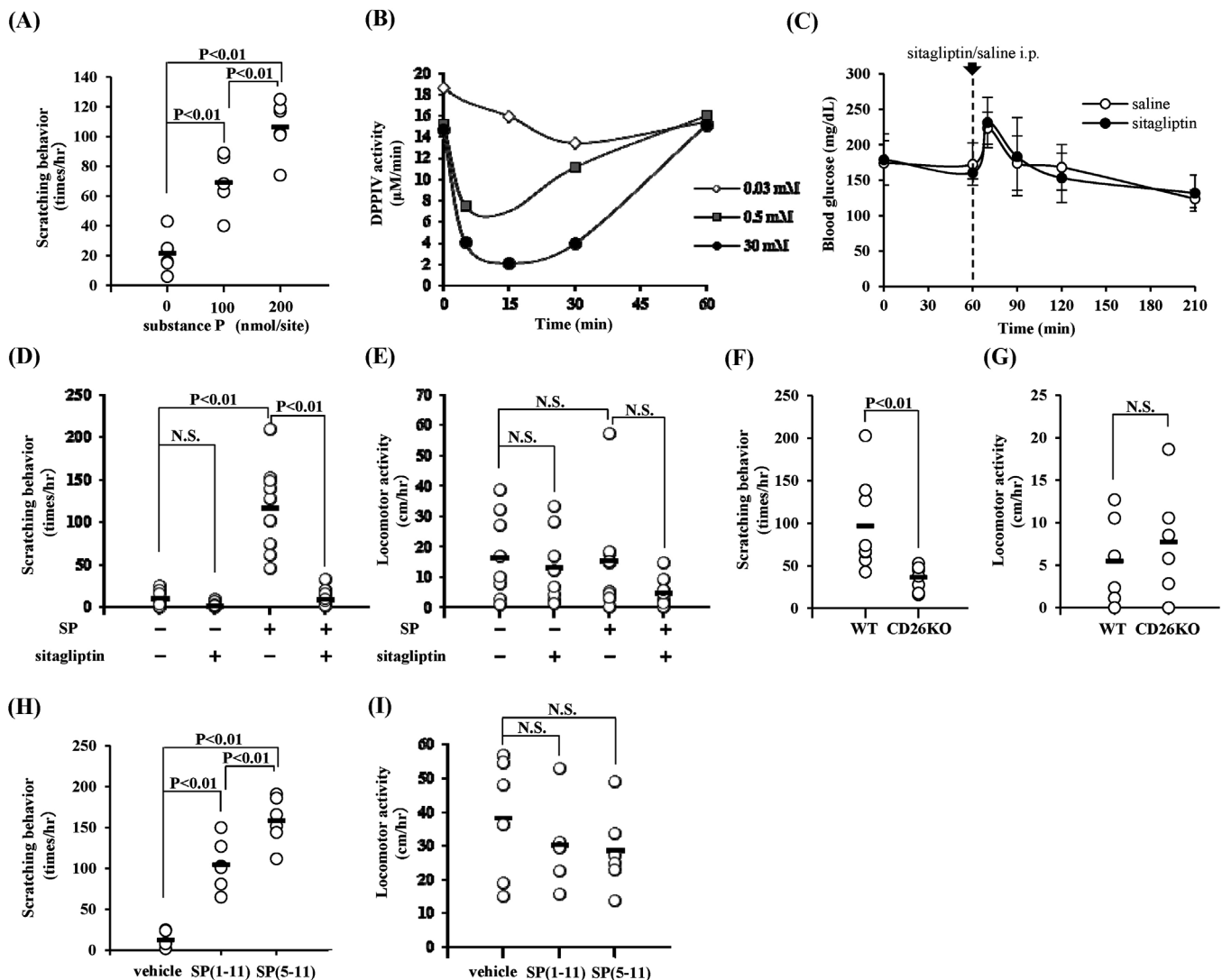


Fig. 3. Treatment with DPPIV inhibitor attenuates SP-induced pruritus. (A) Recombinant full-length SP(1–11) was injected at doses of 0 (saline), 100 or 200 nmol per site by i.d. into the rostral back of C57BL/6 mice. The frequency of scratching behavior was counted for 1 hr as described in Materials and Methods. Mice receiving saline exhibited scratching behavior of 21.5 ± 12.3 times/hr ($n = 6$). On the other hand, mice receiving 100 or 200 nmol of SP exhibited scratching behavior of 68.3 ± 17.9 or 106.3 ± 18.6 times/hr, respectively (each, $n = 6$), showing significant increase of scratching behavior in a dose-dependent manner of SP. Each dot indicates an individual value and the horizontal bar represents average value. (B) Representative plot of mean values of serum DPPIV enzyme activity in mice receiving the DPPIV inhibitor sitagliptin is shown. Sitagliptin was injected at doses of 0.03, 0.5 or 30 mM by i.p. Peripheral blood was harvested at 0, 5, 15, 30 and 60 min after injection, and levels of DPPIV enzyme activity were determined as described in Materials and Methods. Serum levels of DPPIV activity were decreased in a dose-dependent manner of sitagliptin. At 30 mM of sitagliptin, DPPIV enzyme activity in C57BL/6 mice clearly decreased to less than 20% of the value prior to administration, and lasted for at least 30 min. Similar results were observed in independent experiments ($n = 6$). (C) Blood glucose levels in mice receiving the DPPIV inhibitor sitagliptin is shown ($n = 6$). The blood glucose levels were measured at 0 (before 1 hr food deprivation), 60 (before 30 mM sitagliptin i.p. injection), 70, 90, 120 and 210 min. Hypoglycemia was not observed in mice treated with sitagliptin in these experimental conditions. (D) Mice were treated with recombinant full-length SP(1–11) (200 nmol per site) or physiological saline by i.d. and with sitagliptin (30 mM) or saline by i.p. (each, $n = 10$). The frequency of scratching behavior of the rostral back was counted for 1 h by the method as described in Materials and Methods. Scratching behavior was significantly increased in mice treated with 200 nmol of SP compared with control mice (115.9 ± 49.1 v.s. 9.3 ± 9.5 times/hr, $p < 0.01$ v.s. saline cohorts by ANOVA). DPPIV inhibition alone showed no significant changes in scratching behavior (3.3 ± 3.5 times/hr, N.S. denotes 'not significant'). Each dot indicates an individual value and the horizontal bar represents average value. (E) Locomotor activities of mice were measured as total horizontal moving distance during itch behavioral experiment as conducted in (D). There was no significant difference among control mice, mice receiving saline i.d. and sitagliptin i.p., mice receiving SP i.d. and saline i.p., and mice receiving SP i.d. and sitagliptin i.p. (Each, $n = 10$; 16.9 ± 14.1 v.s. 13.4 ± 12.1 v.s. 15.1 ± 16.2 v.s. 4.8 ± 4.7 cm/hr, respectively). Each dot indicates an individual value and the horizontal bar represents average value. N.S. denotes 'not significant' by ANOVA. (F) Wild type C57BL/6 (WT) and CD26 knockout (CD26KO) mice were treated with recombinant full-length SP(1–11) (200 nmol/site) by i.d. The frequency of scratching behavior was counted for 1 hr as described in Materials and Methods. The frequency of CD26KO mice scratching behavior was significantly decreased as compared to wild type mice (each, $n = 8$, 97.0 ± 50.9 v.s. 36.5 ± 23.3 times/hr, $p < 0.01$ by two-tailed Student's *t*-test). Each dot indicates an individual value and the horizontal bar represents average value. (G) Conducted simultaneously with itch behavior experiment as shown in (F), locomotor activities of CD26KO mice were measured as described in Materials and Methods. There was no significant difference in locomotor activity between WT and CD26KO (5.9 ± 4.1 v.s. 7.5 ± 2.5 cm/hr, $p = 0.535$ by two-tailed Student's *t*-test). Each dot indicates an individual value and the horizontal bar represents average value. N.S. denotes 'not significant'. (H) Mice were treated with recombinant full-length SP(1–11), truncated SP(5–11) (200 nmol per site) or control solvent (10%DMSO and 0.00625 M acetate in physiological saline) by i.d. (each, $n = 6$). The frequency of scratching behavior was evaluated by the same method as described in (D). Scratching behavior was significantly increased in mice treated with SP(1–11) (104.5 ± 30.7 times/hr) or SP(5–11) (158.5 ± 29.3 times/hr) than control mice (12.7 ± 9.5 times/hr) (each $p < 0.01$ by ANOVA). Moreover, scratching behavior was significantly increased in mice treated with SP(5–11) compared with mice receiving SP(1–11) ($p < 0.01$ by ANOVA). Each dot indicates an individual value and the horizontal bar represents average value. (I) Locomotor activities of mice were measured as total horizontal moving distance during itch behavioral experiment as conducted in (H). There was no significant difference among mice receiving control solvent, full-length SP(1–11) or truncated SP(5–11) i.d. (38.3 ± 18.0 v.s. 30.2 ± 12.5 v.s. 28.6 ± 12.0 cm/hr). Each dot indicates an individual value and the horizontal bar represents average value. N.S. denotes 'not significant' by ANOVA.

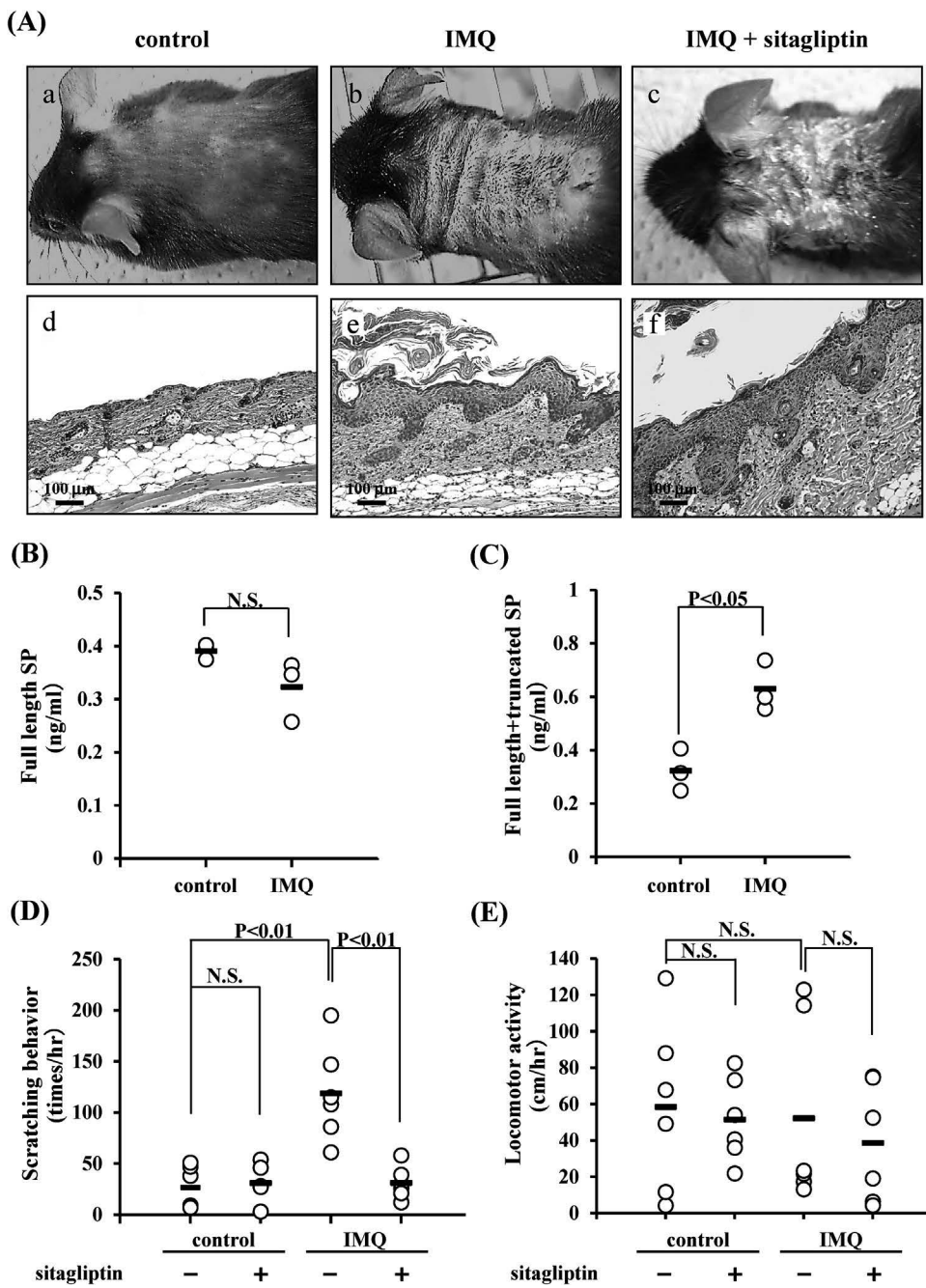


Fig. 4. DPPIV inhibitor attenuates IMQ-induced PSO derived itch. C57BL/6 mice were treated with IMQ cream or control vehicle cream at a daily dose of 30 mg on the rostral part of back for 5 days. On the 6th day, mice were treated with i.p. of sitagliptin (30 mM) or physiological saline, and then subjected to scratching behavior and locomotor activity analyses. (A) Representative macroscopic photographs of back skins of control cream-treated mice (panel a), IMQ cream-treated mice (panel b) or IMQ cream-treated mice receiving the DPPIV inhibitor sitagliptin (panel c) are shown. H&E staining histology of skin specimens obtained from each mouse is shown in panels d, e or f, respectively. Similar results were observed in independent experiments (n=6). Original magnification $\times 100$. Scale bars, 100 μ m. (B) The levels of SP(1–11), (2–11), and (3–11) were measured in sera of IMQ or control cream-treated mice on the 6th day after treatment (each, n=3), utilizing the same ELISA kit as conducted in Fig. 2C. There was no significant difference in the serum levels of SP(1–11), (2–11), and (3–11) between IMQ and control cream-treated mice (0.32 ± 0.06 v.s. 0.39 ± 0.01 ng/ml; $p = 0.11$ by two-tailed Student's *t*-test). Each dot indicates individual value. The horizontal lines in the middle of scattergrams indicate each mean value. N.S. denotes 'not significant'. (C) The levels of SP(4–11) and (5–11), including SP(1–11), (2–11) and (3–11) concentrations, were measured in sera of IMQ or control cream-treated mice on the 6th day after treatment (each, n=3), utilizing the same ELISA kit as conducted in Fig. 2D. The serum levels of SP(4–11) and (5–11) including SP(1–11), (2–11) and (3–11) in IMQ-treated mice were significantly increased as compared with control cream-treated mice (0.63 ± 0.09 v.s. 0.32 ± 0.08 ng/ml; $P < 0.05$ by two-tailed Student's *t*-test). Each dot indicates individual value. The horizontal lines in the middle of scattergrams indicate each mean value. N.S. denotes 'not significant'. (D) The frequency of scratching behavior was counted for 2 hr after injection of sitagliptin or saline. Mice receiving sitagliptin showed significantly decreased IMQ-induced itch scratching behavior compared with IMQ-treated mice receiving saline (each, n=6; 31.0 ± 16.0 v.s. 118.7 ± 47.2 times/hr, $p < 0.01$ by ANOVA). Meanwhile, treatment with the DPPIV inhibitor alone resulted in no significant change in the frequency of scratching behavior in control cream-treated mice (each, n=6; 30.8 ± 17.8 v.s. 26.7 ± 20.9 , $p = 0.989$ by ANOVA). Each dot indicates an individual value and the horizontal bar represents average value. N.S. denotes 'not significant'. (E) Locomotor activities of mice were measured as total horizontal moving distance during itch behavioral experiment as conducted in (D). There was no significant difference among control cream-treated mice receiving saline or sitagliptin, and IMQ-treated mice receiving saline or sitagliptin i.p. (Each, n=6; 58.4 ± 47.3 v.s. 51.4 ± 23.1 v.s. 38.7 ± 32.9 cm/hr, respectively). Each dot indicates an individual value and the horizontal bar represents average value. N.S. denotes 'not significant' by ANOVA.

significant differences in movement length among all cohorts, indicating that the decreased scratching behavior did not result from decreased mouse activity (Fig. 4E). In addition, there was no additional phenotypic and histologic change induced by the administration of sitagliptin (panels c and f of Fig. 4A), similar to those seen in IMQ-treated mice (panels b and e of Fig. 4A). Taken together, our data suggest that treatment with the DPPIV inhibitor sitagliptin attenuates psoriatic itch sensation via a decrease in the truncated form of SP.

3.5. Overexpression of CD26/DPPIV exaggerates IMQ-induced psoriatic itch

Finally, to further determine that DPPIV enzyme activity is associated with pruritus, we used DPPIV-Tg mice to analyze scratching behavior. As shown in Fig. 5A, DPPIV-Tg mice exhibited significant increase in DPPIV enzyme activity in sera compared with parental WT mice (177.5 ± 34.4 v.s. $14.9 \pm 2.6 \mu\text{M}/\text{min}$). Scratching behavior induced by IMQ cream was significantly increased in DPPIV-Tg mice than in WT mice (188.6 ± 66.2 v.s. 107.6 ± 45.9 times/hr) (Fig. 5B). Meanwhile, there was no change in scratching behavior between WT and DPPIV-Tg mice treated with control cream (44.9 ± 19.6 v.s. 40.5 ± 15.5 times/hr), with baseline levels of scratching behavior in both cohorts (Fig. 5B). Moreover, there were no significant differences in movement length between IMQ-treated WT and DPPIV-Tg mice, indicating that the observed increase in scratching behavior did not result from increased mouse activity (Fig. 5C). Taken together with the above data, our findings strongly suggest that increased DPPIV enzyme activity exaggerates psoriatic pruritus and that DPPIV may be a novel target for treatment of itch sensation in psoriasis.

4. Discussion

In the present study, we demonstrated that serum levels of DPPIV enzyme activity was significantly increased in patients with PSO, concomitant with elevation of truncated form of SP. Moreover, overexpression of DPPIV enzyme activity exaggerated itch scratching behavior in psoriatic pruritus murine model induced

by IMQ cream. Furthermore, treatment with the DPPIV inhibitor sitagliptin improved itch scratching behavior in murine pruritus models induced by SP administration or IMQ cream.

Pruritus is an important symptom of PSO. Despite the fact that several studies have been undertaken to investigate the pathogenesis of pruritus in psoriasis, many aspects of this clinical manifestation have not yet been thoroughly examined [1,32]. Therefore, the pathogenesis of this symptom is far from being well-understood and, as a consequence, effective therapy for pruritus in psoriatic patients still remains a significant challenge in the clinical setting [42]. It has been shown previously that keratinocytes expressed high levels of DPPIV and that DPPIV inhibition suppressed keratinocyte proliferation *in vitro*, and partially restored keratinocyte differentiation *in vivo* [43]. It has also been reported that DPPIV activity on keratinocytes was upregulated in PSO [22,44], suggesting a potential role for DPPIV enzyme activity in the pathogenesis of PSO. While other investigators have reported a significant improvement in disease severity in patients with PSO treated with sitagliptin [21,45], the precise mechanisms involved in the effect of DPPIV inhibition on PSO have not been elucidated.

DPPIV is expressed as CD26 on T cells and DPPIV-mediated T cell activation has been demonstrated [46]. Recent report showed that the T-cell bound expression of CD26/DPPIV in psoriatic skin was explicitly present, albeit in small quantities [44]. One hypothesis regarding the potential effect of DPPIV in PSO is that T cell activation mediated by DPPIV is associated with the pathogenesis of PSO [47]. Cytokines and chemokines represent the third key player in the psoriatic chronic immune response [48], and are mediators responsible for the activation and recruitment of infiltrating leucocytes, therefore playing a crucial role in the development and persistence of psoriatic skin lesions [49]. DPPIV likely has a pivotal role in the processing of these molecules [46]. The extracellular protease domain of DPPIV (both on keratinocytes and T cells) can cleave dipeptides from the amino terminus of proteins, such as cytokines and chemokines, which are abundantly present in a chronic immune response in PSO, resulting in alterations in receptor specificity and a subsequent reduction in biological activity. Taken together, it is conceivable that in PSO, a

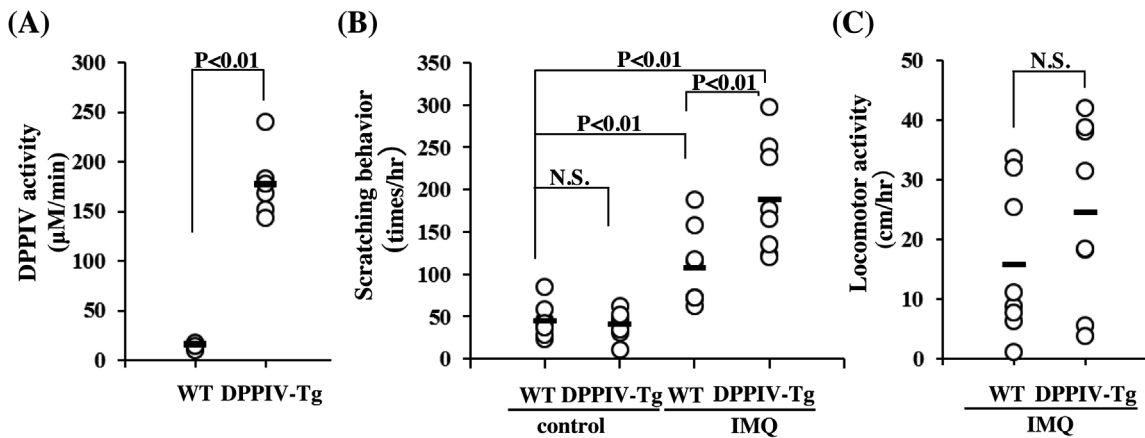


Fig. 5. Overexpression of DPPIV aggravates IMQ-induced psoriatic itch. (A) DPPIV enzyme activities in sera of Wild type C57BL/6 (WT) or DPPIV-Tg mice were determined as described in Materials and Methods. DPPIV-Tg mice exhibited a significant increase in DPPIV enzyme activity in sera compared with parental WT mice (each, $n=6$; 177.5 ± 34.4 v.s. $14.9 \pm 2.6 \mu\text{M}/\text{min}$, $p < 0.01$ by Student's *t*-test). Each dot indicates an individual value and the horizontal bar represents average value. (B) WT and DPPIV-Tg mice were treated with IMQ cream or control vehicle cream at a daily dose of 30 mg on the rostral part of the back for 5 days (each, $n=8$). Control cream-treated WT and DPPIV-Tg mice showed no significant difference in scratching behavior (44.9 ± 19.6 v.s. 40.5 ± 15.5 times/hr, $p = 0.993$ by ANOVA), while IMQ-treated WT or DPPIV-Tg mice exhibited increased scratching behavior, compared with each control cream-treated mice (44.9 ± 19.6 v.s. 107.6 ± 46.9 or 40.5 ± 15.5 v.s. 188.6 ± 66.2 times/hour, respectively; each $p < 0.01$ by ANOVA). Scratching behavior induced by IMQ-treated DPPIV-Tg mice was significantly increased compared with IMQ-treated WT mice (188.6 ± 66.2 v.s. 107.6 ± 46.9 times/hr, $p < 0.01$ by ANOVA). Each dot indicates an individual value and the horizontal bar represents average value. N.S. denotes 'not significant'. (C) Locomotor activities of mice were measured as total horizontal moving distance during itch behavioral experiment as conducted in (B). There was no significant difference between WT and DPPIV-Tg mice treated with IMQ cream (Each, $n=8$; 15.8 ± 12.6 v.s. 24.6 ± 15.1 cm/hr, respectively; $p = 0.228$ by Student's *t*-test). Each dot indicates an individual value and the horizontal bar represents average value.

disease involving critical interplays among activated T cells, keratinocytes and cytokines, DPPIV can influence disease behavior by regulating all three components.

SP is a sensory undecapeptide of the tachykinin family distributed widely in the central and peripheral nervous systems, mediating the sensation of itch via small-diameter C fibers in the skin [50,51]. Previous studies have reported that serum levels of SP were decreased in patients with PSO [52–54]. Meanwhile, since SP is cleaved by DPPIV enzyme and DPPIV enzyme activity is increased in PSO as shown in Figs. 1 and 2, it is important for a detailed understanding of the role of SP in PSO to precisely measure the truncated form of SP separately from full-length SP. In our present study, we evaluated full-length SP(1–11) and truncated forms of SP and demonstrated that there was no change in the serum levels of full-length SP(1–11), SP(2–11) and SP(3–11) between PSO and healthy adult controls. However, we found that DPPIV enzyme activity and truncated form of SP were significantly increased in PSO, and that truncated form of SP(5–11) resulting from DPPIV enzyme activity is associated with an increase in itch sensation. In IMQ-induced PSO model, truncated form of SP was significantly increased in sera compared with control mice, and scratching behavior was decreased by administration of sitagliptin. On the other hand, there were no differences in serum levels of DPPIV enzyme activity between IMQ and control cream-treated mice (data not shown). It is conceivable that the persistent existence of psoriatic skin lesions may be required for the increased serum levels of DPPIV enzyme activity seen in PSO patients, and that SP truncation may result from the increased levels of DPPIV enzyme activity in skin lesions rather than in the circulation [22,24]. Regarding the specific receptors mediating the itch sensation of truncated SP, while SP-mediated itch has been reported to be mediated via full-length SP bound to NK-1R [29,31], future studies will be performed to determine whether truncated form of SP acts on NK-1R as an agonistic mediator or targets other pruritic receptors.

Our current study has conclusively demonstrated that increase in DPPIV enzyme activity exacerbates pruritus in PSO, and that inhibition of DPPIV enzyme reduces severity of itch scratching behavior. Moreover, our results suggest that DPPIV inhibitors are useful as therapeutic agents for pruritus including PSO. Additional studies will be conducted in the near future to better characterize and understand PSO-associated pruritus, which may lead to the development of novel effective antipruritic treatment modalities targeting the CD26/DPPIV molecule.

Conflicts-of-interest disclosure

The authors have no conflict of interest to declare.

Funding sources

This work was supported by a Grant-in-Aid (S1311011) from the Foundation of Strategic Research Projects in Private Universities from the Ministry of Education, Culture, Sports, Science, and Technology, Japan; JSPS KAKENHI Grant Number 15H04879; JSPS KAKENHI Grant Number 15K15324; JSPS KAKENHI Grant Number 16H05345; JSPS KAKENHI Grant Number 26830114; a grant of the Ministry of Health, Labour, and Welfare, Japan (Grant Number 150401-01).

Acknowledgements

The authors thank Dr. Airi Jo-Watanabe (Department of Biochemistry, Juntendo University School of Medicine), Dr. Hyeon-cheol Lee (Department of Biochemistry, Juntendo University School of Medicine), Mr. Nobuaki Takahashi (Institute for

Environmental and Gender Specific Medicine, Juntendo University Graduate School of medicine), Mrs. Hiroko Madokoro (Department of Pathology, Keio University School of Medicine) and Mrs. Yuka Narita (Department of Therapy Development and Innovation for Immune Disorders and Cancers, Juntendo University Graduate School of Medicine) for excellent technical assistances and thorough discussion.

References

- J.C. Szepietowski, A. Reich, Pruritus in psoriasis: an update, *Eur. J. Pain* 20 (1) (2016) 41–46.
- B. Amatya, G. Wennersten, K. Nordlind, Patients' perspective of pruritus in chronic plaque psoriasis: a questionnaire-based study, *J. Eur. Acad. Dermatol. Venereol.* 22 (7) (2008) 822–826.
- S.E. Chang, S.S. Han, H.J. Jung, J.H. Choi, Neuropeptides and their receptors in psoriatic skin in relation to pruritus, *Br. J. Dermatol.* 156 (6) (2007) 1272–1277.
- G. Stinco, G. Trevisan, F. Piccirillo, S. Pezzetta, E. Errichetti, N. di Meo, F. Valent, P. Patroni, Pruritus in chronic plaque psoriasis: a questionnaire-based study of 230 Italian patients, *Acta Dermatovenerol. Croat.* 22 (2) (2014) 122–128.
- J.C. Szepietowski, A. Reich, B. Wisnicka, Pruritus and psoriasis, *Br. J. Dermatol.* 151 (6) (2004) 1284.
- G. Yosipovitch, A. Goon, J. Wee, Y.H. Chan, C.L. Goh, The prevalence and clinical characteristics of pruritus among patients with extensive psoriasis, *Br. J. Dermatol.* 143 (5) (2000) 969–973.
- A. Reich, K. Welz-Kubiak, L. Rams, Apprehension of the disease by patients suffering from psoriasis, *Postepy Dermatol Alergol* 31 (5) (2014) 289–293.
- D.A. Fox, R.E. Hussey, K.A. Fitzgerald, O. Acuto, C. Poole, L. Palley, J.F. Daley, S.F. Schlossman, E.L. Reinherz, Ta1, anovel 105 KD human T cell activation antigen defined by a monoclonal antibody, *J. Immunol.* 133 (3) (1984) 1250–1256.
- D.M. Nanus, D. Engelstein, G.A. Gastl, L. Gluck, M.J. Vidal, M. Morrison, C.L. Finstad, N.H. Bander, A.P. Albino, Molecular cloning of the human kidney differentiation antigen gp160: human aminopeptidase A, *Proc. Natl. Acad. Sci. U. S. A.* 90 (15) (1993) 7069–7073.
- T. Tanaka, D. Camerini, B. Seed, Y. Torimoto, N.H. Dang, J. Kameoka, H.N. Dahlberg, S.F. Schlossman, C. Morimoto, Cloning and functional expression of the T cell activation antigen CD26, *J. Immunol.* 149 (2) (1992) 481–486.
- C. Morimoto, S.F. Schlossman, The structure and function of CD26 in the T-cell immune response, *Immunol. Rev.* 161 (1998) 55–70.
- K. Ohnuma, N.H. Dang, C. Morimoto, Revisiting an old acquaintance: CD26 and its molecular mechanisms in T cell function, *Trends Immunol.* 29 (6) (2008) 295–301.
- T. Tanaka, J. Kameoka, A. Yaron, S.F. Schlossman, C. Morimoto, The costimulatory activity of the CD26 antigen requires dipeptidyl peptidase IV enzymatic activity, *Proc. Natl. Acad. Sci. U. S. A.* 90 (10) (1993) 4586–4590.
- H. Kobayashi, O. Hosono, T. Mimori, H. Kawasaki, N.H. Dang, H. Tanaka, C. Morimoto, Reduction of serum soluble CD26/dipeptidyl peptidase IV enzyme activity and its correlation with disease activity in systemic lupus erythematosus, *J. Rheumatol.* 29 (9) (2002) 1858–1866.
- T. Inamoto, T. Yamada, K. Ohnuma, S. Kina, N. Takahashi, T. Yamochi, S. Inamoto, Y. Katsuoka, O. Hosono, H. Tanaka, N.H. Dang, C. Morimoto, Humanized anti-CD26 monoclonal antibody as a treatment for malignant mesothelioma tumors, *Clin. Cancer Res.* 13 (14) (2007) 4191–4200.
- E. Komiya, K. Ohnuma, H. Yamazaki, R. Hatano, S. Iwata, T. Okamoto, N.H. Dang, T. Yamada, C. Morimoto, CD26-mediated regulation of periostin expression contributes to migration and invasion of malignant pleural mesothelioma cells, *Biochem. Biophys. Res. Commun.* 447 (4) (2014) 609–615.
- R. Pang, W.L. Law, A.C. Chu, J.T. Poon, C.S. Lam, A.K. Chow, L. Ng, L.W. Cheung, X. R. Lan, H.Y. Lan, V.P. Tan, T.C. Yau, R.T. Poon, B.C. Wong, A subpopulation of CD26+ cancer stem cells with metastatic capacity in human colorectal cancer, *Cell Stem Cell* 6 (6) (2010) 603–615.
- B.A. Stecca, B. Nardo, P. Chieco, A. Mazziotti, L. Bolondi, A. Cavallari, Aberrant dipeptidyl peptidase IV (DPP IV/CD26) expression in human hepatocellular carcinoma, *J. Hepatol.* 27 (2) (1997) 337–345.
- Y.X. Sun, E.A. Pedersen, Y. Shiozawa, A.M. Havens, Y. Jung, J. Wang, K.J. Pienta, R. S. Taichman, CD26/dipeptidyl peptidase IV regulates prostate cancer metastasis by degrading SDF-1/CXCL12, *Clin. Exp. Metastasis* 25 (7) (2008) 765–776.
- H. Nagai, S. Fujiwara, Y. Takahashi, C. Nishigori, Ameliorating effect of the novel dipeptidyl peptidase-4 inhibitor teneligliptin on psoriasis: a report of two cases, *J. Dermatol.* 42 (11) (2015) 1094–1097.
- T. Nishioka, M. Shinohara, N. Tanimoto, C. Kumagai, K. Hashimoto, Sitagliptin, a dipeptidyl peptidase-IV inhibitor, improves psoriasis, *Dermatology* 224 (1) (2012) 20–21.
- M. Novelli, P. Savoia, M.T. Fierro, A. Verrone, P. Quaglino, M.G. Bernengo, Keratinocytes express dipeptidyl-peptidase IV (CD26) in benign and malignant skin diseases, *Br. J. Dermatol.* 134 (6) (1996) 1052–1056.
- R.G. van Lingen, M.K. Poll, M.M. Seyger, E.M. de Jong, P.C. van de Kerkhof, P.E. van Erp, Distribution of dipeptidyl-peptidase IV on keratinocytes in the margin zone of a psoriatic lesion: a comparison with hyperproliferation and aberrant differentiation markers, *Arch. Dermatol. Res.* 300 (10) (2008) 561–567.
- D.J. Drucker, Enhancing incretin action for the treatment of type 2 diabetes, *Diabetes Care* 26 (10) (2003) 2929–2940.

- [25] G.A. Herman, A. Bergman, C. Stevens, P. Kotey, B. Yi, P. Zhao, B. Dietrich, G. Golor, A. Schrodter, B. Keymeulen, K.C. Lasseter, M.S. Kipnes, K. Snyder, D. Hilliard, M. Tanen, C. Cilissen, M. De Smet, I. de Lepeleire, K. Van Dyck, A.Q. Wang, W. Zeng, M.J. Davies, W. Tanaka, J.J. Holst, C.F. Deacon, K.M. Gottesdiener, J.A. Wagner, Effect of single oral doses of sitagliptin, a dipeptidyl peptidase-4 inhibitor, on incretin and plasma glucose levels after an oral glucose tolerance test in patients with type 2 diabetes, *J. Clin. Endocrinol. Metab.* 91 (11) (2006) 4612–4619.
- [26] D. Kim, L. Wang, M. Beconi, G.J. Eiermann, M.H. Fisher, H. He, G.J. Hickey, J.E. Kowalchick, B. Leiting, K. Lyons, F. Marsilio, M.E. McCann, R.A. Patel, A. Petrov, G. Scapin, S.B. Patel, R.S. Roy, J.K. Wu, M.J. Wyvratt, B.B. Zhang, L. Zhu, N.A. Thornberry, A.E. Weber, (2R)-4-oxo-4-[3-(trifluoromethyl)-5,6-dihydro[1,2,4]triazolo[4,3-a]pyrazin-7(8H)-yl]-1-(2,4,5-trifluorophenyl)butan-2-amine: a potent, orally active dipeptidyl peptidase IV inhibitor for the treatment of type 2 diabetes, *J. Med. Chem.* 48 (1) (2005) 141–151.
- [27] C. De Felipe, J.F. Herrero, J.A. O'Brien, J.A. Palmer, C.A. Doyle, A.J. Smith, J.M. Laird, C. Belmonte, F. Cervero, S.P. Hunt, Altered nociception, analgesia and aggression in mice lacking the receptor for substance P, *Nature* 392 (6674) (1998) 394–397.
- [28] B. Pernow, P. Substance, *Pharmacol. Rev.* 35 (2) (1983) 85–141.
- [29] M.K. Church, Y. Okayama, S. el-Lati, Mediator secretion from human skin mast cells provoked by immunological and non-immunological stimulation, *Skin Pharmacol.* 4 (Suppl. 1) (1991) 15–24.
- [30] A.E. Kremer, J. Feramisco, P.W. Reeh, U. Beuers, R.P. Oude Elferink, Receptors, cells and circuits involved in pruritus of systemic disorders, *Biochim. Biophys. Acta* 1842 (7) (2014) 869–892.
- [31] M. Schmelz, R. Schmidt, A. Bickel, H.O. Handwerker, H.E. Torebjork, Specific C-receptors for itch in human skin, *J. Neurosci.* 17 (20) (1997) 8003–8008.
- [32] M. Nakamura, M. Toyoda, M. Morohashi, Pruritogenic mediators in psoriasis vulgaris: comparative evaluation of itch-associated cutaneous factors, *Br. J. Dermatol.* 149 (4) (2003) 718–730.
- [33] E. Heymann, R. Mentlein, Liver dipeptidyl aminopeptidase IV hydrolyzes substance P, *FEBS Lett.* 91 (2) (1978) 360–364.
- [34] T. Karl, T. Hoffmann, R. Pabst, S. von Horsten, Extreme reduction of dipeptidyl peptidase IV activity in F344 rat substrains is associated with various behavioral differences, *Physiol. Behav.* 80 (1) (2003) 123–134.
- [35] D. Marguet, L. Baggio, T. Kobayashi, A.M. Bernard, M. Pierres, P.F. Nielsen, U. Ribe, T. Watanabe, D.J. Drucker, N. Wagtmann, Enhanced insulin secretion and improved glucose tolerance in mice lacking CD26, *Proc. Natl. Acad. Sci. U. S. A.* 97 (12) (2000) 6874–6879.
- [36] A.S. Agrawal, T. Garron, X. Tao, B.H. Peng, M. Wakamiya, T.S. Chan, R.B. Couch, C. T. Tseng, Generation of a transgenic mouse model of Middle East respiratory syndrome coronavirus infection and disease, *J. Virol.* 89 (7) (2015) 3659–3670.
- [37] K. Ohnuma, T. Saito, R. Hatano, O. Hosono, S. Iwata, N.H. Dang, H. Ninomiya, C. Morimoto, Comparison of two commercial ELISAs against an in-house ELISA for measuring soluble CD26 in human serum, *J. Clin. Lab. Anal.* 29 (2) (2015) 106–111.
- [38] T. Andrieu, V. Thibault, I. Malet, J. Laporte, B. Bauvois, H. Agut, A. Cahour, Similar increased serum dipeptidyl peptidase IV activity in chronic hepatitis C and other viral infections, *J. Clin. Virol.* 27 (1) (2003) 59–68.
- [39] A. Sedo, R. Malik, Dipeptidyl peptidase IV-like molecules: homologous proteins or homologous activities? *Biochim. Biophys. Acta* 1550 (2001) 107–116.
- [40] L. van der Fots, S. Mourits, J.S. Voerman, M. Kant, L. Boon, J.D. Laman, F. Cornelissen, A.M. Mus, E. Florencia, E.P. Prens, E. Lubberts, Imiquimod-induced psoriasis-like skin inflammation in mice is mediated via the IL-23/IL-17 axis, *J. Immunol.* 182 (9) (2009) 5836–5845.
- [41] K. Sakai, K.M. Sanders, M.R. Youssef, K.M. Yanushefski, L. Jensen, G. Yosipovitch, T. Akiyama, Mouse model of imiquimod-induced psoriatic itch, *Pain* (2016).
- [42] A.S. Raut, R.H. Prabhu, V.B. Patravale, Psoriasis clinical implications and treatment: a review, *Crit. Rev. Ther. Drug Carrier Syst.* 30 (3) (2013) 183–216.
- [43] A. Thielitz, D. Reinhold, R. Vetter, U. Bank, M. Helmuth, R. Hartig, S. Wrenge, I. Wiswedel, U. Lendeckel, T. Kahne, K. Neubert, J. Faust, C.C. Zouboulis, S. Ansorge, H. Gollnick, Inhibitors of dipeptidyl peptidase IV and aminopeptidase N target major pathogenetic steps in acne initiation, *J. Invest. Dermatol.* 127 (5) (2007) 1042–1051.
- [44] R.G. van Lingen, P.C. van de Kerkhof, M.M. Seyger, E.M. de Jong, D.W. van Rens, M.K. Poll, P.L. Zeeuwen, P.E. van Erp, CD26/dipeptidyl-peptidase IV in psoriatic skin: upregulation and topographical changes, *Br. J. Dermatol.* 158 (6) (2008) 1264–1272.
- [45] M. Lynch, A.M. Tobin, T. Aherne, D. O'Shea, B. Kirby, Sitagliptin for severe psoriasis, *Clin. Exp. Dermatol.* 39 (7) (2014) 841–842.
- [46] K. Ohnuma, O. Hosono, N.H. Dang, C. Morimoto, Dipeptidyl peptidase in autoimmune pathophysiology, *Adv. Clin. Chem.* 53 (2011) 51–84.
- [47] M. Diani, G. Altomare, E. Reali, T cell responses in psoriasis and psoriatic arthritis, *Autoimmun. Rev.* 14 (4) (2015) 286–292.
- [48] J. Baliwag, D.H. Barnes, A. Johnston, Cytokines in psoriasis, *Cytokine* 73 (2) (2015) 342–350.
- [49] M.P. Schon, W.H. Boehncke, N. Psoriasis, *Engl. J. Med.* 352 (18) (2005) 1899–1912.
- [50] F.O. Nestle, P. Di Meglio, J.Z. Qin, B.J. Nickoloff, Skin immune sentinels in health and disease, *Nat. Rev. Immunol.* 9 (10) (2009) 679–691.
- [51] T. Akiyama, E. Carstens, Neural processing of itch, *Neuroscience* 250 (2013) 697–714.
- [52] C. Remrod, S. Lonne-Rahm, K. Nordlind, Study of substance P and its receptor neuropeptide-1 in psoriasis and their relation to chronic stress and pruritus, *Arch. Dermatol. Res.* 299 (2) (2007) 85–91.
- [53] B. Amatya, K. Nordlind, C.F. Wahlgren, Responses to intradermal injections of substance P in psoriasis patients with pruritus, *Skin Pharmacol. Physiol.* 23 (3) (2010) 133–138.
- [54] T. Miyagaki, M. Sugaya, H. Suga, S. Morimura, M. Kamata, H. Ohmatsu, H. Fujita, Y. Asano, Y. Tada, T. Kadono, S. Sato, Serum soluble CD26 levels: diagnostic efficiency for atopic dermatitis, cutaneous T-cell lymphoma and psoriasis in combination with serum thymus and activation-regulated chemokine levels, *J. Eur. Acad. Dermatol. Venereol.* 27 (1) (2013) 19–24.

Identification of senescent cell surface targetable protein DPP4

Kyoung Mi Kim,^{1,4} Ji Heon Noh,^{1,4}
 Monica Bodogai,¹ Jennifer L. Martindale,¹
 Xiaoling Yang,¹ Fred E. Indig,¹ Sandip K. Basu,²
 Kei Ohnuma,³ Chikao Morimoto,³
 Peter F. Johnson,² Arya Biragyn,¹
 Kotb Abdelmohsen,¹ and Myriam Gorospe¹

¹National Institute on Aging, National Institutes of Health, Baltimore, Maryland 21224, USA; ²National Cancer Institute, National Institutes of Health, Frederick, Maryland 21702, USA; ³Graduate School of Medicine, Juntendo University, Tokyo 113-8421, Japan

Senescent cell accumulation in aging tissues is linked to age-associated diseases and declining function, prompting efforts to eliminate them. Mass spectrometry analysis revealed that DPP4 (dipeptidyl peptidase 4) was selectively expressed on the surface of senescent, but not proliferating, human diploid fibroblasts. Importantly, the differential presence of DPP4 allowed flow cytometry-mediated isolation of senescent cells using anti-DPP4 antibodies. Moreover, antibody-dependent cell-mediated cytotoxicity (ADCC) assays revealed that the cell surface DPP4 preferentially sensitized senescent, but not dividing, fibroblasts to cytotoxicity by natural killer cells. In sum, the selective expression of DPP4 on the surface of senescent cells enables their preferential elimination.

Supplemental material is available for this article.

Received May 24, 2017; revised version accepted August 2, 2017.

Cell senescence is a state of terminal growth arrest triggered by stress signals such as critically short telomeres, oxidative damage, oncogene activation, and hypoxia (Kuilman et al. 2010). Compared with proliferating cells, senescent cells exhibit an enlarged morphology, distinct metabolic and gene expression patterns, and increased activity of a neutral β -galactosidase (Crowe et al. 2014). They also display a senescence-associated secretory phenotype (SASP) characterized by the production and secretion of proinflammatory factors, angiogenic factors, and matrix metalloproteases that alter tissue function by promoting angiogenesis, attracting immune cells, and remodeling the extracellular matrix (Coppé et al. 2010).

Cell senescence has a range of complex effects on physiology and disease processes. Among its beneficial effects, senescent cells promote tissue morphogenesis and wound healing and suppress fibrosis and tumorigenesis in young organisms (Prieur and Peeper 2008; Muñoz-Espín et al. 2013; Storer et al. 2013; Demaria et al. 2014; Muñoz-Espín and Serrano 2014). On the other hand, extensive detri-

mental effects have been documented for senescent cells accumulating in tissues of older organisms, as they trigger or exacerbate age-related diseases such as cancer, cataracts, arthritis, and atherosclerosis (Baker et al. 2008, 2011; Prieur and Peeper 2008; Muñoz-Espín and Serrano 2014; van Deursen 2014).

The accumulation of senescent cells in aging tissues, as investigated in a genetic mouse model in which senescent cells were selectively eliminated, was found to promote aging-associated declines and diseases. Indeed, the removal of senescent cells from aging mouse tissues—achieved by triggering apoptotic death of cells that expressed the senescence protein p16—enhanced longevity and promoted healthy life span associated with a reduction in tumorigenesis and extended function of the renal, cardiovascular, muscular, and adipose systems (Baker et al. 2011, 2016).

With increasing evidence that senescent cells adversely influence aging-associated declines and diseases, a major goal in the field is to design interventions that recognize and eradicate senescent cells selectively. Senescent cells differ greatly from proliferating cells in the patterns of expressed proteins, including those on the cell surface that can serve as markers and therapeutic targets. Thus, we set out to identify cell surface proteins uniquely present in senescent cells. This strategy is similar to that used to eliminate cancer cells selectively (Rasmussen and Ditzel 2009). Using mass spectrometry (MS) analysis, we identified DPP4 (dipeptidyl peptidase 4; also known as CD26) as a surface protein that was strikingly more abundant in senescent cells. Importantly, senescent cells were preferentially eliminated by antibody-dependent cell-mediated cytotoxicity (ADCC), as the presence of DPP4 on their surface rendered them suitable targets for destruction by natural killer (NK) cells recognizing an anti-DPP4 antibody.

Results and Discussion

Identification of DPP4 as a novel senescent cell surface marker

To find novel surface markers selectively present on the plasma membrane of senescent cells, we used a well-characterized model of cellular senescence: proliferating WI-38 human diploid fibroblasts (HDFs; at population doubling level [PDL] 23) compared with those that had become senescent (PDL59) following extended culture. Senescent HDFs displayed a characteristic flattened and enlarged morphology and exhibited elevated senescence-associated β -galactosidase (SA- β -gal) activity, a distinctive trait of cellular senescence (Fig. 1A). Analysis of the incorporation of 3 H-thymidine or BrdU further indicated that senescent cells had significantly lower proliferating activity (Fig. 1A). We fractionated membrane-associated proteins and cell surface-associated proteins as described (Materials and Methods) and surveyed them by MS

[Keywords: CD26; cell senescence; human diploid fibroblasts]

⁴These authors contributed equally to this work.

Corresponding author: kyoungmi.kim@nih.gov

Article published online ahead of print. Article and publication date are online at <http://www.genesdev.org/cgi/doi/10.1101/gad.302570.117>.

© 2017 Kim et al. This article is distributed exclusively by Cold Spring Harbor Laboratory Press for the first six months after the full-issue publication date (see <http://genesdev.cshlp.org/site/misc/terms.xhtml>). After six months, it is available under a Creative Commons License (Attribution-NonCommercial 4.0 International), as described at <http://creativecommons.org/licenses/by-nc/4.0/>.

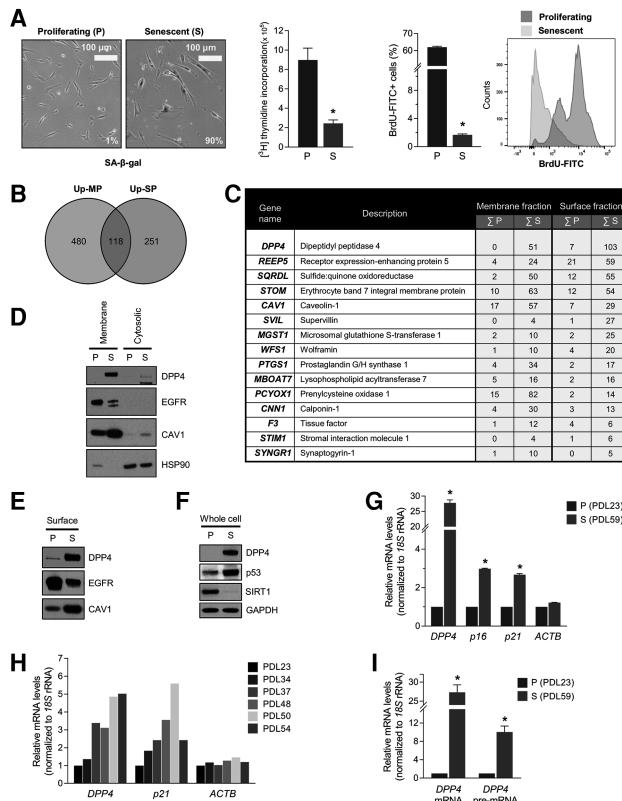


Figure 1. Identification of DPP4 as a novel senescent cell surface marker. *(A, left)* Detection of the senescent marker SA- β -gal in proliferating (P; PDL23) and senescent (S; PDL59) WI-38 HDFs; the percentages of blue cells are indicated. *(Middle)* Measurement of 3 H-thymidine and BrdU incorporation in proliferating and senescent WI-38 cells. *(Right)* Flow cytometry analysis of BrdU-FITC-positive proliferating and senescent cells. *(B)* Venn diagram summarizing the MS analysis; the numbers of proteins more abundant in cell membrane preparations (Up-MP; green) and cell surface preparations (Up-SP; blue) from senescent cells relative to proliferating cells are indicated. *(C)* The top 15 proteins from the intersection in *B*. The numbers indicate the sums of the PSM from two experiments. *(D-F)* Western blot analysis of DPP4 levels in membrane and cytosolic lysates *(D)*, surface proteins *(E)*, and whole-cell lysates *(F)*. (HSP90) Cytosolic protein marker; (CAV1 and EGFR) membrane protein markers; (SIRT1) protein marker of proliferating cells; (p53) protein marker of senescent cells; (GAPDH) loading control protein. *(G-I)* Steady-state levels of *DPP4* mRNA and *DPP4* pre-mRNA quantified by RT-qPCR analysis. Total RNA was prepared from proliferating and senescent cells *(G,I)* or cells at PDLs between PDL23 and PDL54 *(H)*. Senescent markers *p21* mRNA and *p16* mRNAs were included as positive controls, and *ACTB* mRNA was used as a negative control. mRNA levels were normalized to 18S rRNA levels in each sample; mRNAs in PDL23 cells were set as 1 in *G-I*. The graphs in *A*, *G*, and *I* represent the means \pm SEM from three independent experiments. (*) *P*-value < 0.05 .

analysis (see Supplemental Table S1 for complete MS data set). We focused on the proteins that were more abundant among membrane proteins (a fraction that included endoplasmic reticulum, mitochondria, and other intracellular membrane structures) and among cell surface proteins in senescent compared with proliferating fibroblasts. Among the 118 protein candidates at the overlap of the two groups (Fig. 1B), the top 15 proteins and the PSM (peptide spectrum match) count in proliferating relative to senescent cells are listed in Figure 1C. The leading candidate on this list was DPP4 (CD26). DPP4 peptides

detected by MS analysis are indicated (Supplemental Fig. S1A).

To validate these differences in DPP4 levels, we fractionated the membrane, surface-associated, and cytosolic fractions of proliferating and senescent WI-38 HDFs. Western blot analysis (Fig. 1D) revealed that DPP4 levels were robustly elevated in the membrane fraction of senescent fibroblasts but not proliferating fibroblasts or cytosolic fractions (Fig. 1D); membrane-associated proteins EGFR and Caveolin-1 (CAV1) as well as cytosolic protein HSP90 were included to monitor the cell fractionation. DPP4 was also more highly expressed on the cell surface and in whole-cell lysates (Fig. 1E,F) of senescent relative to proliferating WI-38 cells. Proteins present on the cell membrane (EGFR and CAV1), proteins showing altered levels with senescence (EGFR, CAV1, SIRT1, and p53), and a loading control (GAPDH) were also assessed.

We investigated the mechanism that led to the rise in DPP4 levels in senescent cells. RNA isolation from proliferating and senescent cells followed by RT-qPCR analysis revealed that *DPP4* mRNA was markedly higher in senescent cells (Fig. 1G); senescent markers *p16* (*CDKN2A*) mRNA and *p21* (*CDKN1A*) mRNA were also elevated (Fig. 1G). *DPP4* mRNA levels increased gradually with advancing PDLs (Fig. 1H). We quantified *DPP4* pre-mRNA levels as a surrogate measure of de novo *DPP4* mRNA transcription (Fig. 1I); the strong increase in *DPP4* pre-mRNA levels in senescent cells suggested that increased *DPP4* gene transcription was a major mechanism leading to DPP4 increase with senescence.

To test whether DPP4 increased more generally in senescent cells, we triggered senescence by exposing proliferating WI-38 and IMR-90 HDFs to ionizing radiation (IR); 10 d later, SA- β -gal activity was selectively elevated in IR-treated cells. Western blot and RT-qPCR analyses indicated that DPP4 and *DPP4* mRNA (Supplemental Fig. S1B,C) were up-regulated in IR-induced senescent HDFs, although more modestly than in HDFs undergoing replicative senescence (Fig. 1F,G). We further tested whether DPP4 levels were elevated in other models of senescence by exposing human umbilical vein endothelial cells (HUVECs) and human aortic endothelial cells (HAECS) to 4 Gy of IR to elicit senescence; 14 d later, RT-qPCR analysis revealed significantly elevated *DPP4* mRNA in senescent (IR-treated) compared with proliferating (untreated) HUVECs and HAECS (Supplemental Fig. S2A,B). Another trigger of senescence, treatment with doxorubicin (Dox), also led to a rise in *DPP4* mRNA abundance in WI-38 cells (Supplemental Fig. S2C). Moreover, oncogene-induced senescence (OIS) in mouse embryonic fibroblasts (MEFs) expressing the oncogene HRAS^{G12V} via viral transduction also revealed a robust rise in DPP4 levels (Supplemental Fig. S2D). Together, these data indicate that DPP4 levels were highly and broadly elevated in senescent cells relative to proliferating cells at least in part by transcriptional induction of *DPP4* mRNA levels and that DPP4 localized on the surface of the plasma membrane.

Contribution to senescence by DPP4

Given the rise in DPP4 levels in senescent cells, we asked whether DPP4 itself might help promote cellular senescence. To test this possibility, we overexpressed DPP4 in proliferating WI-38 cells by infection with a lentivirus that expressed DPP4-Myc using control viral particles

that expressed only the Myc tag. After selection of infected cells in puromycin for 20 d, protein lysates were prepared, and Western blot analysis was used to assess senescence markers. As shown, markers p16 and p21 were elevated while SIRT1 levels declined in cells overexpressing DPP4 (Fig. 2A), supporting the notion that DPP4 promoted cell senescence. In addition, overexpression of DPP4 in WI-38 cells elevated SA- β -gal activity (Fig. 2B) and decreased 3 H-thymidine incorporation (Fig. 2C).

We further tested whether DPP4 contributed to eliciting senescence by silencing DPP4 in presenescence WI-38 cells (approximately PDL39–PDL45) and assessing senescence markers. As shown, the robust silencing of DPP4 by 72 h after transfection of siRNA (Supplemental Material) led to marked reductions in the levels of p53, p21, and p16 and increased SIRT1 levels, as determined by Western blot analysis (Fig. 2D). Likewise, RT-qPCR analysis

revealed that the levels of senescence markers p21 mRNA, IL1A mRNA, and IL1B mRNA were significantly reduced in the DPP4 siRNA group (Fig. 2E). Additionally, DPP4 silencing increased the number of cells in the population (Fig. 2F) and promoted incorporation of 3 H-thymidine and BrdU (Fig. 2G,H), further indicating that DPP4 contributed to the growth suppression characteristic of senescence. Interestingly, DPP4 silencing reduced the production of reactive oxygen species (ROS) in presenescence cells (Fig. 2I). Taken together, our results indicate that DPP4 enhances fibroblast senescence.

Specific selection of senescent cells using cell surface DPP4

Given that DPP4 was identified as a cell surface protein in senescent cells (Fig. 1B,C), we used confocal microscopy to further investigate this localization. Proliferating and senescent WI-38 HDFs were fixed but not permeabilized in order to detect only proteins present on the outside of the plasma membrane. As shown in Figure 3A, DPP4 signal (red) was virtually undetectable in proliferating cells but was highly abundant in senescent cultures and was found throughout the cell surface. In light of these results, we tested whether DPP4 might be a suitable selection marker for senescent cells. We used two mouse antibodies, anti-DPP4-PE and (control) mIgG-PE, to label proliferating and senescent WI-38 HDFs without fixation or permeabilization to analyze cell surface markers. Labeled samples were analyzed by flow cytometry to assess the presence of DPP4 on the cell surface. MFI (mean fluorescence intensity) analysis revealed that DPP4-labeled cells were enriched eightfold in senescent compared with proliferating WI-38 HDFs (Fig. 3B). Moreover, the number of DPP4-positive cells identified by flow cytometry analysis using DPP4-PE was only 6.05% in proliferating cells but rose to 67.9% in senescent cells (Fig. 3C). In sum, DPP4 levels are markedly elevated on the surface of senescent fibroblasts and serve as a suitable marker for the specific isolation of senescent cells.

With advancing age, senescent cells accumulate in a variety of tissues, including blood. We thus asked whether DPP4-positive cells might be detected in peripheral blood mononuclear cells (PBMCs) from three healthy young individuals (27–36 yr of age) and three healthy old individuals (78–88 yr of age) (Materials and Methods). As shown in Figure 3D, the percentage of DPP4-positive cells (as determined by flow cytometry using the DPP4-PE antibody) was higher in “old” PBMCs than in “young” PBMCs (15.5% vs. 10%). Since most DPP4 signals came from monocytes and lymphocytes, we calculated the percentages of DPP4-positive monocytes and lymphocytes and found that these percentages remained significantly higher in the old donor group than the young donor group (33% vs. 21%); see Supplemental Figure S3 for contour plots of the individual donors. To determine whether DPP4-positive cells were senescent, PBMCs from four donors (ages 27, 27, 60, and 63 yr) were labeled with DPP4-PE and sorted using anti-PE microbeads by MACS (magnetic-activated cell sorting) analysis. After isolation of RNA from the affinity-purified cells, RT-qPCR analysis was used to assess the expression of senescence markers. As shown (Fig. 3E), DPP4-positive cells in each of the four donors expressed higher levels of DPP4 and DPP4 mRNA by Western blot and RT-qPCR analyses, respectively (to verify

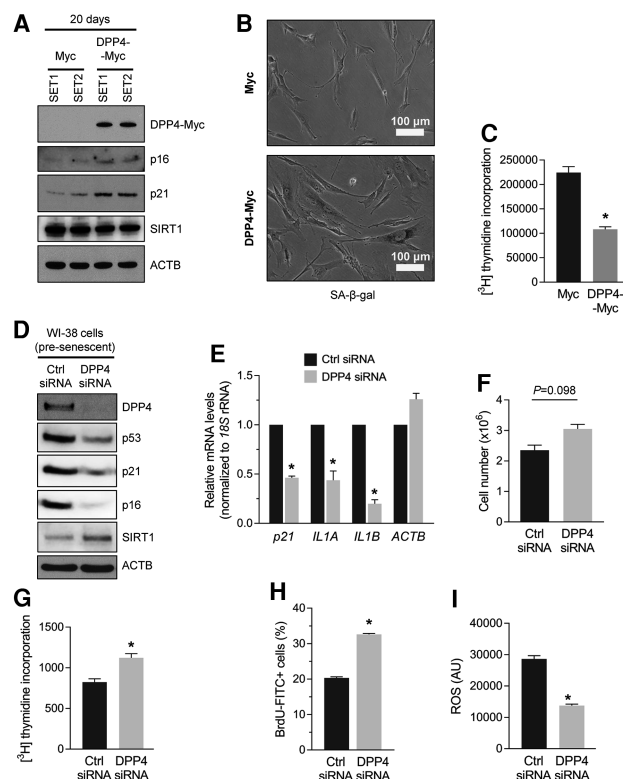


Figure 2. DPP4 contributes to the senescence program. *(A)* Proliferating WI-38 cells were infected with lentiviral particles expressing either Myc tag alone or DPP4-Myc. After 20 d of puromycin selection, cells were harvested, and whole-cell lysates were prepared for Western blot analysis to examine the levels of proteins DPP4-Myc (using anti-DPP4 antibody), p16, p21, and SIRT1 and loading control ACTB (β -Actin); endogenous DPP4 was undetectable. *(B,C)* Detection of the senescent marker SA- β -gal (*B*) and measurement of 3 H-thymidine incorporation (*C*) in the populations described in *A*. *(D–I)* Seventy-two hours after transfecting presenescence WI-38 cells [PDL39–PDL45] with control (Ctrl) siRNA or DPP4 siRNA, the levels of DPP4, p53, p21, p16, SIRT1, and ACTB in whole-cell lysates were assessed by Western blot analysis (*D*); the steady-state levels of p21, IL1A, IL1B, and ACTB mRNAs were calculated by RT-qPCR analysis and normalized to 18S rRNA levels (*E*); cell numbers were quantified (*F*); 3 H-thymidine (*G*) and BrdU (*H*) incorporation was measured; and reactive oxygen species (ROS) production was measured (*I*). The graphs in *C* and *E–I* represent the means \pm SEM from three independent experiments. (*) P -value < 0.05 .

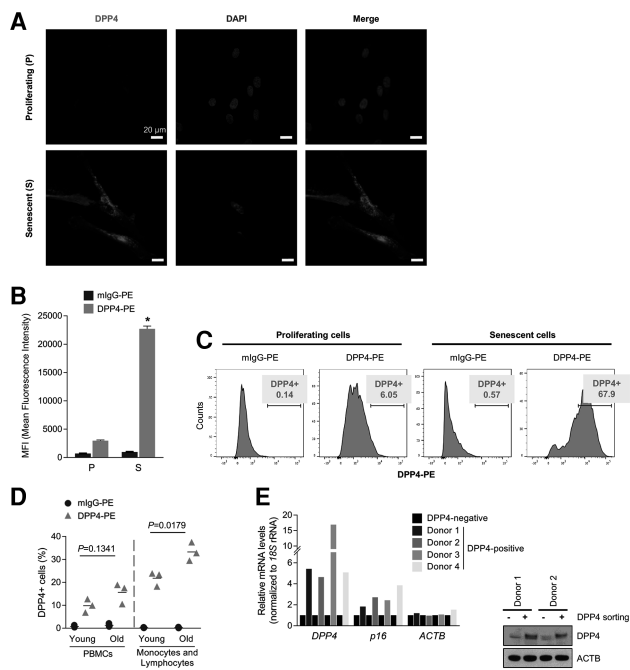


Figure 3. DPP4 is more highly expressed in senescent cells and localizes on the cell surface. (A) Proliferating (P) or senescent (S) WI-38 HDFs were fixed with methanol, and the endogenous DPP4 protein was detected by confocal microscopy. (B, C) WI-38 (proliferating and senescent) HDFs were harvested and incubated with either anti-DPP4-PE or control IgG-PE antibodies. (B) DPP4-positive cells were analyzed by flow cytometry, and the MFI of DPP4-PE in proliferating and senescent cells was quantified. The graph represents the means \pm SEM. from three independent experiments. (*) P -value < 0.05 . (C) Histograms from the flow analysis representing control isotype (left) or DPP4 (right) in proliferating and senescent cells; the percentages of DPP4-PE-positive cells are indicated. The experiment shown is representative of three independent experiments. (D) Human peripheral blood mononuclear cells (PBMCs) obtained from young (27- to 36-yr-old) and old (78- to 88-yr-old) donors were analyzed by flow cytometry using antibodies that recognized DPP4-PE (\blacktriangle) or mouse IgG-PE (\bullet). The graph shows the percentage of DPP4-PE-positive cells. (Left) PBMC populations. (Right) Monocyte and lymphocyte populations. Each data point represents a young ($n = 3$ total) or old ($n = 3$ total) subject; horizontal lines indicate the mean values. (E) Human PBMCs obtained from four donors (27, 27, 60, or 63 yr old) were sorted into DPP4-positive cells and DPP4-negative cells by MACS using a DPP4-PE antibody and anti-PE microbeads. The steady-state levels of DPP4, p16, and ACTB mRNAs were quantified by RT-qPCR analysis after normalization to 18S rRNA levels. Each mRNA in DPP4-negative cells was set as 1.

that the affinity pull-down was successful), and, importantly, all four samples also displayed higher levels of *p16* mRNA, which encodes the major senescence-associated protein *p16*. The data obtained using PBMCs further support the notion that DPP4 also serves as a surface marker for the selection of senescent cells among a heterogeneous cell population.

Selective elimination of DPP4-positive senescent cells by ADCC assay

Our initial goal was to devise a method to eliminate senescent cells selectively using a differentially expressed surface protein. Thus, after establishing that DPP4 is located on the surface of the plasma membrane of senescent

cells (Figs. 1, 3), we set out to test whether we could eliminate senescent cells selectively using an antibody directed at DPP4 and the ADCC assay. Originally developed for cancer therapy, the ADCC assay uses antibodies to recognize a specific antigen on the cell surface and guide NK cells to selectively destroy the antibody-labeled cells (Weiner 2015). We carried out ADCC analysis using increasing concentrations of anti-DPP4 antibody (up to 5 μ g/mL) to bind the DPP4 surface marker and thereby label proliferating and senescent WI-38 fibroblasts. We then isolated NK cells from human PBMCs and added them to the WI-38 cultures, allowing the NK cells to destroy the cells labeled by anti-DPP4 antibody. Treatment with NK cells from eight different donors in the presence of rabbit or humanized anti-DPP4 antibodies (Fig. 4A) indicated that, in every case, senescent cells exhibited stronger reductions in cell viability, as low as ~40% (as seen with "donor 8" of NK cells), compared with proliferating cells. As shown in Supplemental Figure S4, ADCC assay using a control rabbit IgG (rIgG) revealed that this antibody did not affect cell viability in proliferating or senescent cells.

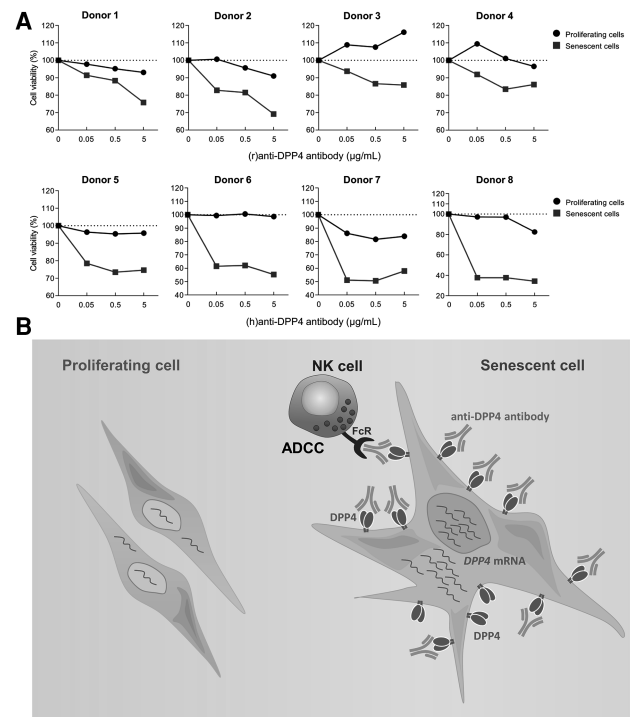


Figure 4. Eliminating DPP4-positive senescent cells by ADCC. (A) Proliferating and senescent WI-38 cells (5×10^4) were incubated without or with 0.05, 0.5, and 5 μ g/mL anti-DPP4 antibody and either 2.5×10^5 NK cells [for rabbit (r)anti-DPP4] or 1.25×10^6 or 2.5×10^6 NK cells [for humanized (h)anti-DPP4 antibody] per well for 4 h. After removing NK cells, WI-38 cells were incubated for another 18 h, and cell viability was measured by the MTT [3-(4,5-dimethylthiazol-2-yl)-2,5-diphenyltetrazolium bromide] assay. Cell numbers were compared with those that received no anti-DPP4 antibody. Donors 1-4 were incubated with (r)anti-DPP4, and donors 5-8 were incubated with (h)anti-DPP4. (B) Proposed model. (Left) In proliferating cells, DPP4 is expressed at low levels or is undetectable. (Right) In senescent cells, DPP4 mRNA levels increase transcriptionally, leading to increased production of DPP4, which localizes as a dimer on the cell surface, exposed to the extracellular space. The abundance and localization of DPP4 in senescent cells enable the selective elimination of senescent cells by ADCC.

Targeting DPP4 to eliminate senescent cells

In sum, we identified DPP4 as a protein robustly up-regulated on the plasma membrane of senescent cells. DPP4 levels increased via transcriptional induction of *DPP4* mRNA in senescent cells. Whether this increase might be mediated via transcription factors HNF and/or STAT1 α in fibroblasts, as shown previously in B lymphocytes and intestinal epithelial cells (Bauvois et al. 2000; Erickson et al. 2000; D'Angelo et al. 2010), remains to be tested. We further found that senescent cells can be selectively targeted by anti-DPP4 antibodies and eliminated. Accordingly, we propose a model (Fig. 4B) in which the highly abundant DPP4 on the exposed surface of a senescent cell allows it to be recognized and eliminated by anti-DPP4 antibody-directed NK-elicited cell death. These results underscore the usefulness of targeting for selective destruction proteins differentially present on the plasma membrane of senescent cells.

DPP4 is best known as a protease that inactivates two hormones named incretins: glucose-dependent insulinotropic peptide (GIP) and glucagon-like peptide-1 (GLP-1). Incretins trigger a rapid release of insulin from pancreatic β cells after a meal; since they suppress a sudden rise in blood glucose, they are particularly beneficial in diabetes (Wu et al. 2016). Although the significance of having elevated DPP4 in senescent cells is unclear, DPP4 might influence some of the changes in glucose homeostasis that occur with aging. For example, a rise in DPP4 levels from accumulating senescent cells could contribute to the impairment of glucose metabolism that leads to hyperglycemia in the elderly. In this regard, it will be interesting to test whether DPP4 inhibitors (e.g., sitagliptin) (Scott 2017), which enhance the so-called "incretin effect" and have been used to treat diabetes, recapitulate the enhanced proliferation and suppressed senescence seen after silencing DPP4 (Fig. 2).

DPP4 and senolytic therapy

Similarly, as incretin-independent actions of DPP4 are emerging, it will be important to study whether the health benefits of DPP4 inhibitors depend partly on their impact on senescent cells irrespective of DPP4-mediated inactivation of incretins. For example, DPP4 present on the plasma membrane of lymphocytes (which we found to be elevated with age) (Fig. 3D) associates with CAV1, a membrane protein that also rises with senescence, leading to the activation of IRAK-1 and NF- κ B (Ohnuma et al. 2005, 2008). Likewise, DPP4 present on the membrane of antigen-presenting cells and inflammatory cells in adipose tissue promotes inflammation independent of its effects on insulin production (Zhong et al. 2013). These actions of DPP4 as well as its interaction with extracellular matrix components such as collagen and fibronectin (Löster et al. 1995; Zhong et al. 2013) might implicate DPP4 as a factor related to SASP traits, which are modulated by NF- κ B and profoundly affect extracellular matrix remodeling.

SASP has been linked to the disease-enhancing impact of senescent cells that accumulate in aging tissues, since SASP factors (cytokines, growth factors, and MMPs) perturb tissue metabolism locally and systemically. Accordingly, senescent cell elimination via genetic manipulation improved age-related pathologies (Baker et al. 2008, 2011, 2016). To achieve the same goal, several drugs called "senolytics" have been identified that selectively destroy

senescent cells. Senolytics ABT737 (Yosef et al. 2016) and ABT263 (Zhu et al. 2016) were BH3 mimetic inhibitors of anti-apoptotic proteins (Bcl-xL, Bcl-2, and Bcl-w) originally developed for cancer therapy, although inhibiting Bcl-xL was found to have severe side effects. Other senolytics, such as dasatinib and quercetin (Roos et al. 2016; Zhu et al. 2016), trigger apoptosis in subsets of senescent cells, while piperlongumine appears to work best in combination with other senolytics (Wang et al. 2016). In this context, the identification of DPP4 as a targetable senescence marker can complement interventions aimed at eliminating senescent cells.

In closing, DPP4 is overexpressed in cancers such as malignant pleural mesothelioma (MPM) and renal cell and colorectal carcinoma. A recent study found that DPP4 was more highly expressed on the plasma membrane of MPM than normal mesothelioma cells (Angevin et al. 2017). Importantly, in preclinical trials, MPM tumor growth was delayed by treatment with anti-DPP4 antibody, suggesting that it was inhibitory in both cultured cells and patients. Antibody modifications such as conjugation with a toxin might enhance the cytotoxic activity of the anti-DPP4 antibody on DPP4-bearing cells. In summary, our findings have identified the cell membrane-associated protein DPP4 senescence marker as a promising target of therapeutic intervention in conditions in which it is desirable to eliminate senescent cells.

Materials and methods

Cells, cell culture, IR, and SA- β -gal assay

The source and culture of HDFs WI-38 and IMR-90, MEFs, HUVECs, and HAECs are indicated in the Supplemental Material. Proliferating WI-38 HDFs were used at PDLs ranging between PDL18 and PDL23, and senescent cells were used after additional culture (PDL47–PDL55). SA- β -gal analysis and siRNA transfections using Lipofectamine 2000 (Invitrogen) are described (Supplemental Material). Human PBMCs were isolated from participants of the Baltimore Longitudinal Study of Aging (BLSA) (Ferrucci 2008) aged 27–36 yr old (young) or 78–88 yr old (old). Proliferating WI-38 cells (approximately PDL25) and IMR-90 cells (approximately PDL25) were rendered senescent by exposure to 10 Gy of IR; cells were harvested 10 d later. Proliferating WI-38 cells were transduced with lentiviruses that expressed either DPP4-Myc or Myc (GeneCopoeia, Inc.) and selected using 1 μ g/mL puromycin for 20 d before harvest.

RNA isolation, reverse transcription, and quantitative real-time PCR

Total RNA was extracted using TriPure isolation reagent (Roche), and cDNA was synthesized using random hexamers and reverse transcriptase (Invitrogen) as described (Supplemental Material). Reactions for qPCR amplification contained SYBR Green master mix (Kapa Biosystems) and were performed using an Applied Biosystems 7300 instrument. The gene-specific primers used are listed in the Supplemental Material.

Protein analysis

The preparation and analysis of cell membrane and cell surface proteins by Western blotting and MS as well as the detection of DPP4 using immunofluorescence are explained in the Supplemental Material.

Flow cytometry of WI-38 cells and PBMCs and MACS

Proliferating and senescent WI-38 cells were counted using a TC20 cell counter (Bio-Rad), washed using FACS buffer (0.5% BSA in PBS), and seeded into 96-well plates. Dead cells were stained with Zombie Aqua fixable viability kit (BioLegend); after washing, human TruStain FcX (BioLegend) was added to block the Fc receptor, and cells were labeled with DPP4-PE

(BD Biosciences) or mIgG-PE (BioLegend) for 15 min at 4°C in the dark. FACS analysis was performed on a Canto II flow cytometer (BD Biosciences) using FlowJo software (FlowJo version 10.2).

Human PBMCs were incubated with DPP4-PE (BD Biosciences) for 10 min at 4°C in the dark to label DPP4-expressing cells and then labeled with anti-PE magnetic microbeads (Miltenyi Biotec, Inc.) for 15 min at 4°C. Magnetically labeled cells were separated by MACS (Supplemental Material). Total RNA was extracted from DPP4-positive and DPP4-negative cells.

ADCC assay

Peripheral blood from participants of the BLSA (National Institute on Aging) and healthy volunteers was collected under Human Subject Protocol 2003054 and Tissue Procurement Protocol 2003-076. White blood cells were isolated by ACK lysis, and PBMCs were isolated using Ficoll (Ficoll-Paque Plus, GE Healthcare) gradients following the manufacturer's instructions. NK cells were isolated from PBMCs using a human NK cell isolation kit (Miltenyi Biotec, Inc.). Proliferating and senescent WI-38 cells growing on 24-well plates (5×10^4 cells per well) were incubated with different concentrations of control rlgG or with rabbit or humanized monoclonal antibodies recognizing 0.05, 0.5, and 5 µg/mL DPP4 for 15 min at 37°C. The isolated NK cells (2.5×10^5 cells per well for rabbit antibody and 1.25×10^6 or 2.5×10^6 for humanized antibody) were added at a ratio of 5:1 (proliferating) or 25:1 or 50:1 (senescent; NK cells:fibroblasts [proliferating or senescent]) and incubated for 4 h at 37°C. NK cells were removed by washing, fibroblasts were returned to the incubator, and, 18 h later, cell viability was analyzed using the MTT [3-(4,5-dimethylthiazol-2-yl)-2,5-diphenyltetrazolium bromide] assay (Sigma).

Acknowledgments

We thank M.K. Evans and N. Noren Hooten for providing HUVECs and HAECs. This work was supported in part by the National Institute on Aging and National Cancer Institute Intramural Research Program and the National Institutes of Health. K.O. and C.M. were supported by Grant-in-Aid (S1311011), grant 150401-01, and Japan Society for the Promotion of Science Grants-in-Aid for Scientific Research (KAKENHI) grants 15H04879, 15K15324, 16H05345, and 16K09878.

References

- Angevin E, Isambert N, Trillet-Lenoir V, You B, Alexandre J, Zalcman G, Vielh P, Farace F, Valleix F, Podoll T, et al. 2017. First-in-human phase 1 of YS110, a monoclonal antibody directed against CD26 in advanced CD26-expressing cancers. *Br J Cancer* **116**: 1126–1134.
- Baker DJ, Perez-Terzic C, Jin F, Pitel KS, Niederländer NJ, Jeganathan K, Yamada S, Reyes S, Rowe L, Hiddingsa HJ, et al. 2008. Opposing roles for p16Ink4a and p19Arf in senescence and ageing caused by BubR1 insufficiency. *Nat Cell Biol* **10**: 825–36.
- Baker DJ, Wijshake T, Tchkonia T, LeBrasseur NK, Childs BG, van de Sluis B, Kirkland JL, van Deursen JM. 2011. Clearance of p16Ink4a-positive senescent cells delays ageing-associated disorders. *Nature* **479**: 232–236.
- Baker DJ, Childs BG, Durik M, Wijers ME, Sieben CJ, Zhong J, Saltness RA, Jeganathan KB, Verzosa GC, Pezeski A, et al. 2016. Naturally occurring p16Ink4a-positive cells shorten healthy lifespan. *Nature* **530**: 184–189.
- Bauvois B, Djavaheri-Mergny M, Rouillard D, Dumont J, Wietzerbin J. 2000. Regulation of CD26/DPP4 gene expression by interferons and retinoic acid in tumor B cells. *Oncogene* **19**: 265–272.
- Coppé JP, Desprez PY, Krtolica A, Campisi J. 2010. The senescence-associated secretory phenotype: the dark side of tumor suppression. *Annu Rev Pathol* **5**: 99–118.
- Crowe EP, Nacarelli T, Bitto A, Lerner C, Sell C, Torres C. 2014. Detecting senescence: methods and approaches. *Methods Mol Biol* **1170**: 425–445.
- D'Angelo A, Bluteau O, Garcia-Gonzalez MA, Gresh L, Doyen A, Garbay S, Robine S, Pontoglio M. 2010. Hepatocyte nuclear factor 1α and β control terminal differentiation and cell fate commitment in the gut epithelium. *Development* **137**: 1573–1582.
- Demaria M, Ohtani N, Youssef SA, Rodier F, Toussaint W, Mitchell JR, Laberge RM, Viig J, Van Steeg H, Dollé ME, et al. 2014. An essential role for senescent cells in optimal wound healing through secretion of PDGF-AA. *Dev. Cell* **31**: 722–733.
- Erickson RH, Lai RS, Kim YS. 2000. Role of hepatocyte nuclear factor 1α and 1β in the transcriptional regulation of human dipeptidyl peptidase IV during differentiation of Caco-2 cells. *Biochem Biophys Res Commun* **270**: 235–239.
- Ferrucci L. 2008. The Baltimore Longitudinal Study of Aging (BLSA): a 50-year-long journey and plans for the future. *J Gerontol A Biol Sci Med Sci* **63**: 1416–1419.
- Kuiman T, Michaloglou C, Mooi WJ, Peepre DS. 2010. The essence of senescence. *Genes Dev* **24**: 2463–2479.
- Löster K, Zeilinger K, Schuppan D, Reutter W. 1995. The cysteine-rich region of dipeptidyl peptidase IV (CD26) is the collagen-binding site. *Biochem Biophys Res Commun* **217**: 341–348.
- Muñoz-Espin D, Serrano M. 2014. Cellular senescence: from physiology to pathology. *Nat Rev Mol Cell Biol* **15**: 482–496.
- Muñoz-Espin D, Cañamero M, Maraver A, Gómez-López G, Contreras J, Murillo-Cuesta S, Rodríguez-Baeza A, Varela-Nieto I, Ruberte J, Collado M, et al. 2013. Programmed cell senescence during mammalian embryonic development. *Cell* **155**: 1104–1118.
- Ohnuma K, Yamochi T, Uchiyama M, Nishibashi K, Iwata S, Hosono O, Kawasaki H, Tanaka H, Dang NH, Morimoto C. 2005. CD26 mediates dissociation of Tollip and IRAK-1 from caveolin-1 and induces upregulation of CD86 on antigen-presenting cells. *Mol Cell Biol* **25**: 7743–7757.
- Ohnuma K, Dang NH, Morimoto C. 2008. Revisiting an old acquaintance: CD26 and its molecular mechanisms in T cell function. *Trends Immunol* **29**: 295–301.
- Prieur A, Peepre DS. 2008. Cellular senescence in vivo: a barrier to tumorigenesis. *Curr Opin Cell Biol* **20**: 150–155.
- Rasmussen N, Ditzel HJ. 2009. Scanning the cell surface proteome of cancer cells and identification of metastasis-associated proteins using a subtractive immunization strategy. *J Proteome Res* **8**: 5048–5059.
- Roos CM, Zhang B, Palmer AK, Ogródniak MB, Pirtskhalava T, Thalji NM, Hagler M, Jurk D, Smith LA, Casaclang Verzosa G, et al. 2016. Chronic senolytic treatment alleviates established vasomotor dysfunction in aged or atherosclerotic mice. *Aging Cell* **15**: 973–977.
- Scott LJ. 2017. Sitagliptin: a review in type 2 diabetes. *Drugs* **77**: 209–224.
- Storer M, Mas A, Robert-Moreno A, Pecoraro M, Ortells MC, Di Giacomo V, Yosef R, Pilpel N, Krizhanovsky V, Sharpe J, Keyes WM. 2013. Senescence is a developmental mechanism that contributes to embryonic growth and patterning. *Cell* **155**: 1119–1130.
- van Deursen JM. 2014. The role of senescent cells in ageing. *Nature* **509**: 439–446.
- Wang Y, Chang J, Liu X, Zhang X, Zhang S, Zhang X, Zhou D, Zheng G. 2016. Discovery of piperlongumine as a potential novel lead for the development of senolytic agents. *Aging* **8**: 2915–2926.
- Weiner GJ. 2015. Building better monoclonal antibody-based therapeutics. *Nat Rev Cancer* **15**: 361–370.
- Wu T, Rayner CK, Horowitz M. 2016. Incretins. *Handb Exp Pharmacol* **233**: 137–171.
- Yosef R, Pilpel N, Tokarsky-Amiel R, Biran A, Ovadya Y, Cohen S, Vadai E, Dassa L, Shahar E, Condiotti R, et al. 2016. Directed elimination of senescent cells by inhibition of BCL-W and BCL-XL. *Nat Commun* **7**: 11190.
- Zhong J, Rao X, Deiuliis J, Braunstein Z, Narula V, Hazey J, Mikami D, Needleman B, Satoskar AR, Rajagopalan S. 2013. A potential role for dendritic cell/macrophage-expressing DPP4 in obesity-induced visceral inflammation. *Diabetes* **62**: 149–157.
- Zhu Y, Tchkonia T, Fuhrmann-Stroissnigg H, Dai HM, Ling YY, Stout MB, Pirtskhalava T, Giorgadze N, Johnson KO, Giles CB, et al. 2016. Identification of a novel senolytic agent, navitoclax, targeting the Bcl-2 family of anti-apoptotic factors. *Aging Cell* **15**: 428–435.



Identification of senescent cell surface targetable protein DPP4

Kyoung Mi Kim, Ji Heon Noh, Monica Bodogai, et al.

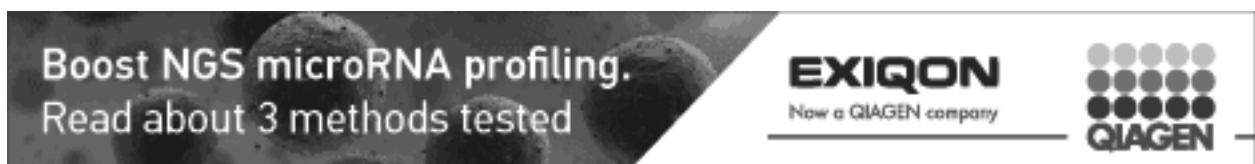
Genes Dev. 2017, **31**: originally published online September 6, 2017
Access the most recent version at doi:10.1101/gad.302570.117

Supplemental Material <http://genesdev.cshlp.org/content/suppl/2017/09/06/gad.302570.117.DC1>

References This article cites 29 articles, 4 of which can be accessed free at:
<http://genesdev.cshlp.org/content/31/15/1529.full.html#ref-list-1>

Creative Commons License This article is distributed exclusively by Cold Spring Harbor Laboratory Press for the first six months after the full-issue publication date (see <http://genesdev.cshlp.org/site/misc/terms.xhtml>). After six months, it is available under a Creative Commons License (Attribution-NonCommercial 4.0 International), as described at <http://creativecommons.org/licenses/by-nc/4.0/>.

Email Alerting Service Receive free email alerts when new articles cite this article - sign up in the box at the top right corner of the article or [click here](#).

An advertisement for EXIQON, a QIAGEN company. The ad features a dark background with a grid of small, light-colored dots. The text 'Boost NGS microRNA profiling. Read about 3 methods tested' is displayed in white. The EXIQON logo is at the top right, followed by the text 'Now a QIAGEN company'. The QIAGEN logo is at the bottom right, consisting of a grid of nine dots and the word 'QIAGEN'.



Data Article

Gene expression microarray data from mouse cerebrum treated with rTMS for 30 days



Tetsurou Ikeda^{a,b,1,*}, Satoru Kobayashi^c, Chikao Morimoto^b

^a Laboratory for Structural Neuropathology, RIKEN Brain Science Institute, 2-1 Hirosawa, Wako-shi, Saitama 351-0198, Japan

^b Clinical Immunology, Institute of Medical Science, The University of Tokyo, 4-6-1 Shirokanedai, Minato-ku, Tokyo 108-8639, Japan

^c Technical Support, Thermo Fisher Scientific K.K., 3-9 Moriya, Kanagawa-ku, Yokohama 221-0022, Japan

ARTICLE INFO

Article history:

Received 28 June 2017

Received in revised form

12 September 2017

Accepted 12 October 2017

Available online 19 October 2017

ABSTRACT

This data article contains complementary tables related to the research article entitled, 'Effects of repetitive transcranial magnetic stimulation on ER stress-related genes and glutamate, γ -aminobutyric acid, and glycine transporter genes in mouse brain' (Ikeda et al. (2017) [1]), which showed that rTMS modulates glutamate, GABA and glycine transporters and regulates ER stress-related genes. Here we provide accompanying data collected using Affymetrix GeneChip microarrays to identify changes in gene expression in mouse cerebrum treated with rTMS for 30 days (Tables 1–10).

© 2017 The Authors. Published by Elsevier Inc. This is an open access article under the CC BY license (<http://creativecommons.org/licenses/by/4.0/>).

Specifications Table

Subject area

Neuroscience

More specific subject area

Psychiatric disorders

Type of data

Tables

How data was acquired

Affymetrix GeneChip RNA microarray

* Corresponding author.

E-mail address: ikedatetsurou@kochi-u.ac.jp (T.o.s. Ikeda).

¹ Present address: Kochi Medical School, Kochi University, Kochi, Japan.

Data format	<i>Filtered, analysed</i>
Experimental factors	<i>Mouse brain treated with rTMS for 30 days</i>
Experimental features	<i>RNA isolation, global gene expression analyses</i>
Data source location	<i>Wako, Saitama, Japan</i>
Data accessibility	<i>Data are contained within this article</i>

Value of the Data

-
- A global gene expression analysis of mouse cerebrum treated with rTMS for 30 days.
 - These data may be useful for comparison with microarray data obtained from rTMS of different durations.
 - Genes identified as differentially expressed in this data set could be useful in further studies on the effects of rTMS on mouse brain.
-

1. Data

Affymetrix GeneChip microarray analyses of mRNA isolated from mouse cerebrum after 30 days of rTMS revealed altered expression of several genes (Tables 1–10), including glutamatergic genes (e.g., glutamate transporter), dopaminergic genes, cholinergic genes, genes of adrenergic signaling in cardiomyocytes and so on.

2. Experimental design, materials and methods

We carried out a comprehensive analysis of altered gene expression in cerebrum following chronic rTMS using a high-density oligonucleotide array (GeneChip; Affymetrix, Santa Clara, CA, USA. MG_U74Av2 probe array), as described elsewhere [2]. Using the Affymetrix algorithm [3] and multiple analysis comparison software for assessing gene expression differences, mRNAs that increased or decreased in the mouse brain following chronic rTMS relative to levels in the control mouse brain were identified. Pathway analysis was used to identify the significant pathway of the differential genes according to KEGG. And also, Gene Ontology (GO) analysis was applied to analyze the main function of the differentially expressed genes according to the gene ontology, which is the key functional classification of NCBI that can organize genes into hierarchical categories and uncover the gene regulatory network based on biological process and molecular function [4].

Using these data, we indicated that rTMS modulates glutamate, GABA and glycine transporters and regulates ER stress-related genes [1].

Table 1
Gene expression matrix after 30 days rTMS on cerebrum.

TC ID	GS	L1	C	L2	C	L3	C	L4	C	*	#	Description
93320_at	Cpt1a	0.44	1	0.15	1	0.3	1	0.17	1	4	0	carnitine palmitoyltransferase 1a, liver acidic (leucine-rich) nuclear phosphoprotein 32 family, member A
93372_at	Anp32a	1.75	1	2.28	1	1.59	1	1.91	1	4	0	coactosin-like 1 (Dictyostelium)
95466_at	Cotl1	2.41	1	1.11	1	2.03	1	0.83	1	4	0	chemokine (C-C motif) ligand 21A (serine); chemokine (C-C motif) ligand 21B (leucine); chemokine (C-C motif) ligand 21C (leucine); predicted gene 10591; predicted gene 13304; predicted gene 1987; predicted gene, 21541; C-C motif chemokine 21c
103012_at	Ccl21a	0.27	1	3.54	1	-1.5	D	1.6	1	3	1	
100307_at	Nfix	1.12	1	0.62	1	0.41	1	-0.05	NC	3	0	nuclear factor I/X
101883_s_at	Xlr3a	0.03	NC	1.16	1	0.74	1	1.79	1	3	0	X-linked lymphocyte-regulated 3A; X-linked lymphocyte-regulated 3B; X-linked lymphocyte-regulated 3C
101921_at	Rab4a	0.46	1	0.27	1	-0.01	NC	0.07	1	3	0	RAB4A, member RAS oncogene family
104175_at	Dlg4	1.09	1	1.46	1	0.41	1	1.15	NC	3	0	disces, large homolog 4 (Drosophila)
93253_at	Mapk1	-0.04	NC	0.34	1	0.34	1	0.71	1	3	0	mitogen-activated protein kinase 1
93924_f_at	Tuba3b	0.4	1	0.15	1	0.11	1	-0.09	NC	3	0	tubulin, alpha 3B
96295_at	Psat1	0.09	NC	0.11	1	0.28	1	0.44	1	3	0	phosphoserine aminotransferase 1
96590_f_at	Otud7b	0.59	NC	0.7	1	0.33	1	0.32	1	3	0	OTU domain containing 7B
99598_g_at	Gna12	0.33	1	0.67	1	-0.1	NC	0.2	MI	3	0	guanine nucleotide binding protein (G protein), alpha inhibiting 2
102009_at	Cyfip2	0.53	1	0.21	1	-0.33	NC	-0.6	D	2	1	cytoplasmic FMR1 interacting protein 2
103275_at	Atp6v0a1	0.52	1	-1.05	D	1.2	1	-0.31	NC	2	1	ATPase, H ⁺ transporting, lysosomal V0 subunit A1
104486_at	A2m	0.27	1	-0.91	D	0.83	1	-0.91	NC	2	1	alpha-2-macroglobulin
104564_at	Scg3	0.47	1	0.32	1	-0.49	D	-0.52	NC	2	1	secretogranin III
104643_at	Wwc1	0.72	1	0.47	1	-0.34	NC	-0.69	D	2	1	WW, C2 and coiled-coil domain containing 1
160189_at	Nudt4	-0.2	NC	-0.84	D	0.63	1	0.4	1	2	1	nudix (nucleoside diphosphate linked moiety X)-type motif 4
162138_s_at	Cbx6	0.21	1	0.27	1	-0.54	D	-0.71	NC	2	1	chromobox 6
93660_at	Camk2a	1.53	1	-0.93	D	2.09	1	-0.27	NC	2	1	calcium/calmodulin-dependent protein kinase II alpha
95301_at	S100a5	0.6	1	0.96	1	-0.86	D	-0.45	NC	2	1	S100 calcium binding protein A5
95785_s_at	Rab7	-0.36	NC	-0.91	D	0.91	1	0.4	1	2	1	RAB7, member RAS oncogene family
96583_s_at	Kif5a	-0.13	NC	-1.32	D	1.6	1	0.36	1	2	1	kinesin family member 5A
97458_at	Gnb1	0.61	1	0.8	1	-0.58	D	-0.62	NC	2	1	guanine nucleotide binding protein (G protein), beta 1
97560_at	Psap	-0.28	NC	-1.49	D	1.74	1	0.37	1	2	1	psaposin
98457_at	Slc4a4	0.72	1	0.35	1	-0.62	NC	-0.92	D	2	1	solute carrier family 4 (anion exchanger), member 4
99458_i_at	Mark2	0.28	1	0.46	1	-0.66	D	-0.5	NC	2	1	MAP/microtubule affinity regulating kinase 2
99481_at	Atp1a2	0.86	1	0.45	1	-0.49	NC	-0.82	D	2	1	ATPase, Na ⁺ /K ⁺ transporting, alpha 2 polypeptide
99882_at	Ids	-0.75	NC	-1.24	D	0.55	1	-0.19	MI	2	1	iduronate 2-sulfatase
100012_at	Laptm5	0.63	1	0.07	NC	0.34	MI	-0.35	NC	2	0	lysosomal-associated protein transmembrane 5
100068_at	Aldh1a1	0.21	1	0.16	1	-0.42	NC	-0.31	NC	2	0	aldehyde dehydrogenase family 1, subfamily A1

100133_at	Fyn	0.35	1	0.55	1	-0.22	NC	0.06	NC	2	0	Fyn proto-oncogene
100154_at	Tapbp	0.8	1	0.21	1	0.28	NC	-0.19	NC	2	0	TAP binding protein
100380_at	Gm10257	0.06	NC	0.26	1	-0.21	NC	0.02	1	2	0	predicted gene 10257; predicted gene 12657; H3 histone, family 3A; H3 histone, family 3B; H3 histone, family 3C; histone H3.3-like; uncharacterized LOC105242736
100494_at	Fgr1	0.48	NC	-0.23	NC	0.71	1	0.29	1	2	0	fibroblast growth factor 1
100573_f_at	Gpi1	0.35	1	0.41	1	-0.13	NC	-0.05	NC	2	0	glucose phosphate isomerase 1
100727_at	Rpl28	0.36	1	0.6	1	-0.26	NC	-0.02	NC	2	0	ribosomal protein L28
100762_at	Sema6a	2.15	1	-0.09	NC	0.39	MI	-1.7	NC	2	0	sema domain, transmembrane domain (TM), and cytoplasmic domain, (semaphorin) 6A

Gnb1, Gna12, Dlg4 and Mapk1 are glutamatergic genes. Fyn, Camk2a and Mapk1 are cholinergic genes. Kif5a is Dopaminergic gene. Mice cerebrum stimulated by rTMS for 30days were denoted as M1 and M2, sham control were denoted as C1 and C2. N=2. All expression ratios were converted into the \log_2 (expression ratio) values. L1: Signal Log Ratio (M1/C1), L2: Signal Log Ratio (M2/C1), L3: Signal Log Ratio (M1/C2), L4: Signal Log Ratio (M1/C2). C1, C2 were normalized with respect to C1 and C2 to obtain expression ratios. Expression Console (EC) Ver.1.4 and Transcriptome Analysis Console (TAC) Ver.3. were used for Comparison Analysis as manufacture procedure. C means data analysis output for a Comparison Analysis illustrating Change p-values with the associated Increase (I) or Decrease (D) call. Increase calls have Change p-values closer to zero and Decrease calls have Change p-values closer to one. Finally, the Change algorithm assesses probe pair saturation, calculates a Change p-values, and assigns an (I), Marginal Increase (MI), No Change (NC), Marginal Decrease (MD), or (D) call for C. Gene with more than 2 significant difference calls was chosen. Abbreviations: TC ID: Transcript Cluster ID, GS: Gene Symbol, *: Total number of increase, #: Total number of decrease. TC ID is available for Pathway analysis.

Table 2
Gene expression matrix after 30 days rTMS on cerebrum.

TC ID	GS	L1	C	L2	C	L3	C	L4	C	*	#	Description
100774_at	Synj2bp	0.34	I	-0.15	I	-0.28	NC	-0.08	NC	2	0	synaptotannin 2 binding protein
100892_at	Ndufaf1	0.4	NC	0.31	I	0.26	NC	0.29	I	2	0	NADH dehydrogenase (ubiquinone) 1 alpha subcomplex, assembly factor 1
100992_at	Phc1	0.43	I	0.24	I	-0.07	NC	-0.28	NC	2	0	polyhomeotic-like 1 (Drosophila) ras homolog gene family, member A
101113_at	Rh0a	0.31	I	0.16	MI	0.18	NC	-0.26	NC	2	0	tubulin, beta 4 A class IV A
101419_at	Tubb4a	0.35	I	0.51	I	-0.27	NC	-0.01	NC	2	0	inositol 1,4,5-triphosphate receptor 2
101441_i_at	Itpn2	0.32	I	0.25	MI	-0.18	NC	-0.57	NC	2	0	S100 protein, beta polypeptide, neural proteasome (prosome, macropain) activator subunit 1 (PA28 alpha)
101467_at	S100b	0.06	NC	0.04	NC	0.53	I	0.44	I	2	0	actin, beta
101510_at	Psmn1	0.21	NC	0.27	I	0.08	NC	0.19	I	2	0	epoxide hydrolase 1, microsomal
101578_f_at	Actb	0.92	I	0.99	I	-0.4	NC	-0.47	NC	2	0	microtubule-associated protein 6
101587_at	Ephx1	0.9	I	0.99	I	-1.13	NC	-1.27	NC	2	0	phospholipase A2, group VII (platelet-activating factor acetylhydrolase, plasma)
101855_at	Map6	0.3	I	0.15	I	-0.01	NC	-0.35	NC	2	0	SWI/SNF related, matrix associated, actin dependent regulator of chromatin, subfamily a, member 2
101923_at	Pla2g7	0.47	I	0.42	I	-0.08	NC	-0.18	NC	2	0	nuclear factor I/X
101930_at	Nfix	0.63	I	0.34	MI	-0.11	NC	-0.34	NC	2	0	RNA 2'-3'-cyclic phosphate and 5'-OH ligase
101960_at	Rtcb	0.24	NC	0.3	I	-0.18	NC	0.04	I	2	0	holocytochrome c synthetase
102007_at	Hccs	0.02	NC	-0.35	NC	0.41	I	0.48	I	2	0	testis specific protein kinase 1
102033_at	Tesk1	0.42	I	0.4	I	0.09	NC	-0.05	NC	2	0	3-phosphoinositide dependent protein kinase 1
102063_at	Pdpk1	0.87	I	0.2	I	-0.2	NC	-0.46	NC	2	0	sparc/osteonectin, cwcv and kazal-like domains proteoglycan 2
102095_f_at	Spock2	0.32	I	0.18	MI	-0.53	NC	-0.73	NC	2	0	prefoldin 2
102252_at	Pfdn2	0.42	I	0.24	I	-0.03	NC	-0.14	NC	2	0	zinc finger, MIz-type containing 2
102271_at	Zmiz2	0.58	I	0.54	I	-0.32	NC	-0.52	NC	2	0	regulator of calcineurin 3
102374_at	Rcan3	0.27	NC	-0.03	NC	0.29	I	0.12	I	2	0	SWI/SNF related, matrix associated, actin dependent regulator of chromatin, subfamily a, member 2
102384_at	Smarca2	0.42	I	0.59	I	-0.31	NC	-0.04	NC	2	0	carbohydrate sulfotransferase 2
102639_at	Chst2	0.47	I	0.4	I	-0.04	NC	-0.21	NC	2	0	zinc finger protein 385A
102691_at	Zfp385a	0.88	I	0.67	I	-0.18	NC	-0.56	NC	2	0	T-box brain gene 1
102700_at	Thr1	0.43	I	0.41	I	-0.37	NC	-0.43	NC	2	0	cytoplasmic FMR1 interacting protein 1
102752_at	Cyfip1	0.43	I	0.31	I	-0.17	NC	-0.32	NC	2	0	adhesion G protein-coupled receptor G1
102787_at	Adgrg1	0.79	I	0.26	I	0.52	NC	-0.42	NC	2	0	annexin A11; predicted gene 2260; predicted gene 2274
102815_at	Anxa11	0.28	I	0.5	I	-0.86	NC	-0.55	NC	2	0	SRY (sex determining region Y)-box 10
102856_at	Sox10	0.39	I	0.45	I	-0.08	NC	-0.14	NC	2	0	tankyrase, TRF1-interacting ankyrin-related ADP-ribose polymerase 2
102912_at	Tnks2	0.28	I	0.34	I	-0.4	NC	-0.2	NC	2	0	sperm antigen with calponin homology and coiled-coil domains 1
102942_at	Spcc1	0.3	I	0.28	I	-0.35	NC	-0.43	NC	2	0	vascular endothelial growth factor B
103001_at	Vegfb	0.46	MI	0.15	I	-0.13	NC	-0.02	NC	2	0	

103029_at	Pdcd4	0.76	1	0.61	1	-0.17	NC	-0.02	NC	2	0
103040_at	Cd83	0.02	NC	0.43	1	-0.12	NC	0.11	1	2	0
103054_at	Polr2a	0.43	1	0.07	NC	0.23	1	-0.06	NC	2	0
103090_at	Uqcc1	-0.41	NC	-0.09	NC	0.21	1	0.33	1	2	0
103299_at	Pld4	0.88	1	0.03	NC	1.18	1	0.36	NC	2	0
103300_at	Abcb7	0.64	1	-0.12	NC	0.41	1	-0.48	NC	2	0
103305_at	Itgb4	0.83	1	2.63	1	0.51	NC	2.83	NC	2	0
103369_at	Klf13	0.77	1	0.36	1	-0.36	NC	-0.43	NC	2	0
103370_at	Lin7c	0.35	1	0.27	1	0	NC	-0.21	NC	2	0
103404_at	Re1re	0.6	1	0.19	1	0.05	NC	-0.15	NC	2	0
103411_at	Gna11	0.23	NC	0.48	1	0.1	NC	0.13	1	2	0
103584_at	Cnmp	0.32	1	0.46	1	-0.37	NC	-0.37	NC	2	0

Actb, Itpr2 and Rho are oxytocin signaling pathway genes. Cyfip1 and Itgb4 are actin cytoskeleton regulation genes. Pdkp1 and Pdcd4 are genes of proteoglycans in cancer. Pla2g7 and Pld4 are ether lipid metabolism genes. Mice cerebrum stimulated by rTMS for 30days were denoted as M1 and M2, sham control were denoted as C1 and C2. N=2. All expression ratios were converted into the \log_2 (expression ratio) values. L1: Signal Log Ratio (M1/C1), L2: Signal Log Ratio (M2/C1), L3: Signal Log Ratio (M1/C2), L4: Signal Log Ratio (M2/C2). C1, C2 were used as a control and M1, M2 were normalized with respect to C1 and C2 to obtain expression ratios. Expression Console (EC) Ver.1.4 and Transcriptome Analysis Console (TAC) Ver.3. were used for Comparison Analysis as manufacture procedure. C means data analysis output for a Comparison Analysis illustrating Change p-values with the associated Increase (I) or Decrease (D) call. Increase calls have Change p-values closer to zero and Decrease calls have Change p-values closer to one. Finally, the Change algorithm assesses probe pair saturation, calculates a Change p-values, and assigns an (I), Marginal Increase (MI), No Change (NC), Marginal Decrease (MD), or (D) call for C. Gene with more than 2 significant difference calls was chosen. Abbreviations; TC ID: Transcript Cluster ID, GS: Gene Symbol, #: Total number of increase, *: Total number of decrease, #: Total number of decrease. TC ID is available for Pathway analysis.

Table 3
Gene expression matrix after 30 days rTMS on cerebrum.

TC ID	GS	L1	C	L2	C	L3	C	L4	C	*	#	Description
103611_at	Cd47	0.55	1	0.59	1	-0.22	NC	-0.18	NC	2	0	CD47 antigen (Rh-related antigen, integrin-associated signal transducer)
103613_at	Aldoart2	1.82	1	1.52	1	1.42	NC	1.55	NC	2	0	aldolase 1 A, retrogene 2
103624_at	Urm1	0.25	NC	-0.2	NC	0.54	1	0.36	1	2	0	ubiquitin related modifier 1 homolog (S. cerevisiae)
103663_at	Pomgntr1	0.35	1	0.32	1	-0.16	NC	0.07	NC	2	0	protein O-linked mannose beta 1,2-N-acetylglucosaminyltransferase
103682_at	Uril	-0.04	NC	0.65	1	-0.23	NC	0.27	1	2	0	UR11 prefoldin-like chaperone
103748_at	Cmip	0.78	1	0.34	1	-0.03	NC	-0.27	NC	2	0	c-Maf inducing protein
103771_at	Rnf208	0.48	1	0.17	1	-0.16	NC	-0.32	NC	2	0	ring finger protein 208
104032_at	Mast3	0.6	1	0.36	1	-0.39	NC	-0.51	NC	2	0	microtubule associated serine/threonine kinase 3
104034_at	Al464131	0.63	1	0.66	1	-0.77	NC	-0.4	NC	2	0	expressed sequence Al464131
104214_at	Slc7a8	0.63	1	0.33	1	0.09	NC	0.16	NC	2	0	solute carrier family 7 (cationic amino acid transporter, y+ system),member 8
104244_at	Mark2	0.95	1	0.63	1	-0.35	NC	-0.5	NC	2	0	MAP/microtubule affinity regulating kinase 2
104250_at	Lrrc8a	0.53	1	0.12	1	-0.36	NC	-0.64	NC	2	0	leucine rich repeat containing 8A
104316_at	Gna13	0.64	1	0.59	1	-0.02	NC	-0.01	NC	2	0	guanine nucleotide binding protein, alpha 13
104352_at	Bird4	0.2	MI	0.41	1	-0.37	NC	-0.33	NC	2	0	bromodomain containing 4
104368_at	Mapre3	0.23	MI	0.56	1	-0.22	NC	-0.09	NC	2	0	microtubule-associated protein, RP/EB family, member 3
104380_at	Sic35a1	-0.23	NC	0.34	1	0.02	NC	0.7	1	2	0	solute carrier family 35 (CMP-sialic acid transporter), member 1
104409_at	Grik5	0.49	1	0.37	1	-0.16	NC	-0.25	NC	2	0	glutamate receptor, ionotropic, kainate 5 (gamma 2)
104415_at	Foxp1	0.47	1	0.2	1	-0.12	NC	-0.18	NC	2	0	forkhead box P1
104514_at	Epn1	0.3	1	0.11	1	-0.17	NC	-0.39	NC	2	0	epsin 1
104546_g_at	Csnk2a1	1.1	1	-0.1	NC	0.97	1	0.13	NC	2	0	casein kinase 2, alpha 1 polypeptide; predicted pseudogene 10031
104634_at	Lims1	0.49	NC	0.73	1	-0.16	NC	0.5	1	2	0	LIM and senescent cell antigen-like domains 1
104650_at	Ache	0.48	1	0.38	1	0.19	NC	-0.12	NC	2	0	acetylcholinesterase
104725_at	Rhoq	0.81	1	0.61	1	0.37	NC	0.02	NC	2	0	ras homolog gene family, member Q
104739_at	Tcta	0.18	NC	-0.34	NC	0.66	1	0.31	1	2	0	T cell leukemia translocation altered gene
104741_at	Zdhhc9	0.8	1	0.14	1	0.75	NC	-0.1	NC	2	0	zinc finger, DHHC domain containing 9
104747_at	Slc1a1	0.42	1	0.44	1	-0.28	NC	-0.35	NC	2	0	solute carrier family 1 (neuronal/epithelial high affinity glutamate transporter, system Xag), member 1
160111_at	Eiflax	-0.38	NC	-0.47	NC	0.48	1	0.31	1	2	0	eukaryotic translation initiation factor 1A, X-linked
160181_at	Syp	0.37	1	0.45	1	-0.43	NC	-0.42	NC	2	0	synaptophysin
160184_at	Ergic1	0.75	1	0.12	NC	0.75	1	-0.22	NC	2	0	endoplasmic reticulum-golgi intermediate compartment (ERGIC) 1
160190_at	Syt4	0.5	1	0.68	1	-0.09	NC	-0.01	NC	2	0	synaptotagmin IV
160196_at	Smap1	0.37	1	0.42	1	-0.59	NC	-0.48	NC	2	0	small ArfGAP 1
160272_at	Cbx3	0.55	1	0.55	1	-0.41	NC	-0.13	NC	2	0	chromobox 3
160414_at	Sic38a10	0.42	1	-0.17	NC	0.28	1	-0.26	NC	2	0	solute carrier family 38, member 10
160417_at	Kif5b	0.34	1	0.7	1	-0.23	NC	0.08	NC	2	0	kinesin family member 5B

160502_at	Creg1	-0.03	NC	-0.22	NC	0.52	MI	0.14	1	2	0	cellular repressor of E1A-stimulated genes 1
160614_at	Pten	0.6	1	0.39	1	-0.13	NC	-0.36	NC	2	0	phosphatase and tensin homolog
160667_at	Evl	0.58	1	0.56	1	-0.2	NC	-0.34	NC	2	0	Ena-vasodilator stimulated phosphoprotein
160743_at	Pole3	0.41	1	-0.13	NC	0.15	1	-0.44	NC	2	0	polymerase (DNA directed), epsilon 3 (p17 subunit)
160754_at	Pygm	0.66	1	0.83	1	-0.34	NC	-0.1	NC	2	0	muscle glycogen phosphorylase
160942_at	Obx6	0.63	1	0.23	1	-0.06	NC	-0.36	NC	2	0	chromobox 6
161015_at	Clysv1	0.11	NC	0.7	1	-0.06	NC	0.71	1	2	0	clavosin 1
161054_at	Spock1	0.62	1	0.44	1	-0.13	NC	-0.05	NC	2	0	sparc/osteonectin, cwcv and kazal-like domains proteoglycan 1
161057_at	Actr10	0.35	1	0.33	1	-0.36	NC	-0.41	NC	2	0	ARP10 actin-related protein 10

Ache is Cholinergic gene. Gril5 and Slc1a1 are Glutamatergic gene. Mice cerebrum stimulated by rTMS for 30days were denoted as M1 and M2, sham control were denoted as C1 and C2. N=2. All expression ratios were converted into the \log_2 (expression ratio) values. L1: Signal Log Ratio (M1/C1), L2: Signal Log Ratio (M2/C1), L3: Signal Log Ratio (M1/C2). L4: Signal Log Ratio (M1/C2). C1, C2 were used as a control and M1, M2 were normalized with respect to C1 and C2 to obtain expression ratios. Expression Console (EC) Ver.1.4 and Transcriptome Analysis Console (TAC) Ver.3. were used for Comparison Analysis illustrating Change p-values with the associated Increase (I) or Decrease (D) call. Increase calls have Change p-values closer to zero and Decrease calls have Change p-values closer to one. Finally, the Change algorithm assesses probe pair saturation, calculates a Change p-values, and assigns an (I), Marginal Increase (MI), No Change (NC), Marginal Decrease (MD), or (D) call for C. Gene with more than 2 significant difference calls was chosen. Abbreviations: TC ID: Transcript Cluster ID, GS: Gene Symbol, *: Total number of increase, #: Total number of decrease. TC ID is available for Pathway analysis.

Table 4
Gene expression matrix after 30 days rTMS on cerebrum.

TC ID	GS	L1	C	L2	C	L3	C	L4	C	*	#	Description
161070_at	Spred2	0.28	1	0.38	1	-0.74	NC	-0.5	NC	2	0	sprouty-related, EVH1 domain containing 2
161167_at	Uck1	2.05	1	-0.84	NC	2.47	1	-0.66	NC	2	0	uridine-cytidine kinase 1
161371_at	Ptpk	1.29	NC	1.29	NC	3.1	1	2.98	1	2	0	protein tyrosine phosphatase, receptor type, K
161819_f_at	Laptm5	0.73	1	0.48	1	-0.11	NC	-0.05	NC	2	0	lysosomal-associated protein transmembrane 5
162134_at	201011101Rik	0.47	1	-0.14	NC	0.47	1	-0.47	NC	2	0	RIKEN cDNA 201011101 gene
162182_f_at	Kcnab2	0.54	1	0.17	1	-0.22	NC	-0.73	NC	2	0	potassium voltage-gated channel, shaker-related subfamily, beta member 2
162332_f_at	Mapre3	0.9	1	1.08	1	0.08	NC	-0.03	NC	2	0	microtubule-associated protein, RP/EB family, member 3
162499_f_at	Ube2d2a	0.48	1	0.38	1	-0.17	NC	-0.17	NC	2	0	ubiquitin-conjugating enzyme E2D 2A
92180_at	H1fx	0.42	1	0.37	1	-0.38	NC	-0.51	NC	2	0	H1 histone family, member X
92196_f_at	Sf3a2	0.37	1	0.29	1	-0.16	NC	-0.27	NC	2	0	splicing factor 3a, subunit 2
92202_g_at	Zbtb16	0.72	1	0.66	1	-0.61	NC	-0.73	NC	2	0	zinc finger and BTB domain containing 16
92227_s_at	Ctnna2	0.08	NC	0.36	1	-0.25	NC	-0.01	1	2	0	catenin (cadherin associated protein), alpha 2
92241_at	Nfic	0.68	1	0.88	1	-0.58	NC	-0.43	NC	2	0	nuclear factor I/C
92247_at	Arhgap5	0.6	1	-0.02	NC	0.31	MI	-0.43	NC	2	0	Rho GTPase activating protein 5
92350_at	Mapre1	0.82	1	0.42	1	0.09	NC	-0.44	NC	2	0	microtubule-associated protein, RP/EB family, member 1
92379_f_at	Ptprz1	0.27	MI	0.49	1	-0.55	NC	-0.2	NC	2	0	protein tyrosine phosphatase, receptor type Z, polypeptide 1
92397_at	Agap1	0.52	1	0.2	1	0.06	NC	-0.46	NC	2	0	ArfGAP with GTPase domain, ankyrin repeat and PH domain 1
92411_at	Hs1bp3	0.44	1	0.12	1	0.3	NC	-0.02	NC	2	0	HCL51 binding protein 3
92426_at	Tspan5	0.33	1	0	NC	0.33	1	-0.14	NC	2	0	tetraspanin 5
92484_at	Hivep2	0.5	1	-0.2	NC	0.36	1	-0.45	NC	2	0	human immunodeficiency virus type I enhancer binding protein 2
92525_i_at	Nacc2	0.33	1	0.82	1	-0.03	NC	0.4	NC	2	0	nucleus accumbens associated 2, BEN and BTB (POZ) domain
												containing
92528_at	Adgrb1	0.37	1	0.17	1	-0.43	NC	-0.55	NC	2	0	adhesion G protein-coupled receptor B1
92586_at	Glud1	0.36	NC	0.39	1	-0.13	NC	0.24	1	2	0	glutamate dehydrogenase 1
92621_at	Pcbp2	0.43	1	0.09	1	-0.08	NC	-0.49	NC	2	0	poly(rC) binding protein 2
92659_at	Rapgef4	-0.28	NC	-0.73	NC	0.98	1	0.66	1	2	0	Rap guanine nucleotide exchange factor (GEF) 4
92678_at	Ddx25	0.22	NC	-0.07	NC	0.17	1	0.12	1	2	0	DEAD (Asp-Glu-Ala-Asp) box polypeptide 25
92795_at	Map4	0.56	1	0.5	1	-0.07	NC	-0.28	NC	2	0	microtubule-associated protein 4
92817_at	Imp3	-0.22	NC	-0.46	NC	0.23	1	-0.03	MI	2	0	IMP3, U3 small nucleolar ribonucleoprotein, homolog (yeast)
92820_at	Usp2	0.64	1	0.54	1	-0.28	NC	-0.34	NC	2	0	ubiquitin specific peptidase 2
92821_at	Usp2	0.42	1	0.29	1	-0.25	NC	-0.27	NC	2	0	ubiquitin specific peptidase 2
92838_at	Fscn1	0.73	1	0.2	NC	0.35	1	-0.16	NC	2	0	fasin homolog 1, actin bundling protein (Strongylocentrotus purpuratus)
92871_at	Sel1l	0.79	1	0.4	1	-0.19	NC	-0.36	NC	2	0	sel-1 suppressor of lin-12-like (C. elegans)
92927_at	Etv1	0.66	1	0.27	NC	0.49	1	0.26	NC	2	0	ets variant 1
92949_at	Pacsin1	0.31	1	0.33	1	-0.23	NC	-0.29	NC	2	0	protein kinase C and casein kinase substrate in neurons 1

92958_at	Foxo3	0.43	1	0.11	1	-0.44	NC	-0.54	NC	2	0
93006_at	Nfic	0.33	1	0.35	MI	-0.39	NC	-0.58	NC	2	0
93047_at	Nup50	0.48	1	-0.61	NC	0.81	1	-0.38	NC	2	0
93055_at	Ankrd46	-0.16	NC	-0.14	NC	0.28	1	0.28	1	2	0
93058_at	Eif1a	0.02	NC	0.35	1	-0.04	NC	0.26	1	2	0
93069_at	Ube2d2a	0.04	NC	0.41	1	-0.04	NC	0.2	1	2	0
93129_at	Cux2	0.51	1	0.43	1	0	NC	-0.28	NC	2	0
93147_f_at	Celf4	0.43	1	0.23	1	-0.2	NC	-0.39	NC	2	0
93246_at	Naa15	0.22	1	0.55	1	-0.27	NC	-0.35	NC	2	0
93284_at	Cirbp	-0.27	NC	0.42	1	-0.02	NC	0.54	1	2	0
93288_at	Arpc2	0.23	MI	0.44	1	-0.31	NC	-0.01	NC	2	0

Kcnab2 and Pacsin1 are Synaptosome genes. Rapgef4, Arhgap5 and Ctnna2 are Leukocyte transendothelial migration genes. Mice cerebrum stimulated by rTMS for 30days were denoted as M1 and M2, sham control were denoted as C1 and C2. N=2. All expression ratios were converted into the \log_2 (expression ratio) values. L1: Signal Log Ratio (M1/C1), L2: Signal Log Ratio (M2/C1), L3: Signal Log Ratio (M1/C2), L4: Signal Log Ratio (M1/C2). C1, C2 were used as a control and M1, M2 were normalized with respect to C1 and C2 to obtain expression ratios. Expression Console (EC) Ver.1.4 and Transcriptome Analysis Console (TAC) Ver.3. were used for Comparison Analysis as manufacture procedure. C means data analysis output for a Comparison Analysis illustrating Change p-values with the associated Increase (I) or Decrease (D) call. Increase calls have Change p-values closer to zero and Decrease calls have Change p-values closer to one. Finally, the Change algorithm assesses probe pair saturation, calculates a Change p-values, and assigns an (I), Marginal Increase (MI), No Change (NC), Marginal Decrease (MD), or (D) call for C. Gene with more than 2 significant difference calls was chosen. Abbreviations; TC ID: Transcript Cluster ID, GS: Gene Symbol, *: Total number of increase, #: Total number of decrease. TC IID is available for Pathway analysis.

Table 5
Gene expression matrix after 30 days rTMS on cerebrum.

TC ID	GS	L1	C	L2	C	L3	C	L4	C	*	#	Description
93374_at	Jph3	0.44	1	0.38	1	-0.25	NC	-0.17	NC	2	0	junctophilin 3
93382_at	Pde1b	0.61	1	0.29	1	0.04	NC	-0.27	NC	2	0	phosphodiesterase 1B, Ca2+-calmodulin dependent
93423_at	Ldoc11	0.51	1	0.31	1	0.21	NC	-0.14	NC	2	0	leucine zipper, down-regulated in cancer 1-like
93548_at	Sec_61b	-0.12	NC	-0.3	NC	0.29	1	0.11	1	2	0	Sec. 61 beta subunit
93645_at	Rgs7	-0.02	NC	0.53	1	-0.03	NC	0.45	1	2	0	regulator of G protein signaling 7
93659_at	Camk2a	1.66	1	-0.95	NC	1.5	1	-0.55	NC	2	0	calcium/calmodulin-dependent protein kinase II alpha
93664_at	Atp1b2	0.78	1	-0.28	NC	0.76	1	-0.15	NC	2	0	ATPase, Na+ /K+ transporting, beta 2 polypeptide
93720_at	Agrp1	0.27	MI	-0.71	NC	0.51	1	-0.23	NC	2	0	1-acylglycerol-3-phosphate O-acyltransferase 1 (lysophosphatidic acid acyltransferase, alpha)
93793_at	Lasp1	0.43	1	0.28	1	-0.14	NC	-0.24	NC	2	0	LIM and SH3 protein 1
93852_at	Mef2a	0.2	1	0.25	1	-0.04	NC	-0.12	NC	2	0	myocyte enhancer factor 2A
93861_f_at	LOC105247328	0.29	1	-0.33	NC	0.56	1	-0.05	NC	2	0	MLV-related proviral Env polyprotein-like
93964_s_at	Ddx6	0.81	1	0.36	1	0.14	NC	-0.46	NC	2	0	DEAD (Asp-Glu-Ala-Asp) box polypeptide 6
93965_f_at	Ddx6	0.88	1	0.59	1	0.23	NC	-0.17	NC	2	0	DEAD (Asp-Glu-Ala-Asp) box polypeptide 6
93994_at	Chpt1	0.4	1	0.27	1	0.15	NC	0.16	NC	2	0	choline phosphotransferase 1
94057_g_at	Scd1	0.32	1	0.43	1	-0.12	NC	-0.03	NC	2	0	stearoyl-Coenzyme A desaturase 1
94077_f_at	Rpm2	0.49	MI	0.29	1	-0.13	NC	-0.27	NC	2	0	ribophorin II
94194_s_at	Hcn2	0.84	1	0.33	1	-0.23	NC	-0.61	NC	2	0	hyperpolarization-activated, cyclic nucleotide-gated K+ 2
94218_at	Tcp1	0.27	1	0.49	1	-0.05	NC	0.35	NC	2	0	t-complex protein 1
94245_at	Vimp	0.08	NC	0.26	1	0.04	NC	0.09	1	2	0	VCP-interacting membrane protein
94257_at	Rraga	0.08	NC	-0.07	NC	0.47	1	0.17	1	2	0	Ras-related GTP binding A
94335_f_at	Ina	0.45	1	0.14	1	-0.25	NC	-0.63	NC	2	0	internexin neuronal intermediate filament protein, alpha
94336_at	Otub1	0.76	1	0.43	1	0	NC	-0.55	NC	2	0	OTU domain, ubiquitin aldehyde binding 1
94353_at	Eif4ebp2	1.04	MI	-0.37	NC	0.4	1	-0.98	NC	2	0	eukaryotic translation initiation factor 4E binding protein 2
94374_at	Wdr13	0.13	NC	0.03	MI	0.06	NC	0.09	MI	2	0	WD repeat domain 13
94456_at	Set	-0.13	NC	0.77	1	-0.14	NC	0.79	1	2	0	SET nuclear oncogene
94819_f_at	Ccm1	0.3	1	0.28	1	-0.4	NC	-0.28	NC	2	0	cyclin I
94832_at	Hnmph2	0.45	NC	0.95	1	0.21	NC	0.83	1	2	0	heterogeneous nuclear ribonucleoprotein H2
94876_f_at	Gorasp2	0.29	1	0.27	1	-0.35	NC	-0.5	NC	2	0	golgi reassembly stacking protein 2
94986_at	Gng3	0.34	1	0.27	1	-0.13	NC	-0.17	NC	2	0	guanine nucleotide binding protein (G protein), gamma 3
95010_at	Traf3	0.29	1	-0.08	NC	0.31	1	-0.02	NC	2	0	TNF receptor-associated factor 3
95159_at	Gm13552	0.1	NC	0.35	1	-0.15	NC	0.22	1	2	0	predicted gene 13552; mitochondrial ribosomal protein S18B
95397_at	D430019H16Rik	0.45	1	0.28	1	0.04	NC	-0.3	NC	2	0	RIKEN cDNA D430019H16 gene
95432_f_at	Tomm70a	0.01	NC	0.35	1	-0.32	NC	0.13	MI	2	0	translocase of outer mitochondrial membrane 70 homolog A (yeast)
95447_at	Mdp1	-0.4	NC	-0.23	NC	0.43	MI	0.41	1	2	0	magnesium-dependent phosphatase 1
95468_at	Egln1	0.4	1	0.11	NC	0.26	1	0.1	NC	2	0	egl-9 family hypoxia-inducible factor 1
95530_at	Gtp2a1	0.13	NC	-0.1	NC	0.29	1	0.13	1	2	0	general transcription factor II A, 1

95721_at	Mapkapk2	0.36	1	-0.21	NC	0.6	1	-0.02	NC	2	0	MAP kinase-activated protein kinase 2
95883_at	Jade1	0.25	MI	0.54	1	-0.54	NC	-0.14	NC	2	0	jade family PHD finger 1
95927_f_at		0.55	MI	0.65	1	-0.2	NC	-0.14	NC	2	0	
96007_at	Ssr3	-0.12	NC	-0.3	NC	0.24	1	0.16	1	2	0	signal sequence receptor, gamma
96056_at	Rhoc	0.57	1	-0.23	NC	0.46	1	-0.12	NC	2	0	ras homolog gene family, member C
96065_at	Lxn	0.55	1	0.73	1	-0.43	NC	0.12	NC	2	0	latexin
96088_at	Ndrg2	0.44	1	0.48	1	-0.28	NC	-0.34	NC	2	0	N-myc downstream regulated gene 2
96102_i_at	Rad23b	-0.07	NC	0.26	1	-0.26	NC	0.12	1	2	0	RAD23b homolog (S. cerevisiae)
96186_at	Lrp10	0.58	1	-0.1	NC	0.42	1	-0.28	NC	2	0	low-density lipoprotein receptor-related protein 10

Rad23b, Sec. 61b, Vimf, Rpn2 and Ssr3 are genes of protein processing in endoplasmic reticulum. Atp1b2 and Camk2a are cAMP signaling pathway genes. Mice cerebrum stimulated by rTMS for 30days were denoted as M1 and M2, sham control were denoted as C1 and C2. N=2. All expression ratios were converted into the \log_2 (expression ratio) values. L1: Signal Log Ratio (M1/C1), L2: Signal Log Ratio (M2/C1), L3: Signal Log Ratio (M1/C2), L4: Signal Log Ratio (M2/C2). C1, C2 were used as a control and M1, M2 were used for Comparison Analysis as manufacture procedure. C means data to obtain expression ratios. Expression Console (EC) Ver.1.4 and Transcriptome Analysis Console (TAC) Ver.3. were used for Comparison Analysis illustrating Change p-values with the associated Increase (I) or Decrease (D) call. Increase calls have Change p-values closer to zero and Decrease calls have Change p-values closer to one. Finally, the Change algorithm assesses probe pair saturation, calculates a Change p-values, and assigns an (I), Marginal Increase (MI), No Change (NC), Marginal Decrease (MD), or (D) call for C. Gene with more than 2 significant difference calls was chosen. Abbreviations: TC ID: Transcript Cluster ID, GS: Gene Symbol, *: Total number of increase, #: Total number of decrease. TC ID is available for Pathway analysis.

Table 6
Gene expression matrix after 30 days rTMS on cerebrum.

TC ID	GS	L1	C	L2	C	L3	C	L4	C	*	#	Description
96191_at	Argef1	0.59	1	0.17	1	0.24	NC	-0.28	NC	2	0	ADP-ribosylation factor guanine nucleotide-exchange factor 1 (brefeldin A-inhibited)
96211_at	Dpp8	0.38	1	-0.08	NC	0.23	MI	-0.23	NC	2	0	dipeptidylpeptidase 8
96255_at	Bnip3l	-0.01	NC	0.37	1	-0.09	NC	0.15	1	2	0	BCL2/adenovirus E1B interacting protein 3-like
96313_at	Rasgrf1	0.71	1	0.76	1	-0.25	NC	-0.19	NC	2	0	RAS protein-specific guanine nucleotide-releasing factor 1
96360_at	Arhgdia	0.33	1	0.13	1	-0.02	NC	-0.17	NC	2	0	Rho GDP dissociation inhibitor (GDI) alpha
96518_at	Wwc1	0.33	1	0.31	1	-0.34	NC	-0.5	NC	2	0	WW, C2 and coiled-coil domain containing 1
96593_at	Elk1	0.74	1	-0.53	NC	1.15	1	0.06	NC	2	0	ELK1, member of ETS oncogene family
96674_at	Tmpo3	-0.17	NC	0.57	1	-0.38	NC	0.14	1	2	0	transportin 3
96725_at	Cic	0.81	1	0.27	1	0.12	NC	-0.54	NC	2	0	capicua homolog (Drosophila)
96731_at	Ddx6	0.39	1	0.38	1	-0.09	NC	-0.34	NC	2	0	DEAD (Asp-Glu-Ala-Asp) box polypeptide 6
96741_at	Phf12	0.46	1	0.48	1	-0.46	NC	-0.17	NC	2	0	PHD finger protein 12
96784_at	Anln	-0.27	NC	-0.1	NC	0.7	1	0.32	1	2	0	anillin, actin binding protein
96811_at	Rab31	-0.01	NC	0.01	NC	0.16	1	0.04	1	2	0	RAB31, member RAS oncogene family
96813_f_at	Otd5	0.35	1	0.53	1	-0.33	NC	-0.1	NC	2	0	OTU domain containing 5
96884_at	Carhsp1	-0.1	NC	0.06	NC	0.49	1	0.51	1	2	0	calcium regulated heat stable protein 1
96920_at	Htra1	0.68	1	0.29	1	-0.24	NC	-0.62	NC	2	0	HtrA serine peptidase 1
96955_at	Atp6v0e2	0.04	NC	0.03	NC	0.17	1	-0.01	1	2	0	ATPase, H ⁺ transporting, lysosomal V0 subunit E2
97210_at	1700037H04Rik	0.76	1	-0.13	NC	0.32	1	-0.16	NC	2	0	RIKEN cDNA 1700037H04 gene
97243_at	Slc9a3r1	0.51	1	0.39	1	-0.18	NC	-0.36	NC	2	0	solute carrier family 9 (sodium/hydrogen exchanger), member 3 regulator 1
97365_at	Coro2b	0.46	1	0.26	1	-0.17	NC	-0.36	NC	2	0	coronin, actin binding protein, 2B
97450_s_at	Aldh7a1	0.46	1	-0.07	NC	0.42	1	-0.22	NC	2	0	aldehyde dehydrogenase family 7, member A1
97487_at	Serpine2	0.32	NC	0.29	1	0.05	NC	0.1	1	2	0	serine (or cysteine) peptidase inhibitor, clade E, member 2
97530_at	Ube2i	0.01	NC	0.18	NC	0.33	1	0.36	1	2	0	ubiquitin-conjugating enzyme E2I
97536_at	Wdtc1	0.68	1	0.03	1	-0.03	NC	-0.49	NC	2	0	WD and tetratricopeptide repeats 1
97740_at	Dusp16	0.46	NC	0.53	1	0.46	NC	0.69	MI	2	0	dual specificity phosphatase 16
97770_s_at	Fam3c	0.53	1	0.63	1	-0.43	NC	-0.49	NC	2	0	family with sequence similarity 3, member C
97776_at	Drd2	0.75	1	1.11	1	0.1	NC	0.27	NC	2	0	dopamine receptor D2
97794_at	Sema7a	2.38	1	-0.83	NC	4.45	1	0.15	NC	2	0	sema domain, immunoglobulin domain (Ig), and GPI membrane anchor, (semaphorin) 7A
97841_at	Chmp2a	0.05	NC	0.37	1	-0.18	NC	0.28	1	2	0	charged multivesicular body protein 2A
97974_at	Zfpml	0.72	1	0.2	1	0.12	NC	-0.54	NC	2	0	zinc finger protein, multitype 1
97998_at	Atn1	0.7	1	0.44	1	0.19	NC	-0.03	NC	2	0	atrophin 1
98004_at	Pkia	0.11	NC	-0.53	NC	1.12	1	0.31	1	2	0	protein kinase inhibitor, alpha
98011_at	Gabbr1	0.24	1	0.3	1	-0.21	NC	-0.23	NC	2	0	gamma-aminobutyric acid (GABA) B receptor, 1
98026_g_at	Evi2a	-0.31	NC	-0.24	NC	0.28	1	0.6	1	2	0	ectropic viral integration site 2a

98073_at	Cux1	0.46	1	0.27	1	0.24	NC	-0.05	NC	2	0
98114_at	Npc1	0.49	1	0.38	1	-0.11	NC	-0.24	NC	2	0
98127_at	Capza2	0.09	NC	0.5	1	-0.11	NC	0.22	1	2	0
98129_at	Tmsb10	0.35	1	0.25	MI	-0.41	NC	-0.72	NC	2	0
98141_at	Eif5b	0.34	1	0.43	1	-0.58	NC	-0.29	NC	2	0
98150_at	Rab11b	0.27	1	0.19	1	-0.23	NC	-0.31	NC	2	0
98169_s_at	Fzd3	0.39	1	-0.49	NC	0.46	1	-0.41	NC	2	0
98454_at	Palm	0.4	1	0.14	MI	0	NC	-0.25	NC	2	0
98477_s_at	Ank3	0.57	1	0.29	1	-0.29	NC	-0.51	NC	2	0

Arfgef1, Rab31, Rab11b, Capza2, and Chmp2a are genes of endocytosis. Mice cerebrum stimulated by rTMS for 30days were denoted as M1 and M2, sham control were denoted as C1 and C2. N=2. All expression ratios were converted into the \log_2 (expression ratio) values. L1: Signal Log Ratio (M1/C1), L2: Signal Log Ratio (M1/C2), C1, C2 were used as a control and M1, M2 were normalized with respect to C1 and C2 to obtain expression ratios. Expression Console (EC) Ver.1.4 and Transcriptome Analysis Console (TAC) Ver.3. were used for Comparison Analysis as manufacture procedure. C means data analysis output for a Comparison Analysis illustrating Change p-values with the associated Increase (I) or Decrease (D) call. Increase calls have Change p-values closer to zero and Decrease calls have Change p-values closer to one. Finally, the Change algorithm assesses probe pair saturation, calculates a Change p-values, and assigns an (I), Marginal Increase (MI), No Change (NC), Marginal Decrease (MD), or (D) call for C. Gene with more than 2 significant difference calls was chosen. Abbreviations: TC ID: Transcript Cluster ID, GS: Gene Symbol, *: Total number of increase, #: Total number of decrease. TC ID is available for Pathway analysis.

Table 7
Gene expression matrix after 30 days rTMS on cerebrum.

TC ID	GS	L1	C	L2	C	L3	C	L4	C	*	#	Description
98543_at	Ctss	-0.18	NC	0.3	1	-0.03	NC	0.25	1	2	0	cathepsin S
98550_at	Set	-0.1	NC	0.46	1	-0.25	NC	0.09	1	2	0	SET nuclear oncogene
98564_f_at	Gm6654	0.39	1	0.47	1	-0.29	NC	-0.2	NC	2	0	predicted pseudogene 6654; 40S ribosomal protein S26-like; ribosomal protein S26
98588_at	Fah	-0.15	NC	-0.21	NC	0.21	1	0.58	1	2	0	fumarylacetoacetate hydrolase
98590_at	Sdc4	0.69	1	0.12	1	-0.42	NC	-0.76	NC	2	0	syndecan 4
98602_at	Rangap1	0.5	1	0.27	1	0.09	NC	-0.01	NC	2	0	RAN GTPase activating protein 1
98616_f_at	Myh7	0.64	1	0.16	1	-0.43	NC	-1.01	NC	2	0	myosin, heavy polypeptide 7, cardiac muscle, beta
98827_i_at	Kif5a	0.24	NC	-1.04	NC	1.74	1	0.33	1	2	0	kinesin family member 5 A
98866_at	Dlx6	0.92	1	1.99	1	0.7	NC	2.14	NC	2	0	distal-less homeobox 6
98925_at	Vamp2	0.91	1	0.33	NC	0.76	1	0.19	NC	2	0	vesicle-associated membrane protein 2
98993_at	Ppp2r5c	0.23	MI	0.35	1	0.08	NC	0.02	NC	2	0	protein phosphatase 2, regulatory subunit B', gamma
99023_at	Pafah1b2	-0.09	NC	-0.42	NC	0.66	1	0.26	1	2	0	platelet-activating factor acetylhydrolase, isoform 1b, subunit 2
99045_at	Eno2	0.36	1	0.34	1	-0.38	NC	-0.49	NC	2	0	enolase 2, gamma neuronal
99085_at	Usp3	0.41	NC	0.22	NC	0.65	1	0.4	1	2	0	ubiquitin specific peptidase 3
99378_f_at	H2-Q4	-0.42	NC	-0.42	NC	0.61	MI	0.53	1	2	0	histocompatibility 2, Q region locus 4
99451_at	Fam102a	0.36	1	0.16	NC	0.62	1	0.11	NC	2	0	family with sequence similarity 102, member A
99465_at	Mep2	0.69	1	0.59	1	0.08	NC	-0.04	NC	2	0	methyl CpG binding protein 2
99504_at	St8sia3	0.38	1	0.2	MI	-0.22	NC	-0.3	NC	2	0	ST8 alpha-N-acetyl-neuraminate alpha-2,8-sialyltransferase 3
99537_at	Ruvbl1	0.03	NC	-0.28	NC	0.48	1	0.1	1	2	0	RuvB-like protein 1
99575_at	Ubqlhn1	0.52	NC	-0.16	NC	0.6	1	0.13	1	2	0	ubiquilin 1
99597_at	Gnai2	0.45	1	0.23	MI	-0.11	NC	-0.34	NC	2	0	guanine nucleotide binding protein (G protein), alpha inhibiting 2
99666_at	Cs	0.39	1	0.14	1	0.06	NC	-0.21	NC	2	0	citrate synthase
99893_at	Fgf13	0.07	NC	-0.57	NC	0.87	1	0.05	1	2	0	fibroblast growth factor 13

Gnai2, Kif5a and Ppp2r5c are dopaminergic synapse genes. Gnai2, Myh7 and Ppp2r5c are genes of adrenergic signaling in cardiomyocytes. Mice cerebrum stimulated by rTMS for 30days were denoted as M1 and M2, sham control were denoted as C1 and C2. N=2. All expression ratios were converted into the log₂(expression ratio) values. L1: Signal Log Ratio (M1/C1), L2: Signal Log Ratio (M2/C1), L3: Signal Log Ratio (M1/C2), L4: Signal Log Ratio (M1/C2). C1, C2 were used as a control and M1, M2 were normalized with respect to C1 and C2 to obtain expression ratios. Expression Console (EC) Ver.1.4 and Transcriptome Analysis Console (TAC) Ver.3. were used for Comparison Analysis as manufacture procedure. C means data analysis output for a Comparison Analysis illustrating Change p-values with the associated Increase (I) or Decrease (D) call. Increase calls have Change p-values closer to zero and Decrease calls have Change p-values closer to one. Finally, the Change algorithm assesses probe pair saturation, calculates a Change p-values, and assigns an (I), Marginal Increase (MI), No Change (NC), Marginal Decrease (MD), or (D) call for C. Gene with more than 2 significant difference calls was chosen. Abbreviations; TC ID: Transcript Cluster ID, GS: Gene Symbol, #: Total number of increase, #: Total number of decrease. TC ID is available for Pathway analysis.

Table 8
Gene expression matrix after 30 days rTMS on cerebrum.

TC ID	GS	L1	C	L2	C	L3	C	L4	C	*	#	Description
102362_i_at	Junb	-2.26	D	-1.89	D	-1.91	D	-1.6	D	0	4	jun B proto-oncogene
102371_at	Nr4a1	-1.99	D	-1.81	D	-1.8	D	-1.72	D	0	4	nuclear receptor subfamily 4, group A, member 1
102661_at	Egr2	-1.29	D	-1.33	D	-1.7	D	-1.69	D	0	4	early growth response 2
102870_at	Dynit1a	-0.68	D	-1.04	D	-0.62	D	-0.91	D	0	4	dynein light chain Tctex-type 1A
104598_at	Dusp1	-1.41	D	-1.38	D	-1.51	D	-1.49	D	0	4	dual specificity phosphatase 1
160172_at	Meg3	-1.61	D	-1.73	D	-0.68	D	-0.89	D	0	4	maternally expressed 3
160173_at	Meg3	-0.91	D	-1.31	D	-0.79	D	-1.15	D	0	4	maternally expressed 3
160901_at	Fos	-2.14	D	-2.01	D	-2.08	D	-1.95	D	0	4	FBJ osteosarcoma oncogene
160970_at	Odf2	-0.95	D	-1.24	D	-1.31	D	-1.54	D	0	4	outer dense fiber of sperm tails 2
161666_f_at	Gadd45b	-0.98	D	-0.99	D	-1.63	D	-1.51	D	0	4	growth arrest and DNA-damage-inducible 45 beta
96302_at	Srsf7	-0.83	D	-0.73	D	-0.82	D	-0.74	MD	0	4	serine/arginine-rich splicing factor 7
97752_at	Snhg11	-1.12	D	-0.63	D	-1.24	D	-0.71	D	0	4	small nucleolar RNA host gene 11
97890_at	Sgk1	-0.8	D	-1.04	D	-1.3	D	-1.59	D	0	4	serum/glucocorticoid regulated kinase 1
99109_at	Ier2	-0.92	D	-1.48	D	-0.87	D	-1.29	D	0	4	immediate early response 2
101058_at	Amy1	-1.11	D	-0.83	D	-1.08	MD	-0.81	NC	0	3	amylase 1, salivary
101583_at	Btg2	-0.58	D	-1.06	D	-0.6	NC	-1.04	D	0	3	B cell translocation gene 2, anti-proliferative
104410_at	Midn	-0.72	D	-0.23	NC	-1.07	D	-0.77	MD	0	3	midnolin
104639_i_at	Tarid	-1.01	D	-0.74	D	-0.55	D	-0.63	NC	0	3	TATA box binding protein (Tbp)-associated factor, RNA polymerase I, D
160487_at	Myl4	-0.35	MD	-0.38	NC	-1.02	D	-0.96	D	0	3	myosin, light polypeptide 4
92424_at	Zfp692	-0.86	D	-0.94	D	-0.42	NC	-0.9	D	0	3	zinc finger protein 692
92542_at	Rsp1	-1.25	D	-0.75	D	-0.96	D	-0.52	NC	0	3	arginine/serine rich protein 1
93411_at	Sema7a	-0.51	D	-0.1	NC	-1.37	D	-0.75	D	0	3	sema domain, immunoglobulin domain (Ig), and GPI membrane anchor, (semaphorin) 7A
93619_at	Per1	-0.9	D	-0.3	NC	-1.01	D	-0.8	D	0	3	period circadian clock 1
98579_at	Egr1	-0.68	D	-0.57	NC	-1.42	D	-1.04	D	0	3	early growth response 1
99347_f_at	Eml5	-0.92	D	-1.48	D	-0.97	NC	-1.44	D	0	3	echinoderm microtubule associated protein like 5
100002_at	Ith3	0.54	I	0.22	NC	-0.65	D	-0.82	D	1	2	inter-alpha trypsin inhibitor, heavy chain 3
100592_at	Gh1m	-0.56	D	-1.06	D	0.52	I	-0.01	NC	1	2	growth hormone inducible transmembrane protein
100599_at	Atf4	-0.82	D	-0.58	D	-0.27	NC	-0.01	MI	1	2	activating transcription factor 4
162457_f_at	Hba-a1	0.7	I	-1.46	D	-0.12	NC	-2.33	D	1	2	hemoglobin alpha, adult chain 1; hemoglobin alpha, adult chain 2
93722_at	Ensa	-0.46	MD	-0.83	D	0.38	I	-0.03	NC	1	2	endosulfine alpha
93909_f_at	Noct	-0.61	D	-0.84	D	0.35	I	0.08	NC	1	2	nocturnin
94781_at	Hba-a1	0.35	I	-1.71	D	-0.38	NC	-2.42	D	1	2	hemoglobin alpha, adult chain 1
97263_s_at	Csnk1d	-0.65	D	-1.23	D	0.13	I	-0.4	NC	1	2	casein kinase 1, delta
99009_at	Nnt	0.77	I	-0.6	D	-0.1	NC	-1.56	D	1	2	nicotinamide nucleotide transhydrogenase
99095_at	Max	-0.62	D	0.36	NC	-0.98	D	0.01	I	1	2	Max protein
100050_at	Id1	-0.75	D	-0.55	NC	-0.64	D	-0.49	NC	0	2	inhibitor of DNA binding 1

Table 8 (continued)

TC ID	GS	L1	C	L2	C	L3	C	I4	C	*	#	Description
100064_f_at	Gja1	0.23	NC	-0.09	NC	-0.62	D	-0.7	D	0	2	gap junction protein, alpha 1
100348_at	Gm40022	-0.82	D	-0.93	MD	-1.22	NC	-1.12	NC	0	2	predicted gene, 40022
100482_at	Zfp598	-0.42	D	-0.81	D	-0.33	NC	-0.64	NC	0	2	zinc finger protein 598
100536_at	Mobp	-0.11	NC	-0.22	NC	-0.72	D	-0.66	D	0	2	myelin-associated oligodendrocytic basic protein
100611_at	Lyz2	0.32	NC	-1.04	D	0.06	NC	-1.05	D	0	2	lysosome 2
101482_at	Ppp1cc	0.08	NC	-0.04	NC	-0.59	D	-0.77	D	0	2	protein phosphatase 1, catalytic subunit, gamma isoform
101580_at	Cox7b	-0.62	D	-0.43	NC	-0.71	D	-0.43	NC	0	2	cytochrome c oxidase subunit VIIb
101596_at	C78859	-0.96	MD	-0.8	MD	-0.66	NC	-0.91	NC	0	2	expressed sequence C78859
101740_at	Adra1a	-0.04	NC	-2.3	D	-1.47	NC	-4.05	D	0	2	adrenergic receptor, alpha 1a

Atf4, Adra1a, Myl4 and Ppp1cc are genes of adrenergic signalling in cardiomyocytes. Fos, Max, Atf4, Dusp1, Gadd45b and Nr4a1 are genes of MAPK signalling pathway. Fos, Atf4 and Ppp1cc are Dopaminergic genes. Csnk1d, Id1 and Ppp1cc are genes of hippo signalling pathway. Csnk1d and Per1 are circadian rhythm genes. Mice cerebrum stimulated by rTMS for 30days were denoted as M1 and M2, sham control were denoted as C1 and C2. N = 2. All expression ratios were converted into the \log_2 (expression ratio) values. L1: Signal Log Ratio (M1/C1), L2: Signal Log Ratio (M2/C1), L3: Signal Log Ratio (M1/C2), L4: Signal Log Ratio (M1/C2). C1, C2 were used as a control and M1, M2 were used for Comparison Analysis as manufacture procedure. C means data analysis output for a Comparison Analysis illustrating Change p-values with the associated Increase (I) or Decrease (D) call. Increase calls have Change p-values closer to zero and Decrease calls have Change p-values closer to one. Finally, the Change algorithm assesses probe pair saturation, calculates a Change p-values, and assigns an (I), Marginal Increase (MI), No Change (NC), Marginal Decrease (MD), or (D) call for C. Gene with more than 2 significant difference calls was chosen. Abbreviations; TC ID: Transcript Cluster ID, GS: Gene Symbol, #: Total number of increase, #: Total number of decrease. TC ID is available for Pathway analysis.

Table 9
Gene expression matrix after 30 days rTMS on cerebrum.

TC ID	GS	L1	C	L2	C	L3	C	L4	C	*	#	Description
101869_s_at	Hbb-b1	0.03	NC	-1.76	D	-0.05	NC	-1.94	D	0	2	hemoglobin, beta adult major chain; hemoglobin, beta adult minor chain; hemoglobin, beta adult s chain; hemoglobin, beta adult t chain
101936_at	Clik4	-0.63	D	-0.73	D	-0.4	NC	-0.3	NC	0	2	CDC like kinase 4
101962_at	Ddx17	-0.73	D	-0.35	NC	-0.58	D	-0.19	NC	0	2	DEAD (Asp-Glu-Ala-Asp) box polypeptide 17
102255_at	Osmr	0.04	NC	-1.08	MD	-3.48	NC	-3.02	MD	0	2	oncostatin M receptor
102431_at	Mapt	-0.01	NC	-0.04	NC	-0.61	D	-0.6	D	0	2	microtubule-associated protein tau
102574_at	Fgf11	2.96	NC	-1.26	D	3.35	NC	-0.77	D	0	2	fibroblast growth factor 11
102779_at	Gadd45b	-1.04	D	-1.15	D	-0.64	NC	-0.62	NC	0	2	growth arrest and DNA-damage-inducible 45 beta
102781_at	Ccnl2	-0.78	D	-0.93	D	-0.72	NC	-0.79	NC	0	2	cyclin L2
103253_at	Lin7b	-0.46	D	-0.39	NC	-0.64	D	-0.56	NC	0	2	lin-7 homolog B (C. elegans)
103427_at	Fbxj3	-0.67	D	-0.63	D	-0.2	NC	-0.39	NC	0	2	F-box and leucine-rich repeat protein 3
103448_at	S100a8	2.13	NC	-2.11	D	1.42	NC	-2.74	D	0	2	S100 calcium binding protein A8 (calgranulin A)
103460_at	Ddit4	-0.34	NC	-0.5	NC	-1.1	D	-1.48	D	0	2	DNA-damage-inducible transcript 4
103534_at	Hbb-b2	0.17	NC	-1.63	D	-0.09	NC	-2.34	D	0	2	hemoglobin, beta adult minor chain
103811_at	Invs	-0.58	NC	-1.39	D	-1.34	NC	-2	D	0	2	inversin
103863_at	Sfr2d1	-0.41	D	-0.66	D	-0.18	NC	-0.29	NC	0	2	SFR2 domain containing 1
103990_at	Fosb	0.08	NC	-1.24	D	-0.3	NC	-1.35	D	0	2	FBX osteosarcoma oncogene B
104155_f_at	Atf3	-1.59	D	-2.13	D	-0.47	NC	-1.05	NC	0	2	activating transcription factor 3
104578_f_at	Actn1	0.08	NC	-0.05	NC	-0.69	D	-0.86	D	0	2	actinin, alpha 1
104640_f_at	Taf1d	-0.02	NC	-0.47	NC	-0.68	D	-0.97	D	0	2	TATA box binding protein (Tbp)-associated factor, RNA polymerase I, D
104701_at	Bhlhe40	-0.38	NC	-0.42	NC	-0.87	D	-0.9	D	0	2	basic helix-loop-helix family, member e40
160140_at	Tbce	-1.09	D	-0.66	NC	-0.92	D	-0.82	NC	0	2	tubulin-specific chaperone E
160182_at	Srsf6	-0.6	D	-0.7	D	-0.45	NC	-0.56	NC	0	2	serine/arginine-rich splicing factor 6
160316_at	AI503316	-0.89	D	-1.11	D	-0.01	NC	-0.74	NC	0	2	expressed sequence AI503316; heterogeneous nuclear ribonucleoprotein U
160407_at	Actr1a	-1.42	D	-2.18	D	-0.11	NC	-0.68	NC	0	2	ARP1 actin-related protein 1 A, centractin alpha
160547_s_at	Txnip	-0.6	NC	-1.07	D	-0.7	NC	-1.28	D	0	2	thioredoxin interacting protein
160564_at	Lcn2	-0.8	NC	-3.16	D	-0.92	NC	-3.84	D	0	2	lipocalin 2
160791_at	Luc7l3	-0.9	D	-0.14	NC	-1.26	D	-0.37	NC	0	2	IUC7-like 3 (S. cerevisiae)
160894_at	Cebpd	-0.15	NC	-1.06	D	-0.34	NC	-1.37	D	0	2	CCAAT/enhancer binding protein (C/EBP), delta
161462_f_at	6820431F20Rik	-1.44	NC	-2.05	D	-1.53	NC	-2.36	D	0	2	cadherin 11 pseudogene; predicted gene, 21811
162093_at	Yars	-0.87	D	-0.94	D	-0.07	NC	-0.35	NC	0	2	tyrosyl-tRNA synthetase
162399_f_at	Atxn2	-0.14	NC	-0.23	NC	-0.94	D	-1.23	D	0	2	ataxin 2
162424_f_at	Ddx17	-0.58	D	-0.11	NC	-0.86	D	-0.23	NC	0	2	DEAD (Asp-Glu-Ala-Asp) box polypeptide 17
162459_f_at	Col6a1	-0.11	NC	-0.78	NC	-3.33	D	-4.01	D	0	2	collagen, type VI, alpha 1
92211_at	Bod1l	-0.56	D	-0.69	D	-0.56	NC	-0.5	NC	0	2	biorientation of chromosomes in cell division 1-like

Table 9 (continued)

TC ID	GS	L1	C	L2	C	L3	C	L4	C	*	#	Description
92233_at	Paxbp1	-0.62	D	-0.93	D	-0.61	NC	-0.68	NC	0	2	PAX3 and PAX7 binding protein 1
92523_at	Kcnj6	0.42	NC	-1.73	D	1.6	NC	-1.02	MD	0	2	potassium inwardly-rectifying channel, subfamily J, member 6
92636_f_at	Gm10177	-0.34	D	-0.09	NC	-0.52	D	-0.23	NC	0	2	predicted gene 10177; predicted gene, 17756; predicted gene 4184; protein transport protein Sec. 61 subunit gamma; protein transport protein Sec. 61 subunit gamma-like; SEC. 61, gamma subunit
92642_at	Car2	-0.42	MD	-0.37	NC	-0.88	D	-0.72	NC	0	2	carbonic anhydrase 2
92665_f_at	3830403N18Rik	-3.41	D	-3.56	NC	-3.93	D	-4.21	NC	0	2	RIKEN cDNA 3830403N18 gene; X-linked lymphocyte-regulated wingless-type MMTV integration site family, member 10B
92751_i_at	Wnt10b	0.49	NC	-1.75	D	-2.13	NC	-4.2	D	0	2	aminolevulinic acid synthase 2, erythroid
92768_s_at	Alas2	-0.01	NC	-1.89	D	-0.66	NC	-2.71	D	0	2	

Ddit4, Col6a1, Fgf11 and Osmr genes of PI3K-AKT signaling pathway. Fbxl3 and Blhhe40 are circadian rhythm genes. Mice cerebrum stimulated by rTMS for 30days were denoted as M1 and M2, sham control were denoted as C1 and C2. N=2. All expression ratios were converted into the \log_2 (expression ratio) values. L1: Signal Log Ratio (M1/C1), L2: Signal Log Ratio (M2/C1), L3: Signal Log Ratio (M1/C2), L4: Signal Log Ratio (M1/C2). C1, C2 were used as a control and M1, M2 were normalized with respect to C1 and C2 to obtain expression ratios. Expression Console (EC) Ver.1.4 and Transcriptome Analysis Console (TAC) Ver.3. were used for Comparison Analysis as manufacture procedure. C means data analysis output for a Comparison Analysis illustrating Change p-values with the associated Increase (I) or Decrease (D) call. Increase calls have Change p-values closer to zero and Decrease calls have Change p-values closer to one. Finally, the Change algorithm assesses probe pair saturation, calculates a Change p-values, and assigns an (I), Marginal Increase (MI), Marginal Decrease (MD), or (D) call for C. Gene with more than 2 significant difference calls was chosen. Abbreviations: TC ID: Transcript Cluster ID, GS: Gene Symbol, *: Total number of increase, #: Total number of decrease. TC ID is available for Pathway analysis.

Table 10
Gene expression matrix after 30 days rTMS on cerebrum.

TC ID	GS	L1	C	L2	C	L3	C	L4	C	*	#	Description
92777_at	Cyr61	-1.09	NC	-1.87	D	-1.21	NC	-2.36	D	0	2	cysteine rich protein 61
92787_at	Ankrnd10	-0.66	D	-1	D	-0.31	NC	-0.69	NC	0	2	ankyrin repeat domain 10
92802_s_at	Plp1	-0.61	D	-0.99	D	0.03	NC	-0.42	NC	0	2	proteolipid protein (myelin) 1
92945_at	Gria2	-0.45	NC	-0.06	NC	-0.96	D	-0.82	D	0	2	glutamate receptor, ionotropic, AMPA2 (alpha 2)
93009_at	Gstm2	-2	D	-4.19	D	-0.85	NC	-2.44	NC	0	2	glutathione S-transferase, mu 2
93126_at	Ckb	-0.01	NC	-0.12	NC	-0.53	D	-0.56	D	0	2	creatine kinase, brain
93274_at	Clk1	-1.11	D	-1.04	D	-0.6	NC	-0.46	NC	0	2	CDC-like kinase 1
93285_at	Dusp6	-0.48	NC	-0.52	NC	-0.58	D	-0.83	D	0	2	dual specificity phosphatase 6
93353_at	Lum	-0.93	D	-0.76	D	0.22	NC	0.25	NC	0	2	lumican
93390_g_at	Prom1	0.11	NC	0.05	NC	-1.44	D	-1.09	D	0	2	prominin 1
93478_at	Dnajc21	-0.14	NC	-0.07	NC	-1.02	MD	-1.39	D	0	2	Dnaj (Hsp40) homolog, subfamily C, member 21
93486_at	Slc27a1	0.53	NC	-0.65	D	-0.4	NC	-1.46	D	0	2	solute carrier family 27 (fatty acid transporter), member 1
93615_at	Pbx3	0.26	NC	0.07	NC	-0.63	D	-0.94	D	0	2	pre B cell leukemia homeobox 3
93666_at	Lmo2	-0.51	D	-0.72	D	0.08	NC	-0.23	NC	0	2	LIM domain only 2
93773_f_at	Zramb2	-0.71	D	-0.4	NC	-0.61	D	-0.41	NC	0	2	zinc finger, RAN-binding domain containing 2
93985_at	Tiparp	-1.11	D	-0.46	NC	-0.74	D	-0.79	NC	0	2	TCDD-inducible poly(ADP-ribose) polymerase
94155_at	Rgs4	-0.56	MD	-0.96	D	0.49	NC	-0.31	NC	0	2	regulator of G-protein signaling 4
94192_at	Gdap10	-0.41	NC	-1.15	D	-0.66	NC	-1.24	D	0	2	ganglioside-induced differentiation-associated-protein 10
94349_at	Khdc1b	-2.59	NC	-4.38	D	0.41	NC	-1.57	D	0	2	KH domain containing 1B
94379_at	Kifib	-1.4	NC	-1.71	D	-1.62	NC	-2.65	D	0	2	kinatin family member 1B
94395_at	Fubp1	-0.48	NC	-0.78	D	-0.99	D	-1.05	NC	0	2	far upstream element (FUSE) binding protein 1
94460_at	Stk38	-0.43	D	-0.79	D	-0.04	NC	-0.37	NC	0	2	serine/threonine kinase 38
94516_f_at	Penk	0.16	NC	0.02	NC	-0.78	D	-0.89	D	0	2	preproenkephalin
94689_at	Gm39971	-0.03	NC	-0.48	NC	-1.15	D	-2	D	0	2	predicted gene, 39971
95001_at	Atkap8	-0.88	D	-1	MD	-0.62	NC	-0.84	NC	0	2	A kinase (PRKA) anchor protein 8
95081_at	Exosc8	-1.38	D	-1.39	D	-0.8	NC	-0.95	NC	0	2	exosome component 8
95134_at	Mid1ip1	-0.92	D	-0.8	D	-0.3	NC	-0.2	NC	0	2	Mid1 interacting protein 1 (gastrulation specific G12-like (zebrafish))
95339_f_at	Mmp12	-2.02	MD	-4.34	D	-1.71	NC	-4.09	NC	0	2	matrix metalloproteinase 12
95418_at	Ras11b	0.02	NC	-0.09	NC	-0.76	D	-0.85	D	0	2	RAS-like, family 11, member B
95674_f_at	Basp1	-0.37	D	-0.21	NC	-0.51	D	-0.3	NC	0	2	brain abundant, membrane attached signal protein 1
95694_at	Top1	-0.2	NC	-0.4	NC	-0.56	D	-0.63	D	0	2	topoisomerase (DNA) I
96464_at	Plxnb2	-0.41	NC	-1.64	D	0.19	NC	-0.78	MD	0	2	plexin B2
96672_at	Hopx	-0.45	D	-0.64	D	-0.29	NC	-0.52	NC	0	2	HOP homeobox
96785_at	Kank3	-0.55	D	-0.33	NC	-1.08	D	-0.92	NC	0	2	KN motif and ankyrin repeat domains 3
96912_s_at	Ctla2a	-0.8	D	-1.02	D	-0.38	NC	-0.77	NC	0	2	cytotoxic T lymphocyte-associated protein 2 alpha; cytotoxic T lymphocyte-associated protein 2 beta

Table 10 (continued)

TC ID	GS	L1	C	L2	C	L3	C	L4	C	*	#	Description
96961_at	Pcgf2	-0.35	NC	-1.18	D	-0.08	NC	-0.74	D	0	2	polycomb group ring finger 2
97142_at	DXErt2d242e	-1.93	D	-2.25	D	-2.93	NC	-3.23	NC	0	2	DNA segment, Chr X, ERATO Doi 242, expressed
97358_at	Adgrl1	0.02	NC	0.08	NC	-0.66	D	-0.5	MD	0	2	adhesion G protein-coupled receptor L1
97759_at	Kcnma1	-0.15	NC	-0.06	NC	-0.87	D	-0.65	D	0	2	potassium large conductance calcium-activated channel, subfamily M, alpha member 1
98474_r_at	Trnaip6	-1.14	D	-0.3	NC	-1.1	MD	0.04	NC	0	2	tumor necrosis factor alpha induced protein 6
98475_at	Matn2	-0.17	NC	-0.29	NC	-0.76	D	-1.16	D	0	2	matrinil 2
99089_at	Mal	-0.28	NC	-0.61	NC	-0.92	D	-1.12	D	0	2	myelin and lymphocyte protein, T cell differentiation protein
99622_at	Klf4	-0.81	NC	-0.52	NC	-2.7	D	-2.56	D	0	2	Kruppel-like factor 4 (gut)
99830_at	Kalrn	-0.16	NC	0.04	NC	-0.89	D	-0.69	D	0	2	kalirin, RhoGEF kinase

Lmo2, Pbx3 and Prom1 are genes of transcriptional misregulation in cancer. Mice cerebrum stimulated by rTMS for 30days were denoted as M1 and M2, sham control were denoted as C1 and C2. N=2. All expression ratios were converted into the \log_2 (expression ratio) values. L1: Signal Log Ratio (M1/C1), L2: Signal Log Ratio (M2/C1), L3: Signal Log Ratio (M2/C2), L4: Signal Log Ratio (M1/C2). C1, C2 were used as a control and M1, M2 were normalized with respect to C1 and C2 to obtain expression ratios. Expression Console (EC) Ver.1.4 and Transcriptome Analysis Console (TAC) Ver.3. were used for Comparison Analysis as manufacture procedure. C means data analysis output for a Comparison Analysis illustrating Change p-values with the associated Increase (I) or Decrease (D) call. Increase calls have Change p-values closer to zero and Decrease calls have Change p-values closer to one. Finally, the Change algorithm assesses probe pair saturation, calculates a Change p-values, and assigns an (I), Marginal Increase (MI), No Change (NC), Marginal Decrease (MD), or (D) call for C. Gene with more than 2 significant difference calls was chosen. Abbreviations; TC ID: Transcript Cluster ID, GS: Gene Symbol, *: Total number of increase, #: Total number of decrease, TC ID is available for Pathway analysis.

Acknowledgements

This work was partly supported by a grant from the Japanese Society for the Promotion of Science (Grant no.17109011). Furthermore, this work was supported by the Global COE Program 'Center of Education and Research for the Advanced Genome-Based Medicine-For personalized medicine and the control of worldwide infectious disease' and MEXT Japan. The authors would like to thank Enago for the English language review. The authors would like to thank Mr. Masaru Kurosawa and Dr. Nobuyuki Nukina for the support for the experiment.

Transparency document. Supporting information

Transparency data associated with this article can be found in the online version at <http://dx.doi.org/10.1016/j.dib.2017.10.034>.

References

- [1] T. Ikeda, W. Kobayashi and C. Morimoto, Effects of repetitive transcranial magnetic stimulation on ER stress-related genes and glutamate, γ -aminobutyric acid, and glycine transporter genes in mouse brain. Submitted.
- [2] S. Kotliarova, N.R. Jana, N. Sakamoto, M. Kurosawa, H. Miyazaki, M. Nekooki, H. Doi, Y. Machida, H.K. Wong, T. Suzuki, C. Uchikawa, Y. Kotliarov, K. Uchida, Y. Nagao, U. Nagaoka, A. Tamaoka, K. Oyanagi, F. Oyama, N. Nukina, Decreased expression of hypothalamic neuropeptides in Huntington disease transgenic mice with expanded polyglutamine-EGFP fluorescent aggregates, *J. Neurochem.* 93 (2005) 641–653.
- [3] R.J. Lipshutz, S.P. Fodor, T.R. Gingras, D.J. Lockhart, High density synthetic oligonucleotide arrays, *Nat. Genet.* 21 (1999) 20–24.
- [4] The Gene Ontology (GO) Project in 2006, *Nucleic Acids Res.* 34 (2006) (2006) D322–D326.

REVIEW ARTICLE
Current Cancer Therapy Reviews, 2017, 13, 76-88

Current and Emerging Therapy for Malignant Pleural Mesothelioma: Focus on CD26/Dipeptidyl Peptidase IV as a Therapeutic Target



Bently P. Doonan¹, Kei Ohnuma², Long H. Dang¹, Chikao Morimoto² and Nam H. Dang^{1,*}

¹*University of Florida, Gainesville, FL, USA;* ²*Juntendo University, Tokyo, Japan*

Abstract: **Background:** Malignant mesothelioma is a largely incurable disease that is refractory to current therapies. CD26 is a multifunctional cell surface protein involved in autoimmune disease, diabetes, and cancer. It has a role in T cell function, extracellular protein modification, as a prognostic factor for cancer, and as a therapeutic target for malignant mesothelioma. New treatment strategies are urgently needed for malignant pleural mesothelioma (MPM), and CD26-targeted therapy represents a novel approach.

Outline: In this review, the most current and up-to-date literature available was reviewed and the current state of malignant mesothelioma treatment is described. Throughout the review the need for new therapeutic approaches is highlighted in the shortcomings of current therapy. CD26 is a target that is fit to take on these shortcomings. In this review we discuss the structure and function of CD26, its role in malignant mesothelioma and the future of anti-CD26 therapy as a versatile immunotherapeutic option.

Conclusion: This review highlights the areas of most promise in treating MPM, these include immune checkpoint blockade, passive immunization, and based on our recently published data, targeting of CD26 with its specific mAb. Finally we describe how the anti-CD26 mAb YS110 was recently evaluated in the first-in-human phase I clinical trial, showing prolonged disease stabilization and a favorable side effect profile. Through better understanding of CD26, new pathways to treating and potentially curing malignant mesothelioma may be discovered.

Keywords: Asbestos, CD26, dipeptidyl peptidase IV, immunotherapy, Malignant Pleural Mesothelioma, YS110.

1. INTRODUCTION

The human leukocyte surface antigen CD26 is an active cell surface peptidase that is structurally identical to dipeptidyl peptidase IV (DPPIV), able to cleave N-terminal dipeptides from peptides with

terminal L-alanine or L-proline residues [1-4]. It is composed of 766 amino acids, the majority of which comprise the extracellular domain of the protein where a peptidase catalytic site is found and where important ligand binding sites for adenosine deaminase (ADA) and fibronectin are located [1-4]. The remainder of the protein structure includes a short 6-peptide cytoplasmic domain and a 23-peptide transmembrane region [4]. Through this peptidase activity CD26/DPPIV has significant effects on enhancing cellular response to external stimuli, effects on glucose homeostasis,

*Address correspondence to this author at the Division of Hematology/Oncology, University of Florida, P.O. Box 100278, Gainesville FL 326100278, USA; Tel: (352) 273-7832; Fax: (352) 273-5006; E-mail: nam.dang@medicine.ufl.edu

T cell stimulation and activation, and the biological behavior of selected human neoplasms. CD26 has relatively widespread expression on leukocytes, fibroblasts, mesothelium, endothelial, epithelial cells, and can be found in kidney, intestine, prostate, pancreas, and liver cells [5]. Since its discovery in 1966 by Hopsu-Havu and Glenner, CD26/DPPIV has been the focus of vigorous study in its pluripotent role in glucose homeostasis, inflammation, and more recently in tumorigenesis and as a therapeutic target in cancer [6]. The various immunomodulatory effects of CD26 have been previously summarized by our group and recently revisited and expanded by Kleemann *et al.* [7, 8]. These works summarize the numerous substrates for DPPIV/CD26 and their far-reaching roles in autoimmune diseases such as multiple sclerosis, asthma, arthritis, and inflammatory bowel disease [7-9]. Likewise, CD26 involvement in malignancy has been extensively reviewed and characterized, including its potential role in terms of its role as a tumor suppressor, cancer biomarker, and therapeutic target [6, 10-14]. Additionally CD26 has been described as a marker for so-called cancer stem cells (CSCs) which have been a highly sought after targets in chemotherapeutic approaches [15]. Given the preponderance of evidence for CD26 involvement in various malignancies, as well as its role in immune activation and the biology of cancer stem cells, CD26 represents an ideal immunotherapeutic target; including for the aggressive, almost always fatal cancer malignant pleural mesothelioma (MPM).

Malignant pleural mesothelioma (MPM) is an aggressive and fatal disease. Over the past 60 years, since its acceptance as an independent oncological process, the incidence of MPM has continued to rise [16]. MPM is almost exclusively a direct result of exposure to asbestos [17]. Chronic pleural inflammation, ionizing radiation, and SV40 virus have been proposed as alternative exposures that can result in MPM, but these account for less than 20% of all cases [17]. Asbestos, a term for naturally occurring families of minerals that separate into thin fibers, has been used for greater than 5000 years for its high tensile strength and fire resistant properties [18]. It wasn't until the 1960s that the direct correlation between asbestos exposure and cancer development was validated and accepted [19]. Since that time, the WHO and International Agency for research in cancer have

defined asbestos as a class I carcinogen responsible for both lung cancer and malignant pleural mesothelioma [18]. Inhaled asbestos fibers end up in the pleura, induce cytotoxic effects, and cause DNA damage and chronic inflammation [20]. This process is constant and smoldering for the next 20-60 years prior to the development of MPM. This long period of latency and protracted asymptomatic period explains the delayed peak in MPM cases and the increasing incidence over the past 40 years [21]. For example, in the US the peak in asbestos consumption occurred in the early 1970s, and its manufacturing was banned in the late 1980s, with total consumption and exposure risk being significantly reduced by the late 1990s; but the peak in MPM diagnoses of roughly 2,500-3,000 cases did not occur until about 2002 [22]. The expected plateau effect for MPM diagnoses for most industrialized nations that have banned the use of asbestos are expected to occur between 2015 and 2030, but countries like Russia, China, Brazil, and India continue to both mine and use asbestos at an alarming rate [23]. China has become the world's largest asbestos-consuming country, has little to no reporting mechanism of its MPM rates, and will likely experience a surge in MPM diagnoses in the future [24]. With this predictable man-made epidemic looming on the horizon, new strategies are required for treating this aggressive disease as current strategies show limited efficacy, poor survival benefit, and have significant morbidity associated with them [18]. In this review, we will discuss the current state of malignant mesothelioma treatment and some of the burgeoning therapies currently in clinical trials. We will also highlight the work done on CD26 expression in MPM, its potential as a biomarker, and its functional role in MPM survival, invasion, and migration. Finally, we will review the ongoing clinical development of an anti-CD26 monoclonal antibody in malignant mesothelioma and its potential far-reaching implications as a novel immunotherapeutic agent.

2. CURRENT THERAPIES

If left untreated, MPM has an average life expectancy of 8 months and a 5-year mortality of greater than 95% [24]. Our best efforts with multimodal therapy may extend this outcome by mere months, further emphasizing the extreme need for improved therapies. Current therapeutic strategies

Table 1. Principal characteristics and benefit of current therapies for MPM.

First Line Therapy	Overall Survival (Months)	Improvement vs. SOC	Study Features/ Limitations	References
None	8	n/a	Na/	Zhang et al. Ann Transl Med 2015
Cisplatin + pemetrexed (SOC)	16.1	0	225 pts, newly diagnosed MPM, ECOG 0-2	Zalcman et al. Lancet 2016
SOC + bevacizumab	18.8	2.7	223 pts, newly diagnosed MPM, ECOG 0-2	Zalcman et al. Lancet 2016
SOC + EPP	21.9	5.8	54 pts, stage I to III MPM, otherwise healthy, ECOG 0-1	Krug et al. J clin oncol 2009
EPP + IMRT	14.2	None	63 pts, able to tolerate EPP, minimal comorbidities	Rice et al. Ann thorac surg 2007
EPP + SOC + hemithoracic RT	29.1	13	42 pts, ECOG 0-1, T1-3 N0-2 (33 pts who entered study could not tolerate all phases of therapy)	Krug et al. J clin oncol 2009
PD + SOC + IMPRINT	20.2	4.4	70 pts, retrospective study over 30 years, high Karnofsky score	Shaikh et al. J of thoracic oncol 2017
CRS-207 + SOC	8.5*	N/A	38 pts, treatment naïve, ECOG 0-1	Jahan et al. J of thoracic oncol 2016

Second Line Therapy	Overall Survival (Months)	Improvement vs. Historic Chemo	Study Features/ Limitations	Reference
Tremelimumab + SOC	10.7	2.0	29 pts, ECOG 0-1, primarily epithelioid histology	Calabro et al. Lancet Respir Med 2015 MESOT-TREM-2012

Abbreviations: MPM (Malignant Pleural Mesothelioma), ECOG (Eastern Cooperative Oncology Group Performance Status), SOC (Standard of Care), pts (patients), EPP (Extrapleural Pneumonectomy), PD (Pleurectomy with Decortication), IMRT (Intensity-modulated Radiation Therapy), CRS-207 (live, attenuated, double-deleted *listeria monocytogenes* engineered to express tumor-associated antigen mesothelin).* (progression free survival, overall survival goal not met to date).

for MPM include surgery, radiation, chemotherapy, and more recently targeted therapy and immunotherapy [25-31]. Table 1 summarizes the mainstays of treatment and the benefit of traditional therapies over systemic chemotherapy. The roles of surgery and radiation as part of MPM treatment are rife with controversy, with these modalities showing limited benefit in patients with advanced disease.

2.1. Multimodal (Surgical Resection, Radiotherapy, and Chemotherapy)

Surgical intervention is difficult to perform, since achieving negative margins when extracting

thin areas of pleura is difficult to accomplish and is associated with a significant level of risk, requiring a high level of familiarity and expertise with the procedure [32]. Two main surgical interventions are currently in use, pleurectomy/decortication (P/D) and Extrapleural Pneumonectomy (EPP) [29]. As illustrated in the MARS trial, EPP, an invasive aggressive debulking procedure showed no benefit when added to chemotherapy/radiation, being associated with a worse median survival when compared with no surgical intervention, and may actually cause harm [33, 34]. However, it is important to note that this study, like many involving MPM, is extremely underpowered and involved only 19 individuals re-

ceiving EPP [34]. With the high morbidity and required technical expertise, this procedure has therefore fallen out of favor except in those patient fortunate enough to be diagnosed at an early-localized stage.

P/D is being evaluated currently in the MARS2 trial to evaluate the role of surgery in MPM therapy, aside from its value in diagnostic biopsy [32]. In a similar vein, radiotherapy has been used in combination with chemotherapy and surgery as part of a trimodal therapeutic approach, or following surgery to prevent tumor seeding of thoracoscopy or thoracotomy scars. Trimodal therapy involves chemotherapy followed by EPP or P/D and intensity modulated radiotherapy as combination treatment for MPM. Results from small trimodal clinical trials suggest that, in certain patient populations, this aggressive multipronged attack may improve overall survival by up to 6 months *vs.* standard of care (SOC) [35]. However, this treatment option is only valuable to those MPM patients with limited burden of disease, excellent performance status, and epithelioid histology [36]. While surgery and radiotherapy may have some role to play in specific MPM cases, the mainstay of treatment for the past 20 years has been systemic chemotherapy.

2.2. Systemic Chemotherapy in Malignant Mesothelioma (SOC)

For a prolonged period of time, there was no consensus as to the optimum systemic chemotherapy used for MPM due to the limited randomized clinical trial data to support one strategy over another. It is important to mention that systemic chemotherapy for MPM is palliative in nature and has been the only intervention to show modest improvement in overall survival [27, 37]. This situation changed in 2003 following the availability of the results of the EMPHACIS phase III trial, which showed the superiority of the combination of cisplatin and pemetrexed over cisplatin alone, which was the most commonly used first line chemotherapy at the time [38, 39]. In this study, median survival was improved from 9.3 to 12.1 months [39]. These data led to the formal approval of the pemetrexed/cisplatin combination as the new SOC for MPM, a development which has not changed in the decade plus since it was first described [37]. Additional studies have validated the use of a different antifolate, raltitrexed, with

cisplatin as an appropriate alternative regimen if pemetrexed is not well-tolerated [40]. Many clinicians also substitute carboplatin for cisplatin to reduce toxicity with little clinical difference in outcomes and without formal FDA approval [41]. Meanwhile, the recently published MAPS study demonstrated the clinical benefit of adding bevacizumab to SOC which resulted in an additional 2.7 month survival benefit though not without risks as the bevacizumab arm had higher reported adverse events across multiple subgroups and significant increases in grade 3-4 arterial and venous thromboembolic events [42]. However, even with this increase in median survival from the addition of bevacizumab plus SOC, MPM typically recurs as an incurable disease, necessitating the development of effective second line therapeutic options. Unlike the case with first line therapy, there is currently no established SOC therapy for disease recurrence or progression following initial management. The most common second line chemotherapy options include the vinca alkaloid vinorelbine, the anti-nucleoside analog gemcitabine, and the re-administration of single agent pemetrexed, which have shown the most promise in terms of tolerability but have failed to improve overall survival [27, 43]. In view of these shortcomings of currently available therapies, novel treatment strategies including targeted strategies and immunotherapy have been explored as both adjunctive and independent options for systemic therapy of MPM.

2.3. Targeted Therapies and Immunotherapy in Malignant Mesothelioma

Given the overwhelming lack of second line options in MPM and the large percentage of patients diagnosed with advanced disease that is not amenable to aggressive multimodal approaches, there has been a focus on targeted therapies with biological agents over the last 10 years, albeit with mostly disappointing results. Targeting various tyrosine kinases and the process of angiogenesis, as well as representing various forms of immunotherapy, these therapies can be broadly subcategorized into small molecule inhibitors, angiogenesis inhibitors, histone deacetylase (HDAC) inhibitors, and gene mutation targeting. The small molecule inhibitors include multitargeting receptor tyrosine kinase inhibitors (mTKIs), selective tyrosine kinase inhibitors (sTKIs), and

proteasome inhibitors. These molecules have garnered much focus in the oncologic world with broad applications in both solid and liquid tumors [44-47]. Unfortunately, phase I and phase II clinical trials involving the mTKIs sorafenib, sunitinib, pazopanib, and desatinib showed either limited anti-mesothelioma activity, the inability to induce remission, and/or unacceptable toxicity [48-52]. These receptor tyrosine kinase inhibitors broadly target EGFR, VEGFR, PDGFR, and C-kit to exert their anticancer effects. While these self-signaling molecules are upregulated in MPM, they do not appear vital to its propagation and are not MPM specific, which likely contributes to the limited efficacy of these drugs. Interestingly, the process of angiogenesis has only been successfully targeted by the monoclonal antibody bevacizumab and not by the above mentioned mTKIs which target VEGFR, or by the biologic agent thalidomide which primarily works through angiogenesis inhibition [53, 54]. Thalidomide was tested in clinical trials as both adjunct to standard of care treatment and as maintenance therapy for MPM patients previously treated with platinum based chemotherapy. The results of these studies showed no benefit to thalidomide as adjunct and no improvement in overall survival (OS) vs supportive care alone as maintenance therapy [27, 54]. Guazelli *et al.*, recently summarized active phase I and phase II clinical trials and highlight that many studies have looked at targeting the EGFR or VEGR pathway with little success to show for it up to this point, this review expertly highlights the current clinical trials that are ongoing from Clinicaltrials.gov [53]. Since EGFR expression is upregulated in the majority of MPM, selective tyrosine kinase inhibitors like erlotinib and gefitinib should theoretically exhibit increased activity against MPM. Unfortunately, similar to the mTKIs, results from phase II clinical trials were disappointing. Limited efficacy and marked resistance to these sTKIs was observed even in the presence of detectable EGFR expression on MPM tumors [55-57]. Similar results to these were seen with the proteasome inhibitor bortezomib, which has been approved for use in multiple myeloma and is currently in clinical trials for multiple other cancers including non-small cell lung cancer and metastatic breast cancer [58]. In two different clinical trials bortezomib failed to show objective response as monotherapy and failed to provide significant OS survival or

disease progression benefit when combined with SOC [59].

HDAC inhibitors, specifically vorinostat, which modify and limit deacetylation of histone and block access genes that are overused by cancer cells for progression and division, showed promising results in early clinical trials [60]. These results prompted the large-scale VANTAGE-014 phase III double blind, randomized placebo control study using vorinostat monotherapy as either second- or third-line therapy for MPM [61]. Results reported in the Lancet in 2015 of this large well designed and well executed study (660 patients enrolled) showed no benefit to vorinostat over placebo in terms of overall survival [61]. Gene mutations have been a hallmark of targeted cancer therapy, but few highly conserved gene mutations in MPM have been identified, and studies involving those found and targeted have failed to result in clinically significant efficacy. The most common mutations observed through molecular genetic analysis of patient MPM samples include BAP1, PTEN/PI3K, CDKN2A/ARF, and NF2 [62-65]. Of these, NF2 has been identified in 40% of MPM and results in inactivation of a protein called Merlin which is involved in cell adhesion and motility. Of potential therapeutic value is the fact that Merlin loss increases cell sensitivity to focal adhesion kinase (FAK) inhibitors [66]. Initial research showed FAK inhibitors, specifically defactinib, along with their MPM cytotoxic effect reduced so called cancer stem cell populations in MPM with potential for more durable prolonged response vs SOC [66]. These results prompted a large phase II COMMAND study which enrolled 372 patients to receive defactinib plus SOC vs placebo plus SOC control arm as first line therapy for MPM [67]. Unfortunately as is often the case in MPM clinical trials, the study was stopped during recruitment when no difference in defactinib vs placebo were observed, even when subdivided to those patients with identifiable merlin loss [68].

Immunotherapy has been on the forefront of cancer therapy for the past 20 years and recent successes in immune checkpoint inhibition, tumor escape mechanism targeting, passive immunotherapy, and dendritic cell vaccines have pushed the field further with ever broadening application [69-71]. Recent advances in immunotherapy and current clinical trials in MPM are well summarized by

Thapa *et al.*, [72]. In their review of current immunologic strategies, the failures of targeting MPM with single agent immunotherapy warrants the use of combination strategies to improve efficacy [72]. One of the more successful pathways of immunotherapy described in their work and others is the use of immune checkpoint inhibition as a novel target in MPM [72]. An example of immune checkpoint inhibition is the strategy of targeting and blocking CTLA-4. CTLA-4 is a cell surface co-factor expressed on the surface of T cells that acts as an inhibitory cofactor for CD80 and CD86 [73]. CTLA-4 competes with CD28 for binding with CD80/86 and when bound sends an inhibitor signal to antigen presenting cells to decrease the inflammatory response and diminish cell activation. This process allows CTLA-4 to protect surrounding cells and the system as a whole from uncontrolled immune stimulation [74]. Tumor cells, including malignant mesothelioma, express increased level of CTLA-4 as a means of blocking anti-tumor immune responses [74]. Inhibition of CTLA-4, or so-called checkpoint inhibition, therefore can restore the anti-tumor immune response, resulting in T cells recognition and attack of tumors that had previously been undetected. In a recent review, Guazelli *et al.* have summarized the role of CTLA-4 targeting in MPM [75]. They and others point out monoclonal antibodies (mAb) directed against CTLA-4 have shown impressive results in melanoma and have been tested in early clinical trials with MPM [75]. The CTLA-4 mAb Tremelimumab has been investigated in the MESOT-TREM-2008, and MESOT-TREM-2012 phase II clinical trials in patients with chemotherapy-resistant MPM [28, 75, 76]. In these studies, Tremelimumab treatment resulted in a disease control rate of 31% when administered every 3 months, and a control rate of 52% when given every 4 weeks, a regimen that led to improved efficacy in other cancers [75-77]. Furthermore, with the shorter dosing time, median OS was improved to 10.7 months compared to historical averages of 8.7 months with second line chemo [77]. These early results have led to an ongoing study comparing Tremelimumab monotherapy *vs* placebo control. Additionally, combination immunotherapies, CTLA-4 blockade combined with anti-PD-L1 therapy is under active investigation and was recently presented at ASCO 2016 with the combination of Tremelimumab and durvalumab

[75]. Like CTLA-4, programmed death ligand 1 (PD-L1) is overexpressed in MPM, particularly the sarcomatoid type, and exerts an inhibitory effect on T cells to suppress the anti-tumor immune response [77]. Binding PD-L1 with ligand specific mAbs therefore blocks this tumor escape mechanism, potentially resulting in greater susceptibility of MPM to immune destruction. In the recent KEYNOTE-028 phase I clinical trial, the PD-1 mAb pembrolizumab was tested in a 25 patient cohort and showed an impressive overall disease control rate of 76% [73, 78]. This has prompted larger phase II investigation to further explore the anti-MPM activity of pembrolizumab [73].

Additional passive immunotherapy strategies in MPM have focused on targeting the tumor-associated antigen Mesothelin. Mesothelin expression is increased in MPM and likely plays a role in cell adhesion and invasion [79, 80]. Strategies focusing on mesothelin targeting have involved the mAb Amatuximab, anti-mesothelin vaccine CRS-207, and the mAb-toxin fusion protein called SS1P [79]. Amatuximab is a chimeric anti-mesothelin mAb that was tested in a phase II multicenter trial of 89 MPM patients in combination with SOC (pemetrexed/cisplatin) *vs* SOC alone, with improved OS in the Amatuximab-containing arm [81]. The anti-mesothelin vaccine CRS-207 is a live, attenuated, derivative of listeria monocytogenes that expressed the mesothelin Ag and activates both innate and adaptive immunity [82]. The synergistic effects of CRS-207 and SOC chemotherapy was tested in a phase I trial of 38 MPM patients which showed encouraging anti-tumor immunity, with a progression free survival of 8.5 months [82]. Encouraging results from this study has led to a large multicenter phase III clinical trial that is currently recruiting. Similarly, the recombinant anti-mesothelin and truncated pseudomonas exotoxin SS1P has shown significant anti-tumor activity and tolerability in a phase I clinical trial [83]. Finally, adoptive transfer of *ex vivo* stimulated dendritic cells, so called dendritic cell vaccination has recently shown activity in MPM. In a trial of 10 patients with MPM, cyclophosphamide was given to reduce activity of T regulatory cells prior to infusion of dendritic cells pulsed with autologous tumor lysate [84]. Results of this small study showed radiographic disease control in 8/10 patients and an impressive OS of greater than 2

years in 7/10 patients [84]. This technique will likely be expanded and further investigated in future years.

3. POTENTIAL APPROACH TO TARGETING CD26 IN MPM

As discussed above, treatment for MPM beyond first line therapy is still unsatisfactory due to limited efficacy, and novel therapeutic approaches are urgently needed for this patient population. While immunotherapy approaches appear promising with encouraging efficacy in multiple small studies, the observed benefit is still relatively short lasting and typically limited to only a few months. Additionally some concerns that arise with all studies involving immunotherapy include utilizing progression free survival (PFS) vs OS as an overall marker of drug efficacy or combining drugs that lack single-agent activity. In a recent study published in the *Journal of Clinical Oncology*, Tan *et al.* performed a meta-analysis of trials with results posted on *ClinicalTrials.gov* where they found a majority of studies showing significant benefit on PFS but not on OS [85]. They highlight the need for studies to look at both PFS and OS and to not use one as a surrogate marker for the other [85]. In separate commentary, Gyawali and Prasad illustrate that multiple trials over the past decade where multiple drugs without proven single-agent efficacy were added together as a novel treatment and showed PFS but rarely showed an effect on OS [86]. They pose in additional manuscript that by combining multiple therapies to extent PFS we run the risk of subjecting patients to unnecessary side effects and risks for little benefit [87]. These compelling examples shed light on the grain of salt mentality that is needed when evaluating the efficacy of immunotherapy. Unfortunately, as is usually the case, most of these trials and analysis did not include studies involving MPM. Given the small treatment arms and aggressive nature of MPM small gains in PFS may indicate improvement in OS but the low power of these studies makes statistical extrapolation difficult and with such a short OS window for these patients even small gains should be looked at as possible treatment strategies. There studies confirm and support the need for improved targeting in diseases like MPM and stresses the importance of single-agent efficacy in therapy design before a drug is pushed forward through clinical trials and

towards FDA approval. Thus, an ideal target in MPM would be one that is highly expressed by malignant mesothelioma cells but absent from normal mesothelioma, and plays a role in tumor proliferation or invasiveness. In addition, therapy specifically targeting this antigen should work in concert with chemotherapy to enhance treatment efficacy without increasing side effect burden, have strong activity as a single agent, and improve both PFS and OS in MPM patients. All these characteristics can be found potentially in the surface antigen CD26.

3.1. CD26 Expression and Function in MPM

CD26 is a multifunctional cell surface receptor with roles in immune regulation, T cell activation, and malignant potential of various cancers. CD26 is highly expressed in MPM and was originally identified as a potential target by our group [88, 89]. Our initial work demonstrated that targeting CD26 with anti-CD26 mAb resulted in *in vitro* growth inhibition of MPM cell line [89]. Subsequently, we showed high CD26 expression on various human MPM types including localized MPM, well-differentiated papillary MPM, and diffuse MPM but not on adenomatoid tumors or reactive mesothelioma cells [88]. Complementing our earlier *in vitro* work, we also demonstrated for the first time the potential for targeting CD26 in MPM with anti-CD26 mAb in an *in vivo* NOD-SCID mouse model of MPM. This initial evaluation for CD26 expression on a small sample population of MPM tissues was then further expanded in a follow-up paper which demonstrated overexpression of CD26 in MPM in more than 120 different MPM surgical samples including epithelioid mesothelioma, biphasic mesothelioma, and sarcomatoid mesothelioma as well as 8 different mesothelioma cell lines [90]. Interestingly, the more aggressive sarcomatoid mesothelioma samples had reduced cell surface CD26 expression but retained cytoplasmic CD26 expression. This work suggested that the morphology of the mesothelioma cell type, which has been used as a prognostic factor in the disease, correlated with CD26 expression and that loss of membranous CD26 was associated with the more aggressive spindle shaped sarcomatoid mesothelioma, raising the possibility that the loss of CD26 in these cells represented an epithelial to mesenchymal transition for MPM potentially responsible for the difficulty in treating and poorer

outcome associated with sarcomatoid MPM [90]. We subsequently showed that CD26 surface expression was associated with improved survival in MPM patients that received chemotherapy and potentially contributed to mesothelioma chemosensitivity [91]. We also demonstrated through *in vitro* investigation that CD26 was associated with enhanced proliferative activity of MPM and through downstream gene activation, CD26 upregulated mechanisms that increased chemotherapy sensitivity [91]. Given the increased surface expression of CD26 in favorable MPM phenotypes, soluble CD26 (sCD26) was investigated as potential biomarker for MPM. We showed in a recent preclinical model of MPM that sCD26 levels were higher in patients with the favorable epithelioid phenotype than those with the aggressive sarcomatoid subtype and through therapeutic monitoring, reduction in sCD26 may indicate progression of disease [92]. Whether sCD26 can be used in high-risk patients, those with previous significant asbestos exposure or those residents of asbestos mining communities, as a screening tool for early detection of disease remains to be determined. Additionally, CD26 expression was identified and characterized as a marker for so called cancer stem cells (CSC) in MPM and was found to be co-expressed with the CSC marker CD24 [93]. In this study we used shRNA knockdown of CD24 and CD26 to determine the effects of gene silencing in the MPM cell line Meso-1 [93]. We showed that through silencing of CD26 but not CD24 MPM cellular invasion was reduced and MPM showed reduced proliferation [93]. Gene knockout of CD26 additionally caused a reduction in the cancer cell signaling molecules IGFBP7, IGFBP3, Wnt5A, and IL7R [93]. These studies also showed CD26 played a role in asymmetric cell division and invasion potential in MPM cell lines [93]. These collective works clearly validated CD26 as a surface receptor upregulated in MPM with various roles in cell proliferation, invasion, and chemosensitivity, while loss of expression correlated with progression of MPM to a more aggressive treatment-resistant phenotype.

These studies on CD26 expression in MPM were subsequently followed by our work evaluating molecular mechanisms for CD26 role in cellular invasiveness. We showed that CD26 promotes invasiveness through the formation of CD26- α 5 β 1 integrin molecular complexes that interact with various cell surface and endothelium receptors and

stimulate extra-cellular matrix metalloproteinases [94]. In addition, the short 6 amino acid cytoplasmic region of CD26 plays a crucial role in MPM migration and invasion through upregulation of periostin [95]. We demonstrated that the lipid raft platforms clustered around CD26, indirect activation and phosphorylation of the proto-oncogene Src occurred resulting in nuclear translocation of the transcription factor Twist1 [95]. Through this mechanism, periostin production is increased, associated with an enhancement in the migratory potential and invasiveness of MPM, contributing to both progression of disease and metastases. CD26 therefore represents a targetable MPM specific molecule with a direct role in the invasiveness and metastatic potential of MPM.

3.2. CD26 Targeting in Malignant Mesothelioma

As mentioned above, proof-of-concept studies using preclinical MPM models demonstrate that targeting CD26 with its specific mAbs is a viable anti-cancer therapeutic approach. Treatment of MPM cell lines with the humanized anti-CD26 mAB, YS110 resulted in p27^{kip1} accumulation leading to cytotoxicity in both *in vitro* and *in vivo* models [88]. Binding of YS110 also had a direct role in regulating binding to extra-cellular matrix proteins, biphasic antitumor immunity through immune activation and direct cytotoxicity, as well as inhibition of distant metastases [88]. In addition, anti-CD26 mAB enhanced nuclear translocation of CD26 with downstream effects resulting in mesothelioma growth suppression [96, 97]. Cellular localization analysis revealed that YS110 caused an increase in transport *via* caveolin-dependent endocytosis and accumulation of CD26 to the nucleus of MPM resulting in suppression of POLR2 gene expression and subsequent growth suppression of MPM cells, while highlighting a secondary anti-tumor mechanism of anti-CD26 mABs [96, 97]. Meanwhile, a recently published paper demonstrated that YS110 caused retarded G2/M cell cycle progression through inhibition of phosphorylation of cdc2 and cdc25C and activation of ERK1/2 [98]. Importantly, a synergistic effect between YS110 and the first line anti-MPM chemotherapeutic agent pemetrexed was observed, as the combination of YS110 and pemetrexed showed superior anti-tumor activity associated with combinatorial G1/S and G2/M cell cycle tran-

sition inhibition than either agent alone in a mouse xenograft model of MPM [98].

These encouraging preclinical results along with our increased understanding of the novel molecular mechanisms involved in CD26 targeting in cancer cells led to the first-in-human phase I study of YS110 in CD26 expressing cancer cells. This recently published study involved 33 patients with CD26⁺ tumors (22 of whom had heavily pre-treated MPM) treated with a standard 3+3 escalation scheme with escalating doses of YS110 [99]. YS110 was generally well tolerated even to doses of 6mg/kg weekly, with maximal tolerated dose not reached and only 2 patients reporting grade 3 or higher anaphylactic or allergic reactions, which entirely resolved with supportive treatment and dose omission [99]. When the study was subsequently amended to add clinically relevant allergies as a new exclusion criterion and to allow for the administration of a systemic steroid prophylaxis prior to each infusion to better control infusions reactions, the safety profile was even further improved with treatment doses being escalated to 6mg/kg without dose limiting toxicities. While there was a transient decrease in total peripheral lymphocyte counts and CD26⁺ lymphocyte subsets following antibody administration, there was no observed autoimmune or infectious disease occurrences [99]. Furthermore, in this first-in-human phase I study, prolonged disease stabilization was observed in a significant number of patients that received YS110 [99, 100]. Thirteen of 26 evaluable patients treated with YS110 had stable disease as the best response for an overall median PFS of 43 days, while 7 patients (including five cases of mesothelioma) experienced prolonged PFS of 184-399 days [99, 100]. Taken together, data from both preclinical studies as well as the recently completed first-in-human phase I clinical trial indicate that additional testing of YS110, which may represent a major breakthrough in the treatment of MPM, in future clinical trials as either single agent therapy or as part of combination therapies with other anti-neoplastic agents, would be warranted.

CONCLUSION

MPM is an ongoing oncological concern. With continued mining and use of asbestos globally in developing countries and major industrialized

nations like China and Russia, MPM cases will predictably increase in the coming decades. When found, treatment strategies include combination surgery, radiation, and chemotherapy; although few patients are diagnosed in time to benefit from definitive surgery, with systemic chemotherapy being thus left for many patients as their only option. While beneficial at reducing symptoms, systemic chemotherapy with pemetrexed and cisplatin (SOC) fails to provide curative benefit for most MPM patients and only extends overall survival by a matter of months. The addition of novel biologic agents such as bevacizumab to standard of care will likely provide modest survival benefit but has yet to become the approved standard. For most patients with MPM, following initial systemic therapy, disease commonly relapses with progression and metastases. Over the past 20 years, many chemo- and immunotherapeutics have been evaluated as potential treatments for MPM with limited benefit. Novel immunotherapy strategies including passive immunotherapy, mesothelin targeting, and checkpoint inhibition targeting have recently shown promise in small phase I and II studies. In this review, we highlight the need for novel therapeutic approaches in MPM and discuss the potential of CD26 as a new molecular target. CD26 is highly expressed in MPM with limited expression in normal mesothelial cells. Unlike other immunotherapeutic targets, CD26 has a direct role in progression, invasion, metastasis, and cancer-stem cell proliferation in MPM. Our recently completed first-in-human phase I clinical trial involving the anti-CD26 mAb YS110 suggests that successful targeting of CD26 may lead potentially to improved disease control and prolonged overall survival with limited toxic side effects in malignant mesothelioma. The successful development of a CD26-targeted approach will enhance the treatment armamentarium available against MPM as we prepare for this predictive epidemic.

LIST OF ABBREVIATIONS

DPPIV	=	Dipeptidyl Peptidase IV
MPM	=	Malignant Pleural Mesothelioma
mAb	=	Monoclonal Antibody
SOC	=	Standard of Care

- CSC = Cancer Stem Cells
 OS = Overall Survival

CONSENT FOR PUBLICATION

Not applicable.

CONFLICT OF INTEREST

Nam H. Dang, Chikao Morimoto, and Kei Ohnuma are stockholders of Y's AC Co, Ltd.

ACKNOWLEDGEMENTS

Declared none.

REFERENCES

- [1] Ohnuma K, Dang NH, Morimoto C. Revisiting an old acquaintance: CD26 and its molecular mechanisms in T cell function. *Trends Immunol* 2008; 29(6): 295-301.
- [2] Boonacker E, Van Noorden CJ. The multifunctional or moonlighting protein CD26/DPPIV. *Eur J Cell Biol* 2003; 82(2): 53-73.
- [3] Hosono O, Ohnuma K, Dang NH, Morimoto C. CD26: A key molecule in immune regulation and autoimmune diseases. *Mod Rheumatol* 2003; 13(3): 199-204.
- [4] Matteucci E, Giampietro O. Dipeptidyl peptidase-4 (CD26): Knowing the function before inhibiting the enzyme. *Curr Med Chem* 2009; 16(23): 2943-51.
- [5] Mortier A, Gouwy M, Van Damme J, Proost P, Struyf S. CD26/dipeptidylpeptidase IV-chemokine interactions: Double-edged regulation of inflammation and tumor biology. *J Leukoc Biol* 2016; 99(6): 955-69.
- [6] Cordero OJ, Salgado FJ, Nogueira M. On the origin of serum CD26 and its altered concentration in cancer patients. *Cancer Immunol Immunother* 2009; 58(11): 1723-47.
- [7] Ohnuma K, Takahashi N, Yamochi T, Hosono O, Dang NH, Morimoto C. Role of CD26/dipeptidyl peptidase IV in human T cell activation and function. *Front Biosci* 2008; 13: 2299-310.
- [8] Kleemann C, Wagner L, Stephan M, Von Hörsten S. Cut to the chase: A review of CD26/dipeptidyl peptidase-4 (DPP4)'S entanglement in the immune system. *Clin Exp Immunol* 2016; 185(1): 1-21.
- [9] Ohnuma K, Inoue H, Uchiyama M, *et al.* T-cell activation via CD26 and caveolin-1 in rheumatoid synovium. *Mod Rheumatol* 2006; 16(1): 3-13.
- [10] Dang NH, Morimoto C. CD26: An expanding role in immune regulation and cancer. *Histol Histopathol* 2002; 17(4): 1213-26.
- [11] Dang NH, Aytac U, Sato K, *et al.* T-large granular lymphocyte lymphoproliferative disorder: Expression of CD26 as a marker of clinically aggressive disease and characterization of marrow inhibition. *Br J Haematol* 2003; 121(6): 857-65.
- [12] Havre PA, Abe M, Urasaki Y, Ohnuma K, Morimoto C, Dang NH. The role of CD26/dipeptidyl peptidase IV in cancer. *Front Biosci* 2008; 13: 1634-45.
- [13] Lam CS, Cheung AH, Wong SK, *et al.* Prognostic significance of CD26 in patients with colorectal cancer. *PLoS One* 2014; 9(5): e98582.
- [14] Ho L, Aytac U, Stephens LC, *et al.* *In vitro* and *in vivo* antitumor effect of the anti-CD26 monoclonal antibody 1F7 on human CD30+ anaplastic large cell T-cell lymphoma Karpas 299. *Clin Cancer Res* 2001; 7(7): 2031-40.
- [15] Davies S, Beckenkamp A, Buffon A. CD26 a cancer stem cell marker and therapeutic target. *Biomed Pharmacother* 2015; 71: 135-8.
- [16] Ai J, Stevenson JP. Current issues in malignant pleural mesothelioma evaluation and management. *Oncoologist* 2014; 19(9): 975-84.
- [17] Robinson BM. Malignant pleural mesothelioma: An epidemiological perspective. *Ann Cardiothorac Surg* 2012; 1(4): 491-6.
- [18] Røe OD, Stella GM. Malignant pleural mesothelioma: History, controversy and future of a manmade epidemic. *Eur Respir Rev* 2015; 24(135): 115-31.
- [19] Riva MA, Carnevale F, Sironi VA, De Vito G, Cesana G. Mesothelioma and asbestos, fifty years of evidence: Chris Wagner and the contribution of the Italian occupational medicine community. *Med Lav* 2010; 101(6): 409-15.
- [20] Bononi A, Napolitano A, Pass HI, Yang H, Carbone M. Latest developments in our understanding of the pathogenesis of mesothelioma and the design of targeted therapies. *Expert Rev Respir Med* 2015; 9(5): 633-54.
- [21] Pasdar EA, Smits M, Stapelberg M, *et al.* Characterisation of mesothelioma-initiating cells and their susceptibility to anti-cancer agents. *PLoS One* 2015; 10(5): e0119549.
- [22] Price B, Ware A. Time trend of mesothelioma incidence in the United States and projection of future cases: An update based on SEER data for 1973 through 2005. *Crit Rev Toxicol* 2009; 39(7): 576-88.
- [23] Markowitz S. Asbestos-related lung cancer and malignant mesothelioma of the pleura: Selected current issues. *Semin Respir Crit Care Med* 2015; 36(3): 334-46.
- [24] Zhang W, Wu X, Wu L, Zhao X. Advances in the diagnosis, treatment and prognosis of malignant pleural mesothelioma. *Ann Transl Med* 2015; 3(13): 182.
- [25] Adusumilli PS. Translational immunotherapeutics: Chemoimmunotherapy for malignant pleural mesothelioma. *Cancer* 2014; 120(21): 3268-71.
- [26] Blomberg C, Nilsson J, Holgersson G, *et al.* Randomized trials of systemic medically-treated malignant

- mesothelioma: A systematic review. *Anticancer Res* 2015; 35(5): 2493-501.
- [27] Buikhuisen WA, Hiddinga BI, Baas P, van Meerbeeck JP. Second line therapy in malignant pleural mesothelioma: A systematic review. *Lung Cancer* 2015; 89(3): 223-31.
- [28] Calabro L, Maio M. Immune checkpoint blockade in malignant mesothelioma. *Semin Oncol* 2015; 42(3): 418-22.
- [29] Cao C, Akhunji Z, Fu B, *et al.* Surgical management of malignant pleural mesothelioma: An update of clinical evidence. *Semin Thorac Cardiovasc Surg* 2015; 27(1): 6-8.
- [30] Christoph DC, Eberhardt WE. Systemic treatment of malignant pleural mesothelioma: New agents in clinical trials raise hope of relevant improvements. *Curr Opin Oncol* 2014; 26(2): 171-81.
- [31] Jing XQ, Zhou L, Sun XD, Yu JM, Meng X. Pemetrexed maintenance therapy following bevacizumab-containing first-line chemotherapy in advanced malignant pleural mesothelioma: A case report and literatures review. *Medicine (Baltimore)* 2016; 95(14): e3351.
- [32] Bertoglio P, Waller DA. The role of thoracic surgery in the management of mesothelioma: An expert opinion on the limited evidence. *Expert Rev Respir Med* 2016; 10(6): 663-72.
- [33] Treasure T, Waller D, Tan C, *et al.* The mesothelioma and radical surgery randomized controlled trial: The mars feasibility study. *J Thorac Oncol* 2009; 4(10): 1254-8.
- [34] Treasure T, Lang-Lazdunski L, Waller D, *et al.* Extra-pleural pneumonectomy versus no extra-pleural pneumonectomy for patients with malignant pleural mesothelioma: Clinical outcomes of the Mesothelioma and Radical Surgery (MARS) randomised feasibility study. *Lancet Oncol* 2011; 12(8): 763-72.
- [35] Thieke C, Nicolay NH, Sterzing F, *et al.* Long-term results in malignant pleural mesothelioma treated with neoadjuvant chemotherapy, extrapleural pneumonectomy and intensity-modulated radiotherapy. *Radiat Oncol* 2015; 10: 267.
- [36] Federico R, Adolfo F, Giuseppe M, *et al.* Phase II trial of neoadjuvant pemetrexed plus cisplatin followed by surgery and radiation in the treatment of pleural mesothelioma. *BMC Cancer* 2013; 13: 22.
- [37] Kondola S, Manners D, Nowak AK. Malignant pleural mesothelioma: An update on diagnosis and treatment options. *Ther Adv Respir Dis* 2016; 10(3): 275-88.
- [38] Reck M, Gatzemeier U. Pemetrexed-cisplatin combination in mesothelioma. *Expert Rev Anticancer Ther* 2005; 5(2): 231-7.
- [39] Vogelzang NJ, Rusthoven JJ, Symanowski J, *et al.* Phase III study of pemetrexed in combination with cisplatin versus cisplatin alone in patients with malignant pleural mesothelioma. *J Clin Oncol* 2003; 21(14): 2636-44.
- [40] van Meerbeeck JP, Gaafar R, Manegold C, *et al.* Randomized phase III study of cisplatin with or without raltitrexed in patients with malignant pleural mesothelioma: An intergroup study of the European Organisation for Research and Treatment of Cancer Lung Cancer Group and the National Cancer Institute of Canada. *J Clin Oncol* 2005; 23(28): 6881-9.
- [41] Habib EE, Fahmy ES. Chemotherapy management of malignant pleural mesothelioma: A phase II study comparing two popular chemotherapy regimens. *Clin Transl Oncol* 2013; 15(11): 965-8.
- [42] Zalcman G, Mazieres J, Margery J, *et al.* Bevacizumab for newly diagnosed pleural mesothelioma in the Mesothelioma Avastin Cisplatin Pemetrexed Study (MAPS): A randomised, controlled, open-label, phase 3 trial. *Lancet* 2016; 387(10026): 1405-14.
- [43] Abdel-Rahman O, Kelany M. Systemic therapy options for malignant pleural mesothelioma beyond first-line therapy: A systematic review. *Expert Rev Respir Med* 2015; 9(5): 533-49.
- [44] Hall RD, Le TM, Haggstrom DE, Gentzler RD. Angiogenesis inhibition as a therapeutic strategy in Non-Small Cell Lung Cancer (NSCLC). *Transl Lung Cancer Res* 2015; 4(5): 515-23.
- [45] Kim SH, Park WS, Joung JY, Seo HK, Lee KH, Chung J. Systemic treatments for metastatic renal cell carcinoma: 10-year experience of immunotherapy and targeted therapy. *Cancer Res Treat* 2016; 48(3): 1092-101.
- [46] Cella D, Beaumont JL. Pazopanib in the treatment of advanced renal cell carcinoma. *Ther Adv Urol* 2016; 8(1): 61-9.
- [47] Siddiqi T, Rosen ST. Novel biologic agents for non-Hodgkin lymphoma and chronic lymphocytic leukemia-part 2: Adoptive cellular immunotherapy, small-molecule inhibitors, and immunomodulation. *Oncology (Williston Park)* 2015; 29(4): 299-308.
- [48] Dubey S, Jänne PA, Krug L, *et al.* A phase II study of sorafenib in malignant mesothelioma: Results of cancer and leukemia group B 30307. *J Thorac Oncol* 2010; 5(10): 1655-61.
- [49] Camidge DR, Blais N, Jonker DJ, *et al.* Sunitinib combined with pemetrexed and cisplatin: Results of a phase I dose-escalation and pharmacokinetic study in patients with advanced solid malignancies, with an expanded cohort in non-small cell lung cancer and mesothelioma. *Cancer Chemother Pharmacol* 2013; 71(2): 307-19.
- [50] Laurie SA, Gupta A, Chu Q, *et al.* Brief report: A phase II study of sunitinib in malignant pleural mesothelioma. The NCIC Clinical Trials Group. *J Thorac Oncol* 2011; 6(11): 1950-4.
- [51] Dudek AZ, Pang H, Kratzke RA, *et al.* Phase II study of dasatinib in patients with previously treated malignant mesothelioma (cancer and leukemia group B 30601): A brief report. *J Thorac Oncol* 2012; 7(4): 755-9.
- [52] Mathy A, Baas P, Dalesio O, van Zandwijk N. Limited efficacy of imatinib mesylate in malignant meso-

- thelioma: A phase II trial. *Lung Cancer* 2005; 50(1): 83-6.
- [53] Guazzelli A, Bakker E, Tian K, Demonacos C, Krstic-Demonacos M, Mutti L. Promising investigational drug candidates in phase I and phase II clinical trials for mesothelioma. *Expert Opin Investig Drugs* 2017; 26(8): 933-944.
- [54] Buikhuisen WA, Burgers JA, Vincent AD, *et al.* Thalidomide versus active supportive care for maintenance in patients with malignant mesothelioma after first-line chemotherapy (NVALT 5): An open-label, multicentre, randomised phase 3 study. *Lancet Oncol* 2013; 14(6): 543-51.
- [55] Govindan R, Kratzke RA, Herndon JE, *et al.* Gefitinib in patients with malignant mesothelioma: A phase II study by the cancer and leukemia group B. *Clin Cancer Res* 2005; 11(6): 2300-4.
- [56] Garland LL, Rankin C, Gandara DR, *et al.* Phase II study of erlotinib in patients with malignant pleural mesothelioma: A southwest oncology group study. *J Clin Oncol* 2007; 25(17): 2406-13.
- [57] Jackman DM, Kindler HL, Yeap BY, *et al.* Erlotinib plus bevacizumab in previously treated patients with malignant pleural mesothelioma. *Cancer* 2008; 113(4): 808-14.
- [58] O'Brien ME, Gaafar RM, Popat S, *et al.* Phase II study of first-line bortezomib and cisplatin in malignant pleural mesothelioma and prospective validation of progression free survival rate as a primary endpoint for mesothelioma clinical trials (European Organisation for research and treatment of cancer 08052). *Eur J Cancer* 2013; 49(13): 2815-22.
- [59] Tada Y, Suzuki T, Shimada H, Hiroshima K, Tatsumi K, Tagawa M. Molecular-targeted therapy for malignant mesothelioma. *Pleura* 2015; 2: 1-11.
- [60] Paik PK, Krug LM. Histone deacetylase inhibitors in malignant pleural mesothelioma: Preclinical rationale and clinical trials. *J Thorac Oncol* 2010; 5(2): 275-9.
- [61] Krug LM, Kindler HL, Calvert H, *et al.* Vorinostat in patients with advanced malignant pleural mesothelioma who have progressed on previous chemotherapy (VANTAGE-014): A phase 3, double-blind, randomised, placebo-controlled trial. *Lancet Oncol* 2015; 16(4): 447-56.
- [62] McMillan R, Zauderer M, Bott M, Ladanyi M. Important recent insights into the genetics and biology of malignant pleural mesothelioma. *Ann Cardiothorac Surg* 2012; 1(4): 462-5.
- [63] de Assis LV, Locatelli J, Isoldi MC. The role of key genes and pathways involved in the tumorigenesis of malignant mesothelioma. *Biochim Biophys Acta* 2014; 1845(2): 232-47.
- [64] Lo Iacono M, Monica V, Righi L, *et al.* Targeted next-generation sequencing of cancer genes in advanced stage malignant pleural mesothelioma: A retrospective study. *J Thorac Oncol* 2015; 10(3): 492-9.
- [65] Jean D, Daubriac J, Le Pimpec-Barthes F, Galateau-Salle F, Jaurand MC. Molecular changes in mesothelioma with an impact on prognosis and treatment. *Arch Pathol Lab Med* 2012; 136(3): 277-93.
- [66] Shapiro IM, Kolev VN, Vidal CM, *et al.* Merlin deficiency predicts FAK inhibitor sensitivity: A synthetic lethal relationship. *Sci Transl Med* 2014; 6(237): 237ra68.
- [67] Fennell DA, Baas P, Kindler HL, *et al.* COMMAND: A phase II randomized, double-blind, placebo-controlled, multicenter study of defactinib as maintenance therapy in subjects with malignant pleural mesothelioma that has not progressed on at least four cycles of pemetrexed/platinum therapy. *J Clin Oncol* 2014; 32: 15.
- [68] Verastem Stops Enrollment Due to Futility in the COMMAND Study of VS-6063 for the Treatment of Malignant Pleural Mesothelioma [press release]. 2015; <http://www.businesswire.com/news/home/20150928005465/en/Verastem-Stops-Enrollment-Due-Futility-COMMAND-Study>
- [69] Maggioni C, Barletta G, Rijavec E, Biello F, Gualco E, Grossi F. Advances in treatment of mesothelioma. *Expert Opin Pharmacother* 2016; 17(9): 1197-205.
- [70] Hassan R, Schweizer C, Lu KF, *et al.* Inhibition of mesothelin-CA-125 interaction in patients with mesothelioma by the anti-mesothelin monoclonal antibody MORAb-009: Implications for cancer therapy. *Lung Cancer* 2010; 68(3): 455-9.
- [71] Calabro L, Maio M. Immune checkpoint blockade in malignant mesothelioma: A novel therapeutic strategy against a deadly disease? *Oncoimmunology* 2014; 3(1): e27482.
- [72] Thapa B, Watkins DN, John T. Immunotherapy for malignant mesothelioma: Reality check. *Expert Rev Anticancer Ther* 2016; 6: 1-10.
- [73] Ceresoli GL, Bonomi M, Sauta MG. Immune checkpoint inhibitors in malignant pleural mesothelioma: Promises and challenges. *Expert Rev Anticancer Ther* 2016; 16(7): 673-5.
- [74] Roncella S, Laurent S, Fontana V, *et al.* CTLA-4 in mesothelioma patients: Tissue expression, body fluid levels and possible relevance as a prognostic factor. *Cancer Immunol Immunother* 2016; 65(8): 909-17.
- [75] Guazzelli A, Bakker E, Krstic-Demonacos M, Lisanti MP, Sotgia F, Mutti L. Anti-CTLA-4 therapy for malignant mesothelioma. *Immunotherapy* 2017; 9(3): 273-80.
- [76] Calabro L, Morra A, Fonsatti E, *et al.* Efficacy and safety of an intensified schedule of tremelimumab for chemotherapy-resistant malignant mesothelioma: An open-label, single-arm, phase 2 study. *Lancet Respir Med* 2015; 3(4): 301-9.
- [77] Marcq E, Pauwels P, van Meerbeeck JP, Smits EL. Targeting immune checkpoints: New opportunity for mesothelioma treatment? *Cancer Treat Rev* 2015; 41(10): 914-24.
- [78] Alley EW, Molife LR, Santoro A, *et al.* Abstract CT103: Clinical safety and efficacy of pembrolizumab (MK-3475) in patients with malignant pleural

- mesothelioma: Preliminary results from KEYNOTE-028. *Cancer Res* 2015; 75(15 Suppl): CT103.
- [79] Remon J, Reguart N, Corral J, Lianes P. Malignant pleural mesothelioma: New hope in the horizon with novel therapeutic strategies. *Cancer Treat Rev* 2015; 41(1): 27-34.
- [80] Servais EL, Colovos C, Rodriguez L, *et al.* Mesothelin overexpression promotes mesothelioma cell invasion and MMP-9 secretion in an orthotopic mouse model and in epithelioid pleural mesothelioma patients. *Clin Cancer Res* 2012; 18(9): 2478-89.
- [81] Hassan R, Kindler HL, Jahan T, *et al.* Phase II clinical trial of amatuximab, a chimeric antimesothelin antibody with pemetrexed and cisplatin in advanced unresectable pleural mesothelioma. *Clin Cancer Res* 2014; 20(23): 5927-36.
- [82] Jahan T, Hassan R, Alley E, *et al.* 2080_PR: CRS-207 with chemotherapy (chemo) in malignant pleural mesothelioma (MPM): Results from a phase 1b trial. *J Thorac Oncol* 2016; 11(4 Suppl): S156.
- [83] Hassan R, Sharon E, Thomas A, *et al.* Phase 1 study of the antimesothelin immunotoxin SS1P in combination with pemetrexed and cisplatin for front-line therapy of pleural mesothelioma and correlation of tumor response with serum mesothelin, megakaryocyte potentiating factor, and cancer antigen 125. *Cancer* 2014; 120(21): 3311-9.
- [84] Cornelissen R, Hegmans JP, Maat AP, *et al.* Extended tumor control after dendritic cell vaccination with low-dose cyclophosphamide as adjuvant treatment in patients with malignant pleural mesothelioma. *Am J Respir Crit Care Med* 2016; 193(9): 1023-31.
- [85] Tan A, Porcher R, Crequit P, Ravaud P, Dechartres A. Differences in treatment effect size between overall survival and progression-free survival in immunotherapy trials: A meta-epidemiologic study of trials with results posted at ClinicalTrials.gov. *J Clin Oncol* 2017; 35(15): 1686-94.
- [86] Gyawali B, Prasad V. Drugs that lack single-agent activity: Are they worth pursuing in combination? *Nat Rev Clin Oncol* 2017; 14(4): 193-4.
- [87] Gyawali B, Prasad V. Combining drugs and extending treatment: A PFS end point is not sufficient. *Nat Rev Clin Oncol* 2017; 14(9): 521-522.
- [88] Inamoto T, Yamada T, Ohnuma K, *et al.* Humanized anti-CD26 monoclonal antibody as a treatment for malignant mesothelioma tumors. *Clin Cancer Res* 2007; 13(14): 4191-200.
- [89] Dang NH, Torimoto Y, Schlossman SF, Morimoto C. Human CD4 helper T cell activation: Functional involvement of two distinct collagen receptors, 1F7 and VLA integrin family. *J Exp Med* 1990; 172(2): 649-52.
- [90] Amatya VJ, Takeshima Y, Kushitani K, Yamada T, Morimoto C, Inai K. Overexpression of CD26/DPPIV in mesothelioma tissue and mesothelioma cell lines. *Oncol Rep* 2011; 26(6): 1369-75.
- [91] Aoe K, Amatya VJ, Fujimoto N, *et al.* CD26 overexpression is associated with prolonged survival and enhanced chemosensitivity in malignant pleural mesothelioma. *Clin Cancer Res* 2012; 18(5): 1447-56.
- [92] Fujimoto N, Ohnuma K, Aoe K, *et al.* Clinical significance of soluble CD26 in malignant pleural mesothelioma. *PLoS One* 2014; 9(12): e115647.
- [93] Yamazaki H, Naito M, Ghani FI, Dang NH, Iwata S, Morimoto C. Characterization of cancer stem cell properties of CD24 and CD26-positive human malignant mesothelioma cells. *Biochem Biophys Res Commun* 2012; 419(3): 529-36.
- [94] Okamoto T, Iwata S, Yamazaki H, *et al.* CD9 negatively regulates CD26 expression and inhibits CD26-mediated enhancement of invasive potential of malignant mesothelioma cells. *PLoS One* 2014; 9(1): e86671.
- [95] Komiya E, Ohnuma K, Yamazaki H, *et al.* CD26-mediated regulation of periostin expression contributes to migration and invasion of malignant pleural mesothelioma cells. *Biochem Biophys Res Commun* 2014; 447(4): 609-15.
- [96] Yamada K, Hayashi M, Du W, *et al.* Localization of CD26/DPPIV in nucleus and its nuclear translocation enhanced by anti-CD26 monoclonal antibody with anti-tumor effect. *Cancer Cell Int* 2009; 9: 17.
- [97] Yamada K, Hayashi M, Madokoro H, *et al.* Nuclear localization of CD26 induced by a humanized monoclonal antibody inhibits tumor cell growth by modulating of POLR2A transcription. *PLoS One* 2013; 8(4): e62304.
- [98] Hayashi M, Madokoro H, Yamada K, *et al.* A humanized anti-CD26 monoclonal antibody inhibits cell growth of malignant mesothelioma *via* retarded G2/M cell cycle transition. *Cancer Cell Int* 2016; 16: 35.
- [99] Angevin E, Isambert N, Trillet-Lenoir V, *et al.* First-in-human phase 1 of YS110, a monoclonal antibody directed against CD26 in advanced CD26-expressing cancers. *Br J Cancer* 2017; 116: 1926.
- [100] Nakano T, Kuribayashi K, Mikami K. Possible new therapeutic agents for malignant pleural mesothelioma: Anti-CD26 monoclonal antibody and naftopidil. *Expert Rev Anticancer Ther* 2016; 8: 1-3.

Pancreas Fat and β Cell Mass in Humans With and Without Diabetes: An Analysis in the Japanese Population

Rie Murakami,¹ Yoshifumi Saisho,¹ Yuusuke Watanabe,¹ Jun Inaishi,¹ Tami Tsuchiya,¹ Kinsei Kou,^{1,2} Seiji Sato,^{1,3} Minoru Kitago,⁴ Yuko Kitagawa,⁴ Taketo Yamada,^{5,6} and Hiroshi Itoh¹

¹Department of Internal Medicine, Keio University School of Medicine, Tokyo 160-8582, Japan;

²Department of Internal Medicine, Hiratsuka City Hospital, Kanagawa 254-0065, Japan; ³Shinseikai Sato Hospital, Fukushima 965-0877, Japan; ⁴Department of Surgery, Keio University School of Medicine, Tokyo 160-8582, Japan; ⁵Department of Pathology, Keio University School of Medicine, Tokyo 160-8582, Japan; and ⁶Department of Pathology, Saitama Medical University, Saitama 350-0495, Japan

Context: The mechanisms by which β cell mass is reduced in patients with type 2 diabetes remain unclear. It has been postulated that ectopic fat deposits in the pancreas induce β cell apoptosis, leading to the development of diabetes.

Objective: The aim of this study was to clarify the effects of intrapancreatic fat on β and α cell mass in humans with and without diabetes.

Design and Subjects: Using our tissue database, pancreas sections of 72 Japanese nondiabetic (NDM) autopsy cases and 50 diabetic and 49 age- and body mass index (BMI)-matched NDM patients who underwent pancreatic surgery were analyzed. In addition to histological grading, intrapancreatic fat area (IPFA) was quantified as fractional intralobular, but not interlobular, fat area to the whole pancreas area.

Results: Although IPFA was positively correlated with age and BMI, there was no significant difference in IPFA between cases with and without diabetes. Moreover, no association was found between IPFA and either β or α cell area, or glycated hemoglobin.

Conclusion: These findings suggest that pancreatic fat deposits have little effect on β cell mass and the development of diabetes in humans. (*J Clin Endocrinol Metab* 102: 3251–3260, 2017)

Type 2 diabetes (T2DM) is characterized by a deficit of β cell mass (1–4). Although it has been reported that the deficit of β cell mass in patients with T2DM is attributable to an increase in β cell apoptosis (1), the mechanisms that cause β cell apoptosis remain uncertain.

Obesity is an established risk factor for T2DM (5, 6). When fat supply exceeds the capacity of subcutaneous fat storage, spilled-over fat leads to ectopic fat deposits in not only visceral adipose tissue, but also various organs, including the pancreas (7, 8). It has been reported that fatty acids induce β cell apoptosis in *in vitro* and *in vivo*

studies of rodents (9, 10), the so-called lipotoxicity hypothesis. In Zucker Diabetic Fatty rats, β cell dysfunction and apoptosis were accompanied by excess lipid accumulation in islets, suggesting that excess lipid accumulation in the pancreas induces β cell apoptosis (9, 10).

However, conflicting results regarding the relationship between pancreatic fat content and β cell function or dysglycemia have been shown in human studies (7, 11–13). Although pancreatic fat content measured by magnetic resonance imaging or magnetic resonance spectrometry (MRS) has been shown to correlate with β

cell function and/or dysglycemia (14–16), we have previously reported no significant difference in pancreatic fat content measured by computed tomography (CT) imaging between subjects with and without T2DM (17).

One of the major reasons for this inconsistency may be the difficulty of measurement of pancreatic fat content. Because the pancreas is surrounded by fat tissue in the retroperitoneal space, it is difficult to precisely exclude the fat outside the pancreas. Although attempts to improve the accuracy of pancreatic fat measurement using imaging tools have been made (14, 18, 19), it remains impossible to completely distinguish interlobular fat (*i.e.*, fat outside the pancreas) from intralobular fat of the pancreas due to the intricate lobular structure of the pancreas. Moreover, in contrast to the liver, in which fat is diffusely distributed within hepatocytes, pancreatic fat is mainly present in adipocytes within the pancreas (20), and thereby the distribution of fat is not homogeneous within the pancreas, which accounts for the difficulty of assessment of pancreatic fat content by imaging methods.

In view of these limitations of imaging studies, we conducted a histological evaluation of intrapancreatic fat content using pancreas samples from 72 autopsy cases and 50 patients with and 49 without diabetes who underwent pancreatic surgery in an attempt to gain more insight into the relationship between pancreatic fat and β cell mass and diabetes.

Research Design and Methods

Subjects

This study was approved by the Ethics Committee of the Keio University School of Medicine. The cases have been reported in our prior studies (3, 21). For autopsy cases, specimens of pancreas obtained at autopsy were acquired with the permission of the bereaved families. For patients who underwent pancreatic surgery, written informed consent was obtained from each patient, whereas it was waived for patients who had

discontinued hospital visits at the time of study enrollment ($n = 40$).

A total of 72 autopsy cases without diabetes [nondiabetic (NDM)-1 group] and 99 patients who underwent pancreatic surgery [50 diabetic (DM) patients and 49 patients without diabetes (NDM-2 group)] were included in this study. The characteristics of the cases, which have been previously reported (3, 21), are summarized in Table 1. All subjects were Japanese.

Autopsy cases

Potential cases were first identified by retrospective analysis of the Keio University autopsy database. To be included, cases were required to have (1) been aged 20 to 69 years, (2) had a full autopsy within 24 hours of death, (3) medical information prior to death, (4) no history of diabetes, pancreatitis, pancreatic tumor, or pancreatic surgery, (5) no use of glucocorticoids, and (6) pancreatic tissue stored that was of adequate size and quality. Cases were excluded if pancreatic tissue had undergone autolysis.

Surgical cases

As previously described (3), subjects who underwent pancreatic surgery and whose resected pancreas sample contained adequate normal pancreas for histological analysis were included in the study. Of these, 41 patients had been diagnosed with T2DM before the diagnosis of pancreatic tumors, and eight patients were diagnosed with pancreatic cancer and diabetes at the same time. There was no case of type 1 diabetes or case in which glutamic acid decarboxylase antibody was positive.

Glycemic markers

In autopsy cases, glycated hemoglobin (HbA1c) measured within 1 year prior to death was obtained from the medical records (21). In patients who underwent pancreatic surgery, information including HbA1c, casual plasma glucose, and serum C-peptide immunoreactivity levels was obtained from the medical records, as previously described (3). HbA1c was measured by high-performance liquid chromatography and expressed as National Glycohemoglobin Standardization Program and International Federation of Clinical Chemistry values. Serum C-peptide immunoreactivity was measured by chemiluminescent enzyme immunoassay.

Table 1. Characteristics of Subjects

	Total	Autopsy Cases		Surgical Cases
		NDM-1	NDM-2	DM
N	171	72	50	49
Sex (male/female)	107/64	46/26	26/24	35/14
Age (y)	58 \pm 15	47 \pm 12	64 \pm 14	67 \pm 9
Height (m)	1.63 \pm 0.09	1.65 \pm 0.09	1.61 \pm 0.08	1.63 \pm 0.09
Weight (kg)	61.9 \pm 14.3	66.2 \pm 16.7	58.6 \pm 10.5	58.9 \pm 12.2
BMI (kg/m ²)	23.0 \pm 4.1	24.1 \pm 5.0	22.5 \pm 2.7	21.9 \pm 3.5
Casual plasma glucose (mmol/L) ^a	6.4 \pm 2.1	5.2 \pm 1.0	6.2 \pm 1.2	8.3 \pm 2.5
HbA1c (%) ^a	6.3 \pm 1.6	5.3 \pm 0.7	5.6 \pm 0.5	7.8 \pm 1.6
HbA1c (mmol/mol) ^a	45 \pm 17	34 \pm 7	38 \pm 6	61 \pm 18
Pancreas head/body or tail (n)	27/144	7/65	6/44	14/35

Data are expressed as mean \pm SD. Note that NDM-2 and DM groups were matched for age and BMI, as previously reported (3).

^aCasual plasma glucose and HbA1c levels were measured in 169 cases and 132 cases, respectively.

Pancreatic tissue processing

The pancreas was fixed in formaldehyde and then embedded in paraffin for subsequent analysis. Autopsy specimens were sampled from the body or tail portion of the pancreas, except for seven specimens sampled from the head of the pancreas. Seventy-nine and 20 surgical specimens were sampled from the body or tail portion and the head portion, respectively. Five-micrometer sections were cut from the tumor-free region and stained for light microscopy as follows: (1) with hematoxylin-eosin, (2) for insulin (peroxidase staining) with hematoxylin, (3) for glucagon with hematoxylin, (4) for insulin and Ki67 for assessment of β cell replication, and (5) for insulin and single-stranded DNA or cleaved poly(adenosine 5'-diphosphate-ribose) polymerase-1 for assessment of β cell apoptosis, as previously described (3, 21).

Morphometric analysis

As previously described (3, 21, 22), to quantify fractional β cell area (BCA), the entire pancreatic section was imaged at $\times 200$ magnification ($\times 20$ objective) using a Mirax Scan and Mirax Viewer (Carl Zeiss MicroImaging GmbH, Göttingen, Germany). The ratio of BCA to total pancreas area was digitally measured using Image Pro Plus software (Media Cybernetics, Silver Springs, MD). Likewise, the ratio of α cell area (ACA) to total pancreas area was also digitally measured, and the ratio of ACA to BCA was determined in each case. Intraobserver coefficient of variance (computed in five cases studied on five occasions) and interobserver variance were approximately 7% and 12%, respectively (3, 21). All measurements were conducted twice, and the mean of the two measurements was used.

To conduct further morphometric analysis, scattered β cells, insulin-positive duct cells, and β cell replication were quantified in randomly selected areas of the pancreas that contained more than 100 islets in each case, using a Mirax Viewer (Carl Zeiss MicroImaging GmbH). Scattered β cells were defined as a cluster of three or fewer β cells in acinar tissue, and the density of scattered β cells was determined as the number of scattered β cells/pancreas area (mm^2). Likewise, the density of islets and individual islet size were also determined in the same area. Insulin-positive duct cells were also counted and expressed as the number of insulin-positive duct cells/pancreas area (mm^2). The frequency of β cell replication was expressed as the percentage of islets.

Assessment of intrapancreatic fat content

Intrapancreatic fat content was graded based on histological evaluation [none (–) to severe (+++)] (Fig. 1). Because pancreatic fat is extracted during specimen dehydration, intrapancreatic fat appears as lobulated spaces within the pancreas lobes. These intrapancreatic adipocytes were confirmed by perilipin staining (antiperilipin A antibody-carboxyterminal end; ab61682, Abcam, Cambridge, United Kingdom). These intrapancreatic fat areas (IPFAs) were also quantified using Image Pro Plus software (Media Cybernetics). Only pancreatic fat within parenchymal tissue (*i.e.*, intralobular fat), but not interlobular fat (*i.e.*, fat outside the pancreas), was measured as IPFA. Thus, IPFA was calculated as a fraction of total pancreatic area.

Statistical analysis

Data are presented as mean \pm standard deviation (SD) in the text and tables unless otherwise indicated. Non-normally

distributed data are presented as median and interquartile range (IQR). Mann-Whitney *U* test was used to assess differences between two groups, and comparisons among the three groups were performed by Kruskal-Wallis test. Spearman correlation analysis was carried out for correlation analysis. Multivariate analysis was used to adjust for confounding factors such as age and body mass index (BMI). All analyses were performed using the Statistical Package for the Social Sciences (version 23; SPSS, Chicago, IL), and $P < 0.05$ was considered statistically significant.

Results

Intrapancreatic fat content in subjects with and without diabetes

Intrapancreatic adipocytes were diffusely distributed within the pancreatic lobes, and as the number of adipocytes increased, they formed clusters, which were readily distinguishable from other structures such as vessels, ducts, and interlobular adipocytes (Fig. 1). Adipocytes were not observed within the islets. Histological grade of intrapancreatic fat content was closely correlated with IPFA (Table 2). IPFA varied among subjects (median, 0.51%; IQR, 0.17% to 1.27%). There was no difference in IPFA between samples from the head portion of the pancreas ($n = 27$) and those from the body or

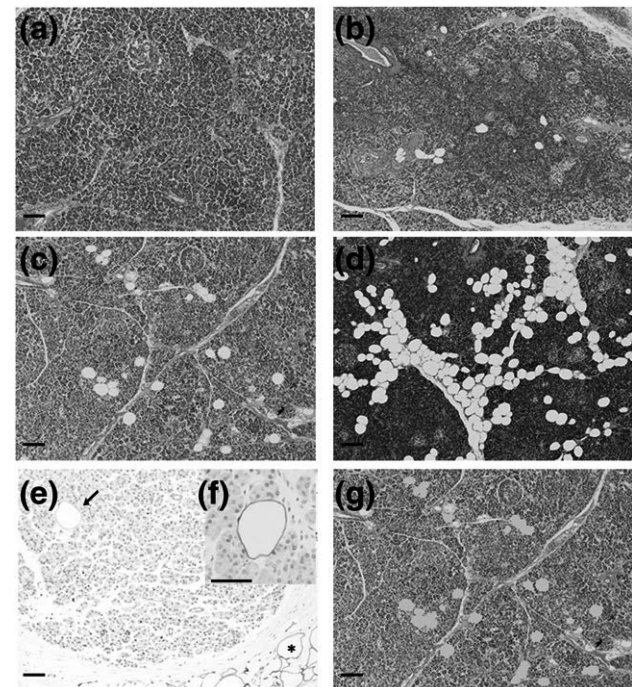


Figure 1. (a-d) Representative photomicrographs of histological grades of intrapancreatic fat content. (a) Grade (–). (b) Grade (+). (c) Grade (++) (d) Grade (+++). (e) Intrapancreatic adipocytes were confirmed by perilipin staining (brown). Interlobular pancreatic adipocytes are indicated by asterisk. (f) Higher magnification ($\times 40$ objective) of intrapancreatic adipocyte. (g) IPFA was carefully quantified as a fraction of IPFA (shown in orange), but not interlobular fat area, to the total pancreas area. Scale bar = 100 μm .

Table 2. Characteristics of Subjects According to Histological Grade of Intrapancreatic Fat Content

Intrapancreatic Fat Content	(-)	(+)	(++) to (+++)	P ^a
N (%)	33 (19)	80 (47)	58 (34)	
Sex (male/female)	24/9	46/34	37/21	0.31
Age (y)	54 ± 15	56 ± 16	61 ± 13	0.04
Height (m)	1.64 ± 0.09	1.63 ± 0.09	1.63 ± 0.09	0.82
Weight (kg)	60.0 ± 13.4	60.1 ± 11.5	65.7 ± 17.5	0.04
BMI (kg/m ²)	21.9 ± 3.3	22.4 ± 3.2	24.5 ± 5.1	<0.01
DM (%)	39	19	36	0.08
Casual plasma glucose (mmol/L) ^b	6.6 ± 2.3	6.2 ± 2.1	6.7 ± 1.9	0.28
HbA1c (%) ^b	6.7 ± 1.8	6.1 ± 1.5	6.4 ± 1.4	0.22
HbA1c (mmol/mol) ^b	50 ± 20	43 ± 17	46 ± 15	0.22
IPFA (%)	0.07 (0.04–0.17)	0.40 (0.19–0.66)	1.82 (0.97–2.66)	<0.01

Data are expressed as mean ± SD or median (IQR).

^aP for Kruskal-Wallis test or χ^2 test among three groups.

^bCasual plasma glucose and HbA1c levels were measured in 169 and 132 cases, respectively.

tail portion of the pancreas (n = 144; median, 0.50%; IQR, 0.17% to 1.09% vs median, 0.52%; IQR, 0.17% to 1.31%; P = 0.61) [Supplemental Fig. 2(a)]. There was no difference in IPFA between autopsy cases (NDM-1) and surgical cases (NDM-2) (median, 0.45%; IQR, 0.12% to

1.20% vs median, 0.51%; IQR, 0.26 to 0.99; P = 0.39) [Fig. 2(a)]. Although we previously reported a significant reduction in BCA in patients with diabetes compared with age- and BMI-matched patients without diabetes (NDM-2) (1.48% ± 1.08% vs 0.80% ± 0.54%, P < 0.001) (3),

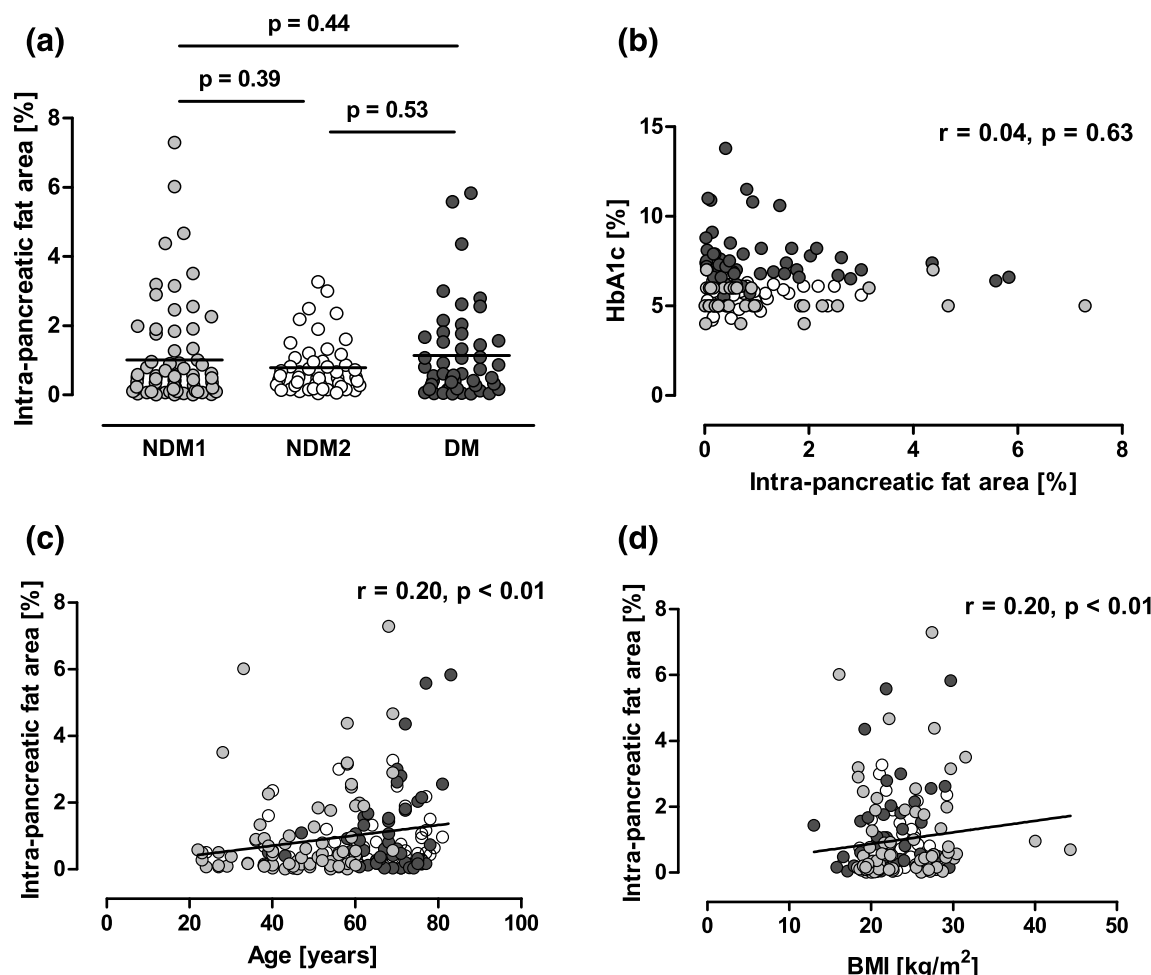


Figure 2. (a) IPFA in autopsy cases without diabetes (NDM-1), surgical cases with diabetes (DM), and surgical cases without diabetes matched for age and BMI (NDM-2). (b–d) Correlations between IPFA and (b) HbA1c, (c) age, and (d) BMI. Light-gray circles show autopsy cases. Dark-gray and white circles show surgical cases with and without diabetes, respectively.

there was no difference in IPFA between the two groups (median, 0.51%; IQR, 0.04% to 3.27% vs median, 0.61%; IQR, 0.03% to 5.83%; $P = 0.53$) [Fig. 2(a)]. In view of the fact that there was no significant difference in intrapancreatic fat content either between autopsy and surgical cases or between cases with and without diabetes, we conducted subsequent analyses in the combined cases as well as within each group.

Factors associated with intrapancreatic fat content

Characteristics of the subjects according to the histological grade of intrapancreatic fat content are shown in Table 2 and Supplemental Table 1 for surgical cases. Histological grade of intrapancreatic fat content was associated with age and BMI, but not with HbA1c or plasma glucose level. As well as histological grade, IPFA was significantly correlated with age and BMI in the total cases (both $r = 0.20$, $P < 0.01$) [Fig. 2(c) and 2(d)], but not with HbA1c [Fig. 2(b)]. In surgical cases, the duration of obesity as well as current BMI, but not maximum BMI, tended to associate with intrapancreatic fat content ($P = 0.07$ and 0.66, respectively) (Supplemental Table 1). The results were not markedly changed when the analysis was conducted only in the DM group (Supplemental Table 2). There was no significant correlation between IPFA and casual plasma glucose or serum C-peptide immunoreactivity level (Supplemental Table 2; Supplemental Fig. 1).

Relationships between intrapancreatic fat content and BCA, ACA, and islet morphology

There was no difference in either BCA or ACA among the groups according to the histological grade of intrapancreatic fat content [Fig. 3(a) and 3(b)], and there was no significant correlation between IPFA and BCA or ACA ($r = 0.05$, $P = 0.56$ and $r = -0.12$, $P = 0.12$) [Fig. 3(f) and 3(g)]. ACA/BCA ratio was also not associated with histological grade or IPFA [Fig. 3(c) and 3(i)]. When the NDM-1, NDM-2, and DM groups were analyzed separately (Supplemental Table 2), BCA and ACA were positively correlated with IPFA in the DM group ($r = 0.30$, $P = 0.04$ and $r = 0.30$, $P = 0.04$, respectively), and ACA was negatively correlated with IPFA in the NDM-1 group ($r = -0.28$, $P = 0.02$). However, the significant correlations were attenuated after adjustment for age and BMI (Supplemental Table 2).

Difference in mean islet size was also statistically significant among the histological grading groups ($P = 0.03$) [Fig. 3(e)], but no association between IPFA and mean islet size was detected ($r = 0.00$, $P = 0.99$) [Fig. 3(j)]. These results were not changed when the analyses were conducted in each group separately (*i.e.*, NDM-1,

NDM-2, and DM groups) (Supplemental Table 2). There was no association between IPFA and islet density ($r = -0.10$, $P = 0.21$) [Fig. 3(i)].

Relationships between intrapancreatic fat content and markers of β cell turnover

Intrapancreatic fat content assessed as histological grade or IPFA was not associated with either frequency of β cell replication, insulin-positive duct cells, or scattered β cells (Fig. 4). No β cell apoptosis was observed in these cases, as previously reported (3, 21).

Discussion

The current study, applying histological evaluation of intrapancreatic fat content, showed the following: (1) There was no significant difference in intrapancreatic fat content between subjects with and without diabetes. (2) No association between intrapancreatic fat content and β cell mass, islet morphology, or markers of β cell turnover was observed. (3) There was no correlation between intrapancreatic fat content and HbA1c level. (4) Intrapancreatic fat content increased with age and obesity in humans.

T2DM is characterized by a deficit of β cells, presumably due to an increase in β cell apoptosis (1). However, the mechanisms by which β cell apoptosis increases in patients with T2DM remain unclear. A longitudinal cohort in the UK Prospective Diabetes Study suggested that β cell dysfunction begins over 10 years before the onset of T2DM (23). Reduced β cell mass in patients with prediabetes has also been reported (1, 24, 25), suggesting that β cell loss occurs even before the onset of T2DM.

Ectopic fat deposits are a hallmark of metabolic syndrome and T2DM (8, 26). Rodent studies have suggested the possibility that ectopic fat deposits in the pancreas induce β cell apoptosis and the development of hyperglycemia (9, 10), the so-called lipotoxicity hypothesis. Since then, the association between pancreas fat content and β cell function or glucose tolerance status has been actively investigated (7, 11–13).

Tushuizen *et al.* (14) first reported, using MRS, that pancreatic fat content was increased in patients with T2DM, and pancreatic fat content was negatively associated with β cell function in NDM subjects. However, the small sample size (12 with T2DM, 24 without diabetes) with an almost significant difference in BMI between the two groups has been pointed out as a limitation of that study (27). We have previously reported, using CT scan images of over 2000 subjects, that there was no significant difference in pancreas fat content between age-, sex-, and BMI-matched subjects with and without T2DM (17).

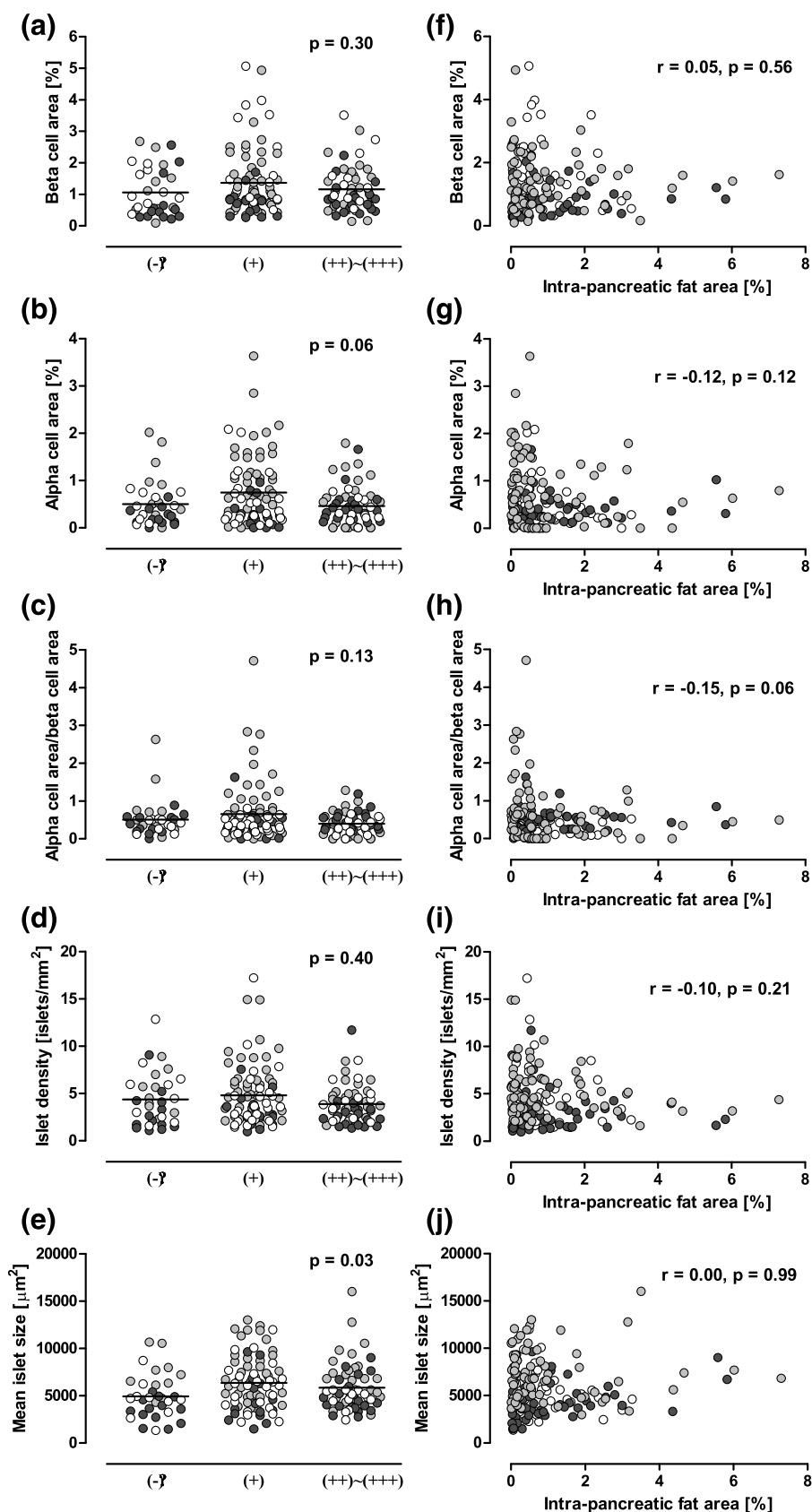


Figure 3. (a–e) Comparisons among groups according to histological grade of intrapancreatic fat content: (a) BCA, (b) ACA, (c) ACA/BCA ratio, (d) islet density, and (e) mean islet size. (f–j) Correlations between IPFA and (f) BCA, (g) ACA, (h) ACA/BCA ratio, (i) islet density, and (j) mean islet size. Light-gray circles show autopsy cases. Dark-gray and white circles show surgical cases with and without diabetes, respectively.

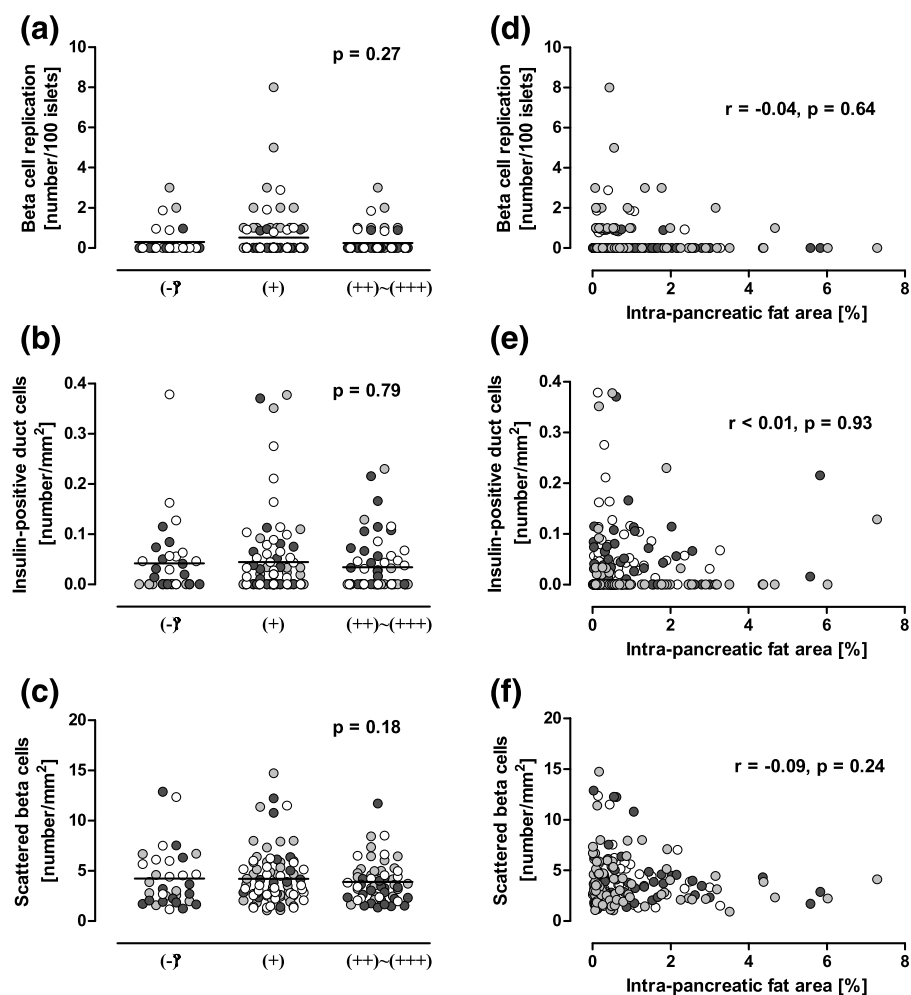


Figure 4. (a–c) Comparisons among three groups according to histological grade of intrapancreatic fat content: frequency of (a) β cell replication, (b) insulin-positive duct cells, and (c) scattered β cells. (d–f) Correlations between IPFA and frequency of (d) β cell replication, (e) insulin-positive duct cells, and (f) scattered β cells. Light-gray circles show autopsy cases. Dark-gray and white circles show surgical cases with and without diabetes, respectively.

Furthermore, these inconsistent results of imaging studies may be in part due to difficulties in accurate measurement of pancreatic fat (11). The pancreas is surrounded by fat in the retroperitoneal space and consists of an intricate lobular structure, making it inevitably difficult to distinguish intrapancreatic fat from fat outside the pancreas. In this study, to overcome these limitations of imaging studies, by conducting histological assessment of intrapancreatic fat content, we reported that there was no relationship between intrapancreatic fat content and β cell mass or dysglycemia in humans.

Our findings are also in line with prior histological studies assessing pancreas fat in subjects with diabetes, which have shown no difference in pancreatic fat content in subjects with and without T2DM (17, 20, 28, 29). Our study applied quantification of intrapancreatic fat content in a relatively large number of subjects with a wide range of age and BMI, and we believe our findings are more objective and robust compared with those of these prior histological studies. Our conclusion that there is no

association between intrapancreatic fat content and diabetes is also supported by the finding of no association between intrapancreatic fat content and β cell mass.

Recent rodent studies have suggested that dedifferentiation of β cells and conversion from β to α cells is one of the mechanisms of β cell loss in T2DM (30), although histological studies in humans have suggested that β cell dedifferentiation has only a minor role, and presumably β cell apoptosis is a major cause of β cell loss in patients with T2DM (31), in line with the observation of reduced islet size in patients with T2DM (3, 32, 33). In this study, we found no significant relationship between IPFA and either BCA or ACA/BCA ratio, suggesting that intrapancreatic fat content is unlikely to be associated with this intriguing possibility.

Recently, several studies showing no association between pancreatic fat and T2DM have also been published. Begovatz *et al.* (18) conducted an assessment of intrapancreatic fat by magnetic resonance imaging/MRS in 56 subjects with and without dysglycemia. In that

study, they measured intrapancreatic fat carefully after excluding the fat outside the pancreas and found no association between intrapancreatic fat content and β cell function or dysglycemia (18). Yamazaki *et al.* (34) conducted a longitudinal study showing that pancreatic fat assessed by CT imaging was not associated with the development of T2DM independently of obesity. Moreover, whereas it has been reported that the improvement of dysglycemia by a very low-calorie diet in adults with T2DM was associated with improvement of pancreatic fat content (35), Gow *et al.* (36) did not find such an association between pancreatic fat and improvement of hyperglycemia during treatment with a very low-calorie diet in young people with T2DM. Taking these results together, to date, there is no concrete evidence for a causal association of pancreatic fat with the development of diabetes. Further studies to improve the accuracy of intrapancreatic fat measurement *in vivo* in humans are warranted. Also, because intra- and interlobular pancreatic fat content are both increased with aging and obesity, future studies should be carefully conducted to exclude these important confounders.

As with other studies, our study was not free from limitations. First, we assessed intrapancreatic fat in a section of the pancreas. Intrapancreatic fat content may differ among different portions of the pancreas. However, it has been reported that the proportion of fat content did not differ among the head, body, and tail portions of the pancreas (37, 38), and we found no significant difference in IPFA between samples from the head of the pancreas and those from the body or tail of the pancreas [Supplemental Fig. 2(a)]. Also, the results did not change when the analyses were conducted using only samples from the body or tail of the pancreas ($n = 144$, data not shown). It should also be noted that β cell mass was assessed as fractional BCA in a section of the pancreas, although it is widely used as a measure of β cell mass, as discussed previously (3, 21). Nonetheless, it should be kept in mind that the individual values may not be truly representative for any particular pancreas, although we believe that the overall conclusions are valid because of the large number of subjects studied. Whereas increased pancreatic fat infiltration has been reported in patients with pancreatic ductal adenocarcinoma (39), we found no significant difference in IPFA between patients with and without pancreatic cancer (median, 0.57%; IQR, 0.33% to 1.14% vs median, 0.56%; IQR, 0.20% to 1.35%; $P = 0.94$) [Supplemental Fig. 2(b)]. Second, the histological measurement of fat was indirect, because fat is removed during tissue processing and section staining. However, the morphological features of adipocytes were readily identified, and we also confirmed the presence of adipocytes in the pancreas by perilipin staining (Fig. 1).

We also assessed the intrapancreatic fat content using a grading system and confirmed consistent results between the two methods. Although we did not assess lipid content within islets, close correlations among IPFA, pancreatic triacylglycerol content (20), and islet triacylglycerol content (9) have been reported in rodent models. Thus, it is reasonable to assume that IPFA reflects islet triglyceride content. Third, we could not assess β cell function in most of the subjects. Thus, although we found no association between IPFA and BCA, we cannot exclude the possibility that IPFA is associated with β cell dysfunction. However, the absence of association between IPFA and HbA1c, C-peptide immunoreactivity, or presence of diabetes suggests that the effect of IPFA on β cell function is, if any, modest. Although we could not exclude the possibility that patients with pancreatic diabetes, but not T2DM, were included in this study, we found no significant difference in IPFA between subjects with duration of diabetes ≤ 3 years ($n = 23$) and those with duration of diabetes > 3 years ($n = 26$; median, 0.61%; IQR, 0.17% to 1.53% vs median, 0.59%; IQR, 0.26% to 1.71%; $P = 0.41$). Finally, this study included only Japanese subjects. We have reported that there was no significant correlation between β cell mass and BMI in Japanese subjects with and without T2DM (3, 21), suggesting that the adaptive increase in β cell mass in response to obesity is minimal in the Japanese population. Thus, our findings may not be applicable to other ethnicities, and future studies including multiple ethnic groups are needed.

In conclusion, there was no correlation between intrapancreatic fat content and β cell mass or turnover, or dysglycemia. These findings suggest that ectopic fat deposits in the pancreas may not be responsible for the development of diabetes in humans.

Acknowledgments

We thank Yuko Madokoro, Department of Pathology, Keio University School of Medicine, for technical assistance and Wendy Gray for editing the manuscript.

Address all correspondence and requests for reprints to: Yoshifumi Saisho, MD, PhD, Department of Internal Medicine, Keio University School of Medicine, 35 Shinanomachi, Shinjuku-ku, Tokyo 160-8582, Japan. E-mail: ysaisho@keio.jp.

This study was supported by funding from the Japan Diabetes Foundation, Keio Gijuku Academic Development Funds, and Japan Society for the Promotion of Science Grants-in-Aid for Scientific Research (JSPS KAKENHI) Grant Number JP15K09399 (to Y.S.).

Author contributions: Y.S. designed and performed the research. R.M., J.I., and K.K. contributed to the data analysis. R.M., Y.S., Y.W., J.I., T.T., K.K., S.S., M.K., Y.K., T.Y., and H.I.

contributed to the discussion and reviewed and edited the manuscript. Y.S. is the guarantor of this work and, as such, had full access to all the data in the study and takes responsibility for the integrity of the data and the accuracy of the data analysis.

Disclosure Summary: The authors have nothing to disclose.

References

1. Butler AE, Janson J, Bonner-Weir S, Ritzel R, Rizza RA, Butler PC. Beta-cell deficit and increased beta-cell apoptosis in humans with type 2 diabetes. *Diabetes*. 2003;52(1):102–110.
2. Rahier J, Guiot Y, Goebel RM, Sempoux C, Henquin JC. Pancreatic beta-cell mass in European subjects with type 2 diabetes. *Diabetes Obes Metab*. 2008;10(Suppl 4):32–42.
3. Inaishi J, Saisho Y, Sato S, Kou K, Murakami R, Watanabe Y, Kitago M, Kitagawa Y, Yamada T, Itoh H. Effects of obesity and diabetes on alpha- and beta-cell mass in surgically resected human pancreas. *J Clin Endocrinol Metab*. 2016;101(7):2874–2882.
4. Saisho Y. β -cell dysfunction: its critical role in prevention and management of type 2 diabetes. *World J Diabetes*. 2015;6(1):109–124.
5. Guh DP, Zhang W, Bansback N, Amarsi Z, Birmingham CL, Anis AH. The incidence of co-morbidities related to obesity and overweight: a systematic review and meta-analysis. *BMC Public Health*. 2009;9:88.
6. Hu Y, Bhupathiraju SN, de Koning L, Hu FB. Duration of obesity and overweight and risk of type 2 diabetes among US women. *Obesity (Silver Spring)*. 2014;22(10):2267–2273.
7. van Raalte DH, van der Zijl NJ, Diamant M. Pancreatic steatosis in humans: cause or marker of lipotoxicity? *Curr Opin Clin Nutr Metab Care*. 2010;13(4):478–485.
8. Sattar N, Gill JM. Type 2 diabetes as a disease of ectopic fat? *BMC Med*. 2014;12:123.
9. Lee Y, Lingvay I, Szczepaniak LS, Ravazzola M, Orci L, Unger RH. Pancreatic steatosis: harbinger of type 2 diabetes in obese rodents. *Int J Obes*. 2010;34(2):396–400.
10. Lee Y, Hirose H, Ohneda M, Johnson JH, McGarry JD, Unger RH. Beta-cell lipotoxicity in the pathogenesis of non-insulin-dependent diabetes mellitus of obese rats: impairment in adipocyte-beta-cell relationships. *Proc Natl Acad Sci USA*. 1994;91(23):10878–10882.
11. Saisho Y. Pancreas volume and fat deposition in diabetes and normal physiology: consideration of the interplay between endocrine and exocrine pancreas. *Rev Diabet Stud*. 2016;13(2-3):132–147.
12. Pezzilli R, Calzulli L. Pancreatic steatosis: is it related to either obesity or diabetes mellitus? *World J Diabetes*. 2014;5(4):415–419.
13. Smits MM, van Geenen EJM. The clinical significance of pancreatic steatosis. *Nat Rev Gastroenterol Hepatol*. 2011;8(3):169–177.
14. Tushuizen ME, Bunck MC, Pouwels PJ, Bontemps S, van Waesberghe JH, Schindhelm RK, Mari A, Heine RJ, Diamant M. Pancreatic fat content and beta-cell function in men with and without type 2 diabetes. *Diabetes Care*. 2007;30(11):2916–2921.
15. Szczepaniak LS, Victor RG, Mathur R, Nelson MD, Szczepaniak EW, Tyer N, Chen I, Unger RH, Bergman RN, Lingvay I. Pancreatic steatosis and its relationship to β -cell dysfunction in humans: racial and ethnic variations. *Diabetes Care*. 2012;35(11):2377–2383.
16. Heni M, Machann J, Staiger H, Schwenzer NF, Peter A, Schick F, Claussen CD, Stefan N, Häring H-U, Fritsche A. Pancreatic fat is negatively associated with insulin secretion in individuals with impaired fasting glucose and/or impaired glucose tolerance: a nuclear magnetic resonance study. *Diabetes Metab Res Rev*. 2010;26(3):200–205.
17. Saisho Y, Butler AE, Meier JJ, Monchamp T, Allen-Auerbach M, Rizza RA, Butler PC. Pancreas volumes in humans from birth to age one hundred taking into account sex, obesity, and presence of type-2 diabetes. *Clin Anat*. 2007;20(8):933–942.
18. Begovatz P, Koliaki C, Weber K, Strassburger K, Nowotny B, Nowotny P, Müsseg K, Bunke J, Pacini G, Szendrodi J, Roden M. Pancreatic adipose tissue infiltration, parenchymal steatosis and beta cell function in humans. *Diabetologia*. 2015;58(7):1646–1655.
19. Lingvay I, Esser V, Legendre JL, Price AL, Wertz KM, Adams-Huet B, Zhang S, Unger RH, Szczepaniak LS. Noninvasive quantification of pancreatic fat in humans. *J Clin Endocrinol Metab*. 2009;194(10):4070–4076.
20. Pinnick KE, Collins SC, Londos C, Gauguier D, Clark A, Fielding BA. Pancreatic ectopic fat is characterized by adipocyte infiltration and altered lipid composition. *Obesity (Silver Spring)*. 2008;16(3):522–530.
21. Kou K, Saisho Y, Satoh S, Yamada T, Itoh H. Change in β -cell mass in Japanese nondiabetic obese individuals. *J Clin Endocrinol Metab*. 2013;98(9):3724–3730.
22. Saisho Y, Butler AE, Manesso E, Flashoff D, Rizza RA, Butler PC. β -cell mass and turnover in humans: effects of obesity and aging. *Diabetes Care*. 2013;36(1):111–117.
23. U.K. Prospective Diabetes Study Group. U.K. prospective diabetes study 16. Overview of 6 years' therapy of type II diabetes: a progressive disease. *Diabetes*. 1995;44(11):1249–1258.
24. Meier JJ, Breuer TG, Bonadonna RC, Tannapfel A, Uhl W, Schmidt WE, Schrader H, Menge BA. Pancreatic diabetes manifests when beta cell area declines by approximately 65% in humans. *Diabetologia*. 2012;55(5):1346–1354.
25. Yoneda S, Uno S, Iwahashi H, Fujita Y, Yoshikawa A, Kozawa J, Okita K, Takiuchi D, Eguchi H, Nagano H, Imagawa A, Shimomura I. Predominance of β -cell neogenesis rather than replication in humans with an impaired glucose tolerance and newly diagnosed diabetes. *J Clin Endocrinol Metab*. 2013;98(5):2053–2061.
26. Kusminski CM, Shetty S, Orci L, Unger RH, Scherer PE. Diabetes and apoptosis: lipotoxicity. *Apoptosis*. 2009;14(12):1484–1495.
27. Saisho Y, Butler AE, Butler PC. 2008 Pancreatic fat content and beta-cell function in men with and without type 2 diabetes: response to Tushuizen et al. *Diabetes Care*. 2008;31(5):e38–e39.
28. Olsen TS. Lipomatosis of the pancreas in autopsy material and its relation to age and overweight. *Acta Pathol Microbiol Scand [A]*. 1978;86A(5):367–373.
29. Clark A, Wells CA, Buley ID, Cruickshank JK, Vanhegan RI, Matthews DR, Cooper GJ, Holman RR, Turner RC. Islet amyloid, increased A-cells, reduced B-cells and exocrine fibrosis: quantitative changes in the pancreas in type 2 diabetes. *Diabetes Res*. 1988;9(4):151–159.
30. Talchai C, Xuan S, Lin HV, Sussel L, Accili D. Pancreatic β cell dedifferentiation as a mechanism of diabetic β cell failure. *Cell*. 2012;150(6):1223–1234.
31. Butler AE, Dhawan S, Hoang J, Cory M, Zeng K, Fritsch H, Meier JJ, Rizza RA, Butler PC. Beta-cell deficit in obese type 2 diabetes, a minor role of beta-cell dedifferentiation and degranulation. *J Clin Endocrinol Metab*. 2016;101(2):523–532.
32. Sato S, Saisho Y, Inaishi J, Kou K, Murakami R, Yamada T, Itoh H. Effects of glucocorticoid treatment on beta- and alpha-cell mass in Japanese adults with and without diabetes. *Diabetes*. 2015;64(8):2915–2927.
33. Westermark P, Wilander E. The influence of amyloid deposits on the islet volume in maturity onset diabetes mellitus. *Diabetologia*. 1978;15(5):417–421.
34. Yamazaki H, Tsuboya T, Katanuma A, Kodama Y, Tauchi S, Dohke M, Maguchi H. Lack of independent association between fatty pancreas and incidence of type 2 diabetes mellitus: 5-year Japanese cohort study. *Diabetes Care*. 2016;39(10):1677–1683.
35. Lim EL, Hollingsworth KG, Aribisala BS, Chen MJ, Mathers JC, Taylor R. Reversal of type 2 diabetes: normalisation of beta cell function in association with decreased pancreas and liver triacylglycerol. *Diabetologia*. 2011;54(10):2506–2514.
36. Gow ML, Baur LA, Johnson NA, Cowell CT, Garnett SP. Reversal of type 2 diabetes in youth who adhere to a very-low-energy diet: a pilot study. *Diabetologia*. 2017;60(3):406–415.

37. Li J, Xie Y, Yuan F, Song B, Tang C. Noninvasive quantification of pancreatic fat in healthy male population using chemical shift magnetic resonance imaging: effect of aging on pancreatic fat content. *Pancreas*. 2011;40(2):295–299.
38. Idilman IS, Tuzun A, Savas B, Elhan AH, Celik A, Idilman R, Karcaaltincaba M. Quantification of liver, pancreas, kidney, and vertebral body MRI-PDFF in non-alcoholic fatty liver disease. *Abdom Imaging*. 2015;40(6):1512–1519.
39. Hori M, Takahashi M, Hiraoka N, Yamaji T, Mutoh M, Ishigamori R, Furuta K, Okusaka T, Shimada K, Kosuge T, Kanai Y, Nakagama H. Association of pancreatic fatty infiltration with pancreatic ductal adenocarcinoma. *Clin Transl Gastroenterol*. 2014;5:e53.



A novel phenylphthalimide derivative, pegylated TC11, improves pharmacokinetic properties and induces apoptosis of high-risk myeloma cells via G2/M cell-cycle arrest



Shuji Aida ^a, Masashi Hozumi ^a, Daiju Ichikawa ^a, Kazuki Iida ^a, Yuko Yonemura ^b, Noriko Tabata ^b, Taketo Yamada ^c, Maiko Matsushita ^a, Takeshi Sugai ^d, Hiroshi Yanagawa ^{a, b}, Yutaka Hattori ^{a, *}

^a Clinical Physiology & Therapeutics, Keio University Faculty of Pharmacy, Tokyo, Japan

^b IDAC Theranostics Inc., Tokyo, Japan

^c Department of Pathology, Saitama Medical University, Saitama, Japan

^d Organic and Biocatalytic Chemistry, Keio University Faculty of Pharmacy, Tokyo, Japan

ARTICLE INFO

Article history:

Received 29 August 2017

Accepted 31 August 2017

Available online 1 September 2017

Keywords:

Multiple myeloma
Pegylation of low molecule compounds
Phenylphthalimide derivative
G2/M arrest
Celebron

ABSTRACT

Despite the development of new drugs for multiple myeloma (MM), the prognosis of MM patients with high-risk cytogenetic abnormalities such as t (4; 14) and del17p remains poor. We reported that a novel phenylphthalimide derivative, TC11, induced apoptosis of MM cells *in vitro* and *in vivo*, and TC11 directly bound to α -tubulin and nucleophosmin-1 (NPM1). However, TC11 showed low water solubility and poor pharmacokinetic properties. Here we synthesized a water-soluble TC11-derivative, PEG(E)-TC11, in which HOEtO-TC11 is pegylated with PEG through an ester bond, and we examined its anti-myeloma activity. We observed that PEG(E)-TC11 and its hydrolyzed product, HOEtO-TC11, induced G2/M arrest and the apoptosis of MM cells. Intraperitoneal administration of PEG(E)-TC11 to xenografted mice revealed improved pharmacokinetic properties and significantly delayed tumor growth. TC11 and its derivatives did not bind to cereblon (CRBN), which is a responsible molecule for thalidomide-induced teratogenicity. These results suggest that PEG(E)-TC11 is a good candidate drug for treating high-risk MM.

© 2017 Elsevier Inc. All rights reserved.

1. Introduction

Multiple myeloma (MM) is a hematological malignancy that is characterized by the proliferation of malignant plasma cells. MM comprises 13% of hematological malignancies, and it is the second most frequent after malignant lymphoma [1]. MM usually occurs in elderly individuals, and the patients show symptoms such as anemia, nephropathy, bone lytic lesions, hypercalcemia, and amyloidosis [2].

Recent advances in the treatment of MM using newly developed drugs have significantly improved the prognosis of MM patients. For example, immunomodulatory drugs (IMiDs) such as thalidomide, lenalidomide, and pomalidomide and proteasome inhibitors

including bortezomib, carfilzomib and ixazomib play central roles in MM treatment [3–5]. However, IMiDs have substantial limitations when they are used to treat MM [6,7]. For example, thalidomide has a high level of teratogenicity, and newborn infants whose mothers have taken thalidomide have suffered from phocomelia [8]. A second problem is that IMiDs show only limited effects against the MM of patients with high-risk chromosomal abnormalities such as t (4; 14) and del17p (deletion of TP53 gene). The MM patients with these cytogenetic abnormalities showed significantly shorter survival than those with a normal karyotype [9]. Thus, the drug design of novel IMiDs that are non-teratogenic as well as highly effective for high-risk MM cells is strongly desired.

IMiDs are multifunctional compounds, and their molecular mechanisms have not been fully elucidated. It was reported that IMiDs directly bind to cereblon (CRBN), a component of E3 ubiquitin ligase complex, and the IMiDs induced teratogenicity and showed antitumor effects [10–13]. A proteome analysis revealed various CRBN substrates, and it was reported that the degradation

* Corresponding author. Division of Clinical Physiology and Therapeutics, Keio University Faculty of Pharmacy, 1-5-30 Shiba-koen, Minato-ku, Tokyo 105-8512, Japan.

E-mail address: hattori-yt@pha.keio.ac.jp (Y. Hattori).

of IKZF1 (ikaros) and IKZF3 (aiolos) by IMiDs are important for the induction of apoptosis of MM cells [14]. More recently, Eichner et al. reported that IMiDs inhibited CCRN chaperone function and abrogated cell surface CD147–MCT1 expression [15]. This effect by IMiDs was closely related to teratogenicity. Taken together, these findings indicate that CCRN mediates biological actions of IMiDs, and that various downstream CCRN substrates demonstrate multifunctional effects of IMiDs.

We reported that a novel phenylphthalimide derivative, 2-(2,6-diisopropylphenyl)-5-amino-1H-isoindole-1,3-dione (TC11) induced the apoptosis of high-risk MM cells *in vivo* and *in vitro* and inhibited the differentiation of osteoclasts. We also demonstrated that TC11 directly bound to α -tubulin and the protein nucleophosmin-1 (NPM1) by an *in vitro* virus (IVV) method [16,17]. A major drawback of TC11 was its low water solubility, which hampered its absorption into blood and limited its antitumor effects when it was intraperitoneally administered in tumor-bearing mice.

In the present study, we attempted to improve the solubility of TC11 in water by linking TC11 with polyethylene glycol (PEG) through an ester bond, and we designated the resulting derivative PEG(E)-TC11. We found that PEG(E)-TC11 was very efficiently absorbed into the bloodstream and showed significantly high maximum blood concentrations compared to TC11.

PEG(E)-TC11 effectively inhibited the growth of MM cell xenografts in SCID mice. Our histopathological observations of xeno-grafted mice administered PEG(E)-TC11 showed the apoptosis of MM cells. To elucidate the mechanisms underlying the ability of PEG(E)-TC11 to induce the apoptosis of MM cells with high-risk cytogenetic abnormalities, we also examined the effects of PEG(E)-TC11 on cell-cycle regulation.

2. Materials & methods

2.1. Synthesis of compounds, PEG(E)-TC11 and hydroxyethoxy-TC11

PEG(E)-TC11 was synthesized from 4-hydroxyphthalic acid by the following six steps. Nitration of 4-hydroxyphthalic acid by guanidine nitrate in 85% sulfuric acid at 0°–5 °C for 3 h afforded a mixture of 5-nitro- and 3-nitro-4-hydroxyphthalic acids with the ratio of 1 to 1 at 96% yield (step 1), which was then refluxed in dehydrated toluene containing P_2O_5 at 100 °C overnight to give a mixture of 5-nitro- and 3-nitro-4-hydroxyphthalic acid anhydrides at the ratio of 1 to 0.6 in 51% yield (step 2).

Nitrophthalimide derivatives were obtained by refluxing a mixture of 5-nitro- and 3-nitrophthalic acid anhydrides and 2,6-diisopropylaniline in acetic acid at 140 °C overnight at 96% yield (step 3), and separated from each other by silica gel column chromatography. Reaction of the isolated 5-nitrophthalimide derivative with ethylene bromohydrin in DMF at 110 °C overnight yielded 4-hydroxyethoxy-5-nitrophthalimide derivative at 81% yield (step 4), which was pegylated with mPEG11-COOH with a molecular weight of 550 (step 5) followed by catalytic hydrogenation to finally give PEG(E)-TC11 (step 6). Hydroxyethoxy-TC11 (HOEtO-TC11) was also obtainable by the catalytic hydrogenation of 4-hydroxyethoxy-5-nitrophthalimide derivative prepared in step 4. The chemical structures of synthetic compounds were confirmed by 1H NMR spectroscopy and mass spectrometry.

2.2. Cell lines

The human MM cell lines KMM1, KMS11, KMS21, KMS27, KMS28, and KMS34 were established and provided by Dr. T. Ohtuki (Kawasaki Medical University, Kurashiki, Japan). The human MM cell line MUM24 was established in our laboratory [18]. All cell lines

were cultured in RPMI1640 medium (Sigma-Aldrich, St. Louis, MO) containing 10% fetal bovine serum (FBS) (Gibco, Grand Island, NY) and 1% Pen-Strep (Gibco) at 37 °C and 5% CO₂.

2.3. High-performance liquid chromatography (HPLC)

PEG(E)-TC11 was mixed with 10% FBS containing RPMI1640 medium at 37 °C, and 2, 6, 12, 24 or 48 h later, samples were collected and refined by solid phase extraction (Sep-Pak®, Waters, Milford, MA), and liquefied out 1 mL of acetonitrile. All samples were analyzed by high-performance liquid chromatography (HPLC). The Inertsil ODS-3 column (GL Science, Tokyo) was used. The mobile phases were acetonitrile and distilled water (50:50). The flow rate was 0.7 ml/min. The compounds were detected by fluorescence. The excitation wavelength was 380 nm, and the fluorescence wavelength was 530 nm.

2.4. Cell viability assay

MM cells (2×10^4 cells per well) were seeded in 96-well plates and incubated with various concentrations (0–30 μ M) of TC11, PEG(E)-TC11, or HOEtO-TC11 at 37 °C for 48 h. The cell viability was assessed by a Cell Proliferation Kit I (MTT) (Roche Diagnostics, Indianapolis, IN) according to the manufacturer's handling instructions.

2.5. Apoptosis detection assay

KMS34 cells (8×10^5 per well) were seeded in six-well plates and incubated with 10 μ M of TC11 or PEG(E)-TC11 at 37 °C for 24, 48, or 72 h. The cells were then collected and stained with FITC-labeled Annexin-V and propidium iodide (PI) (Biovision, Milpitas, CA). A flow cytometry analysis was performed with a BD LSR II system (BD Biosciences, San Jose, CA).

2.6. Cell-cycle assay

KMS34 cells (8×10^5 per well) were seeded in six-well plates and incubated with 3 μ M of TC11, PEG(E)-TC11, or HOEtO-TC11 at 37 °C for 12, 24, or 36 h. The cells were then collected and fixed in 70% ethanol, and incubated at 4 °C overnight. The cells were suspended in phosphate-buffered saline (PBS) plus 0.1 mg/mL RNaseA and incubated at room temperature for 30 min. After incubation, the cells were stained by PI in the dark for 30 min. The cells were then analyzed by a FACSCalibur (BD Biosciences).

2.7. *In vivo* tumor growth assay

The *in vivo* tumor growth assay was performed as described with several modifications [19]. Briefly, 3×10^7 KMS11 cells were subcutaneously inoculated into 5-week-old male ICR/SCID mice (Clea Japan, Tokyo). When the plasmacytoma reached 50 mm³, the intraperitoneal injections of drugs were started: 186 μ mol/kg of TC11 or PEG(E)-TC11 dissolved in 10% DMSO (Sigma-Aldrich)/1% Tween80 (Sigma-Aldrich)/saline (Otsuka Pharmaceuticals, Tokyo), or saline. Drugs or control (10% DMSO/1% Tween80/saline, or saline) was injected intraperitoneally twice every 3 days for 14 days. The tumor volume was calculated as width \times length² \times 0.52 [20].

2.8. Histopathologic assay

The histopathologic analysis was performed as described [19]. After 14-day treatment with PEG(E)-TC11 or control, the mice were sacrificed and the isolated plasmacytoma were fixed with 10% formalin and embedded in paraffin. Plasmacytomas were sliced at

5 μ m and stained with hematoxylin and eosin (H.E.). Anti-human cleaved PARP (Asp214) polyclonal antibody (Cell Signaling Technology Japan, Tokyo), anti-cleaved caspase-3 (Asp175) polyclonal antibody (Cell Signaling Technology Japan) were used for immunohistochemistry.

2.9. Pharmacokinetics study

To evaluate the pharmacokinetics after the intraperitoneal injection of TC11 or PEG(E)-TC11 in 5-week-old male ICR mice (Clea Japan), we extracted peripheral blood from the tail veins using heparin-coated hematocrit tubes (Terumo, Tokyo). Peripheral blood samples were centrifuged immediately at 3400 g for 15 min at 4 °C. Ten μ L of plasma and standard were refined by solid phase extraction (Sep-Pak[®]) and liquated out with 1 mL acetonitrile and analyzed by HPLC.

2.10. Surface plasmon resonance analysis

We performed a surface plasmon resonance (SPR) analysis with a Biacore 3000 system (GE Healthcare, Buckinghamshire, UK) to determine the binding kinetics of drugs to CRBN. All experiments were performed at 25 °C using TBS buffer (25 mM Tris-HCl, pH 7.4, 137 mM NaCl, 3 mM KCl). CRBN was immobilized onto the sensor chip NTA (GE Healthcare). To determine the dissociation constants, we injected three different concentrations of TC11, PEG(E)-TC11, HOEtO-TC11, thalidomide and lenalidomide (Santa Cruz Biotechnology, Santa Cruz, CA). The injection periods for association and dissociation were 300 s. The binding data were analyzed with 1:1 binding with the mass transfer model using the BIA evaluation software, ver. 4.1 (Biacore).

2.11. Statistical analysis

We performed a one-way analysis of variance (ANOVA) followed by the Tukey test for unpaired results to evaluate differences between more than two groups. Differences were considered to be significant when p-values <0.05 were obtained. All statistical analyses were conducted using the IBM SPSS Statistics program, ver. 23 (IBM, Armonk, NY).

3. Results

3.1. The pegylation of TC11 increased the water solubility

To examine the water solubility of pegylated TC11, we measured the saturated concentrations of TC11 and PEG(E)-TC11 in 100 mM Tris-HCl (pH 7.5) by HPLC. Although TC11 showed a low saturated concentration (2 mg/100 mL), PEG(E)-TC11 saturated with an approx. 4500 times higher concentration (8894 mg/100 mL).

The chemical structure of PEG(E)-TC11 is shown in Fig. 1A. When PEG(E)-TC11 was dissolved in RPMI1640 medium containing 10% FBS, PEG branches were immediately excised from TC11. Consequently, HOEtO-TC11 was produced (Fig. 1B), which we hypothesized would show biological activities after the hydrolysis of PEG(E)-TC11 in blood. A time-course increase in the HOEtO-TC11 concentration was observed when PEG(E)-TC11 was incubated with 10% FBS containing RPMI1640 medium (Fig. 1C). These results suggested that PEG(E)-TC11 was probably hydrolyzed and converted into HOEtO-TC11 by serum esterase.

3.2. PEG(E)-TC11 inhibited cell proliferation and induced the apoptosis of MM cells with high-risk cytogenetic abnormalities

To examine whether PEG(E)-TC11 inhibits the proliferation of

MM cells, we performed an MTT assay using eight MM cell lines including those with high-risk cytogenetic abnormalities. PEG(E)-TC11 inhibited the proliferation of all eight MM cell lines in a dose-dependent manner regardless of the existence of cytogenetic change (Fig. 2A). Since PEG(E)-TC11 was immediately hydrolyzed to HOEtO-TC11, we also examined the growth inhibitory activity of HOEtO-TC11, and we found that HOEtO-TC11 also significantly inhibited all of the MM cell lines. Very interestingly, water-soluble PEG(E)-TC11 and HOEtO-TC11 much more potently inhibited the proliferation of MM cells compared to TC11 against the KMM1, KMS11, KMS21, KMS34, and MUM24 cells. The exact reason for the superior growth inhibition by their water-soluble forms has not been elucidated.

We examined whether PEG(E)-TC11 induced the apoptosis of MM cells. We performed Annexin V/PI staining of MUM24 cells. The treatment of MM cells with 10 μ M of PEG(E)-TC11 or TC11 increased in the annexin V+/PI- and annexin V+/PI+ fractions in a time-dependent manner (Fig. 2B).

3.3. PEG(E)-TC11 also inhibited cell proliferation in vivo in KMS11-xenografted mice

We next evaluated the anti-myeloma effect of PEG(E)-TC11 and TC11 *in vivo* using KMS11-xenografted mice. KMS11 cells have high-risk cytogenetic abnormalities including t (4; 14) and del17p. PEG(E)-TC11 and TC11 were administered intraperitoneally to the xenografted mice (186 μ mol/kg) for 14 days. The PEG(E)-TC11- and TC11-treated mice showed significantly reduced tumor growth compared to the control mice (Fig. 3A). Neither compound resulted in serious systemic toxicity such as significant weight loss or abnormal behavior. PEG(E)-TC11 tended to reveal more potent tumor growth inhibition than TC11, although the difference was not significant. In one of the PEG(E)-TC11-treated mice, the skin xenografted tumor completely disappeared. These results suggest that PEG(E)-TC11 also has more potent antitumor activity *in vivo* than TC11, which is probably due to the change of pharmacokinetics in the mice by the increased water solubility.

In our histopathological examination of PEG(E)-TC11 treated xenografts, the hematoxylin-eosin staining revealed the aggregation of nuclei in the PEG(E)-TC11 treated mice. The immunohistochemical staining revealed that PARP- and cleaved-caspase3-positive cells were increased in the PEG(E)-TC11 treated mice. These results indicated that PEG(E)-TC11 exhibited antitumor activity via apoptosis *in vivo* (Fig. 3B).

3.4. PEG(E)-TC11 showed higher blood concentrations in mice compared to TC11

To evaluate the pharmacokinetics of PEG(E)-TC11, we examined the plasma concentrations of PEG(E)-TC11 and those of TC11 in ICR mice over time after a single injection of 186 μ mol/kg PEG(E)-TC11 or TC11. The results demonstrated that the PEG modification of TC11 significantly increased the peak blood concentration (Cmax) from 2.6 to 24.4 μ M and extended the elimination half-life (t1/2) from 1.4 to 2.2 h (Fig. 3C). These results suggested that the pegylation of water-insoluble TC11 increased the absorption from the peritoneal cavity to the blood, resulting in an increase in the Cmax value. We also speculated that the above-mentioned alteration of pharmacokinetics led to the increased tumor growth inhibition by PEG(E)-TC11 compared to TC11.

3.5. PEG(E)-TC11 induced G2/M cell-cycle arrest in MM cells

To investigate the mechanisms of induction of MM cell death, we performed a cell-cycle analysis by flow cytometry. Three μ M of

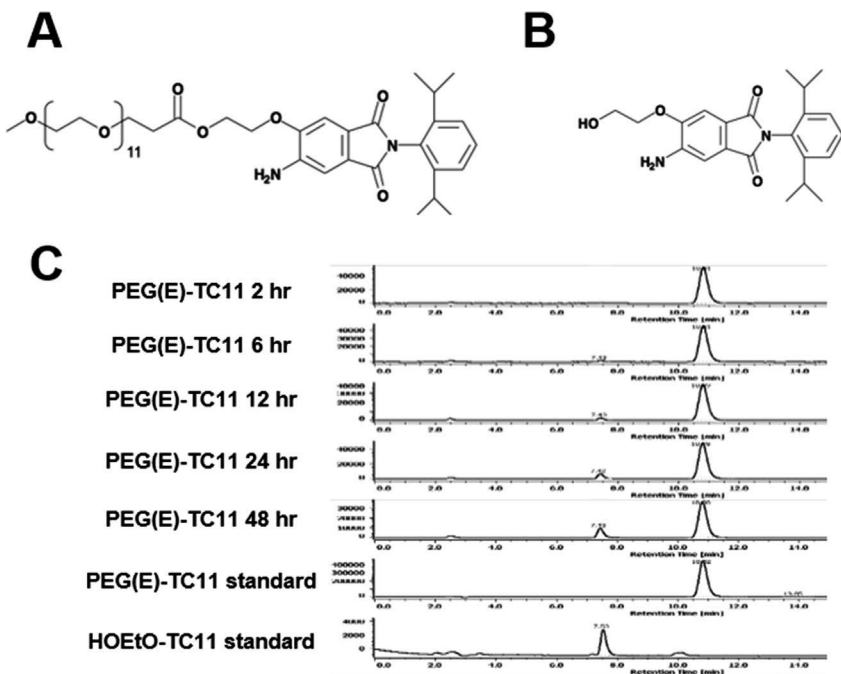


Fig. 1. The chemical structures of the TC11 derivatives. The chemical structures of PEG(E)-TC11 (A) and HOEtO-TC11 (B). The HPLC chromatogram of PEG(E)-TC11 and its hydrolyzed product HOEtO-TC11 (C). The peak of PEG(E)-TC11 and HOEtO-TC11 appeared in approx. 10.9 min and 7.5 min, respectively.

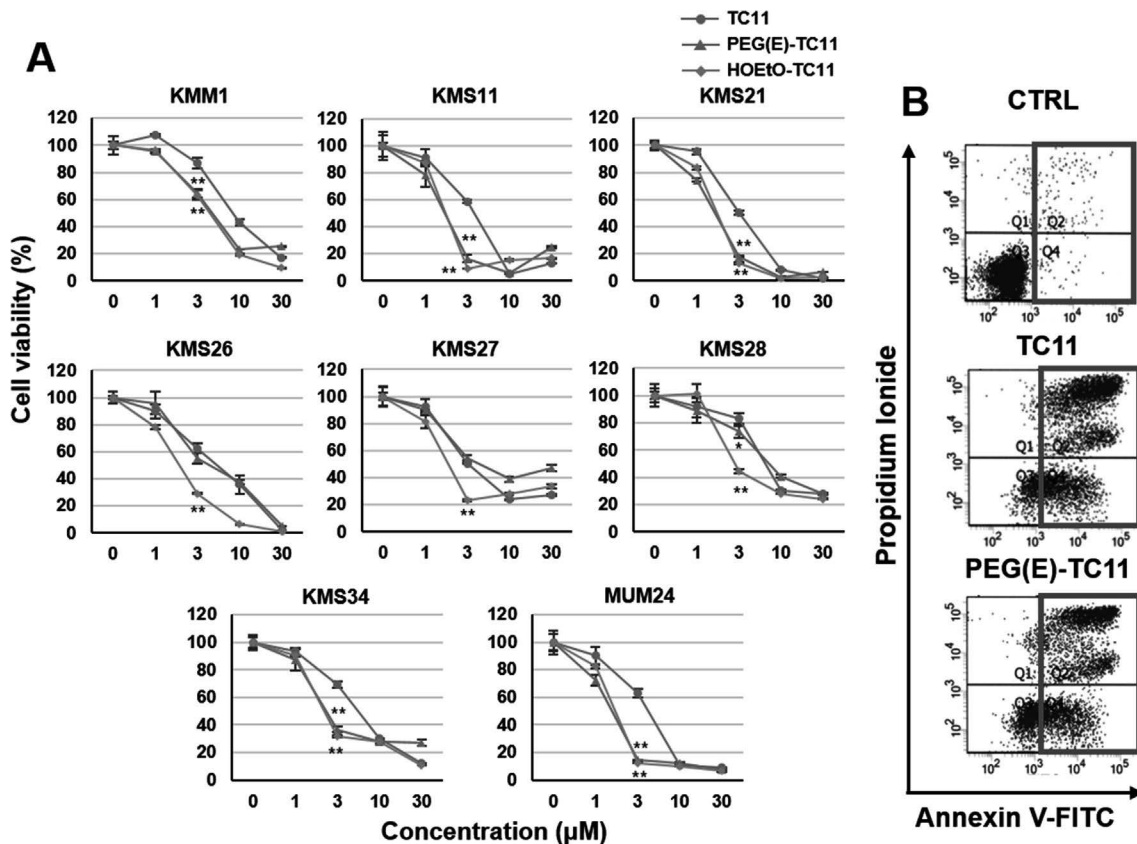


Fig. 2. The anti-myeloma effect of PEG(E)-TC11 in vitro. A: Human myeloma cell lines KMM1, KMS11, KMS21, KMS26, KMS27, KMS28, KMS34, and MUM24 were incubated with the indicated concentrations of the drugs for 48 h. The viable cell numbers were determined by MTT assay. Values are mean \pm SD, n = 3. *p < 0.05, **p < 0.01 (Tukey test vs. TC11). B: Flow cytometry analysis of apoptotic cells. MUM24 was incubated with 10 μ M of TC11 or PEG(E)-TC11 for 48 h, and the cells were then stained with FITC-labeled Annexin-V and PI and analyzed with a BD LSR II system.

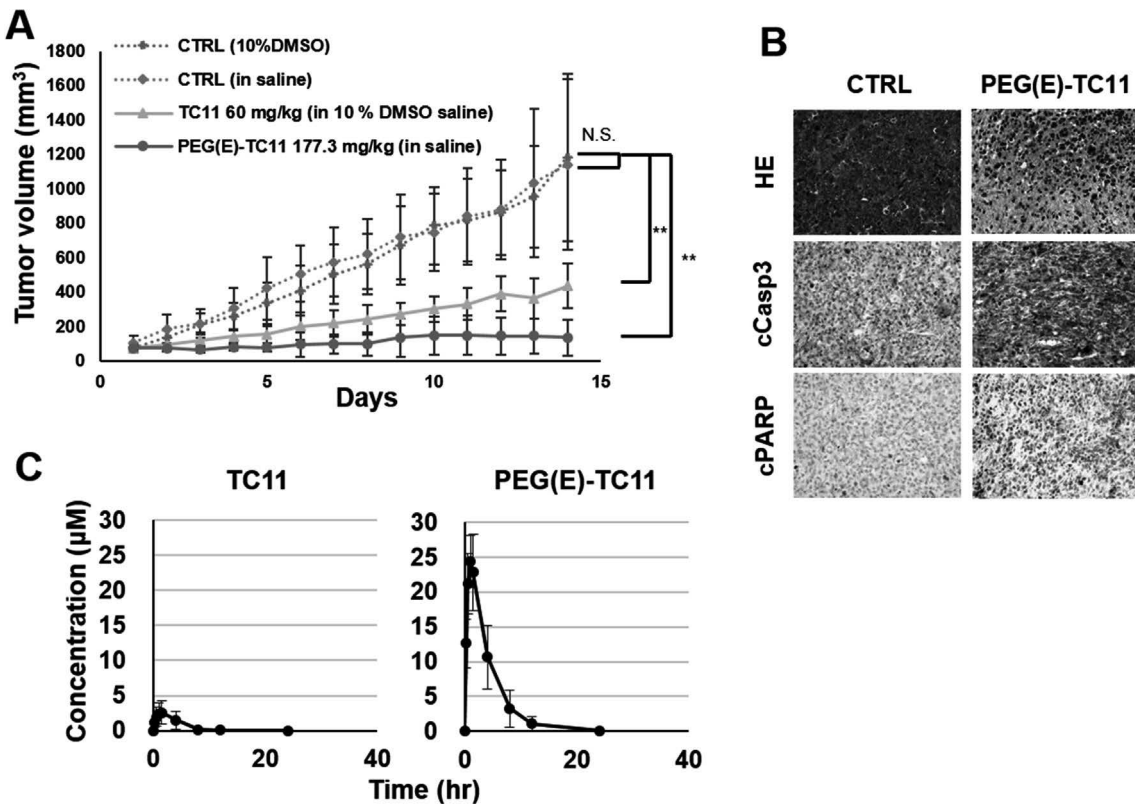


Fig. 3. The anti-myeloma effect of PEG(E)-TC11 *in vivo*. **A:** The growth curve of plasmacytoma. KMS11-inoculated mice were treated with 186 μ M/kg of TC11 or PEG(E)-TC11 twice every 3 days for 2 weeks. After observation, the mice were sacrificed and isolated plasmacytomas were fixed with 10% formalin. Values are mean \pm SD, n = 6–7. **p < 0.01 (Tukey test vs. control [Saline]). **B:** Histopathological examination of the KMS11-derived plasmacytomas. The plasmacytomas were sliced and stained with H.E., anti-human cleaved PARP (Asp214) polyclonal antibody and anti-cleaved caspase-3 (Asp175) polyclonal antibody. **C:** Pharmacokinetics study of TC11 and PEG(E)-TC11. Plasma concentrations of TC11 or HOEtO-TC11 in mice after a single injection of 186 μ M/kg of TC11 or HOEtO-TC11 were determined by HPLC.

PEG(E)-TC11 and TC11 both significantly induced cell-cycle arrest in a time-dependent manner. After 1-day drug exposure, the G2/M fractions were 18.8% in the control, 60.40% in the TC11 treatment, and 68.40% in the PEG(E)-TC11 treatment (Fig. 4A).

3.6. Anti-myeloma effects of PEG(E)-TC11 and TC11 are independent of the CRBN pathway

It was reported that IMiDs were known to induce cytotoxicity and teratogenicity via their binding to CRBN. It is important to determine whether or not PEG(E)-TC11 binds to CRBN, and to address this question, we performed the SPR assay. As shown in Fig. 4B, PEG(E)-TC11, TC11 and HOEtO-TC11 did not bind to CRBN, whereas thalidomide and lenalidomide directly bound to CRBN with high affinities; their binding affinities (K_D) were 5.66×10^{-7} and 3.65×10^{-6} M, respectively. These results indicated that TC11 and its derivatives did not interact with CRBN. The treatments with PEG(E)-TC11, HOEtO-TC11, and TC11 resulted in the growth inhibition of MM cells independently from CRBN binding (Fig. 4B).

3.7. Discussion

Various drugs have been developed to treat MM. In particular, IMiDs are effective for relapsed and refractory MM patients and have extended the survival rate of untreated patients [3,5]. However, IMiDs have two substantial limitations; their teratogenicity and limited effects against high-risk MM patients [6,21].

We reported that a novel phthalimide derivative, TC11, induced the apoptosis of high-risk MM cells *in vitro* and *in vivo* [16,17]. One

of the major drawbacks of TC11 for further preclinical development is its low water solubility, and to overcome this problem, we synthesized pegylated TC11, which shows much higher water saturated concentrations compared to TC11.

Pegylation is commonly used for increasing water solubility and changing pharmacokinetic parameters. It has been used for improving the bioavailability and extending the blood retention time of water-insoluble drugs such as camptothecin, paclitaxel, and interferon [22–24]. Generally, pegylation is expected to increase the maximum blood concentration (Cmax) value and to elongate the elimination half-life (t1/2). For example, the Cmax and t1/2 of interferon-gamma (IFN- γ) are 3411 pg/ml and 0.9 h, and those of pegylated-IFN- γ are 567,297 pg/ml and 29.1 h, respectively [25].

In the present study, the pegylation of TC11 resulted in an eightfold-higher Cmax, probably due to the increase of absorption from the peritoneal cavity to the bloodstream. However, the elongation of t1/2 by TC11 pegylation was only 1.8-fold. Considering the ester-binding structure between PEG and TC11, we suspect that the immediate hydrolyzation and dissociation of a PEG branch from TC11 is a cause of the limited elongation of t1/2. It was reported that carboxylesterase activity is much higher in mouse plasma compared to human plasma [26]. We therefore suspect that PEG(E)-TC11 was immediately hydrolyzed to HOEtO-TC11 by carboxylesterase in the blood.

We examined whether the modification of chemical structure by pegylation would alter the antitumor activity of TC11. As shown in Fig. 2A, PEG(E)-TC11 and its hydrolyzate HOEtO-TC11 both significantly inhibited the growth of all eight MM cell lines [16]. In our earlier study, we identified α -tubulin and NPM1 as TC11-

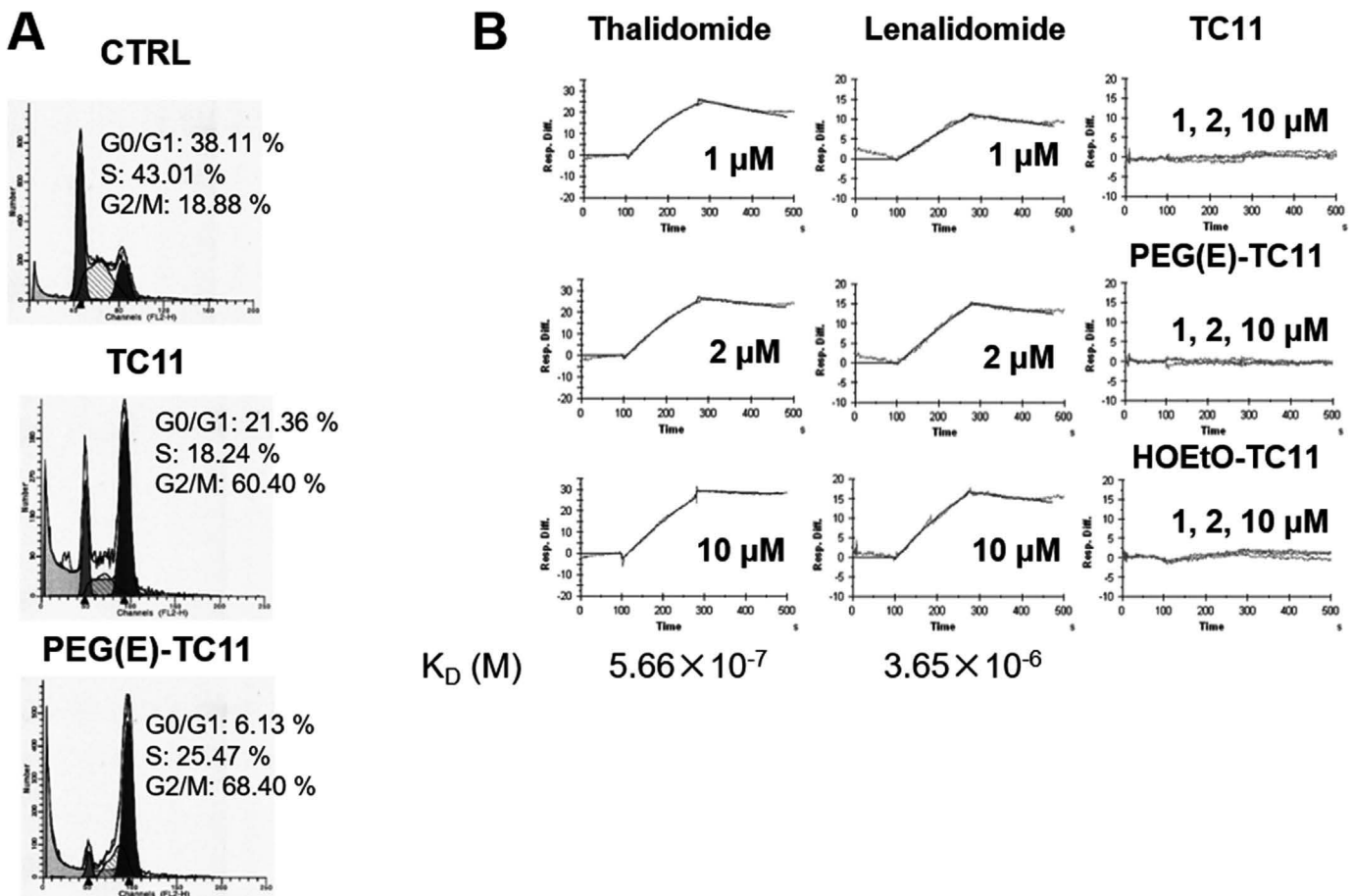


Fig. 4. PEG(E)-TC11 and TC11 induced G2/M arrest in a CRBN-independent manner. **A:** Cell-cycle analysis of PEG(E)-TC11-, TC11- and HOEtO-TC11-treated cells. KMS34 cells were incubated with 3 μM of TC11, PEG(E)-TC11 or HOEtO-TC11 for 24 h; the cells were then fixed with 70% EtOH and labeled with PI and analyzed by a FACSCalibur. **B:** The SPR analysis of the ability of TC11 and its derivatives to bind to CRBN. CRBN was immobilized onto the sensor chip NTA followed by SPR analysis. Left panels, the affinity of thalidomide to CRBN; middle panels, the affinity of lenalidomide; right panels, the affinity of TC11 and its derivatives.

binding proteins that are involved in cell-cycle regulation [17]. As shown in Fig. 4A, PEG(E)-TC11 and HOEtO-TC11 more clearly induced G2/M arrest compared to TC11. The reason why PEG(E)-TC11 and HOEtO-TC11 induced cell-cycle arrest more potently than TC11 is not clear.

We also confirmed the anti-myeloma effect of PEG(E)-TC11 *in vivo* using xenografts of KMS11 cells which harbored cytogenetic abnormalities such as t(4; 14) translocation and del17p. In the PEG(E)-TC11-injected mice, the KMS11 xenografts proliferated more slowly compared to those in the TC11-treated mice, although the difference in the growth inhibition between PEG(E)-TC11 and TC11 was not statistically significant. We speculate that the potentiated growth inhibition of PEG(E)-TC11 is brought about by the alteration of pharmacokinetics as described earlier.

Deletion of the TP53 tumor suppressor gene is one of the representative high-risk cytogenetic abnormalities in MM and other hematological malignancies [9]. TP53 plays a central role in the G1/S checkpoint of the cell cycle [27]. Drugs used to treat MM such as lenalidomide induced apoptosis via G1/S arrest [28,29]. However, MM cells with deletion of TP53 gene did not reveal G1/S arrest by treatment with lenalidomide (data not shown). To the contrary, TC11 and its derivatives induced G2/M arrest independent of TP53 function. We thus consider TC11 and its derivatives effective for high-risk MM with deletion of TP53 gene.

In 2010, it was reported that IMiDs directly bound to CRBN, which mediated teratogenicity as well as antitumor effects [10–12].

In the present study, we determined the binding dissociation constants (K_D) of PEG(E)-TC11 and TC11 to CRBN by an SPR analysis. Thalidomide and lenalidomide bound to CRBN with high affinity, whereas TC11 and its derivatives did not bind to CRBN at any concentration. Ito et al. reported that the knock-down of CRBN gene abrogated thalidomide-induced teratogenicity in zebrafish embryos [12]. If CRBN is a responsible molecule for thalidomide-induced teratogenicity, TC11 and its derivatives are expected to be safe compounds lacking CRBN-mediated teratogenicity.

In conclusion, our present findings demonstrated that a novel pegylated phenylphthalimide derivative, PEG(E)-TC11, has anti-myeloma effect for MM that has high-risk cytogenetic abnormalities *in vitro* and *in vivo*. In addition, PEG(E)-TC11 improved the pharmacological properties of TC11 such as absorption from the peritoneal cavity to the bloodstream. PEG(E)-TC11 inhibited cell growth via G2/M arrest in a CRBN-independent manner. Thus, PEG(E)-TC11 should be considered as a candidate compound for overcoming high-risk MM.

Acknowledgements

We thank Dr. Takemi Ohtsuki for the gift of MM cell lines and Yuka Masaharu for her helpful scientific assistance. This work was supported in part by a Grant-in-Aid for Scientific Research and a grant from the Private University Strategic Research Base Development Program of the Ministry of Education, Culture, Sports,

Science and Technology (MEXT) of Japan, International Myeloma Foundation Japan's Grants, Japanese Society of Myeloma (JSM) Research Award, and Keio Gijuku Academic Development Funds.

Transparency document

Transparency document related to this article can be found online at <http://dx.doi.org/10.1016/j.bbrc.2017.08.159>.

References

- [1] M.A. Dimopoulos, E. Terpos, Multiple myeloma, *Ann. Oncol.* 21 (Suppl 7) (2010) 143–150 vii.
- [2] A. Palumbo, K. Anderson, Multiple myeloma, *N. Eng. J. Med.* 364 (2011) 1046–1060.
- [3] P.G. Richardson, E. Blood, C.S. Mitsiades, et al., A randomized phase 2 study of lenalidomide therapy for patients with relapsed or relapsed and refractory multiple myeloma, *Blood* 108 (2006) 3458–3464.
- [4] M.V. Mateos, J.M. Hernandez, M.T. Hernandez, et al., Bortezomib plus melphalan and prednisone in elderly untreated patients with multiple myeloma: results of a multicenter phase 1/2 study, *Blood* 108 (2006) 2165–2172.
- [5] M.A. Dimopoulos, A. Anagnostopoulos, D. Weber, Treatment of plasma cell dyscrasias with thalidomide and its derivatives, *J. Clin. Oncol.* 21 (2003) 4444–4454.
- [6] H. Avet-Loiseau, J. Soulier, J.P. Fermand, et al., Impact of high-risk cytogenetics and prior therapy on outcomes in patients with advanced relapsed or refractory multiple myeloma treated with lenalidomide plus dexamethasone, *Leukemia* 24 (2010) 623–628.
- [7] H. Chang, A. Jiang, C. Qi, et al., Impact of genomic aberrations including chromosome 1 abnormalities on the outcome of patients with relapsed or refractory multiple myeloma treated with lenalidomide and dexamethasone, *Leuk. Lymphoma* 51 (2010) 2084–2091.
- [8] Y. Hattori, T. Iguchi, Thalidomide for the treatment of multiple myeloma, *Congenit. Anom. (Kyoto)* 44 (2004) 125–136.
- [9] S.Z. Usmani, P. Rodriguez-Otero, M. Bhutani, et al., Defining and treating high-risk multiple myeloma, *Leukemia* 29 (2015) 2119–2125.
- [10] J. Kronke, N.D. Udeshi, A. Narla, et al., Lenalidomide causes selective degradation of IKZF1 and IKZF3 in multiple myeloma cells, *Science* 343 (2014) 301–305.
- [11] J. Kronke, E.C. Fink, P.W. Hollenbach, et al., Lenalidomide induces ubiquitination and degradation of CK1alpha in del(5q) MDS, *Nature* 523 (2015) 183–188.
- [12] T. Ito, H. Ando, T. Suzuki, et al., Identification of a primary target of thalidomide teratogenicity, *Science* 327 (2010) 1345–1350.
- [13] E.S. Fischer, K. Bohm, J.R. Lydeard, et al., Structure of the DDB1-CRBN E3 ubiquitin ligase in complex with thalidomide, *Nature* 512 (2014) 49–53.
- [14] C.C. Bjorklund, L. Lu, J. Kang, et al., Rate of CRL4(CRBN) substrate Ikaros and Aiolos degradation underlies differential activity of lenalidomide and pomalidomide in multiple myeloma cells by regulation of c-Myc and IRF4, *Blood Cancer J.* 5 (2015) e354.
- [15] R. Eichner, M. Heider, V. Fernandez-Saiz, et al., Immunomodulatory drugs disrupt the cereblon-CD147-MCT1 axis to exert antitumor activity and teratogenicity, *Nat. Med.* 22 (2016) 735–743.
- [16] H. Shihido, F. Terada, N. Tabata, et al., A phthalimide derivative that inhibits centrosomal clustering is effective on multiple myeloma, *PLoS One* 7 (2012) e38878.
- [17] M. Matsushita, Y. Ozaki, Y. Hasegawa, et al., A novel phthalimide derivative, TC11, has preclinical effects on high-risk myeloma cells and osteoclasts, *PLoS One* 10 (2015) e0116135.
- [18] Y. Hattori, W. Du, T. Yamada, et al., A myeloma cell line established from a patient refractory to thalidomide therapy revealed high-risk cytogenetic abnormalities and produced vascular endothelial growth factor, *Blood Cancer J.* 3 (2013) e115.
- [19] W. Du, Y. Hattori, T. Yamada, et al., NK4, an antagonist of hepatocyte growth factor (HGF), inhibits growth of multiple myeloma cells: molecular targeting of angiogenic growth factor, *Blood* 109 (2007) 3042–3049.
- [20] D. Tomioka, N. Maebara, K. Kuba, et al., Inhibition of growth, invasion, and metastasis of human pancreatic carcinoma cells by NK4 in an orthotopic mouse model, *Cancer Res.* 61 (2001) 7518–7524.
- [21] U. Klein, A. Jauch, T. Hielscher, et al., Chromosomal aberrations +1q21 and del(17p13) predict survival in patients with recurrent multiple myeloma treated with lenalidomide and dexamethasone, *Cancer* 117 (2011) 2136–2144.
- [22] R.B. Greenwald, Y.H. Choe, J. McGuire, et al., Effective drug delivery by PEGylated drug conjugates, *Adv. Drug Deliv. Rev.* 55 (2003) 217–250.
- [23] J.S. Choi, B.W. Jo, Enhanced paclitaxel bioavailability after oral administration of pegylated paclitaxel prodrug for oral delivery in rats, *Int. J. Pharm.* 280 (2004) 221–227.
- [24] J.H. Hoofnagle, L.B. Seeff, Peginterferon and ribavirin for chronic hepatitis C, *N. Eng. J. Med.* 355 (2006) 2444–2451.
- [25] C.M. Fam, S.P. Eisenberg, S.J. Carlson, et al., PEGylation improves the pharmacokinetic properties and ability of interferon gamma to inhibit growth of a human tumor xenograft in athymic mice, *J. Interferon Cytokine Res.* 34 (2014) 759–768.
- [26] T. Satoh, M. Hosokawa, Structure, function and regulation of carboxylesterases, *Chem. Biol. Interact.* 162 (2006) 195–211.
- [27] S.J. Kuerbitz, B.S. Plunkett, W.V. Walsh, et al., Wild-type p53 is a cell cycle checkpoint determinant following irradiation, *Proc. Natl. Acad. Sci. U. S. A.* 89 (1992) 7491–7495.
- [28] A.K. Gandhi, J. Kang, L. Capone, et al., Dexamethasone synergizes with lenalidomide to inhibit multiple myeloma tumor growth, but reduces lenalidomide-induced immunomodulation of T and NK cell function, *Curr. Cancer Drug Targets* 10 (2010) 155–167.
- [29] D. Verhelle, L.G. Corral, K. Wong, et al., Lenalidomide and CC-4047 inhibit the proliferation of malignant B cells while expanding normal CD34+ progenitor cells, *Cancer Res.* 67 (2007) 746–755.

Utility of Survivin, BAP1, and Ki-67 immunohistochemistry in distinguishing epithelioid mesothelioma from reactive mesothelial hyperplasia

KEI KUSHITANI¹, VISHWA JEET AMATYA¹, AMANY SAYED MAWAS², RUI SUZUKI¹, YOSHIHIRO MIYATA³, MORIHITO OKADA³, KOUKI INAI¹, TAKUMI KISHIMOTO⁴ and YUKIO TAKESHIMA¹

¹Department of Pathology, Institute of Biomedical and Health Sciences, Hiroshima University, Hiroshima 734-8551, Japan; ²Department of Pathology and Clinical Pathology, Faculty of Veterinary Medicine, South Valley University, Qena 83523, Egypt; ³Department of Surgical Oncology, Research Center for Radiation Casualty Medicine, Research Institute for Radiation Biology and Medicine, Hiroshima University, Hiroshima 734-8551; ⁴Department of Internal Medicine, Okayama Rosai Hospital, Okayama 702-8055, Japan

Received June 30, 2017; Accepted November 20, 2017

DOI: 10.3892/ol.2018.7765

Abstract. Histological distinction between epithelioid mesothelioma (EM) and reactive mesothelial hyperplasia (RMH) can be challenging. The aim of this study was to assess the diagnostic utility of Survivin, Ki-67, and loss of BRCA1-associated protein 1 (BAP1) expressions in distinguishing EM from RMH using immunohistochemistry. Formalin-fixed, paraffin-embedded specimens from 78 cases of EM and 80 cases of RMH were immunohistochemically examined for Survivin, BAP1, and Ki-67. In addition, receiver operating characteristic curve analyses were performed to establish the cut-off values for Survivin and Ki-67 labelling indices. Survivin (cut-off value: 5%) had 67.7% sensitivity and 100% specificity, while Ki-67 (cut-off value: 10%) had 85.1% sensitivity and 87.5% specificity, and BAP1 had 66.2% sensitivity and 100% specificity for the differentiation of EM from RMH. Among the combinations of two markers, the combination of Survivin and BAP1 (Survivin-positive and/or BAP1-loss finding) had the highest diagnostic accuracy (sensitivity: 89.8%; specificity: 100%; accuracy: 95.3%). We recommend using the combination of Survivin and BAP1 to distinguish EM from RMH.

Introduction

Malignant mesothelioma (MM) is a relatively rare but highly aggressive malignant neoplasm arising from mesothelial cells of the pleura, peritoneum, pericardium, and tunica vaginalis.

It is well-correlated with occupational and environmental asbestos exposure. (1,2) The incidence of MM has increased in many countries; (3) in Japan, mortality due to MM has increased since the 1990s, and is predicted to peak in the 2030s (4).

Epithelioid mesothelioma (EM) must be differentiated from reactive mesothelial hyperplasia (RMH), which is a non-neoplastic condition frequently caused by pleuritis, peritonitis, or serosal invasion of other cancers. Due to the close resemblance of EM to RMH, differentiation by routine histological observation alone can be challenging.

Various established and novel immunohistochemical markers have been utilized to distinguish EM from other malignancies (5-8) and RMH (6,9-17). Multiple potential immunohistochemical markers, including Ki-67, desmin, epithelial membrane antigen (EMA), p53, glucose transporter 1, insulin-like growth factor 2 messenger RNA binding protein-3 and BRCA1-associated protein 1 (BAP1) have been evaluated. However, despite the use of these immunohistochemical markers, the distinction between EM and RMH remains challenging in some cases.

Recently, detection of *p16* (*CDKN2A*) homozygous deletion (*p16* HD) using fluorescence *in situ* hybridization (FISH) has been used to differentiate MM from RMH, with 100% specificity. However, the sensitivity of this marker for pleural EM varies between 45 and 86%, while its sensitivity for peritoneal EM ranges from 14 to 41% in different laboratories (10,18-20). In our unpublished experience, *p16* HD (detected by FISH) was present in 63.2% (12/19) of EM cases, but absent in all RMH cases (0/20). Although the detection of *p16* HD using FISH may be considered highly specific, its sensitivity in differentiating EM from RMH is not very high. In addition, FISH analysis cannot be applied in all cases or in all pathology laboratories, given its high cost and stringent experimental requirements.

We recently reported that phorbol 12-myristate-13-acetate-induced protein-1 (PMAIP-1; Noxa) and baculoviral IAP repeat-containing 5 (BIRC5; Survivin) mRNA expression levels are significantly higher in EM than in non-neoplastic pleural tissue, and discussed the utility of anti-Noxa antibody

Correspondence to: Professor Yukio Takeshima, Department of Pathology, Institute of Biomedical and Health Sciences, Hiroshima University, 1-2-3 Kasumi, Minami-ku, Hiroshima 734-8551, Japan
E-mail: ykotake@hiroshima-u.ac.jp

Key words: BAP1, immunohistochemistry, Ki-67, mesothelioma, reactive mesothelial hyperplasia, survivin

for the distinction between EM and RMH (21). However, the utility of Survivin IHC for the differentiation of benign and malignant mesothelial proliferation has not yet been assessed.

Here, we studied the utility of Survivin and Ki-67 expressions along with the loss of BAP1 expression in distinguishing benign from malignant mesothelial proliferation.

Materials and methods

Patients and histological samples. We used formalin-fixed, paraffin-embedded (FFPE) specimens from 78 patients with a definite histological diagnosis of EM who had undergone thoracoscopic pleural biopsy, pleurectomy/decortication, extra-pleural pneumonectomy, or autopsy between 2000 and 2016. FFPE histological samples from surgical specimens obtained from 80 patients with a histological diagnosis of RMH were obtained via thoracoscopic biopsy, laparoscopic biopsy, or surgical resection between 2005 and 2016. These samples were retrieved from the archives of the Department of Pathology at Hiroshima University (Hiroshima, Japan). Each of the tumour specimens was independently reviewed by three pathologists (K.K., V.J.A, and Y.T.), and all cases of mesothelioma were diagnosed according to currently accepted World Health Organization Histological Criteria (6,22).

The tissue samples were retrieved from the archive of the Department of Pathology at Hiroshima University's Institute of Biomedical and Health Sciences. The collection of tissue specimens for this study was carried out in accordance with the 'Ethics Guidelines for Human Genome/Gene Research' enacted by the Japanese Government. Ethical approval was obtained from the institutional ethics review committee (Hiroshima University E-974). All experimental procedures were in accordance with the with ethical guidelines.

Immunohistochemical procedures. Immunohistochemical staining of sections from the FFPE tissue samples was performed using Ventana BenchMark GX (Roche Diagnostics, Basel, Switzerland). In brief, after deparaffinization using EZ-Prep (Roche Diagnostics) and antigen retrieval using Cell Conditioning 1 buffer at 95°C for 32 min, sections were incubated with primary antibodies. The primary antibodies were anti-Survivin (cat. no. AF886, polyclonal, dilution of 1:200; R&D systems, Minneapolis, MN, USA), anti-BAP1 (C-4, dilution of 1:50; Santa Cruz Biotechnology, Inc., Dallas, TX, USA), and anti-Ki-67 (MIB-1, dilution of 1:25; Dako, Glostrup, Denmark). Incubation with secondary antibodies and detection was performed using the Ventana UltraView Universal DAB Detection kit.

Nuclear staining of Survivin, BAP1, and Ki-67 in EM or RMH cells with the same or higher intensity than internal positive controls was regarded as positive staining. Negative staining of BAP1 was defined as completely absent nuclear staining in the target cells in the presence of a positive internal control such as lymphocytes or stromal cells. Although some cases had weak cytoplasmic positivity for Survivin and BAP1, we have not included cases with only cytoplasmic positivity for Survivin and BAP1 for evaluation in this study. Immunoreactivity of Survivin and Ki-67 was evaluated using a labelling index (% of positive cells) in the 'hot spot' exhibiting the highest number of positive cells compared to the rest

of the lesion. We evaluated at least 100 (maximum 500) EM or RMH cells in high power fields (x400). Counting of labelling indices of Survivin and Ki-67 was performed by three pathologists (K.K., V.J.A, and Y.T.) independently; the mean of three numbers was then calculated.

Statistical analysis. Receiver operating characteristic (ROC) curve analysis was performed to establish the cut-off values for the Survivin and Ki-67 labelling indices. The cut-off points were determined based on the Youden index. All statistical analyses were performed using EZR (Saitama Medical Center, Jichi Medical University, Saitama, Japan), a graphical user interface for R (The R Foundation for Statistical Computing, Vienna, Austria). More precisely, it is a modified version of R commander designed to add statistical functions frequently used in biostatistics (23).

Sensitivity, specificity, positive predictive values, negative predictive values, and diagnostic accuracies were calculated for each marker and combinations of two markers.

Results

Survivin expression and cut-off value. Representative immunohistochemical staining images for EM and RMH are shown in Fig. 1. Survivin expression was significantly higher in EM than in RMH. The mean of the Survivin labelling indices in EM [mean, 9.3; range, 0-24.5, standard deviation (SD), 6.5] was significantly higher than that in RMH (mean, 1.2; range, 0-4.0, SD, 1.2) (t-test, P-value <0.001). Distributions of the Survivin labelling indices in EM and RMH are shown in Fig. 2A.

The cut-off value for the Survivin IHC assay led by the result of ROC analysis was 4.000 (Fig. 2B). Based on the ROC analysis, and in consideration of convenience in practical pathological diagnosis, we set the cut-off value for the Survivin IHC assay at 5%. Immunoreactivity of Survivin was classified as negative (positivity of less than 5% of the mesothelioma cells or non-neoplastic mesothelial cells) or positive (positivity of over 5% of the mesothelioma or mesothelial cells).

Forty-two of 62 (67.7%) EM cases were positive for Survivin. In contrast, none of the RMH cases were positive for Survivin (Table I).

Ki-67 expression and cut-off value. Representative immunohistochemical staining images for EM and RMH are shown in Fig. 3. Ki-67 expression was also significantly higher in EM than in RMH. The mean of the Ki-67 labelling indices in EM (mean, 32.6; range, 1.0-90.0; SD, 22.1) was significantly higher than that in RMH (mean, 3.5; range, 0-20.0, SD, 4.2) (t-test, P-value <0.001). Distributions of the Ki-67 labelling indices in EM and RMH are shown in Fig. 4A.

The cut-off value for the Ki-67 IHC assay led by the result of ROC analysis was 10.333 (Fig. 4B). Based on the ROC analysis, and in consideration of convenience in practical pathological diagnosis, we set the cut-off value for the Ki-67 IHC assay at 10%. Immunoreactivity of Ki-67 was classified as negative (positivity of less than 10% of the mesothelioma cells or non-neoplastic mesothelial cells) or positive (positivity of over 10% of the mesothelioma or mesothelial cells).

Fifty-seven of 67 (85.1%) EM cases and 7 of 56 (12.5%) RMH cases were positive for Ki-67 (Table I).

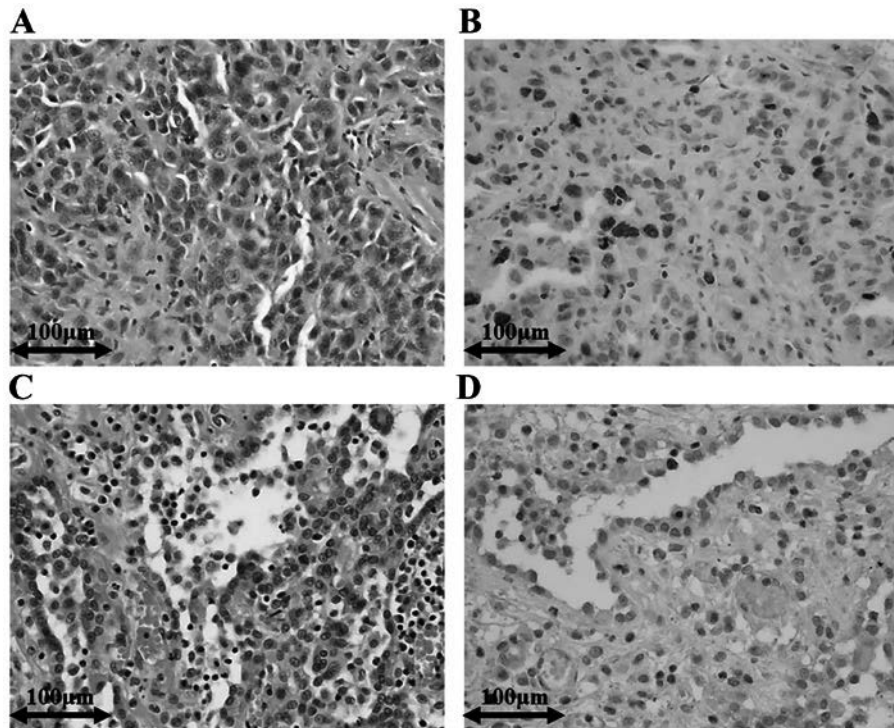


Figure 1. Representative histological images of Survivin IHC. (A) EM with H&E staining. (B) Survivin IHC in EM; labelling index, 18.1. (C) RMH with H&E stain. (D) Survivin IHC in RMH; labelling index, 1.3. IHC, immunohistochemistry; EM, epithelioid mesothelioma; RMH, reactive mesothelial hyperplasia; H&E, haematoxylin and eosin.

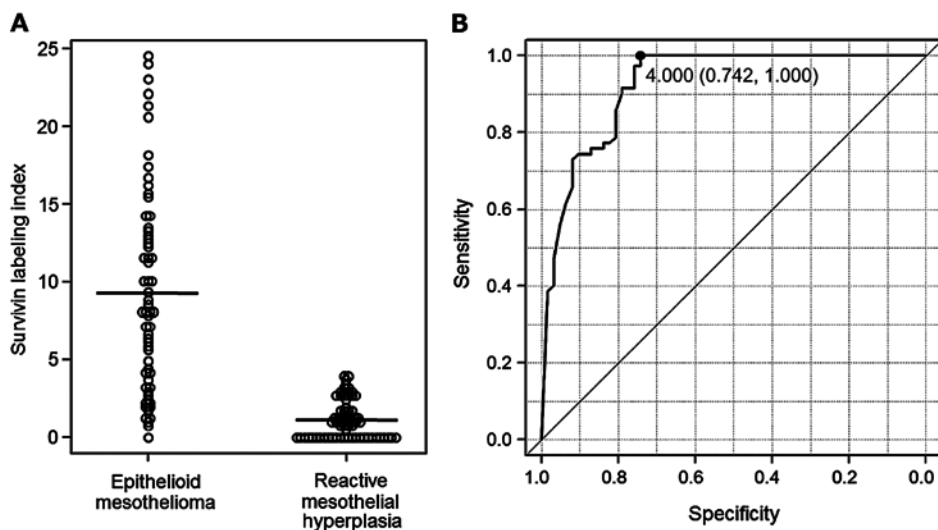


Figure 2. (A) Distribution of Survivin labelling index in epithelioid mesothelioma and reactive mesothelial hyperplasia. The horizontal line in the dot chart shows the mean. (B) ROC analysis. ROC curve was estimated using Survivin labelling index. Cut-off value based on the Youden index is also shown. ROC, receiver operating characteristic.

BAP1 expression. Loss of nuclear BAP1 expression was observed in 49 of 74 (66.2%) cases of EM (Table I). Almost all cases without BAP1 expression had a homogenous expression loss pattern. No heterogeneous loss patterns were observed. In contrast, nuclear BAP1 expression was preserved in all 78 RMH cases (Table I). Representative immunohistochemical staining images for EM and RMH are shown in Fig. 5.

Utilities of each marker and combinations of two markers. The sensitivity and specificity of each marker and combinations of

two markers for the distinction between EM and RMH are shown in Table II. Among three single markers and six combination patterns of two markers, 'Survivin-positive and/or BAP1-loss' finding showed the highest diagnostic accuracy (95.3%).

Discussion

Accurate histopathological differentiation between MM and RMH is extremely important, not only for clinical management, but also for the appropriate operation of the public

Table I. Immunohistochemical findings of Survivin, Ki-67, and BAP1 in epithelioid mesothelioma and reactive mesothelial hyperplasia.

Immunohistochemical data	Epithelioid mesothelioma			Reactive mesothelial hyperplasia		
	n (%)	Negative	Positive	n (%)	Negative	Positive
Survivin expression	42/62 (67.7)	20	42	0/70	70	0
Ki-67 expression	57/67 (85.1)	10	57	7/56 (12.5)	49	7
BAP1-loss	49/74 (66.2)	25	49	0/78	78	0

BAP1, BRCA1-associated protein 1.

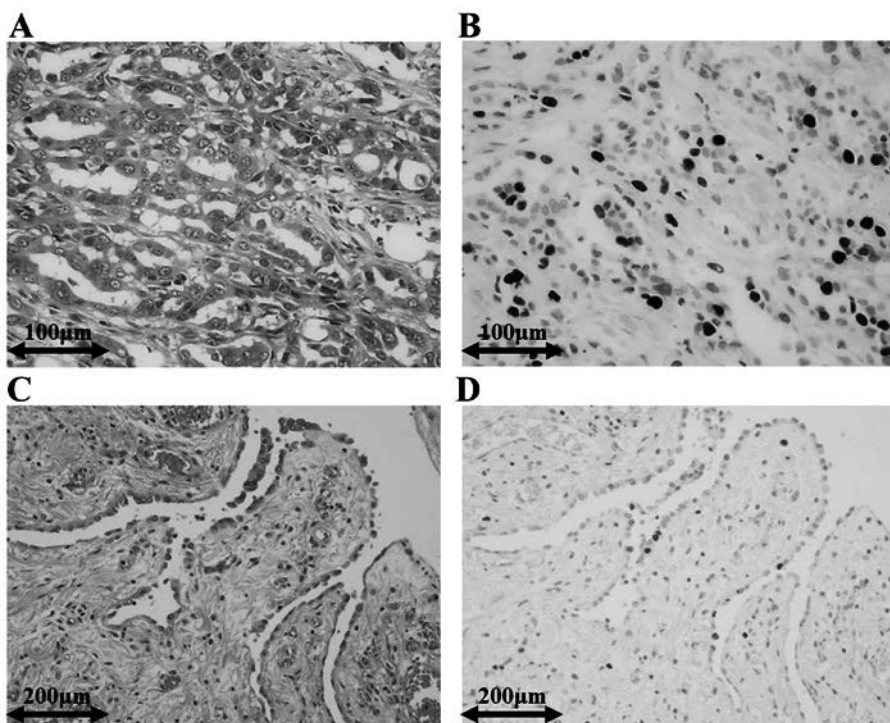


Figure 3. Representative histological images of Ki-67 IHC. (A) EM with H&E stain. (B) Ki-67 IHC in EM; labelling index, 35.0. (C) RMH with H&E stain. (D) Ki-67 IHC in RMH; labelling index, 8.7. IHC, immunohistochemistry; EM, epithelioid mesothelioma; RMH, reactive mesothelial hyperplasia; H&E, haematoxylin and eosin.

compensation system for victims of environmental and occupational asbestos exposure and their dependents. To obtain a better marker for EM, we evaluated the diagnostic utilities of Survivin, BAP1, and Ki-67 in differentiating EM from RMH. We found that the sensitivity and specificity of the nuclear Survivin labelling index following the use of a properly determined cut-off value was appropriate in distinguishing EM from RMH. The utility of Survivin IHC for the differentiation between benign and malignant mesothelial proliferation has not been reported to date. To the best of our knowledge, this is the first report evaluating the utility of Survivin IHC in differentiating EM from RMH.

Survivin is the smallest member of the inhibitor of apoptosis (IAP) family, and is expressed highly in most human foetal tissues and cancers. However, it is completely absent in terminally-differentiated tissues. Survivin functions as a regulator of both cell division and apoptosis. The function of

Survivin differs according to cellular localization. Cytosolic Survivin is believed to function as an apoptotic suppressor, while nuclear Survivin is postulated to regulate cell division (24). Overexpression of Survivin is associated with tumour progression and poor prognosis in many types of human malignancies, including MM (25,26). In fact, several reports indicate that Survivin is a promising marker for the diagnosis of malignant pleural effusion (27). Survivin has also been reported to be associated with anti-tumour activity and outcomes of chemotherapy in MM, and is a new therapeutic target for the treatment of MM (28-30).

While the Survivin labelling indices of the EM cases in our study were similar to those reported by Meerang *et al* (25), they were significantly lower than those reported by Hmeljak *et al* (median, 67; mean, 63; range, 9.7-94.9; SD, 20.8) (26). This discrepancy in Survivin expression may be due to differences in staining technique, source of antibodies used for analysis,

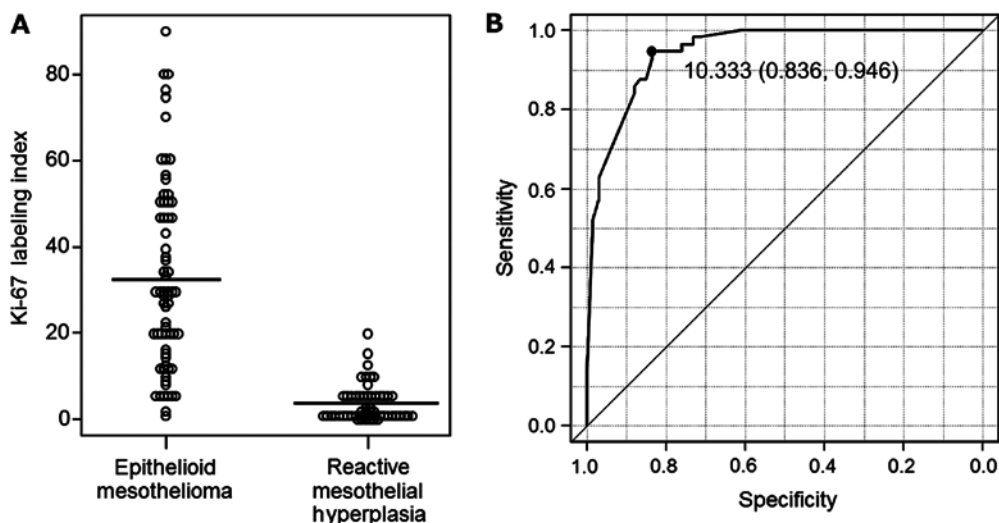


Figure 4. (A) Distributions of Ki-67 labelling index in epithelioid mesothelioma and reactive mesothelial hyperplasia. The horizontal line in the dot chart shows the mean. (B) ROC analysis. ROC curve was estimated using Ki-67 labelling index. Cut-off value based on the Youden index is also shown. ROC, receiver operating characteristic.

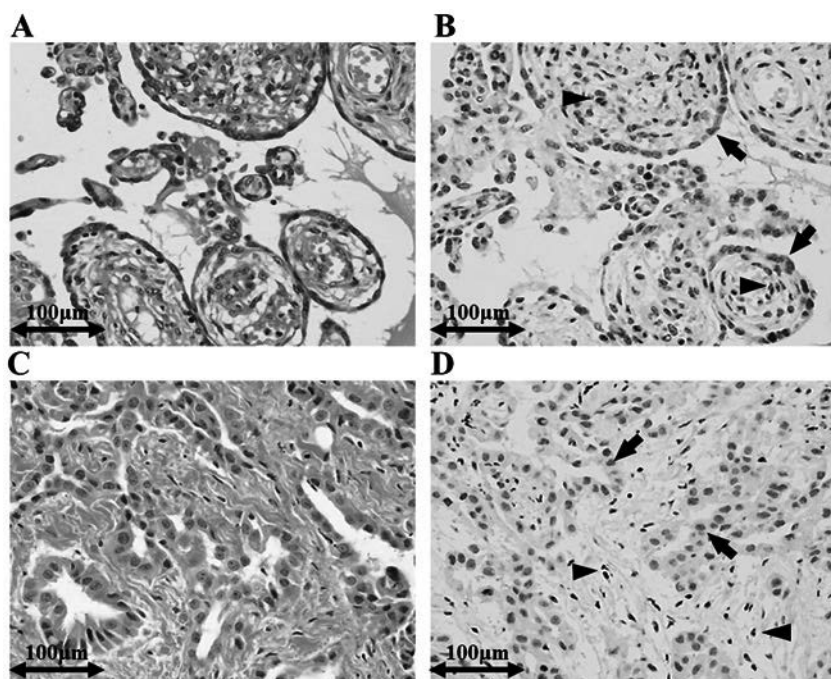


Figure 5. Representative histological images of BAP1 IHC. (A) RMH with H&E stain. (B) BAP1 IHC in RMH. Nuclear staining of the mesothelial cells (arrows) demonstrated the same intensity as that of internal positive controls (arrowheads; stromal cells). (C) EM with H&E stain. (D) BAP1 IHC in EM. Nuclear staining was not observed in tumour cells (loss of expression). Strong nuclear staining was observed in internal positive controls (arrowheads; stromal cells). IHC, immunohistochemistry; EM, epithelioid mesothelioma; RMH, reactive mesothelial hyperplasia; H&E, haematoxylin and eosin; BAP1, BRCA1-associated protein 1.

and the quantification technique. In our study, we used fully automated immunohistochemical staining utilising equipment from Roche for reproducible results. We also used commercially available antibodies from reputable sources and evaluated nuclear reactivity alone. Evaluation of nuclear reactivity was reproducible and was independently confirmed by 3 pathologists.

Several studies have determined that germline mutations in the gene for *BAP1* predispose individuals to developing various tumours, including MM, cutaneous melanocytic tumours,

uveal melanoma, lung adenocarcinoma, and meningioma (31). These studies suggest that germline mutations in *BAP1* result in a 'tumour predisposition syndrome' linking *BAP1* to many other cancers. Somatic mutations in the *BAP1* gene have also been relatively frequently reported in MMs, uveal melanomas, and renal cell carcinomas (31). *BAP1* is encoded by the *BAP1* gene, which is located on the short arm of chromosome 3 (3p21). *BAP1* is a deubiquitinase targeting histones and the host cell factor-1 transcriptional co-factor, and plays a role in transcriptional regulation, chromatin modulation, cell cycle

Table II. Sensitivity, specificity, PPVs, NPVs and diagnostic accuracies of each marker and combinations of two markers for the differential diagnosis between epithelioid mesothelioma and reactive mesothelial hyperplasia.

Immunohistochemical findings	Sensitivity (%)	Specificity (%)	PPV (%)	NPV (%)	Accuracy (%)
Survivin-positive	67.7	100.0	100.0	77.8	84.8
BAP1-loss	66.2	100.0	100.0	75.7	83.6
Ki-67-positive	85.1	87.5	89.1	83.1	86.2
Survivin-positive and/or BAP1-loss	89.8	100.0	100.0	92	95.3
Both Survivin-positive and BAP1-loss	39.0	100	100.0	65.7	71.9
Survivin-positive and/or Ki-67-positive	91.1	86.3	87.9	89.8	88.8
Both Survivin-positive and Ki-67-positive	66.1	100.0	100.0	72.9	82.2
BAP1-loss and/or Ki-67-positive	96.9	92.1	94.3	95.9	94.8
Both BAP1-loss and Ki-67-positive	53.8	100	100.0	64.3	74.8

PPV, positive predictive values; NPV, negative predictive values; BAP1, BRCA1-associated protein 1.

regulation, and DNA repair (31,32). Several different alterations in the *BAP1* gene have been described, including large deletions of exons leading to loss of the N-terminal region, or to premature protein termination, focal deletions, frameshift mutations due to insertions or deletions, splice site mutations, and base substitutions leading to nonsense and missense mutations. Frameshift mutations and missense and nonsense substitutions are the most common sequence alterations. Truncating mutations frequently result in loss of the nuclear localization signal and/or the C-terminal protein-binding domain, while missense mutations interfere with the ubiquitin hydrolase function of BAP1 (31). As the detection of these alterations in *BAP1* has been made possible in recent years using immunohistochemistry (IHC), immunohistochemical detection of BAP1 loss has also been reported to be useful in distinguishing MM from RMH. However, the sensitivity of this assay in differentiating MM from RMH does not exceed 70% (10-13). Several studies indicate that the loss of nuclear BAP1 expression as assessed by IHC is closely correlated with genetic alterations in BAP1 (33-35).

In the present study, the frequency of BAP1 loss in EM was 66.2% (49/74), similar to those found in previous reports (10-13). Recently, Hida *et al* reported a focal heterogeneous BAP1 staining pattern in mesothelioma cases (10). However, in our study, almost all EM cases had either a uniform positive staining pattern or completely negative staining for BAP1. There were some EM cases that appeared to have focal staining for BAP1; however, careful observation of these cases under high power magnification confirmed that these focal positive cells were in fact inflammatory cells infiltrating into the mesothelioma or stromal cells. We classified such cases as cases with no loss of BAP1 expression. This may be the reason for the observed heterogeneous BAP1 staining pattern in mesothelioma. However, other reasons, such as differences in staining techniques and improper processing of the tumour, may also contribute to apparent differences between studies.

The specificity of a Survivin labelling index of over 5% and a loss of BAP1 expression was 100%. However, sensitivity of Survivin labelling index (67.7%) and loss of BAP1 expression (66.2%) alone are not sufficient for differential

diagnosis. Although diagnostic accuracies of Survivin (84.8%) and BAP1 (83.6%) as single markers were inferior to that of EMA (95.5%), (21) the diagnostic accuracy of the combination of Survivin and BAP1 (Survivin-positive and/or BAP1-loss) was 95.3%, which was almost similar to EMA. Recently, Shinozaki-Ushiku *et al* proposed using a combination of BAP1 and enhancer of zeste homolog 2 (EZH2) expression to differentiate between MM from RMH; the sensitivity of this combination was 90%, while the specificity was absolute (36). The sensitivity (89.8%) and specificity (100%) of the combination of Survivin and BAP1 IHC in this study was comparable to those of previous reports (36).

A positive correlation between nuclear Survivin and Ki-67 labelling indices was previously reported by Meerang *et al* (25). We observed a similar correlation between Survivin and Ki-67 labelling indices in our study (data not shown). Although this correlation was present in both EM and RMH, it was more conspicuous in EM. Ki-67 protein is present during all active phases of the cell cycle (G1, S, G2, and mitosis), but is absent in resting cells (G0). Therefore, Ki-67 is well known as a so-called 'proliferation marker', and the Ki-67 labelling index is often correlated with the clinical course of cancer (37,38). On the other hand, nuclear Survivin plays important roles in the regulation of mitosis. Survivin expression is found to be dominant only in the G2/M phase, and Survivin is known to localize to components of the mitotic spindle during the metaphase and anaphase of mitosis (39,40). Therefore, both nuclear Survivin and Ki-67 may be considered proliferation markers. We can thus explain both the high expression of Survivin and Ki-67 in EM compared to RMH, and the positive correlation between the nuclear Survivin and Ki-67 labelling indices.

Although various studies have reported the usefulness of Ki-67 IHC in differentiating EM from RMH, (14-17) it is not routinely utilized for the confirmation of mesothelioma due to its low sensitivity and specificity.

The sensitivity, specificity, and diagnostic accuracy of Ki-67 (85.1, 87.5, and 86.2%, respectively) in this study were almost the same or slightly higher compared with previous reports (14,15,17). These values were relatively high but not sufficient for differential diagnosis by single marker. However, the diagnostic accuracy

of the combination of Ki-67 and BAP1 was 94.8%, which was almost the same as that of the combination of Survivin and BAP1.

We evaluated the utility of Survivin, BAP1, and Ki-67 IHC in distinguishing EM from RMH. Based on our results, 'Survivin-positive and/or BAP1-loss' finding strongly suggest EM, therefore we recommend the use of a combination of Survivin and BAP1. In addition, further evaluation of the Ki-67 labelling index may be useful for accurate differential diagnosis.

Acknowledgements

The authors would like to thank the Technical Centre of Hiroshima University for technical assistance. This study was funded in part by the Japanese Ministry of Health, Labour, and Welfare.

References

1. Robinson BW, Musk AW and Lake RA: Malignant mesothelioma. *Lancet* 366: 397-408, 2005.
2. Roggli VL, Sharma A, Butnor KJ, Sporn T and Vollmer RT: Malignant mesothelioma and occupational exposure to asbestos: A clinicopathological correlation of 1445 cases. *Ultrastruct Pathol* 26: 55-65, 2002.
3. Delgermaa V, Takahashi K, Park EK, Le GV, Hara T and Sorahan T: Global mesothelioma deaths reported to the World Health Organization between 1994 and 2008. *Bull World Health Organ* 89: 716-724, 2011.
4. Murayama T, Takahashi K, Natori Y and Kurumata N: Estimation of future mortality from pleural malignant mesothelioma in Japan based on an age-cohort model. *Am J Ind Med* 49: 1-7, 2006.
5. Churg A, Roggli V, Galateau-Salle F, Cagle PhT, Gibbs AR, Hasleton PhS, Henderson DW, Vignaud JM, Inai K, Praet M, *et al*: Tumours of the pleura. In: WHO Classification of Tumours of the Lung, Pleura, Thymus and Heart. Travis WD, Brambilla E, Burke AP, Marx A and Nicholson AG (eds). IARC Press, Lyon, pp153-181, 2015.
6. Husain AN, Colby T, Ordonez N, Krausz T, Attanoos R, Beasley MB, Borczuk AC, Butnor K, Cagle PT, Chirieac LR, *et al*: Guidelines for pathologic diagnosis of malignant mesothelioma: 2012 update of the consensus statement from the International Mesothelioma Interest Group. *Arch Pathol Lab Med* 137: 647-667, 2013.
7. Ordóñez NG: Application of immunohistochemistry in the diagnosis of epithelioid mesothelioma: A review and update. *Hum Pathol* 44: 1-19, 2013.
8. Kushitani K, Amatya VJ, Okada Y, Katayama Y, Mawas AS, Miyata Y, Okada M, Inai K, Kishimoto T and Takeshima Y: Utility and pitfall of immunohistochemistry in the differential diagnosis between epithelioid mesothelioma and poorly differentiated lung squamous cell carcinoma. *Histopathology* 70: 375-384, 2017.
9. Minato H, Kurose N, Fukushima M, Nojima T, Usuda K, Sagawa M, Sakuma T, Ooi A, Matsumoto I, Oda M, *et al*: Comparative immunohistochemical analysis of IMP3, GLUT1, EMA, CD146, and desmin for distinguishing malignant mesothelioma from reactive mesothelial cells. *Am J Clin Pathol* 141: 85-93, 2014.
10. Hida T, Hamasaki M, Matsumoto S, Sato A, Tsujimura T, Kawahara K, Iwasaki A, Okamoto T, Oda Y, Honda H and Nabeshima K: BAP1 immunohistochemistry and p16 FISH results in combination provide higher confidence in malignant pleural mesothelioma diagnosis: ROC analysis of the two tests. *Pathol Int* 66: 563-570, 2016.
11. Hwang HC, Sheffield BS, Rodriguez S, Thompson K, Tse CH, Gown AM and Churg A: Utility of BAP1 immunohistochemistry and p16 (CDKN2A) FISH in the diagnosis of malignant mesothelioma in effusion cytology specimens. *Am J Surg Pathol* 40: 120-126, 2016.
12. McGregor SM, Dunning R, Hyrek E, Vigneswaran W, Husain AN and Krausz T: BAP1 facilitates diagnostic objectivity, classification, and prognostication in malignant pleural mesothelioma. *Hum Pathol* 46: 1670-1678, 2015.
13. Cigognetti M, Lonardi S, Fisogni S, Balzarini P, Pellegrini V, Tironi A, Bercich L, Bugatti M, Rossi G, Murer B, *et al*: BAP1 (BRCA1-associated protein 1) is a highly specific marker for differentiating mesothelioma from reactive mesothelial proliferations. *Mod Pathol* 28: 1043-1057, 2015.
14. Kimura F, Okayasu I, Kakinuma H, Satoh Y, Kuwao S, Saegusa M and Watanabe J: Differential diagnosis of reactive mesothelial cells and malignant mesothelioma cells using the cell proliferation markers minichromosome maintenance protein 7, geminin, topoisomerase II alpha and Ki-67. *Acta Cytol* 57: 384-390, 2013.
15. Kimura F, Kawamura J, Watanabe J, Kamoshida S, Kawai K, Okayasu I and Kuwao S: Significance of cell proliferation markers (Minichromosome maintenance protein 7, topoisomerase IIalpha and Ki-67) in cavital fluid cytology: Can we differentiate reactive mesothelial cells from malignant cells? *Diagn Cytopathol* 38: 161-167, 2010.
16. Hasteh F, Lin GY, Weidner N and Michael CW: The use of immunohistochemistry to distinguish reactive mesothelial cells from malignant mesothelioma in cytologic effusions. *Cancer Cytopathol* 118: 90-96, 2010.
17. Taheri ZM, Mehrafza M, Mohammadi F, Khoddami M, Bahadori M and Masjedi MR: The diagnostic value of Ki-67 and repp86 in distinguishing between benign and malignant mesothelial proliferations. *Arch Pathol Lab Med* 132: 694-697, 2008.
18. Churg A, Sheffield BS and Galateau-Salle F: New markers for separating benign from malignant mesothelial proliferations: Are we there yet? *Arch Pathol Lab Med* 140: 318-321, 2016.
19. Hiroshima K, Wu D, Hasegawa M, Koh E, Sekine Y, Ozaki D, Yusa T, Walts AE, Marchevsky AM, Nabeshima K, *et al*: Cytologic differential diagnosis of malignant mesothelioma and reactive mesothelial cells with fish analysis of p16. *Diagn Cytopathol* 44: 591-598, 2016.
20. Walts AE, Hiroshima K, McGregor SM, Wu D, Husain AN and Marchevsky AM: BAP1 immunostain and CDKN2A (p16) FISH analysis: Clinical applicability for the diagnosis of malignant mesothelioma in effusions. *Diagn Cytopathol* 44: 599-606, 2016.
21. Kushitani K, Amatya VJ, Mawas AS, Miyata Y, Okada M and Takeshima Y: Use of anti-noxa antibody for differential diagnosis between epithelioid mesothelioma and reactive mesothelial hyperplasia. *Pathobiology* 83: 33-40, 2016.
22. Travis WD, Brambilla E, Nicholson AG, Yatabe Y, Austin JHM, Beasley MB, Chirieac LR, Dacic S, Duhig E, Flieder DB, *et al*: The 2015 World Health Organization Classification of Lung Tumors: Impact of genetic, clinical and radiologic advances since the 2004 classification. *J Thorac Oncol* 10: 1243-1260, 2015.
23. Kanda Y: Investigation of the freely available easy-to-use software 'EZR' for medical statistics. *Bone Marrow Transplant* 48: 452-458, 2013.
24. Garg H, Suri P, Gupta JC, Talwar GP and Dubey S: Survivin: A unique target for tumor therapy. *Cancer Cell Int* 16: 49, 2016.
25. Meerang M, Bérdar K, Friess M, Bitanahirwe BK, Soltermann A, Vrugt B, Felley-Bosco E, Bueno R, Richards WG, Seifert B, *et al*: Low merlin expression and high survivin labeling index are indicators for poor prognosis in patients with malignant pleural mesothelioma. *Mol Oncol* 10: 1255-1265, 2016.
26. Hmeljak J, Erčulj N, Dolžan V, Pižem J, Kern I, Kovač V, Cemazar M and Cör A: Is survivin expression prognostic or predictive in malignant pleural mesothelioma? *Virchows Arch* 462: 315-321, 2013.
27. Chen S, Wang Y, An L, Fei ZT and Li T: The diagnostic value of survivin in malignant pleural effusion: A meta-analysis. *Clin Chim Acta* 441: 142-147, 2015.
28. Bertino P, Panigada M, Soprana E, Bianchi V, Bertilaccio S, Sanvito F, Rose AH, Yang H, Gaudino G, Hoffmann PR, *et al*: Fowlpox-based survivin vaccination for malignant mesothelioma therapy. *Int J Cancer* 133: 612-623, 2013.
29. De Cesare M, Cominetti D, Doldi V, Lopergolo A, Deraco M, Gandellini P, Friedlander S, Landesman Y, Kauffman MG, Shacham S, *et al*: Anti-tumor activity of selective inhibitors of XPO1/CRM1-mediated nuclear export in diffuse malignant peritoneal mesothelioma: The role of survivin. *Oncotarget* 6: 13119-13132, 2015.
30. Goričar K, Kovač V, Franko A, Dodič-Fikfak M and Dolžan V: Serum survivin levels and outcome of chemotherapy in patients with malignant mesothelioma. *Dis Markers* 2015: 316739, 2015.
31. Murali R, Wiesner T and Scolyer RA: Tumours associated with BAP1 mutations. *Pathology* 45: 116-126, 2013.
32. Scheuermann JC, de Ayala Alonso AG, Oktaba K, Ly-Hartig N, McGinty RK, Fraterman S, Wilm M, Muir TW and Müller J: Histone H2A deubiquitinase activity of the Polycomb repressive complex PR-DUB. *Nature* 465: 243-247, 2010.

33. Bott M, Brevet M, Taylor BS, Shimizu S, Ito T, Wang L, Creaney J, Lake RA, Zakowski MF, Reva B, *et al*: The nuclear deubiquitinase BAP1 is commonly inactivated by somatic mutations and 3p21.1 losses in malignant pleural mesothelioma. *Nat Genet* 43: 668-672, 2011.
34. Testa JR, Cheung M, Pei J, Below JE, Tan Y, Sementino E, Cox NJ, Dogan AU, Pass HI, Trusa S, *et al*: Germline BAP1 mutations predispose to malignant mesothelioma. *Nat Genet* 43: 1022-1025, 2011.
35. Yoshikawa Y, Sato A, Tsujimura T, Emi M, Morinaga T, Fukuoka K, Yamada S, Murakami A, Kondo N, Matsumoto S, *et al*: Frequent inactivation of the BAP1 gene in epithelioid-type malignant mesothelioma. *Cancer Sci* 103: 868-874, 2012.
36. Shinozaki-Ushiku A, Ushiku T, Morita S, Anraku M, Nakajima J and Fukayama M: Diagnostic utility of BAP1 and EZH2 expression in malignant mesothelioma. *Histopathology* 70: 722-733, 2017.
37. Scholzen T and Gerdes J: The Ki-67 protein: From the known and the unknown. *J Cell Physiol* 182: 311-322, 2000.
38. Brown DC and Gatter KC: Monoclonal antibody Ki-67: Its use in histopathology. *Histopathology* 17: 489-503, 1990.
39. Altieri DC: Validating survivin as a cancer therapeutic target. *Nat Rev Cancer* 3: 46-54, 2003.
40. Kim JY, Chung JY, Lee SG, Kim YJ, Park JE, Yoo KS, Yoo YH, Park YC, Kim BG and Kim JM: Nuclear interaction of Smac/DIABLO with survivin at G2/M arrest prompts docetaxel-induced apoptosis in DU145 prostate cancer cells. *Biochem Biophys Res Commun* 350: 949-954, 2006.



This work is licensed under a Creative Commons Attribution-NonCommercial-NoDerivatives 4.0 International (CC BY-NC-ND 4.0) License.



A phase I trial of afatinib and bevacizumab in chemo-naïve patients with advanced non-small-cell lung cancer harboring EGFR mutations: Okayama Lung Cancer Study Group Trial 1404

Takashi Ninomiya^{a,*}, Naoyuki Nogami^b, Toshiyuki Kozuki^b, Daijiro Harada^b, Toshio Kubo^{a,c}, Kadoaki Ohashi^d, Shoichi Kuyama^e, Kenichiro Kudo^e, Akihiro Bessho^f, Nobuaki Fukamatsu^f, Nobukazu Fujimoto^g, Keisuke Aoe^h, Takuo Shibayamaⁱ, Keisuke Sugimoto^j, Nagio Takigawa^k, Katsuyuki Hotta^l, Katsuyuki Kiura^a

^a Department of Respiratory Medicine and Allergy, Okayama University Hospital, 2-5-1, Shikata-cho, Okayama, Japan

^b Department of Thoracic Oncology and Medicine, National Hospital Organization, Shikoku Cancer Center, 160, Minamiumemoto-ko, Matsuyama, Japan

^c Center for Oncology, Okayama University Hospital, 2-5-1, Shikata-cho, Okayama, Japan

^d Department of Hematology, Oncology and Respiratory Medicine, Okayama University Graduate School of Medicine, Dentistry and Pharmaceutical Sciences, 2-5-1, Shikata-cho, Okayama, Japan

^e Department of Respiratory Medicine, Iwakuni Clinical Center, 1-1-1, Atago-cho, Iwakuni, Japan

^f Department of Respiratory Medicine, Japanese Red Cross Okayama Hospital, 2-1-1, Aoe, Okayama, Japan

^g Department of Medical Oncology, Okayama Rosai Hospital, 1-10-25, Chikkomidorimachi, Okayama, Japan

^h Department of Medical Oncology, National Hospital Organization, Yamaguchi-Ube Medical Center, 685, Higashikiwa, Ube, Japan

ⁱ Department of Respiratory Medicine, National Hospital Organization, Okayama Medical Center, 1711-1, Tamasu, Okayama, Japan

^j Department of Respiratory Medicine, Japanese Red Cross Kobe Hospital, 1-3-1, Wakihamakaigann-dori, Chuo-ku, Kobe, Japan

^k Department of General Internal Medicine 4, Kawasaki Medical School, 2-6-1, Nakasange, Okayama, Japan

^l Center for Innovative Clinical Medicine, Okayama University Hospital, 2-5-1, Shikata-cho, Okayama, Japan



ARTICLE INFO

Keywords:

Non-small-cell lung cancer

EGFR

Bevacizumab

Afatinib

EGFR-TKI

Phase Ib

ABSTRACT

Objective: In advanced epidermal growth factor receptor (EGFR)-mutant non-small-cell lung cancer (NSCLC), treatment with afatinib, a second-generation EGFR-tyrosine kinase inhibitor (TKI), confers a significant survival benefit over platinum-based chemotherapy. The first-generation EGFR-TKIs gefitinib and erlotinib in combination with bevacizumab have improved progression-free survival. We hypothesized that the combination of afatinib with bevacizumab would further improve efficacy, and conducted a phase I trial to test this hypothesis.

Materials and methods: Untreated patients with advanced EGFR-mutant NSCLC were enrolled. The primary endpoint was safety. Two doses of afatinib, 40 mg/day (level 0) and 30 mg/day (level -1), were evaluated in combination with 15 mg/kg bevacizumab every 3 weeks. Optimal dosing was determined by dose-limiting toxicity (DLT), with the concentration at which ≤ 4 of 12 patients experienced toxicity considered the recommended dose.

Results: Nineteen patients were enrolled (level 0:5, level -1:14). Three of the five patients at level 0 experienced a DLT, which indicated that this dose was unfeasible. Three patients at level -1 developed a DLT of grade 3 non-hematological toxicity, which was soon resolved. Grade 3 or worse adverse events were experienced by all five patients at dose level 0 (diarrhea in 2, skin rash in 1, hypoxia in 1, and paronychia in 1), and by three patients at level -1 (diarrhea in 2 and anorexia in 1). Among 16 evaluable patients, 1 had a complete response, 12 had partial responses, and 0 had progressive disease.

Conclusion: Afatinib plus bevacizumab (level -1) was well tolerated and showed evidence of favorable disease control. This combination therapy may represent a potent therapeutic option for patients with EGFR-mutant NSCLC.

* Corresponding author at: Department of Respiratory Medicine and Allergy, Okayama University Hospital, 2-5-1, Shikata-cho, Okayama, 700-8558, Japan.
E-mail address: tninomiya5@okayama-u.ac.jp (T. Ninomiya).

1. Introduction

Lung cancer is a leading cause of death worldwide. The major pathological subtype of lung cancer is non-small-cell lung cancer (NSCLC); in some NSCLCs, activating mutations in the epidermal growth factor receptor (EGFR) gene have been reported [1]. In this subgroup of patients, an EGFR-tyrosine kinase inhibitor (EGFR-TKI) was found to prolong progression-free survival (PFS) compared with standard platinum-based chemotherapy [2–7]. While the median overall survival (OS) of this patient subgroup reaches almost 2 years with EGFR-TKI treatment, this is still insufficient. To prolong PFS and OS, more effective treatments are needed.

Afatinib, a second-generation EGFR-TKI, is an irreversible inhibitor of the ErbB family that is expected to inhibit tumors with activating EGFR mutations more strongly than are reversible EGFR-TKIs. Our preclinical study revealed that afatinib prolonged survival compared with gefitinib in an *egfr*-driven mouse lung cancer model [8]. In a clinical study, afatinib significantly improved outcomes in treatment-naïve patients with NSCLC harboring EGFR mutations compared with gefitinib [9]. In a combined analysis of phase III studies comparing afatinib with platinum-based chemotherapy, afatinib significantly prolonged both PFS and OS [10], while first-generation EGFR-TKIs (gefitinib or erlotinib) prolonged PFS but not OS [2,3]. Thus, second-generation EGFR-TKIs are suggested to achieve better outcomes than those of first-generation inhibitors.

Vascular endothelial growth factor (VEGF)-A, by binding to the VEGF receptor (VEGFR)-2, promotes angiogenesis in the tumor microenvironment and indirectly promotes tumor growth. We previously described the synergistic effects of afatinib and bevacizumab, a recombinant monoclonal antibody targeting VEGF-A [8]. In our pre-clinical study, the combination of bevacizumab with afatinib was more effective than afatinib alone in a xenograft model of NSCLC cells harboring EGFR mutations. Clinically, we and another group have already shown favorable PFS with acceptable toxicity profiles for combination therapy consisting of bevacizumab and first-generation EGFR-TKIs in untreated EGFR-mutant tumors [11–13]. The median PFSs of patients treated with erlotinib/bevacizumab therapy and gefitinib/bevacizumab therapy were 16.0 months and 14.4 months, respectively. However, combination therapy of bevacizumab with the second-generation EGFR-TKI afatinib had not been evaluated clinically.

Against this background, we hypothesized that the combination of bevacizumab with afatinib would yield improved efficacy. As the first step to test this hypothesis, we initiated a phase I trial of this combination therapy in chemo-naïve patients with advanced NSCLC harboring EGFR mutations.

2. Materials and methods

2.1. Study design

This open-label, phase I study was conducted in 16 institutions in Japan (UMIN000015944). The study protocol was approved by the institutional review boards of each participating center. Written informed consent was obtained from each patient prior to the study. This study was performed in accordance with the Declaration of Helsinki and all relevant Japanese laws and regulations.

The aim of this study was to evaluate the feasibility and recommended dose of combination therapy in chemo-naïve patients with advanced NSCLC harboring EGFR mutations. The primary outcome measure was dose-limiting toxicity (DLT). Secondary outcome measures were the objective response rate, PFS, OS, and specific toxicity.

2.2. Patients

Those patients who met the following criteria were eligible: histologically or cytologically confirmed stage IIIB/IV or postoperative

recurrent non-squamous NSCLC with activating EGFR mutations (either exon 19 deletion or Leu858Arg), age ≥ 20 years, Eastern Cooperative Oncology Group performance status of 0 or 1, adequate organ function, and life expectancy of 3 months or more. Those who received previous EGFR-TKI therapy or radiation therapy for lung tumors were excluded. Tumor samples were screened by PCR-based hypersensitive EGFR mutation testing in local laboratories, according to standard testing practices.

Major exclusion criteria included confirmation of the Thr790Met mutation, presence of symptomatic brain metastasis or leptomeningeal carcinomatosis, history or presence of hemoptysis, bloody sputum or a coagulation disorder, tumor invading or abutting major blood vessels, tumor cavitation, or coexisting or previous interstitial lung disease.

2.3. Treatment regimen

Six patients were first scheduled to receive 40 mg afatinib daily plus 15 mg/kg intravenous bevacizumab repeated at 3-week intervals (level 0) until disease progression or unacceptable toxicity was observed. If no more than two patients experienced DLT, an additional six patients were treated at the same dose. If no more than two patients experienced DLT in both sets (a rate of DLT $< 33.3\%$), we concluded this dose schedule to be feasible and planned a subsequent phase II trial. Otherwise, we repeated the same treatment of 30 mg/day afatinib and 15 mg/kg bevacizumab (level -1). If four or fewer patients experienced DLT (a rate of DLT $< 33.3\%$), this level was recommended; if not, further investigation of this combination therapy was not pursued.

2.4. Safety and efficacy assessment

Severity of toxicity was assessed according to the Common Terminology Criteria for Adverse Events v 4.0. Although all treatment courses were analyzed to determine the DLT and maximum tolerated dose, the decision to lower the dose level was based on toxicity during the first 28 days from initiation of the combination therapy. A DLT was defined as any of the following adverse drug reactions: grade 4 hematological toxicity, grade 4 hypertension, grade 3 or worse non-hematological toxicity other than hypertension, grade 2 non-hematological toxicity lasting ≥ 7 days despite supportive care, grade 2 or worse left ventricular function or renal function, grade 1 or worse pneumonitis, or inability to receive the second course of bevacizumab due to bevacizumab toxicity.

Antitumor activity was assessed radiologically (by computed tomography or magnetic resonance imaging) every 2 months. All responses were defined according to the criteria of RECIST 1.1. If a patient had a documented complete response (CR) or partial response (PR), a confirmatory evaluation was performed after 4 weeks. Disease control was defined as the best tumor response among CR, PR, and stable disease (SD) that had been confirmed and sustained for at least 6 weeks. The response rate (RR) was defined as the number of patients with the best tumor response (CR or PR) among all patients with measurable lesions. OS was defined as the time from the date of registration to death from any cause. PFS was defined as the time from the date of registration to the date of the detection of progressive disease or of death from any cause. OS and PFS were assessed by the Kaplan-Meier method.

3. Results

3.1. Patient characteristics

From December 2014 to July 2016, 19 patients were enrolled, of whom 5 were treated at dose level 0 and 14 at dose level -1 . The clinical characteristics of all patients are listed in Table 1. Three patients were withdrawn for toxicity (Fig. 1).

Table 1
Patient characteristics by dose level.

Characteristics	All patients (n = 19)	Level 0 (n = 5)	Level -1 (n = 14)
Age (years)			
Median	67.0	65.0	67.5
Range	40–76	42–68	40–76
Sex			
Male	10	3	7
Female	9	2	7
ECOG performance status			
0	10	4	6
1	9	1	8
Histology			
Adenocarcinoma	19	5	14
Disease status			
IV	9	3	6
Postoperative recurrence	10	2	8
EGFR mutation			
Exon 19 deletion	8	2	6
Exon 21 L858R	11	3	8
Brain metastasis			
Positive	9	2	7
Negative	10	3	7

Dose level 0: afatinib (40 mg once daily) plus bevacizumab (15 mg/kg intravenously repeated at 3-week intervals). Dose level -1: afatinib (30 mg once daily) plus bevacizumab (15 mg/kg intravenously repeated at 3-week intervals).

ECOG, Eastern Cooperative Oncology Group.

3.2. DLTs

Three of five patients at dose level 0 experienced DLTs: grade 3 diarrhea (n = 2) and hypoxia (n = 1); thus, we concluded that this dose level was unfeasible. At level -1, 3 of 14 patients developed DLTs: grade 3 diarrhea (n = 2) and anorexia (n = 1). Although we originally planned to enroll only 12 patients in level -1, 14 patients were ultimately included due to the timing of patient enrollment. The rate of DLT was 60% at dose level 0 and 21.4% at dose level -1. The maximum tolerated/recommended dose was determined to be 30 mg afatinib once daily with 15 mg/kg of bevacizumab repeated at 3-week intervals. All DLTs resolved soon after discontinuation of afatinib. Four patients who experienced DLT of grade 3 diarrhea reduced their dosage of afatinib and resumed treatment after recovering. Those patients who experienced hypoxia or anorexia stopped therapy, based on the investigator's decision and the patients' requests, respectively.

Table 2
Adverse events.

Adverse Event	n (%)	
	Any Grade	Grade 3 ^b
Dose level 0 (n = 5)		
Diarrhea	5 (100)	2 (40) ^a
Rash acneiform	4 (80)	1 (20)
Paronychia	4 (80)	1 (20)
Hypertension	3 (60)	0
AST/ALT increase	2 (40)	0
Hypoxia	1 (20)	1 (20) ^a
Fatigue	1 (20)	0
Bleeding	1 (20)	0
Mucositis oral	1 (20)	0
Proteinuria	1 (20)	0
Dose level -1 (n = 14)		
Rash acneiform	13 (93)	1 (7)
Diarrhea	12 (86)	2 (14) ^a
Paronychia	7 (50)	0
Nausea/Vomiting	4 (29)	0
Hypertension	4 (29)	0
Proteinuria	4 (29)	0
Anorexia	3 (21)	1 (7) ^a
Mucositis Oral	3 (21)	1 (7)
Fatigue	3 (21)	0
Bleeding	1 (7)	0

Dose level 0: afatinib (40 mg once daily) plus bevacizumab (15 mg/kg intravenously repeated at 3-week intervals). Dose level -1: afatinib (30 mg once daily) plus bevacizumab (15 mg/kg intravenously repeated at 3-week intervals).

AST/ALT, aspartate aminotransferase/alanine aminotransferase ratio.

^a DLTs comprised grade 3 diarrhea (n = 4), hypoxia (n = 1), and anorexia (n = 1).

^b There were no grade 4 or 5 adverse events.

3.3. Adverse events

The frequent (> 25%) adverse events were acneiform rash, diarrhea, paronychia, hypertension, and proteinuria. The main grade 3 toxicities are listed in Table 2. All patients at dose level 0 and 4 of 14 patients (29%) at level -1 had grade 3 toxicities. There were no grade 4 or 5 toxicities. Three patients at level 0 and five patients at level -1 required dose reductions for toxicity. Three patients at level 0 and one patient at level -1 discontinued the protocol therapy for toxicity, and two patients at level -1 discontinued for anorexia (Fig. 1).

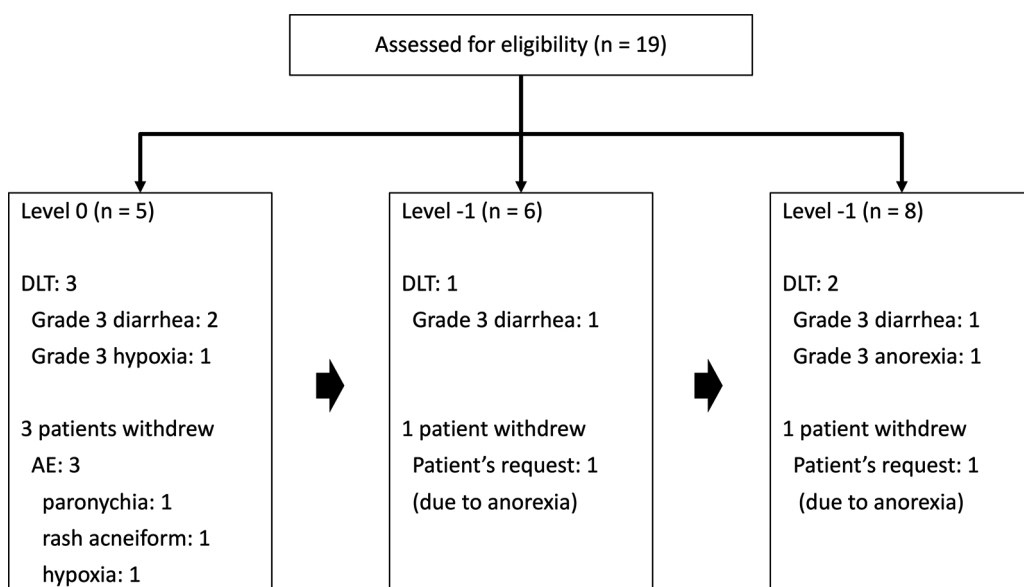


Fig. 1. Flow chart showing the study progression. Abbreviations: DLT, dose limiting toxicity; AE, adverse event.

Table 3
Response and disease control rates.

	No. of Patients (n = 16)	%
Response		
Complete response	1	6.3
Partial response	12	75.0
Stable disease	3	18.8
Progressive disease	0	0
Response rate (95% CI)	13	81.3 (62.1–100)
Disease control rate	16	100

A total of 16 patients who had measurable lesions were evaluated (Level 0, n = 4, Level –1, n = 12).

Disease control implies complete response, partial response, and stable disease. CI, confidence interval.

3.4. Treatment activity

Of 19 patients, 16 had baseline measurable lesions. Of these 16 patients, 1 had a confirmed CR and 12 a PR for an overall RR of 81.3% (95% confidence interval: 62.1–100%) in our intent-to-treat analysis (Table 3). There was no disease progression in any of the patients, and the disease control rate (DCR, summation percentage of CR, PR, and SD) was 100%. A waterfall plot for the 15 response-evaluable patients with at least one follow-up scan is presented in Fig. 2A. The treatment duration, treatment dose, and dose reduction or discontinuation of afatinib due to toxicity for each patient are shown in Fig. 2B. No disease progression has been reported at this time (median follow-up: 104 [range: 41–536] days).

4. Discussion

This is the first trial to assess the combination of a second-generation EGFR-TKI with an angiogenesis inhibitor. In the dose level 0 group, the rate of DLT was 60%, and the two patients without DLT required dose reductions for toxicity. Therefore, this dose level was not considered feasible. In the dose level –1 group, the rate of DLT was 21.4%, which met the primary end point. Of the 14 patients at this level, 7 were able to continue therapy at this dose, and we concluded that this does should be investigated further.

The most frequent toxicity was rash acneiform (17/19 patients), followed by diarrhea (16/19 patients). Specifically, diarrhea rapidly increased around day 10–14, when it reached grade 3, and was considered a DLT, although the toxicity immediately resolved after cessation of afatinib. The other grade 3 toxicities also resolved immediately. The bevacizumab toxicities noted were bleeding, hypertension, and proteinuria, but all were grade 1 or 2.

The LUX-Lung 3 (LL3) study was a large, prospective, randomized trial comparing afatinib with cisplatin-based chemotherapy for patients with advanced EGFR mutant NSCLC [6]. Included in this trial was a cohort of 54 Japanese patients treated with afatinib alone. Within this group, adverse events included diarrhea (100%), rash acneiform (100%), nail effects (92.6%), and stomatitis (92.6%) [14]. Time to first onset of diarrhea was within 14 days after starting afatinib for most patients. In terms of grade 3 toxicities, diarrhea occurred in 22.2%, rash acneiform in 20.4%, nail effects in 25.9%, and stomatitis in 7.4%, respectively. These safety profiles were generally consistent with that of our dose level –1. Adverse events leading to dose reduction occurred in 75.9% in the LL3 study. Here, dose level 0 was deemed too toxic, with all patients requiring either a dose reduction or discontinuation of therapy.

In a phase II trial comparing bevacizumab and erlotinib combination therapy with erlotinib monotherapy (JO25567), more grade 3 or worse adverse events were reported in the combination therapy group (91% vs 53%) [11]. In a similar phase II trial examining the use of bevacizumab and gefitinib combination therapy (OLCSG1001), grade 2

or worse rash was seen in 15% of patients [12], compared to only 2–5% for gefitinib monotherapy [2,3,15]. Taken together, these studies show that toxicities caused by EGFR-TKIs are exacerbated by the addition of bevacizumab. In this trial, afatinib-associated toxicities were also expected to worsen with the addition of bevacizumab, necessitating a lower recommended afatinib dose of 30 mg/day.

Like the LL3 trial, the LUX-Lung 6 (LL6) trial was also a large, prospective, randomized trial that compared afatinib with cisplatin-based chemotherapy for patients with advanced EGFR mutant NSCLC. The LL3 study was conducted globally and included Japanese patients, while the LL6 study was limited to patients in China, Thailand, and South Korea [6,7]. In a post hoc analysis of LL3 and LL6, afatinib trough plasma concentrations after treatment at the 40 mg dose were found to be higher on day 22 in patients whose doses were subsequently reduced to 30 mg due to toxicity, compared with those who remained on the 40 mg dose, with similar plasma concentrations observed in both groups on day 43 [16]. Furthermore, total treatment time tended to be longer in patients requiring a dose reduction compared to those maintained at the same dose, with similar PFS times in each group. This tolerability-guided dose adjustment of afatinib is thought to have played an important role in determining patient outcomes, allowing patients to maintain adequate plasma concentrations and continue effective therapy. In the LL3 study, Japanese patients were more likely to require a dose reduction (to 30 mg or 20 mg) due to adverse events than the overall study population (75.9% vs. 57.2%, respectively). Nevertheless, the median PFS was similar to that observed in the overall population (13.8 months vs. 11.1 months, respectively) [14]. In the present study evaluating afatinib combined with bevacizumab, the recommended afatinib dose (30 mg/day) should yield adequate plasma concentrations in all patients.

In two different phase II trials assessing the use of erlotinib alone or in combination with bevacizumab, the overall RR and DCR were 69% and 100%, respectively for the JO25567 trial [11], compared with 78% and 92%, respectively, for the BELIEF trial [13]. In the OLCSG1001 phase II trial of bevacizumab alone or combined with gefitinib, the overall RR and DCR were 73.8% and 97.6%, respectively [12]. The finding that almost no patients showed early refractory responses might be a feature of these combination therapies of EGFR-TKIs and bevacizumab. The overall RR of 81.3% and DCR of 100% in the present trial indicates that the combination therapy we evaluated might also have this effect. The PFS and OS data are still immature.

The current study had several limitations. Although toxicities were evaluated using the pre-defined criteria set forth in the protocol, the follow-up time may have been too short, as no disease progression was observed. Furthermore, the scope of this trial was limited, assessing only a small number of patients from a handful of institutes in a single country. Observation gathered over a longer period of time, as well as in a larger cohort of patients, will be necessary, particularly for side effects such as paronychia, hypertension, renal toxicity, thrombosis, and bleeding, as these would be more common during prolonged therapy. To that end, we have just initiated a larger randomized trial comparing the combination of afatinib and bevacizumab with afatinib alone (UMIN000027432). In this trial, 100 patients (50 patients per group) will be enrolled, enabling better assessment of the safety and efficacy of these treatments over longer treatment times, and across a larger number of patients.

In summary, the combination therapy of bevacizumab with afatinib, at doses of 30 mg/day afatinib and 15 mg/kg bevacizumab, was feasible and potentially effective.

Contributors

All authors contributed to the protocol writing. TN, TK, and KH also took part in the trial design and set-up. TN, TK, and KH participated in the sample size calculation. NN, DH, KO, SK, AB, NF, KA, TS, NT, KS, KK, and NF contributed to the subject enrollment.

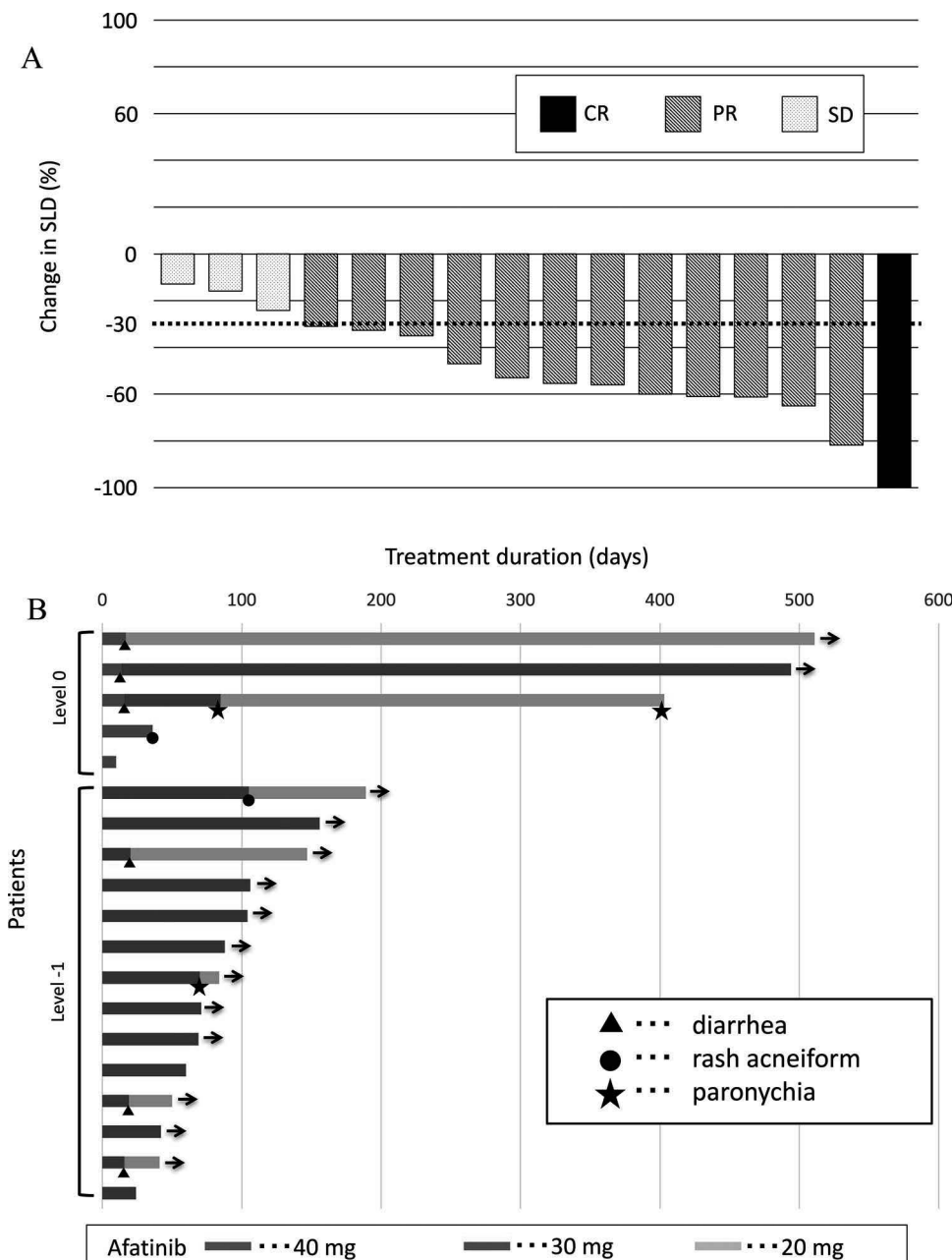


Fig. 2. A. Waterfall plot for the patients with measurable lesions. Abbreviations: SLDsum of the longest diameters; CRcomplete response; PRpartial response; SDstable disease. B. Swimmer plot for all patients.

Trial sponsorship and financing information

This research received no specific grant from any funding agency in the public, commercial, or not-for-profit sectors.

Conflict of interest

TN received honoraria outside the current work from MSD, Boehringer-Ingelheim, and Chugai Pharmaceutical. NN received honoraria outside the current work from AstraZeneca, Ono Pharmaceutical, Astellas, Taiho Pharmaceutical, Eli Lilly Japan, Pfizer Inc. Japan, Boehringer-Ingelheim, and Chugai Pharmaceutical. TK received honoraria outside the current work from AstraZeneca, Ono Pharmaceutical, BMS, Kyowa Hakko Kirin, Eli Lilly Japan, Pfizer Inc. Japan, Boehringer-Ingelheim, and Chugai Pharmaceutical. TK has also received research funding outside the current work from AstraZeneca, Ono Pharmaceutical, BMS, Eli Lilly Japan, MSD, and Chugai Pharmaceutical. DH received honoraria outside the current work from

Ono Pharmaceutical, BMS, Kyowa Hakko Kirin and Yakult Honsha Co. Ltd. KO has received a research grant from Novartis Pharmaceuticals Japan. SK received honoraria outside the current work from Ono Pharmaceutical, BMS, Eli Lilly Japan, Boehringer-Ingelheim, Meiji Seika Pharma Co., and Chugai Pharmaceutical. AB received honoraria outside the current work from AstraZeneca, Novartis, Eli Lilly Japan, Taiho Pharmaceutical, Pfizer Inc. Japan and Chugai Pharmaceutical. AB has also received research funding outside the current work from AstraZeneca and Amgen. NF received honoraria outside the current work from KISSEI Co. Ltd. KA received honoraria outside the current work from AstraZeneca, Eli Lilly Japan, Ono Pharmaceutical, and BMS. NT has received honoraria outside the current work from Eli Lilly Japan, AstraZeneca, Daiichi-Sankyo Pharmaceutical, Chugai Pharmaceutical, Taiho Pharmaceutical, Pfizer Inc. Japan, Boehringer-Ingelheim, and Ono Pharmaceutical, and research funding from AstraZeneca, Pfizer Inc. Japan, Kyowa Hakko Kirin, Eli Lilly Japan, Chugai Pharmaceutical, Nippon Kayaku Co. Ltd, Taiho Pharmaceutical, Takeda Pharmaceutical Co. Ltd, and

Boehringer-Ingelheim, and Ono Pharmaceutical. KH received honoraria outside the current work from AstraZeneca, Ono Pharmaceutical, Astellas, Novartis, BMS, MSD, Eli Lilly Japan, Daiichi-Sankyo Pharmaceutical, Boehringer-Ingelheim, Nihon Kayaku, Taiho Pharmaceutical, and Chugai Pharmaceutical. KH has also received research funding outside the current work from AstraZeneca, Boehringer-Ingelheim, Ono Pharmaceutical, Astellas, Novartis, BMS, Eli Lilly Japan, MSD, and Chugai Pharmaceutical. KK has received honoraria from Eli Lilly Japan, Nihon Kayaku, AstraZeneca, Daiichi-Sankyo Pharmaceutical, Chugai Pharmaceutical, Taiho Pharmaceutical, and Sanofi-Aventis. All of the other authors declare no conflicts of interest regarding this study.

Acknowledgements

The authors wish to acknowledge and thank the coordinators and all the other investigators who contributed to this study as independent data-monitoring committee members, including Drs. Yoshiko Ogata, Makoto Sakugawa (Japanese Red Cross Okayama Hospital), Tomoko Yamagishi, Sae Wada (Okayama Rosai Hospital), Daisuke Minami, Takamasa Nakasuka (Okayama Medical Center), Daisuke Nojima (Iwakuni Medical Center), Nobuaki Ochi (Kawasaki Medical School General Medical Center), Yusuke Hata, Hirohisa Kano (Okayama University Hospital), Yosuke Toyota (Fukuyama Medical Center), Mikio Kataoka, and Masafumi Fujii. This study has been conducted with support from the Center for Innovative Clinical Medicine, Okayama University Hospital.

References

- [1] T.J. Lynch, D.W. Bell, R. Sordella, S. Gurubhagavatula, R.A. Okimoto, B.W. Brannigan, P.L. Harris, S.M. Haserlat, J.G. Supko, F.G. Haluska, D.N. Louis, D.C. Christiani, J. Settleman, D.A. Haber, Activating mutations in the epidermal growth factor receptor underlying responsiveness of non-small-cell lung cancer to gefitinib, *N. Engl. J. Med.* 350 (2004) 2129–2139, <http://dx.doi.org/10.1056/NEJMoa040938>.
- [2] M. Maemondo, A. Inoue, K. Kobayashi, S. Sugawara, S. Oizumi, H. Isobe, A. Gemma, M. Harada, H. Yoshizawa, I. Kinoshita, Y. Fujita, S. Okinaga, H. Hirano, K. Yoshimori, T. Harada, T. Ogura, M. Ando, H. Miyazawa, T. Tanaka, Y. Saito, K. Hagiwara, S. Morita, T. Nukiwa, North-East Japan Study Group, Gefitinib or chemotherapy for non-small-cell lung cancer with mutated EGFR, *N. Engl. J. Med.* 362 (2010) 2380–2388, <http://dx.doi.org/10.1056/NEJMoa0909530>.
- [3] T. Mitsudomi, S. Morita, Y. Yatabe, S. Negoro, I. Okamoto, J. Tsurutani, T. Seto, M. Satouchi, H. Tada, T. Hirashima, K. Asami, N. Katakami, M. Takada, H. Yoshioka, K. Shibata, S. Kudoh, E. Shimizu, H. Saito, S. Toyooka, K. Nakagawa, M. Fukuoka, West Japan Oncology Group, Gefitinib versus cisplatin plus docetaxel in patients with non-small-cell lung cancer harbouring mutations of the epidermal growth factor receptor (WJTOG3405): an open label, randomised phase 3 trial, *Lancet Oncol.* 11 (2010) 121–128, [http://dx.doi.org/10.1016/S1470-2045\(09\)70364-X](http://dx.doi.org/10.1016/S1470-2045(09)70364-X).
- [4] C. Zhou, Y.-L. Wu, G. Chen, J. Feng, X.-Q. Liu, C. Wang, S. Zhang, J. Wang, S. Zhou, S. Ren, S. Lu, L. Zhang, C. Hu, C. Hu, Y. Luo, L. Chen, M. Ye, J. Huang, X. Zhi, Y. Zhang, Q. Xiu, J. Ma, L. Zhang, C. You, Erlotinib versus chemotherapy as first-line treatment for patients with advanced EGFR mutation-positive non-small-cell lung cancer (OPTIMAL, CTONG-0802): a multicentre, open-label, randomised, phase 3 study, *Lancet Oncol.* 12 (2011) 735–742, [http://dx.doi.org/10.1016/S1470-2045\(11\)70184-X](http://dx.doi.org/10.1016/S1470-2045(11)70184-X).
- [5] R. Rosell, E. Carcereny, R. Gervais, A. Vergnenegre, B. Massuti, E. Felip, R. Palmero, R. Garcia-Gomez, C. Pallares, J.M. Sanchez, R. Porta, M. Cobo, P. Garrido, F. Longo, T. Moran, A. Insa, F. De Marinis, R. Corre, I. Bover, A. Illiano, E. Dansin, J. de Castro, M. Milella, N. Reguart, G. Altavilla, U. Jimenez, M. Provencio, M.A. Moreno, J. Terrasa, J. Muñoz-Langa, J. Valdivia, D. Isla, M. Domine, O. Molinier, J. Mazières, N. Baize, R. Garcia-Campelo, G. Robinet, D. Rodriguez-Abreu, G. Lopez-Vivanco, V. Gebbia, L. Ferrera-Delgado, P. Bombaron, R. Bernabe, A. Bearz, A. Artal, E. Cortesi, C. Rolfo, M. Sanchez-Ronco, A. Drozdowskyj, C. Queralt, I. de Aguirre, J.L. Ramirez, J.J. Sanchez, M.A. Molina, M. Taron, L. Paz-Ares, Spanish Lung Cancer Group in collaboration with Groupe Français de Pneumo-Cancérologie, Associazione Italiana Oncologia Toracica, Erlotinib versus standard chemotherapy as first-line treatment for European patients with advanced EGFR mutation-positive non-small-cell lung cancer (EURTAC): a multicentre, open-label, randomised phase 3 trial, *Lancet Oncol.* 13 (2012) 239–246, [http://dx.doi.org/10.1016/S1470-2045\(11\)70393-X](http://dx.doi.org/10.1016/S1470-2045(11)70393-X).
- [6] L.V. Sequist, J.C.-H. Yang, N. Yamamoto, K. O'Byrne, V. Hirsh, T. Mok, S.L. Geater, S. Orlov, C.-M. Tsai, M. Boyer, W.-C. Su, J. Bennouna, T. Kato, V. Gorbunova, K.H. Lee, R. Shah, D. Massey, V. Zazulina, M. Shahidi, M. Schuler, Phase III study of afatinib or cisplatin plus pemetrexed in patients with metastatic lung adenocarcinoma with EGFR mutations, *J. Clin. Oncol.* 31 (2013) 3327–3334, <http://dx.doi.org/10.1200/JCO.2012.44.2806>.
- [7] Y.-L. Wu, C. Zhou, C.-P. Hu, J. Feng, S. Lu, Y. Huang, W. Li, M. Hou, J.H. Shi, K.Y. Lee, C.-R. Xu, D. Massey, M. Kim, Y. Shi, S.L. Geater, Afatinib versus cisplatin plus gemcitabine for first-line treatment of Asian patients with advanced non-small-cell lung cancer harbouring EGFR mutations (LUX-Lung 6): an open-label, randomised phase 3 trial, *Lancet Oncol.* 15 (2014) 213–222, [http://dx.doi.org/10.1016/S1470-2045\(13\)70604-1](http://dx.doi.org/10.1016/S1470-2045(13)70604-1).
- [8] T. Ninomiya, N. Takigawa, E. Ichihara, N. Ochi, T. Murakami, Y. Honda, T. Kubo, D. Minami, K. Kudo, M. Tanimoto, K. Kiura, Afatinib prolongs survival compared with gefitinib in an epidermal growth factor receptor-driven lung cancer model, *Mol. Cancer Ther.* 12 (2013) 589–597, <http://dx.doi.org/10.1158/1535-7163.MCT-12-0885>.
- [9] K. Park, E.-H. Tan, K. O'Byrne, L. Zhang, M. Boyer, T. Mok, V. Hirsh, J.C.-H. Yang, K.H. Lee, S. Lu, Y. Shi, S.-W. Kim, J. Laskin, D.-W. Kim, C.D. Arvis, K. Kölbeck, S.A. Laurie, C.-M. Tsai, M. Shahidi, M. Kim, D. Massey, V. Zazulina, L. Paz-Ares, Afatinib versus gefitinib as first-line treatment of patients with EGFR mutation-positive non-small-cell lung cancer (LUX-Lung 7): a phase 2B, open-label, randomised controlled trial, *Lancet Oncol.* 17 (2016) 577–589, [http://dx.doi.org/10.1016/S1470-2045\(16\)30033-X](http://dx.doi.org/10.1016/S1470-2045(16)30033-X).
- [10] J.C.-H. Yang, Y.-L. Wu, M. Schuler, M. Sebastian, S. Popat, N. Yamamoto, C. Zhou, C.-P. Hu, K. O'Byrne, J. Feng, S. Lu, Y. Huang, S.L. Geater, K.Y. Lee, C.-M. Tsai, V. Gorbunova, V. Hirsh, J. Bennouna, S. Orlov, T. Mok, M. Boyer, W.-C. Su, K.H. Lee, T. Kato, D. Massey, M. Shahidi, V. Zazulina, L.V. Sequist, Afatinib versus cisplatin-based chemotherapy for EGFR mutation-positive lung adenocarcinoma (LUX-Lung 3 and LUX-Lung 6): analysis of overall survival data from two randomised, phase 3 trials, *Lancet Oncol.* 16 (2015) 141–151, [http://dx.doi.org/10.1016/S1470-2045\(14\)71173-8](http://dx.doi.org/10.1016/S1470-2045(14)71173-8).
- [11] T. Seto, T. Kato, M. Nishio, K. Goto, S. Atagi, Y. Hosomi, N. Yamamoto, T. Hida, M. Maemondo, K. Nakagawa, S. Nagase, I. Okamoto, T. Yamamaka, K. Tajima, R. Harada, M. Fukuoka, N. Yamamoto, Erlotinib alone or with bevacizumab as first-line therapy in patients with advanced non-squamous non-small-cell lung cancer harbouring EGFR mutations (JO25567): an open-label, randomised, multicentre, phase 2 study, *Lancet Oncol.* 15 (2014) 1236–1244, [http://dx.doi.org/10.1016/S1470-2045\(14\)70381-X](http://dx.doi.org/10.1016/S1470-2045(14)70381-X).
- [12] E. Ichihara, K. Hotta, N. Nogami, S. Kuyama, D. Kishino, M. Fujii, T. Kozuki, M. Tabata, D. Harada, K. Chikamori, K. Aoe, H. Ueoka, S. Hosokawa, A. Bessho, A. Hisamoto-Sato, T. Kubo, I. Oze, N. Takigawa, M. Tanimoto, K. Kiura, Phase II trial of gefitinib in combination with bevacizumab as first-line therapy for advanced non-small cell lung cancer with activating EGFR gene mutations: the Okayama Lung Cancer Study Group Trial 1001, *J. Thorac Oncol.* 10 (2015) 486–491, <http://dx.doi.org/10.1097/JTO.0000000000000434>.
- [13] R. Rosell, U. Dafni, E. Felip, A. Curioni-Fontecedro, O. Gautschi, S. Peters, B. Massuti, R. Palmero, S.P. Aix, E. Carcereny, M. Früh, M. Pless, S. Popat, A. Kotsakis, S. Cuffe, P. Bidoli, A. Favaretto, P. Froesch, N. Reguart, J. Puente, L. Coate, F. Barlesi, D. Rauch, M. Thomas, C. Camps, J. Gómez-Codina, M. Majem, R. Porta, R. Shah, E. Hanrahan, R. Kammer, B. Ruepp, M. Rabaglio, M. Kassapian, N. Karachaliou, R. Tam, D.S. Shames, M.A. Molina-Vila, R.A. Stahel, B.E.L.I.E.F. collaborative group, Erlotinib and bevacizumab in patients with advanced non-small-cell lung cancer and activating EGFR mutations (BELIEF): an international, multicentre, single-arm, phase 2 trial, *Lancet Respir. Med.* 5 (2017) 435–444, [http://dx.doi.org/10.1016/S2213-2600\(17\)30129-7](http://dx.doi.org/10.1016/S2213-2600(17)30129-7).
- [14] T. Kato, H. Yoshioka, I. Okamoto, A. Yokoyama, T. Hida, T. Seto, K. Kiura, D. Massey, Y. Seki, N. Yamamoto, Afatinib versus cisplatin plus pemetrexed in Japanese patients with advanced non-small cell lung cancer harboring activating EGFR mutations: subgroup analysis of LUX-lung 3, *Cancer Sci.* 106 (2015) 1202–1211, <http://dx.doi.org/10.1111/cas.12723>.
- [15] T.S. Mok, Y.-L. Wu, S. Thongprasert, C.-H. Yang, D.-T. Chu, N. Sajio, P. Sunpaweravong, B. Han, B. Margono, Y. Ichinose, Y. Nishiwaki, Y. Ohe, J.-J. Yang, B. Chewaskulyong, H. Jiang, E.L. Duffield, C.L. Watkins, A.A. Armour, M. Fukuoka, Gefitinib or carboplatin–paclitaxel in pulmonary adenocarcinoma, *N. Engl. J. Med.* 361 (2009) 947–957, <http://dx.doi.org/10.1056/NEJMoa0810699>.
- [16] J.C.-H. Yang, L.V. Sequist, C. Zhou, M. Schuler, S.L. Geater, T. Mok, C.-P. Hu, N. Yamamoto, J. Feng, K. O'Byrne, S. Lu, V. Hirsh, Y. Huang, M. Sebastian, I. Okamoto, N. Dickgreber, R. Shah, A. Märtens, D. Massey, S. Wind, Y.-L. Wu, Effect of dose adjustment on the safety and efficacy of afatinib for EGFR mutation-positive lung adenocarcinoma: post hoc analyses of the randomized LUX-Lung 3 and 6 trials, *Ann. Oncol.* 27 (2016) 2103–2110, <http://dx.doi.org/10.1093/annonc/mdw322>.

ARTICLE

Open Access

Therapeutic potential of targeting S100A11 in malignant pleural mesothelioma

Hiroki Sato¹, Masakiyo Sakaguchi², Hiromasa Yamamoto¹, Shuta Tomida³, Keisuke Aoe^{4,5}, Kazuhiko Shien¹, Takahiro Yoshioka⁶, Kei Namba¹, Hidejiro Torigoe¹, Junichi Soh¹, Kazunori Tsukuda¹, Hiroyuki Tao^{5,7}, Kazunori Okabe^{5,7}, Shinichiro Miyoshi¹, Harvey I. Pass⁸ and Shinichi Toyooka^{1,6}

Abstract

Malignant pleural mesothelioma (MPM) is an aggressive tumor with an unfavorable prognosis. The standard therapeutic approaches are limited to surgery, chemotherapy, and radiotherapy. Because the consequent clinical outcome is often unsatisfactory, a different approach in MPM treatment is required. S100A11, a Ca^{2+} -binding small protein with two EF-hands, is frequently upregulated in various human cancers. Interestingly, it has been found that intracellular and extracellular S100A11 have different functions in cell viability. In this study, we focused on the impact of extracellular S100A11 in MPM and explored the therapeutic potential of an S100A11-targeting strategy. We examined the secretion level of S100A11 in various kinds of cell lines by enzyme-linked immunosorbent assay. Among them, six out of seven MPM cell lines actively secreted S100A11, whereas normal mesothelial cell lines did not secrete it. To investigate the role of secreted S100A11 in MPM, we inhibited its function by neutralizing S100A11 with an anti-S100A11 antibody. Interestingly, the antibody significantly inhibited the proliferation of S100A11-secreting MPM cells in vitro and in vivo. Microarray analysis revealed that several pathways including genes involved in cell proliferation were negatively enriched in the antibody-treated cell lines. In addition, we examined the secretion level of S100A11 in various types of pleural effusions. We found that the secretion of S100A11 was significantly higher in MPM pleural effusions, compared to others, suggesting the possibility for the use of S100A11 as a biomarker. In conclusion, our results indicate that extracellular S100A11 plays important roles in MPM and may be a therapeutic target in S100A11-secreting MPM.

Introduction

Malignant pleural mesothelioma (MPM) is a highly invasive and aggressive tumor that develops in the mesothelial lining of the pleura. The median survival of patients with MPM from the time of diagnosis is usually less than 1 year^{1,2}. While surgical resection is the treatment of first choice for early-stage disease, recurrence of the disease often makes the prognosis poorer. In addition, most MPM cases are of advanced-stage disease, for which

the benefits of a standard chemotherapeutic regimen with cisplatin and pemetrexed are very limited. These considerations demand the development of novel therapeutic strategies for MPM.

Proteins of the S100 family are small molecules (ranging from 9 to 14 kDa) with two EF-hands and in humans, the family is composed of 20 different members (S100A1–S100A16, S100 β , S100G, S100P, and S100Z). This group of proteins modulates a variety of cellular processes, including cell proliferation, differentiation, and intracellular signaling by functioning both as intracellular Ca^{2+} sensors and as extracellular factors^{3–5}.

S100A11, also called S100C or calgizzarin, was cloned from chicken gizzard in 1991⁶. We previously reported that S100A11 has two ambivalent functions in the cells.

Correspondence: Shinichi Toyooka (toyooka@md.okayama-u.ac.jp)

¹Department of General Thoracic Surgery and Breast and Endocrinological Surgery, Okayama University Graduate School of Medicine, Dentistry and Pharmaceutical Sciences, Okayama, Japan

²Department of Cell Biology, Okayama University Graduate School of Medicine, Dentistry and Pharmaceutical Sciences, Okayama, Japan

Full list of author information is available at the end of the article

© The Author(s) 2018



Open Access This article is licensed under a Creative Commons Attribution 4.0 International License, which permits use, sharing, adaptation, distribution and reproduction in any medium or format, as long as you give appropriate credit to the original author(s) and the source, provide a link to the Creative Commons license, and indicate if changes were made. The images or other third party material in this article are included in the article's Creative Commons license, unless indicated otherwise in a credit line to the material. If material is not included in the article's Creative Commons license and your intended use is not permitted by statutory regulation or exceeds the permitted use, you will need to obtain permission directly from the copyright holder. To view a copy of this license, visit <http://creativecommons.org/licenses/by/4.0/>.

Namely, in the cytoplasmic compartment, S100A11 inhibits the growth of normal human keratinocytes in response to high Ca^{2+} or transforming growth factor $\beta^{7,8}$. Contrarily, the binding of extracellular S100A11 to the receptor for advanced glycation end products (RAGE) enhances the production of epidermal growth factor family proteins, resulting in growth stimulation^{5,9}. Based on these findings, we have studied the biological activity of S100A11 by focusing both on intracellular and extracellular S100A11. As for the function of intracellular S100A11, we have shown that the intracellular S100A11–ANXA2 complex helps plasma membrane repair, which was critical for survival and metastasis, in metastatic breast cancer cell line¹⁰. Additionally, it is reported that intracellular S100A11 promotes pseudopodial actin dynamics, which plays a critical role in tumor metastasis and the suppression of S100A11 results in inhibition of cell migration and invasion, and the reversion of Epithelial to mesenchymal transition (EMT) in various metastatic cell lines¹¹. Regarding extracellular S100A11, we have recently reported that, in mesothelioma cells, S100A11 dimerizes in the peroxisome after transportation of monomeric S100A11 through the interaction with PEX14, an essential component of peroxisomal import machinery, and actively secreted¹². However, despite advances in the understanding of the biological activity and mechanisms of this protein, little is known about its therapeutic or diagnostic potential. In this study, we investigated the relationship between extracellular S100A11 and MPM, and explored the possibility of an intervention in S100A11 function for MPM treatment and diagnosis.

Results

Secretion levels of S100A11 in malignant cell lines and overexpression of S100A11 in MPM

We first examined the secretion level of S100A11 in the culture media of various cell lines by enzyme-linked immunosorbent assay (ELISA). Seven MPM, 2 normal mesothelial, 12 lung cancer, 3 gastric cancer, 3 colorectal cancer, and 3 breast cancer cell lines were used for this analysis, and the result is shown in Fig. 1a. We detected increased levels of S100A11 in cancer cells with various secretion levels. Of interest, there was the marked difference in S100A11 secretion between MPM cells and normal cells. All examined MPM cell lines except for MSTO-211H commonly secreted S100A11, whereas no secretion was observed in normal mesothelial cell lines. MPM cell lines were classified into three categories based on the secretion level of S100A11: High (YUMC44, H290, and H28), Low (HP-1, H2452, and H2052), and None (MSTO-211H). To investigate the correlation between S100A11 secretion and protein expression, protein expression levels of S100A11 in MPM and normal

mesothelial cell lines were determined by western blot analysis. S100A11 was significantly overexpressed in MPM cell lines, compared to normal mesothelial cell lines (Fig. 1b). To confirm the same phenomenon in clinical MPM specimens, three histological subtypes of MPM tissues, epithelioid, sarcomatoid, and biphasic type, were obtained from the patients who underwent surgery at the Okayama University Hospital and then studied for S100A11 expression. We also prepared the paraffin blocks filled with H2452 and MeT-5A cells to use as a positive and negative control, respectively. Immunohistochemistry demonstrated that S100A11 was mainly localized in the cytoplasm or nucleus and was strongly positive in MPM cells, but not in surrounding normal lung cells. Representative images are shown in Fig. 1c. Taken together, these results suggest that S100A11 is aberrantly overexpressed in MPM at both cultured cells and clinical samples and secreted from MPM cells.

Inhibition of the amount of extracellular S100A11 in MPM cells

Next, we examined the involvement of extracellular S100A11 in the growth regulation of MPM cells. As shown in Fig. 2a, MTT assay revealed that administration of the purified S100A11 recombinant protein to the cultures promoted cellular proliferation of MPM cell lines (H2452 and H2052) in a dose-dependent manner up to the point of 100 ng/ml. The growth induction stimulated by extracellular foreign S100A11 at the concentration of 1000 ng/ml was almost equal in H2452 cells or tended to little bit decline in H2052 cells when compared to those at the concentration of 100 ng/ml. While the highest concentration (10,000 ng/ml) commonly worked as growth inhibition in the both cell lines. These results provided us an optimal concentration of extracellular S100A11 (100 ng/ml) in growth stimulation of MPM cells. To inhibit the function of secreted S100A11, we used an anti-S100A11 antibody (Proteintech Group), which has been previously reported as a neutralizing antibody for S100A11¹³. Similarly, we confirmed that the screened antibody decreased the quantity of S100A11 in the cell culture media (Fig. 2b). The effect was continued for about 48 h and then expired at later time point, probably due to the consumption of the antibody life. We also confirmed that mouse control IgG had no effect on cell growth of MPM cell lines (H2052 and H2452, data not shown). Based on these results, the anti-S100A11 antibody was administered on day 1 and day 3 in culture system. We found that cellular growth of “Low” cells (H2452 and H2052) was both highly suppressed by an anti-S100A11 antibody with a final concentration of 100 ng/ml in culture media (Fig. 2c, top). On the other hand, in “High” cells (H290 and H28), the same concentration of the anti-S100A11 antibody did not show any appreciable effect on their cell

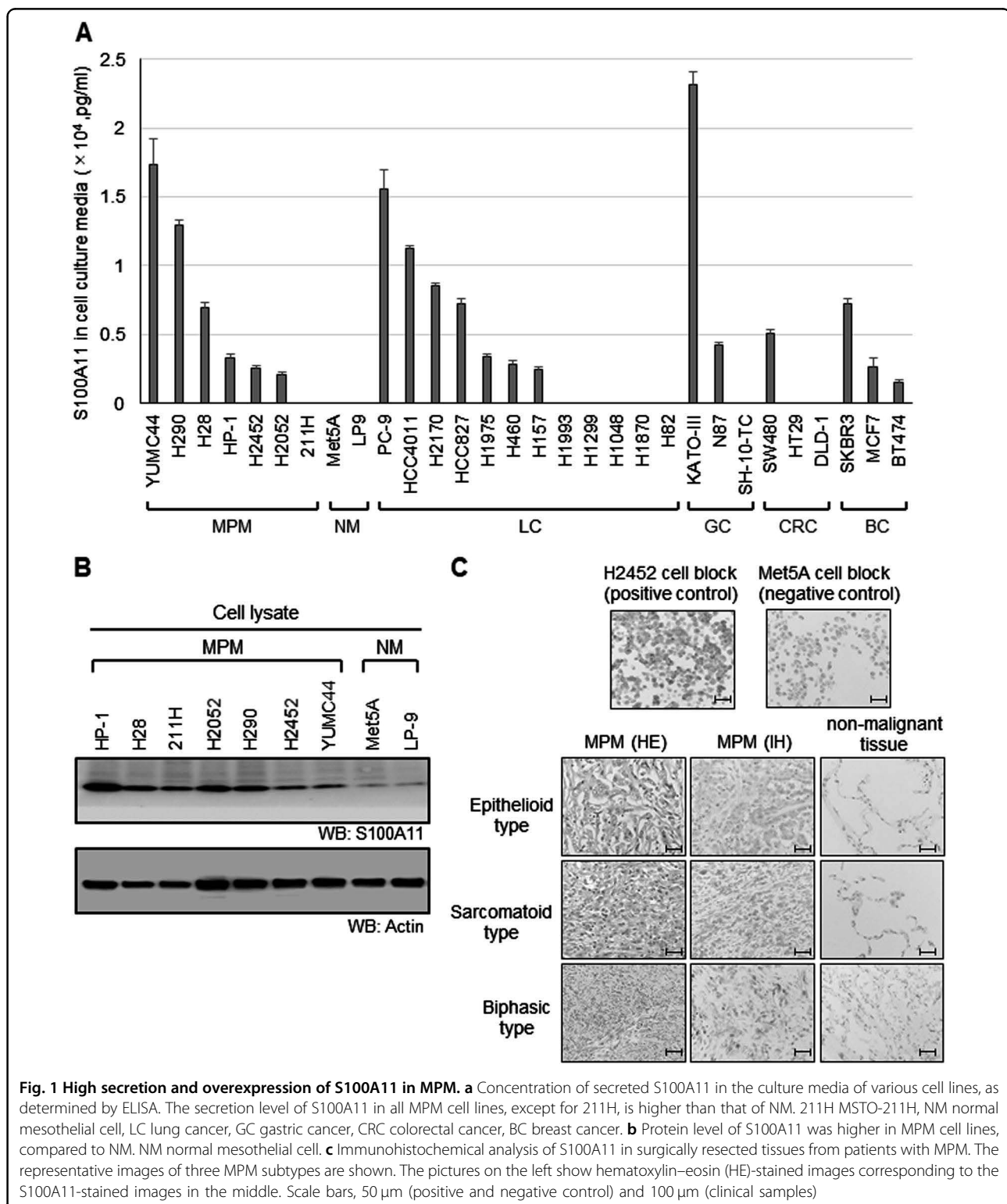
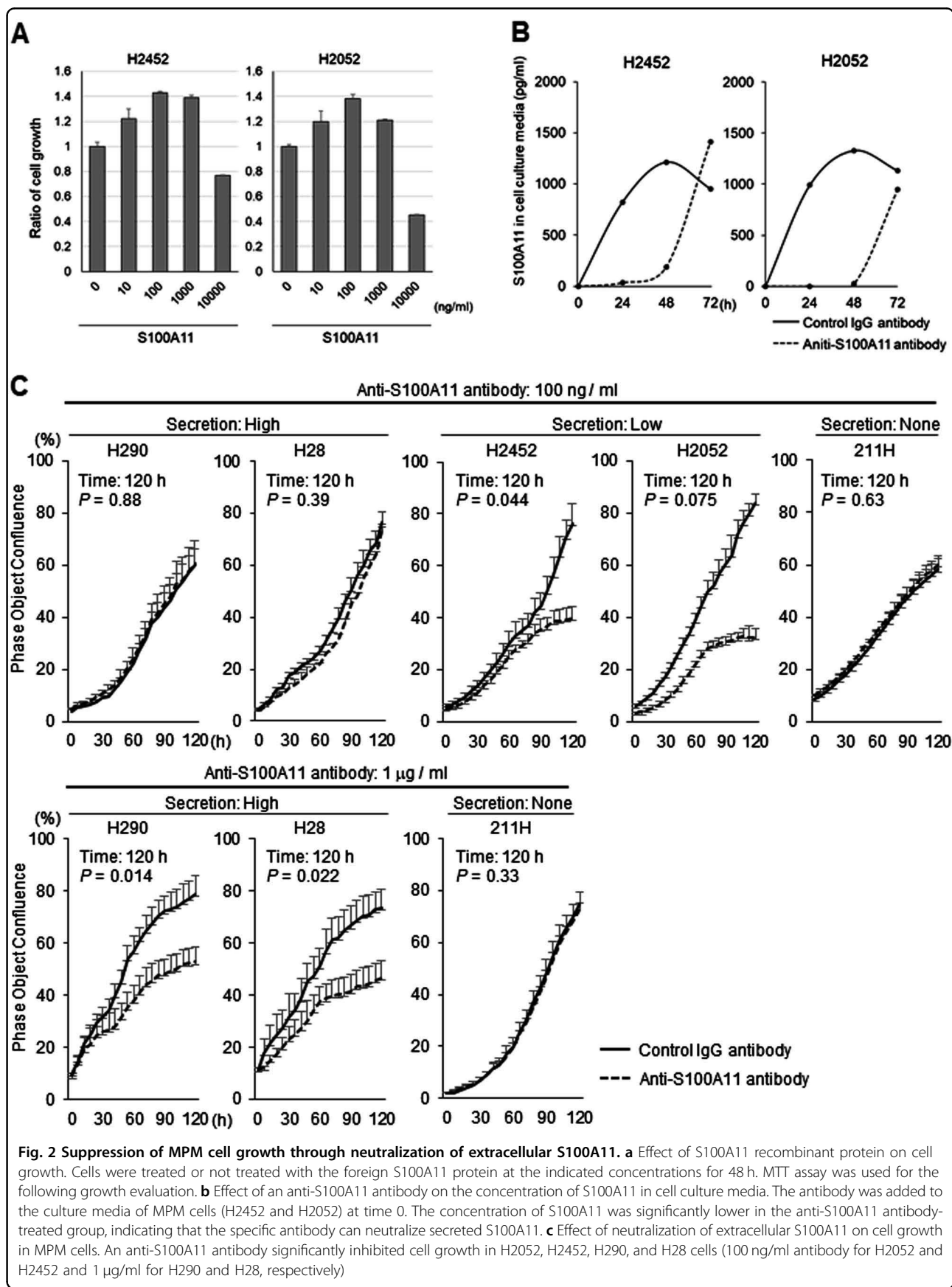


Fig. 1 High secretion and overexpression of S100A11 in MPM. **a** Concentration of secreted S100A11 in the culture media of various cell lines, as determined by ELISA. The secretion level of S100A11 in all MPM cell lines, except for 211H, is higher than that of NM. 211H MSTO-211H, NM normal mesothelial cell, LC lung cancer, GC gastric cancer, CRC colorectal cancer, BC breast cancer. **b** Protein level of S100A11 was higher in MPM cell lines, compared to NM. NM normal mesothelial cell. **c** Immunohistochemical analysis of S100A11 in surgically resected tissues from patients with MPM. The representative images of three MPM subtypes are shown. The pictures on the left show hematoxylin–eosin (HE)-stained images corresponding to the S100A11-stained images in the middle. Scale bars, 50 μ m (positive and negative control) and 100 μ m (clinical samples)

growth. Facing to the issue, we increased the antibody dose up to 1 μ g/ml. The higher dose gave suppression of cell growth even in these cell lines (Fig. 2c, bottom). As for “None” cells (MSTO-211H), the antibody did not affect

the cell growth, regardless of dose (Fig. 2c). To further evaluate the effect of anti-S100A11 antibody on the migration and invasion of MPM, we performed a Boyden chamber assay. Microscopy images of the Boyden



chamber assay are shown in Supplementary Fig. S1A and S1B. Migration and invasion were significantly suppressed in MPM cells treated with the antibody. To confirm the used antibody specificity, we tried to assess whether replenishing foreign S100A11 protein in the culture could cancel the antibody-mediated anticancer behaviors in vitro. As shown in Supplementary Fig. S1A–C, we found that this procedure effectively enfeebled cancer preventive benefits of the antibody in all the three experimental contexts, migration, invasion, and growth of MPM cell lines (H2452 and H2052).

There is a close relationship between cellular growth and cell cycle condition. This prompted us to examine whether cell cycle can be affected by the extracellular S100A11. Cyclins D and B were reliable good makers for cell cycle G1/S-phase and G2/M-phase, respectively, so that we investigated the expression levels of them after stimulation of the cells with 100 ng/ml of S100A11. By the western blot analysis approach, we found that Cyclin D but not Cyclin B was significantly induced with time dependency after the addition of S100A11 in MPM cultures (H2452 and H2052) (Fig. S1D). In addition, we found that anti-apoptotic Bcl-2 protein was significantly elevated with a similar manner to those of Cyclin D in both H2452 and H2052 cells (Fig. S1D). These results suggest that the secreted S100A11 positively regulates not only cell cycle, especially in a specific activation of the G1 phase and following G1/S transition through an induction of Cyclin D, but also survival via induction of Bcl-2.

The alteration of downstream signaling affected by the anti-S100A11 antibody and the S100A11 recombinant protein

To gain insight into the intracellular signaling events induced by the neutralization of extracellular S100A11, we investigated the key molecules regarding to cancer progression. MPM cells were cultured with the anti-S100A11 antibody (1 µg/ml), S100A11 recombinant protein (100 ng/ml), or mouse control IgG (1 µg/ml). Lysates were extracted every 6 h and subjected to western blot analysis (Supplementary Fig. S2). As a result, we found that the treatment with the anti-S100A11 antibody significantly suppressed the constitutive phosphorylation of endogenous STAT3 in H2452 and H2052 cells. Unexpectedly, in cases of AKT and MAPK, both phosphorylation status were commonly upregulated temporary at once at 6 h and then tended to be gradually suppressed with a time-dependent manner (Supplementary Fig. S2A). This may be possibly explained by compensation of the STAT3 downregulation. Next as a converse experiment, we stimulated the cells with extra recombinant S100A11 under the absence of the antibody in culture. The addition of S100A11 recombinant protein in turn activated the downstream proteins, STAT3, AKT, and MAPK

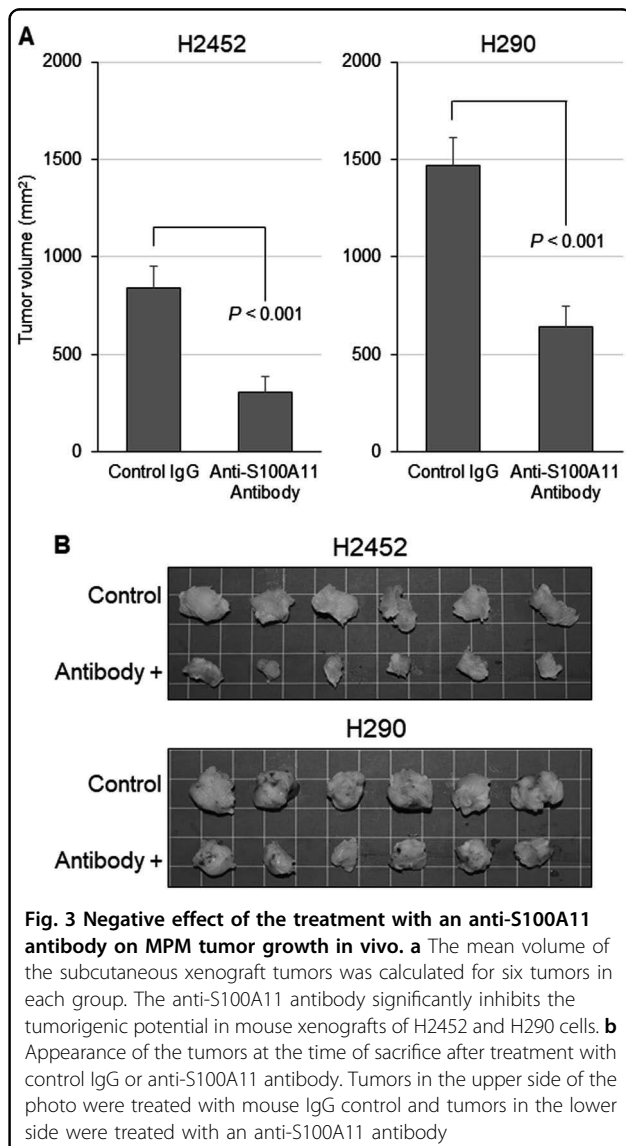
(Supplementary Fig. S2B). To further specify the central pathway related to the extracellular S100A11-induced proliferation of MPM cells, we tried to inhibit the intracellular activations of STAT3, MEK, and PI3K and assessed the following cellular proliferations. Unexpectedly, we found that either Stattic: STAT3 inhibitor, Trametinib: MEK inhibitor, or Taselisib: PI3K inhibitor, effectively suppressed the S100A11-stimulated cellular proliferation with a similar inhibitory degree, suggesting that these molecules play a crucial role in cellular growth and they cooperatively function toward same way regarding growth upregulation under the downstream of RAGE upon S100A11 binding (Supplementary Fig. S2D). Taken together, these results strongly suggest that the secreted S100A11 plays a critical role on MPM progression through upregulation of cell growth, motility, and invasion with an autocrine manner and the extracellular S100A11 is becoming a prominent molecule for therapeutic target of the MPM progression.

An anti-S100A11 antibody inhibits the tumorigenic potential in a mouse xenograft model of MPM

We investigated the antitumor effect of the validated anti-S100A11 neutralizing antibody on the MPM in a xenograft mouse model, using H2452 and H290 cells. We subcutaneously injected tumor cells and the anti-S100A11 antibody, and evaluated the effect of the antibody on the tumorigenic potential. As shown in Fig. 3a, b, the tumor growth in the antibody-administered group was significantly suppressed, compared to those of the control group.

Microarray analysis of H2052 and H2452 cells treated with an S100A11 neutralizing antibody

To reveal the mechanisms involved in the anticancer activity induced by neutralization of extracellular S100A11, we carried out gene expression microarray analysis. The details of the expression profile studies are reported in Supplementary Table S1. Clustering analysis based on the transcripts showed a clear distinction between the cell lines treated or untreated with the antibody (Fig. 4). Next, a gene set enrichment analysis (GSEA) was performed to clarify the groups of genes affected by anti-S100A11 antibody administration. We found that several pathways, including genes involved in cell proliferation (HALLMARK_MITOTIC_SPINDLE), (HALLMARK_P53_PATHWAY 1), (HALLMARK_PI3K_AKT_MTOR_SIGNALING), and (HALLMARK_KRAS_SIGNALING_DN), and a subgroup of genes related to protein secretion (HALLMARK_PROTEIN_SECRETION) were negatively enriched in the antibody-treated cell lines (Table 1). These results are consistent with our in vitro and in vivo data.



Function of RAGE as a receptor for S100A11

To explore the function of RAGE as a receptor for S100A11 in MPM, we first confirmed the positive expression of RAGE in MPM cell lines by western blot analysis (Fig. 5a). To prevent the intrinsic RAGE activation caused by ligand binding, we used sRAGE, which acts as decoy to compete with S100A11, the ligand for the cellular RAGE, and examined a series of effector molecules regarding to RAGE downstream signaling. MPM cells were treated or not treated with S100A11 recombinant protein (100 ng/ml) under the presence or absence of sRAGE (1 µg/ml). Twenty-four hours later, the treated-cell lysates were prepared and then subjected to western blot analysis. We found that blockage of RAGE signaling suppressed the phosphorylation of STAT3 and MAPK induced by S100A11 stimulation (Fig. 5b). Additionally,

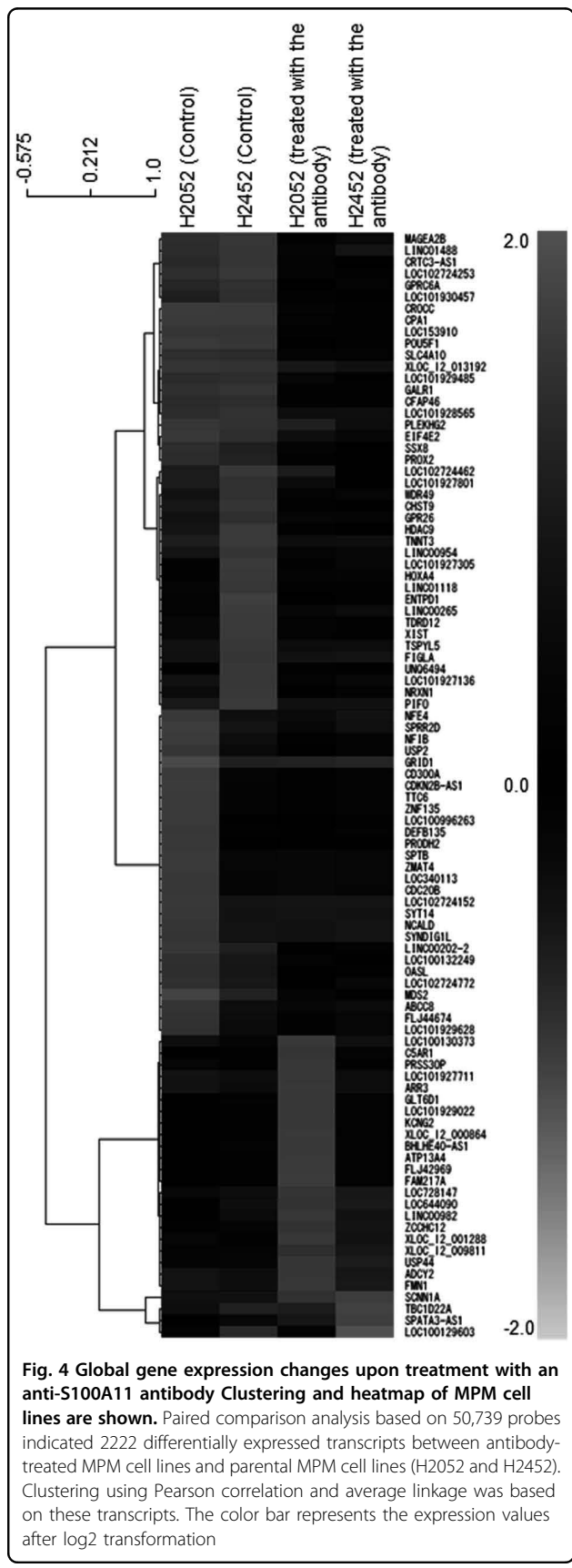


Table 1 Enriched pathways in the parental and antibody-treated cell lines

	ES	FDR q-val
GSEA pathway (parental cell line, $n = 2$)		
HALLMARK_PANCREAS_BETA_CELLS	0.83	0.274
HALLMARK_REACTIVE_OXIGEN_SPECIES_PATHWAY	0.6	0.274
HALLMARK_COAGULATION	0.52	1.000
HALLMARK_PEROXISOME	0.51	0.995
HALLMARK_MYC_TARGETS_V2	0.44	0.926
HALLMARK_GLYCOLYSIS	0.42	0.722
GSEA pathway (anti-S100A11 antibody-treated cell line, $n = 2$)		
HALLMARK_PI3K_AKT_MTOR_SIGNALING	-0.56	0.819
HALLMARK_PROTEIN_SECRETION	-0.47	0.47
HALLMARK_KRAS_SIGNALING_DN	-0.47	0.811
HALLMARK_MYOGENESIS	-0.47	0.87
HALLMARK_MITOTIC_SPINDLE	-0.33	0.887
HALLMARK_P53_PATHWAY	-0.35	0.409

ES enriched score, FDR false discovery rate

MTT assays revealed that sRAGE mitigated growth promotion in both H2452 and H2052 cells, indicating that S100A11–RAGE axis plays a pivotal role in MPM progression in response to the secreted extracellular S100A11 (Fig. 5c).

Secretion levels of S100A11 in pleural effusions

To explore the possibility of using S100A11 as a useful marker for diagnosis of MPM, we examined the secretion levels of S100A11 in several types of pleural effusions. We obtained pleural effusions from 29 MPM patients (biphasic type: $n = 10$, epithelioid type: $n = 15$, sarcomatoid type: $n = 4$), 11 benign asbestosis (BA) patients, and 12 patients who underwent thoracic surgery at the Okayama University Hospital and the National Hospital Organization Yamaguchi-Ube Medical Center (Ube, Yamaguchi, Japan). Postoperative pleural effusions were obtained from lung cancer ($n = 10$) or pulmonary cyst ($n = 2$) patients after postoperative day 2. The concentration of S100A11 was measured by ELISA. As shown in Fig. 6, the level of S100A11 was remarkably elevated in pleural effusion obtained from MPM patients when compared to that obtained from BA patients as a benchmark ($P = 0.014$). Furthermore, we found that the secretion level of S100A11 was significantly higher in pleural effusion from BA patients than that from postoperative patients ($P = 0.041$).

Discussion

In this study, we found that extracellular S100A11, via RAGE, has a critical role in tumor progression of MPM. The blockage of extracellular S100A11 with a neutralizing antibody inhibited the cell proliferation, migration, and invasion of MPM cells. Additionally, in a mouse xenograft model, tumorigenesis of MPM cells was markedly inhibited by an anti-S100A11 antibody. These results suggest that extracellular S100A11 is a potential therapeutic target for MPM. Interestingly, we found that protein expression levels of S100A11 are not correlated with secretion levels in various cells lines, suggesting that intracellular increasing in stock level of S100A11 protein is not essential factor for its secretory mechanism. In fact, MSTO-211H showed no secretion of S100A11 even though plenty of S100A11 protein was stored in cells. To clarify the reason of this discrepancy at the molecular level, further comprehensive investigation with focusing on secretory pathways of leaderless proteins is indispensable.

One of the interesting features of S100A11 is to possess different functions depending on its location and on different cell types, as we reported previously⁹. Accumulating evidence indicates that S100A11 expression is upregulated in various cancers and promote cancer development^{14–17}. However, this is not common in all cancer species, for example, low expression of S100A11 in bladder cancers is associated with poor survival in the patients¹⁸. Therefore, S100A11 might act sometimes as an oncogene, and sometimes as a suppressor gene, and have a key role in the progression of malignant tumors based on the balance of its ambivalent effect, which may be different depending on cancer types. When considering the use of this protein for treatment, the targeting of intracellular S100A11 would require the unitarily control of its two different functions. Thus, it is more convenient to focus on extracellular S100A11 for developing new therapeutic strategies for MPM.

RAGE, which was first identified as a RAGE, is known to bind different ligands, such as amyloid-beta peptide, HMGB1 (amphoterin), and some members of the S100 family, including S100A11^{19–21}. We found that RAGE-positive MPM cells constitutively express and secrete S100A11, the S100A11–RAGE axis is greatly involved in sustained phosphorylation of downstream effector molecules, STAT3, MAPK, and PI3K–AKT, and the blockage of S100A11–RAGE connection using either sRAGE or S100A11 neutralizing antibody effectively inhibits cell growth of MPM cells. For the S100A11-mediated growth upregulation, Cyclin D and Bcl-2 might be critically relevant. How are these molecules induced under the RAGE activation? One hint may come from the Fig. S2D. The S100A11-induced Cyclin D but not Bcl-2 was significantly downregulated by the STAT3, MEK and PI3K

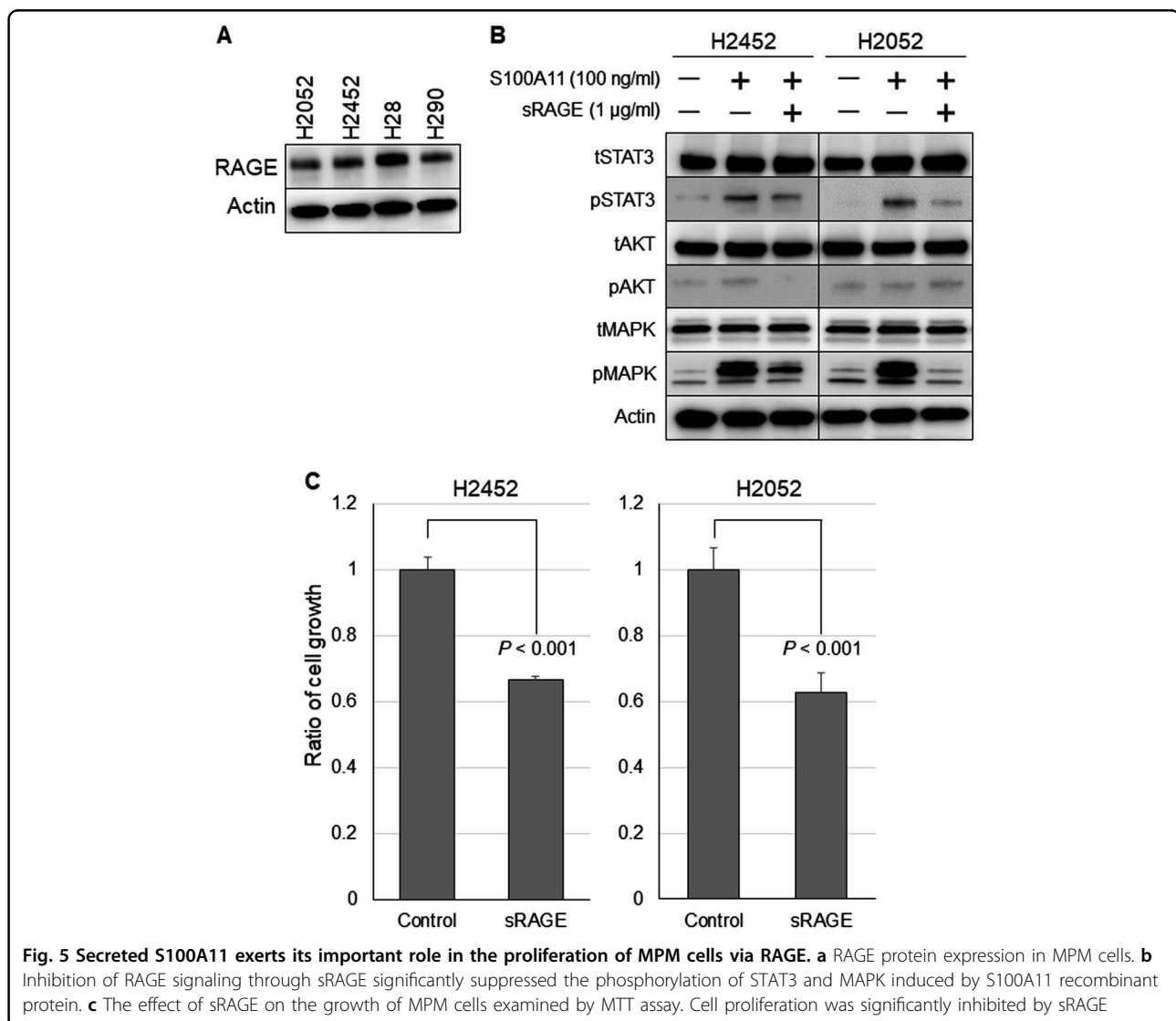


Fig. 5 Secreted S100A11 exerts its important role in the proliferation of MPM cells via RAGE. **a** RAGE protein expression in MPM cells. **b** Inhibition of RAGE signaling through sRAGE significantly suppressed the phosphorylation of STAT3 and MAPK induced by S100A11 recombinant protein. **c** The effect of sRAGE on the growth of MPM cells examined by MTT assay. Cell proliferation was significantly inhibited by sRAGE

inhibitors, suggesting that the molecules regarding pathways coordinately regulate Cyclin D expression after the RAGE activation upon S100A11 binding. Through this study, we hence strongly recognized a significant role of secreted S100A11 in mesothelioma progression.

In our experiments, growth inhibitory effect of sRAGE was limited and insufficient in comparison with the that of anti-S100A11 antibody, indicating that an additional S100A11 receptor, such as CD36, might activate survival or proliferative pathways in the cells^{9,22}. Moreover, RAGE has been shown to have many distinct biological functions. For instance, van Zoelen and colleagues²³ demonstrated that RAGE signaling contributed to an effective antibacterial defense during *Escherichia coli* infection (inhibition of bacterial outgrowth and dissemination), and RAGE deficiency resulted in enhanced organ injuries due to liver necrosis. Thus, the adverse effects due to the

inhibition of RAGE signaling are still unclear and as a therapeutic target for MPM, it seems more convenient to inhibit extracellular S100A11 than RAGE at present.

Although "High" cells (H290 and H28) displayed resistance to the S100A11 antibody at lower concentration (100 ng/ml), the effect of S100A11 antibody was shown when much higher concentration of it (1 μ g/ml) was used. Thus, the secretion of S100A11 in MPM cells was prerequisite for the antibody approach and measurement of the secretion level of S100A11 was quite important index to predict an effectiveness of the S100A11 antibody. We hence examined the secretion level of S100A11 in pleural effusion. The concentration of S100A11 in MPM pleural effusions was significantly higher than that in pleural effusions of BA and postoperative patients, though the amount of secreted S100A11 is high in pleural effusions from both patients with MPM and BA. Generally, BA is

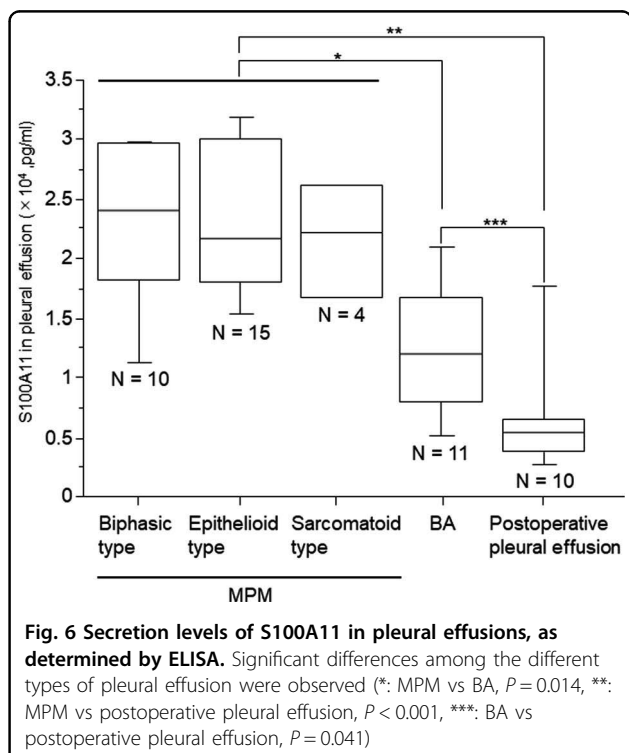


Fig. 6 Secretion levels of S100A11 in pleural effusions, as determined by ELISA. Significant differences among the different types of pleural effusion were observed (*: MPM vs BA, $P = 0.014$, **: MPM vs postoperative pleural effusion, $P < 0.001$, ***: BA vs postoperative pleural effusion, $P = 0.041$)

not regarded as a precancerous lesion of mesothelioma. Taking it into account, we consider that MPM cells actively secrete S100A11 in pleural effusion. These results suggest that S100A11 can be not only a therapeutic target but also an early diagnosis marker. In addition, it is of note mentioning that the concentration of S100A11 in the pleural effusions of patients with BA was significantly higher than that of postoperative patients. The association between high expression of proteins of the S100 protein family and inflammatory diseases has been reported^{24–27}; this along with our results suggest that S100A11 may be involved in chronic inflammation.

In conclusion, we showed that extracellular S100A11 plays an important role in MPM progression and neutralization of extracellular S100A11 directly linked to marked suppression of MPM developments in vitro and in vivo. Our results suggest that extracellular S100A11 can be a novel, selective and effective therapeutic target in S100A11-secreting MPM, since normal cells displayed no secretion phenotype of S100A11.

Materials and methods

Cell lines and reagents

We used seven human MPM cell lines [NCI-H28 (H28), NCI-H290 (H290), NCI-H2052 (H2052), NCI-H2452 (H2452), HP-1, YUMC44, and MSTO-211H], two human normal mesothelial cell lines (MeT-5A and LP-9), 10 human lung cancer cell lines [HCC827, PC-9, HCC4011, NCI-H1975 (H1975), NCI-H1993 (H1993),

NCI-H1299 (H1299), NCI-H460 (H460), NCI-H2170 (H2170), NCI-H157 (H157), and NCI-H82 (H82)], two human extrapulmonary small-cell cancer cell lines [NCI-H1048 (H1048) and NCI-H1870 (H1870)], three gastric cancer cell lines [KATO III, NCI-N87 (N87), and SH-10-TC], three colorectal cancer cell lines (SW480, HT29, and DLD-1), and three breast cancer cell lines (MCF-7, BT474, and SK-BR-3). Two MPM cell lines (HP-1 and H2452) were established by one of the authors (H.I.P.)²⁸. Three MPM cell lines (H28, H290, and H2052 obtained in 2002), two lung cancer cell lines (HCC4011 and H82 obtained in 2008), and two extrapulmonary small-cell cancer cell lines (H1048 and H1870 obtained in 2008) were kindly gifted by Dr. Adi F. Gazdar (Hamon Center for Therapeutic Oncology Research and Department of Pathology, University of Texas Southwestern Medical Center at Dallas, Dallas, TX, USA)²⁹. YUMC44 cell line was established by one of the authors (H.Y.)³⁰. MSTO-211H, MeT-5A, N87 cell lines, seven lung cancer cell lines (HCC827, H1975, H1993, H1299, H460, H2170, and H157), three breast cancer cell lines (MCF-7, BT474, and SK-BR-3), and three colorectal cancer cell lines (Sw480, HT29, and DLD-1) were purchased from the American Type Culture Collection (Manassas, VA, USA). Two gastric cancer cell lines (KATO III and SH-10-TC) were obtained from the Cell Resource Center for Biomedical Research Institute of Development Aging and Cancer, Tohoku University (Sendai, Miyagi, Japan). LP-9 cell line was purchased from the Coriell Cell Repository (Camden, NJ, USA). PC-9 cell line was purchased from Riken Cell Bank (Tsukuba, Ibaragi, Japan). The cell lines within 30 passages were used in this study and the cumulative culture length was less than 6 months. For cell lines with long-term preservation in liquid nitrogen, DNA fingerprinting analysis by short tandem repeat profiling (the PowerPlex 1.2 System, Promega) was performed for the cell authentication. All the cell lines, except for LP-9 and breast cancer cell lines, were maintained in RPMI-1640 medium (Sigma-Aldrich, St Louis, MO, USA, Product No. R8758) supplemented with 10% fetal bovine serum (FBS). The three breast cancer cell lines were cultured in Dulbecco's modified Eagle's medium (Sigma-Aldrich, Product No. D6429) with 10% FBS. LP-9 was cultured in Ham's F12 medium (Sigma-Aldrich, Product No. N4888)/Medium 199 (Sigma-Aldrich, Product No. M7653) (1:1 mixture) with 10% FBS, 2 mM L-glutamine (Thermo Fisher Scientific, Waltham, MA, USA, catalog #25030-081), 1.7 nM epidermal growth factor (Sigma-Aldrich, Product No. E9644), and 1100 nM hydrocortisone (Sigma-Aldrich, Product No. H0888). All the cell lines were grown in a humidified incubator with 5% CO₂ at 37°C and routinely tested for mycoplasma by Venor GeM OneStep kit (Minerva Biolabs, Berlin, Germany, Product No. 11-8050). Soluble receptor for

advanced glycation end products (RAGE) Fc chimera (sRAGE) (R&D Systems, Minneapolis, MN, USA, accession #Q15109), static (Abcam, Cambridge, MA, USA, ab120952), trametinib (GSK-1120212) (LC Laboratories, Woburn, MA, USA, catalog #T-8132), Taselisib (GDC-0032) (Selleckchem, Houston, TX, USA, catalog #S7103), and the mouse IgG-isotype control (Abcam, ab37355) were obtained from the designated sources. S100A11 recombinant protein was prepared as described previously⁵.

Determination of the concentration of S100A11 by ELISA

The concentration of S100A11 was measured using the CircuLex S100A11 ELISA Kit (Circulex, Nagano, Japan, Code No. CY-8063) according to the manufacturer's protocol. The standard curve for the ELISA was obtained using various concentrations of recombinant human S100A11. Samples were diluted 5- to 10-fold. The absorbance was measured at the dual wavelengths of 450/540 nm using the Flex Station 3 microplate reader (Sunnyvale, CA, USA) and the concentration of S100A11 (in pg/ml) was calculated according to the standard curve.

Western blot analysis

The detailed protocol has been described previously³¹. The primary antibodies used for western blot analyses were as follows: EGFR (catalog #4267), phospho- (p)-EGFR (Tyr1068) (#3777), Stat3 (#12640), p-Stat3 (Tyr705) (#9145), Akt (#9272), p-Akt (Ser473) (#4060), p44/p42 MAPK (#9102), p-p44 / p42 MAPK (#9101), Cyclin B1 (#4138), Cyclin D1 (#2922), Bcl-2 (#2872) (Cell Signaling Technology, Danvers, MA, USA), S100A11 (Medical & Biological Laboratories, Nagoya, Japan, catalog #CY-M1037), and β-actin (used as a loading control) (Merck Millipore, Billerica, MA, USA, catalog # MAB1501). The following secondary antibodies were used: goat anti-rabbit (catalog #sc-2030) or anti-mouse (catalog #sc-2031) immunoglobulin G (IgG)-conjugated horseradish peroxidase (Santa Cruz Biotechnology, Dallas, TX, USA). To detect specific signals, the membranes were examined using the ECL Prime Western Blotting Detection System (GE Healthcare, Amersham, UK, Code No. RPN2235) and LAS-3000 imager (Fujifilm, Tokyo, Japan).

Immunohistochemical analysis of clinical samples

MPM tissues were obtained from patients who underwent surgery at the Okayama University Hospital, in Okayama City, Japan. The experimental protocol was approved by the Institutional Review Board/Ethical Committee of the Okayama University Graduate School of Medicine, Dentistry and Pharmaceutical Sciences and Okayama University Hospital (Permit Number: 1508-027) and informed consent, including publication of patient

photos, was obtained from all the patients. Tissue samples were fixed in 10% formaldehyde and embedded in paraffin. The immunohistochemical (IHC) staining for S100A11 was performed using an S100A11 primary antibody (R&D Systems, accession #P31949). The detailed protocol for the IHC staining has been described previously³².

Cell proliferation assays

To examine the effect of the anti-S100A11 antibody (Proteintech Group, Chicago, IL, USA, catalog #10237-1-AP) on cell proliferation, the IncuCyte Zoom Live Cell Imaging System (Essen Biosciences, Ann Arbor, Michigan, USA) was used. In brief, 1.0×10^4 cells were seeded into each well of a 24-well plate. After 24 h of incubation, the plates were placed in the Incucyte Zoom system. Images were taken every 6 h for the indicated amount of time. The percent of confluence over time was calculated using the Incucyte Zoom software. For experiments testing the effect of sRAGE on cell proliferation, the thiazolyl blue tetrazolium bromide (MTT) (Sigma-Aldrich, catalog #M2128) dye reduction method was used, as described previously³³.

Cell migration and invasion assays

Cell migration and invasion were analyzed using a Boyden chamber assay. The cells were cultured with an antibody (100 ng/ml) for 24–48 h (for migration assays) or 48–72 h (for invasion assays). The detailed protocol has been described previously³⁴.

Xenograft model

The protocol was approved by the Animal Care and Use Committee of Okayama University (Permit Number: OKU-2016205). Six-week-old NOD/SCID female mice were purchased from Charles River Laboratories (Yokohama, Kanagawa, Japan). To evaluate the effect of the anti-S100A11 neutralizing antibody, mice were randomly divided into two groups: an antibody-administered group and a control group ($n = 3$ for each group). Each cell line (5×10^6 cells) suspended in 200 μL RPMI-1640 media and Matrigel Basement Membrane Matrix (Corning, NY, USA, catalog #354234) was subcutaneously injected into the backs of the mice either with 1 μg/ml anti-S100A11 antibody (proteintech Group) or mouse IgG-isotype control (two tumors per mouse). The injection was repeated five times every 3 days. Four weeks after the first injection, the mice were sacrificed and the tumors were harvested, measured, and photographed. The tumor volume was calculated using the empirical formula $V = 1/2 \times [(\text{shortest diameter})^2 \times (\text{the longest diameter})]$. No randomization and no blinding was performed. Sample size estimates were based on our previous experience.

Microarray and GSEA

Before and after treatment of H2052 and H2452 cells with the anti-S100A11 antibody (Proteintech Group), total RNAs were extracted from cell lines using an RNeasy Mini Kit (Qiagen, Venlo, the Netherlands, catalog #74104). Purified total RNA samples were hybridized on the Human Whole Genome DNA Microarray system (SurePrint G3 Human 8x60K ver. 2.0, Agilent Technologies, Santa Clara, CA) to obtain the altered gene expression profile. The fold change in the expression of individual genes was calculated and genes with fold changes exceeding 2-fold or below 2-fold were considered up- and downregulated, respectively (Supplementary Table S1). The specific enrichment of gene sets was further analyzed using the GSEA software (GSEA ver. 2.0) downloaded from the GSEA Website (<http://software.broadinstitute.org/gsea/index.jsp>).

Statistical analyses

All in vitro experiments were performed at least three times. Data are expressed as the mean \pm standard deviation. All data were analyzed using the JMP® 9.0.0 software for Windows (SAS Institute, Inc., Cary, NC, USA). The Student's *t*-tests was used to compare means of continuous scores between two independent groups. Otherwise, the Mann-Whitney *U*-test was used. An *F*-test to compare variances was performed, if necessary. All statistical tests were two-sided, and probability values less than 0.05 indicated statistically significant differences.

Acknowledgements

The authors thank Dr. Takehiro Matsubara (Biobank, Okayama University Graduate School of Medicine, Dentistry and Pharmaceutical Sciences, Okayama, Japan) and Ms. Fumiko Isobe (Department of General Thoracic Surgery and Breast and Endocrinological Surgery, Okayama University Graduate School of Medicine, Dentistry and Pharmaceutical Sciences, Okayama, Japan) for their technical supports. This study was supported by a Management Expenses Grants.

Author details

¹Department of General Thoracic Surgery and Breast and Endocrinological Surgery, Okayama University Graduate School of Medicine, Dentistry and Pharmaceutical Sciences, Okayama, Japan. ²Department of Cell Biology, Okayama University Graduate School of Medicine, Dentistry and Pharmaceutical Sciences, Okayama, Japan. ³Department of Bioinformatics, Okayama University Graduate School of Medicine, Dentistry and Pharmaceutical Sciences, Okayama, Japan. ⁴Department of Medical Oncology, National Hospital Organization Yamaguchi-Ube Medical Center, Ube, Yamaguchi, Japan. ⁵Department of Clinical Research, National Hospital Organization Yamaguchi-Ube Medical Center, Ube, Yamaguchi, Japan. ⁶Department of Clinical Genomic Medicine, Okayama University Graduate School of Medicine, Dentistry and Pharmaceutical Sciences, Okayama, Japan. ⁷Department of Thoracic Surgery, National Hospital Organization Yamaguchi-Ube Medical Center, Ube, Yamaguchi, Japan. ⁸Department of Cardiothoracic Surgery, New York University Langone Medical Center, New York, NY, USA

Conflict of interest

The authors declare that they have no competing interests.

Publisher's note

Springer Nature remains neutral with regard to jurisdictional claims in published maps and institutional affiliations.

Supplementary Information: The online version of this article (<https://doi.org/10.1038/s41389-017-0017-3>) contains supplementary material.

Received: 27 June 2017 Accepted: 21 September 2017

Published online: 24 January 2018

References

1. Milano, M. T. & Zhang, H. Malignant pleural mesothelioma: a population-based study of survival. *J. Thorac. Oncol.* **5**, 1841–1848 (2010).
2. Robinson, B. W. & Lake, R. A. Advances in malignant mesothelioma. *N. Engl. J. Med.* **353**, 1591–1603 (2005).
3. Bresnick, A. R., Weber, D. J. & Zimmer, D. B. S100 proteins in cancer. *Nat. Rev. Cancer* **15**, 96–109 (2015).
4. Donato, R. S100: a multigenic family of calcium-modulated proteins of the EF-hand type with intracellular and extracellular functional roles. *Int. J. Biochem. Cell. Biol.* **33**, 637–668 (2001).
5. Sakaguchi, M. et al. S100A11, an dual mediator for growth regulation of human keratinocytes. *Mol. Biol. Cell.* **19**, 78–85 (2008).
6. Todoroki, H., Kobayashi, R., Watanabe, M., Minami, H. & Hidaka, H. Purification, characterization, and partial sequence analysis of a newly identified EF-hand type 13-kDa Ca(2+)-binding protein from smooth muscle and non-muscle tissues. *J. Biol. Chem.* **266**, 18668–18673 (1991).
7. Sakaguchi, M. et al. S100C/A11 is a key mediator of Ca(2+)-induced growth inhibition of human epidermal keratinocytes. *J. Cell. Biol.* **163**, 825–835 (2003).
8. Sakaguchi, M. et al. Truncation of annexin A1 is a regulatory lever for linking epidermal growth factor signaling with cytosolic phospholipase A2 in normal and malignant squamous epithelial cells. *J. Biol. Chem.* **282**, 35679–35686 (2007).
9. Sakaguchi, M. & Huh, N. H. S100A11, a dual growth regulator of epidermal keratinocytes. *Amino Acids* **41**, 797–807 (2011).
10. Jaiswal, J. K. et al. S100A11 is required for efficient plasma membrane repair and survival of invasive cancer cells. *Nat. Commun.* **5**, 3795 (2014).
11. Shankar, J. et al. Pseudopodial actin dynamics control epithelial-mesenchymal transition in metastatic cancer cells. *Cancer Res.* **70**, 3780–3790 (2010).
12. Saho, S. et al. Active secretion of dimerized S100A11 induced by the peroxisome in mesothelioma cells. *Cancer Microenviron.* **9**, 93–105 (2016).
13. Fan, C. et al. S100A11 mediates hypoxia-induced mitogenic factor (HIMF)-induced smooth muscle cell migration, vesicular exocytosis, and nuclear activation. *Mol. Cell. Proteom.* **10**(M110), 000901 (2011).
14. Anania, M. C. et al. S100A11 overexpression contributes to the malignant phenotype of papillary thyroid carcinoma. *J. Clin. Endocrinol. Metab.* **98**, E1591–E1600 (2013).
15. Hao, J. et al. Selective expression of S100A11 in lung cancer and its role in regulating proliferation of adenocarcinomas cells. *Mol. Cell. Biochem.* **359**, 323–332 (2012).
16. Ohuchida, K. et al. S100A11, a putative tumor suppressor gene, is overexpressed in pancreatic carcinogenesis. *Clin. Cancer Res.* **12**, 5417–5422 (2006).
17. Oue, N. et al. Gene expression profile of gastric carcinoma: identification of genes and tags potentially involved in invasion, metastasis, and carcinogenesis by serial analysis of gene expression. *Cancer Res.* **64**, 2397–2405 (2004).
18. Memon, A. A. et al. Down-regulation of S100C is associated with bladder cancer progression and poor survival. *Clin. Cancer Res.* **11**, 606–611 (2005).
19. Hori, O. et al. The receptor for advanced glycation end products (RAGE) is a cellular binding site for amphoterin. Mediation of neurite outgrowth and co-expression of rage and amphoterin in the developing nervous system. *J. Biol. Chem.* **270**, 25752–25761 (1995).
20. Rauvala, H. & Rouhiainen, A. RAGE as a receptor of HMGB1 (Amphoterin): roles in health and disease. *Curr. Mol. Med.* **7**, 725–734 (2007).
21. Yan, S. D. et al. RAGE and amyloid-beta peptide neurotoxicity in Alzheimer's disease. *Nature* **382**, 685–691 (1996).
22. Cecil, D. L. et al. Inflammation-induced chondrocyte hypertrophy is driven by receptor for advanced glycation end products. *J. Immunol.* **175**, 8296–8302 (2005).

23. van Zoelen, M. A. *et al.* Receptor for advanced glycation end products facilitates host defense during *Escherichia coli*-induced abdominal sepsis in mice. *J. Infect. Dis.* **200**, 765–773 (2009).
24. Algernissen, B., Sitzmann, J., LeMotte, P. & Czarnetzki, B. Differential expression of CRABP II, psoriasin and cytokeratin 1 mRNA in human skin diseases. *Arch. Dermatol. Res.* **288**, 426–430 (1996).
25. Hirono, K. *et al.* Expression of myeloid-related protein-8 and -14 in patients with acute Kawasaki disease. *J. Am. Coll. Cardiol.* **48**, 1257–1264 (2006).
26. Hofmann, M. A. *et al.* RAGE mediates a novel proinflammatory axis: a central cell surface receptor for S100/calgranulin polypeptides. *Cell* **97**, 889–901 (1999).
27. Sorg, C. The calcium binding proteins MRP8 and MRP14 in acute and chronic inflammation. *Behring Inst. Mitt.* **91**, 126–137 (1992).
28. Pass, H. I. *et al.* Characteristics of nine newly derived mesothelioma cell lines. *Ann. Thorac. Surg.* **59**, 835–844 (1995).
29. Phelps, R. M. *et al.* NCI/Navy Medical Oncology Branch cell line data base. *J. Cell. Biochem. Suppl.* **24**, 32–91 (1996).
30. Suzawa, K. *et al.* Establishment and molecular characterization of cell lines from Japanese patients with malignant pleural mesothelioma. *Oncol. Lett.* **11**, 705–712 (2016).
31. Shien, K. *et al.* Knockdown of the epidermal growth factor receptor gene to investigate its therapeutic potential for the treatment of non-small-cell lung cancers. *Clin. Lung Cancer* **13**, 488–493 (2012).
32. Shien, K. *et al.* Prognostic impact of cancer stem cell-related markers in non-small cell lung cancer patients treated with induction chemoradiotherapy. *Lung Cancer* **77**, 162–167 (2012).
33. Sato, H. *et al.* Targeting the miR-200c/LIN28B axis in acquired EGFR-TKI resistance non-small cell lung cancer cells harboring EMT features. *Sci. Rep.* **7**, 40847 (2017).
34. Tanaka, N. *et al.* Frequent methylation and oncogenic role of microRNA-34b/c in small-cell lung cancer. *Lung Cancer* **76**, 32–38 (2012).

A Phase II Study of Trastuzumab Emtansine in HER2-Positive Non-Small Cell Lung Cancer

Katsuyuki Hotta, MD, PhD, MPH,^{a,b,*} Keisuke Aoe, MD, PhD,^c
 Toshiyuki Kozuki, MD, PhD,^d Kadoaki Ohashi, MD, PhD,^a Kiichiro Ninomiya, MD,^a
 Eiki Ichihara, MD, PhD,^a Toshio Kubo, MD, PhD,^a Takashi Ninomiya, MD, PhD,^a
 Kenichi Chikamori, MD, PhD,^c Daijiro Harada, MD, PhD,^d Naoyuki Nogami, MD, PhD,^d
 Taizo Hirata, MD, PhD,^a Shiro Hinotsu, MD, PhD,^b Shinichi Toyooka, MD, PhD,^e
 Katsuyuki Kiura, MD, PhD^a

^aDepartment of Respiratory Medicine, Okayama University Hospital, Okayama, Japan

^bCenter of Innovative Clinical Medicine, Okayama University Hospital, Okayama, Japan

^cDepartment of Medical Oncology, National Hospital Organization Yamaguchi-Ube Medical Center, Ube, Japan

^dDepartment of Thoracic Oncology, National Hospital Organization Shikoku Cancer Center, Matsuyama, Japan

^eGeneral Thoracic Surgery and Breast and Endocrinological Surgery, Okayama University Graduate School of Medicine, Okayama, Japan

Received 10 September 2017; revised 26 October 2017; accepted 31 October 2017

Available online - 4 December 2017

ABSTRACT

Trastuzumab emtansine (T-DM1), an anti-erb-b2 receptor tyrosine kinase 2 (HER2) antibody-drug conjugate, has been shown to significantly improve survival in HER2-positive breast cancer. We report a phase II trial of T-DM1 monotherapy in relapsed NSCLC with documented HER2 positivity (an immunohistochemistry [IHC] score of 3+, both an IHC score of 2+ and fluorescence in situ hybridization positivity, or exon 20 mutation). This study was terminated early because of limited efficacy. The demographic characteristics in the 15 assessable patients were as follows: median age, 67 years; male sex, 47%; performance status of 0 to 1, 80%; HER2 status IHC 3+, 33%; HER status IHC 2+/fluorescence in situ hybridization-positive, 20%; and exon 20 mutation, 47%. The median number of delivered cycles was 3 (range 1–11). One patient achieved a partial response with an objective response rate of 6.7% (90% confidence interval: 0.2–32.0). With a median follow-up time of 9.2 months, the median progression-free survival time and median survival time were 2.0 and 10.9 months, respectively. Grade 3 or 4 adverse events included thrombocytopenia (40%) and hepatotoxicity (20%) without any treatment-related deaths. T-DM1 had a limited efficacy for HER2-positive NSCLC in our cohort. Applying the concept of precision medicine to tumors appears challenging; thus, additional molecular approaches are warranted.

© 2017 International Association for the Study of Lung Cancer. Published by Elsevier Inc. All rights reserved.

Keywords: Non-small cell lung cancer; HER2; trastuzumab emtansine; precision medicine

Introduction

Recent driver oncogene-based precision therapy has dramatically changed the treatment strategy for NSCLC, representatively targeting *EGFR* and *ALK* receptor tyrosine kinase gene (*ALK*) aberrations. However, outcomes in other lung cancers remain poor even with standard chemotherapy.^{1,2} Consequently, further development of novel oncogenes and corresponding targeted therapeutic agents is warranted.

*Corresponding author.

Disclosure: Dr. Hotta has received honoraria outside the current work from AstraZeneca, Ono Pharmaceutical, Astellas, Novartis, Bristol-Myers Squibb, Merck Sharp Dohme, Eli Lilly Japan, Daiichi-Sankyo Pharmaceutical, Boehringer-Ingelheim, Nihon Kayaku, Taiho Pharmaceutical, and Chugai Pharmaceutical. Dr. Hotta also has received research funding outside the current work from AstraZeneca, Boehringer-Ingelheim, Ono Pharmaceutical, Astellas, Novartis, Bristol-Myers Squibb, Eli Lilly Japan, Merck Sharp Dohme, and Chugai Pharmaceutical. Dr. Ohashi has received a research grant from Novartis Pharmaceuticals Japan. Dr. Katsuyuki Kiura has received honoraria from Eli Lilly Japan, Nihon Kayaku, AstraZeneca, Daiichi-Sankyo Pharmaceutical, Chugai Pharmaceutical, Taiho Pharmaceutical, and Sanofi-Aventis. The remaining authors declare no conflict of interest.

Trial Registration: A Study of Trastuzumab Emtansine in Patients with HER2-Positive, Recurrent Metastatic Non-Small Cell Lung Cancer. UMIN000017709.

Address for correspondence: Katsuyuki Hotta, MD, PhD, MPH, Center for Innovative Clinical Medicine, Okayama University Hospital, 2-5-1, Shikata-cho, Okayama 700 8558, Japan. E-mail: khotta@okayama-u.ac.jp

© 2017 International Association for the Study of Lung Cancer. Published by Elsevier Inc. All rights reserved.

ISSN: 1556-0864

<https://doi.org/10.1016/j.jtho.2017.10.032>

In addition, erb-b2 receptor tyrosine kinase 2 (HER2) aberrations have been detected, accounting for 4.7% to 10% of NSCLC in terms of grade 3+ HER2 immunohistochemistry (IHC) expression.³ Additionally, the large epidemiological studies have identified tumors with positive HER2 fluorescence in situ hybridization (FISH) in 1.7% and HER2-mutant tumors in 3.6%.⁴

Trastuzumab emtansine (T-DM1) is a novel antibody-drug conjugate that uses trastuzumab, an anti-HER2 antibody, to deliver the maytansinoid antimicrotubule agent DM1, which binds to microtubules in a manner similar to that of vinca alkaloids.⁵ T-DM1 has been shown to confer a survival benefit over the standard regimen applied in HER2-positive, relapsed breast cancer.⁶

As for NSCLC, the Calu 3 lung carcinoma cell line (HER2-IHC 3+) showed preclinically dose-dependent inhibition of cell growth after T-DM1 treatment.⁵ Moreover, lung tumors with erb-b2 receptor tyrosine kinase 2 gene (*HER2*) insertion mutations in exon 20, a confirmed driver oncogene, showed dramatic shrinkage with HER2-targeted therapy.⁷ These studies suggested that T-DM1 might be effective against both HER2-positive lung and breast cancers.

However, few prospective studies of HER2-targeted therapy for lung cancer have been conducted, prompting us to launch this phase II trial.

Methods

Study Population and Intervention

Patients who met the eligibility criteria, including HER2 positivity,⁸ were enrolled for registration at three institutes in Japan: Yamaguchi-Ube Medical Centre, Shikoku Cancer Centre, and Okayama University Hospital. T-DM1 was kindly provided by Chugai Pharmaceuticals. Patients had to have had one or more lines of prior chemotherapy. Written informed consent was obtained from all patients before applying the study procedures. This study was approved by the institutional review boards.

Patients received T-DM1 intravenously, at a dose of 3.6 mg/kg over 90 minutes on day 1 of each 21-day cycle until the disease progressed or unmanageable toxic effects developed, as similar to the protocol for breast cancer.⁶

HER2 Tests

HER2 status was assessed in the laboratory (SRL, Tokyo, Japan) by using tumor formalin-fixed, paraffin-embedded archived tissues; no cytologic specimens were allowed, but biopsy or surgical specimens were. The level of HER2 protein expression was determined by IHC by using the Ventana I-VIEW PATHWAY anti-HER-2/neu (4B5) (Roche, Basel, Switzerland).⁹ IHC scores of 3+ and 2+ were considered strongly and weakly positive, respectively.⁹ FISH assays were also performed using the

PathVision HER-2 DNA probe kit (Vysis/Abbott Laboratories, Downers Grove, IL) to ascertain negativity or positivity according to a cutoff value of 2.0 (of the median ratio of HER2 to chromosome 17 copy numbers). We conducted a separate validation study to review the IHC and FISH specimens to define their positivity (unpublished data, Hotta K, 2017). Mutation analysis was performed by direct sequencing at a central laboratory (Genetic Labo, Japan) to detect known mutations (M774_A775insAYVM, A775_G776insYVMA, G776L insC, G776V insC, and P780_Y781insGSP).⁴

Finally, in this trial, HER2 was defined as positive in the presence of an IHC score of 3+, an IHC score of 2+ and FISH positivity, or an exon 20 insertion mutation.

Statistical Analysis

The primary end point was the objective response rate (ORR), which was centrally confirmed by three independent board members with the Response Evaluation Criteria in Solid Tumors (version 1.1) every 6 weeks. Secondary outcome end points included safety, overall survival, and progression-free survival (PFS). We considered the lower limit of interest to be 10%.¹⁰ Assuming that a 20% or more increase in historical data in ORR would be clinically meaningful, we needed 30 patients with a one-sided α of 0.05 and $1-\beta$ of 0.8, considering a 10% dropout rate, according to the Simon minimax design. We also planned to conduct an interim analysis after the first 15 patients had been registered; early study termination would be considered if the ORR was obtained in no more than one patient. The confidence interval (CI) of the ORR was calculated with a confidence coefficient of two-tailed 90% and 95%.

Regarding the efficacy analysis, waterfall and swimmer plots were also produced. The PFS and overall survival times were calculated from the date of registration to the first documented date of disease progression and date of death, respectively, by the Kaplan-Meier method. Statistical analyses were conducted with STATA software (version 14.0, StataCorp LP, College Station, TX).

Results

Patients

This study was terminated early because of the limited efficacy, which did not satisfy the criteria in the interim analysis; this led to only 16 of the 30 patients planned being registered between September 2015 and November 2016. Among them, 15 were considered assessable for further analysis: one patient was excluded because of a protocol deviation in the registration process. The patients' characteristics are listed in Table 1. Regarding HER2 status, 33% of cases were scored IHC 3+, 20% were scored IHC 2+/FISH positive, and 47% showed the

mutations. All 15 patients were followed up sufficiently to allow assessment of the primary end point.

Treatment Delivery

The treatment delivery is summarized in Table 2. The median delivered number of cycles to each patient was 3 (Table 2). Four patients (27%) required dose reduction during the second cycle or later because of adverse events (AEs) (see Table 2). Treatment was ultimately discontinued in all patients, mainly on account of disease progression (see Table 2).

ORR and Survival

A partial response was centrally confirmed in a female patient with a HER2-mutant tumor (Table 3). Thus, the ORR (the primary end point) was 6.7% (90% CI: 0.2%–32.0%, 95% CI: 0.3%–27.9%), whereas seven patients (46.7%) each had stable disease and progressive disease (Fig. 1A). When patients were stratified by type of HER2 aberration, no tumor shrinkage was seen in the subgroup with an IHC score of 3+ or IHC 2+/FISH-positive tumors (n = 8) (Fig. 1B and Table 3). With a median follow-up time of 9.2 months, the median PFS time was 2.0 months (90% CI: 1.2–4.0, 95% CI: 1.4–4.0),

Table 2. Treatment Delivery (N = 15)

Characteristic	Value
Total no. of treatment cycles, median (range)	3 (1-11)
Cycles received	
≥4 cycles	6 patients (40%)
3 cycles	2 patients (13%)
2 cycles	5 patients (33%)
1 cycle	2 patients (13%)
No. of patients with dose reduction	4 (27%)
Reasons for dose reduction	
Thrombocytopenia	2 patients
AST elevation	1 patient
Infusion reaction	1 patient
No. of patients who discontinued treatment	15 (100%)
Reasons for discontinuation of treatment	
Disease progression	12
Adverse events ^a	2
Attending doctor's discretion	1

^aInterstitial pneumonia (grade 2) and prolonged thrombocytopenia (grade 3) in one patient each.

AST, aspartate transaminase.

whereas the median survival time was 10.9 months (90% CI: 2.3–, 95% CI: 4.4–12.0) (Fig. 2A and B).

Table 1. Patient Characteristics (N = 15)

Characteristic	Value
Median age (range), y	67 (45–77)
Sex	
Male/female	7 (47%)/8 (53%)
Smoking status	
Never/ever	10 (67%)/5 (33%)
ECOG PS	
0	2 (13%)
1	10 (67%)
2	3 (20%)
Adenocarcinoma histologic type	15 (100%)
Stage IV/recurrence ^a	9 (60%)/6 (40%)
HER2 positivity	
IHC 3+	5 (33%)
IHC 2+/FISH-positive	3 (20%)
Exon 20 mutations	7 (47%)
A775_G776insYVMA	5 (33%)
P780_Y781insGSP	1 (7%)
G776VinsC	1 (7%)
Other driver oncogenes	
EGFR	2 (13%) ^b
EML4-ALK	0
Median No. of prior chemotherapy regimens (range)	4 (1–7)

^aPostoperative recurrence.

^bExon 19 deletion and exon 21 point mutation in one patient each.

ECOG, Eastern Cooperative Oncology Group; PS, performance status; HER2, erb-b2 receptor tyrosine kinase 2; IHC, immunohistochemistry; FISH, fluorescence in situ hybridization; EML4, echinoderm microtubule-associated protein-like 4 gene; ALK, anaplastic lymphoma kinase.

Safety

All grade 3 to 4 AEs are listed in Table 4. Almost all of the AEs were known ones, primarily thrombocytopenia (n = 6 [40%]) and hepatotoxicity (n = 3 [20%]). Among the 15 patients, there was no case of treatment-related death.

Grade 3 acute renal failure with a serum creatinine level of 3.08 mg/dL developed in one patient. The AE was

Table 3. Objective Response

	CR	PR	Stable Disease		PD
			Overall cohort (N = 15)	7 (46.7%)	
Subgroups by HER2 aberration pattern					
IHC/FISH-positive (n = 8)	0	0	3 (37.5%)	5 (62.5%)	
Mutant-positive (n = 7)	0	1 (14.3%)	4 (57.1%)	2 (28.6%)	
A775_G776insYVMA (n = 5)	0	1	3	1	
G776VinsC (n = 1)	0	0	0	1	
P780_Y781insGSP (n = 1)	0	0	1	0	

Note: The objective response rate (i.e., the primary end point) was centrally confirmed by three independent extramural review board members and evaluated according to the Response Evaluation Criteria in Solid Tumors (version 1.1) every 6 weeks.

CR, complete response; PR, partial response; PD, progressive disease; HER2, erb-b2 receptor tyrosine kinase 2 IHC, immunohistochemistry; FISH, fluorescence in situ hybridization.

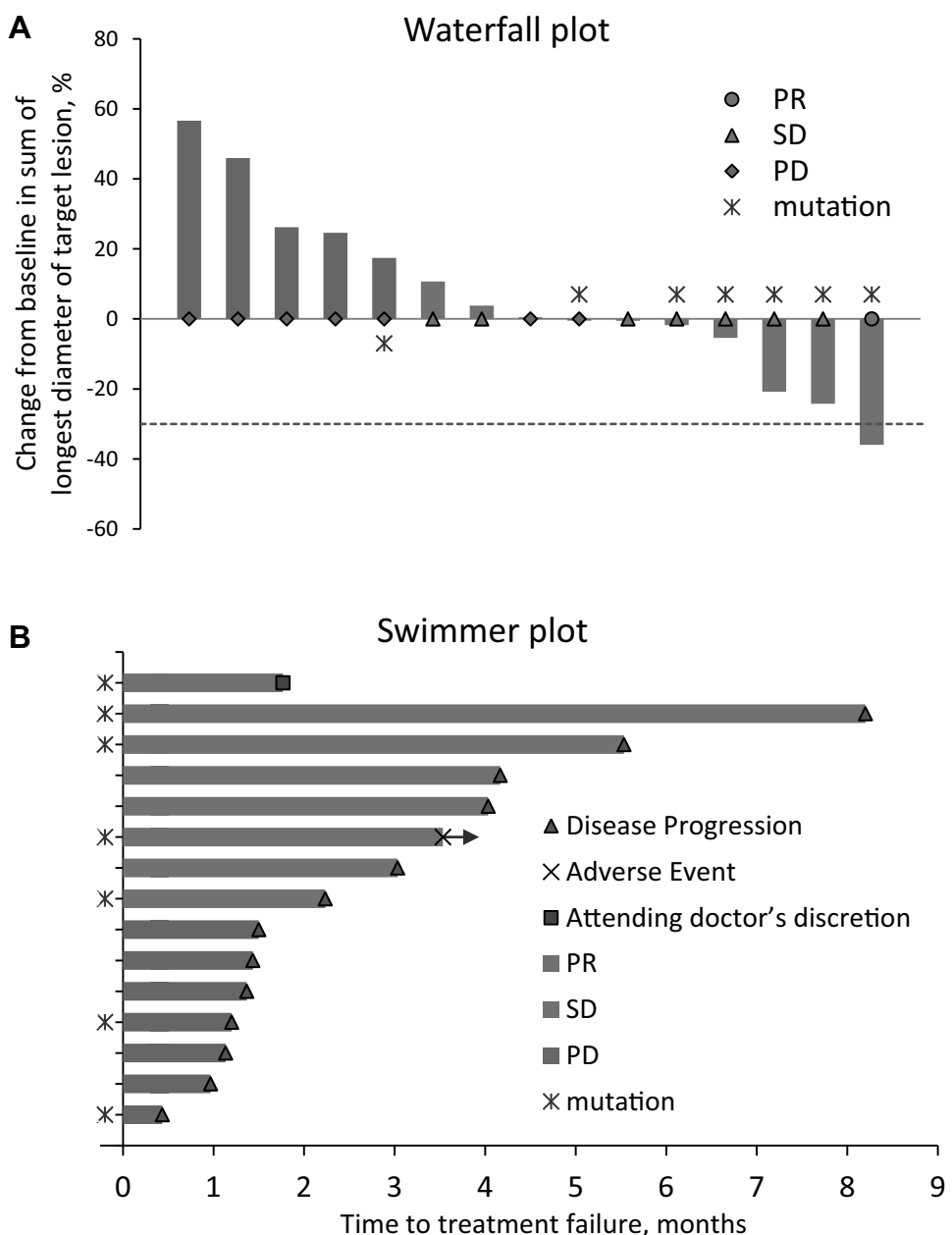


Figure 1. Objective response rate (N = 15). Waterfall plot (A) and swimmer plot (B). In the case of one responder, the attending physician judged progressive disease (PD) at an earlier time in the treatment course than did the independent radiologic review committee. PR, partial response.

recovered to grade 0 within 1 week during provision of appropriate supportive care. Interstitial pneumonia was observed in one patient (grade 2) during the fifth cycle, as detected by computed tomography. No further examination with bronchoscopy was performed in this case and the AE was resolved shortly thereafter without any steroid or oxygen therapy but just discontinuation of T-DM1.

Discussion

In this study, 1 of 15 patients (6.7%) responded to T-DM1, which did not meet the primary end point (see

Table 3). The median PFS and median survival times were 2.0 and 10.9 months, respectively. The AE profiles were almost the same as those obtained in trials for approval for use in breast cancer.⁶

The investigational agent did not show high efficacy in this study (see Table 3 and Fig. 1), which is similar to the results of the very recent trials investigating HER2-targeted therapy in lung cancer (Supplementary Table 1). In particular, IHC 3+ or IHC 2+/FISH-positive tumors were rarely responsive to the investigational agent in this study (see Fig. 1 and Table 3). Although the precise reason remains unknown, it could be

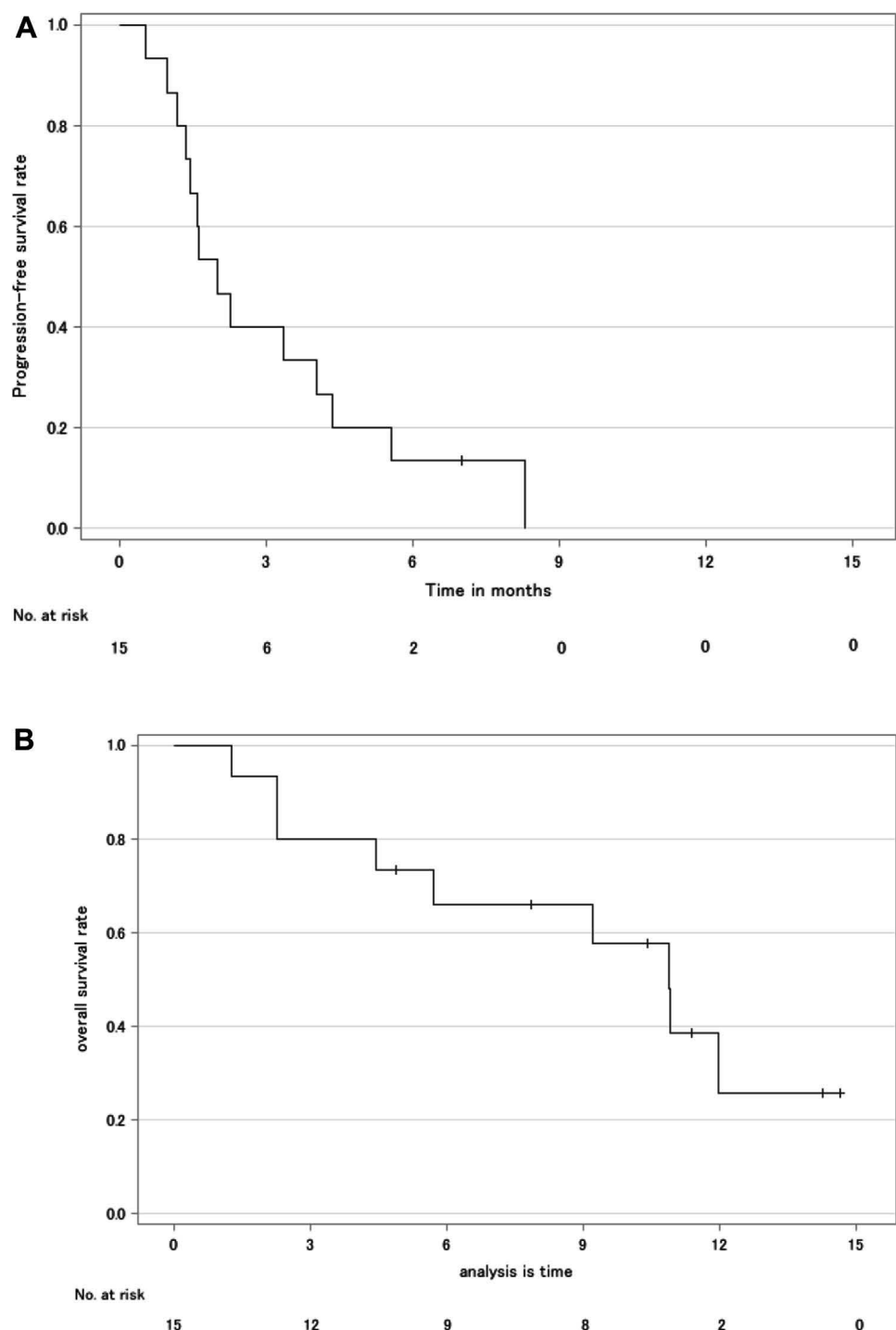


Figure 2. Survival (N = 15). Progression-free survival (A) and overall survival (B).

attributable to tumor heterogeneity, which was detected in 30% of the NSCLC cases.¹¹ It may be that only strongly HER2-immunostained cells were killed in the tumors after exposure to T-DM1, whereas the weakly stained cells might have escaped cell death and continued to grow. Unfortunately, we did not obtain or analyze tumor specimens at the time of disease progression. Further

molecular analyses are warranted to elucidate the mechanisms underlying these tumors.

Another reason for the low sensitivity could be molecularly inappropriate patient selection. We might have overestimated HER2 IHC positivity because in the present study, we used the scoring system for IHC status that is applied to gastric cancer, which is less strict than

Table 4. Grade 3 to 4 Adverse Events

Category	Grade 3	Grade 4	Grades 3-4
Thrombocytopenia	5 (33%)	1 (7%)	6 (40%)
Hypokalemia	1 (7%)	0 (0%)	1 (7%)
Hyperuricemia	0 (0%)	1 (7%)	1 (7%)
AST/ALT level increase	1 (7%)	0 (0%)	1 (7%)
γ -GTP level increase	1 (7%)	0 (0%)	1 (7%)
LFT result abnormality	1 (7%)	0 (0%)	1 (7%)
Decreased appetite	1 (7%)	0 (0%)	1 (7%)
Nausea	1 (7%)	0 (0%)	1 (7%)
Acute renal failure	1 (7%)	0 (0%)	1 (7%)
Gingivitis	1 (7%)	0 (0%)	1 (7%)
Lung infection	1 (7%)	0 (0%)	1 (7%)

Note: No treatment-related deaths were observed.

ALT, Alanine transaminase; AST, aspartate transaminase; LFT, liver function test; γ -GTP, γ -glutamyltransferase.

that used for breast cancer.⁹ Furthermore, the sensitivity of HER2-targeted agents was dependent on the IHC staining intensity.¹²

Regarding HER2-mutant tumors, we designed this study to limit the types of mutations to those confirmed as driver oncogenes in previous reports⁴ but did not exclude tumors with co-mutation in the phosphatidylinositol-4,5-bisphosphate 3-kinase catalytic subunit alpha gene (*PIK3CA*); such mutation was reported as a potential intrinsic resistance mechanism, possibly leading to the low sensitivity.

The current study had several limitations. First, it used a single-arm design, and various potential biases could not be eliminated. Additionally, the study comprised a small number of patients recruited from only a few institutes in one country, thus lowering the likelihood of confirmatory results. The relationship between type of HER2 mutations and efficacy also remains unknown. Our study results should be interpreted together with those of relevant previous studies (see Supplementary Table 1).

In conclusion, T-DM1 showed limited efficacy against HER2-positive NSCLCs in our cohort. It seems that the concept of precision medicine is difficult to apply to tumors. Additional molecular approaches are warranted for precision medicine in the treatment of HER2-positive tumors.

Acknowledgments

This research was supported by a specific grant from the Japan Agency for Medical Research and Development, which is funded by the Japanese government. No additional external funding was received for this study. The investigational agent was kindly provided by Chugai Pharmaceuticals. All of the authors contributed to the writing of the study protocol. Kadoaki Ohashi, Katsuyuki Hotta, Taizo Hirata, Kiichiro Ninomiya, and Katsuyuki

Kiura also participated in the trial design and setup. Kadoaki Ohashi, Katsuyuki Hotta, Kiichiro Ninomiya, and Katsuyuki Kiura calculated the required sample size.

Appendix

The contributing members of the HER2-CS Group are as follows:

Steering Committee: K. Hotta, K. Ohashi, K. Ninomiya, T. Hirata, S. Hinotsu, S. Toyooka, and K. Kiura.

Advisers on the HER2 aberration analysis: H. Yanai (Okayama University Hospital) and M. Takata (Kyoto University).

Independent Data and Safety Monitoring Committee: T. Kato (Kanagawa Cancer Center), J. Sasaki (Kitazato University), and N. Ebi (Iizuka Hospital).

Drug supplier: Chugai Pharmaceutical Co. Ltd.

Study site investigators: K. Hotta, K. Ohashi, K. Ninomiya, M. Tabata, A. Sato, E. Ichihara, T. Kubo, T. Ninomiya, T. Hirata, D. Minami, Y. Kato, H. Higo, G. Makimoto, Y. Toyota, N. Oda, M. Nakanishi, T. Tamura, H. Kayatani, K. Kudo, K. Nishii, S. Senoo, H. Kano, H. Watanabe, T. Ando, T. Nakasuka, N. Hara, J. Itano, H. Nakashima, S. Toyooka, and K. Kiura (Okayama University Hospital); K. Aoe, K. Chikamori, K. Oishi, T. Maeda, D. Kishino, R. Okamoto, H. Ueoka, and H. Kamei (Yamaguchi-Ube Medical Center); and T. Kozuki, D. Harada, A. Nishioka, Y. Minemoto, and N. Nogami (Shikoku Cancer Center Hospital).

This study was conducted with dedicated support from the following persons:

HER2-CS Group: S. Harita, G. Ikeda, M. Yasugi, E. Kurimoto, K. Nakano, and K. Gemba (Chugoku Central Hospital); T. Moritaka and K. Inoue (Ehime Prefectural Central Hospital); S. Miyoshi, N. Hamaguchi, R. Ito, and Y. Sano (Ehime University Hospital); I. Takata and A. Mitani (Fukuyama City Hospital); N. Ishikawa, T. Nishisaka, H. Shoda, A. Nishida, K. Hamai, and S. Tamamoto (Hiroshima Prefectural Hospital); M. Yamasaki (Hiroshima Red Cross Hospital and Atomic-bomb Survivors Hospital); K. Fujitaka, T. Masuda, S. Miyamoto, and N. Hattori (Hiroshima University Hospital); K. Sugimoto, S. Fujii, and Y. Ueda (Japanese Red Cross Kobe Hospital); A. Bessho, S. Hosokawa, Y. Sakugawa, N. Fukamatsu, and K. Ogata (Japanese Red Cross Okayama Hospital); T. Murakami (Japanese Red Cross Society Himeji Hospital); Y. Ueda (Kagawa Prefectural Central Hospital); S. Bandoh and N. Kanaji (Kagawa University Hospital); N. Takigawa, H. Yamane, N. Ochi, and Y. Honda (Kawasaki Hospital); M. Oka and M. Kittaka (Kawasaki Medical School Hospital); T. Kubota and A. Yokoyama (Kochi Medical School Hospital); H. Yoshioka, T. Tanaka, T. Yokoyama, and E. Sato (Kurashiki Central Hospital); Y. Shiota and N. Horita (Kure Kyosai Hospital); T. Kanematsu (Matsuyama Red Cross

Hospital); Y. Awaya, A. Nakamasu, and Y. Sano (Miyoshi Central Hospital); I. Murakami (NHO Higashi-Hiroshima Medical Center); S. Kuyama, K. Kudo, T. Tamura, T. Umeno, and D. Morichika (NHO Iwakuni Medical Center); T. Shibayama, K. Fujiwara, and Sato K (NHO Okayama Medical Center); K. Nishii (Okayama Health Foundation Hospital); Fujimoto N, Fuchimoto Y, and T. Kishimoto (Okayama Rosai Hospital); H. Kawai and K. Watanabe (Okayama Saiseikai General Hospital); K. Tokumo (Onomichi General Hospital); T. Murakami (Onomichi Municipal Hospital); T. Isobe and Y. Tsubata (Shimane University School of Medicine); M. Inoue (Shimonoseki City Hospital); H. Ichikawa (Takamatsu Hospital); Y. Nishioka, M. Hanibuchi, and H. Goto (Tokushima University Hospital); T. Sumikawa (Tottori Prefectural Central Hospital); M. Kodani, H. Suyama, H. Makino, Y. Ueda, N. Kinoshita, and E. Shimizu (Tottori University Hospital); H. Obata and H. Ikegami (Yamaguchi-ken Saiseikai Shimonoseki General Hospital); and Y. Kunihiro, T. Kobayashi, K. Ueda, M. Hayashi, M. Kamiya, and J. Murakami (Yamaguchi University Hospital).

LC-SCRUM group: S. Matsumoto and K. Goto.

Center for Innovative Clinical Medicine, Okayama University Hospital: K. Miyake, K. Ueda, H. Okuda, N. Kondoh, M. Fukata, S. Kuroda, S. Sugihara, M. Nakabayashi, N. Hiramatsu, S. Hinotsu, K. Zama, W. Ishii, Y. Ohe, C. Harada, M. Yoshida, K. Kamikawa, J. Sakurai, and K. Shikata.

Supplementary Data

Note: To access the supplementary material accompanying this article, visit the online version of the *Journal of Thoracic Oncology* at www.jto.org and at <https://doi.org/10.1016/j.jtho.2017.10.032>.

References

1. Hotta K, Fujiwara Y, Matsuo K, et al. Recent improvement in the survival of patients with advanced non-small-cell lung cancer enrolled into phase III trials of first-line systemic chemotherapy. *Cancer*. 2007;109:939-948.
2. Hotta K, Matsuo K, Ueoka H, Kiura K, Tabata M, Tanimoto M. Addition of platinum compounds to a new agent in patients with advanced non-small-cell lung cancer: a literature based meta-analysis of randomised trials. *Ann Oncol*. 2004;15:1782-1789.
3. Kuyama S, Hotta K, Tabata M, et al. Impact of HER2 gene and protein status on the treatment outcome of cisplatin-based chemoradiotherapy for locally advanced non-small cell lung cancer. *J Thorac Oncol*. 2008;3:477-482.
4. Mazières J, Peters S, Lepage B, et al. Lung cancer that harbors an HER2 mutation: epidemiologic characteristics and therapeutic perspectives. *J Clin Oncol*. 2013;31:1997-2003.
5. Lewis Phillips GD, Li G, Dugger DL, et al. Targeting HER2-positive breast cancer with trastuzumab-DM1, an antibody-cytotoxic drug conjugate. *Cancer Res*. 2008;68:9280-9290.
6. Verma S, Miles D, Gianni L, et al. Trastuzumab emtansine for HER2-positive advanced breast cancer. *New Engl J Med*. 2012;367:1783-1791.
7. Perera SA, Li D, Shimamura T, et al. HER2YVMA drives rapid development of adenocarcinoma lung tumors in mice that are sensitive to BIBW2992 and rapamycin combination therapy. *Proc Nat Acad Sci U S A*. 2009;106:474-479.
8. Ohashi K, Hotta K, Hirata T, et al. Trastuzumab emtansine in HER2+ recurrent metastatic non-small-cell lung cancer: study protocol. *Clin Lung Cancer*. 2017;18:92-95.
9. Bang YJ, Van Cutsem E, Feyereislova A, et al. Trastuzumab in combination with chemotherapy versus chemotherapy alone for treatment of HER2-positive advanced gastric or gastro-oesophageal junction cancer (ToGA): a phase 3, open-label, randomised controlled trial. *Lancet*. 2010;376:687-697.
10. Shepherd FA, Dancey J, Ramlau R, et al. Prospective randomized trial of docetaxel versus best supportive care in patients with non-small-cell lung cancer previously treated with platinum-based chemotherapy. *J Clin Oncol*. 2000;18:2095-2103.
11. Kobyakov DS, Avdalyan AM, Klimachev VV, Lazarev AF, Lushnikova EL, Nepomnyaschikh LM. Non-small cell lung cancer: HER2 oncogene status. *Arkh Patol*. 2015;77(2):3-9 [in Russian].
12. Stinchcombe T, Stahel RA, Bubendorf L, et al. Efficacy, safety, and biomarker results of trastuzumab emtansine (T-DM1) in patients (pts) with previously treated HER2-overexpressing locally advanced or metastatic non-small cell lung cancer (mNSCLC) [abstract]. *J Clin Oncol*. 2017;35(suppl):8509.

Anamorelin (ONO-7643) for the Treatment of Patients With Non-Small Cell Lung Cancer and Cachexia: Results From a Randomized, Double-Blind, Placebo-Controlled, Multicenter Study of Japanese Patients (ONO-7643-04)

Nobuyuki Katakami, MD¹; Junji Uchino, MD^{2,3}; Takuma Yokoyama, MD⁴; Tateaki Naito, MD⁵; Masashi Kondo, MD^{6,7}; Kouzo Yamada, MD⁸; Hiromoto Kitajima, MD⁹; Kozo Yoshimori, MD¹⁰; Kazuhiro Sato, MD¹¹; Hiroshi Saito, MD¹²; Keisuke Aoe, MD¹³; Tetsuya Tsuji, MD¹⁴; Yuichi Takiguchi, MD¹⁵; Koichi Takayama, MD²; Naoyuki Komura, MS¹⁶; Toru Takiguchi, MS¹⁶; and Kenji Eguchi, MD¹⁷

BACKGROUND: Cachexia, described as weight loss (mainly in lean body mass [LBM]) and anorexia, is common in patients with advanced cancer. This study examined the efficacy and safety of anamorelin (ONO-7643), a novel selective ghrelin receptor agonist, in Japanese cancer patients with cachexia. **METHODS:** This double-blind clinical trial (ONO-7643-04) enrolled 174 patients with unresectable stage III/IV non-small cell lung cancer (NSCLC) and cachexia in Japan. Patients were randomized to daily oral anamorelin (100 mg) or a placebo for 12 weeks. The primary endpoint was the change from the baseline LBM (measured with dual-energy x-ray absorptiometry) over 12 weeks. The secondary endpoints were changes in appetite, body weight, quality of life, handgrip strength (HGS), and 6-minute walk test (6MWT) results. **RESULTS:** The least squares mean change (plus or minus the standard error) in LBM from the baseline over 12 weeks was 1.38 ± 0.18 and -0.17 ± 0.17 kg in the anamorelin and placebo groups, respectively ($P < .0001$). Changes from the baseline in LBM, body weight, and anorexia symptoms showed significant differences between the 2 treatment groups at all time points. Anamorelin increased prealbumin at weeks 3 and 9. No changes in HGS or 6MWT were detected between the groups. Twelve weeks' treatment with anamorelin was safe and well tolerated in NSCLC patients. **CONCLUSIONS:** Anamorelin significantly increased LBM and improved anorexia symptoms and the nutritional state, but not motor function, in Japanese patients with advanced NSCLC. Because no effective treatment for cancer cachexia is currently available, anamorelin can be a beneficial treatment option. *Cancer* 2017;000:000-000. © 2017 American Cancer Society.

KEYWORDS: anamorelin (ONO-7643), cachexia, lean body mass, non-small cell lung cancer, randomized controlled trial.

INTRODUCTION

Cachexia is commonly related to many clinically important conditions, such as anorexia, inflammation, and degradation of skeletal muscle protein, in which muscle wasting plays a key role. Cachexia is frequently observed in patients with cancer (50%-80%) and leads to approximately 20% of deaths among cancer patients.¹⁻⁵ Moreover, cancer cachexia not only is associated with higher rates of toxicity from chemotherapeutic drugs⁶ but also leads to a poor prognosis as well as reduced quality of life (QOL).⁷

Cancer cachexia cannot be completely reversed with conventional nutritional support,⁸ and there are limited pharmacological therapies useful for the management of cachexia.

Corresponding author: Nobuyuki Katakami, MD, Division of Integrated Oncology, Institute of Biomedical Research and Innovation, 2-2 Minatojima Minamimachi, Chuo-Ku, Hyogo 650-0047, Japan; nkatakami@kcho.jp

¹Division of Integrated Oncology, Institute of Biomedical Research and Innovation, Kobe, Japan; ²Department of Pulmonary Medicine, Kyoto Prefectural University of Medicine, Kyoto, Japan; ³Department of Respiratory Medicine, Fukuoka University School of Medicine, Fukuoka, Japan; ⁴Department of Respiratory Medicine, Kyorin University Hospital, Mitaka, Japan; ⁵Division of Thoracic Oncology, Shizuoka Cancer Center, Shizuoka, Japan; ⁶Department of Respiratory Medicine Graduate School of Medicine, Nagoya University, Nagoya, Japan; ⁷Department of Respiratory Medicine, Fujita Health University, Toyoake, Japan; ⁸Department of Thoracic Oncology, Kanagawa Cancer Center, Yokohama, Japan; ⁹Department of Respiratory Medicine, National Hospital Organization Shikoku Cancer Center, Matsuyama, Japan; ¹⁰Department of Clinical Oncology, Japan Anti-Tuberculosis Association, Fukujyuji Hospital, Kiyose, Japan; ¹¹Department of Respiratory Medicine, Nagaoka Red Cross Hospital, Nagaoka, Japan; ¹²Department of Respiratory Medicine, Aichi Cancer Center Aichi Hospital, Aichi, Japan; ¹³Department of Medical Oncology, National Hospital Organization Yamaguchi-Ube Medical Center, Ube, Japan; ¹⁴Department of Rehabilitation Medicine, Keio University School of Medicine, Tokyo, Japan; ¹⁵Department of Medical Oncology, Graduate School of Medicine, Chiba University, Chiba, Japan; ¹⁶Ono Pharmaceutical Co, Ltd, Osaka, Japan; ¹⁷Health Science on Supportive Medicine for Intractable Diseases, Teikyo University School of Medicine, Tokyo, Japan

See editorial on pages 000-000, this issue.

The clinical trial registration was JapicCTI-142451 (<http://www.clinicaltrials.jp/user/search/directCteDetail.jsp?clinicalTrialId=14228>).

We thank all the patients as well as the caregivers, investigators, and onsite staff who contributed to this clinical trial.

Additional supporting information may be found in the online version of this article.

DOI: 10.1002/cncr.31128, **Received:** June 19, 2017; **Revised:** September 8, 2017; **Accepted:** September 14, 2017, **Published online** Month 00, 2017 in Wiley Online Library (wileyonlinelibrary.com)

Ghrelin, a peptide hormone produced by ghrelin-producing endocrine cells in the gut, acts as a regulator of hunger, which is also involved in the regulation of food intake.⁹⁻¹¹ Furthermore, ghrelin induces the secretion of growth hormone and thereby acts as a growth hormone secretagogue.^{12,13}

Anamorelin (ONO-7643) is an orally active, high-affinity, selective agonist of the ghrelin receptor.^{14,15} Previous phase 1 and 2 trials have demonstrated the safety and efficacy of anamorelin treatment for increasing body weight, lean body mass (LBM), and food intake.¹⁶⁻¹⁸ Two multinational phase 3 clinical studies in patients with advanced non–small cell lung cancer (NSCLC) and cachexia reported that anamorelin administration for 12 weeks increased LBM and body weight and substantially improved the symptoms of anorexia/cachexia.¹⁹

A randomized, double-blind, phase 2 trial investigated 50 and 100 mg of anamorelin versus a placebo in Japanese patients with NSCLC and cachexia; treatment with 100 mg of anamorelin in that study demonstrated improvements in LBM, body weight, appetite, and QOL with no tolerability issues.²⁰ Therefore, in the current study, 100 mg of anamorelin was selected to confirm its action in increasing LBM in Japanese patients with NSCLC and cachexia.

MATERIALS AND METHODS

Study Design

We conducted a multicenter (43 sites in Japan), randomized, double-blind, placebo-controlled trial that comprised an observation/run-in period of 2 weeks, a treatment period of 12 weeks, and a follow-up period of 4 weeks. Visits during the treatment period were planned at weeks 0, (baseline/randomization), 1, 3, 6, 9, and 12. All procedures followed during this study were in accordance with the spirit of the Declaration of Helsinki, the study protocol, the standards specified under the Pharmaceutical Affairs Act of Japan (article 80, paragraph 2 and article 14, paragraph 3), and Good Clinical Practice (effective as of April 1, 1997; Japanese Ministry of Health and Welfare Ordinance No. 28). Ethics committee approval for the study was obtained from each center.

Patients

This study included patients with stage III or IV NSCLC who were not to undergo an operation, were 20 years old or older, had involuntary weight loss $\geq 5\%$ within the last 6 months, had anorexia, had 2 or more applicable symptoms (fatigue, malaise, reduced overall muscular strength, and arm muscle circumference [in centimeters] < 10 th

percentile), and had more than 1 of the following conditions: albumin level < 3.2 g/dL, C-reactive protein level > 5.0 mg/L, hemoglobin level < 12 g/dL, Eastern Cooperative Oncology Group (ECOG) performance status (PS) of 0 to 2, and estimated life expectancy ≥ 4 months. Anorexia, malaise, fatigue, and reduced muscular strength needed to be grade 1 or higher according to the National Cancer Institute's Common Terminology Criteria for Adverse Events (version 4.0). The following formula was used to ascertain the arm muscle circumference:

$$\text{Arm muscle circumference (cm)} = \text{Arm circumference (cm)} - 3.14 \times \text{Triceps skinfold thickness (mm)}/10.$$

Patients were excluded if they had known symptomatic brain metastases or uncontrolled diabetes. Written informed consent was obtained from each patient. All eligible patients were randomized by a centralized allocation center and were further stratified by the enrollment site and reductions in weight during the last 6 months (5%–10% and $>10\%$). The randomization methodology used a randomization table and sealed envelopes to randomize the patients.

Interventions and Concomitant Therapies

After enrollment, patients were randomly assigned to either 100 mg of anamorelin or a placebo once daily throughout the therapy period. In this study, patients were enrolled regardless of their treatment history with chemotherapy for NSCLC, but they were prohibited from newly taking epidermal growth factor receptor tyrosine kinase inhibitors during the treatment period because of their possible effect on the QOL assessment.

During the study period, radiotherapy (other than palliative radiation therapy for bone metastases or radiation therapy for metastases in the brain), general corticosteroids, growth hormone formulations, medroxyprogesterone, megestrol acetate, Chinese herbal drugs, antiarrhythmic drugs, antitumor anthracyclines, inhibitors and inducers of cytochrome P450 3A4, and other experimental treatments were not permitted.

Efficacy Assessments

The primary endpoint of the trial was the mean change in LBM (estimated by dual-energy x-ray absorptiometry [DEXA]) from the baseline over the 12-week treatment period. The secondary endpoints of the study were changes in the body weight, body composition (ascertained by DEXA), appetite, Cancer Fatigue Scale (CFS) score, ECOG PS, Karnofsky Performance Scale (KPS) score, handgrip strength (HGS), Quality-of-Life Questionnaire for Cancer Patients Treated With Anticancer

Drugs (QOL-ACD) score, 6-minute walk test (6MWT) results, and serum biomarkers. The LBM and other body composition-related variables, ECOG PS, KPS, HGS, 6MWT, and serum biomarkers were determined at the baseline and in weeks 3, 6, 9, and 12. The body weight, QOL-ACD score, and CFS score were determined at the baseline and in weeks 1, 3, 6, 9, and 12. In addition, the efficacy parameters were recorded after treatment discontinuation.

Body composition was determined via DEXA with either the GE Lunar system (GE, Wauwatosa, Wisconsin) or the Hologic system (Hologic, Bedford, Massachusetts). DEXA was used to assess the LBM, fat mass, bone mineral content, and overall body mass by means of standardized methods. A grip dynamometer (Tracker Freedom Wireless Grip; JTECH Medical, Midvale, Utah) was used for the measurement of HGS.

The QOL-ACD (see online supporting information) is a self-rated measure assessing the condition of a patient during the last few days according to a 1 to 5 scale, and it is composed of 4 domains (functional, physical, mental, and psychosocial) and a global face scale developed as a generic questionnaire for assessing QOL in Japanese cancer patients receiving chemotherapy.²¹ The CFS is a self-rated scale evaluating current fatigue in cancer patients, and it has 3 dimensions (physical fatigue, affective fatigue, and cognitive fatigue). The scale is composed of 15 items scored on a 1 to 5 scale for a maximum score of 60, with higher scores indicating more severe fatigue. ECOG PS and KPS were used to quantify the PS of the patients. After a \geq 12-hour fast, blood samples were collected for the estimation of insulin-like growth factor 1 (IGF-1), insulin-like growth factor-binding protein 3 (IGFBP-3), and prealbumin. Laboratory tests were performed at each study site.

Safety

The safety parameters included the vital signs, electrocardiography (centrally assessed) with all 12 leads, status of the tumor (evaluated by investigators using Response Evaluation Criteria in Solid Tumors [RECIST] guidelines), clinical laboratory tests, and adverse events (AEs). AEs were reported with the National Cancer Institute's Common Terminology Criteria for Adverse Events (version 4.0), and they were classified according to the system organ class/preferred term.

Statistical Analysis

Analyses were performed according to the predetermined study protocol and statistical analysis plan. The full

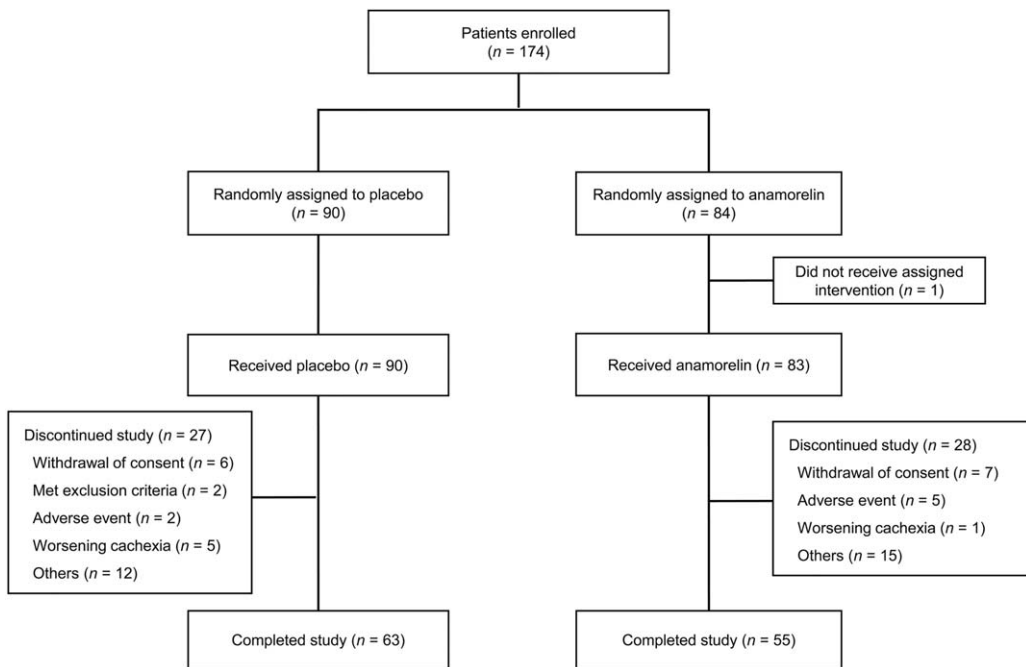
analysis set (FAS) was used for the analysis of all efficacy variables. The FAS comprised all eligible patients who had undergone a minimum of 1 efficacy assessment after the initiation of the study drug. The safety analysis set was used for the analysis of safety data and comprised all patients who had received the study drug at least once.

The findings of a phase 2 trial (ONO-7643-03), in which the mean difference in LBM (according to DEXA) between 100 mg of anamorelin and the placebo was 0.89 ± 1.94 kg, were used to determine the sample size for this study.²⁰ At least 76 patients were required in each treatment arm to reject the null hypothesis at $P < .05$ and a power of 80%. Under the assumption that approximately 10% of the patients would withdraw/drop out of the study, a total of 170 patients (85 patients per group) were to be enrolled. Descriptive statistics were used to summarize the baseline parameters. An analysis of covariance for repeated measurement data, using the study arm, time point, and prior reductions in weight (5%-10% and $>10\%$) as fixed factors and the baseline value as a covariate, was used to analyze efficacy parameters. The difference in the least squares mean from the initiation of treatment to a specific point of time was determined for both groups. The least squares mean differences between patients who received anamorelin and those who received the placebo were determined with 95% confidence intervals (CIs). A study arm-point of time interaction was incorporated for the assessment of secondary endpoints (differences in the body mass composition, QOL-ACD score, CFS score, body weight, KPS, serum biomarkers, HGS, and 6MWT results). Descriptive statistics were used to assess safety parameters and are reported as numbers and percentages of patients. The total incidence of AEs and adverse drug reactions (ADRs) was compared between the study groups with the chi-square test. There was no adjustment for the multiplicity of statistical testing, and an imputation method was not used for missing data.

RESULTS

Patients

A total of 174 patients were enrolled in this study from May 2014 to October 2015. Ninety of these 174 patients were randomized to the placebo group, and 84 were randomized to the 100-mg anamorelin group (Fig. 1). One patient did not receive treatment. One patient treated with 100 mg of anamorelin failed to meet the inclusion criteria and hence was excluded from the FAS. The FAS comprised 172 patients, with 90 and 82 in the placebo

**Figure 1.** Enrollment and outcomes.

and anamorelin groups, respectively. There were 11 deaths in the placebo group and 5 deaths in the anamorelin group. AEs led to treatment discontinuation in 2 patients from the placebo group and in 5 patients from the anamorelin group. The baseline characteristics of the 2 groups were similar (Table 1).

LBM

As shown in Figure 2, the increase in LBM over 12 weeks was found to be significantly larger in the anamorelin-treated patients versus the placebo-treated patients, with least squares means and standard errors of 1.38 ± 0.18 and -0.17 ± 0.17 kg, respectively. Overall, the change in the anamorelin-treated patients versus the placebo-treated patients was 1.56 kg (95% CI, 1.11 - 2.00 kg; $P < .0001$). At week 3 and thereafter, a significant difference ($P < .0001$) in the LBM gain in comparison with the baseline was noted between the treatment groups.

Body Weight

In comparison with the placebo, anamorelin induced a significant weight gain (Fig. 2), which is in agreement with anamorelin's mechanism of action and the LBM gain. The body weight gain was evident at week 1 of treatment and continued thereafter.

Other Body Composition Parameters

In comparison with the placebo, anamorelin significantly increased other body composition parameters, including the total body mass, fat mass, appendicular LBM (arms and legs), and trunk LBM (Supporting Table 1 [see online supporting information]).

QOL-ACD

Throughout the study period from week 1, the anamorelin-treated patients showed significant improvements in comparison with the placebo-treated patients in the QOL-ACD scores for items 7 to 11 ("physical condition"), item 8 ("Did you have a good appetite?"), item 9 ("Did you enjoy your meals?"), and item 11 ("Did you lose any weight?"; Fig. 3A-D). The efficacy of anamorelin was not definite in other domains.

Other Secondary Endpoints

The effects of 100 mg of anamorelin on CFS, HGS, and 6MWT are shown in Figure 2 and Supporting Table 2 (see online supporting information). There were marginal effects on CFS, HGS, and 6MWT. In comparison with the placebo group, the anamorelin group showed significant increases in the serum IGF-1, IGFBP-3, and prealbumin levels (Fig. 4A-C).

TABLE 1. Demographics and Baseline Characteristics of the Patients

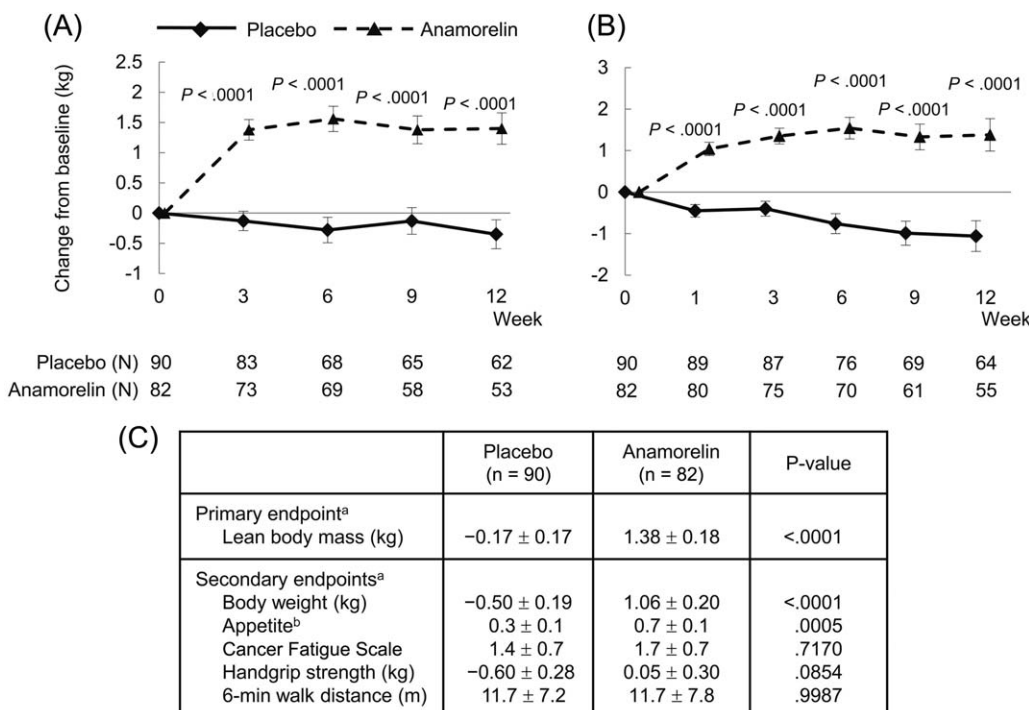
Parameter	Placebo (n = 90)	Anamorelin (n = 84)
Sex, No. (%)		
Male	57 (63.3)	59 (70.2)
Female	33 (36.7)	25 (29.8)
Age, mean \pm SD, y	67.2 \pm 7.9	67.6 \pm 9.9
Weight, mean \pm SD, kg	49.73 \pm 8.32	52.23 \pm 9.43
BMI, mean \pm SD, kg/m ²	19.27 \pm 2.31	19.81 \pm 2.60
Weight loss, No. (%)		
5-10	52 (57.8)	50 (60.2)
>10	38 (42.2)	33 (39.8)
Missing	-	1
Body composition (DEXA), mean \pm SD, kg		
LBM	37.06 \pm 6.34	38.88 \pm 7.06
Body fat	10.68 \pm 4.21	11.29 \pm 5.04
BMC	1.90 \pm 0.56	2.06 \pm 0.57
Total body mass	49.63 \pm 8.61	52.23 \pm 9.73
Grip strength, mean \pm SD, kg		
Dominant hand	26.70 \pm 8.01	27.87 \pm 9.35
Nondominant hand	25.12 \pm 7.01	26.41 \pm 8.30
6-min walk distance, mean \pm SD, m	375.7 \pm 88.4	379.6 \pm 89.6
QOL-ACD, mean \pm SD	70.9 \pm 13.0	74.9 \pm 13.0
Cancer Fatigue Scale, mean \pm SD	23.8 \pm 9.7	24.4 \pm 9.7
ECOG PS, No. (%)		
0	13 (14.4)	9 (10.8)
1	65 (72.2)	64 (77.1)
2	12 (13.3)	10 (12.0)
Missing	-	1
NSCLC type per histological criteria, No. (%)		
Adenocarcinoma	71 (78.9)	67 (79.8)
Squamous cell	16 (17.8)	14 (16.7)
Other	1 (1.1)	2 (2.4)
Unknown	2 (2.2)	1 (1.2)
Disease stage		
IIIA	1 (1.1)	3 (3.6)
IIIB	11 (12.2)	6 (7.1)
IV	60 (66.7)	49 (58.3)
Recurrence	18 (20.0)	26 (31.0)
Time from diagnosis to starting study drug, mean \pm SD, d	609.4 \pm 741.7	768.7 \pm 698.0
Previous history of chemotherapy (No. of times), No. (%)		
0	2 (2.2)	2 (2.4)
1	31 (34.4)	20 (23.8)
2	18 (20.0)	19 (22.6)
\geq 3	39 (43.3)	43 (51.2)
Concomitant cancer therapy, No. (%)		
Chemotherapy	70 (77.8)	64 (76.2)
EGFR TKI	29 (32.2)	23 (27.7)
Radiation	6 (6.7)	7 (8.3)
Supportive care	19 (21.1)	18 (21.7)
Missing	-	1

Abbreviations: BMC, bone mineral content; BMI, body mass index; DEXA, dual-energy x-ray absorptiometry; ECOG, Eastern Cooperative Oncology Group; EGFR, epidermal growth factor receptor; LBM, lean body mass; NSCLC, non–small cell lung cancer; PS, performance status; QOL-ACD, Quality-of-Life Questionnaire for Cancer Patients Treated With Anticancer Drugs (Kurihara Group Questionnaire); SD, standard deviation; TKI, tyrosine kinase inhibitor.

Safety

On the basis of the RECIST criteria, a complete response and a partial response were observed in 1 (1.5%) and 3 patients (4.5%), respectively, in the anamorelin-treated group and in 0 (0.0%) and 2 patients (2.7%), respectively, in the placebo group. Stable disease was observed in 21 (31.3%) and 22 patients (29.7%) in the anamorelin-treated and placebo groups, respectively. Thirty-eight of the anamorelin-treated patients (56.4%) showed

progressive disease, whereas 47 patients (63.5%) in the placebo group did. Non–complete response/non–progressive disease cases were observed for 4 (6.0%) and 3 patients (4.1%) in the anamorelin-treated and placebo groups, respectively. The median survival times were found to be similar for the 2 groups (8.08 months [95% CI, 5.98–11.56 months] for anamorelin and 8.21 months [95% CI, 6.67–12.39 months] for the placebo; hazard ratio, 1.17 [95% CI, 0.82–1.67]; $P = .3762$).



^aLeast squares mean ± standard error for change from baseline over 12 weeks.

^bAppetite was evaluated with QOL-ACD item 8 "Did you have a good appetite?"

Figure 2. Time-course changes for the anamorelin and placebo groups in (A) lean body mass and (B) body weight and (C) changes in primary and secondary efficacy measures from the baseline over 12 weeks. QOL-ACD indicates Quality-of-Life Questionnaire for Cancer Patients Treated With Anticancer Drugs.

Table 2 summarizes the overall incidences of AEs and ADRs. The frequency of AEs was found to be similar in the anamorelin group and the placebo group. On the other hand, the anamorelin group reported a significantly higher number of ADRs in comparison with the placebo group; however, all the ADRs were grade 3 or lower. The most common ADRs were first-degree atrioventricular block and rash, which were followed by increased γ -glutamyltransferase and diabetes mellitus. All these events were grade 1 or 2 except for 1 case of rash.

DISCUSSION

The current study demonstrated that anamorelin significantly improved LBM and body weight in Japanese patients with NSCLC and cachexia in comparison with a placebo. Significant improvements in LBM and body weight were observed in the anamorelin group at the early time points of week 3 and week 1, respectively, in comparison with the placebo group, and they were sustained thereafter during the 12-week study period.

The National Comprehensive Cancer Network clinical guidelines for the management of

anorexia/cachexia define the primary treatment goals as promoting weight gain/stabilization and relieving symptoms of anorexia.²² Similarly, the clinical practice guidelines on cancer cachexia given by the European Palliative Care Research Collaborative specify that the treatment goals for cachexia should be a reversal of the loss of body weight and muscle mass and that the minimum objective must be the maintenance of body weight and the prevention of further body weight loss.²³ The results of the current study satisfy the treatment goals in these guidelines.

As for appetite, a considerable increase was reported in the anamorelin group versus the placebo group as early as week 1, and it was subsequently sustained throughout the study period. The increased level of prealbumin, a nutritional state marker, suggested increased food intake. Decreases in appetite and food intake are considered to be the main underlying causes for the worsening of the physical and psychological status in cancer patients.²⁴ Anorexia leads to QOL deterioration in cancer patients²⁵ and is also a prognostic factor.²⁶ Therefore, oncologists should consider ensuring sufficient energy and protein intake for all cancer patients.²⁷

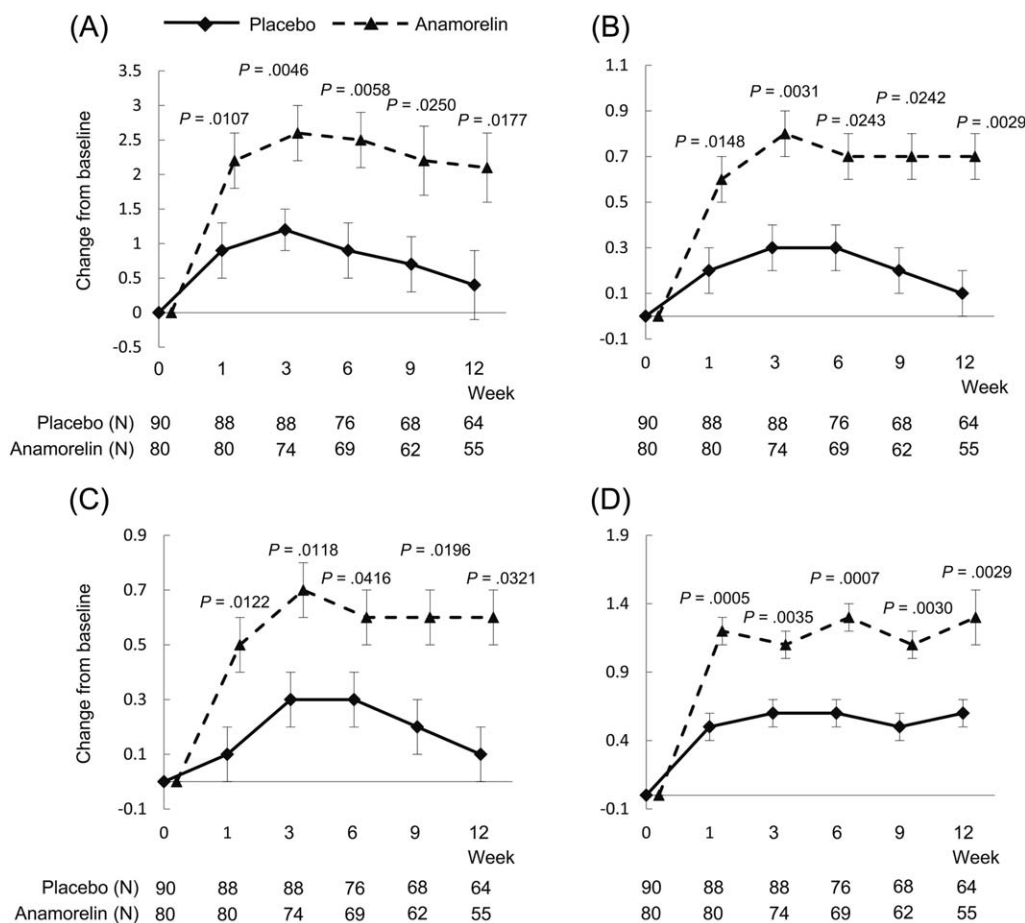


Figure 3. Time-course changes for the anamorelin and placebo groups in the QOL-ACD scores for (A) items 7 to 11 ("physical condition"), (B) item 8 ("Did you have a good appetite?"), (C) item 9 ("Did you enjoy your meals?"), and (D) item 11 ("Did you lose any weight?"). QOL-ACD indicates Quality-of-Life Questionnaire for Cancer Patients Treated With Anticancer Drugs.

Under the present conditions, where there are no effective treatment methods for cancer cachexia, anamorelin may have great clinical significance by preventing weight loss and ameliorating anorexia.

In contrast, in the assessment of motor function, including HGS and 6MWT results, no improvement was observed after anamorelin administration. Previous researchers have suggested that patients who are affected by long-term illness and systemic inflammation may display an unusual association between muscle mass and muscular strength.²⁸⁻³⁰ Furthermore, the most suitable measure for muscle strength in advanced cancer patients is unidentified. The 6MWT measurements may have been affected by respiratory insufficiency in patients with NSCLC. The cause of cachexia is multifactorial, and pharmacological treatment alone may not be able to bring about a complete reversal of all features of the syndrome (especially improvements in motor function). Therefore,

it is expected that a multimodal treatment combining medicine, exercise, and nutrition may improve the condition and symptoms of cachexia, including motor function.

In general, patients in the 2 treatment groups showed similar overall survival times and tumor responses as assessed by RECIST, and this indicated that the therapy had no effect on the progression of the disease. In addition, patient characteristics such as the disease stage and previous use of chemotherapy and prevailing factors that affect the prognosis were similar between the 2 treatment arms.

In comparison with patients receiving the placebo, the frequency of ADRs was significantly higher in patients receiving anamorelin; however, most deaths and treatment discontinuations were caused by disease progression and not by the study drugs. In comparison with the placebo-treated patients, first-degree atrioventricular

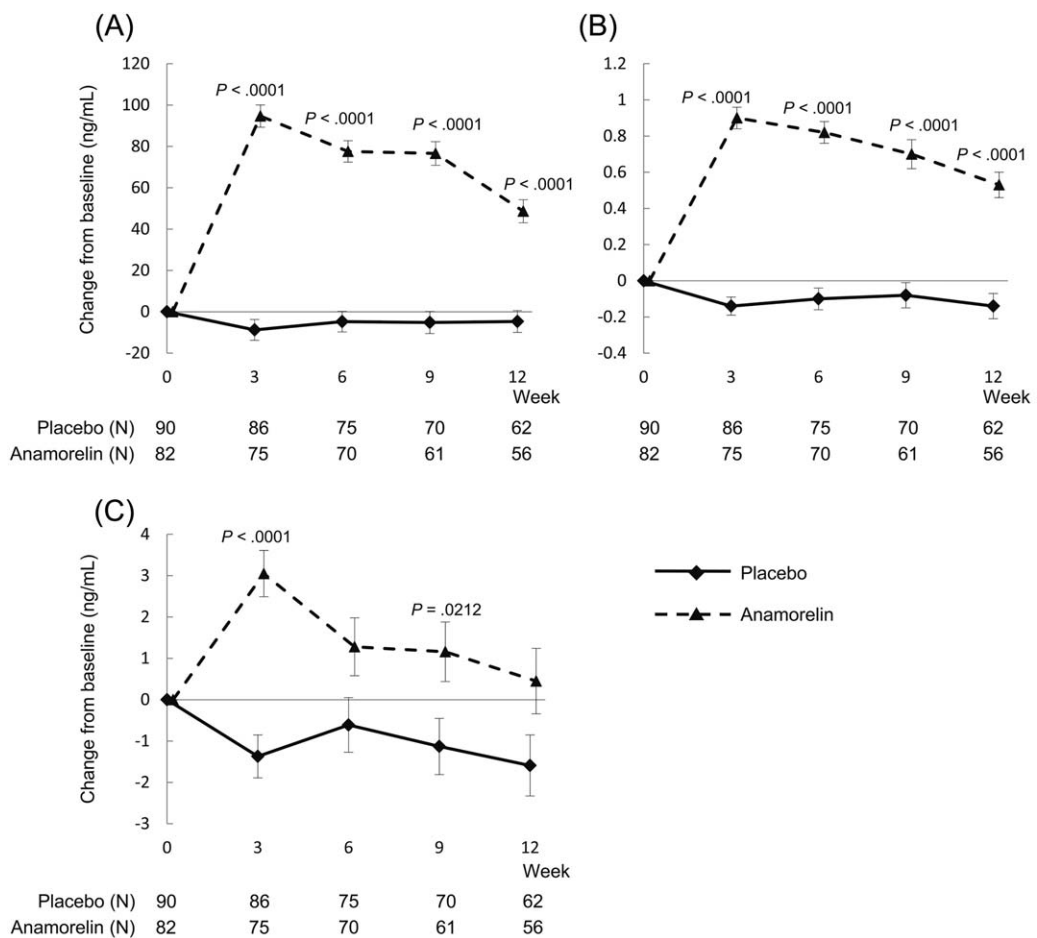


Figure 4. Time-course changes for the anamorelin and placebo groups in (A) insulin-like growth factor 1, (B) insulin-like growth factor-binding protein 3, and (C) prealbumin.

block and rash occurred at rates $\geq 5\%$, and they had a higher incidence in the anamorelin-treated patients. However, all first-degree atrioventricular block cases were grade 1, and only 1 case of rash was grade 3; this suggests no major risk. The frequencies of these ADRs were observed to be higher in the current study versus the multinational phase 3 studies.¹⁹ The frequent electrocardiogram measurements might have caused the higher incidence of first-degree atrioventricular block. Although no apparent cause of rash has been identified, we think that there is a possibility that this might have been influenced by chemotherapy applied during the study. In agreement with previous studies,^{19,20} increases in blood glucose levels were more frequently observed with anamorelin treatment; this was, however, controllable. The changes in glucose homeostasis might have been caused by effects of IGF-1 and growth hormone on glucose metabolism or by a possible effect of the reversal of cancer anorexia/cachexia syndrome. These findings suggest that

anamorelin is safe and well tolerated in Japanese cancer patients with cachexia.

The current research had some shortcomings. First, we could not confirm the efficacy of anamorelin by functional measures of HGS and 6MWT. Second, its efficacy for fatigue was not confirmed. The lack of a treatment effect observed for CFS may have arisen because fatigue associated with cancer is a problematic manifestation to ameliorate in patients with advanced cancer and particularly in patients with more symptomatic disease.^{31,32} This is partly due to the multiple and complex causes of fatigue, including chemotherapy, anemia, nutritional issues, and pain.³³

The efficacy of anamorelin in the current study for increasing LBM and body weight and improving anorexia symptoms and the nutritional state with no improvement in motor function is consistent with the recent results of 2 multinational phase 3 studies with anamorelin.¹⁹

TABLE 2. Safety

	Placebo (n = 90)	Anamorelin (n = 83)
AEs, No. (%)	73 (81.1)	74 (89.2)
AEs		
Difference vs placebo, % (95% CI)		8.0 (-2.4, 18.5)
P		.1390
SAEs, No. (%)	8 (8.9)	16 (19.3)
Discontinuations due to AEs, No. (%)	2 (2.2)	3 (3.6)
ADRs, No. (%)	20 (22.2)	34 (41.0)
ADRs		
Difference vs placebo, % (95% CI)		18.7 (5.1, 32.4)
P		.0079
Serious ADRs, No. (%)	0 (0.0)	2 (2.4)
Discontinuations due to ADRs, No. (%)	1 (1.1)	2 (2.4)
Deaths, No. (%)	11 (12.2)	5 (6.0)
ADRs by grade, No. (%)		
1/2	18 (20.0)	28 (33.7)
3	2 (2.2)	6 (7.2)
ADRs in >2% of patients, No. (%)		
First-degree atrioventricular block	0 (0.0)	5 (6.0)
Tachycardia	0 (0.0)	2 (2.4)
Edema	0 (0.0)	2 (2.4)
Peripheral edema	0 (0.0)	2 (2.4)
Pyrexia	0 (0.0)	2 (2.4)
γ-Glutamyltransferase increase	1 (1.1)	3 (3.6)
Glycosylated hemoglobin increase	1 (1.1)	2 (2.4)
Diabetes mellitus	0 (0.0)	3 (3.6)
Hyperglycemia	1 (1.1)	2 (2.4)
Headache	1 (1.1)	2 (2.4)
Rash	1 (1.1)	5 (6.0)
Hypertension	0 (0.0)	2 (2.4)
Hot flush	0 (0.0)	2 (2.4)

Abbreviations: ADR, adverse drug reaction; AE, adverse event; CI, confidence interval; SAE, severe adverse event.

Although anamorelin cannot improve motor function or survival, it may be of great importance for alleviating anorexia, a highly unmet medical need, to help patients with advanced cancer to enjoy their meals and thereby achieve better QOL.

On the basis of our findings, once daily administration of 100 mg of anamorelin showed favorable results for LBM gains in Japanese patients with NSCLC and cachexia; hence 100 mg could be the desired dose for such patients. Anamorelin therapy was associated with augmentation of IGF-1 and IGFBP-3 levels, and this suggests an increase in the synthesis of proteins that can have direct growth effects on skeletal muscle. Moreover, anamorelin was associated with favorable improvements in appetite and increases in prealbumin, and this indicates an improved nutritional status. Even though the incidences of ADRs and treatment discontinuations due to AEs were higher in the anamorelin group, most of the treatment discontinuations were associated with the progression of disease and not with anamorelin. The efficacy of anamorelin to improve LBM and anorexia was thus confirmed in Japanese patients with NSCLC and cachexia. Because no effective treatment for cancer cachexia is currently

available, anamorelin can be one of the beneficial treatment options.

FUNDING SUPPORT

The study sponsor, Ono Pharmaceutical Co, Ltd (Osaka, Japan), was involved in the study design, provision of study materials, data collection and interpretation, and writing of the report.

CONFLICT OF INTEREST DISCLOSURES

Nobuyuki Katakami reports personal fees from AstraZeneca, Eli Lilly, Pfizer, Boehringer Ingelheim, Ono, Taiho, and Novartis Pharma KK and grants from MSD, Astellas, AstraZeneca, Eisai, Amgen, Shionogi, Daiichi Sankyo, Chugai, Eli Lilly, Boehringer Ingelheim, Bristol-Myers Squibb, Maruishi, and Merck Serono outside the submitted work. Tateaki Naito reports personal fees from Ono during the conduct of the study. Masashi Kondo reports personal fees from Ono, Chugai, Pfizer, Novartis, Eli Lilly, Taiho, and AstraZeneca and grants from Eli Lilly outside the submitted work. Hiroshi Saito reports personal fees from Ono during the conduct of the study; grants from Taiho and Merck Serono outside the submitted work; and personal fees from Pfizer, AstraZeneca, and Kyowa Hakko Kirin outside the submitted work. Yuichi Takiguchi reports grants and personal fees from Ono, AstraZeneca, Taiho, Nippon Boehringer Ingelheim, and Chugai outside the submitted work. Koichi Takayama reports personal fees from Ono during the conduct of the study and personal fees from AstraZeneca, Eli Lilly,

Chugai, and Ono outside the submitted work. Naoyuki Komura and Toru Takiguchi are employees of Ono. Kenji Eguchi reports grants from Ono outside the submitted work.

AUTHOR CONTRIBUTIONS

Nobuyuki Katakami: Conception and design, acquisition of data, data analysis and interpretation, manuscript writing, and final approval of manuscript. **Junji Uchino:** Acquisition of data, manuscript writing, and final approval of manuscript. **Takuma Yokoyama:** Acquisition of data, manuscript writing, and final approval of manuscript. **Tateaki Naito:** Acquisition of data, manuscript writing, and final approval of manuscript. **Masashi Kondo:** Acquisition of data, manuscript writing, and final approval of manuscript. **Kouzo Yamada:** Acquisition of data, manuscript writing, and final approval of manuscript. **Hiromoto Kitajima:** Acquisition of data, manuscript writing, and final approval of manuscript. **Kozo Yoshimori:** Acquisition of data, manuscript writing, and final approval of manuscript. **Kazuhiro Saito:** Acquisition of data, manuscript writing, and final approval of manuscript. **Hirosi Saito:** Conception and design, acquisition of data, data analysis and interpretation, manuscript writing, and final approval of manuscript. **Keisuke Aoe:** Conception and design, acquisition of data, data analysis and interpretation, manuscript writing, and final approval of manuscript. **Tetsuya Tsuji:** Conception and design, data analysis and interpretation, manuscript writing, and final approval of manuscript. **Yuichi Takiguchi:** Conception and design, acquisition of data, data analysis and interpretation, manuscript writing, and final approval of manuscript. **Koichi Takayama:** Conception and design, data analysis and interpretation, manuscript writing, and final approval of manuscript. **Naoyuki Komura:** Conception and design, data analysis and interpretation, manuscript writing, and final approval of manuscript. **Toru Takiguchi:** Conception and design, data analysis and interpretation, manuscript writing, and final approval of manuscript. **Kenji Eguchi:** Conception and design, data analysis and interpretation, manuscript writing, and final approval of manuscript.

REFERENCES

1. Bruera E. ABC of palliative care. Anorexia, cachexia, and nutrition. *BMJ*. 1997;315:1219-1222.
2. Dewys WD, Begg C, Lavin PT, et al. Prognostic effect of weight loss prior to chemotherapy in cancer patients. Eastern Cooperative Oncology Group. *Am J Med*. 1980;69:491-497.
3. Reuben DB, Mor V, Hiris J. Clinical symptoms and length of survival in patients with terminal cancer. *Arch Intern Med*. 1988;148:1586-1591.
4. von Haehling S, Anker SD. Treatment of cachexia: an overview of recent developments. *J Am Med Dir Assoc*. 2014;15:866-872.
5. von Haehling S, Anker SD. Prevalence, incidence and clinical impact of cachexia: facts and numbers—update 2014. *J Cachexia Sarcopenia Muscle*. 2014;5:261-263.
6. Fearon K, Arends J, Baracos V. Understanding the mechanisms and treatment options in cancer cachexia. *Nat Rev Clin Oncol*. 2013;10:90-99.
7. von Haehling S, Anker SD. Cachexia as a major underestimated and unmet medical need: facts and numbers. *J Cachexia Sarcopenia Muscle*. 2010;1:1-5.
8. Fearon K, Strasser F, Anker SD, et al. Definition and classification of cancer cachexia: an international consensus. *Lancet Oncol*. 2011;12:489-495.
9. Neary NM, Small CJ, Wren AM, et al. Ghrelin increases energy intake in cancer patients with impaired appetite: acute, randomized, placebo-controlled trial. *J Clin Endocrinol Metab*. 2004;89:2832-2836.
10. Wren AM, Seal LJ, Cohen MA, et al. Ghrelin enhances appetite and increases food intake in humans. *J Clin Endocrinol Metab*. 2001;86:5992.
11. Akamizu T, Takaya K, Irako T, et al. Pharmacokinetics, safety, and endocrine and appetite effects of ghrelin administration in young healthy subjects. *Eur J Endocrinol*. 2004;150:447-455.
12. Kojima M, Hosoda H, Date Y, Nakazato M, Matsuo H, Kangawa K. Ghrelin is a growth-hormone-releasing acylated peptide from stomach. *Nature*. 1999;402:656-660.
13. Smith RG, Cheng K, Schoen WR, et al. A nonpeptidyl growth hormone secretagogue. *Science*. 1993;260:1640-1643.
14. Currow DC, Abernethy AP. Anamorelin hydrochloride in the treatment of cancer anorexia-cachexia syndrome. *Future Oncol*. 2014;10:789-802.
15. Zhang H, Garcia JM. Anamorelin hydrochloride for the treatment of cancer-anorexia-cachexia in NSCLC. *Expert Opin Pharmacother*. 2015;16:1245-1253.
16. Garcia JM, Friend J, Allen S. Therapeutic potential of anamorelin, a novel, oral ghrelin mimetic, in patients with cancer-related cachexia: a multicenter, randomized, double-blind, crossover, pilot study. *Support Care Cancer*. 2013;21:129-137.
17. Garcia JM, Polvino WJ. Effect on body weight and safety of RC-1291, a novel, orally available ghrelin mimetic and growth hormone secretagogue: results of a phase I, randomized, placebo-controlled, multiple-dose study in healthy volunteers. *Oncologist*. 2007;12:594-600.
18. Garcia JM, Polvino WJ. Pharmacodynamic hormonal effects of anamorelin, a novel oral ghrelin mimetic and growth hormone secretagogue in healthy volunteers. *Growth Horm IGF Res*. 2009;19:267-273.
19. Temel JS, Abernethy AP, Currow DC, et al. Anamorelin in patients with non-small-cell lung cancer and cachexia (ROMANA 1 and ROMANA 2): results from two randomised, double-blind, phase 3 trials. *Lancet Oncol*. 2016;17:519-531.
20. Takayama K, Katakami N, Yokoyama T, et al. Anamorelin (ONO-7643) in Japanese patients with non-small cell lung cancer and cachexia: results of a randomized phase 2 trial. *Support Care Cancer*. 2016;24:3495-3505.
21. Matsumoto T, Ohashi Y, Morita S, et al. The Quality of Life Questionnaire for Cancer Patients Treated With Anticancer Drugs (QOL-ACD): validity and reliability in Japanese patients with advanced non-small-cell lung cancer. *Qual Life Res*. 2002;11:483-493.
22. National Comprehensive Cancer Network. NCCN clinical practice guidelines in oncology: palliative care. http://www.nccn.org/professionals/physician_gls/f_guidelines.asp. Accessed December 28, 2016.
23. Radbruch L, Elsner F, Trotterberg P, Strasser F, Fearon K. Clinical Practice Guidelines on Cancer Cachexia in Advanced Cancer Patients With a Focus on Refractory Cachexia. Aachen, Germany: European Palliative Care Research Collaborative; 2010.
24. Pilil K, Juhler M, Jakobsen J, Jarden M. Controlled rehabilitative and supportive care intervention trials in patients with high-grade gliomas and their caregivers: a systematic review. *BMJ Support Palliat Care*. 2016;6:27-34.
25. Takayama K, Atagi S, Imamura F, et al. Quality of life and survival survey of cancer cachexia in advanced non-small cell lung cancer patients—Japan nutrition and QOL survey in patients with advanced non-small cell lung cancer study. *Support Care Cancer*. 2016;24:3473-3480.
26. Quinten C, Coens C, Mauer M, et al. Baseline quality of life as a prognostic indicator of survival: a meta-analysis of individual patient data from EORTC clinical trials. *Lancet Oncol*. 2009;10:865-871.
27. Aapro M, Arends J, Bozzetti F, et al. Early recognition of malnutrition and cachexia in the cancer patient: a position paper of a European School of Oncology task force. *Ann Oncol*. 2014;25:1492-1499.
28. Chen L, Nelson DR, Zhao Y, Cui Z, Johnston JA. Relationship between muscle mass and muscle strength, and the impact of comorbidities: a population-based, cross-sectional study of older adults in the United States. *BMC Geriatr*. 2013;13:74.

29. Dobs AS, Boccia RV, Croot CC, et al. Effects of enobosarm on muscle wasting and physical function in patients with cancer: a double-blind, randomised controlled phase 2 trial. *Lancet Oncol.* 2013;14:335-345.
30. Park SW, Goodpaster BH, Strotmeyer ES, et al. Decreased muscle strength and quality in older adults with type 2 diabetes: the Health, Aging, and Body Composition Study. *Diabetes.* 2006;55: 1813-1818.
31. Jean-Pierre P, Morrow GR, Roscoe JA, et al. A phase 3 randomized, placebo-controlled, double-blind, clinical trial of the effect of modafinil on cancer-related fatigue among 631 patients receiving chemotherapy: a University of Rochester Cancer Center Community Clinical Oncology Program Research Base study. *Cancer.* 2010;116: 3513-3520.
32. Minton O, Berger A, Barsevick A, et al. Cancer-related fatigue and its impact on functioning. *Cancer.* 2013;119(suppl 11):2124-2130.
33. Neefjes EC, van der Vorst MJ, Blauwhoff-Buskermolen S, Verheul HM. Aiming for a better understanding and management of cancer-related fatigue. *Oncologist.* 2013;18:1135-1143.

Identification of DAB2 and Intelectin-1 as Novel Positive Immunohistochemical Markers of Epithelioid Mesothelioma by Transcriptome Microarray Analysis for its Differentiation From Pulmonary Adenocarcinoma

Masatsugu Kuraoka, MD,*†‡ Vishwa J. Amatya, MBBS, PhD,* Kei Kushitani, MD, PhD,* Amany S. Mawas, MVSc,*§ Yoshihiro Miyata, MD, PhD,|| Morihito Okada, MD, PhD,|| Takumi Kishimoto, MD, PhD,¶ Kouki Inai, MD, PhD,*# Takashi Nishisaka, MD, PhD,† Taijiro Sueda, MD, PhD,‡ and Yukio Takeshima, MD, PhD*

Abstract: As there are currently no absolute immunohistochemical positive markers for the definite diagnosis of malignant epithelioid mesothelioma, the identification of additional “positive” markers that may facilitate this diagnosis becomes of clinical importance. Therefore, the aim of this study was to identify novel positive markers of malignant mesothelioma. Whole genome gene expression analysis was performed using RNA extracted from formalin-fixed paraffin-embedded tissue sections of epithelioid mesothelioma and pulmonary adenocarcinoma. Gene expression analysis revealed that disabled homolog 2 (DAB2) and Intelectin-1 had significantly higher expression in epithelioid mesothelioma compared with that in pulmonary adenocarcinoma. The increased mRNA expression of DAB2 and Intelectin-1 was validated by reverse transcriptase polymerase chain reaction of RNA from tumor tissue and protein expression was validated by Western blotting of 5 mesothelioma cell lines. The utility of DAB2 and Intelectin-1 in the differential diagnosis of epithelioid mesothelioma and pulmonary adenocarcinoma was examined by an immunohistochemical study of 75 cases of epithelioid mesothelioma

From the Departments of *Pathology; †Surgery, Institute of Biomedical and Health Sciences; ‡Department of Surgical Oncology, Research Institute for Radiation Biology and Medicine, Hiroshima University; †Department of Clinical Research and Laboratory, Hiroshima Prefectural Hospital; #Pathologic Diagnostic Center Inc., Hiroshima, Japan; ¶Department of Internal Medicine, Okayama Rosai Hospital, Okayama, Japan; and §Department of Pathology and Clinical Pathology, South Valley University, Qena, Egypt.

Part of this study was performed at the Analysis Center of Life Science, Hiroshima University.

Conflicts of Interest and Source of Funding: T.K., K.I., and Y.T. has received grant from the Japanese Ministry of Health, Labour and Welfare Organization. The authors have disclosed that they have no significant relationships with, or financial interest in, any commercial companies pertaining to this article.

Correspondence: Yukio Takeshima, MD, PhD, Department of Pathology, Hiroshima University Institute of Biomedical and Health Sciences, Hiroshima University, 1-2-3 Kasumi, Minami-ku, Hiroshima 734-8551, Japan (e-mail: ykotake@hiroshima-u.ac.jp).

Supplemental Digital Content is available for this article. Direct URL citations appear in the printed text and are provided in the HTML and PDF versions of this article on the journal's Website, www.ajsp.com. Copyright © 2017 Wolters Kluwer Health, Inc. All rights reserved.

and 67 cases of pulmonary adenocarcinoma. The positive rates of DAB2 and Intelectin-1 expression in epithelioid mesothelioma were 80.0% and 76.0%, respectively, and 3.0% and 0%, respectively, in pulmonary adenocarcinoma. Immunohistochemically, the sensitivity and specificity of DAB2 was 80% and 97% and those of Intelectin-1 were 76% and 100% for differentiation of epithelioid mesothelioma from pulmonary adenocarcinoma. In conclusion, DAB2 and Intelectin-1 are newly identified positive markers of mesothelioma and have potential to be included in future immunohistochemical marker panels for differentiation of epithelioid mesothelioma from pulmonary adenocarcinoma.

Key Words: DAB2, Intelectin-1, gene expression analysis, immunohistochemistry, epithelioid mesothelioma, pulmonary adenocarcinoma

(Am J Surg Pathol 2017;00:000–000)

Malignant mesothelioma is a rare and fatal malignant tumor.¹ In Japan, the mesothelioma death rate is increasing, approaching 1500 deaths in 2015, increased from 500 in 1995 according to Vital Statistics data published by the Ministry of Health, Labour and Welfare, Japan.² Similarly, the death rate due to mesothelioma is increasing globally, including the UK and Ireland,³ the United States and other developing countries.⁴ Asbestos exposure is the main risk factor for malignant pleural mesothelioma, including both occupational and environmental exposure. The time interval between first exposure to asbestos and diagnosis of mesothelioma is speculated to range from 20 to 50 years. Apart from the relatively long time it takes for asbestos to cause disease, delayed onset of symptoms can contribute to late-stage diagnosis and by then, the cancer spreads into the thoracic cavity and is more difficult to treat. Therefore, accurate diagnosis of mesothelioma is essential for its correct management.

A common site of origin of malignant mesothelioma is the pleura followed by other tissues including the peritoneum, pericardium, and tunica vaginalis. Malignant

mesothelioma is classified into 3 major histologic subtypes: epithelioid, sarcomatoid, and biphasic as described in the 2015 World Health Organization (WHO) histologic classification of tumors of lung and pleura, 2015.⁵ Epithelioid mesothelioma, which constitutes more than 60% of all mesothelioma, is the most common histologic subtype, and has a relatively better prognosis than sarcomatoid or biphasic mesothelioma. Epithelioid mesothelioma shows various histologic patterns including tubulopapillary, micropapillary, acinar, adenomatoid, and solid. As epithelioid mesothelioma closely resembles other malignant tumors showing pseudomesotheliomatous growth patterns, such as those of primarily lung carcinoma, breast carcinoma, and cancer that affects the lining of internal organs, the diagnosis of malignant mesothelioma is challenging, both histopathologically and clinically. Currently, the final diagnosis of malignant mesothelioma requires thorough reviewing of clinico-radiologic and pathologic findings (gross examination and histologic findings in tissue samples) with adequate immunohistochemical and/or genetic analyses. As an immunohistochemical marker with absolute sensitivity and specificity is not yet available, the search for additional novel immunohistochemical markers is critical.

The aim of this study was to identify novel positive immunohistochemical markers by analysis of whole gene expression data using microarray gene chips. We performed gene expression analysis on epithelioid cells dissected from formalin-fixed paraffin-embedded (FFPE) tissue of epithelioid mesothelioma and pulmonary adenocarcinoma and identified several novel genes that are differentially expressed between epithelioid mesothelioma and pulmonary adenocarcinoma. Of these, we identified disabled homolog 2 (DAB2) and Intelectin-1 as potential novel positive immunohistochemical markers of epithelioid mesothelioma for differentiation from pulmonary adenocarcinoma.

MATERIALS AND METHODS

Patients and Histologic Samples

The materials included in this study were obtained from the archives of the Department of Pathology, Hiroshima University. The study group consisted of 75 patients with epithelioid mesothelioma who had undergone thoracoscopic pleural biopsy, pleurectomy/decortication, extrapleural pneumonectomy, or autopsy between 2000 and 2016. Between 2005 and 2016, 67 pulmonary adenocarcinoma cases were also obtained by thoracoscopic surgical segmentectomy or lobectomy of lung harboring adenocarcinoma. All microscopic slides were reviewed and reclassified using the current WHO histologic classification of tumors of lung and pleura, 2015⁶ by 4 pathologists (M.K., K.K., V.J.A., and Y.T.). Pathologic diagnosis of each case was confirmed by histologic findings and an immunohistochemical marker panel recommended by Guidelines for Pathologic Diagnosis of Malignant Mesothelioma: 2012 Update of the Consensus Statement from the International Mesothelioma Interest

Group (IMIG)⁷ and current 2015 WHO histologic classification of tumors of the lung, pleura, thymus, and heart.⁶

Anonymized tissue samples were provided by the Department of Pathology for gene expression and immunohistochemical analysis. This study was carried out in accordance with the Ethics Guidelines for Human Genome/Gene Research enacted by the Japanese Government for the collection of tissue specimens and was approved by the institutional ethics review committee (Hiroshima University E-974).

Gene Expression Analysis

Identification of Genes With Marked Difference Between Epithelioid Mesothelioma and Pulmonary Adenocarcinoma

FFPE sections from 6 epithelioid mesothelioma cases and 6 pulmonary adenocarcinoma cases were used for gene expression analysis. RNA extraction for gene expression analysis was performed from papillary or solid growth of tumor cells in each specimen. Five 10 µm thick FFPE tumor tissue sections, each approximately 1 cm in diameter, were processed for total RNA extraction using the Maxwell RSC RNA FFPE Kit (Promega KK, Tokyo, Japan) according to the manufacturer's protocol. Briefly, after deparaffinization and lysis with proteinase K, the samples were treated with DNase I for 15 minutes at room temperature. Following this, RNA purification was carried out according to the manufacturer's protocol using a Maxwell RSC automation instrument (Promega KK). RNA quality check and quantification was performed as described previously⁸ and RNA with an absorbance ratio of ≥ 1.9 between 260 and 280 nm was used for microarray analysis. The Human Transcriptome 2.0 GeneChip Array (Affymetrix, Santa Clara, CA) containing gene transcript sets of 44,699 protein coding and 22,829 nonprotein coding clusters was used to analyze gene expression profiles. Total RNA was amplified and labeled with a 3' IVT Labeling Kit (Affymetrix) before hybridization onto the GeneChip. Briefly, 100 ng total RNA was amplified with GeneChip 3' IVT Pico kit (Affymetrix) to generate 30 µg of SenseRNA according to the manufacturer's protocol. SenseRNA (25 µg) was labeled with a 3' IVT Labeling Kit (Affymetrix) and hybridized to a Human Transcriptome 2.0 GeneChip (Affymetrix) as described previously.⁸ The data were analyzed using the Gene Expression Console Software (Affymetrix), and further statistical analyses were performed using the Subio Software Platform (Subio, Amami-shi, Japan) to plot graphs and for fold change of expression and hierarchical clustering.

Validation of Gene Expression Analysis

Real-time Reverse Transcriptase Polymerase Chain Reaction

The same 6 cases of epithelioid mesothelioma and pulmonary adenocarcinoma that were analyzed for gene expression profiling were used to validate the microarray

expression data by mRNA expression. The relative mRNA expression of DAB2 and Intelectin-1 was assessed with SYBR Green-based real-time reverse transcriptase polymerase chain reaction (RT-PCR) using GAPDH as a control. A total of 100 ng of RNA was used for mRNA expression with a VeryQuest SYBR Green 1-step RT-PCR Master Mix (Affymetrix) using a Stratagene Mx3000P qPCR System (Agilent Technologies, Santa Clara, CA). The primer pairs used for amplification of DAB2 and Intelectin-1 were DAB2-F: GTA GAA ACA AGT GCA ACC AAT GG, DAB2-R: GCC TTT GAA CCT TGC TAA GAG A, ITLN1-F: ACG TGC CCA ATA AGT CCC C, ITLN1-R: CCG TTG TCA GTC CAA CAC TTT C. Primers for GAPDH were GAPDH-F: ACA ACT TTG GTA TCG TGG AAG G, GAPDH-R: GCC ATC ACG CCA CAG TTT C. Data analysis was performed using the $\Delta\Delta$ CT method for relative quantification. Briefly, threshold cycles (CT) for GAPDH (control) and DAB2 and Intelectin-1 (samples) were determined in triplicate. The relative expression (r_1) was calculated using the formula: $r_1 = 2^{-(CT_{\text{sample}} - CT_{\text{normal}})}$.

Western Blotting

Total proteins were extracted from 5 commercially available mesothelioma cell lines (ACC-MESO-1, CRL-5915, ACC-MESO-4, CRL-5946, HMMME) using cell lysis protein extraction reagent (Cell-LyEX1 kit, TOYO B-Net, Tokyo, Japan). Approximately 25 μ g of protein was subjected to electrophoresis on a Novex 10% Bis-Tris gel using a Bolt mini gel tank (Thermo Fisher Scientific, Yokohama, Japan). The proteins were then transferred to a Hybond-P PVDF membrane (GE Healthcare, Buckinghamshire, UK) using a Mini Blot Module (Thermo Fisher Scientific). After treating with blocking buffer, the transfer membrane was incubated with anti-DAB2 antibody (1:2000 rabbit polyclonal, catalog #HPA028888; Sigma-Aldrich, St. Louis, MO), anti-Human Intelectin-1 (1:2000, mouse monoclonal 3G9; Immuno-Biological Laboratories, Gunma, Japan) overnight at 4°C. This was followed by streptavidin-labeled anti-mouse or anti-rabbit secondary antibodies (Cell Signaling Technology, Tokyo, Japan) and Immunostar LD (Wako Pure Chemicals, Tokyo, Japan) as a chemiluminescent detection reagent. Anti-GAPDH antibody (rabbit polyclonal, Santa Cruz Biotechnology, CA) was used as control. The blot membrane was captured by scanning with C-DiGit Blot Scanner (LI-COR) for detection of proteins of interest.

Immunohistochemical Procedures and Evaluation of Expression of DAB2 and Intelectin-1

Immunohistochemistry was performed using 3 μ m tissue sections prepared from the best representative FFPE blocks of epithelioid mesothelioma and pulmonary adenocarcinoma cases. Immunohistochemical staining was performed using the Ventana Benchmark GX automated immunohistochemical station (Roche Diagnostics, Tokyo, Japan). Cell Condition buffer #1 at 95°C for 32 minutes (Roche Diagnostics) was used for antigen retrieval. The sections were then incubated with primary antibodies to

calretinin (rabbit monoclonal, SP65, prediluted; Roche Diagnostics), podoplanin (mouse monoclonal, D2-40, Prediluted; Nichirei Bioscience, Tokyo, Japan), Wilms' tumor gene product (WT1) (mouse monoclonal, 6F-H12, 1:25; Dako, Glostrup, Denmark), DAB2 (rabbit polyclonal, catalog #HPA028888, 1:200; Sigma-Aldrich), and Intelectin-1 (mouse monoclonal, 3G9, 1:1000; Immuno-Biological Laboratories). Incubation with the secondary antibody and detection was performed with Ventana ultraView Universal DAB Detection Kit.

Immunoreactivity was scored as either negative (no immunostaining) or positive. Cells showing nuclear staining for calretinin and WT1, cytoplasmic staining for DAB2 and Intelectin-1, or membranous staining for podoplanin (clone: D2-40) were recorded as "positive." Positive immunoreactivity was further scored as 1+ for up to 10% of tumor cells showing positive immunostaining, 2+ for 10% to 50% positive tumor cells, and 3+ for >50% positive tumor cells. Statistical analyses were performed using the Fisher exact test. Sensitivity, specificity, positive predictive value, negative predictive value, and accuracy rate were calculated using a simple 2 \times 2 table.

RESULTS

Differential Gene Expression and Validation in Epithelioid Mesothelioma and Pulmonary Adenocarcinoma

Of the 44,699 protein coding and 22,829 nonprotein coding transcripts on the Human Transcriptome 2.0 GeneChip Array, 902 statistically significant mRNA transcripts were differentially expressed, with a greater than 1.3-fold difference, between epithelioid mesothelioma and pulmonary adenocarcinoma (Fig. 1). Hierarchical clustering of 426 protein coding mRNA transcripts revealed 197 upregulated mRNA transcripts in epithelioid mesothelioma, including CALB2, WT1, DAB2, and Intelectin-1, and 229 upregulated mRNA transcripts in pulmonary adenocarcinoma, including CEACAM6 and NAPSA (Fig. 2; Supplementary Table S1, Supplemental Digital Content 1, <http://links.lww.com/PAS/A504>).

Real-time RT-PCR showed relative mRNA expression of DAB2 and Intelectin-1 was significantly higher in epithelioid mesothelioma than that in pulmonary adenocarcinoma (data not shown). Western blot analysis showed DAB2 and Intelectin-1 protein expression in all 5 commercially available mesothelioma cells lines with an electrophoretic band of 80 kDa with DAB2 and 1 or 2 electrophoretic bands in the range of 30 to 40 kDa with the Intelectin-1 antibody (Fig. 3).

Immunohistochemical Expression Profiles in Epithelioid Mesothelioma and Pulmonary Adenocarcinoma

The expression of positive mesothelioma markers are summarized in Table 1 and the representative images for DAB2 and Intelectin-1 expression in epithelioid mesothelioma and pulmonary adenocarcinoma are pre-

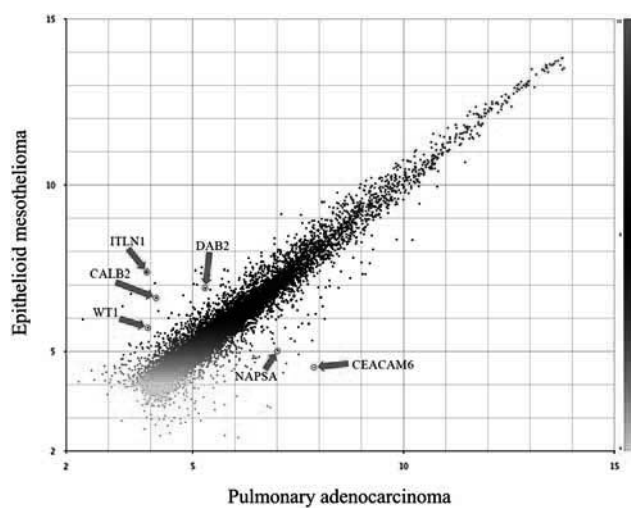


FIGURE 1. Scatter plot diagram showing differential expression of various genes between epithelioid mesothelioma and pulmonary adenocarcinoma. Note, DAB2 and Intelectin-1 locate toward the epithelioid mesothelioma, in addition to previously known mesothelioma positive markers, CALB2 (calretinin) and WT1, while NAPSA (Napsin-A) and CEACAM6 (major gene for CEA), positive pulmonary adenocarcinoma markers, locate towards pulmonary adenocarcinoma.

sented in Figures 4 and 5, respectively. The staining pattern for each marker in 2 tumor types is described in the following sections.

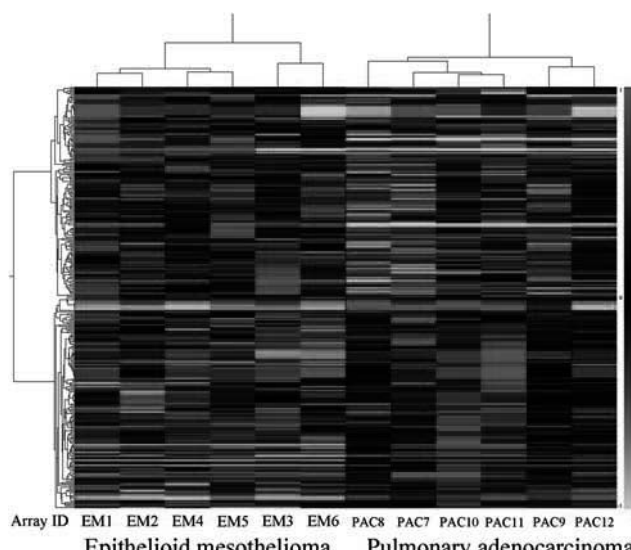


FIGURE 2. Supervised hierarchical clustering of differentially expressed genes between epithelioid mesothelioma and pulmonary adenocarcinoma. The hierarchical clustering of 426 protein coding mRNA transcripts revealed 197 upregulated mRNA transcripts in epithelioid mesothelioma and 229 upregulated mRNA transcripts in pulmonary adenocarcinoma. See detailed data in Supplementary Table S1 (Supplemental Digital Content 1, <http://links.lww.com/PAS/A504>).

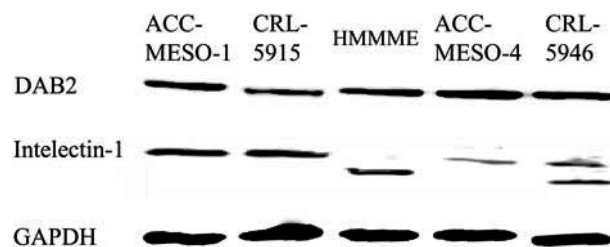


FIGURE 3. Western blot showing DAB2 and Intelectin-1 expression in mesothelioma cell lines. DAB2 expression is present in all 5 mesothelioma cell lines as a single band; however, Intelectin-1 expression is present as either a single or double band.

DAB2 and Intelectin-1 Expression

The expression of DAB2 and Intelectin-1 was localized in the cytoplasm of tumor cells in epithelioid mesothelioma cases. Positive DAB2 expression was observed in 60 of 75 epithelioid mesotheliomas (80.0%) and 2 of 67 pulmonary adenocarcinomas (3.0%). In half of epithelioid mesotheliomas, DAB2 immunoreactivity was generally strong and diffuse (score 3+). In contrast, pulmonary adenocarcinomas showing DAB2 expression was focal (score 1+). In addition, DAB2 expression in alveolar macrophages in pulmonary adenocarcinomas was a helpful internal positive control. Positive Intelectin-1 expression was observed in 57 of 75 epithelioid mesotheliomas (76.0%), with most of them showing score 3+, whereas none of the 67 pulmonary adenocarcinomas were positive for Intelectin-1.

Calretinin, D2-40, and WT1 Expression

Positive calretinin expression was recorded for 74 of 75 epithelioid mesotheliomas (98.7%) and 17 of 67 pulmonary adenocarcinomas (25.4%). In epithelioid mesotheliomas, immunoreactivity was generally strong and diffuse (score 3+). In contrast, staining score in pulmonary adenocarcinomas was 1+ and 2+. There were no score 3+ cases in pulmonary adenocarcinomas. Positive D2-40 expression was observed in 71 of 75 epithelioid mesotheliomas (94.7%), with most of them showing score 3+, whereas only 7 pulmonary adenocarcinomas (10.4%) were focally positive (score 1+ and 2+) for D2-40. Positive WT1 expression was recorded in 62 of 75 epithelioid mesotheliomas (82.7%), whereas none of 67 pulmonary adenocarcinomas (0%) were positive for WT1.

Sensitivity and Specificity of Each Marker for Differential Diagnosis of Epithelioid Mesothelioma and Pulmonary Adenocarcinoma

The sensitivity and specificity of each marker for the differential diagnosis between epithelioid mesothelioma and pulmonary adenocarcinoma are shown in Table 2. Sensitivity of Intelectin-1 (76%) was lowest among 5 positive markers; however, its specificity (100%) was absolute. Sensitivity (80.0%) and specificity (97.0%) of

TABLE 1. Immunohistochemical Findings for Epithelioid Mesothelioma and Pulmonary Adenocarcinoma

Marker	n/N (%)	Epithelioid Mesothelioma				Pulmonary Adenocarcinoma			
		Immunoreactivity Score*				Immunoreactivity Score*			
		0	1+	2+	3+	0	1+	2+	3+
DAB2	60/75 (80.0)	15	12	18	30	2/67 (3.0)	65	2	0
Intelectin-1	57/75 (76.0)	18	17	4	36	0/67 (0)	67	0	0
Calretinin	74/75 (98.7)	1	7	2	65	17/67 (25.4)	50	10	7
Podoplanin (D2-40)	71/75 (94.7)	4	5	6	60	7/67 (10.4)	60	5	2
WT1	62/75 (82.7)	13	18	7	37	0/67 (0)	67	0	0

*0, negative; 1+, <10% positive; 2+, 10% to 50% positive; 3+, 50% < positive.

DAB2 were nearly those of WT1. Specificity of calretinin (74.6%) was lowest among 5 markers.

DISCUSSION

Pathologically, the role of immunohistochemistry in distinguishing pleural epithelioid mesothelioma from pulmonary adenocarcinoma has received much attention especially in the last 20 years. Currently, there are many immunohistochemical markers available for distinguishing epithelioid mesothelioma from pulmonary adenocarcinoma. Among these, calretinin, cytokeratin 5/6, podoplanin (D2-40), and WT1 are the preferred positive markers for epithelioid mesothelioma. Carcinoembryonic antigen (CEA), MOC31 (epithelial-related antigen), Ber-EP4, BG-8, thyroid transcription factor-1, claudin-4, and napsin-A are the preferred positive markers for pulmonary adenocarcinoma. The IMIG 2012 guidelines recommended the consideration of 2 mesothelial and 2 carcinoma markers, based on morphology at initial observation.⁷ In practice, immunohistochemical examination, most laboratories use calretinin, D2-40, and WT1 for diagnosis of epithelioid mesothelioma. However, pathologists must interpret the results of staining by these markers carefully, as specificity of calretinin (74.6% in this study, 90% to 95% in IMIG 2012 guidelines) and D2-40 (88.9% in this study, up to 85% in IMIG 2012 guidelines) is not absolute; additionally, WT1 shows low sensitivity (82.7% in this study, approximately 90% to 100% in IMIG 2012 guidelines). Therefore, novel positive immunohistochemical markers, other than calretinin, D2-40, or WT1, are necessary for increasing the accuracy of epithelioid mesothelioma diagnosis.

Recent development of molecular techniques enabled gene expression analysis from RNA extracted from archival FFPE tumor tissues using GeneChip technology. This method is very useful to find new diagnostic markers, especially in rare tumors, including malignant mesothelioma. We have recently reported the identification of a novel marker, MUC4, for differentiating pleural sarcomatoid mesothelioma from pulmonary sarcomatoid carcinoma by analyzing gene expression data from a gene chip microarray.⁸ In this study, we performed gene expression microarray analysis of 6 cases of mesothelioma and 6 cases of pulmonary adenocarcinoma to identify differentially expressed gene products in epithelioid mesothelioma and

pulmonary adenocarcinoma. We found that the expression of DAB2 and Intelectin-1 in epithelioid mesothelioma was significantly higher than that in pulmonary adenocarcinoma and this was validated by real-time RT-PCR analysis of mRNA extracted from the same tissue source and Western blot analysis of proteins extracted from mesothelioma cell lines. Immunohistochemical analysis showed that expression of DAB2 and Intelectin-1 in epithelioid mesotheliomas was significantly higher than that in pulmonary adenocarcinomas. These novel positive mesothelial markers, DAB2 and/or Intelectin-1, contribute in accurate mesothelioma diagnosis, in addition to known positive markers (calretinin, D2-40, and WT1). In the present study, we analyzed gene expression analysis of only 6 cases of epithelioid mesothelioma and 6 cases of pulmonary adenocarcinoma, and found many differentially expressed genes mentioned in Supplementary Table S1 (Supplemental Digital Content 1, <http://links.lww.com/PAS/A504>). As the analysis of substantially larger number will make these findings more credible, we plan to include more cases in the future.

DAB2, a mitogen-responsive phosphoprotein, is expressed in normal ovarian epithelial cells, but is downregulated or absent from ovarian carcinoma cell lines, suggesting its role as a tumor suppressor.⁹ Decreased DAB2 expression has been reported in various human cancers, including esophageal,¹⁰ lung,¹¹ ovarian,⁹ prostate,¹² and breast¹³ cancers. DAB2 downregulation in these cancers were reported partly due to miRNA targeting DAB2^{10,14} or promoter hypermethylation.^{13,15} However, the biological significance or expression of DAB2 has not yet been reported in malignant mesothelioma. In the present study, we found increased expression of DAB2 in epithelioid mesothelioma compared with that in pulmonary adenocarcinoma by gene expression microarray analysis. We also confirmed this increased expression of DAB2 in epithelioid mesothelioma by real-time RT-PCR and western blot. From the differential analysis of DAB2 expression between epithelioid mesothelioma and pulmonary adenocarcinoma by immunohistochemical study, we found higher sensitivity and specificity in epithelioid mesothelioma of >80%. In 2 of the 67 cases of pulmonary adenocarcinoma, DAB2 expression was identified in tumor cells but with a low immunoreactivity score. DAB2 expression in pulmonary adenocarcinomas was present in inflammatory cell infiltration, mainly macrophages; therefore, precaution must be taken by the physician

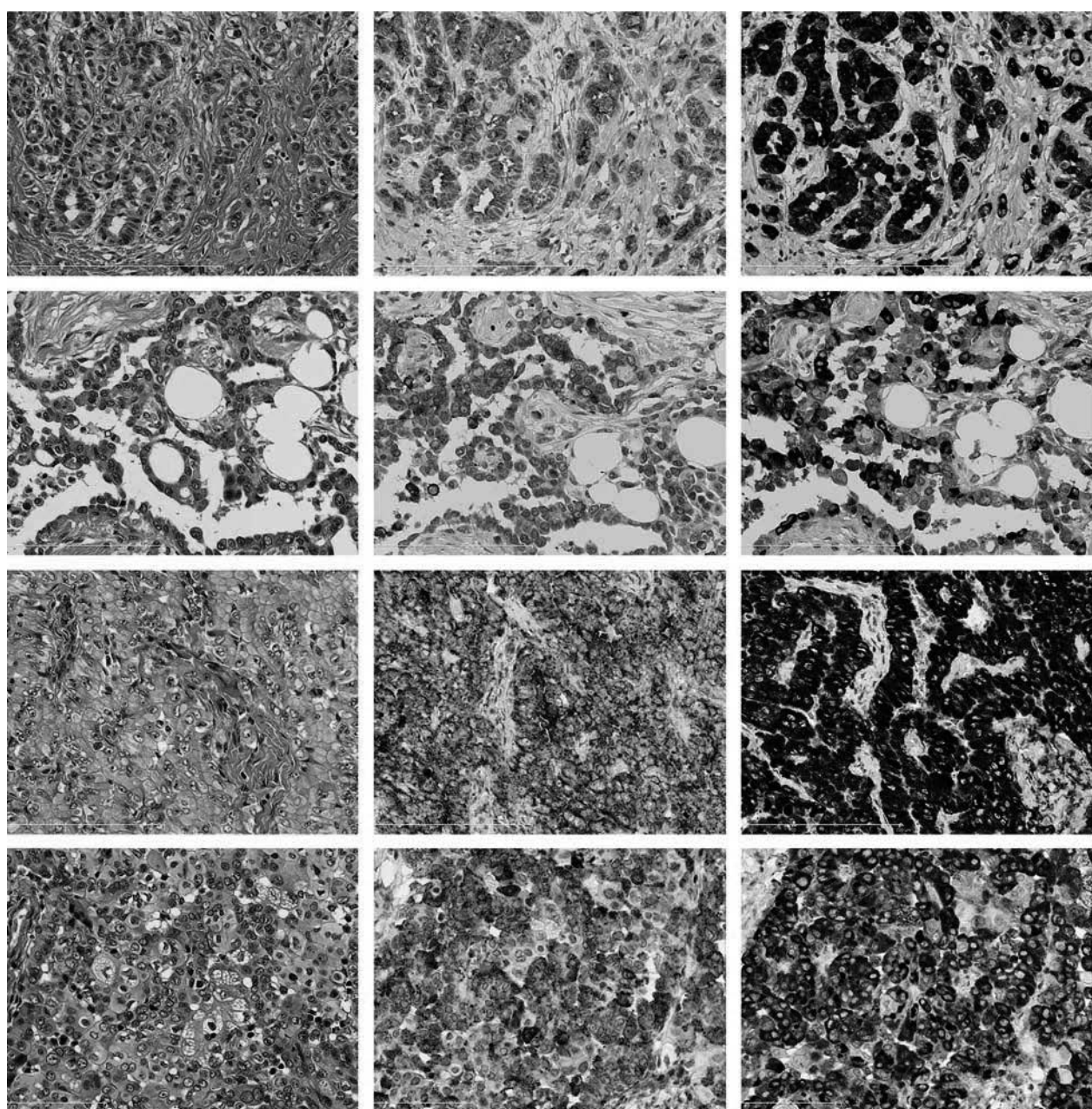


FIGURE 4. DAB2 and Intelectin-1 expression in epithelioid mesothelioma. Various histomorphologic patterns of epithelioid mesothelioma showing prominent expression of DAB2 (middle column) and Intelectin-1 (right column). Each row shows epithelioid mesothelioma with corresponding DAB2 and Intelectin-1 immunohistochemistry.

when interpreting pulmonary adenocarcinoma results for DAB2 expression.

Human Intelectin-1, also known as omentin, is a galactose-binding lectin that is usually expressed in the heart and small intestine as a host defense lectin that binds to bacterial galactofuranose.¹⁶ Intelectin-1 is mainly expressed in the intestinal goblet cells and omentum, and occasionally in the thymus, bronchus, heart, liver, kidney collecting tubule cells, bladder umbrella, and mesothelial cells.¹⁷ Recently, the overexpression of Intelectin-1 in human malignant pleural mesothelioma and its secretion

into pleural effusions indicated toward it being a potential biomarker.^{17,18} It was reported that Intelectin-1 was not expressed in various cancers, except in some mucus-producing adenocarcinomas.¹⁹ In the present study, we observed high expression of Intelectin-1 mRNA in epithelioid mesothelioma, definite expression of Intelectin-1 in mesothelioma cell lines by western blot analysis, and in 57 of 75 mesothelioma tissue samples by immunohistochemical analysis. In addition, we also found Intelectin-1 expression in non-neoplastic mesothelial lining cells and goblet cells in bronchi and bronchioles

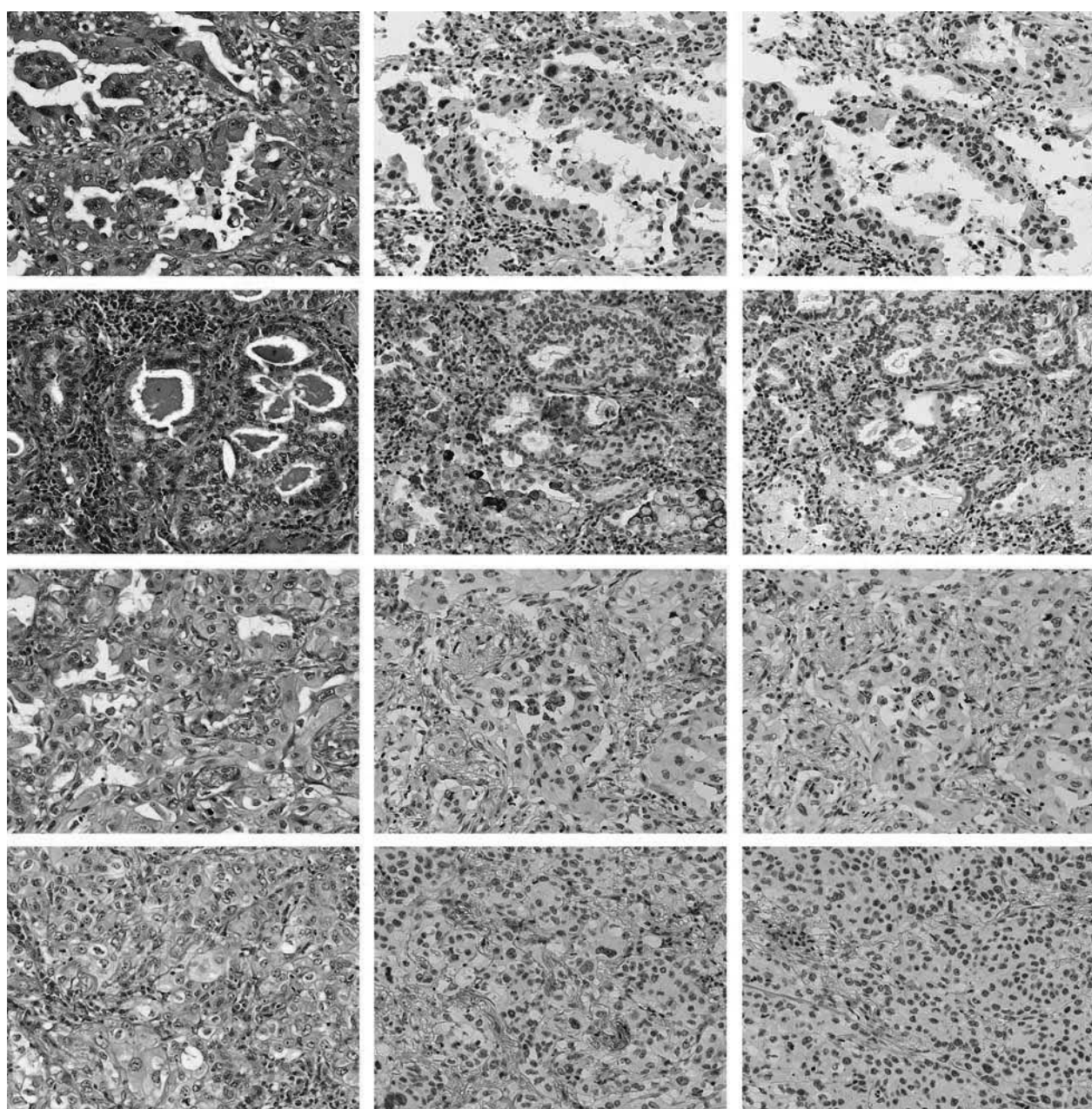


FIGURE 5. DAB2 and Intelectin-1 expression in pulmonary adenocarcinoma. Various histomorphologic patterns of pulmonary adenocarcinoma showing no expression of DAB2 (middle column) and Intelectin-1 (right column). Each row shows pulmonary adenocarcinoma with corresponding DAB2 and Intelectin-1 immunohistochemistry. There is focal reactivity of DAB2 in alveolar macrophages and lymphocytes, which need to be interpreted with care.

TABLE 2. Sensitivity and Specificity of Immunohistochemical Positive Markers for Differential Diagnosis of Epithelioid Mesothelioma from Pulmonary Adenocarcinoma

Immunohistochemical Markers	Sensitivity (%)	Specificity
INT-1 +	76.0	100
DAB2 +	80.0	97.0
Calretinin +	98.7	74.6
D2-40 +	94.7	89.6
WT-1 +	82.7	100

(data not shown). No Intelectin-1 expression was recorded in any pulmonary adenocarcinoma cases, confirming its potential as a novel positive mesothelial marker. The functional roles of DAB2 and Intelectin-1 expression in epithelioid mesothelioma need further analysis, which is beyond the scope of this study.

In conclusion, we identified 2 novel positive markers of epithelioid mesothelioma, DAB2 and Intelectin-1, by using gene expression microarray analysis and confirmed their utility to differentiate epithelioid mesothelioma from

pulmonary adenocarcinoma by immunohistochemical study. Further validation of immunohistochemical staining of these markers by other institutes is warranted.

ACKNOWLEDGMENTS

The authors thank Ms Yukari Go of the Technical Center in Hiroshima University for excellent technical assistance and Ms Naomi Fukuhara for editorial assistance.

REFERENCES

1. Robinson BW, Lake RA. Advances in malignant mesothelioma. *N Engl J Med.* 2005;353:1591–1603.
2. Mortality rate due to mesothelioma in Japan: Ministry of Health, Labor & Welfare. Available at: www.mhlw.go.jp/toukei/saikin/hw/jinkou/tokusyu/chuuhisyu15/dl/chuuhisyu.pdf. Accessed January 6, 2017.
3. Mesothelioma statistics: cancer research, UK. 2015. Available at: www.cancerresearchuk.org/health-professional/cancer-statistics/statistics-by-cancer-type/mesothelioma. Accessed January 6, 2017.
4. Delgermaa V, Takahashi K, Park EK, et al. Global mesothelioma deaths reported to the World Health Organization between 1994 and 2008. *Bull World Health Organ.* 2011;89:716–724, 724A–724C.
5. Travis WD, Noguchi M, Yatabe Y, et al. Epithelioid mesothelioma. In: Travis WD, Brambilla E, Burke AP, et al, eds. *WHO Classification of Tumours of the Lung, Pleura, Thymus and Heart.* Lyon: IARC; 2015:156–164.
6. Travis WD, Noguchi M, Yatabe Y, et al. Adenocarcinoma. In: Travis WD, Brambilla E, Burke AP, et al, eds. *WHO Classification of Tumours of the Lung, Pleura, Thymus and Heart.* Lyon: IARC; 2015:26–37.
7. Husain AN, Colby T, Ordonez N, et al. Guidelines for pathologic diagnosis of malignant mesothelioma: 2012 update of the consensus statement from the International Mesothelioma Interest Group. *Arch Pathol Lab Med.* 2013;137:647–667.
8. Amatya VJ, Kushitani K, Mawas AS, et al. MUC4, a novel immunohistochemical marker identified by gene expression profiling, differentiates pleural sarcomatoid mesothelioma from lung sarcomatoid carcinoma. *Mod Pathol.* 2017. Doi:10.1038/modpathol.2016.181.
9. Mok SC, Chan WY, Wong KK, et al. DOC-2, a candidate tumor suppressor gene in human epithelial ovarian cancer. *Oncogene.* 1998;16:2381–2387.
10. Li C, Ding C, Chen T, et al. Micro ribonucleic acid-93 promotes proliferation and migration of esophageal squamous cell carcinoma by targeting disabled 2. *Thorac Cancer.* 2015;6:524–533.
11. Du L, Zhao Z, Ma X, et al. miR-93-directed downregulation of DAB2 defines a novel oncogenic pathway in lung cancer. *Oncogene.* 2014;33:4307–4315.
12. Zhou J, Hernandez G, Tu SW, et al. The role of DOC-2/DAB2 in modulating androgen receptor-mediated cell growth via the non-genomic c-Src-mediated pathway in normal prostatic epithelium and cancer. *Cancer Res.* 2005;65:9906–9913.
13. Bagadi SA, Prasad CP, Srivastava A, et al. Frequent loss of DAB2 protein and infrequent promoter hypermethylation in breast cancer. *Breast Cancer Res Treat.* 2007;104:277–286.
14. Chao A, Lin CY, Lee YS, et al. Regulation of ovarian cancer progression by microRNA-187 through targeting disabled homolog-2. *Oncogene.* 2012;31:764–775.
15. Li C, Chen J, Chen T, et al. Aberrant hypermethylation at sites 86 to 226 of DAB2 gene in non-small cell lung cancer. *Am J Med Sci.* 2015;349:425–431.
16. Tsuji S, Uehori J, Matsumoto M, et al. Human intelectin is a novel soluble lectin that recognizes galactofuranose in carbohydrate chains of bacterial cell wall. *J Biol Chem.* 2001;276:23456–23463.
17. Washimi K, Yokose T, Yamashita M, et al. Specific expression of human intelectin-1 in malignant pleural mesothelioma and gastrointestinal goblet cells. *PLoS One.* 2012;7:e39889.
18. Tsuji S, Tsuura Y, Morohoshi T, et al. Secretion of intelectin-1 from malignant pleural mesothelioma into pleural effusion. *Br J Cancer.* 2010;103:517–523.
19. Zheng L, Weng M, Qi M, et al. Aberrant expression of intelectin-1 in gastric cancer: its relationship with clinicopathological features and prognosis. *J Cancer Res Clin Oncol.* 2012;138:163–172.

石綿ばく露によるびまん性胸膜肥厚と中皮腫・肺癌発生に関する検討

岸本 卓巳, 藤本 伸一

岡山労災病院アスベスト研究センター

(平成29年2月24日受付)

要旨:【目的】職業性石綿ばく露によって発症したびまん性胸膜肥厚に合併する肺癌および中皮腫の頻度と症例の詳細について検討した。

【対象と方法】労災補償あるいは石綿健康被害救済法のびまん性胸膜肥厚の胸部画像の認定基準を満たした224例について、平成22年4月から平成28年2月までに肺癌および中皮腫を発症した症例の頻度と症例の詳細について検討した。対照群として、同時期に低線量CT検査を行った石綿健康管理手帳健診対象者2,130例を選択した。

【結果】びまん性胸膜肥厚224例中、中皮腫を発症した症例はなかったが、肺癌発症例は8例(3.6%)あった。観察期間から人口10万人あたり610.3人/年と高率であった。一方、対照群では56例(2.6%)で、人口10万人あたり443.9人/年であった。

肺癌発症症例はすべて男性で、年齢の中央値は72歳と高齢者が多かった。組織型は小細胞癌4例、腺癌3例、扁平上皮癌1例で、すべてが喫煙者であった。職業性石綿ばく露は中等度以上のばく露者が多く、ばく露期間の中央値33.5年、潜伏期間は54年と長かった。そのうち、著しい呼吸機能障害のある症例は5例で、石綿肺を伴うものが3例、伴わないものが2例であった。

【考察】石綿ばく露によって発症するびまん性胸膜肥厚症例は一定以上の石綿ばく露量を必要とすると言われているが、今回肺癌を発症した症例についても同様で、なおかつ重喫煙者が多かった。肺癌発生頻度は石綿健康管理手帳を有する人々より高く55~74歳で30パック・年以上の喫煙男性を対象としたNational Lung Screening Trial(以下、NLST)の10万対645人年と同等であった。また特に発症頻度が高いと報告されている中皮腫の発症は過去6年間1症例もなかったが、その理由は明らかではなかった。

【結論】6年間の観察期間中、著しい呼吸機能障害を有するびまん性胸膜肥厚に発症した肺癌は労災補償対象とされているがわずか2例(0.89%)であり、喫煙との関連が大きかった。また、中皮腫合併は1例もなかった。

(日職災医誌, 65:153-159, 2017)

キーワード

石綿ばく露, びまん性胸膜肥厚, 肺癌

はじめに

石綿ばく露によるびまん性胸膜肥厚とは限局性胸膜肥厚である胸膜plaquerに対して、広範囲で肺の一葉以上を巻き込むような胸膜の線維化(臓側胸膜の病変で、通常は壁側胸膜との癒着を来たしている)である。胸膜plaquerとの画像上の相違にはcrow's feetと円形無気肺所見が重要である¹。日本では平成15年から著しい呼吸機能障害を伴う症例は労災補償対象疾病となり、平成22年からは石綿健康被害救済法(以下、救済法とする)の対象ともなった。びまん性胸膜肥厚は臓側と壁側胸膜あ

るいは胸膜と横隔膜の癒着から主に拘束性呼吸機能障害を来すとともに拡散能低下が生じると報告されている^{2,3}。しかし、その成因とともに、本疾患に関わる累積石綿ばく露量や、中皮腫や肺癌の合併頻度等不明な点も少なくない。今回、職業性石綿ばく露によるびまん性胸膜肥厚症例のうち中皮腫あるいは肺癌を合併した症例について検討したので報告する。

目的

職業性石綿ばく露によって発症したびまん性胸膜肥厚に合併する肺癌および中皮腫の頻度と症例の詳細につい

表1 びまん性胸膜肥厚 224 例中、原発性肺癌を合併した症例

症例	年齢	性別	著しい呼吸機能障害	肺癌組織型	喫煙歴	喫煙指数	職業病	ばく露年数(年)	潜伏期間(年)	両側性 片側性	石綿肺の有無	胸膜ブラーク		肺内石綿小体数本/g
												限局性	広範囲	
1	64	男性	あり	小細胞癌	30本×15年	450	造船・保温	31	33	両側性	PR2/2		+	198,654
2	74	男性	あり	腺癌	20本×35年	700	造船・配管	45	59	両側性	PR1/1		+	ND
3	71	男性	なし	腺癌	30本×55年	1,650	石綿運搬	3	51	右側 片側性	なし		+	ND
4	73	男性	あり	扁平上皮癌	40本×50年	2,000	塗装	35	53	両側性	PR1/1	+		ND
5	68	男性	なし	腺癌	30本×20年	600	ボード成型	45	53	両側性	なし	+	+	10,601
6	68	男性	なし	小細胞癌	40本×38年	1,320	水道配管	32	43	両側性	なし	+		ND
7	73	男性	あり	小細胞癌	20本×48年	960	建設業	54	67	両側性	なし	+		ND
8	81	男性	あり	小細胞癌	20本×50年	1,000	内装作業	29	55	両側性	なし	+		5,300

て検討する。

対象と方法

平成 22 年 4 月 1 日から平成 28 年 2 月 1 日までに全国労災病院や研究協力者の病院及び石綿健康被害救済法により認定された職業性石綿ばく露によって発症したびまん性胸膜肥厚症例 224 例を対象とした。対象症例要件として労災補償あるいは石綿健康被害救済法の認定基準である胸部レントゲン写真上の胸膜肥厚の範囲が片側であれば片側胸郭の 2 分の 1 以上、両側の場合には両側胸郭の 4 分の 1 以上であって、石綿ばく露作業従事期間が 3 年以上ある症例とした。このうち、著しい呼吸機能障害を伴う症例は 176 例、そうでない症例が 48 例であった。すなわち、176 例は労災補償あるいは救済法の対象となった症例である。これら症例のうち平成 28 年 2 月 1 日までに病理組織学的に中皮腫と診断された症例あるいは肺癌と確定診断された症例について検討した。

検討項目は年齢、性別、著しい呼吸機能障害の有無、肺癌の組織型、喫煙歴、職業歴・年数・肺癌発生までの潜伏期間、胸部画像所見としてのびまん性胸膜肥厚の範囲、石綿肺、胸膜ブラークの有無及び肺内石綿小体数である。なお、肺癌の病期、組織型は肺癌取扱い規約（第 7 版）に則った。

対照は平成 22 年 4 月 1 日から平成 28 年 2 月 1 日までに岡山労災病院・富山労災病院・千葉労災病院・香川労災病院・北海道中央労災病院・玉野三井病院・近畿中央胸部疾患センター・山口宇部医療センターの 8 施設における石綿健康管理手帳健診受診者 2,080 例および、石綿ばく露歴を有する現役労働者のうち低線量 CT 撮影に文書で同意した 50 例の計 2,130 例とした。

結果

対象 224 例のうち性別では男性 218 例 (97.3%)、女性 6 例 (2.7%) であった。診断時年齢は 44 歳から 91 歳（中央値 72 歳）で、中皮腫を発症した症例は皆無であった。また、肺癌を発症した症例は 8 例 (3.6%) であった。観察期間を考慮した肺癌発生率は人口 10 万人当たり 610.3

人/年であった。一方、対照とした低線量 CT を撮影した 2,130 例のうち性別は男性 2,048 例 (96.2%)、女性 82 例 (3.8%) であった。診断時年齢は 48 歳から 96 歳（中央値 72 歳）で、胸膜ブラークを認めた症例は 1,904 例 (89.4%) であった。また、平成 28 年 2 月までの肺癌発生率は 56 例 (2.6%) であった。観察期間を考慮した肺癌発生率は人口 10 万人当たり 433.9 人/年であった⁴⁾。一方、中皮腫は 7 例 (0.3%) であった。

びまん性胸膜肥厚に肺癌を発症した 8 例の詳細は表 1 に示す。

年齢は 64 歳から 81 歳（中央値 72 歳）で全例男性であった。著しい呼吸機能障害があった症例は 5 例であった。肺癌組織型では小細胞癌 4 例、腺癌 3 例、扁平上皮癌 1 例であった。8 例はすべて喫煙者で、喫煙指数は 450 から 2,000 で、中央値は 980 と重喫煙者が大半であった。職業性石綿ばく露歴では造船、配管、石綿運搬など中等度以上のばく露量を受ける作業歴があり、職業性ばく露期間も 3~54 年間（中央値 33.5 年）であった。初回ばく露から肺癌発生までの潜伏期間は 33~67 年（中央値 54 年）と長かった。画像上、びまん性胸膜肥厚は 1 例を除いて両側性で、石綿肺の合併が 3 例あった。また、全例に胸膜ブラークを認め、そのうち 3 例では胸部レントゲン写真上で胸膜ブラークを認めるか胸郭の 4 分の 1 以上の広範囲ブラークを認めた。また、肺内石綿小体を測定できた 3 例中全例で肺癌発生頻度を 2 倍以上にする肺乾燥重量 1gあたり 5,000 本以上⁵⁾が検出された。

上述のごとく肺癌を発生した 8 例中 5 例では著しい呼吸機能障害があり、労災あるいは救済法の対象となる症例である。そのうち症例 1, 2, 4 は石綿肺合併症例であり、昭和 53 年の石綿肺癌認定基準の 1 型以上の石綿肺に合併した肺癌として認定を受けるべき症例である。

また、症例 3, 5, 6 は著しい呼吸機能障害がないため、びまん性胸膜肥厚として労災あるいは救済法で認定されない症例である。しかし、他の認定要件である胸膜ブラークあるいは広範囲胸膜ブラークと職業性石綿ばく露歴があるため石綿肺癌として認定される症例であるため、石綿肺癌認定基準としてのびまん性胸膜肥厚の基準は必要

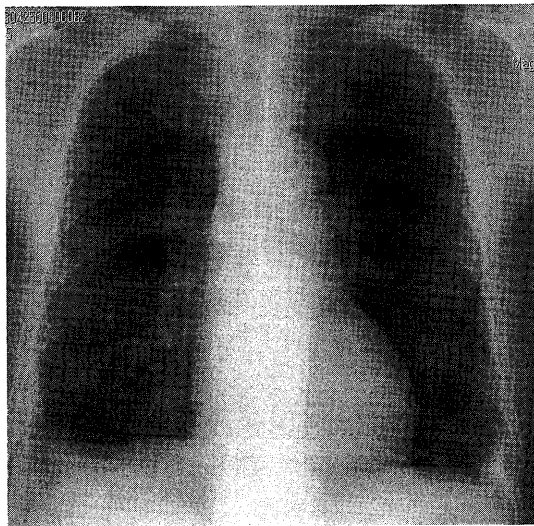


図1 平成X-4年 胸部レントゲン写真正面像で両側びまん性胸膜肥厚を来たした症例である。

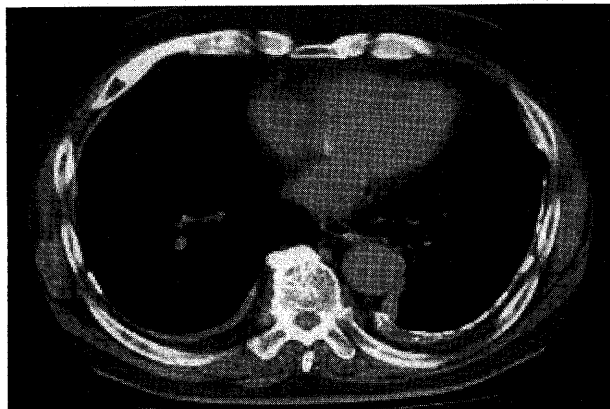


図2 平成X-4年 胸部CT 縦隔条件では両側びまん性胸膜肥厚は一部に石灰化胸膜plaquesを伴う。

としない。

労災認定基準である著しい呼吸機能障害を伴うびまん性胸膜肥厚症例で石綿肺を伴わない症例は症例7, 8の2例のみとなる。そこで、この2例について症例を呈示する。

症例7は73歳、男性で、主訴は体重減少である。職歴では大工として約54年間の職業性石綿ばく露歴がある。喫煙歴としては20本/日、48年間と重喫煙者である。

現病歴では近医で高血圧と糖尿病を加療中であった。平成X-4年7月にびまん性胸膜肥厚のため労災認定をうけている。診断時の呼吸機能検査は、VC: 2.15L, %VC: 63.9%, FEV_{1.0}: 0.97L, 1秒率%: 45.1%, %1秒量: 36.8%であり、著しい混合性呼吸機能障害を伴っていた。動脈血ガス分析においては、PH: 7.34, PaO₂: 79.4mmHg, PaCO₂: 43.3mmHgとほぼ正常であった。

診断時の平成X-4年4月の胸部レントゲン写真(図1)は、両側の肋横角の消失と両側の胸膜肥厚を認め、両側胸壁の4分の1以上のびまん性胸膜肥厚の基準を満

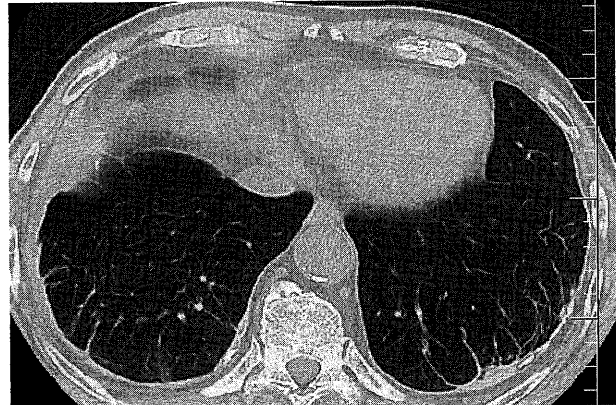


図3 平成X-4年 胸部CT 肺野条件で両側胸壁に crow's feet signを認める。

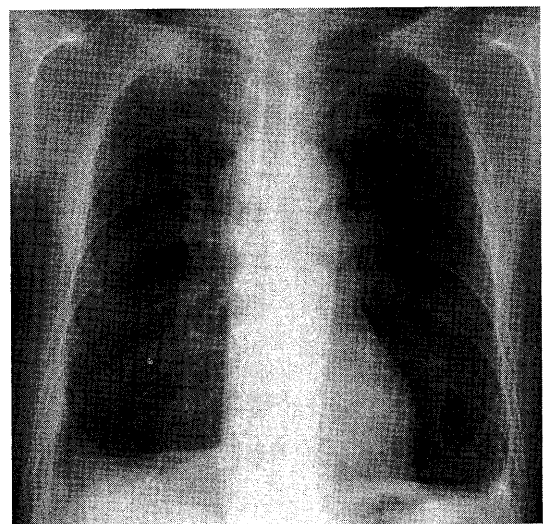


図4 肺癌発生時の胸部レントゲン写真正面像では右肺尖部に腫瘍陰影を認める。

たしていた。また、図2, 3の如く胸部CTにて胸膜plaquesではなく、びまん性胸膜肥厚であることを確認した。平成X年9月に血清CEAの上昇と体重減少のため前医で精査を施行したところ、胸部レントゲン写真にて腫瘍陰影を認め、精査加療目的で平成X年10月に当院に紹介となった。胸部レントゲン写真(図4)では、右肺尖部に腫瘍陰影を認めた。胸部CT(図5)では、右肺S1に38mm大の腫瘍とリンパ節#4R, #7, #10Rに腫大を認めた。経気管支肺生検と超音波気管支鏡ガイド下針生検を施行し、小細胞肺癌と診断した。全身精査の結果、T2aN2M0 cStage IIIAと診断した。年齢と肺機能を考慮し化学療法単独での治療方針となった。平成X年10月から化学療法を行い奏効しているため生存中である。

症例8は81歳の男性で、主訴は労作時呼吸困難である。喫煙歴は20本/日、50年間の過去喫煙者である。職歴では、内装作業を26歳から29年間行っており、職業性石綿ばく露歴を有する。

平成X年6月の初診時の胸部レントゲン上(図6)両

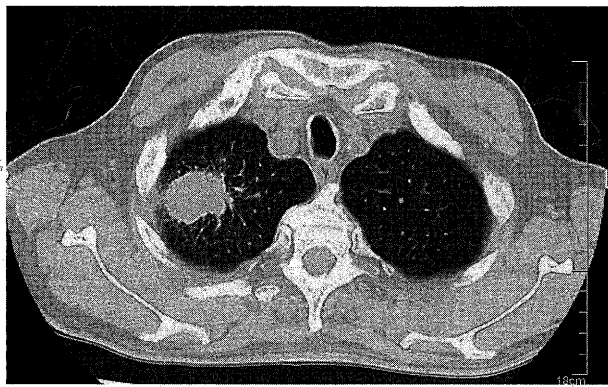


図5 胸部CTでは右肺S1に53×38mm大の辺縁不明瞭な腫瘍陰影を認める。

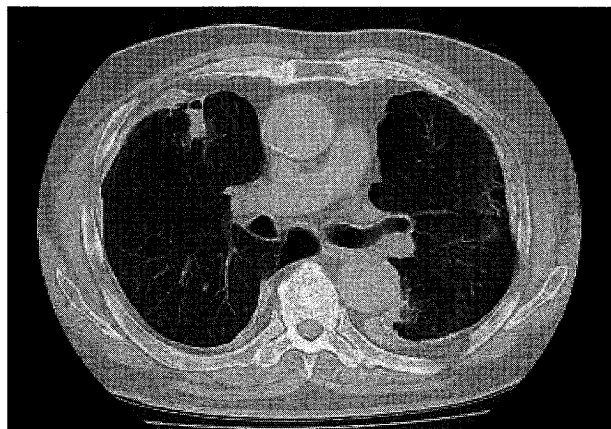


図7 初診時の胸部CT写真 右円形無気肺と左crow's feet signを認める。



図6 胸部レントゲン写真正面像では両側石灰化胸膜プラークと両側に胸郭の2分の1以上のびまん性胸膜肥厚を認める。

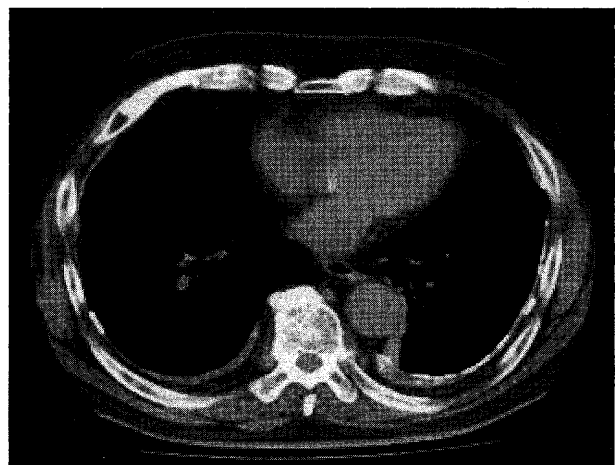


図8 両側に石灰化胸膜プラークを認め、左側石灰化プラークは胸壁内側の2分の1以上を占める。

側びまん性胸膜肥厚があり、肋横角は鈍であり、両側石灰化胸膜プラークを認めた。同日の胸部CT肺野条件では右肺S4に円形無気肺を認めるとともに肺の気腫性変化を伴っていた(図7)。肺野に石綿肺を示唆する線維性変化を認めなかった。一方、胸部CT縦隔条件(図8)では左側胸膜に石灰化を伴う広範囲プラークを認めた。

呼吸機能1次検査では、VC:2.29L, FEV_{1.0}:1.59L, %VC:70.6%, 1秒率:70.98%, %1秒量:65.1%であったが、動脈血ガス分析にてpH:7.367, PaO₂:58.2mmHg, PaCO₂:44.3mmHg, A-aDO₂:37.8mmHgと低酸素血症を認めた。PaO₂が60mmHg以下であったため、著しい呼吸機能障害があると認められ、労災認定を受けた。

当初は労作時呼吸困難のみで安静時には呼吸困難がなかったが、その後徐々に呼吸不全が進行し、PaO₂が50mmHg未満となったため在宅酸素療法が導入された。

平成X+3年11月に両側に急性肺炎を合併した。抗生素による治療を開始したが、完全には回復せず、人工呼吸器による呼吸管理が必要となった。平成X+3年12

月に胸部CTを撮影したところ図9に認められるように左肺S3に径2cm大の腫瘍陰影を認め、左肺門部リンパ節腫大を来たしていることが明らかとなった。リンパ節腫大は対側肺門部にも認めたため画像上、T1N3M0の原発性肺癌と診断した。その後、慢性呼吸不全急性増悪により平成X+4年2月に死亡した。剖検にて組織学的に混合型小細胞癌(扁平上皮癌成分を含む)であると診断された。また、肺内石綿小体数を算定したところ5,300本/g肺乾燥重量であった。

考 察

石綿肺のないびまん性胸膜肥厚有所見は石綿肺ほどではないが、中皮腫のリスクが高い。たとえばKarjarainenら⁶は石綿肺1,287例、良性石綿胸膜疾患4,708例を追跡した結果、肺癌リスクは1.3倍(95%CI:1.0~1.8)で、中皮腫リスクは5.5倍(95%CI:1.5~14.1)であったと報告している。また、石綿セメント労働者を対象とした検討では、石綿肺ほど頻度は高くないが、びまん性胸膜肥厚

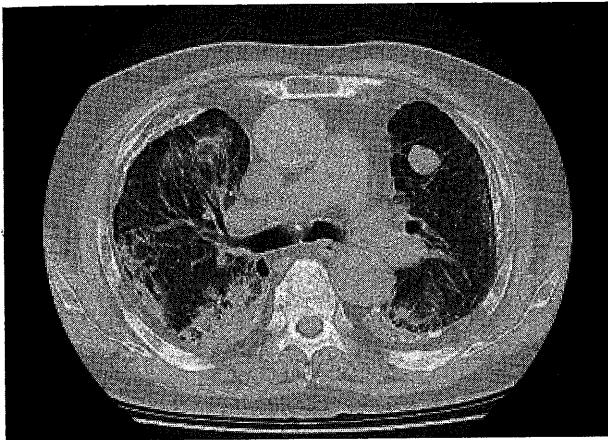


図 9a 左肺 S3 領域に辺縁が明瞭な腫瘍陰影を認める。

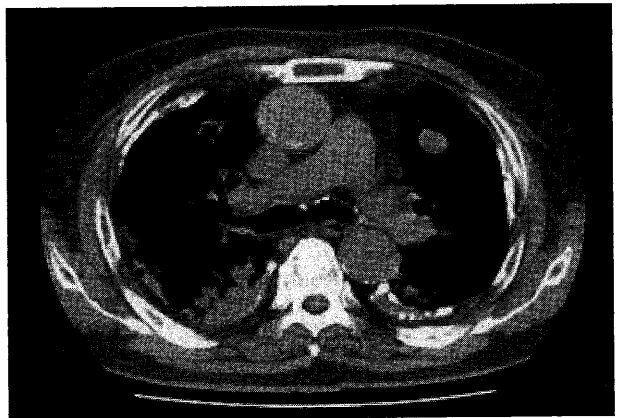


図 9b 左肺 S3 に腫瘍陰影を認める。

の発症頻度は石綿ばく露量が多いほど高いと報告されている⁷。今回、我々は胸部画像上の基準を満たす職業性石綿ばく露のあるびまん性胸膜肥厚 224 例を約 6 年経過観察した。この間、肺癌の発症は 8 例(3.6%)であったが、中皮腫発生例は 1 例もなかった。肺癌発生率は 610.3 人/年であった。これは 55~74 歳で 30 パック・年以上の喫煙者を対象とした NLST の⁸10 万対 645 人/年と同等の肺癌発生率であった。

また、発生頻度が有意に高いと報告されている中皮腫の発生はなく明らかに低発症率であった。その理由としてびまん性胸膜肥厚の本態は臓側胸膜の広範囲な線維化で壁側胸膜との癒着が高頻度で起こっているため、壁側胸膜に発症する胸膜中皮腫の発生母地が癒着により縮小していたために偶然合併がなかった可能性も想定されたが、約 6 年間の経過観察だけでは不十分である。

肺癌発生については 224 例中 8 例の 3.6% であったが、石綿肺合併がなく、著しい呼吸機能障害のない症例を除くと労災認定の対象となった症例は 2 例(0.89%)で 1% にも満たなかった。

症例 7 は喫煙指数が 960 であり、呼吸機能検査上も混合性呼吸機能障害を呈し、%1 秒量が 36.8% と著しい低下をきたしており、呼吸機能障害及び肺癌発症と喫煙が大きく関わっていると考えられる。職業歴では 54 年間の職業性石綿ばく露があり、石灰化胸膜プラークが明らかであるため労災での石綿肺癌の認定は容易である。一方、職業性石綿ばく露歴が明らかにならなかった場合でも左下部胸膜には片側の 4 分の 1 を超える石灰化胸膜プラークを認めることにより石綿健康被害救済法においても認定されるべき事案である。

症例 8 は職業性石綿ばく露によりびまん性胸膜肥厚を発症し著しい呼吸機能障害を来たし、約 4 年間の経過で慢性呼吸不全に肺炎を合併し死亡した。剖検によって診断を確定した原発性肺癌である。労災認定上の著しい呼吸機能障害を合併したびまん性胸膜肥厚に合併した原発性肺癌として労災認定の対象ではあった。本症例は石綿

健康被害救済法においても広範囲胸膜プラークあるいは肺内石綿に小体数が 5,000 本/g 以上あったことにより、石綿肺癌として認定されるべき症例である。その他の 6 例についても石綿肺合併の 3 例は問題なく補償・救済の対象症例であるとともに、著しい呼吸機能障害のなかった症例においても日本の認定基準は労災補償・救済の対象となっているから社会的な問題はない。

びまん性胸膜肥厚発症に対する石綿ばく露量に関しては、Helsinki クライテリア 2014⁹において、両側性びまん性胸膜肥厚は中等度また高度の石綿ばく露と関連していることが多い、肺癌起因性に関して考慮されるべきであると述べられている。今回報告した 8 例においても職業歴とその期間から考慮した場合、石綿中等度以上ばく露があったであろうと推察している。

症例 7, 8 は労災補償における著しい呼吸機能障害と 3 年以上の職業性石綿ばく露があり、画像上の認定基準を満たす肺癌症例である。しかし、その他の認定基準を満たすためこの基準を満たさなくても問題にはならない。石綿健康被害救済法においてもこの 2 例で認められたように広範囲胸膜プラークに合併した肺癌が認定されるようになったため、本症例のような事案についても不利益はなくなった。

一方、石綿ばく露者を対象とした際に肺癌を合併する症例については喫煙との関連が大きいことは様々な疫学研究からも明白である。今回の 8 例全例が喫煙者でその大半は重喫煙者であり、そのうち 5 例は喫煙と関連の深い小細胞癌及び扁平上皮癌であった。Hammond らの疫学調査¹⁰では石綿ばく露と喫煙は相乗効果を示し、非石綿ばく露の非喫煙者を対照とすると肺癌発生率が 53.2 倍になると報告している。また、日本の認定基準によつて石綿肺癌と認定された 252 症例において、その 91.6% が現在あるいは過去喫煙者であったとの我々の報告¹¹からも明らかである。以上のような結果から石綿健康管理手帳を取得しているような過去の石綿ばく露者に対する禁煙活動は肺癌発生を抑制する意味でも重要であると思

われる。

利益相反：利益相反基準に該当無し

文 献

- 1) Gevenois PA, de Maertelaer V, Madani A, et al: Asbestosis, pleural plaques and diffuse pleural thickening: three distinct benign responses to asbestos exposure. *Eur Respir J* 11: 1021—1027, 1998.
- 2) Kee ST, Gamsu G, Blance P: Causes of pulmonary impairment in asbestos-exposed individuals with diffuse pleural thickening. *Am J Respir Crit Care Med* 154: 789—793, 1996.
- 3) Yates DH, Browne K, Stidolph PN, et al: Asbestos-related bilateral diffuse pleural thickening: natural history of radiographic and lung functional abnormalities. *Am J Respir Crit Care Med* 153: 301—309, 1996.
- 4) 玄馬顯一, 加藤勝也, 芦澤和人, 他: 石綿健康管理手帳健診受診者を対象とした低線量 CT についての検討—CT撮影により発見された肺癌・中皮腫症例を中心に—, 平成 27 年度労災疾病臨床研究事業報告書. 2016, pp 82—98.
- 5) Asbestos, asbestosis, and cancer: the Helsinki criteria for diagnosis and attribution. *Scand J Work Environ Health* 23: 311—316, 1997.
- 6) Karjalainen A, Pukkala E, Kauppinen T, Partanen T: Incidence of cancer among Finnish patients with asbestos-related pulmonary or pleural fibrosis. *Cancer Cause Control* 10: 51—57, 1999.
- 7) Finkelstein MM, Vingilis JJ: Radiographic abnormalities among asbestos cement workers. An exposure-response study. *Am Rev Respir Dis* 129: 17—22, 1984.
- 8) National Lung Screening Trial Research Team, Aberle DR, Adams AM, et al: Reduced lung-cancer mortality with low-dose computed tomographic screening. *N Engl J Med* 365: 395—409, 2011.
- 9) Wolff H, Vehmas T, Oksa P, et al: Asbestos, asbestosis, and cancer, the Helsinki criteria for diagnosis and attribution 2014:recommendations. *Scand J Work Environ Health* 41: 5—15, 2015.
- 10) Hammond EC, Selikoff IJ, Seidman H: Asbestos exposure, cigarette smoking and death rates. *ANN NY Acad Sci* 330: 473—490, 1979.
- 11) Kishimoto T, Gemba K, Fujimoto N, et al: Clinical study of asbestos-related lung cancer in Japan with special reference to occupational history. *Cancer Sci* 101: 1194—1198, 2010.

別刷請求先 〒702-8055 岡山市南区築港緑町 1—10—25
岡山労災病院アスベスト研究センター長
岸本 卓巳

Reprint request:

Takumi Kishimoto, M.D., PhD
Chief of Asbestos Research Center, Okayama Rosai Hospital,
1-10-25, Chikko-midorimachi, Minami-ku, Okayama, 702-8055,
Japan

日本医師会雑誌 第146巻・特別号(2)

THE JOURNAL OF THE JAPAN MEDICAL ASSOCIATION

環境による健康リスク

監修　車谷 典男
編集　村田 勝敬
川本 俊弘
五十嵐 隆
島 正之

編集協力



日本医師会

<http://www.med.or.jp/>

アスベストの発がん機序

岸本卓巳

アスベストとは、アスペクト比3以上の纖維

- 性珪酸塩であり、クロシドライト(青石綿)、アモサイト(茶石綿)、クリソタイル(白石綿)のほか3種類の角閃石を称する。

クロシドライト、アモサイトは体内での半減期が20年以上と長く体内に留まって炎症を惹起し、慢性炎症が発がん性につながる。一方、クリソタイルは珪素(Si)とマグネシウム(Mg)の珪酸塩で中空構造のため、もろく崩壊しやすく、マクロファージによって処理され、体外へ排出されやすい。

アスベストによる炎症の機序としては炎症細胞、特に好中球から有意に高い活性酸素の産生を促す。この活性酸素が中皮細胞を障害してがん化の引き金となる。慢性炎症に関係するアディポサイトカイン[たとえば、単球走化性タンパク-1(monocyte chemotactic protein-1; MCP-1)]の産生制御に障害が起こることでアディポサイトカインが大量に放出され、その直接作用あるいは中皮細胞の遊走(migration)に障害が生じることが発がんにつながる。クロシドライト、アモサイトは活性酸素産生能が高く、また4-ヒドロキシ-2-ノネナールにより細胞内タンパクの切断や酸化変異をきたすが、クリソタイルではこのような作用が弱い。一方、クリソタイルは強力な溶血作用を有するとともに、クリソタイルに付着したヘモグロビンが酸化されたDNAにダメージをきたす。そして局所への鉄過剰状態が引き起こされるため中皮細胞のがん化を招来するとともに、ヒストン/DNAに対するアスベストの親和性と中皮細胞へのアスベスト纖維の侵入により遺伝子変異をきたし発がんにつながるとの報告もある。纖維の形状では5μm以上、直径0.25μm未満の長くて細いアスベスト纖維が中皮腫あるいは肺がん頻度を増加させ、特に5~10μmの纖維が肺がんの発生に最も強く関与しているといわれている。

アスベストによる発がんに関する遺伝子異常

について以下の報告がある。

- ① p16染色体のCDKN2A、p19染色体のARF遺伝子はアスベストによる発がんの抑制遺伝子であるため、この両遺伝子の不活性化が発がんの要因となる。
- ② 家族内発がんとして重要なBRCA1-associated protein-1(BAP1)のgermline変異は中皮腫発症の重要な因子である。
- ③ neurofibromin 2(NF2)遺伝子の欠失、変異によりHippo pathwayが障害され、yes-associated protein(YAP)の核移行や遺伝子制御を行うリン酸化が弱められることが中皮腫発がんに重要である。特にYAPにより高発現された遺伝子のなかでもphospholipase-C beta-4(PLCB4)遺伝子が重要である。
- ④ DNA修復遺伝子であるERCC1 N118N、XRCC1 R339Qの存在がアスベストによる発がんに関与している。

アスベストの発がん性および発がん機序については現時点で確認されていることは以上であるが、未だに解明されていない点も多く、今後の研究に委ねられている。

参考文献

- 1) Chew SH, Okazaki Y, Nagai H, et al: Cancer-promoting role of adipocytes in asbestos-induced mesothelial carcinogenesis through dysregulated adipocytokine production. *Carcinogenesis* 2014; 35: 164-172.
- 2) Altomare DA, Menges CW, Xu J, et al: Losses of both products of the Cdkn2a/Arf locus contribute to asbestos-induced mesothelioma development and cooperate to accelerate tumorigenesis. *PLoS One* 2011; 6: e18828.
- 3) Kakiuchi T, Takahara T, Kasugai Y, et al: Modeling mesothelioma utilizing human mesothelial cells reveals involvement of phospholipase-C beta 4 YAP-active mesothelioma cell proliferation. *Carcinogenesis* 2016; bgw084.



A phase II trial of carboplatin plus S-1 for elderly patients with advanced non-small-cell lung cancer with wild-type epidermal growth factor receptor: The Okayama Lung Cancer Study Group Trial 1202

Shoichi Kuyama^{a,1}, Nobuaki Ochi^{b,1}, Akihiro Bessho^c, Katsuyuki Hotta^d, Genyo Ikeda^e, Daizo Kishino^f, Toshio Kubo^g, Daijiro Harada^h, Nobukazu Fujimotoⁱ, Masamoto Nakanishi^a, Takahiro Umeno^{a,c}, Toshiaki Okada^{e,j}, Kenichi Chikamori^f, Tomoko Yamagishi^{b,i}, Kadoaki Ohashi^g, Eiki Ichihara^g, Nagio Takigawa^{b,*}, Mitsune Tanimoto^{a,k}, Katsuyuki Kiura^g

^a Department of Respiratory Medicine, Iwakuni Clinical Center, Iwakuni, Japan

^b Department of General Internal Medicine 4, Kawasaki Medical School, Okayama, Japan

^c Department of Respiratory Medicine, Japanese Red Cross Okayama Hospital, Okayama, Japan

^d Center for Innovative Clinical Medicine, Okayama University Hospital, Okayama, Japan

^e Department of Respiratory Medicine, Chugoku Central Hospital, Fukuyama, Japan

^f Department of Medical Oncology, Yamaguchi-Ube Medical Center, Ube, Japan

^g Department of Allergy and Respiratory Medicine, Okayama University Hospital, Okayama, Japan

^h Department of Thoracic Oncology and Medicine, Shikoku Cancer Center, Matsuyama, Japan

ⁱ Department of Medical Oncology, Okayama Rosai Hospital, Okayama, Japan

^j Department of Respiratory Medicine, Fukuyama Medical Center, Fukuyama, Japan

^k Graduate School of Medicine, Dentistry, and Pharmaceutical Sciences, Okayama, Japan



ARTICLE INFO

Keywords:

Carboplatin

Elderly

Non-small cell lung cancer

S-1

Thymidine phosphorylase

ABSTRACT

Introduction: S-1 is an oral fluoropyrimidine-based combination of tegafur, gimeracil, and oteracil potassium. Although the combination of S-1 with carboplatin is a first-line chemotherapy regimen for advanced non-small cell lung cancer (NSCLC), the efficacy and safety of the regimen in the elderly remain unknown.

Methods: The patient inclusion criteria were previously untreated advanced NSCLC, wild-type epidermal growth factor receptor, aged 70 years or more, and a performance status (PS) of 0–2. The patients received oral S-1 (40 mg/m², twice daily) for 2 weeks and carboplatin (area under the curve: 5) on day 1 every 4 weeks as induction treatment. After four induction cycles, S-1 alone (40 mg/m², twice daily) was administered for 2 weeks every 4 weeks as a maintenance therapy until disease progression. The primary endpoint was the overall response rate (ORR), which was expected to exceed 20%, and the secondary endpoints included the disease control rate (DCR), progression-free survival (PFS), overall survival (OS), and the toxicity profile. The associations between clinical outcomes and expression of genes such as thymidylate synthase and thymidine phosphorylase in the tumors were evaluated.

Results: Thirty-three patients were enrolled between March 2013 and June 2015. The median age was 78 (range 70–89) years, and 51.5% had a PS of 0. The ORR was 30.3% (95% confidence interval (CI): 14.6–46.0) and the DCR 57.6% (95% CI: 40.7–74.4). Grade 3/4 toxicities included thrombocytopenia (42.4%), neutropenia (33.3%), and anemia (27.3%). There was one treatment-related death due to aspiration pneumonia following febrile neutropenia. The median PFS and OS were 134 days (95% CI: 79–173) and 479 days (95% CI: 250–571), respectively. Low thymidine phosphorylase expression was associated with the DCR ($P < 0.01$).

Conclusion: This study met the predetermined primary endpoint, and the regimen seems to be a favorable treatment option.

* Corresponding author.

E-mail addresses: ntakigaw@gmail.com, ntakigaw@med.kawasaki-m.ac.jp (N. Takigawa).

¹ Drs. Kuyama and Ochi equally contributed to this work and they are both first authors.

1. Introduction

Lung cancer is the leading cause of cancer-related death worldwide [1]. Non-small cell lung cancer (NSCLC) accounts for approximately 85% of lung cancers [2]. Oncogenic drivers such as epidermal growth factor receptor (EGFR) mutations [3] and echinoderm microtubule-associated protein-like 4-anaplastic lymphoma kinase (EML4–ALK) [4] have been identified in NSCLC. However, only two targeted drugs are available clinically: EGFR-tyrosine kinase inhibitor (TKI) and ALK-TKI [3,5]. Therefore, it is necessary to develop effective chemotherapies without severe adverse effects for patients who do not benefit from targeted therapy.

Lung cancer patients 60 years or older have relatively high cancer mortality rates regardless of sex [1]. Monotherapy using cytotoxic agents is the standard chemotherapy choice in elderly patients without an EGFR mutation or the EML4–ALK fusion gene [6–9]. A subset analysis of a large phase III trial revealed that the survival benefit from chemotherapy was not influenced by age, and the baseline quality of life and functional status were the best indicators for selecting treatment-fitted elderly patients [10]. Some recent phase III trials have evaluated the effectiveness of platinum-doublet chemotherapy in the elderly [11–13]. Their results were controversial because of early termination of the trials and differences in the regimens/schedules; however, combination chemotherapy in fit elderly patients was promising; thus, the decision to use systemic chemotherapy should not be based on age alone [14].

S-1 is an oral fluoropyrimidine anticancer agent combining tegafur, gimeracil, and oteracil potassium. The overall response rate (ORR) and disease control rate (DCR) for S-1 monotherapy were 22.6–27.6% and 65.5–70.0%, respectively. The median progression-free survival (PFS) and overall survival (OS) were 3.1–4.0 and 11.2–12.1 months, respectively [15–17]. Grade 3/4 toxicities were observed in 6.9–16.7% of the patients [15–18]. In a study of long-term S-1 monotherapy following docetaxel plus cisplatin therapy in patients with curatively resected NSCLC, Niho et al. observed grade 3/4 toxicities during S-1 monotherapy, including anemia in 7.3% and neutropenia in 3.7% [18]. S-1 monotherapy appears to be effective and feasible. Two recent phase III trials for advanced NSCLC showed the non-inferiority of S-1 combined with carboplatin or cisplatin compared with standard platinum doublet chemotherapy [19,20]. Although S-1 plus platinum is considered a standard regimen for advanced NSCLC, its efficacy in the elderly remains unclear.

We have reported clinical trials using S-1 for patients with locally advanced NSCLC, including elderly patients (> 70 years old) [21–24]. We also examined the combination of docetaxel and S-1 in patients with previously treated NSCLC, including the elderly [25]. We believe that S-1 is efficacious and safe for NSCLC patients, even the elderly. Therefore, we conducted this phase II study of carboplatin plus S-1 followed by S-1 monotherapy in elderly patients with NSCLC (Clinical trial number: UMIN000009345).

2. Materials and methods

2.1. Patient selection

This multicenter phase II trial was conducted in accordance with the Declaration of Helsinki and was approved by the institutional review board of each participating institution.

Chemotherapy-naïve patients aged ≥ 70 years old with pathologically confirmed NSCLC harboring stage IIIB or IV wild-type EGFR, an Eastern Cooperative Oncology Group performance status (PS) 2 or lower, and a measurable lesion according to the Response Evaluation Criteria in Solid Tumors (RECIST) criteria ver. 1.1 were eligible for this study. EGFR mutations were analyzed in biopsied samples using commercial assays, such as PNA-LNA PCR clamp, PCR-Invader, and Scorpion-ARMS. Additional inclusion criteria were a white blood cell

count $\geq 3000/\text{mm}^3$, absolute neutrophil count $\geq 1500/\text{mm}^3$, platelet count $> 150,000/\text{mm}^3$, hemoglobin level $\geq 9.0\text{ g/dL}$, serum bilirubin level $\leq 1.5\text{ mg/dL}$, aspartate aminotransferase and alanine aminotransferase levels ≤ 2.5 -fold the normal ranges, creatinine level $\leq 1.5\text{ mg/dL}$, and arterial oxygen pressure $\geq 60\text{ mmHg}$. Patients were excluded if they had symptomatic brain metastasis, interstitial lung disease, a massive effusion requiring drainage, or severe comorbidities such as uncontrolled diabetes or cardiac disease or if they were taking warfarin sodium or dabigatran etexilate. All patients provided written informed consent.

2.2. Treatment schedule

Carboplatin was given as an intravenous infusion (area under the curve: 5) on day 1, and S-1 (80 mg/m² divided into two doses, after breakfast and dinner) was given orally on days 1–14, every 4 weeks. After four cycles of the combination therapy, S-1 monotherapy (same dose and schedule as that used for induction therapy) was continued until disease progression. The S-1 dose was based on the body surface area (BSA) as follows: BSA < 1.25 m², 80 mg/day; 1.25 m² \leq BSA < 1.5 m², 100 mg/day; and 1.5 m² \leq BSA, 120 mg/day. Although a dose reduction for carboplatin was not permitted, the S-1 dose was reduced from 120 to 100 mg/day, 100–80 mg/day, or 80–60 mg/day based on toxicity. Only one dose reduction was allowed. Second-line chemotherapy or further treatments were given at the physician's discretion.

2.3. Patient assessment

Patient assessment, including a physical examination, chest x-ray, complete blood count, and biochemical profile, was repeated once a week during the first cycle and at least once per subsequent cycle. Tumor response was evaluated by computed tomography using RECIST ver. 1.1 at least once every two cycles until disease progression. A response of at least 4 weeks duration was confirmed as a complete or partial response, and stable disease was defined as disease lasting at least 6 weeks from initiation of the treatment protocol. DCR was defined according to the complete response, partial response, and stable disease rates together. Response was confirmed by an independent extramural review. Toxicities were assessed according to the National Cancer Institute–Common Toxicity Criteria for Adverse Events ver. 4.0.

2.4. Gene profiling analysis

Tissue samples were collected from patients who participated in this study and provided additional written informed consent. For quantification, 10 μm slices from paraffin-embedded specimens were set aside. RNA was isolated from tumor tissues using the RNeasy FFPE Kit (Qiagen, Chatsworth, GA, USA). cDNA was prepared using the High Capacity Reverse Transcription Kit from Life Technologies (Foster City, CA, USA), according to the manufacturer's instruction. The expression levels of the following six genes were determined by TaqMan real-time PCR (TaqMan array card; Life Technologies) after TaqMan assay-based pre-amplification: thymidylate synthase (TS), thymidine phosphorylase (TP), dihydropyrimidine dehydrogenase (DPD), orotate phosphoribosyl transferase (OPRT), vascular endothelial growth factor (VEGF), and excision repair cross-complementing gene 1 (ERCC1). The array card included ACTB, GAPDH, and RPLP0 as reference genes based on their validated roles as housekeeping genes [26,27]. The relationships between gene expression and outcomes, including the response, PFS, and OS rates, were evaluated.

2.5. Statistical analysis

The primary endpoint of this study was the ORR, and secondary endpoints included the DCR, PFS, OS, and toxicity profile. OS was

Table 1
Patient characteristics.

Characteristic	n (%)
Age, median (range), years	78 (70–89)
Sex	
Male	28 (84.9)
Female	5 (15.2)
ECOG performance status	
0/1/2	17/13/3 (51.5/39.4/9.1)
Histology	
Adenocarcinoma	19 (57.6)
Squamous cell carcinoma	13 (39.4)
Not otherwise specified	1 (3.0)
Tumor stage	
Recurrence/IIIB/IV	3/5/25 (9.1/15.2/75.8)
Current/former/never smoker	2/26/5 (6.1/78.8/15.2)
Brinkman Index	
< 400	8 (24.2)
≥ 400	25 (75.8)
Median (range)	840 (0–1800)

Abbreviations: ECOG, Eastern Cooperative Oncology Group.

evaluated from the date of study entry to death. The final analysis was planned for 1 year after the last patient was registered.

Assuming that an ORR of 20% would support the potential usefulness of the therapy, whereas an ORR of 5% would be at the lower limit of interest, with alpha = 0.10 and beta = 0.20, the estimated accrual was 28 patients for this study. Given the possibility of variance inflation due to censoring or protocol violation, the sample size was set at 32 patients. Survival was estimated using the Kaplan–Meier method. The difference among survival curves was evaluated using the log-rank test. Patient characteristics and gene expression profiles or treatment response were compared between groups using the χ^2 test. The statistical analyses were performed using Stata for Windows, ver. 14.0 (Stata, College Station, TX, USA).

3. Results

3.1. Patient characteristics

We enrolled 33 patients between Mar 2013 and June 2015 in this study. Table 1 shows the baseline patient characteristics. The median age was 78 (range 70–89) years. The proportion of males was 84.8%, and patients with adenocarcinoma and squamous cell carcinoma comprised 57.6% (19/33) and 39.4% (13/33), respectively. Most patients were current or former smokers (84.9%), and the median Brinkman index was 840.

3.2. Treatment

The median number of induction treatment (carboplatin plus S-1) cycles was 3 (range 1–4), and 15 patients (45.5%) subsequently received maintenance S-1 monotherapy. Four cycles of combination chemotherapy were completed by 42.4% (14/33) of the patients. The main reasons for discontinuation during induction were prolonged neutropenia and thrombocytopenia. Dose reduction was necessary during the induction phase in 36.4% (12/33) of the patients, while no reductions were necessary during the maintenance phase. At the time of analysis on July 30, 2016, 21.2% (7/33) of patients were alive and received subsequent chemotherapy, and one patient continued S-1 maintenance therapy.

3.3. Response and survival analyses

The response was assessed in 32 of the 33 enrolled patients; the remaining patient dropped out of the study because of a grade 3 skin toxicity during the first course of treatment before the radiological

Table 2
Objective treatment response and survival.

	n	%
Complete response	0	0.0
Partial response	10	30.3
Stable disease	9	27.3
Progressive disease	13	39.4
Not assessable	1	3.0
Overall response rate (95% CI)	10	30.3 (14.6–46.0)
Disease control rate (95% CI)	19	57.6 (40.7–74.4)
Survival		
Median PFS (days) (95% CI)	134 (79–173)	
Median OS (days) (95% CI)	479 (250–571)	
1-y survival rate (%) (95% CI)	54.1 (35.7–69.3)	

Abbreviations: CI, confidence interval; OS, overall survival; PFS, progression-free survival.

evaluation. The proportion of patients who achieved a response was 30.3% (10/33; 95% confidence interval [CI]: 14.6–46.0, 90% CI: 17.2–43.4), which met the primary endpoint of an ORR $\geq 20\%$ (lower limit of 90% CI 17.2 > the lower limit of interest 5%). The DCR was 57.6% (95% CI: 40.7–74.4, Table 2). Table 3 shows the subgroup analysis of the treatment responses and survival according to histology. There was no significant difference in the ORR between patients with squamous cell carcinoma and those with adenocarcinoma ($p = 0.94$, χ^2 test). The median follow-up was 808 (range 293–1204) days, the median PFS was 134 days (95% CI: 79–173), and the median survival time (MST) was 479 days (95% CI: 250–571). Fig. 1A and B show the PFS and OS curves for all patients, respectively. The 1-year survival rate was 54.1% (95% CI: 35.7–69.3). The PFS curves were similar between patients with adenocarcinoma and those with squamous cell carcinoma (Fig. 2A). Although the MST was longer in patients with adenocarcinoma than in those with squamous cell carcinoma (571 vs. 250 days; Fig. 2B), the difference was not significant ($p = 0.06$).

3.4. Post-study chemotherapy

Overall, 70.0% (23/33) of the patients received subsequent post-study systemic chemotherapy (Table S1). Of these, 14 patients (42.4%) received further chemotherapy. The median post-study treatment line was 1 (range 0–5). Although most of the patients received single-agent chemotherapy, four received combination chemotherapy (amrubicin plus erlotinib, gemcitabine plus vinorelbine, or docetaxel plus bevacizumab). The patients were administered the following agents: docetaxel (31.6%), pemetrexed (31.6%), nab-paclitaxel (23.7%), and

Table 3
Objective response and survival rates according to tumor histology.

	ADC (n = 19)		SCC (n = 13)	
	No.	%	No.	%
Complete response	0	0.0	0	0.0
Partial response	6	31.6	4	30.8
Stable disease	5	26.3	4	30.8
Progressive disease	8	42.1	4	30.8
Not assessable	0	0.0	1	7.7
Overall response rate (95% CI)	6	31.6 (10.7–52.5)	4	30.8 (0.06–55.9)
Disease control rate (95% CI)	11	57.9 (35.7–80.1)	8	61.5 (35.1–88.0)
Survival				
Median PFS (days) (95% CI)	148 (64–193)		95 (68–244)	
Median OS (days) (95% CI)	571 (317–763)		250 (95–374)	
1-y survival rate (%) (95% CI)	73.3 (47.2–87.9)		30.8 (9.5–55.4)	

Abbreviations: ADC, adenocarcinoma; CI, confidence interval; OS, overall survival; PFS, progression-free survival; SCC, squamous cell carcinoma.

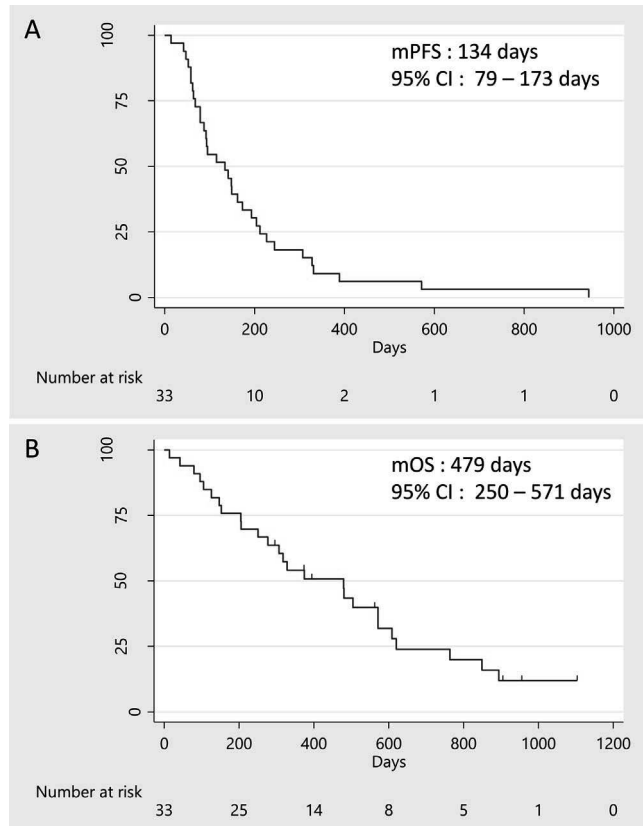


Fig. 1. Progression-free and overall survival curves for all patients.

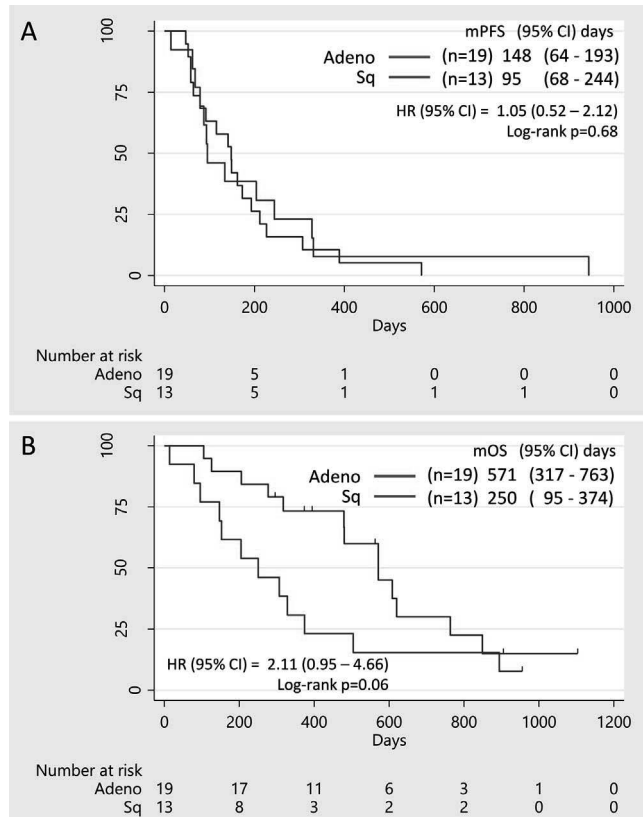


Fig. 2. Progression-free and overall survival curves according to tumor histology.

Table 4
Incidence of adverse events.

Adverse event	Grade 3 (%)	Grade 3 or higher (%)
General		
Fatigue	0.0	0.0
Anorexia	0.0	0.0
Nausea	0.0	0.0
Vomiting	0.0	0.0
Skin rash	0.0	0.0
Febrile neutropenia	9.1	12.1
Pneumothorax	0.0	3.0
Erythema multiforme	0.0	3.0
Hematological		
Neutropenia	24.2	33.3
Anemia	27.3	27.3
Thrombocytopenia	33.3	42.4
Biochemical		
AST/ALT elevation	0.0	0.0
Creatinine elevation	0.0	0.0

Abbreviations: ALT, alanine amino transferase; AST, aspartate amino transferase.

others (13.2%). One patient received alectinib, because the EML4–ALK fusion gene was detected later. One patient received nivolumab.

3.5. Gene profiling analysis

Gene expression analyses were performed in 17 of the 33 patients. The expression of six genes (TS, TP, DPD, OPRT, ERCC1, and VEGF) was successfully measured in these 17 patients. Fig. S1 shows the PFS and OS curves. The cut-off values were based on the median expression level of each gene. In the histological subgroup analysis (Fig. S2), TS expression was higher in the patients with squamous cell carcinoma, albeit not significantly ($p = 0.085$, χ^2 test). Low TP expression was significantly correlated with a better DCR ($p = 0.004$, χ^2 test). Figs. S3 and S4 show the distribution of gene expression stratified according to response. There were no significant differences in the PFS or OS stratified by each gene (Figs. S5 and S6).

3.6. Safety

Table 4 shows the adverse event profile. The majority of the grade 3 or higher adverse events were thrombocytopenia (42.4%), neutropenia (33.3%), and anemia (27.3%). One patient developed grade 3 skin toxicity (erythema multiforme) just before beginning the second cycle of carboplatin/S-1. He recovered fully after discontinuing all suspected drugs, including S-1, and received prednisolone 30 mg/day for several days. Because we could not rule out S-1-related skin toxicity, we decided to discontinue the protocol treatment. Two deaths (6.1%) occurred during the study. One patient died after four cycles of maintenance S-1 monotherapy of a spontaneous pneumothorax due to ruptured bullae in the contralateral lung; death was thus considered to be unrelated to the S-1 treatment. The other died of aspiration pneumonia following febrile neutropenia and was deemed a treatment-related death.

4. Discussion

This phase II trial met the pre-designed primary endpoint (ORR $\geq 20\%$), with a favorable survival outcome and moderate toxicities, in elderly patients with advanced NSCLC. Low TP expression in tumors might serve as a marker predictive of a better DCR.

Standard chemotherapy regimens have been established for elderly NSCLC patients in the last two decades. In 1999, an Italian group reported the first results from a phase III trial of vinorelbine monotherapy compared with supportive care alone for the elderly. The survival outcome was significantly better in the chemotherapy arm (MST: 6.4

months in the vinorelbine arm vs. 4.8 months in the supportive care arm) [7]. Subsequently, a phase III trial comparing vinorelbine, gemcitabine, and both drugs together showed no survival benefit in the combination arm [8]. Thus, single-agent monotherapy was proposed as the standard regimen for the elderly. A Japanese group evaluated the efficacy of docetaxel versus vinorelbine. Previously untreated stage IIIB/IV NSCLC patients, ≥ 70 years of age with a PS of 2 or lower, were enrolled. Although there was no significant difference in OS between the two treatment arms, PFS and ORR were significantly better in the docetaxel arm than in the vinorelbine arm (median PFS: 5.5 months vs. 3.1 months, $p < 0.001$; ORR: 22.7% vs. 9.9%, $p = 0.019$) [9]. We also found that docetaxel was effective in select elderly patients (> 75 years old) with advanced NSCLC [28]. Thus, docetaxel monotherapy was proposed as the standard treatment for the elderly in Japan.

Two phase III trials of S-1 combined platinum doublet chemotherapy showed possible survival benefit in patients with squamous cell carcinoma than those with adenocarcinoma [20,29]. On the contrary, possible survival benefit was observed in the adenocarcinoma group in our study (Fig. 2B). Thus, it remains unclear whether the combination of S-1 with platinum has different efficacy between adenocarcinoma and squamous cell carcinoma. Further investigations are warranted.

Chemotherapy-related adverse events are likely to arise in the elderly, probably because of their impaired organ functions and comorbidities compared with younger patients. Grade 3/4 neutropenia is associated with serious complications. The previously reported [9] incidence of grade 3/4 neutropenia (82.9%) caused by docetaxel monotherapy was greater than that in the present study (33.3%). Therefore, the carboplatin/S-1 combination seems to be safer than docetaxel monotherapy in terms of neutropenia.

Age is an important factor when choosing a chemotherapy regimen. Although the benefits of chemotherapy are similar regardless of age, toxicities generally are more common in the elderly [30]. In a randomized phase III trial, Quoix et al. compared carboplatin and weekly paclitaxel with monotherapy in elderly patients with advanced NSCLC [31]. Grade 3/4 hematological toxicities were significantly more frequent in the combination chemotherapy group than in the monotherapy group. The incidence of treatment-related deaths with the combination therapy was also high (4.4% vs. 1.3%). However, both PFS and OS were significantly longer in patients treated with the combination therapy (median PFS: 6.0 vs. 2.8 months, MST: 10.3 vs. 6.2 months) [31]. Table S2 shows the results from representative trials of platinum combination therapy conducted in elderly (≥ 70 years) patients with NSCLC. The median PFS and MST ranged from 4.7 to 6.2 months and from 10.3 to 17.0 months, respectively. The survival benefit observed in our study was comparable with that in those studies [12,13,31,32]. The efficacy and safety of S-1 plus carboplatin have not been evaluated in the elderly. In addition, no related subset analyses have been reported [19,33–35]. Compared with those studies, the response and survival benefit in our study were comparable or better, but the incidence of adverse events was higher (Tables S2 and S3).

The expression of six genes, TS, TP, DPD, OPRT, VEGF, and ERCC1, were evaluated in this study. High TS expression is often observed in squamous cell carcinoma and is associated with a poor treatment response to fluorouracil [36–38]. However, there were no significant differences in PFS or OS according to TS expression, which might be because of the small sample size. By contrast, lower TP expression was significantly correlated with a better DCR. Low TP expression led to a better response and survival in gastric cancer patients [37,39]. TP is an enzyme involved in pyrimidine nucleotide metabolism, and low TP expression might be advantageous for tumor shrinkage or stabilization by S-1. TP was recently found to be the same molecule as platelet-derived endothelial cell growth factor, which stimulates the chemotaxis of endothelial cells and angiogenesis [40,41], and high TP expression was correlated with increased angiogenesis and a poor prognosis [42–46]. Therefore, the importance of TP expression in NSCLC should be

clarified.

There were some limitations to our study. First, this was a single-arm study. Patient selection bias could not be eliminated. Second, the significance of S-1 maintenance has not been established. Only one report has examined S-1 maintenance therapy for advanced NSCLC [47], although it has been evaluated for other malignancies and in an adjuvant setting for NSCLC [48–52]. Suzuki, et al. reported S-1 maintenance therapy following four cycles of carboplatin and S-1 induction therapy in patients with advanced squamous cell lung cancer [47]. The median age was 72 years (range, 57–89 years), and 19 patients (37.3%) were aged > 75 years. The treatment seemed feasible and tolerable even in the population including elderly. Further studies are needed to reveal the efficacy and survival benefit of S-1 maintenance therapy. Third, tissue samples were collected for gene expression analysis in only 52% (33/67) of the subjects. The relationship between TP gene expression and treatment outcome should be verified in future studies. Fourth, we could not evaluate quality of life, comorbidities, number of medications, or functional and cognitive status, which should be evaluated in future studies of NSCLC in the elderly.

In conclusion, carboplatin plus S-1 had favorable efficacy and tolerable toxicity for the elderly with NSCLC. This study met the pre-designed primary endpoint, and the regimen seems to be a treatment option. We need to conduct further studies to evaluate whether this combination is superior to the standard first-line treatment for the elderly.

Disclosure

KH received honoraria outside the current work from AstraZeneca, Ono Pharmaceutical, Astellas, Novartis, BMS, MSD, Eli Lilly Japan, Daiichi-Sankyo Pharmaceutical, Boehringer-Ingelheim, Nihon Kayaku, Taiho Pharmaceutical, and Chugai Pharmaceutical. KH also has received research funding outside the current work from AstraZeneca, Boehringer-Ingelheim, Ono Pharmaceutical, Astellas, Novartis, BMS, Eli Lilly Japan, MSD, and Chugai Pharmaceutical. NT has received honoraria from Eli Lilly Japan, AstraZeneca, Daiichi-Sankyo Pharmaceutical, Chugai Pharmaceutical, Taiho Pharmaceutical, Pfizer Inc. Japan, Boehringer-Ingelheim, and Ono Pharmaceutical, and research funding from AstraZeneca, Pfizer Inc. Japan, Kyowa Hakko Kirin, Eli Lilly Japan, Chugai Pharmaceutical, Nippon Kayaku Co. Ltd, Taiho Pharmaceutical, Takeda Pharmaceutical Co. Ltd, Boehringer-Ingelheim, and Ono Pharmaceutical. KK has received honoraria from Chugai Pharmaceutical, Eli Lilly Japan, Pfizer Inc. Japan, Novartis Pharm, and Taiho Pharmaceutical, and research funding from AstraZeneca, Boehringer-Ingelheim, Nippon Kayaku Co. Ltd, Daiichi-Sankyo Pharmaceutical, and Shionogi Co. Ltd. All other authors declare that they have no conflict of interest.

Acknowledgement

Molecular analysis of this study was funded by Taiho Pharmaceutical Co., Ltd.(Tokyo, Japan).

Appendix A. Supplementary data

Supplementary data associated with this article can be found, in the online version, at <http://dx.doi.org/10.1016/j.lungcan.2017.08.010>.

References

- [1] R.L. Siegel, K.D. Miller, A. Jemal, Cancer statistics 2016, CA Cancer J. Clin. 66 (2016) 7–30.
- [2] R. Siegel, D. Naishadham, A. Jemal, Cancer statistics 2012, CA Cancer J. Clin. 62 (2012) 10–29.
- [3] T.J. Lynch, D.W. Bell, R. Sordella, S. Gurubhagavatula, R.A. Okimoto, B.W. Brannigan, P.L. Harris, S.M. Haserlat, J.G. Supko, F.G. Haluska, D.N. Louis, D.C. Christiani, J. Settleman, D.A. Haber, Activating mutations in the epidermal

- growth factor receptor underlying responsiveness of non-small-cell lung cancer to gefitinib, *N. Engl. J. Med.* 350 (2004) 2129–2139.
- [4] M. Soda, Y.L. Choi, M. Enomoto, S. Takada, Y. Yamashita, S. Ishikawa, S. Fujiwara, H. Watanabe, K. Kurashina, H. Hatanaka, M. Bando, S. Ohno, Y. Ishikawa, H. Aburatani, T. Niki, Y. Sohara, Y. Sugiyama, H. Mano, Identification of the transforming EML4-ALK fusion gene in non-small-cell lung cancer, *Nature* 448 (2007) 561–566.
- [5] E.L. Kwak, Y.-J. Bang, D.R. Camidge, A.T. Shaw, B. Solomon, R.G. Maki, S.-H.I. Ou, B.J. Dezube, P.A. Jänne, D.B. Costa, M. Varella-Garcia, W.-H. Kim, T.J. Lynch, P. Fidias, H. Stubbs, J.A. Engelman, L.V. Sequist, W. Tan, L. Gandhi, M. Minn-Kenudson, G.C. Wei, S.M. Shreeve, M.J. Ratain, J. Settleman, J.G. Christensen, D.A. Haber, K. Wilner, R. Salgia, G.I. Shapiro, J.W. Clark, A.J. Iafrate, Anaplastic lymphoma kinase inhibition in non-small-cell lung cancer, *N. Engl. J. Med.* 363 (2010) 1693–1703.
- [6] G. Frasci, V. Lorusso, N. Panza, P. Comella, G. Nicolella, A. Bianco, G. De Cataldis, A. Iannelli, D. Bilancia, M. Belli, B. Massidda, F. Piantedosi, G. Comella, M. De Lena, Gemcitabine plus vinorelbine versus vinorelbine alone in elderly patients with advanced non-small-cell lung cancer, *J. Clin. Oncol.* 18 (2000) 2529–2536.
- [7] C. Gridelli, The ELVIS trial: a phase III study of single-agent vinorelbine as first-line treatment in elderly patients with advanced non-small cell lung cancer. Elderly Lung Cancer Vinorelbine Italian Study, *Oncologist* 6 (Suppl. 1) (2001) 4–7.
- [8] C. Gridelli, F. Perrone, C. Gallo, S. Cigolari, A. Rossi, F. Piantedosi, S. Barbera, F. Ferraro, E. Piazza, F. Rosetti, M. Clerici, O. Bertetto, S.F. Robbiati, L. Frontini, C. Sacco, F. Castiglione, A. Favaretto, S. Novello, M.R. Migliorino, G. Gasparini, D. Galetta, R.V. Iaffaioli, V. Gebbia, MILES Investigators, Chemotherapy for elderly patients with advanced non-small-cell lung cancer: the Multicenter Italian Lung Cancer in the Elderly Study (MILES) phase III randomized trial, *J. Natl. Cancer Inst.* 95 (2003) 362–372.
- [9] S. Kudoh, K. Takeda, K. Nakagawa, M. Takada, N. Katakami, K. Matsui, T. Shinkai, T. Sawa, I. Goto, H. Semba, T. Seto, M. Ando, T. Satoh, N. Yoshimura, S. Negoro, M. Fukuoka, Phase III study of docetaxel compared with vinorelbine in elderly patients with advanced non-small-cell lung cancer: results of the West Japan Thoracic Oncology Group Trial (WJTOG 9904), *J. Clin. Oncol.* 24 (2006) 3657–3663.
- [10] P. Maione, F. Perrone, C. Gallo, L. Manzione, F. Piantedosi, et al., Pretreatment quality of life and functional status assessment significantly predict survival of elderly patients with advanced non-small-cell lung cancer receiving chemotherapy: a prognostic analysis of the multicenter Italian lung cancer in the elderly study, *J. Clin. Oncol.* 23 (2005) 6865–6872.
- [11] E. Quoix, G. Zalcman, J.-P. Oster, V. Westeel, E. Pichon, A. Lavolé, J. Dauba, D. Debieuvre, P.-J. Souquet, L. Bigay-Game, E. Dansin, M. Poudenx, O. Molinier, F. Vaylet, D. Moro-Sibilot, D. Herman, J. Bennouna, J. Tredaniel, A. Ducolomé, M.-P. Lebitas, L. Baudrin, S. Laporte, B. Milleron, Intergroupe Francophone de Cancérologie Thoracique, Carboplatin and weekly paclitaxel doublet chemotherapy compared with monotherapy in elderly patients with advanced non-small-cell lung cancer: IFCT-0501 randomised, phase 3 trial, *Lancet* 378 (2011) 1079–1088.
- [12] T. Abe, K. Takeda, Y. Ohe, S. Kudoh, Y. Ichinose, H. Okamoto, N. Yamamoto, H. Yoshioka, K. Minato, T. Sawa, Y. Iwamoto, H. Saka, J. Mizusawa, T. Shibata, S. Nakamura, M. Ando, A. Yokoyama, K. Nakagawa, N. Saito, T. Tamura, Randomized phase III trial comparing weekly docetaxel plus cisplatin versus docetaxel monotherapy every 3 weeks in elderly patients with advanced non-small-cell lung cancer: the intergroup trial JCOG0803/WJOG4307L, *J. Clin. Oncol.* 33 (2015) 575–581.
- [13] H. Tsukada, A. Yokoyama, K. Goto, T. Shinkai, M. Harada, M. Ando, T. Shibata, Y. Ohe, T. Tamura, N. Saito, Randomized controlled trial comparing docetaxel-cisplatin combination with weekly docetaxel alone in elderly patients with advanced non-small-cell lung cancer: Japan Clinical Oncology Group (JCOG) 0207†, *Jpn. J. Clin. Oncol.* 45 (2015) 88–95.
- [14] G.A. Masters, S. Temin, C.G. Azzoli, G. Giaccone, S. Baker, J.R. Brahmer, P.M. Ellis, A. Gajra, N. Rackear, J.H. Schiller, T.J. Smith, J.R. Straw, D. Trent, D.H. Johnson, American society of clinical oncology clinical practice, systemic therapy for stage IV non-small-cell lung cancer: american society of clinical oncology clinical practice guideline update, *J. Clin. Oncol.* 33 (2015) 3488–3515.
- [15] O. Nishiyama, H. Taniguchi, Y. Kondoh, K. Takada, K. Baba, H. Saito, Y. Sugino, M. Yamamoto, T. Ogasawara, M. Kondo, K. Imaizumi, Y. Hasegawa, R. Suzuki, K. Shimokata, Central Japan Lung Study Group, Phase II study of S-1 monotherapy as a first-line treatment for elderly patients with advanced nonsmall-cell lung cancer: the Central Japan Lung Study Group trial 0404, *Anticancer Drugs* 22 (2011) 811–816.
- [16] M. Wada, M. Yamamoto, S. Ryuge, Y. Nagashima, N. Hayashi, S. Maki, S. Otani, K. Katono, A. Takakura, T. Yanaihara, S. Igawa, M. Yokoba, H. Mitsuishi, M. Kubota, M. Katagiri, N. Masuda, Phase II study of S-1 monotherapy in patients with previously treated, advanced non-small-cell lung cancer, *Cancer Chemother. Pharmacol.* 69 (2012) 1005–1011.
- [17] T. Kasai, Y. Nakamura, M. Fukuda, T. Kitazaki, S. Nagashima, H. Takatani, H. Nakano, K. Nakatomi, T. Ikeda, H. Yamaguchi, K. Tsukamoto, M. Oka, S. Kohno, A phase II study of S-1 for previously untreated elderly patients with advanced non-Small cell lung cancer, *Chemotherapy* 61 (2016) 93–98.
- [18] S. Niho, N. Ikeda, H. Michimae, K. Suzuki, H. Sakai, T. Kaburagi, K. Minato, T. Kato, H. Okamoto, T. Seto, Y. Hosomi, K. Shimizu, F. Oshita, H. Kunio, M. Tsuboi, M. Takeuchi, K. Watanabe, Feasibility trial for adjuvant chemotherapy with docetaxel plus cisplatin followed by single agent long-term administration of S-1 chemotherapy in patients with completely resected non-small cell lung cancer: thoracic Oncology Research Group Study 0809, *Br. J. Cancer* 109 (2013) 545–551.
- [19] I. Okamoto, H. Yoshioka, S. Morita, M. Ando, K. Takeda, T. Seto, N. Yamamoto, H. Saka, K. Asami, T. Hirashima, S. Kudoh, M. Satouchi, N. Ikeda, Y. Iwamoto, T. Sawa, M. Miyazaki, K. Tamura, T. Kurata, M. Fukuoka, K. Nakagawa, Phase III trial comparing oral S-1 plus carboplatin with paclitaxel plus carboplatin in chemotherapy-naïve patients with advanced non-small-cell lung cancer: results of a west Japan oncology group study, *J. Clin. Oncol.* 28 (2010) 5240–5246.
- [20] K. Kubota, H. Sakai, N. Katakami, M. Nishio, A. Inoue, H. Okamoto, H. Isobe, H. Kunio, Y. Takiguchi, K. Kobayashi, Y. Nakamura, H. Ohmatsu, S. Sugawara, K. Minato, M. Fukuda, A. Yokoyama, M. Takeuchi, H. Michimae, A. Gemma, S. Kudoh, Tokyo Cooperative Oncology Group, A randomized phase III trial of oral S-1 plus cisplatin versus docetaxel plus cisplatin in Japanese patients with advanced non-small-cell lung cancer: TCOG0701 CATS trial, *Ann. Oncol.* 26 (2015) 1401–1408.
- [21] K. Chikamori, D. Kishino, N. Takigawa, K. Hotta, N. Nogami, H. Kamei, S. Kuyama, K. Gemba, M. Takemoto, S. Kanazawa, H. Ueoka, Y. Segawa, S. Takata, M. Tabata, K. Kiura, M. Tanimoto, Okayama Lung Cancer Study Group, A phase I study of combination S-1 plus cisplatin chemotherapy with concurrent thoracic radiation for locally advanced non-small cell lung cancer, *Lung Cancer* 65 (2009) 74–79.
- [22] N. Takigawa, K. Kiura, K. Hotta, S. Hosokawa, N. Nogami, K. Aoe, K. Gemba, K. Fujiwara, S. Harita, M. Takemoto, K. Hime, T. Shinkai, Y. Fujiwara, S. Takata, M. Tabata, S. Kanazawa, M. Tanimoto, Okayama Lung Cancer Study Group, A phase I study of S-1 with concurrent thoracic radiotherapy in elderly patients with localized advanced non-small cell lung cancer, *Lung Cancer* 71 (2011) 60–64.
- [23] K. Aoe, N. Takigawa, K. Hotta, T. Maeda, D. Kishino, N. Nogami, M. Tabata, S. Harita, T. Okada, T. Kubo, S. Hosokawa, K. Fujiwara, K. Gemba, M. Yasugi, T. Kozuki, Y. Kato, K. Katsui, S. Kanazawa, H. Ueoka, M. Tanimoto, K. Kiura, A phase II study of S-1 chemotherapy with concurrent thoracic radiotherapy in elderly patients with locally advanced non-small-cell lung cancer: the Okayama Lung Cancer Study Group Trial 0801, *Eur. J. Cancer* 50 (2014) 2783–2790.
- [24] N. Nogami, N. Takigawa, K. Hotta, Y. Segawa, Y. Kato, T. Kozuki, I. Oze, D. Kishino, K. Aoe, H. Ueoka, S. Kuyama, S. Harita, T. Okada, S. Hosokawa, K. Inoue, K. Gemba, T. Shibayama, M. Tabata, M. Takemoto, S. Kanazawa, M. Tanimoto, K. Kiura, A phase II study of cisplatin plus S-1 with concurrent thoracic radiotherapy for locally advanced non-small-cell lung cancer: the Okayama Lung Cancer Study Group Trial 0501, *Lung Cancer* 87 (2015) 141–147.
- [25] Y. Segawa, K. Kiura, K. Hotta, N. Takigawa, M. Tabata, K. Matsuo, H. Yoshioka, H. Hayashi, H. Kawai, K. Aoe, T. Maeda, H. Ueoka, M. Tanimoto, A randomized phase II study of a combination of docetaxel and S-1 versus docetaxel monotherapy in patients with non-small cell lung cancer previously treated with platinum-based chemotherapy: results of Okayama Lung Cancer Study Group (OLCSG) Trial 0503, *J. Thorac. Oncol.* 5 (2010) 1430–1434.
- [26] A. Bonanomi, D. Kojic, B. Giger, Z. Rickenbach, L. Jean-Richard-Dit-Bressel, C. Berger, F.K. Niggli, D. Nadal, Quantitative cytokine gene expression in human tonsils at excision and during histoculture assessed by standardized and calibrated real-time PCR and novel data processing, *J. Immunol. Methods* 283 (2003) 27–43.
- [27] S. Pérez, L.J. Royo, A. Astudillo, D. Escudero, F. Alvarez, A. Rodríguez, E. Gómez, J. Otero, Identifying the most suitable endogenous control for determining gene expression in hearts from organ donors, *BMC Mol. Biol.* 8 (2007) 114.
- [28] N. Takigawa, Y. Segawa, D. Kishino, K. Fujiwara, Y. Tokuda, N. Seki, T. Shinkai, Y. Watanabe, S. Hiraki, T. Kozuki, K. Gemba, M. Tabata, K. Kiura, H. Ueoka, M. Tanimoto, Clinical and pharmacokinetic study of docetaxel in elderly non-small-cell lung cancer patients, *Cancer Chemother. Pharmacol.* 54 (2004) 230–236.
- [29] H. Yoshioka, I. Okamoto, S. Morita, M. Ando, K. Takeda, T. Seto, N. Yamamoto, H. Saka, S. Atagi, T. Hirashima, S. Kudoh, M. Satouchi, N. Ikeda, Y. Iwamoto, T. Sawa, Y. Nakanishi, K. Nakagawa, Efficacy and safety analysis according to histology for S-1 in combination with carboplatin as first-line chemotherapy in patients with advanced non-small-cell lung cancer: updated results of the West Japan Oncology Group LETS study, *Ann. Oncol.* 24 (2013) 1326–1331.
- [30] G.A. Masters, S. Temin, C.G. Azzoli, G. Giaccone, S. Baker, J.R. Brahmer, P.M. Ellis, A. Gajra, N. Rackear, J.H. Schiller, T.J. Smith, J.R. Straw, D. Trent, D.H. Johnson, American society of clinical oncology clinical practice, systemic therapy for stage IV non-small-cell lung cancer: american society of clinical oncology clinical practice guideline update, *J. Clin. Oncol.* 33 (2015) 3488–3515.
- [31] E. Quoix, G. Zalcman, J.-P. Oster, V. Westeel, E. Pichon, A. Lavolé, J. Dauba, D. Debieuvre, P.-J. Souquet, L. Bigay-Game, E. Dansin, M. Poudenx, O. Molinier, F. Vaylet, D. Moro-Sibilot, D. Herman, J. Bennouna, J. Tredaniel, A. Ducolomé, M.-P. Lebitas, L. Baudrin, S. Laporte, B. Milleron, Intergroupe Francophone de Cancérologie Thoracique, Carboplatin and weekly paclitaxel doublet chemotherapy compared with monotherapy in elderly patients with advanced non-small-cell lung cancer: IFCT-0501 randomised, phase 3 trial, *Lancet* 378 (2011) 1079–1088.
- [32] Y.-M. Chen, R.-P. Perng, J.-F. Shih, J. Whang-Peng, A phase II randomized study of vinorelbine alone or with cisplatin against chemo-naïve inoperable non-small cell lung cancer in the elderly, *Lung Cancer* 61 (2008) 214–219.
- [33] K. Tamura, I. Okamoto, T. Ozaki, T. Kashii, K. Takeda, M. Kobayashi, K. Matsui, T. Shibata, T. Kurata, K. Nakagawa, M. Fukuoka, Phase I/II study of S-1 plus carboplatin in patients with advanced non-small cell lung cancer, *Eur. J. Cancer* 45 (2009) 2132–2137.
- [34] K. Kaira, N. Sunaga, N. Yanagitani, H. Imai, M. Utsugi, Y. Iwasaki, K. Shimizu, H. Iijima, H. Tsurumaki, Y. Tomizawa, T. Hisada, T. Ishizuka, R. Saito, M. Mori, Phase 2 study of S-1 plus carboplatin in patients with advanced non-small cell lung cancer, *Lung Cancer* 68 (2010) 253–257.
- [35] A. Sekine, H. Satoh, T. Baba, S. Ikeda, R. Okuda, T. Shinohara, S. Komatsu, E. Hagiwara, T. Iwasawa, T. Ogura, T. Kato, Safety and efficacy of S-1 in combination with carboplatin in non-small cell lung cancer patients with interstitial lung disease: a pilot study, *Cancer Chemother. Pharmacol.* 77 (2016) 1245–1252.
- [36] T. Miyoshi, K. Kondo, H. Toba, M. Yoshiida, H. Fujino, K. Kenzaki, S. Sakiyama, M. Takehisa, A. Tangoku, Predictive value of thymidylate synthase and dihydropyrimidine dehydrogenase expression in tumor tissue, regarding the efficacy of

- postoperatively administered UFT (tegafur + uracil) in patients with non-small cell lung cancer, *Anticancer Res.* 27 (2007) 2641–2648.
- [37] P.P. Grimminger, P.M. Schneider, R. Metzger, D. Vallböhmer, A.H. Hölscher, P.V. Danenberg, J. Brabender, Low thymidylate synthase, thymidine phosphorylase, and dihydropyrimidine dehydrogenase mRNA expression correlate with prolonged survival in resected non-small-cell lung cancer, *Clin. Lung Cancer* 11 (2010) 328–334.
- [38] M. Takeda, I. Okamoto, N. Hirabayashi, M. Kitano, K. Nakagawa, Thymidylate synthase and dihydropyrimidine dehydrogenase expression levels are associated with response to S-1 plus carboplatin in advanced non-small cell lung cancer, *Lung Cancer* 73 (2011) 103–109.
- [39] W. Ichikawa, T. Takahashi, K. Suto, Y. Shirota, Z. Nihei, M. Shimizu, Y. Sasaki, R. Hirayama, Simple combinations of 5-FU pathway genes predict the outcome of metastatic gastric cancer patients treated by S-1, *Int. J. Cancer* 119 (2006) 1927–1933.
- [40] T. Sumizawa, T. Furukawa, M. Haraguchi, A. Yoshimura, A. Takeyasu, M. Ishizawa, Y. Yamada, S. Akiyama, Thymidine phosphorylase activity associated with platelet-derived endothelial cell growth factor, *J. Biochem.* 114 (1993) 9–14.
- [41] K. Miyadera, T. Sumizawa, M. Haraguchi, H. Yoshida, W. Konstanty, Y. Yamada, S. Akiyama, Role of thymidine phosphorylase activity in the angiogenic effect of platelet derived endothelial cell growth factor/thymidine phosphorylase, *Cancer Res.* 55 (1995) 1687–1690.
- [42] K. Reynolds, F. Farzaneh, W.P. Collins, S. Campbell, T.H. Bourne, F. Lawton, A. Moghaddam, A.L. Harris, R. Bicknell, Association of ovarian malignancy with expression of platelet-derived endothelial cell growth factor, *J. Natl. Cancer Inst.* 86 (1994) 1234–1238.
- [43] K. Maeda, Y.S. Chung, Y. Ogawa, S. Takatsuka, S.M. Kang, M. Ogawa, T. Sawada, N. Onoda, Y. Kato, M. Sowa, Thymidine phosphorylase/platelet-derived endothelial cell growth factor expression associated with hepatic metastasis in gastric carcinoma, *Br. J. Cancer* 73 (1996) 884–888.
- [44] Y. Takebayashi, S. Akiyama, S. Akiba, K. Yamada, K. Miyadera, T. Sumizawa, Y. Yamada, F. Murata, T. Aikou, Clinicopathologic and prognostic significance of an angiogenic factor thymidine phosphorylase, in human colorectal carcinoma, *J. Natl. Cancer Inst.* 88 (1996) 1110–1117.
- [45] T.S. O'Brien, S.B. Fox, A.J. Dickinson, H. Turley, M. Westwood, A. Moghaddam, K.C. Gatter, R. Bicknell, A.L. Harris, Expression of the angiogenic factor thymidine phosphorylase/platelet-derived endothelial cell growth factor in primary bladder cancers, *Cancer Res.* 56 (1996) 4799–4804.
- [46] Y. Imazano, Y. Takebayashi, K. Nishiyama, S. Akiba, K. Miyadera, Y. Yamada, S. Akiyama, Y. Ohi, Correlation between thymidine phosphorylase expression and prognosis in human renal cell carcinoma, *J. Clin. Oncol.* 15 (1997) 2570–2578.
- [47] S. Suzuki, M. Karayama, N. Inui, T. Fujisawa, N. Enomoto, Y. Nakamura, S. Kuroishi, H. Matsuda, K. Yokomura, N. Koshimizu, M. Toyoshima, S. Imokawa, K. Asada, M. Masuda, T. Yamada, H. Watanabe, T. Suda, Continuation maintenance therapy with S-1 in chemotherapy-naïve patients with advanced squamous cell lung cancer, *Invest. New Drugs* 34 (2016) 490–496.
- [48] G. Nakayama, Y. Kodera, H. Yokoyama, N. Okuda, T. Watanabe, C. Tanaka, N. Iwata, N. Ohashi, M. Koike, M. Fujiwara, A. Nakao, Modified FOLFOX6 with oxaliplatin stop-and-go strategy and oral S-1 maintenance therapy in advanced colorectal cancer: CCOG-0704 study, *Int. J. Clin. Oncol.* 16 (2011) 506–511.
- [49] H. Shinchi, K. Maemura, Y. Mataki, H. Kurahara, M. Sakoda, S. Ueno, Y. Hiraki, M. Nakajo, S. Natsugoe, S. Takao, A phase II study of oral S-1 with concurrent radiotherapy followed by chemotherapy with S-1 alone for locally advanced pancreatic cancer, *J. Hepatobiliary Pancreat. Sci.* 19 (2012) 152–158.
- [50] Y. Urata, I. Okamoto, M. Takeda, Y. Hattori, K. Okuno, T. Shimada, T. Kurata, H. Kaneda, M. Miyazaki, M. Terashima, K. Tanaka, S. Morita, K. Nakagawa, S. Negoro, M. Satouchi, Phase 2 study of S-1 and carboplatin plus bevacizumab followed by maintenance S-1 and bevacizumab for chemotherapy-naïve patients with advanced nonsquamous non-small cell lung cancer, *Cancer* 119 (2013) 2275–2281.
- [51] Q.H. Ke, S.Q. Zhou, J.Y. Yang, W. Du, G. Liang, Y. Lei, F. Luo, S-1 plus gemcitabine chemotherapy followed by concurrent radiotherapy and maintenance therapy with S-1 for unresectable pancreatic cancer, *World J. Gastroenterol.* 20 (2014) 13987–13992.
- [52] N. Okumura, M. Sonobe, K. Okabe, H. Nakamura, M. Kataoka, M. Yamashita, M. Nakata, K. Kataoka, Y. Yamashita, J. Soh, H. Yoshioka, K. Hotta, K. Matsuo, J. Sakamoto, S. Toyooka, H. Date, Feasibility of adjuvant chemotherapy with S-1 plus carboplatin followed by single-agent maintenance therapy with S-1 for completely resected non-small-cell lung cancer: results of the Setouchi Lung Cancer Group Study 1001, *Int. J. Clin. Oncol.* 22 (2017) 274–282.

Case Report

Esophagobronchial Fistula in a Patient with Squamous Cell Carcinoma of the Lung: A Case Report

Taichi Ozeki^a Michiko Asano^b Nobukazu Fujimoto^c Jun Nishimura^a
Kenji Takada^a Yosuke Miyamoto^b Yasuko Fuchimoto^b Sae Wada^b
Shinji Ozaki^b Takumi Kishimoto^a

^aDepartment of Medicine, Okayama Rosai Hospital, Okayama, Japan; ^bDepartment of Pulmonary Medicine, Okayama Rosai Hospital, Okayama, Japan; ^cDepartment of Medical Oncology, Okayama Rosai Hospital, Okayama, Japan

Keywords

Fistula · Squamous cell carcinoma · Chemoradiotherapy · Cisplatin · Docetaxel · Lung tumor

Abstract

A 73-year-old man was referred to our hospital after a 2-week history of bloody sputum and cough. Computed tomography (CT) images of the chest showed a mass grouped with mediastinal lymph nodes, and bronchoscopy showed a projecting mass in the right main bronchus. After a transbronchial biopsy, the patient was diagnosed with squamous cell carcinoma (T4N2M0 stage IIIB). The patient was treated with systemic chemotherapy, consisting of cisplatin (40 mg/m², days 1 and 8) and docetaxel (30 mg/m², days 1 and 8), and concurrent thoracic irradiation at a daily dose of 2 Gy. On day 35 of treatment, the patient complained of a sore throat and cough. A CT of the chest showed punctate low-attenuation foci between the esophagus and bronchus. Gastrointestinal endoscopy and bronchoscopy demonstrated a fistula in the middle intrathoracic esophagus and the left main bronchus. The patient's symptoms gradually improved, and the fistula was closed after the suspension of chemoradiotherapy. Radiotherapy was resumed and completed on day 82. However, on day 108, he developed a fever and cough, and a tumor with fistula was revealed in the right main bronchus. He had an esophageal stent inserted, but he later died of sudden hemoptysis.

© 2017 The Author(s)
Published by S. Karger AG, Basel

Introduction

An esophagobronchial fistula represents a connection between the esophagus and the bronchus, resulting from direct neoplastic infiltration and necrosis between the esophagus, bronchi, and mediastinum [1]. A fistula could also be induced by necrosis or cytoreduction of the tumor, though there is no clear evidence that treatment modalities such as chemotherapy or radiotherapy increase the incidence of fistula formation [2]. We report on a patient with squamous cell carcinoma of the lung who developed an esophagobronchial fistula twice in his clinical course. The first one developed during chemoradiotherapy, and the second one was thought to be due to extension of the tumor.

Case Report

A 72-year-old Japanese man was referred to our hospital after 2 weeks of bloody sputum and cough. He had a history of hypertension but was not treated with medication. He had smoked between the ages of 20 and 72 years, and had been exposed to asbestos at shipyards for 15 years. Physical examination revealed a slight wheeze in the bilateral lungs, and no superficial lymph nodes were palpated. A blood test revealed elevated white blood cells, C-reactive protein, and serum calcium levels. Tumor markers were slightly elevated in carcinoembryonic antigen (13.4 ng/mL) and cytokeratin 19 fragment (12.9 ng/mL). Computed tomography (CT) of the chest showed a 60-mm mass grouped with mediastinal lymph nodes, which invaded the right main bronchus (Fig 1a, b). After a transbronchial biopsy of the mass, the diagnosis of squamous cell carcinoma was made. The staging workup, including magnetic resonance imaging of the brain and whole-body fluorine-18 2-fluoro-2-deoxy-d-glucose positron emission tomography, revealed his disease as cT4N2M0, stage IIIB.

The patient was treated with systemic chemotherapy, consisting of cisplatin (40 mg/m², days 1 and 8) and docetaxel (30 mg/m², days 1 and 8), and concurrent thoracic irradiation at a daily dose of 2 Gy. On day 35 of treatment, he complained of a sore throat and cough, and a CT of the chest showed punctate low-attenuation foci between the esophagus and bronchus (Fig. 1c). Gastrointestinal endoscopy and bronchoscopy demonstrated a fistula in the middle intrathoracic esophagus and the left main bronchus, respectively (Fig. 2a, b). After the suspension of chemoradiotherapy and abstaining from eating, his symptoms gradually improved and the fistula was closed on day 52 (Fig. 2c). Radiotherapy at 2 Gy was resumed every other day and 60 Gy was completed on day 82. The fistula remained closed and the patient was discharged after the second course of chemotherapy.

However, he was referred to our hospital for a sore throat and fever again on day 108. A CT of the chest showed a clear connection between the esophagus and the right main bronchus (Fig. 3a), and there was ground glass opacity spread in the right lower lung. Bronchoscopy demonstrated a mass with the fistula in the right main bronchus (Fig. 3b). Pathological analyses of the mass showed poorly differentiated squamous cell carcinoma. Based on these findings, the patient was diagnosed with a relapse of the cancer. He had an esophageal stent inserted; however, he died of sudden hemoptysis on day 146. An autopsy was not allowed.

Discussion

The development of an esophagobronchial fistula is a devastating and life-threatening complication. The incidence of fistula in lung cancer is rare compared with that in esophageal cancer (0.16 vs. 4.9%). A fistula may occur in lung cancer when the tumor makes contact with the esophagus [2]. In the current case, the tumor was located in the mediastinal space and close to the middle intrathoracic esophagus. The first fistula was considered the result of tumor necrosis and damage to the mucous membrane induced by chemoradiotherapy, because the fistula developed in the left main bronchus and the initial tumor in the right main bronchus disappeared at that time. This speculation was also supported by the finding that the fistula improved after 3 weeks' interruption of chemoradiotherapy. On the other hand, the second fistula was considered the result of tumor progression, because the fistula was associated with a tumor that had the same histology as the initial tumor. To our knowledge, this is the first report of an esophagobronchial fistula developing twice in 1 patient by different mechanisms.

An esophagobronchial fistula is a serious complication and the survival time is around 8 months [3]. Direct surgical closure, chemotherapy, and radiotherapy [4] may be used to close the fistula. However, the utility of these treatments was not established, and stent insertion is currently recommended in such situations for symptomatic relief [5]. An esophageal stent was inserted in the current case; however, long-term symptomatic relief was not obtained due to massive hemoptysis.

Chemoradiotherapy is a standard treatment option for locally advanced lung cancer [6], even in cases where the tumor is located close to or invades the esophagus. In such cases, physicians should be extremely cautious about the development of esophagobronchial fistula during and after treatment. In addition to the CT scanning, gastrointestinal endoscopy, before and during treatment, might be considered for early detection of a fistula. In conclusion, we reported a case of squamous cell carcinoma of the lung in a patient who twice developed an esophagobronchial fistula that was caused by different mechanisms.

Acknowledgement

This study was supported by The Research, Development, and Dissemination of Projects Related to Nine Fields of Occupational Injuries and Illnesses of the Japan Labour Health and Welfare Organization and by grants-in-aid from the Ministry of Health, Labor and Welfare, Japan.

Statement of Ethics

The authors have no ethical conflicts to disclose.

Disclosure Statement

The authors declare that they have no conflict of interest.

References

- 1 Chan KP, Eng P, Hsu AA, Huat GM, Chow M: Rigid bronchoscopy and stenting for esophageal cancer causing airway obstruction. *Chest* 2002;122:1069–1072.
- 2 Martini N, Goodner JT, D'Angio GJ, Beattie EJ Jr: Tracheoesophageal fistula due to cancer. *J Thorac Cardiovasc Surg* 1970;59:319–324.
- 3 Herth FJ, Peter S, Baty F, Eberhardt R, Leuppi JD, Chhajed PN: Combined airway and oesophageal stenting in malignant airway-oesophageal fistulas: a prospective study. *Eur Respir J* 2010;36:1370–1374.
- 4 Yamada S, Takai Y, Ogawa Y, Kakuto Y, Sakamoto K: Radiotherapy for malignant fistula to other tract. *Cancer* 1989;64:1026–1028.
- 5 Kvale PA, Simoff M, Prakash UB; American College of Chest Physicians: Lung cancer. Palliative care. *Chest* 2003;123(suppl):284S–311S.
- 6 Segawa Y, Kiura K, Takigawa N, Kamei H, Harita S, Hiraki S, Watanabe Y, Sugimoto K, Shibayama T, Yonei T, Ueoka H, Takemoto M, Kanazawa S, Takata I, Nogami N, Hotta K, Hiraki A, Tabata M, Matsuo K, Tanimoto M: Phase III trial comparing docetaxel and cisplatin combination chemotherapy with mitomycin, vindesine, and cisplatin combination chemotherapy with concurrent thoracic radiotherapy in locally advanced non-small-cell lung cancer: OLCSG 0007. *J Clin Oncol* 2010;28:3299–3306.

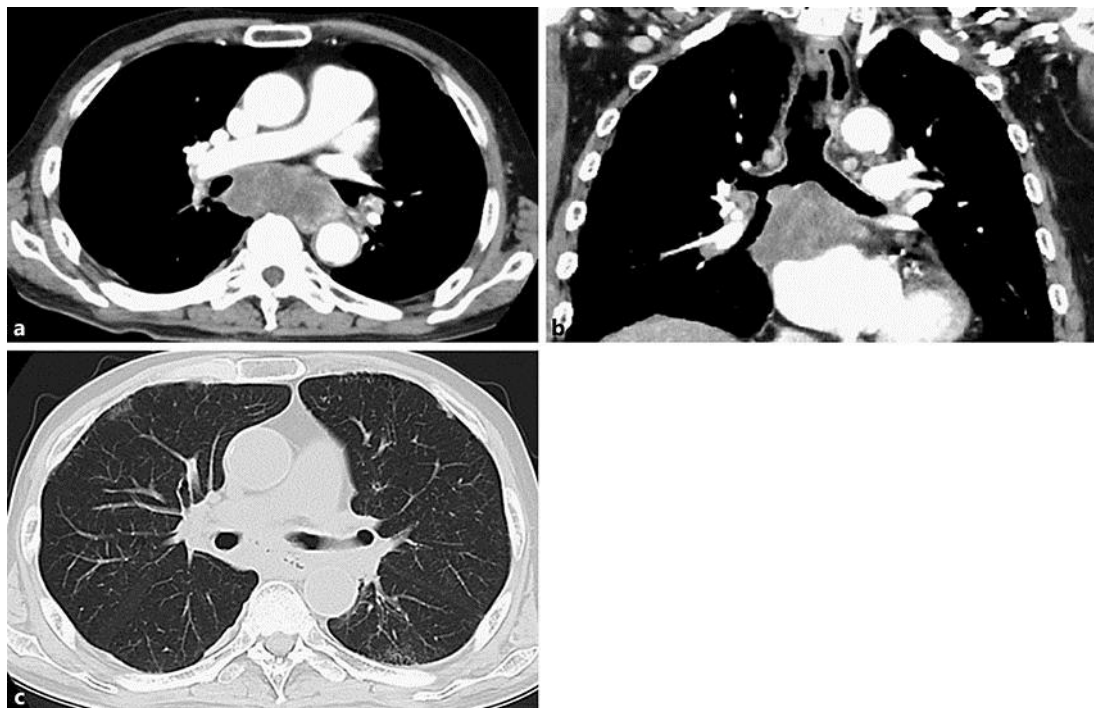


Fig. 1. Computed tomography (CT) of the chest at the initial presentation showing a mass grouped with mediastinal lymph nodes, which invaded the right main bronchus: axial view (a) and coronal view (b). c The CT of the chest on day 35 of treatment demonstrated punctate low-attenuation foci between the esophagus and bronchus.

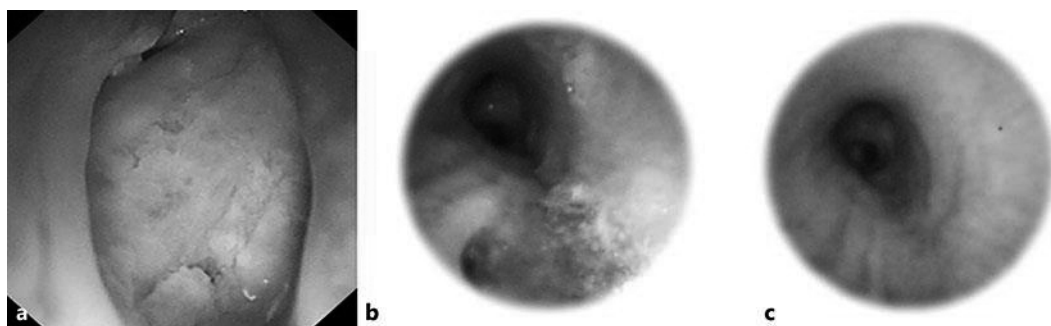


Fig. 2. Gastrointestinal endoscopy and bronchoscopy demonstrated a fistula in the middle intrathoracic esophagus (a) and the left main bronchus (b), respectively. After the suspension of chemoradiotherapy and abstaining from eating, the fistula was closed (c).

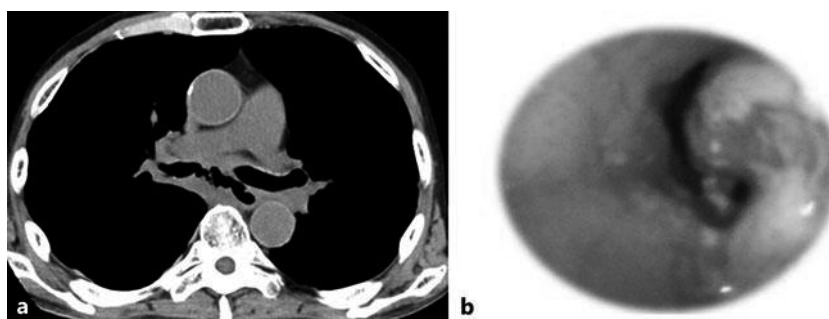


Fig. 3. a Computed tomography of the chest on day 108, showing a connection between the esophagus and the right main bronchus. b Bronchoscopy demonstrated a tumor with the fistula in the right main bronchus.

Case Report

Adenocarcinoma of the Lung Acquiring Resistance to Afatinib by Transformation to Small Cell Carcinoma: A Case Report

Jun Nishimura^a Yosuke Miyamoto^b Nobukazu Fujimoto^c Taichi Ozeki^a
Kenji Takada^a Michiko Asano^b Yasuko Fuchimoto^b Sae Wada^b
Shinji Ozaki^b Takumi Kishimoto^a

^aDepartment of Medicine, Okayama Rosai Hospital, Okayama, Japan; ^bDepartment of Pulmonary Medicine, Okayama Rosai Hospital, Okayama, Japan; ^cDepartment of Medical Oncology, Okayama Rosai Hospital, Okayama, Japan

Keywords

Adenocarcinoma · Afatinib · Small cell carcinoma · Irinotecan · Drug resistance · Transformation

Abstract

A 65-year-old woman visited our hospital due to right chest pain and dyspnea on exertion. Chest radiography revealed decreased permeability of the right lung. Computed tomography demonstrated a huge mass in the right upper lobe and right pleural effusion. Right pleural effusion cytology yielded a diagnosis of adenocarcinoma and was positive for mutation of epidermal growth factor receptor (EGFR; exon 21 L858R). Afatinib was selected for the initial treatment. Multiple tumors regressed remarkably, but then rapidly progressed 3 months later. We performed re-biopsy to detect the mechanism of resistance to afatinib. Histopathology revealed a mixture of small cell carcinoma (SCC) and adenocarcinoma harboring same EGFR mutation. To the best of our knowledge, this is the first report of transformation to SCC after treatment with afatinib.

© 2017 The Author(s)
Published by S. Karger AG, Basel

Introduction

Lung cancers harboring epidermal growth factor receptor (EGFR) mutations usually respond to EGFR tyrosine kinase inhibitors (TKIs), but most acquire resistance [1, 2]. Transformation of the tumor has been reported to be one of the mechanisms of acquired resistance after treatment with first-generation EGFR-TKIs [3]. However, few reports have described transformation during treatment with the second-generation EGFR-TKI afatinib [4]. We report a case of adenocarcinoma of the lung that acquired resistance to afatinib via transformation to small cell carcinoma (SCC).

Case Report

A 65-year-old woman visited our hospital due to right chest pain and dyspnea on exertion. A chest radiograph revealed decreased permeability of the right lung (Fig. 1a). Computed tomography (CT) demonstrated a huge mass in the right upper lobe (Fig. 1b) and right pleural effusion. In addition, multiple masses were detected on the left lung, liver, and left adrenal gland, as well as mediastinal lymphadenopathy. Pathological examination of the right pleural effusion and a transbronchial biopsy from the right upper bronchus yielded a diagnosis of adenocarcinoma of the lung. Because an EGFR mutation (exon 21 L858R) was detected, treatment with afatinib was initiated.

Multiple tumors remarkably regressed in 1 month, but paronychia (grade 3) appeared in 2 months. Due to difficulties in daily life, the treatment was interrupted for 2 weeks. CT images 3 months after the initial treatment demonstrated growth of the tumors in the lung. We performed another transbronchial biopsy to determine the mechanisms of resistance to afatinib. Histopathological examination revealed a mixture of SCC and adenocarcinoma (Fig. 2) harboring the same EGFR mutation as the initial biopsy specimen. Systemic chemotherapy consisting of cisplatin and irinotecan was administered, but no tumor regression was evident and carcinomatous pericarditis occurred. In addition, the patient complained of consciousness disorder and convulsions. Lumbar puncture identified adenocarcinoma cells in the cerebrospinal fluid. The patient was diagnosed with carcinomatous meningitis and erlotinib treatment was administered. However, no symptomatic improvement occurred and the patient died 5 months after the initial diagnosis. Autopsy was not allowed.

Discussion

In lung cancers harboring EGFR mutations, EGFR-TKIs demonstrate a favorable response, but drug resistance emerges in most cases. A transformation of adenocarcinoma to SCC is one of the resistance mechanisms in first-generation EGFR-TKIs and occurs in 14% of resistant cases, in which the same EGFR mutation is found before and after the changes [5]. An amplification of MET, a high affinity tyrosine kinase receptor for hepatocyte growth factor, and a T790M mutation have been reported as resistance mechanisms of the second-generation EGFR-TKI afatinib [4]. However, to the best of our knowledge, this is the first report of transformation to SCC after afatinib treatment.

In the current case, SCC cells were found 3 months after the initial treatment with afatinib. After the chemotherapy for SCC, the carcinomatous meningitis progressed rapidly. Thus, we hypothesized that a very early stage of SCC development was observed in the cur-

rent case. Although there is a possibility that adenocarcinoma and SCC coexisted from the initial diagnosis, a transbronchial biopsy from the same spot demonstrated adenocarcinoma alone at the time of the initial diagnosis and adenocarcinoma and SCC at the re-biopsy. We consider these findings to support our hypothesis.

When resistance to an EGFR-TKI occurs in lung cancer harboring an EGFR mutation, re-biopsy is recommended to reveal the resistance mechanisms. For cases with a T790M mutation in exon 20, osimertinib has been reported to be a promising treatment option [6]. Recently, the utility of liquid biopsy has been reported for the detection of the T790M mutation [7]. However, to date, SCC transformation cannot be detected by liquid biopsy. In cases in which EGFR-TKI treatment fails, re-biopsy should be applied to reveal the resistance mechanisms and aid in the selection an appropriate treatment.

Favorable results of systemic chemotherapy consisting of platinum and etoposide or irinotecan have been reported in cases of SCC transformation [8], but little response was observed in the current case and the adenocarcinoma progressed rapidly. The effect of EGFR-TKIs for transformed SCC is reported to be limited [9]. A treatment strategy for transformed SCC and existing adenocarcinoma should be established.

In conclusion, we reported a case of EGFR-mutated adenocarcinoma of the lung that transformed to SCC.

Acknowledgments

This work was supported by “the research and development and the dissemination projects related to the 9 fields of occupational injuries and illnesses” of the Japan Labour Health and Welfare Organization and by grants-in-aid from the Ministry of Health, Labor and Welfare, Japan.

Statement of Ethics

The authors have no ethical conflicts to disclose.

Disclosure Statement

The authors have no conflicts of interest to declare.

References

- 1 Maemondo M, Minegishi Y, Inoue A, Kobayashi K, Harada M, Okinaga S, Morikawa N, Oizumi S, Tanaka T, Isobe H, Kudoh S, Hagiwara K, Nukiwa T, Gemma A: First-line gefitinib in patients aged 75 or older with advanced non-small cell lung cancer harboring epidermal growth factor receptor mutations: NEJ 003 study. *J Thorac Oncol* 2012;7:1417–1422.
- 2 Rosell R, Carcereny E, Gervais R, Vergnenegre A, Massuti B, Felip E, Palmero R, Garcia-Gomez R, Pallares C, Sanchez JM, Porta R, Cobo M, Garrido P, Longo F, Moran T, Insa A, De Marinis F, Corre R, Bover I, Illiano A, Dansin E, de Castro J, Millela M, Reguart N, Altavilla G, Jimenez U, Provencio M, Moreno MA, Terrasa J, Munoz-Langa J, Valdivia J, Isla D, Domine M, Molinier O, Mazieres J, Baize N, Garcia-Campelo R, Robinet G, Rodriguez-Abreu D, Lopez-Vivanco G, Gebbia V, Ferrera-Delgado L, Bombaron P, Bernabe R, Bearz A, Artal A, Cortesi E, Rolfo C, Sanchez-Ronco M, Drozdowskyj A, Queralt C, de Aguirre I, Ramirez JL, Sanchez JJ, Molina MA, Taron M, Paz-Ares L: Erlotinib versus standard chemotherapy as

- first-line treatment for European patients with advanced EGFR mutation-positive non-small-cell lung cancer (EURTAC): a multicentre, open-label, randomised phase 3 trial. *Lancet Oncol* 2012;13:239–246.
- 3 Yu HA, Arcila ME, Rekhtman N, Sima CS, Zakowski MF, Pao W, Kris MG, Miller VA, Ladanyi M, Riely GJ: Analysis of tumor specimens at the time of acquired resistance to EGFR-TKI therapy in 155 patients with EGFR-mutant lung cancers. *Clin Cancer Res* 2013;19:2240–2247.
- 4 Wu SG, Liu YN, Tsai MF, Chang YL, Yu CJ, Yang PC, Yang JC, Wen YF, Shih JY: The mechanism of acquired resistance to irreversible EGFR tyrosine kinase inhibitor-afatinib in lung adenocarcinoma patients. *Oncotarget* 2016;7:12404–12413.
- 5 Sequist LV, Waltman BA, Dias-Santagata D, Digumarthy S, Turke AB, Fidias P, Bergethon K, Shaw AT, Gettinger S, Cosper AK, Akhavanfard S, Heist RS, Temel J, Christensen JG, Wain JC, Lynch TJ, Vernovsky K, Mark EJ, Lanuti M, Iafrate AJ, Mino-Kenudson M, Engelman JA: Genotypic and histological evolution of lung cancers acquiring resistance to EGFR inhibitors. *Sci Transl Med* 2011;3:75ra26.
- 6 Mok TS, Wu YL, Ahn MJ, Garassino MC, Kim HR, Ramalingam SS, Shepherd FA, He Y, Akamatsu H, Theelen WS, Lee CK, Sebastian M, Templeton A, Mann H, Marotti M, Ghiorghiu S, Papadimitrakopoulou VA: Osimertinib or platinum-pemetrexed in EGFR T790M-positive lung cancer. *N Engl J Med* 2017;376:629–640.
- 7 Sueoka-Aragane N, Katakami N, Satouchi M, Yokota S, Aoe K, Iwanaga K, Otsuka K, Morita S, Kimura S, Negoro S: Monitoring EGFR T790M with plasma DNA from lung cancer patients in a prospective observational study. *Cancer Sci* 2016;107:162–167.
- 8 Oser MG, Niederst MJ, Sequist LV, Engelman JA: Transformation from non-small-cell lung cancer to small-cell lung cancer: molecular drivers and cells of origin. *Lancet Oncol* 2015;16:e165–e172.
- 9 Niederst MJ, Sequist LV, Poirier JT, Mermel CH, Lockerman EL, Garcia AR, Katayama R, Costa C, Ross KN, Moran T, Howe E, Fulton LE, Mulvey HE, Bernardo LA, Mohamoud F, Miyoshi N, VanderLaan PA, Costa DB, Janne PA, Borger DR, Ramaswamy S, Shioda T, Iafrate AJ, Getz G, Rudin CM, Mino-Kenudson M, Engelman JA: RB loss in resistant EGFR mutant lung adenocarcinomas that transform to small-cell lung cancer. *Nat Commun* 2015;6:6377.

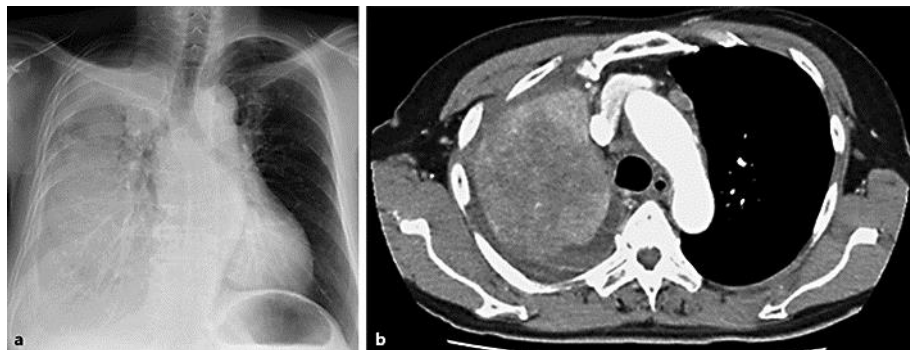


Fig. 1. **a** Chest radiograph showing decreased permeability of the right lung. **b** CT image of the chest demonstrating a huge mass in the right lung and right pleural effusion.

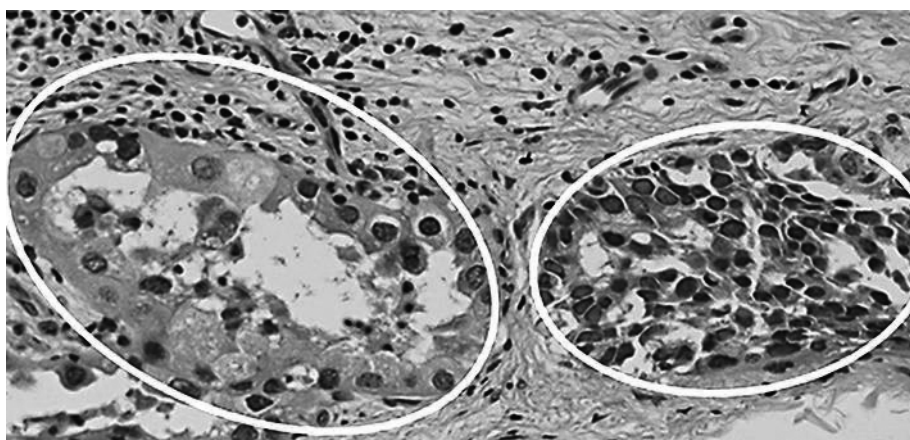


Fig. 2. Pathological analysis of the transbronchial re-biopsy specimen revealed adenocarcinoma (left circle) and small cell carcinoma (right circle).

Association of immunoglobulin G4 and free light chain with idiopathic pleural effusion

Y. Murata,^{*†‡} K. Aoe,^{*}
Y. Mimura-Kimura ,^{*}
T. Murakami,^{*} K. Oishi,^{*†‡}
T. Matsumoto,^{*} H. Ueoka,^{*}
K. Matsunaga,[§] M. Yano[‡] and
Y. Mimura ,^{*}

^{*}The Department of Clinical Research, [†]The Department of Respiratory Medicine, National Hospital Organization Yamaguchi-Ube Medical Center, Ube, Japan, [‡]Division of Cardiology, The Department of Medicine and Clinical Science, and [§]The Department of Respiratory Medicine and Infectious Disease, Yamaguchi University Graduate School of Medicine, Ube, Japan

Summary

The cause of pleural effusion remains uncertain in approximately 15% of patients despite exhaustive evaluation. As recently described immunoglobulin (Ig)G4-related disease is a fibroinflammatory disorder that can affect various organs, including the lungs, we investigate whether idiopathic pleural effusion includes IgG4-associated etiology. Between 2000 and 2012, we collected 830 pleural fluid samples and reviewed 35 patients with pleural effusions undiagnosed after pleural biopsy at Yamaguchi-Ube Medical Center. Importantly, IgG4 immunostaining revealed infiltration of IgG4-positive plasma cells in the pleura of 12 patients (34%, IgG4⁺ group). The median effusion IgG4 level was 41 mg/dl in the IgG4⁺ group and 27 mg/dl in the IgG4⁻ group ($P < 0.01$). The light and heavy chains of effusion IgG4 antibodies of patients in the IgG4⁺ group were heterogeneous by two-dimensional electrophoresis, indicating the absence of clonality of the IgG4 antibodies. Interestingly, the κ light chains were more heterogeneous than the λ light chains. The measurement of the κ and λ free light chain (FLC) levels in the pleural fluids showed significantly different κ FLC levels (median: 28.0 *versus* 9.1 mg/dl, $P < 0.01$) and κ/λ ratios (median: 2.0 *versus* 1.2, $P < 0.001$) between the IgG4⁺ and IgG4⁻ groups. Furthermore, the κ/λ ratios were correlated with the IgG4⁺/IgG⁺ plasma cell ratios in the pleura of the IgG4⁺ group. Taken together, these results demonstrate the involvement of IgG4 in certain idiopathic pleural effusions and provide insights into the diagnosis, pathogenesis and therapeutic opportunities of IgG4-associated pleural effusion.

Keywords: fibrinous pleuritis, free light chain, IgG4-related disease, pleural effusion

Accepted for publication 13 June 2017
Correspondence: Y. Mimura, Department of Clinical Research, NHO Yamaguchi-Ube Medical Center, 685 Higashi-Kiwa, Ube, 755-0241, Japan.
E-mail: mimuray@yamaguchi-hosp.jp

Introduction

Pleural effusion remains common, originating from a wide range of pathologies including congestive heart failure, pneumonia and cancer [1]. A diagnostic algorithm for the differentiation of a pleural effusion proposed by Light *et al.* has been widely accepted [2] and recommended in the British Thoracic Society pleural disease guideline [3]. Nonetheless, the cause of the pleural effusion remains unclear in a substantial percentage of patients with persistently exudative effusions after the history, physical examination and biochemical and cytological tests of pleural fluid [4–6]. No diagnosis has been established for up to 15% of patients, despite invasive procedures such as thoracoscopy or open pleural biopsy [4,6,7]. Therefore, a new

approach is needed to detect the cause(s) of undiagnosed pleural effusions [8–11]. Because immunoglobulin G4 (IgG4)-related disease is recognized as a fibroinflammatory condition of unknown cause that can affect multiple organs including the lungs and pleura [12,13], IgG4 might be related to certain idiopathic pleural effusions.

Hamano *et al.* originally reported elevated serum IgG4 concentrations in patients with autoimmune pancreatitis [14], and IgG4-related autoimmune disease has been proposed as a new clinicopathological entity characterized by IgG4⁺ plasma cell infiltration [15]. High serum IgG4 levels and infiltration of IgG4⁺ plasma cells have also been reported in other organs, including salivary and lacrimal glands [15–18]. Although the criteria for diagnosis of

IgG4-related disease in the lung have not been established, elevated serum IgG4 concentrations and histopathological examinations, such as marked lymphoplasmacytic infiltration including IgG4⁺ cells and fibrosis, have been recommended [19–21]. Taniguchi *et al.* have reported interstitial pneumonia associated with autoimmune pancreatitis and marked infiltration of IgG4⁺ plasma cells in the pulmonary alveolar septum [22]. Common radiological findings of IgG4-related lung disease include hilar and mediastinal lymphadenopathy, thickening of perilymphatic interstitium with or without subpleural and/or peribronchovascular consolidation, and the pathological examination reveals lymphoplasmacytic infiltration with fibrosis, which correlates well with the radiological manifestations [23].

It has been reported that pleural effusion may occur in association with systemic IgG4-related disease [16,24–30]. Conversely, there have been a few case reports on isolated IgG4-related pleural effusion [26,31,32], but little is known about the involvement of IgG4 in the pleural effusion. In this study, we hypothesize that idiopathic pleural effusions include IgG4-associated aetiology and demonstrate pleural infiltration of IgG4⁺ plasma cells in a substantial percentage of patients with idiopathic pleural effusion.

Methods

Patients

Idiopathic pleural effusion was defined as any persistent, exudative pleural effusion that remains undiagnosed after the history and physical examination, biochemical and cytological studies of pleural fluid, radiographic examinations and histopathological analysis of biopsied specimens [4,6]. Diagnosis of idiopathic pleural effusion was made after a minimum of 1-year follow-up (range = 1–10 years), with detailed exploration including computed tomographic (CT) scanning to exclude other causes of effusion such as malignant pleural mesothelioma and carcinomatous pleuritis, according to previous studies that mainly performed follow-up of 1–2 years [4,7,33–36]. In this retrospective study, we accumulated 830 pleural fluid samples at Yamaguchi-Ube Medical Center between 2000 and 2012 and reviewed 35 patients with undiagnosed pleural effusions who underwent thoracoscopy and pleural biopsy, after excluding three patients who had a malignancy during follow-up. Biochemical data were obtained for the sera and pleural fluids when thoracentesis was conducted. Biological and bacterial analyses of sera and pleural fluids, CT scan, cytological and histological examination did not demonstrate malignancy or infectious disease in patients with pleural effusions. The patients' pleural fluids were stored at –80°C until use. This study was approved by the institutional review board of NHO Yamaguchi-Ube Medical Center (Approval no. 26–2). Written informed consent was

obtained from each patient or their family for the use of data and samples.

IgG4 immunohistochemistry

The parietal pleura were obtained from biopsy specimens. Immunostaining for IgG or IgG4 was performed by activation of the pleura with 0.1% trypsin, incubation with rabbit polyclonal anti-human IgG antibody (Dako, Glostrup, Denmark; cat. no. A0423) or biotinylated mouse monoclonal anti-human IgG4 antibody (clone HP-6025; Sigma B3648; Sigma, St Louis, MO, USA) [37,38] and HistoFine® Simple Stain™ Max PO Multi (Nichirei Biosciences, Tokyo, Japan; cat. no. 724152), and development with 3,3'-diaminobenzidine (Nichirei Bioscience; cat. no. 715301). The average number of IgG4⁺ plasma cells within three high-power fields (HPFs) was calculated, and patients with the presence of > 10 IgG4⁺ plasma cells/HPF and an IgG4⁺/IgG⁺ cell ratio of > 40%, as described for biopsy specimens [23,38,39], were assigned to the IgG4⁺ group.

Immunoglobulin analysis of pleural fluids

IgG1, IgG2, IgG3, IgG4, IgM, IgA and IgE in pleural fluids were quantitated with Bio-Plex Pro Assays Human Isotyping 7-Plex (Bio-Rad, Hercules, CA, USA), according to the manufacturer's instructions. Bio-Plex Suspension Array System was operated with Bio-Plex Manager (version 6.0).

Purification of IgG4 antibodies from pleural fluids

IgG4 was purified from pleural fluids by diethylaminoethyl (DEAE)-cellulose ion exchange chromatography and subsequently by affinity chromatography on anti-IgG4 antibody-coupled Sepharose-4. Pleural fluid was dialyzed against 0.01 M phosphate buffer (pH 7.0). DEAE-cellulose (DE52; Whatman Biosystems, Chalfont St Giles, UK) in a column (φ1 × 30 cm) was equilibrated with 0.01 M phosphate buffer (pH 7.0). The dialyzed pleural fluid (20 ml) was passed onto the DEAE column and the fall-through fractions containing IgG were collected. IgG4 in the IgG of the fall-through fractions was purified with anti-IgG4-coupled Sepharose-4 that had been prepared by coupling monoclonal anti-IgG4 antibody (clone HP-6025; Sigma) to CNBr-activated Sepharose-4 (GE) according to the manufacturer's instructions. The bound IgG4 was eluted with 0.1 M glycine-HCl (pH 2.7) and neutralized immediately with 1 M Tris.

Two-dimensional electrophoresis (2-DE) of effusion IgG4 antibodies

2-DE of purified IgG4 was performed as described previously [40,41]. Briefly, isoelectric focusing (IEF) gel solution contained 8.5 M urea, acrylamide/Bis (5% T, 3% C), 10% glycerol, 1.3 mM lysine and a mixture of Pharmalyte pH 3–10 (1.25%) and pH 5–8 (1.25%) (GE), which was degassed and polymerized by adding ammonium persulphate and TEMED

to concentrations of 0.05 and 0.1%, respectively. Purified IgG4 was reduced in the presence of 5% β -mercaptoethanol at room temperature for 1 h, and urea was added to a concentration of 8.5 M immediately before loading onto the capillary IEF gel (ϕ 1 mm \times 5 cm). IEF was run in Mini-PROTEAN 2-D Electrophoresis Cell (Bio-Rad) at 200 V for 15 min, 400 V for 15 min and 750 V for 2.5 h. After IEF, capillary gel was equilibrated with sodium dodecyl sulphate (SDS) sample buffer containing 5% β -mercaptoethanol for 30 min. After washing the capillary gel with SDS running buffer, SDS-polyacrylamide gel electrophoresis (SDS-PAGE) was performed at 25 mA constant per gel. After transferring the proteins onto PVDF membranes, γ 4, κ and λ chains on the blots were probed with biotinylated anti-IgG4 (Sigma; cat. no. B3648)/horseradish peroxidase-conjugated Extavidin (Sigma; cat. no. E2886), peroxidase-conjugated anti- κ and anti- λ light chain antibodies (Bio-Rad; cat. nos STAR127P and STAR129P), respectively.

Free light chain (FLC) analysis of pleural fluids

The levels of κ and λ FLCs in pleural fluids were measured by latex-based immunoassay using Freelite kappa kit and Freelite lambda kit (The Binding Site, Birmingham, UK). The measurement with Freelite was performed by The BN II System (Siemens, Munich, Germany) at a qualified clinical laboratory of SRL Inc. (Tokyo, Japan). The diagnostic ranges for serum κ FLC, λ FLC and κ/λ FLC ratio are 3.3–19.4 mg/l, 5.7–26.3 mg/l and 0.26–1.65, respectively [42].

Statistical analysis

The Mann–Whitney *U*-test was used to assess differences in the laboratory data, pleural fluid immunoglobulin levels and FLC levels between the IgG4⁺ and IgG4⁻ groups. The immunoglobulin data are expressed as median and interquartile range (IQR) unless stated otherwise. A correlation coefficient was obtained using Pearson's equation. $P < 0.05$ was considered statistically significant. All statistical analyses were conducted using IBM SPSS statistics (version 22.0; IBM, Armonk, NY, USA).

Results

Characteristics of patients' pleural fluids and pleura

Clinical and demographic information of 35 patients with idiopathic pleural effusion was obtained from the medical records (Tables 1 and 2). Biopsies from the parietal pleura of these patients demonstrated diffuse sclerosing inflammation, but no malignant cells were identified. Fibrosis was pronounced on the side of the pleural cavity, while storiform fibrosis was not seen. Diffuse lymphoplasmacytic infiltration was observed in 16 of 35 patients (Fig. 1a,b). No obliterative phlebitis was observed. IgG4 immunostaining was performed to examine whether IgG4⁺ plasma cells were present

Table 1. Clinical characteristics of patients with pleural effusions of unknown cause

	IgG4 ⁻ group (n = 23)	IgG4 ⁺ group (n = 12)	P
Age (years)	70 (63–78)	76 (73–80)	0.092
Sex (male/female)	22/1	12/0	0.851
Serum			
Total protein (g/dl)	7.1 (6.4–7.3)	7.2 (6.7–7.6)	0.420
Albumin/globulin	1.00 (0.80–1.30)	1.05 (0.85–1.20)	0.932
LDH (IU/l)	186 (164–235)	181 (164–227)	0.797
CRP (mg/dl)	1.48 (0.75–2.14)	0.83 (0.27–1.83)	0.161
Pleural fluid			
Total protein (g/dl)	4.3 (3.9–5.0)	4.5 (3.6–5.2)	1.000
LDH (IU/l)	356 (197–577)	221 (145–340)	0.049
CRP (mg/dl)	0.89 (0.51–1.24)	0.34 (0.17–1.31)	0.085
ADA (U/l)	21.7 (16.4–23.5)	21.5 (15.9–29.5)	0.719
LDH in pleural fluid/serum	1.60 (1.29–3.00)	1.19 (0.77–1.95)	0.079

Data are presented as median (interquartile range). LDH = lactate dehydrogenase; CRP = C-reactive protein; ADA = adenosine deaminase. The normal ranges for total protein, albumin/globulin ratio, LDH and CRP in serum are 6.0–8.3 g/dl, 1.0–2.0, 120–240 IU/l and < 0.3 mg/dl, respectively. The normal range for pleural fluid ADA is < 30 U/l [2].

in the pleura of the 35 patients (Fig. 1c–h). IgG4⁺ plasma cells were variably detected, and the cut-off for IgG4 positivity was set to 10 IgG4⁺ plasma cell counts per HPF, as proposed for biopsy specimens [23,39]. Of 35 patients, 12 patients showing > 10 IgG4⁺ plasma cells/HPF were assigned to the IgG4⁺ group (median = 31; range = 20–70; Tables 1 and 2) and 23 patients with \leq 10 IgG4⁺ plasma cells/HPF to the IgG4⁻ group (median = 0.3; range = 0–5). All patients in the IgG4⁺ group showed IgG4⁺/IgG⁺ cell ratios greater than 40% (Table 2). The patients in the IgG4⁺ group were older men with a median age of 76 years, and biochemical analysis showed lower median effusion LDH and CRP levels for this group (Table 1).

Immunoglobulin analysis of pleural fluids

Effusion IgG4 levels were significantly higher in the IgG4⁺ group than in the IgG4⁻ group (median = 41 *versus* 27 mg/dl, $P < 0.01$, Fig. 2d). The proportion of IgG4 to the total IgG was also higher in the IgG4⁺ group than in the IgG4⁻ group (median = 3.2 *versus* 1.9%, $P < 0.01$, Fig. 2h), which confirms higher IgG4 production in the pleura of the former group. The pleural fluid IgA levels were also elevated in the IgG4⁺ group (median = 403 *versus* 193 mg/dl, Fig. 2f), in contrast to those of IgG1, IgG2, IgG3, IgM and IgE (Fig. 2a–c,e,g).

Clonality of the IgG4 antibodies of patients in the IgG4⁺ group

To exclude the possibility of malignant lymphoma and multiple myeloma, the clonality of the effusion IgG4

Table 2. Clinical features of patients in the immunoglobulin IgG4⁺ group.

n	Age/sex	Effusion IgG4, mg/dl	IgG4 ⁺ PC counts/HPF*	CT scan findings						Follow-up period (years)
				IgG4 ⁺ /IgG ⁺ PC ratio (%)	Respiratory symptom	Pleura	Pulmonary lesion	Mediastinal lymphadenopathy	Extrapulmonary lesion	
1	75M	1133.1	48	85	Dyspnoea on effort	(-)	(-)	(-)	(-)	6
2	81M	20.3	70	93	Abnormality of X-ray	Pleural plaque	(-)	(-)	(-)	2
3	68M	239.6	45	75	Dyspnoea on effort	Pleural plaque and thickening	Ground glass attenuation	(-)	(-)	5
4	76M	44.1	31	48	Abnormality of X-ray	Pleural thickening	Fibrosis	(-)	(-)	3
5	73M	60.1	24	65	Cough	Pleural thickening	Consolidation	(-)	(-)	9
6	73M	37.6	20	75	Abnormality of X-ray	Pleural plaque	Round atelectasis	(-)	(-)	10
7	73M	36.7	22	70	Abnormality of X-ray	(-)	Pneumocytosis nodule	(-)	(-)	9
8	84M	36.3	26	81	Abnormality of X-ray	Pleural plaque and thickening	(-)	(-)	(-)	3
9	77M	36.5	31	69	Abnormality of X-ray	(-)	Consolidation	(-)	(-)	3
10	78M	36.3	29	54	Abnormality of X-ray	Pleural plaque	(-)	(-)	(-)	5
11	67M	50.7	35	79	Dyspnoea on effort	Pleural plaque	(-)	(-)	(-)	6
12	81M	50.6	57	51	Abnormality of X-ray	(-)	(-)	(-)	(-)	1

*PC = plasma cell; HPF = high-power field ($\times 400$); CT = computed tomography.

antibodies of patients in the IgG4⁺ group was examined by 2-DE (Fig. 3). The control human IgG4, κ myeloma protein, was separated into four $\gamma 4$ H chain spots with different isoelectric points and one κ L chain spot, but no λ L chain spot (Fig. 3a–c). In contrast, the H and L chains of the IgG4 antibodies of the patients were more heterogeneous in terms of isoelectric point and molecular weight (Fig. 3d–i). In particular, both κ and λ L chains were detected, indicating that their IgG4 antibodies are polyclonal. The numbers of the spots of the κ and λ chains were 10 and 5–6, respectively, which suggests that the κ chain predominates in the effusion IgG4 antibodies of the patients.

Free light chains (FLC) analysis of pleural fluids

As the κ chain was associated predominantly with IgG4 H chain in the patients (Fig. 3), it was presumed that the κ -type was also predominant in the FLCs of the pleural fluids of the IgG4⁺ group. FLCs are produced in excess of the H chains during immunoglobulin synthesis and secreted into the circulation. The FLC assay was developed originally to support the diagnosis of L chain multiple myeloma, and has been used to assess the excess of one L chain isotype over another by using κ/λ ratio as a surrogate for clonal expansion [43–45]. Interestingly, the κ FLC levels were higher in the patients of the IgG4⁺ group than in the IgG4⁻ group (median = 30.1 *versus* 9.1 mg/dl, $P < 0.01$) (Fig. 4a), whereas the median λ FLC levels were not significantly different (Fig. 4b). Importantly, the median κ/λ FLC ratio was above the normal range and significantly higher in the IgG4⁺ group than in the IgG4⁻ group (2.0 *versus* 1.2, $P < 0.001$) (Fig. 4c). In a comparison of patients between the IgG4⁻ and IgG4⁺ groups, the receiver operating characteristic (ROC) curve for the κ/λ FLC ratio had a sensitivity of 0.87, a specificity of 0.83 at a cut-off value of 1.42 with an area under the curve (AUC) of 0.88 (Fig. 5). In addition, the κ/λ FLC ratios were found to be correlated with the IgG4⁺ plasma cell counts/HPF and the IgG4⁺/IgG⁺ cell ratios in the pleura of the IgG4⁺ group (Fig. 6). These results are consistent with the predominance of the κ chain in the 2-DE patterns of the effusion IgG4 antibodies (Fig. 3).

Discussion

The aetiology of exudative pleural effusion sometimes remains unknown, despite thoracoscopy and histological examination of pleural biopsy specimens. In this study, we have shown that 34% of patients with idiopathic pleural effusion are associated with IgG4. To our knowledge, this study is the first to investigate the incidence of IgG4-associated pleural effusion in patients with idiopathic pleural effusion. A pleural marker that might be related to this pleural effusion is also discussed.

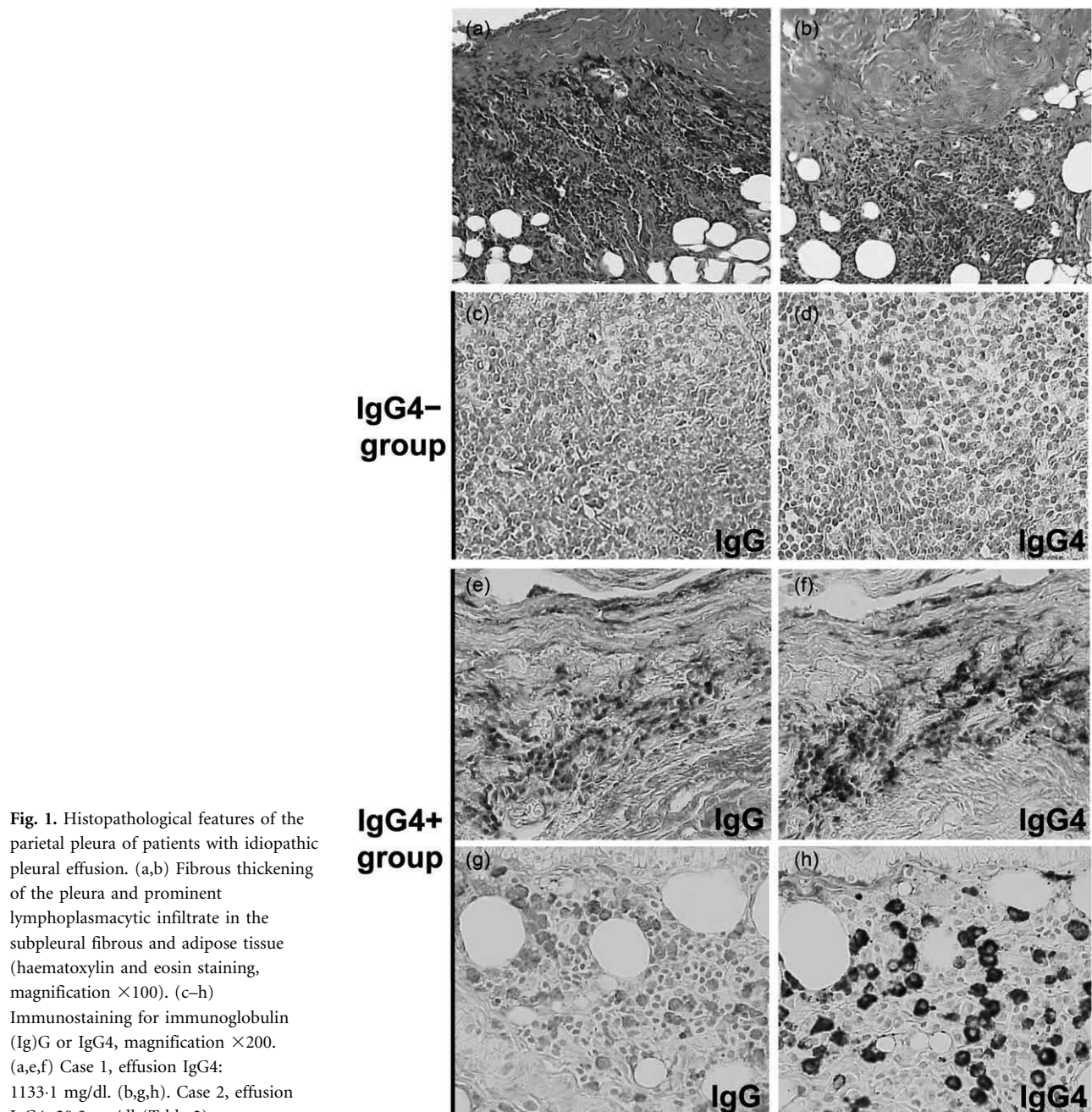


Fig. 1. Histopathological features of the parietal pleura of patients with idiopathic pleural effusion. (a,b) Fibrous thickening of the pleura and prominent lymphoplasmacytic infiltrate in the subpleural fibrous and adipose tissue (haematoxylin and eosin staining, magnification $\times 100$). (c–h) Immunostaining for immunoglobulin (Ig)G or IgG4, magnification $\times 200$. (a,e,f) Case 1, effusion IgG4: 1133.1 mg/dl. (b,g,h) Case 2, effusion IgG4: 20.3 mg/dl (Table 2).

Pleural effusions are manifested in some systemic IgG4-related disease. In previous case reports on IgG4-related disease, pleural effusion occurred as one of the symptoms of the systemic disease involving pancreas, salivary glands, etc. Nodular lesions and bronchovascular involvement are the most common pulmonary manifestations, and various combinations of pulmonary abnormalities are often found in the same patients [23,46,47]. In contrast, the patients in this study did not show multi-organ system involvement other than pleuritis. Considering the elevated effusion IgG4 levels, tissue IgG4⁺ plasma cell numbers and IgG4⁺/IgG⁺ plasma cell ratios (Table 2), however, the IgG4-associated aetiology is

evident for the patients in the IgG4⁺ group of this study. The patients in the IgG4⁺ group were elderly men and less inflammatory compared with those in the IgG4⁻ group (Table 1), which is in agreement with characteristics of IgG4-related disease that affects predominantly older men and progresses slowly with relatively weak inflammation signs [48]. IgG4 antibodies are considered generally to be anti-inflammatory [49,50], but their pathogenic effects have also been reported [51,52]. At present, it is unclear whether the increased production of IgG4 antibody is a causative factor of the pleural effusion or a bystander phenomenon associated with chronic inflammatory reactions.

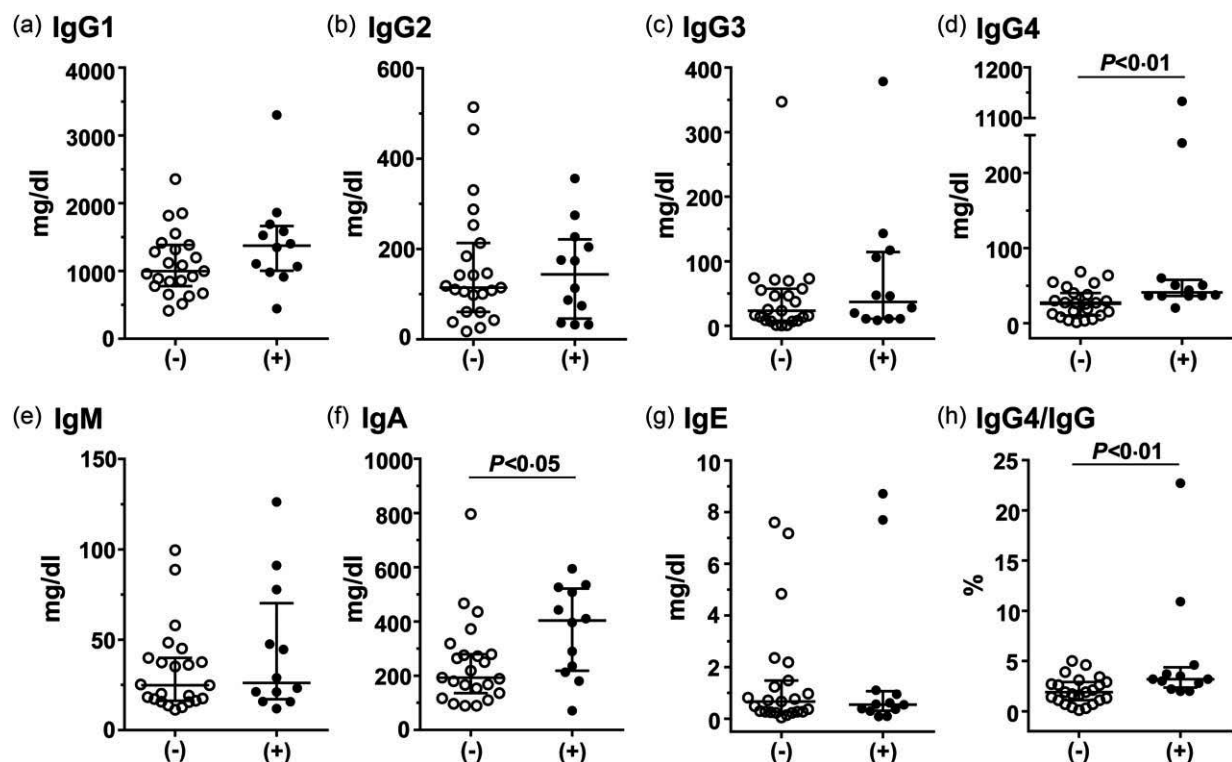


Fig. 2. Comparison of pleural fluid levels of immunoglobulins between the immunoglobulin (Ig)G4[−] and IgG4⁺ groups. (−), IgG4[−] group; (+), IgG4⁺ group. Median and interquartile ranges are shown.

In differential diagnosis, sarcoidosis and multi-centric Castleman's disease were ruled out by clinical and radiological findings, including lack of mediastinal/hilar or extrapulmonary lymphadenopathy in the chest X-ray and CT scan examinations (Table 2). Although lymphoma/myeloma needs to be suspected when the IgG4 levels are

markedly high, in this study the IgG4 antibodies were polyclonal and no patient developed malignancy during at least 1-year follow-up (median 5 years, Table 2). Interestingly, the effusion IgG4 levels did not correlate with the extent of pleural infiltration of IgG4⁺ plasma cells (cases 1 and 2, Fig. 1, Table 2). Although the effusion IgG4 level of case 2

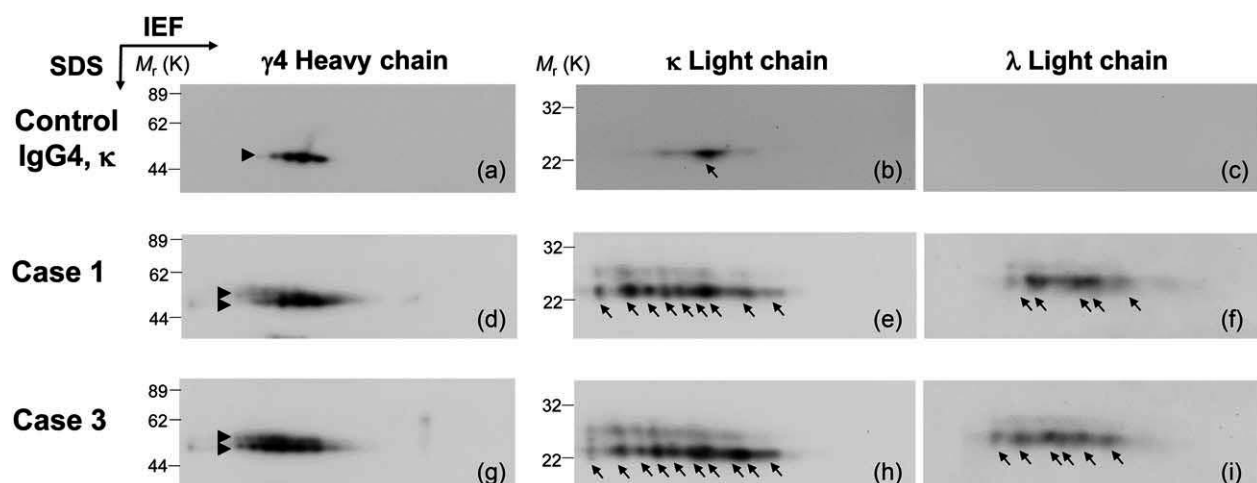


Fig. 3. Analysis of the clonality of the effusion immunoglobulin (Ig)G4 antibodies of patients in the IgG4⁺ group by two-dimensional electrophoresis (2-DE). Control IgG4 κ myeloma protein from Sigma (cat no. I4639) (a–c). Effusion IgG4 antibodies of representative cases with abnormal IgG4 levels (d–i). The H and L chains were probed with anti-IgG4-Fc (left), anti-κ chain (middle) and anti-λ chain (right) antibodies.

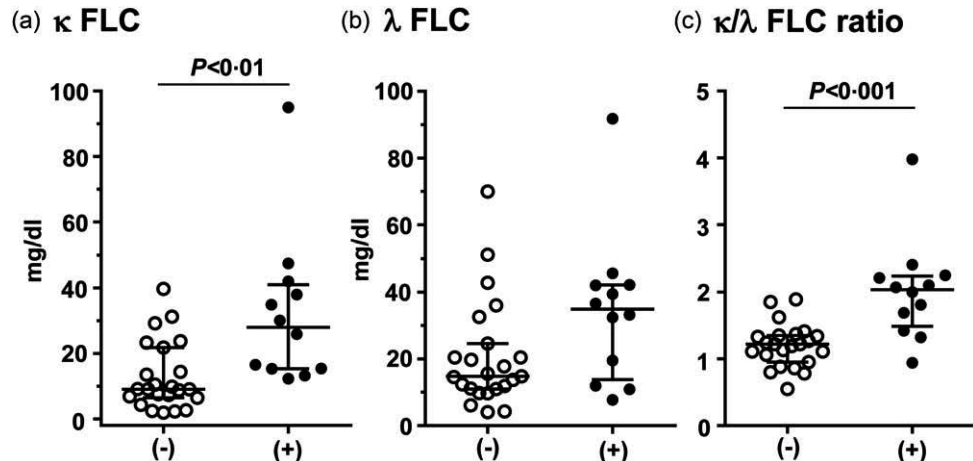


Fig. 4. Comparison of pleural fluid levels of the κ and λ free L chains (FLC) (a,b) and κ/λ ratio (c). Median and interquartile ranges are shown. (–), Immunoglobulin (Ig)G4[–] group; (+), IgG4⁺ group.

in the IgG4⁺ group was as low as 20.3 mg/dl, IgG4 immunostaining exhibited dense infiltration of IgG4⁺ plasma cells in the pleura (Fig. 1h). The discrepancy between serum IgG4 concentrations and immunohistochemical findings has also been noted in IgG4-related disease [53]. Therefore, a biomarker other than IgG4 is needed to support the diagnosis of this pleural effusion. The measurements of FLC in the pleural fluid may be considered.

Elevated FLC levels (Fig. 4a,b) are likely to reflect the activation of polyclonal B cells that infiltrate in the pleura. Higher κ FLC levels and κ/λ ratios in the IgG4⁺ group than in the IgG4[–] group may be useful to discriminate the

IgG4-associated pleural effusion (Fig. 4). Over-production of serum FLC and high serum κ/λ ratios have been shown recently to correlate with the disease activity of systemic lupus erythematosus [54], rheumatoid arthritis, primary Sjögren's syndrome [55] and IgG4-related disease [56]. However, the reason for the high κ/λ ratios in these diseases is not known. One possibility to explain the high κ/λ ratios in the IgG4⁺ group is dominant selection of V κ genes by possible antigen(s) that elicit pleuritis. It has been reported that the κ/λ ratios of granulocyte-macrophage colony-stimulating factor (GM-CSF) autoantibodies in the sera of patients with autoimmune pulmonary alveolar proteinosis are correlated with disease severity [57]. The study suggests the occurrence of selective expansion of λ -type anti-GM-CSF antibody-positive B cell clones in the peripheral lymphatic tissues. However, neither autoantigens nor disease-specific IgG4 autoantibodies have been identified in IgG4-related disease [12]. A second possibility is a preferential association of the κ L chains with the $\gamma 4$ and α H chains because the levels of IgG4 and IgA were elevated in the pleural fluids (Fig. 2). The κ L chains have been shown to be associated preferentially with IgG4 and IgA H chains from the analyses of subclass distribution in 659 IgG myeloma sera [58] and 176 IgG and 62 IgA myeloma proteins [59]. These studies show the mean κ/λ ratios for the IgG4 myeloma proteins as 3.0 ($n = 24$ [58]) and 2.7 ($n = 11$ [59]) and that for IgA as 2.1 ($n = 42$ [59]). The correlations of the effusion κ/λ FLC ratios with the IgG4⁺ cell counts and IgG4⁺/IgG⁺ cell ratios in the pleura are in agreement with this notion (Fig. 6). It has been reported that FLC can confer mast cell-dependent hypersensitivity in mice and that increased κ FLC monomer and dimer levels and high κ/λ ratios are often found in the cerebrospinal fluid of patients with multiple sclerosis [60,61]. The pleural effusions in the IgG4⁺ group may be attributable to the accumulation of κ FLCs.

IgG4-related pleural lesions are reported to be steroid-responsive [26,32,62]. Considering B cell activation as a

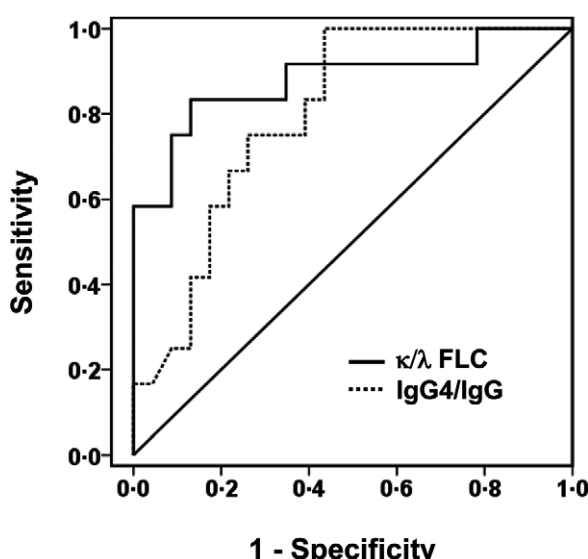


Fig. 5. Receiver operating characteristic (ROC) analysis on diagnostic utility of immunoglobulin (Ig)G4 and κ/λ ratio for distinguishing patients between the IgG4[–] and IgG4⁺ groups. Cut-off value for κ/λ ratio, 1.42; sensitivity, 0.87; specificity, 0.83. Area under the curve (AUC), 0.88; 95% confidence interval (CI) for the AUC, 0.74 – 1.00. Cut-off value for IgG4/IgG ratio, 2.75%; sensitivity, 0.75; specificity, 0.74; AUC, 0.80; 95% CI for the AUC, 0.66–0.94.

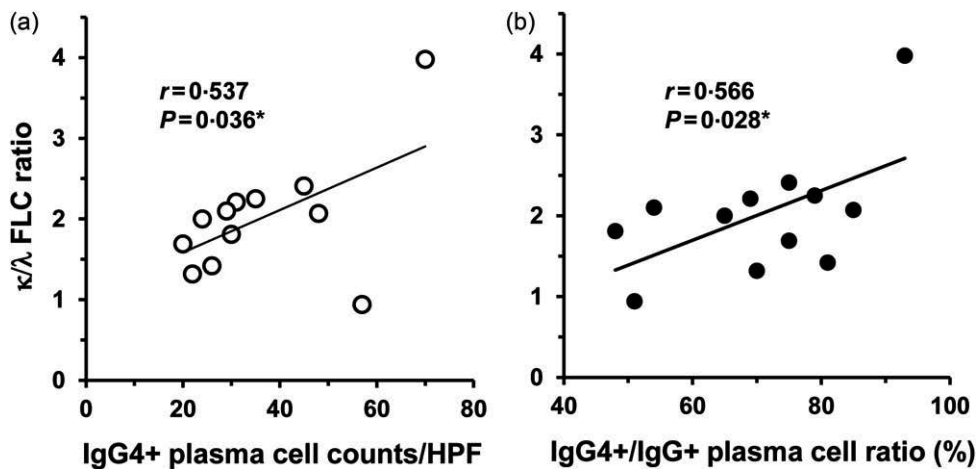


Fig. 6. Correlation of the effusion κ/λ free L chains (FLC) ratio with immunoglobulin (Ig)G4⁺ plasma cell counts (a) and IgG4⁺/IgG⁺ plasma cell ratio (b) in the pleura of patients in the IgG4⁺ group. *One-tailed *P*-value.

possible mechanism for the pleural effusion in our study, the same therapeutic strategy with immunosuppressive agents may be applicable to our cases. One patient in the IgG4⁺ group who had suffered recurrent pleural effusions (Case 1, Table 2) received corticosteroids, which ameliorated the pleural effusion. Conversely, pleural effusions resolved spontaneously in a subset of patients, and so watchful waiting may be appropriate in some patients with mild pleural effusion or asymptomatic pleuritis, as described for IgG4-related disease in other organs [63]. However, criteria to justify treatment of IgG4-related pleural lesions need to be established by future prospective studies.

This study has several limitations. This is a retrospective study with a small number of patients. One patient was followed-up for 1 year, although more than 1-year follow-up is recommended for detection of occult pleural malignancy [7,33,36]. It was not possible in all patients to assess the development of an extra-pleural IgG4-related lesion during follow-up. As serum samples were not available, the serum levels of IgG4, κ and λ FLCs could not be analysed. Immunoglobulins including IgG4 were quantitated by a capture sandwich immunoassay, which is different from nephelometry used in the literature, and so the IgG4 concentrations in this study cannot be compared directly with those in the previous reports on IgG4-related disease.

Acknowledgements

We thank Masami Murakami and Masazumi Tanaka for technical assistance. This study was supported in part by Japan Society for the Promotion of Science under JSPS KAKENHI Grant no. 23590578 (Y. M.).

Disclosure

The authors declare no conflicts of interest.

References

- 1 Porcel JM, Azzopardi M, Koegelenberg CF, Maldonado F, Rahman NM, Lee YC. The diagnosis of pleural effusions. *Expert Rev Respir Med* 2015; **9**:801–15.
- 2 Light RW. Pleural diseases, 6th edn. Philadelphia, PA: Lippincott Williams & Wilkins, 2013.
- 3 Hooper C, Lee YC, Maskell N, BTS Pleural Guideline Group. Investigation of a unilateral pleural effusion in adults: British Thoracic Society Pleural Disease Guideline 2010. *Thorax* 2010; **65**: ii4–17.
- 4 Ferrer JS, Munoz XG, Orriols RM, Light RW, Morell FB. Evolution of idiopathic pleural effusion: a prospective, long-term follow-up study. *Chest* 1996; **109**:1508–13.
- 5 Light RW. The undiagnosed pleural effusion. *Clin Chest Med* 2006; **27**:309–19.
- 6 Aleman C, Sanchez L, Alegre J *et al.* Differentiating between malignant and idiopathic pleural effusions: the value of diagnostic procedures. *Q J Med* 2007; **100**:351–9.
- 7 Davies HE, Nicholson JE, Rahman NM, Wilkinson EM, Davies RJ, Lee YC. Outcome of patients with nonspecific pleuritis/ fibrosis on thoracoscopic pleural biopsies. *Eur J Cardiothorac Surg* 2010; **38**:472–7.
- 8 Aoe K, Hiraki A, Murakami T *et al.* Diagnostic significance of interferon-gamma in tuberculous pleural effusions. *Chest* 2003; **123**:740–4.
- 9 Aoe K, Hiraki A, Murakami T *et al.* Relative abundance and patterns of correlation among six cytokines in pleural fluid measured by cytometric bead array. *Int J Mol Med* 2003; **12**:193–8.
- 10 Aoe K, Hiraki A, Maeda T *et al.* Soluble receptor-binding cancer antigen expressed on SiSo cells in pleural fluid: a potential diagnostic marker for malignant pleural effusion. *Chest* 2004; **126**:1195–7.
- 11 Porcel JM. Pleural fluid biomarkers: beyond the Light criteria. *Clin Chest Med* 2013; **34**:27–37.
- 12 Stone JH, Zen Y, Deshpande V. IgG4-related disease. *N Engl J Med* 2012; **366**:539–51.
- 13 Della-Torre E, Lanzillotta M, Doglioni C. Immunology of IgG4-related disease. *Clin Exp Immunol* 2015; **181**:191–206.
- 14 Hamano H, Kawa S, Horiuchi A *et al.* High serum IgG4 concentrations in patients with sclerosing pancreatitis. *N Engl J Med* 2001; **344**:732–8.

- 15 Kamisawa T, Funata N, Hayashi Y *et al.* A new clinicopathological entity of IgG4-related autoimmune disease. *J Gastroenterol* 2003; **38**:982–4.
- 16 Zen Y, Inoue D, Kitao A *et al.* IgG4-related lung and pleural disease: a clinicopathologic study of 21 cases. *Am J Surg Pathol* 2009; **33**:1886–93.
- 17 Stone JH, Khosroshahi A, Hilgenberg A, Spooner A, Isselbacher EM, Stone JR. IgG4-related systemic disease and lymphoplasma-cytic aortitis. *Arthritis Rheum* 2009; **60**:3139–45.
- 18 Yamamoto M, Ohara M, Suzuki C *et al.* Elevated IgG4 concentrations in serum of patients with Mikulicz's disease. *Scand J Rheumatol* 2004; **33**:432–3.
- 19 Masaki Y, Dong L, Kurose N *et al.* Proposal for a new clinical entity, IgG4-positive multiorgan lymphoproliferative syndrome: analysis of 64 cases of IgG4-related disorders. *Ann Rheum Dis* 2009; **68**:1310–5.
- 20 Umebara H, Okazaki K, Masaki Y *et al.* A novel clinical entity, IgG4-related disease (IgG4RD): general concept and details. *Mod Rheumatol* 2012; **22**:1–14.
- 21 Matsui S, Yamamoto H, Minamoto S, Waseda Y, Mishima M, Kubo K. Proposed diagnostic criteria for IgG4-related respiratory disease. *Respir Investig* 2016; **54**:130–2.
- 22 Taniguchi T, Ko M, Seko S *et al.* Interstitial pneumonia associated with autoimmune pancreatitis. *Gut* 2004; **53**:770; author reply 770–1.
- 23 Matsui S, Hebisawa A, Sakai F *et al.* Immunoglobulin G4-related lung disease: clinicoradiological and pathological features. *Respirology* 2013; **18**:480–7.
- 24 Miyake K, Moriyama M, Aizawa K *et al.* Peripheral CD4⁺ T cells showing a Th2 phenotype in a patient with Mikulicz's disease associated with lymphadenopathy and pleural effusion. *Mod Rheumatol* 2008; **18**:86–90.
- 25 Rossi G, Marchionni A, Guicciardi N, Cadioli A, Cavazza A. Recurrent pleural and pericardium effusions in a white woman with IgG4-related syndrome. *Am J Surg Pathol* 2009; **33**:802–3.
- 26 Yamamoto H, Suzuki T, Yasuo M *et al.* IgG4-related pleural disease diagnosed by a re-evaluation of chronic bilateral pleuritis in a patient who experienced occasional acute left bacterial pleuritis. *Intern Med* 2011; **50**:893–7.
- 27 Sekiguchi H, Horie R, Utz JP, Ryu JH. IgG4-related systemic disease presenting with lung entrapment and constrictive pericarditis. *Chest* 2012; **142**:781–3.
- 28 Ishida M, Hodohara K, Furuya A *et al.* Concomitant occurrence of IgG4-related pleuritis and periaortitis: a case report with review of the literature. *Int J Clin Exp Pathol* 2014; **7**:808–14.
- 29 Choi JH, Sim JK, Oh JY *et al.* A case of IgG4-related disease presenting as massive pleural effusion and thrombophlebitis. *Tuberc Respir Dis (Seoul)* 2014; **76**:179–83.
- 30 Waheed W, Nickerson J, Ambaye AB, Babi MA, Tandan R. IgG4-related neuromyopathy associated with recurrent pleural effusion. *J Clin Neuromuscul Dis* 2015; **16**:210–9.
- 31 Kojima M, Nakazato Y, Kaneko Y, Sugihara S, Masawa N, Nakamura N. Cytological findings of IgG4-related pleural effusion: a case report. *Cytopathology* 2013; **24**:338–40.
- 32 Corcoran JP, Culver EL, Psallidas I *et al.* A 63-year-old man with a recurrent right-sided pleural effusion. *Thorax* 2015; **70**:504–7.
- 33 El Solh AA, Abdo T, Pineda L, Ramadan F, Berbary E. A longitudinal study of idiopathic exudative lymphocytic pleural effusion in older people. *J Am Geriatr Soc* 2005; **53**:1957–60.
- 34 Bintcliffe OJ, Hooper CE, Rider IJ *et al.* Unilateral pleural effusions with more than one apparent etiology. A prospective observational study. *Ann Am Thorac Soc* 2016; **13**:1050–6.
- 35 DePew ZS, Verma A, Wigle D, Mullon JJ, Nichols FC, Maldonado F. Nonspecific pleuritis: optimal duration of follow-up. *Ann Thorac Surg* 2014; **97**:1867–71.
- 36 Janssen JP, Ramlal S, Mravunac M. The long-term follow up of exudative pleural effusion after nondiagnostic thoracoscopy. *J Bronchol* 2004; **11**:169–74.
- 37 Pifferi M, Di Cicco M, Bush A, Caramella D, Chilos M, Boner AL. Uncommon pulmonary presentation of IgG4-related disease in a 15-year-old boy. *Chest* 2013; **144**:669–71.
- 38 Deshpande V, Zen Y, Chan JK *et al.* Consensus statement on the pathology of IgG4-related disease. *Mod Pathol* 2012; **25**:1181–92.
- 39 Chari ST. Diagnosis of autoimmune pancreatitis using its five cardinal features: introducing the Mayo Clinic's HISORt criteria. *J Gastroenterol* 2007; **42**:39–41.
- 40 Mimura Y, Kabat EA, Tanaka T, Fujimoto M, Takeo K, Nakamura K. Microheterogeneity of mouse antidiextran monoclonal antibodies. *Electrophoresis* 1995; **16**:116–23.
- 41 Mimura Y, Nakamura K, Tanaka T, Fujimoto M. Evidence of intra- and extracellular modifications of monoclonal IgG polypeptide chains generating charge heterogeneity. *Electrophoresis* 1998; **19**:767–75.
- 42 Katzmann JA, Clark RJ, Abraham RS *et al.* Serum reference intervals and diagnostic ranges for free kappa and free lambda immunoglobulin light chains: relative sensitivity for detection of monoclonal light chains. *Clin Chem* 2002; **48**:1437–44.
- 43 Bradwell AR, Carr-Smith HD, Mead GP *et al.* Highly sensitive, automated immunoassay for immunoglobulin free light chains in serum and urine. *Clin Chem* 2001; **47**:673–80.
- 44 Drayson M, Tang LX, Drew R, Mead GP, Carr-Smith H, Bradwell AR. Serum free light-chain measurements for identifying and monitoring patients with nonsecretory multiple myeloma. *Blood* 2001; **97**:2900–2.
- 45 Bradwell AR, Carr-Smith HD, Mead GP, Harvey TC, Drayson MT. Serum test for assessment of patients with Bence Jones myeloma. *Lancet* 2003; **361**:489–91.
- 46 Fujinaga Y, Kadoya M, Kawa S *et al.* Characteristic findings in images of extra-pancreatic lesions associated with autoimmune pancreatitis. *Eur J Radiol* 2010; **76**:228–38.
- 47 Hamano H, Arakura N, Muraki T, Ozaki Y, Kiyosawa K, Kawa S. Prevalence and distribution of extrapancreatic lesions complicating autoimmune pancreatitis. *J Gastroenterol* 2006; **41**:1197–205.
- 48 Umebara H, Nakajima A, Nakamura T *et al.* IgG4-related disease and its pathogenesis-cross-talk between innate and acquired immunity. *Int Immunol* 2014; **26**:585–95.
- 49 Aalberse RC, Stapel SO, Schuurman J, Rispens T. Immunoglobulin G4: an odd antibody. *Clin Exp Allergy* 2009; **39**:469–77.
- 50 van der Neut Kolfschoten M, Schuurman J, Losen M *et al.* Anti-inflammatory activity of human IgG4 antibodies by dynamic Fab arm exchange. *Science* 2007; **317**:1554–7.
- 51 Cornell LD, Chicano SL, Deshpande V *et al.* Pseudotumors due to IgG4 immune-complex tubulointerstitial nephritis associated with autoimmune pancreatocentric disease. *Am J Surg Pathol* 2007; **31**:1586–97.

- 52 Deshpande V, Chicano S, Finkelberg D *et al.* Autoimmune pancreatitis: a systemic immune complex mediated disease. *Am J Surg Pathol* 2006; **30**:1537–45.
- 53 Sah RP, Chari ST. Serologic issues in IgG4-related systemic disease and autoimmune pancreatitis. *Curr Opin Rheumatol* 2011; **23**:108–13.
- 54 Aggarwal R, Sequeira W, Kokebie R *et al.* Serum free light chains as biomarkers for systemic lupus erythematosus disease activity. *Arthritis Care Res (Hoboken)* 2011; **63**:891–8.
- 55 Gottenberg JE, Aucouturier F, Goetz J *et al.* Serum immunoglobulin free light chain assessment in rheumatoid arthritis and primary Sjögren's syndrome. *Ann Rheum Dis* 2007; **66**:23–7.
- 56 Grados A, Ebbo M, Boucraut J *et al.* Serum immunoglobulin free light chain assessment in IgG4-related disease. *Int J Rheumatol* 2013; **2013**:426759.
- 57 Nei T, Urano S, Itoh Y *et al.* Light chain (kappa/lambda) ratio of GM-CSF autoantibodies is associated with disease severity in autoimmune pulmonary alveolar proteinosis. *Clin Immunol* 2013; **149**:357–64.
- 58 Skvaril F, Morell A, Barandun S. The IgG subclass distribution in 659 myeloma sera. *Vox Sang* 1972; **23**:546–51.
- 59 Aucouturier P, Preud'Homme JL. Subclass distribution of human myeloma proteins as determined with monoclonal antibodies. *Immunol Lett* 1987; **16**:55–7.
- 60 Redegeld FA, van der Heijden MW, Kool M *et al.* Immunoglobulin-free light chains elicit immediate hypersensitivity-like responses. *Nat Med* 2002; **8**:694–701.
- 61 Kaplan B, Livneh A, Sela BA. Immunoglobulin free light chain dimers in human diseases. *ScientificWorldJournal* 2011; **11**:726–35.
- 62 Gajewska ME, Rychwicka-Kielek BA, Sorensen K, Kubik M, Hilberg O, Bendstrup E. Immunoglobulin G4-related pleuritis - a case report. *Respir Med Case Rep* 2016; **19**:18–20.
- 63 Khosroshahi A, Wallace ZS, Crowe JL, *et al.* International consensus guidance statement on the management and treatment of IgG4-related disease. *Arthritis Rheumatol* 2015; **67**:1688–99.



Contents lists available at ScienceDirect

Biochemical and Biophysical Research Communications

journal homepage: www.elsevier.com/locate/ybbrc



Inhibition of VEGF-dependent angiogenesis by the anti-CD82 monoclonal antibody 4F9 through regulation of lipid raft microdomains



Sayaka Nomura ^a, Satoshi Iwata ^{a,1}, Ryo Hatano ^{a,1}, Eriko Komiya ^b, Nam H. Dang ^c, Noriaki Iwao ^d, Kei Ohnuma ^{e,*,1}, Chikao Morimoto ^{a, e, 1}

^a Division of Clinical Immunology, Advanced Clinical Research Center, The Institute of Medical Science, The University of Tokyo, 4-6-1 Shirokanedai, Minato-ku, Tokyo, 108-8639, Japan

^b Department of Therapy Development and Innovation for Immune Disorders and Cancers, Graduate School of Medicine, Juntendo University, 2-1-1, Hongo, Bunkyo-ku, Tokyo, 113-8421, Japan

^c Division of Hematology/Oncology, University of Florida, 1600 SW Archer Road- Box 100278, Room MSB M410A, Gainesville, FL, 32610, USA

^d Department of Hematology, School of Medicine, Juntendo University, 2-1-1, Hongo, Bunkyo-ku, Tokyo, 113-8421, Japan

^e Department of Rheumatology and Allergy, IMSUT Hospital, The Institute of Medical Science, The University of Tokyo, 4-6-1 Shirokanedai, Minato-ku, Tokyo, 108-8639, Japan

ARTICLE INFO

Article history:

Received 5 April 2016

Accepted 18 April 2016

Available online 19 April 2016

Keywords:

CD82

4F9

VEGF

VEGFR2

Angiogenesis

ABSTRACT

CD82 (also known as KAI1) belongs to the tetraspanin superfamily of type III transmembrane proteins, and is involved in regulating cell adhesion, migration and proliferation. In contrast to these well-established roles of CD82 in tumor biology, its function in endothelial cell (EC) activity and tumor angiogenesis is yet to be determined. In this study, we show that suppression of CD82 negatively regulates vascular endothelial growth factor (VEGF)-induced angiogenesis. Moreover, we demonstrate that the anti-CD82 mAb 4F9 effectively inhibits phosphorylation of VEGF receptor 2 (VEGFR2), which is the principal mediator of the VEGF-induced angiogenic signaling process in tumor angiogenesis, by regulating the organization of the lipid raft microdomain signaling platform in human EC. Our present work therefore suggests that CD82 on EC is a potential target for anti-angiogenic therapy in VEGFR2-dependent tumor angiogenesis.

© 2016 Elsevier Inc. All rights reserved.

1. Introduction

CD82 (also known as KAI1) belongs to the tetraspanin superfamily of type III transmembrane proteins, and is involved in the regulation of cell adhesion, migration and proliferation through the

activation of downstream signaling processes [1]. We previously showed that CD82 was preferentially expressed on CD4⁺CD45RO⁺ memory T cells and that treatment with the anti-CD82 monoclonal antibody (mAb) 4F9 co-immobilized with a submitogenic dose of anti-CD3 mAb led to marked T cell proliferation [2]. Moreover, we dissected key aspects of the CD82-and β 1 integrin-mediated signaling pathways through studies with Jurkat T cells with marginal expression of Cas-L/NEDD9 as well as those involving CD82-mediated tyrosine phosphorylation of Cas-L in peripheral T cells and H9 cells [3]. Meanwhile, CD82 expression on cancer cells suppresses tumor progression [1]. CD82 was originally identified as a suppressor of metastasis in a genetic screening assay for rat AT6.1 prostate cancer cells [4]. Subsequent studies showed that CD82 functions as a wide-spectrum suppressor of invasion and metastasis during cancer progression in many solid tumors [1,5]. Mechanistically, CD82 inhibits receptor tyrosine kinases (RTKs) (e.g., epidermal growth factor receptor and hepatocyte growth factor

Abbreviations: BSA, bovine serum albumin; EC, endothelial cell; HUVEC, human umbilical vein endothelial cell; IL-6, interleukin-6; IL-6R, interleukin-6 receptor; mAb, monoclonal antibody; RTK, receptor tyrosine kinase; shCD82, shRNA against CD82; shRNA, short hairpin RNA; VEGF, vascular endothelial growth factor; VEGFR, vascular endothelial growth factor receptor; [³H]-TdR, tritiated thymidine.

* Corresponding author. Department of Therapy Development and Innovation for Immune Disorders and Cancers, Graduate School of Medicine, Juntendo University, 2-1-1, Hongo, Bunkyo-ku, Tokyo, 113-8421, Japan.

E-mail address: kohnuma@juntendo.ac.jp (K. Ohnuma).

¹ Department of Therapy Development and Innovation for Immune Disorders and Cancers, Graduate School of Medicine, Juntendo University, 2-1-1, Hongo, Bunkyo-ku, Tokyo 113-8421, Japan.

receptor) and integrin signaling by promoting their internalization [6,7]. Recent studies demonstrated that CD82 expressed on melanoma cells suppresses environmental angiogenesis by inhibiting the production of interleukin-6 (IL-6) and vascular endothelial growth factor (VEGF) in melanoma cells [8].

Cancer angiogenesis is another fundamental process involved in tumor growth as it ensures adequate supply of oxygen and nutrients to promote cell growth and motility through the development of new blood vessels, potentially causing cancer progression and metastasis [9]. Angiogenesis involves coordinated endothelial cell (EC) proliferation, migration, branching and tube formation [10]. The VEGF family is a group of key proteins involved in the angiogenic pathway and is highly expressed in many tumor types [11]. Following increased production of VEGF induced by hypoxia, inflammatory cytokines, activation of oncogenes or silencing of onco-suppressor genes, the VEGF receptors (VEGFRs), which are expressed in tumor environmental vascular ECs, are activated to mediate cancer angiogenesis, promoting tumor growth and metastasis [12–14]. Therefore, suppression of cancer angiogenesis pathway by such agents as the anti-VEGF mAb bevacizumab, anti-VEGFR2 mAb ramucirumab, or the RTK inhibitors sorafenib and sunitinib represents novel treatment approaches for anticancer therapy [9,12,15].

Although CD82 is also expressed on EC as well as many neoplasms [1], a role for CD82 in EC activity and angiogenesis has not yet been clearly established. Recent study using *Cd82*-null mice showed that perturbation of CD82-ganglioside-CD44 signaling attenuates pathological angiogenesis by inhibiting EC movement [16], while *Cd82*-null mice display normal vessel development without obvious vascular defects [17]. Although VEGF-dependent EC activity plays an essential role in angiogenesis [18], a functional role for CD82 in association with VEGF/VEGFRs in EC activity has not yet been elucidated.

In this study, we show that suppression of CD82 negatively regulates VEGF-induced angiogenesis. Moreover, we demonstrate that the anti-CD82 mAb 4F9 effectively inhibits phosphorylation of VEGFR2, which is the principal mediator of the VEGF-induced angiogenic signaling process, by regulating the organization of the signaling platform, *i.e.*, lipid raft microdomains, in human EC. As a result, our present study suggests that CD82 on EC is a potential target for anti-angiogenic therapy in tumor angiogenesis.

2. Materials and methods

2.1. Antibodies, reagents and cells

Anti-human CD82 mAb 4F9 (mouse IgG1) was established in our laboratory as reported elsewhere [2]. Anti-VEGFR2 rabbit mAb (55B11), anti-phospho-VEGFR2 rabbit mAb (19A10) and anti-CD31 mouse mAb (89C2) were purchased from Cell Signaling Technology (USA). Suramin and recombinant human VEGF were purchased from Sigma–Aldrich (USA) and R&D Systems (USA), respectively. Human umbilical vein endothelial cells (HUVECs) were purchased from KURABO (Japan) and cultured according to the manufacturer's instruction. 293 FT cells for production of lentivirus particles were obtained from the ATCC (USA).

2.2. Generation of CD82-knockdown HUVECs using short hairpin (sh) RNA

Four clones of lentiviral shRNA against human CD82 (shCD82-*RNA*) and one control shRNA were purchased from Sigma–Aldrich (MISSION™ TRC shRNA Target Set), and each sequence of shCD82-*RNA* is shown in Supplemental Table. Each vector contained GFP tag as a selection marker. Lentivirus particles of shRNA

were produced by 293 FT cells utilizing ViraPower™ Lentiviral Packaging Mix (Invitrogen, USA). After transfection of each shRNA lentivirus particle, GFP-positive HUVECs were purified using BD FACSaria cell sorter (BD Biosciences, USA), and expression of CD82 was confirmed by flow cytometry by the same method as described previously [3].

2.3. Cell migration and proliferation assays

HUVEC migration was assessed using 96-well microchamber plates (BD BioCoat Angiogenesis System, BD Biosciences). Cells were starved for 20 h in HuMedia-EB2 (KURABO) containing 0.1% bovine serum albumin (BSA). Cells were then harvested, resuspended in HuMedia-EB2 containing 0.1% BSA with indicated concentrations of anti-CD82 mAb 4F9 or suramin, and placed in the upper chamber of fibronectin-coated FluoroBlock Cell Culture Inserts (BD Biosciences) at a cell density of 5×10^4 cells per well. Cell migration was initiated by placing medium containing 10 ng/ml VEGF and 0.1% fetal bovine serum to the bottom chamber. After 18 h of incubation, cells were stained with 4 ng/ml calcein AM. Fluorescence in the cells that had migrated through the pores of the fluorescence blocking membrane was directly measured through the bottom of the chambers in a fluorescence plate reader at excitation/emission wavelengths of 485/530 nm (SpectraMax Gemini EM, Molecular Devices, USA) and analyzed using SoftMax Pro 5.2 software (Molecular Devices).

Cell proliferation was measured using [³H]-thymidine ([³H]-Tdr) incorporation assay. HUVECs were seeded in HuMedia-EG2 (KURABO) containing indicated concentrations of mAbs or VEGF in collagen-coated 96-well plates (BD Biosciences) at a density of 2.5×10^4 cells per well. [³H]-Tdr (1 μ Ci/mL) was added and the cells were cultured for a further 18 h. Cells were then harvested and their radioactivity level was measured with a Liquid Scintillation Counter (Wallac 1205 Beta Plate; Perkin–Elmer Life Sciences, USA).

2.4. 2-D angiogenesis assay

After treatment with indicated concentrations of mAbs, VEGF or suramin, HUVECs were cultured utilizing the Angiogenesis Kit with the manufacturer's instruction (KURABO). The media containing each concentration of mAbs, VEGF or suramin were changed at 4, 7, 9 days, and cells were immunostained with anti-CD31 mAb at 11 days. Tube formation of HUVECs was examined by photography under a microscope (Nikon DIAPHOT 300, Nikon, Japan) and quantified in 5 random fields utilizing Angiogenesis Image Analyzer v.2.0.0 (KURABO).

2.5. Measurement of phosphorylation of VEGFR2

HUVECs were cultured in HuMedia-EG2 with 4F9 or control mouse IgG (each 10 μ g/ml) for 12 h, followed by addition of VEGF (10 ng/ml). Cells were harvested at the indicated incubation period with VEGF, and lysates were then subjected to Western blot analysis according to the method described previously [19].

2.6. Lipid raft fractionation

HUVECs were cultured in HuMedia-EG2 with 4F9 or control mouse IgG (each 10 μ g/ml) for 12 h, followed by a 5 min incubation period with VEGF (10 ng/ml). Cells were then harvested, and cell lysates were prepared for fractionation by sucrose density gradient ultracentrifugation by the same method as described previously [19].

2.7. Statistical analysis

Data were analyzed by two-tailed Student's *t* test for two group comparison or by ANOVA test for multiple comparison testing followed by the Tukey–Kramer *post-hoc* test. The level of significance was $p < 0.05$. The calculations were conducted using Prism6.0 software (GraphPad Software, USA).

3. Results

3.1. Knockdown of CD82 decreases EC migration, proliferation and angiogenesis

To determine the role of CD82 in vascular morphogenesis, we first examined cellular activity using a gene ablation approach. For this purpose, we used HUVECs in this study to address the functional role of human CD82 as an angiogenesis model. We first confirmed expression of CD82 in HUVECs by flow cytometry. As shown in Supplemental Fig. S1, cell surface expression of CD82 in HUVECs was clearly observed using the anti-CD82 mAb 4F9. Using 4 different shRNAs against CD82, we then established 4

clones of CD82-knockdown HUVECs with a lentivirus transfection system (shCD82-283, 300, 643 and 949). As shown in Supplemental Fig. S2, expression of cell surface CD82 was significantly decreased in each CD82-knockdown HUVECs than that in control shRNA-transfected HUVECs. Utilizing these shRNA HUVECs, we performed 2-D angiogenesis assay of fibroblast-coculture system. As shown in Fig. 1A, each CD82-knockdown HUVEC exhibited a significant decrease in the level of angiogenesis compared to control shRNA HUVEC. We next examined cell migration and proliferation. As shown in Fig. 1B, with increased doses of VEGF, control shRNA HUVECs displayed enhanced migratory activity. In contrast, CD82-knockdown HUVEC (shCD82-300 clone) exhibited a significant decrease in migratory activity while being cultured with VEGF (** in Fig. 1B). Moreover, cell proliferation decreased significantly in CD82-knockdown HUVEC (shCD82-300 clone) than control shRNA HUVECs (** in Fig. 1C). Other shCD82-HUVEC clones including shCD82-283, 643 and 949 exhibited decreased levels of migration and proliferation similar to those of shCD82-300 HUVEC (data not shown). These results suggest that the CD82 molecule plays a role in EC motility and angiogenesis.

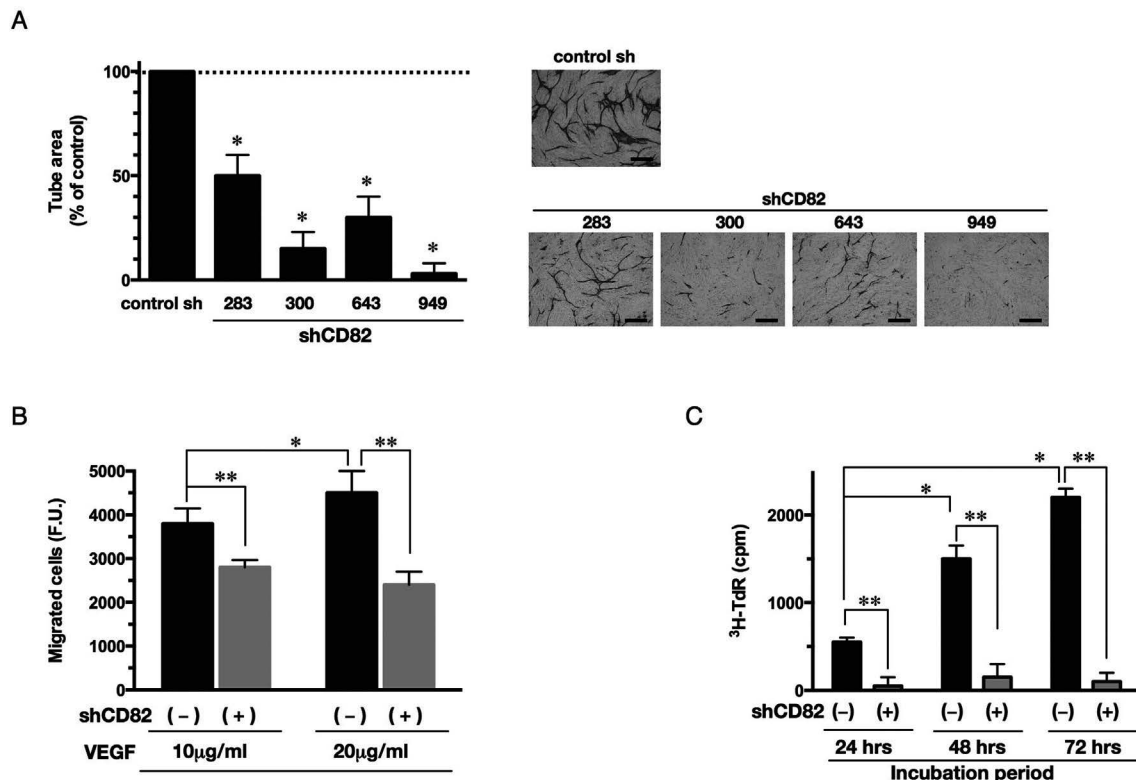


Fig. 1. Silencing of CD82 expression inhibited HUVEC tube formation, migration and proliferation. Four clones of CD82-knockdown HUVEC (shCD82-283, 300, 643 and 949) and one clone of control shRNA HUVEC were established by lentivirus-based shRNA transfection system. (A) Each shRNA HUVEC was cultured in wells seeded with normal human dermal fibroblasts, and was incubated in HuMedia-EG2 containing 10 ng/ml of VEGF. Angiogenesis was quantified by measuring CD31-stained area in 5 random fields utilizing Angiogenesis Image Analyzer. Left panel shows the results presented as the percentage of the mean values obtained in the percentage of tube area in control shRNA HUVECs. The mean values of percentage of tube area \pm S.E. are shown ($n = 5$ experiments with triplicates), and the horizontal dotted line indicates a 100% level of control shRNA HUVECs. A significant decrease in angiogenesis of each CD82-knockdown HUVEC is indicated (* $P < 0.001$ vs. control shRNA). Representative microphotographs of tube formation of each shRNA HUVEC were shown in the right five panels (brown cells are anti-CD31 immunohistochemistry). Scale bars indicate 25 μ m (B) CD82-knockdown HUVECs (shCD82-300) (shCD82 (+)) or control shRNA transfected HUVECs (shCD82 (-)) were seeded on the upper chamber of fibronectin-coated culture inserts with the lower chamber containing VEGF (10 or 20 ng/ml). The number of cells that migrated through the inserts in the lower chamber was measured as Calcein AM positive cells and the mean values \pm S.E. of fluorescence units (F.U.) are shown ($n = 5$ experiments with triplicates). A significant increase in migration of control shRNA HUVECs was observed in a dose-dependent manner of VEGF (* $P < 0.05$). In contrast, a significant decrease in migration of shCD82 HUVECs was indicated in 10 and 20 ng/ml of VEGF (** $P < 0.001$ vs. control shRNA). (C) CD82-knockdown HUVECs (shCD82-300) (shCD82 (+)) or control shRNA transfected HUVECs (shCD82 (-)) were incubated with 10 ng/ml of VEGF. Proliferation of HUVECs was monitored by measuring [³H]-thymidine (TdR) incorporation at 24, 48 or 72 h of culture. The mean values of [³H]-TdR incorporation \pm S.E. are shown ($n = 5$ experiments with triplicates). A significant increase in proliferation of control shRNA HUVECs was observed in a time course of culture (* $P < 0.05$). In contrast, a significant decrease in proliferation was indicated in shCD82 HUVECs (** $P < 0.001$ vs. control shRNA). (For interpretation of the references to colour in this figure legend, the reader is referred to the web version of this article.)

3.2. Anti-CD82 mAb 4F9 inhibits EC migration, proliferation and angiogenesis

We previously established the anti-CD82 mAb 4F9, which exerted a comitogenic effect on T cell costimulatory signaling pathway and caused cell spreading in H9 cells [2,3]. While these data indicate that 4F9 has a functional effect on CD82-expressing cells, we next hypothesized that EC activity is also regulated by treatment with 4F9. To assess the role of 4F9 in EC activity and angiogenesis, we therefore performed angiogenesis, migration or proliferation assays following 4F9 treatment. As shown in Fig. 2A, 4F9 treatment significantly decreased angiogenesis in a dose-dependent manner. In addition, this inhibitory effect of 4F9 on angiogenesis was comparable to that of suramin treatment, which is a potent inhibitor of VEGF (** in Fig. 2A). Furthermore, we assessed cell migration and proliferation of HUVECs following 4F9 treatment. As shown in Fig. 2B, cell migration was reduced by treatment with 4F9 in a dose-dependent manner, an inhibitory effect that was comparable to that of suramin (** in Fig. 2B). Moreover, while no change in proliferative activity was observed after 24 h of 4F9 treatment, cell proliferation decreased significantly following a 48 h incubation period with 4F9 in a dose-dependent manner (Fig. 2C). In addition, 4F9 treatment exhibited a significant decrease in angiogenesis, migratory and proliferative activity while being cultured with high doses of exogenous VEGF up

to 100 ng/ml (data not shown). These data strongly suggest that ligation of CD82 by the anti-CD82 mAb 4F9 leads to suppression of VEGF-dependent angiogenesis.

3.3. Anti-CD82 mAb 4F9 inhibits phosphorylation of VEGFR2 via control of CD82 distribution in lipid rafts

The VEGF family members bind three different RTK receptors: VEGFR1 (Flt-1), VEGFR2 (Flt-1-KDR) and VEGFR3 [12]. Among them, VEGFR2 is the principal mediator of VEGF-induced angiogenesis signaling in EC [12,20]. We next examined the effect of 4F9 treatment on VEGFR2 phosphorylation in HUVECs. As shown in Fig. 3A, 4F9 treatment in HUVECs significantly decreased phosphorylation of VEGFR2 by exogenous VEGF treatment, compared to that of control IgG. These data suggest that 4F9 inhibitory effect on EC activity is mediated at least partly via decreased VEGFR2 phosphorylation.

Previous work has shown that CD82 and VEGFR2 are components of lipid rafts and that CD82 is internalized through lipid rafts [16,21]. We therefore hypothesized that 4F9 treatment affects VEGFR2 phosphorylation by regulating CD82 in lipid rafts. To determine whether distribution of CD82 molecules in lipid rafts is altered by 4F9 treatment, we next analyzed the distribution pattern of CD82 in light density fractions by discontinuous sucrose gradient centrifugation. As shown in Fig. 3B, a slight proportion of CD82 is

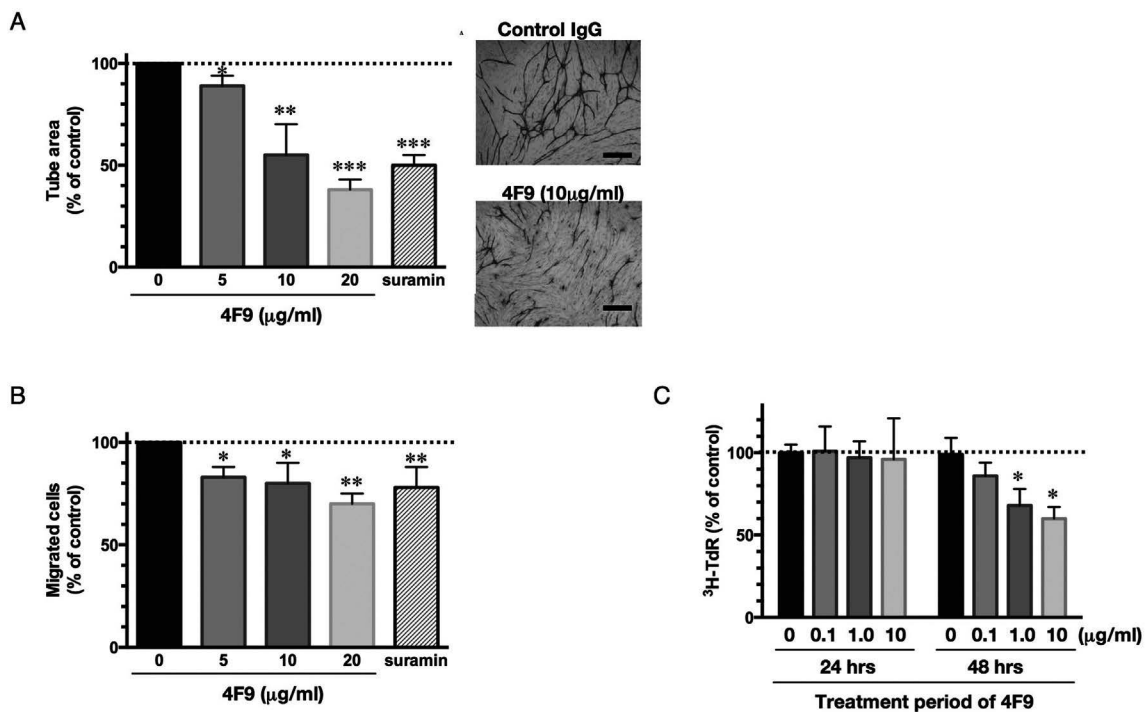


Fig. 2. Anti-CD82 mAb 4F9 inhibited HUVEC angiogenesis, migration and proliferation. (A) HUVECs were incubated with control mouse IgG (20 μ g/ml, as indicated at 0 μ g/ml of 4F9), 4F9 (5, 10, and 20 μ g/ml) or suramin (50 μ M), stained and measured for angiogenesis by the same method as in Fig. 1A. Left panel shows the results expressed as the percentage of the mean values obtained in the percentage of tube area in control IgG treated HUVECs. The mean values of percentage of tube area \pm S.E. ($n = 5$ experiments with triplicates), and the horizontal dotted line indicates a 100% level of control IgG treatment. A significant decrease in angiogenesis was indicated in a dose-dependent manner for 4F9 as well as for suramin (* $P < 0.05$, ** $P < 0.01$ or *** $P < 0.0001$ vs. control IgG). Representative microphotographs of tube formation of control IgG or 4F9-treated HUVECs were shown in the right two panels (brown cells are anti-CD31 immunohistochemistry). Scale bars indicate 25 μ m. (B) Following treatment with control mouse IgG (20 μ g/ml, as indicated at 0 μ g/ml of 4F9), 4F9 (5, 10, and 20 μ g/ml) or suramin (50 μ M), HUVECs were seeded on the upper chamber of fibronectin-coated inserts with the lower chamber containing VEGF (10 ng/ml). The migrated cells were measured by the same method as in Fig. 1B. The results are expressed as the percentage of the mean values obtained in the fluorescence levels of control IgG treated HUVECs (\pm S.E. of five independently performed experiments with triplicates). The horizontal dotted line indicates a 100% level of control IgG treatment. A significant decrease in cell migration was indicated in a dose-dependent manner for 4F9 as well as for suramin (* $P < 0.05$ or ** $P < 0.001$ vs. control IgG). (C) Following treatment with control mouse IgG (10 μ g/ml, as indicated at 0 μ g/ml of 4F9), 4F9 (0.1, 1.0, and 10 μ g/ml), HUVECs were incubated with 10 ng/ml of VEGF. Proliferation of HUVECs was monitored by measuring [3 H]-TdR incorporation at 24 or 48 h of culture. The mean values of [3 H]-TdR incorporation \pm S.E. are shown ($n = 5$ experiments with triplicates), and the horizontal dotted line indicates a 100% level of control IgG treatment. A significant decrease in proliferation after 48 h of culture was observed in a dose-dependent manner for 4F9. (* $P < 0.001$ as calculated by Student's *t* test). (For interpretation of the references to colour in this figure legend, the reader is referred to the web version of this article.)

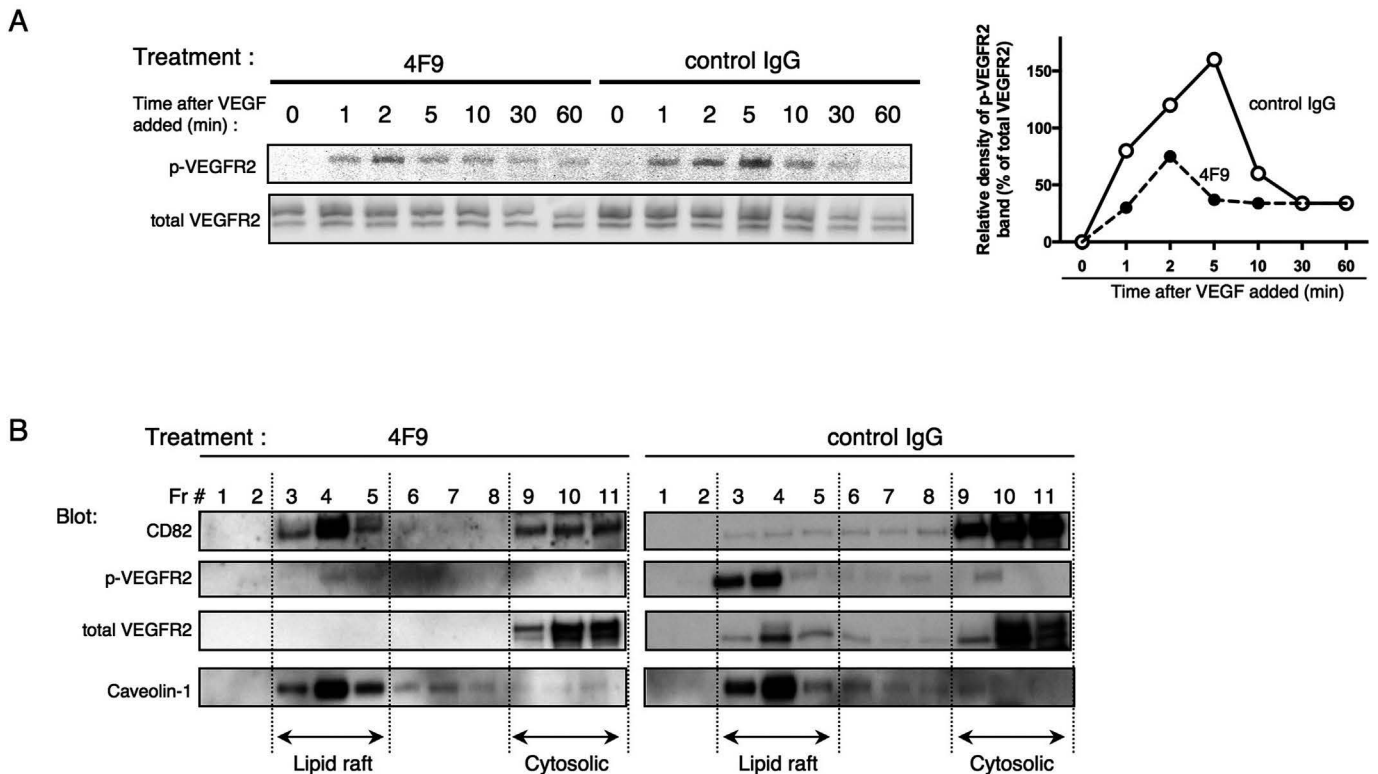


Fig. 3. Anti-CD82 mAb 4F9 inhibited phosphorylation of VEGFR2 via control of CD82 distribution in lipid rafts. **(A)** Following treatment with 4F9 or control mouse IgG (each 10 μ g/ml) for 12 h, HUVECs were incubated with 10 ng/ml of VEGF for the indicated time periods. Cells were harvested, and cell lysates were subjected to Western blot analysis for phosphorylated (upper of left panel) or total VEGFR2 (lower of left panel). Phosphorylated VEGFR2 (p-VEGFR2) proteins in each time point were quantified by measuring p-VEGFR2 band density and are presented as the percentage of each corresponding band density of total VEGFR2 (right panel). In control IgG treated HUVECs, levels of phosphorylation of VEGFR2 increased from 1 to 10 min after VEGF addition (solid line). On the other hand, 4F9 treatment significantly decreased phosphorylation levels of VEGFR2 (dashed line). Similar results were obtained in three independent experiments. **(B)** HUVECs were treated with 4F9 or control mouse IgG (each 10 μ g/ml) for 12 h, followed by incubation with 10 ng/ml of VEGF for 5 min. Light density lipid raft or heavy density cytosolic fractions were prepared by sucrose gradient ultracentrifugation. The distribution of CD82, p-VEGFR2, total VEGFR2 and caveolin-1 was determined by immunoblotting with specific antibodies. Caveolin-1 was a representative of lipid raft proteins and was used as a quantity control indicating equal amounts in the experiments (bottom panels). Fraction number (Fr#) 3–5 or 9–11 contains lipid raft or cytosolic fractions, respectively. After 4F9 treatment, CD82 molecule was recruited in the lipid raft fractions (upper panels), and VEGFR2 (both phosphorylated and total VEGFR2) were segregated from lipid raft to cytosolic fractions (middle two panels). Similar results were obtained in three independent experiments.

present in lipid raft fractions, while being mainly presented in the cytosolic fraction, in HUVECs treated with control IgG (upper right panel). On the other hand, 4F9 treatment markedly increased CD82 distribution in lipid raft fractions (left upper panel of Fig. 3B). These data suggest that engagement of CD82 by 4F9 alters its distribution level in lipid rafts. We next analyzed phosphorylation of VEGFR2 and its distribution in lipid rafts following 4F9 treatment. Upon treatment with control IgG, VEGF-induced phosphorylation of VEGFR2 was observed in lipid raft fractions, while phosphorylation level of VEGFR2 decreased following 4F9 treatment (second upper panels in Fig. 3B). Moreover, 4F9 treatment abrogated recruitment of VEGFR2 in lipid rafts (second lower panels of Fig. 3B), while distribution of the other lipid raft molecule caveolin-1 was not affected by 4F9 treatment (bottom panels of Fig. 3B). These data indicate that ligation of CD82 by 4F9 abrogates recruitment of VEGFR2 in lipid rafts and decreases VEGF-mediated phosphorylation of VEGFR2. Taken together with the data above, our findings strongly suggest that 4F9 treatment inhibits VEGF-dependent angiogenesis through control of distribution of CD82 and VEGFR2 in lipid rafts.

4. Discussion

In this study, we showed that knockdown of CD82 expression decreased migration, proliferation and angiogenesis in HUVECs.

Moreover, treatment with the anti-CD82 mAb 4F9 inhibited VEGF-dependent EC migration, proliferation and angiogenesis. Finally, we demonstrated that inhibition of HUVECs activity by 4F9 was achieved via CD82-dependent regulation of VEGFR2 recruitment in lipid rafts.

In contrast to the well-known characteristics of CD82 in tumor cell biology [1], its role in regulating vascular function is heretofore unclear. Recent study using *Cd82*-null mice showed that perturbation of CD82-ganglioside-CD44 signaling attenuates pathological angiogenesis by inhibiting EC movement [16], while *Cd82*-null mice display normal vessel development without obvious vascular defects [17]. In human vascular biology, VEGF is one of key proteins involved in the cancer angiogenesis pathway [9,13]. Sustained VEGF expression from cancer cells leads to the development and maintenance of a vascular network that promotes tumor growth and metastasis [13]. Binding of VEGF to VEGFR2 on ECs induces a downstream signaling process critical to EC motility, proliferation and survival [18]. Although VEGF-dependent EC activity plays an essential role in angiogenesis [18], a functional role for CD82 in association with VEGF/VEGFRs in EC activity has not yet been clearly established. Our data are novel and significant in that they demonstrate the association between CD82 and the regulation of VEGF-dependent EC functions, with knockdown of CD82 in HUVECs resulting in decrease of VEGF-dependent EC migration, proliferation and angiogenesis.

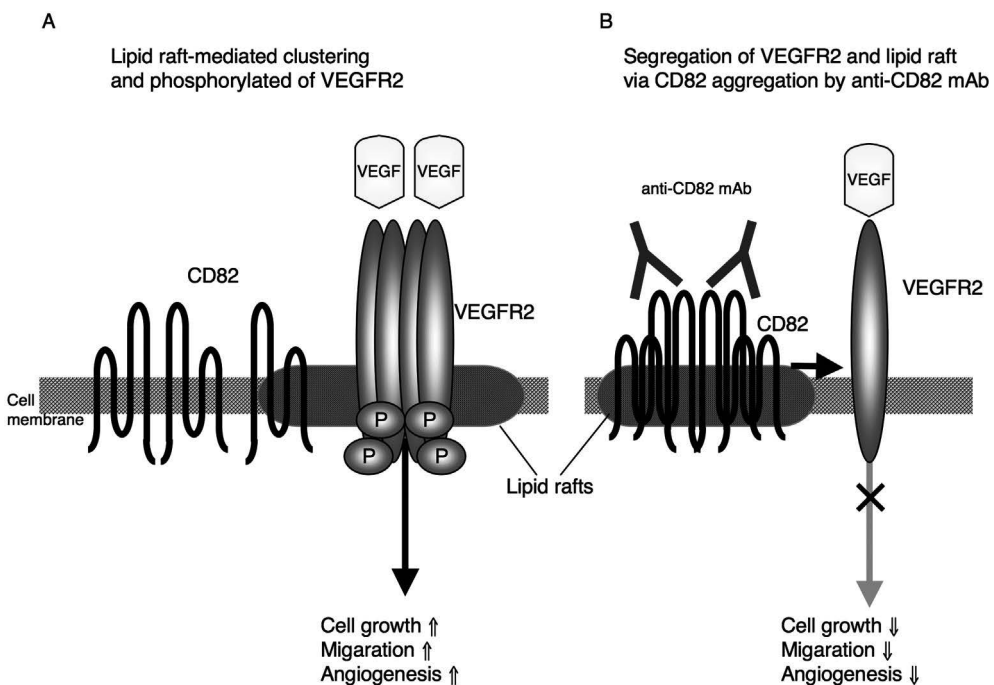


Fig. 4. Model for the regulation of VEGFR2 phosphorylation in lipid rafts via ligation of CD82 molecules by 4F9.

Targeting cancer angiogenesis has been a recent focus as anti-cancer therapy [9]. Studies on the role of VEGF in tumor progression have mostly been directed to the cancer angiogenesis effect exerted by VEGF and VEGFR on tumor environmental vascular network [9,22]. In the present study, we clearly demonstrated that the anti-CD82 mAb 4F9 inhibits EC migration, proliferation and angiogenesis. Since endothelial CD82 regulates VEGF-dependent tumor angiogenesis, 4F9 can be a novel drug candidate for anticancer therapy.

Binding of VEGF to VEGFR2 induces VEGFR2 dimerization and subsequent autophosphorylation of the intracellular tyrosine kinase domains, resulting in EC proliferation, movement and angiogenesis [12,20,23]. Our biochemical analysis demonstrates that 4F9 treatment affects the distribution of CD82 and VEGFR2 in lipid rafts, associated with decreased VEGFR2 phosphorylation and inhibition of EC migration, proliferation and angiogenesis. On the basis of our current results, we propose a model to describe the molecular mechanisms involved in 4F9 regulation of CD82 role in VEGF-dependent EC activity (Fig. 4); in physiological condition, CD82 molecules are mostly present outside of lipid rafts, which mediate clustering and phosphorylation of VEGFR2 upon VEGF binding (Fig. 4A). After ligation of CD82 molecules by 4F9, CD82 aggregates in lipid rafts with segregation of VEGFR2 out of lipid rafts, leading to attenuation of VEGF-dependent signaling (Fig. 4B). CD82 therefore plays an important role in VEGF-dependent EC activity as a membrane domain organizer.

Along with VEGF, IL-6 also plays a role of EC activity in melanoma angiogenesis [8]. It has been reported that the gp130 molecule involved in the IL-6 receptor (IL-6R) complex partially exists in lipid rafts and serves to activate signaling complex through lipid raft aggregation [24]. It is possible that CD82 regulates IL-6/IL-6R pathway-related EC activity via organization of membrane micro-domains, a topic which will be examined in future studies.

In summary, the anti-CD82 mAb 4F9 effectively inhibits phosphorylation of VEGFR2 through the organization of lipid raft microdomains in human EC. Our present study hence suggests that CD82 on EC is potentially a suitable target for anti-angiogenic

therapy in tumor angiogenesis.

The authors declare no competing financial interests

S.N. and S.I. contributed to the conception and design of the study, or acquisition of data, R.H., E.K. and N.I. contributed to analysis and interpretation of data, K.O. and C.M. designed the research, interpreted the data and wrote the paper, N.H.D. interpreted the data, assisted with the paper, and proofread the manuscript. All authors showed final approval of the version to be submitted.

Acknowledgements

This study was supported in part by a grant of the Ministry of Education, Science, Sports and Culture, Japan (K.O. and C.M.) (15H04879 and 15K15324), a grant of the Ministry of Health, Labour and Welfare, Japan (C.M.) and a Grant-in-Aid (S1311011) from the Foundation of Strategic Research Projects in Private Universities from the Ministry of Education, Culture, Sports, Science, and Technology, Japan (C.M.).

Appendix A. Supplementary data

Supplementary data related to this article can be found at <http://dx.doi.org/10.1016/j.bbrc.2016.04.081>.

Transparency document

Transparency document related to this article can be found online at <http://dx.doi.org/10.1016/j.bbrc.2016.04.081>.

References

- [1] M. Zoller, Tetraspanins: push and pull in suppressing and promoting metastasis, *Nat. Rev. Cancer* 9 (2009) 40–55.
- [2] Y. Nojima, T. Hirose, K. Tachibana, et al., The 4F9 antigen is a member of the

- tetra spans transmembrane protein family and functions as an accessory molecule in T cell activation and adhesion, *Cell Immunol.* 152 (1993) 249–260.
- [3] S. Iwata, H. Kobayashi, R. Miyake-Nishijima, et al., Distinctive signaling pathways through CD82 and $\beta 1$ integrins in human T cells, *Eur. J. Immunol.* 32 (2002) 1328–1337.
- [4] J.T. Dong, P.W. Lamb, C.W. Rinker-Schaeffer, et al., KAI1, a metastasis suppressor gene for prostate cancer on human chromosome 11p11.2, *Science* 268 (1995) 884–886.
- [5] F.A. Malik, A.J. Sanders, W.G. Jiang, KAI-1/CD82, the molecule and clinical implication in cancer and cancer metastasis, *Histol. Histopathol.* 24 (2009) 519–530.
- [6] E. Odintsova, T. Sugiura, F. Berditchevski, Attenuation of EGF receptor signaling by a metastasis suppressor, the tetraspanin CD82/KAI-1, *Curr. Biol.* 10 (2000) 1009–1012.
- [7] S.C. Sridhar, C.K. Miranti, Tetraspanin KAI1/CD82 suppresses invasion by inhibiting integrin-dependent crosstalk with c-Met receptor and Src kinases, *Oncogene* 25 (2006) 2367–2378.
- [8] Y. Tang, M. Bhandaru, Y. Cheng, et al., The role of the metastasis suppressor gene KAI1 in melanoma angiogenesis, *Pigment. Cell Melanoma Res.* 28 (2015) 696–706.
- [9] H.L. Goel, A.M. Mercurio, VEGF targets the tumour cell, *Nat. Rev. Cancer* 13 (2013) 871–882.
- [10] W. Risau, Mechanisms of angiogenesis, *Nature* 386 (1997) 671–674.
- [11] L. Coultas, K. Chawengsaksophak, J. Rossant, Endothelial cells and VEGF in vascular development, *Nature* 438 (2005) 937–945.
- [12] N. Ferrara, H.-P. Gerber, J. LeCouter, The biology of VEGF and its receptors, *Nat. Med.* 9 (2003) 669–676.
- [13] P. Carmeliet, R.K. Jain, Angiogenesis in cancer and other diseases, *Nature* 407 (2000) 249–257.
- [14] K. Nagao, K. Oka, HIF-2 directly activates CD82 gene expression in endothelial cells, *Biochem. Biophys. Res. Commun.* 407 (2011) 260–265.
- [15] H. Hurwitz, L. Fehrenbacher, W. Novotny, et al., Bevacizumab plus irinotecan, fluorouracil, and leucovorin for metastatic colorectal cancer, *N. Engl. J. Med.* 350 (2004) 2335–2342.
- [16] Q. Wei, F. Zhang, M.M. Richardson, et al., CD82 restrains pathological angiogenesis by altering lipid raft clustering and CD44 trafficking in endothelial cells, *Circulation* 130 (2014) 1493–1504.
- [17] J.I. Risinger, M. Custer, L. Feigenbaum, et al., Normal viability of Kai1/Cd82 deficient mice, *Mol. Carcinog.* 53 (2013) 610–624.
- [18] N. Ferrara, T. Davis-Smyth, The biology of vascular endothelial growth factor, *Endocr. Rev.* 18 (1997) 4–25.
- [19] T. Ishii, K. Ohnuma, A. Murakami, et al., CD26-mediated signaling for T cell activation occurs in lipid rafts through its association with CD45RO, *Proc. Natl. Acad. Sci. U. S. A.* 98 (2001) 12138–12143.
- [20] C. Fontanella, E. Ongaro, S. Bolzonello, et al., Clinical advances in the development of novel VEGFR2 inhibitors, *Ann. Transl. Med.* 2 (2014) 123.
- [21] L. Labrecque, I. Royal, D.S. Surprenant, et al., Regulation of vascular endothelial growth factor receptor-2 activity by caveolin-1 and plasma membrane cholesterol, *Mol. Biol. Cell* 14 (2003) 334–347.
- [22] J. Folkman, Tumor angiogenesis: therapeutic implications, *N. Engl. J. Med.* 285 (1971) 1182–1186.
- [23] A. Kiba, H. Sagara, T. Hara, et al., VEGFR-2-specific ligand VEGF-E induces non-edematous hyper-vascularization in mice, *Biochem. Biophys. Res. Commun.* 301 (2003) 371–377.
- [24] P.B. Sehgal, G.G. Guo, M. Shah, et al., Cytokine signaling: STATs in plasma membrane rafts, *J. Biol. Chem.* 277 (2002) 12067–12074.

PRIMARY RESEARCH

Open Access



A humanized anti-CD26 monoclonal antibody inhibits cell growth of malignant mesothelioma via retarded G2/M cell cycle transition

Mutsumi Hayashi^{1,2}, Hiroko Madokoro¹, Koji Yamada³, Hiroko Nishida¹, Chikao Morimoto⁴, Michiie Sakamoto¹ and Taketo Yamada^{1,5*}

Abstract

Background: Malignant Mesothelioma (MM) is a highly aggressive tumor with poor prognosis. Multimodal treatments and novel molecular targeted therapies against MM are in high demand in order to treat this disease effectively. We have developed a humanized monoclonal antibody YS110 against CD26 expressed in 85 % of MM cases. CD26 is thought to be involved in tumor growth and invasion by interacting with collagen and fibronectin, or affecting signal transduction processes.

Methods: We evaluated the direct anti-tumor effect of YS110 against MM cell lines, NCI-H2452 and JMN, and investigated its effects on cell cycle and on the cell cycle regulator molecules. In addition, we investigated synergistic effects of YS110 and anti-tumor agent pemetrexed (PMX) against MM cell line both in vitro and in vivo.

Results: YS110 suppressed the proliferation of NCI-H2452 cells by approximately 20 % in 48 h. Based on cell cycle analysis, percentage of cells in G2/M phase increased 8.0 % on the average after YS110 treatment; in addition, cell cycle regulator p21 cip/waf1 was increased and cyclin B1 was decreased after YS110 treatment. Inhibitory phosphorylation of both cdc2 (Tyr15) and cdc25C (Ser216) were elevated. Furthermore, activating phosphorylation of p38 MAPK (Thr180/Tyr182) and ERK1/2 (Thr202/Tyr204) were augmented at 24 h after YS110 treatment. PMX rapidly induced CD26 expression on cell surface and the treatment with both YS110 and PMX inhibited in vivo tumor growth accompanied by a synergistic reduction in the MIB-1 index.

Conclusion: This is a first report of a novel anti-proliferative mechanism of the humanized anti-CD26 monoclonal antibody YS110, which resulted in G2/M cell cycle delay through regulation of quantity and activity of various cell cycle regulating molecules.

Keywords: Mesothelioma, CD26, Monoclonal antibody, G2/M transition, Pemetrexed

Background

Malignant mesothelioma (MM) is an aggressive cancer of the pleura, peritoneal cavity, pericardium, and scrotum and has a poor prognosis. MM is associated with occupational exposure to asbestos and, despite

legislation introduced by many industrialized countries, the incidence is not expected to peak until 2020 due to the long latency between initial exposure and disease expression [1]. As single modality approach to treatment has failed to extend survival, multimodal treatment and novel molecular targeted therapies are highly sought after. Although extrapleural pneumonectomy (EPP) is a preferred treatment option, median survival among patients receiving EPP alone is less than 10 months [2]. EPP followed by high-dose radiation therapy (RT) has

*Correspondence: taketo@saitama-med.ac.jp

⁵ Department of Pathology, Saitama Medical University, 38 Morohongo, Saitama, Moroyama-machi 350-0495, Japan
Full list of author information is available at the end of the article

been shown to prolong median survival to 33.8 months in patients with Stage 1 and Stage 2 MM but survival remained 10 months in patients with Stage 3 and Stage 4 MM [2]. A Phase 3 trial showed that combination of pemetrexed and cisplatin improved survival over cisplatin alone for inoperable patients [3]. According to recent multicenter trials of trimodality treatment that consisted of neoadjuvant chemotherapy (cisplatin and pemetrexed), EPP, and adjuvant RT led in the USA [2] and Europe [4], median survival of patients who completed the therapy was 29.1 months compared to 18.4 months in controls. Since the trimodality approach seems to be limited and because not all patient can tolerate aggressive therapies, novel molecular targeted therapies are highly desirable. To date, a number of molecular targeted agents have been evaluated in MM. While tyrosine kinase inhibitors against epidermal growth factor receptor (EGFR) and platelet-derived growth factor receptor (PDGFR) did not show clinically significant effects, histone deacetylase inhibitor (HDACI) and anti-angiogenic agents showed some clinical benefits and are undergoing Phase 3 trials [5]; however, none of these agents have been incorporated into clinical practice and efforts must continue in the area of both clinical research and search for novel target molecules.

CD26 is an 110 kD glycoprotein anchored in the cellular membrane with dipeptidyl peptidase IV activity. CD26 is also known as a co-stimulatory molecule of the T lymphocyte. CD26 binds to caveolin-1 on antigen-presenting cells and the interaction triggers signal transduction process leading to T cell proliferation and cytokine production [6]. Several recent studies have shown that CD26 is highly expressed in several malignancies, including MM, lung adenocarcinoma, hepatocellular carcinoma, prostate cancer, and thyroid cancer [7]. CD26 expression evaluated by immunohistochemistry was positive in 85 % of tested MM cases [8, 9]. Moreover, CD26 is thought to be involved in tumor growth and invasion through its interaction with collagen and fibronectin or by regulating activity of chemotactic peptides through its DPPIV activity. Furthermore, CD26 has been reported to be involved in signal transduction processes, including the p38 MAPK pathway. Though the mechanisms of action of CD26 have not been clarified, its enzymatic activity does not appear essential for its role in signal transduction process [10]. Considering its high rate of overexpression in MM and suspected function in tumor progression, we have developed a humanized an anti-CD26 antibody, designated YS110, as a targeted therapy against CD26-positive malignancies, including MM. We have previously reported the anti-tumor effects of YS110 against MM cells [11]. In addition to the anti-tumor effect via antibody-dependent-cell-mediated-cytotoxicity, YS110 showed direct

anti-tumor effect via p27^{kip1} accumulation [11]; however, the molecular mechanism of direct anti-tumor effect of YS110 against MM cell lines remains unknown.

The molecular mechanisms underlying the direct anti-tumor effect of several monoclonal antibodies have been investigated; for example, the anti-HER-2 antibody (Trastuzumab) and anti-EGFR antibody (Cetuximab) result in G1/S cell cycle arrest by upregulating the CDK inhibitor p27^{kip1} via multiple signaling pathways [12, 13]. The anti-CD20 antibody (rituximab) can induce cell death of malignant B cell lymphoma cells in vitro via inhibition of the p38 MAPK, ERK1/2, and AKT anti-apoptotic survival pathways [14]. Most therapeutic antibodies against cancers that affect the cell cycle, including antibodies mentioned above, result in G1/S arrest. So far, only one anti-cancer antibody, the anti-human type 1 insulin-like growth factor receptor (IGF-IR) antibody A12 against androgen-independent prostate cancer cell line LuCaP 35 V, has been reported to cause G2/M cell cycle delay although its molecular mechanism is not yet understood [15].

In this study, we focused on evaluating the direct in vitro effect of the humanized anti-CD26 monoclonal antibody YS110 against the MM cell line NCI-H2452 and investigated its effect on the cell cycle and on cell cycle-regulating molecules. YS110 inhibited growth of YS110 with G2/M cell cycle arrest and altered the expression or phosphorylation state of cell cycle molecules. Furthermore, pemetrexed (PMX), a standard reagent against mesothelioma, rapidly induced CD26 expression on the cell surface and treatment with both YS110 and PMX inhibited in vivo tumor growth in a synergistic manner. This is the first report describing a novel anti-proliferative mechanism of the humanized anit-CD26 monoclonal antibody YS110, which resulted in G2/M cell cycle delay, through regulation of quantity and activity of various cell cycle-regulating molecules.

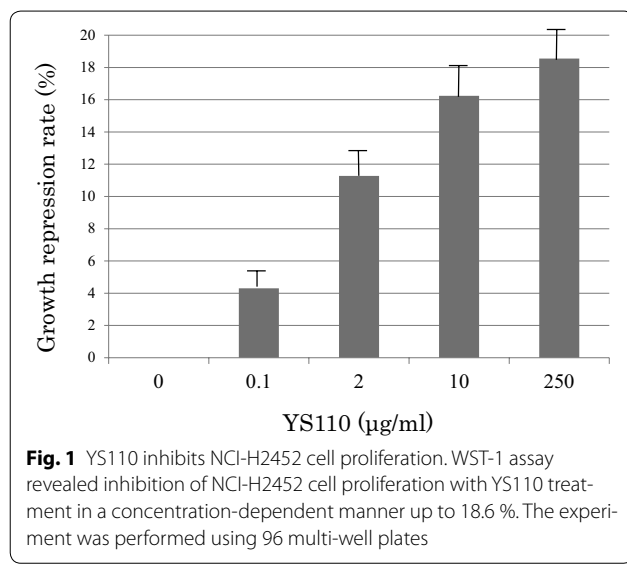
Results

YS110 inhibits mesothelioma cell proliferation

YS110 inhibits proliferation of the mesothelioma cell line NCI-H2452 in a concentration-dependent manner (Fig. 1). Maximum of growth inhibition was 18.3 % at 250 µg/mL of YS110. Based on this result, we used YS110 at 2 µg/mL, which showed 11.2 % of growth inhibition, in the following experiments.

YS110 induced G2/M cell cycle delay in mesothelioma cells

To investigate the mechanism responsible for the growth inhibition caused by YS110, cell-cycle distribution was determined by flow cytometry analysis. At 24 h after YS110 treatment, the percentage of cells in



the G2/M phase increased compared to the control. The representative experiment is shown (Fig. 2a). On the average of ten experiments, the percentage of G2/M phase cells were significantly increased after YS110 treatment ($p < 0.05$) (Fig. 2b). This cell cycle delay may be compatible with repression of cell proliferation. Furthermore, in another CD26 positive MM cell line NCI-H28, the percentage of cells in G2/M phase increased by 5 % on the average after YS110 treatment though its significance could not be proved statistically (data not shown).

YS110 alters cell cycle regulators

We investigated the alterations caused by YS110 treatment in the quantity and activation state of cell cycle regulators responsible for G2/M transition. At 24 h after YS110 treatment, the cell cycle regulator p21 increased while the positive regulatory subunit cyclin B1 decreased. Inhibitory phosphorylation of cdc2 on Tyr15 and inhibitory phosphorylation of cdc25C on Ser216, an upstream inhibitory regulator of cdc2, was elevated (Fig. 3a). Cdc25C phosphorylated on Ser216 is known to be sequestered into cytoplasm and refrained from contact with cdc2 [16]. After YS110 treatment for 24 h, cytoplasmic whole cdc25C was elevated while nuclear whole cdc25C was decreased, as confirmed by densitometry analysis (Fig. 3b). At 6 h and 12 h after YS110 treatment, the amount of phosphorylated cdc2 and phosphorylated cdc25C were varied among experiments despite consistent increase at 24 h. No significant change in cdc25A and cdc25B was observed (data not shown).

YS110 elevates activating phosphorylation of p38 MAPK and ERK1/2

In order to determine the upstream regulator of cdc25C phosphorylation caused by YS110 treatment, expression and activation status of several molecules known to regulate cell cycle through cdc25C phosphorylation were examined. Activating phosphorylation of p38 MAPK (Thr180/Tyr182) and ERK1/2 (Thr202/Tyr204) were elevated 24 h after YS110 treatment (Fig. 4a). No significant change in chk1, chk2, or c-TAK1 was observed (data not shown). While the p38 inhibitor SB203580 failed to block G2/M arrest caused by YS110 (data not shown), the MEK1/2 inhibitor U0126 blocked G2/M arrest caused by YS110 according to cell cycle analysis using flowcytometry (Fig. 4b).

Pemetrexed (PMX) increased CD26 expression in mesothelioma cells in vitro

CD26 expression on the cell surface of JMN cells increased 15 % from 6 to 6.5 % 24 h after treatment with 10 µM of PMX based on flowcytometry analysis (Fig. 5a). In order to confirm the augmented expression of CD26 in JMN cells, Western blot analysis was performed. CD26 protein expression was rapidly induced in whole cell lysates by treatment with 10 µM of PMX at 1 h after PMX treatment; most augmentation of CD26 expression at 6 h and then this augmented expression continued to 24 h after PMX treatment (Fig. 5b). In order to examine the altered expression of CD26 in NCI-H2452 cells, Western blot analysis was performed. CD26 protein expression in NCI-H2452 cells was also rapidly induced in whole cell lysates by treatment with 10 µM of PMX at 1 h after PMX treatment; most augmentation of CD26 expression at 6 h and then this augmented expression continued to 24 h after PMX treatment (Fig. 5b).

Effective inhibition of in vivo mesothelioma cell growth by combined treatment with both YS110 and PMX

Combination effects of YS110 and PMX were examined using xenograft models with JMN cells transplanted into NOG mice subcutaneously. Mice were then monitored for the development and progression of tumors and the tumor size was determined by caliper measurement. Tumor size in mice treated with both YS110 and PMX was smaller than mice treated with only YS110 or PMX (data not shown). The weight of tumors with YS110 treatment was insignificantly reduced (Fig. 6A). PMX treatment induced a significant reduction in tumor weight ($p < 0.05$); the combination of YS110 and PMX treatment synergistically reduced tumor weight compared with YS110 single treatment and PMX single treatment ($p < 0.05$).

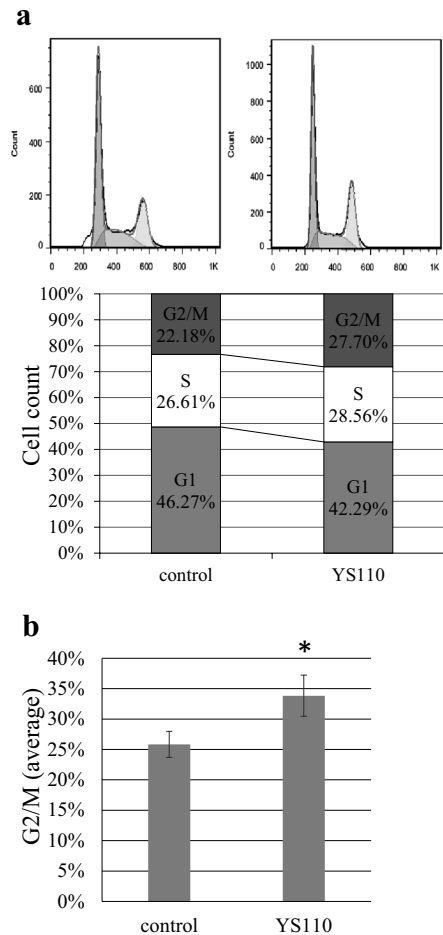


Fig. 2 YS110 induces G2/M cell cycle delay in NCI-H2452 cells. **a** Flowcytometry analysis using propidium iodide staining revealed that the percentage of G2/M phase cells increased while the percentage of G1 phase cells was reduced in NCI-H2452 cells treated 24 h with 2 μ g/mL of YS110. A representative experiment is shown. **b** The average percentage of G2/M phase cells in NCI-H2452 cells treated 24 h with 2 μ g/mL of YS110 was significantly increased (* $p < 0.05$)

Combination effects of tumor growth *in vivo* were examined by measuring the MIB-1 index histologically. The MIB-1 index was significantly decreased in tumors after YS110 or PMX single treatment compared with controls ($p < 0.05$; Fig. 6B, C). Combinatory treatment with YS110 and PMX significantly reduced the MIB-1 index compared to single treatment ($p < 0.05$; Fig. 6B, C).

Histology of the tumor derived from JMN cells in the xenograft model is shown in Fig. 6C. Sarcomatous mesothelioma is shown in HE staining (Fig. 6C-a) and stained with anti-CD26 polyclonal antibody (R&D) (Fig. 6C-b). The MIB-1 index was measured by immunohistochemistry using the anti-Ki-67 (MIB-1) monoclonal antibody. Staining of Ki-67 antigens in nucleus was shown in tumors treated with control IgG (Fig. 6C-c), YS110

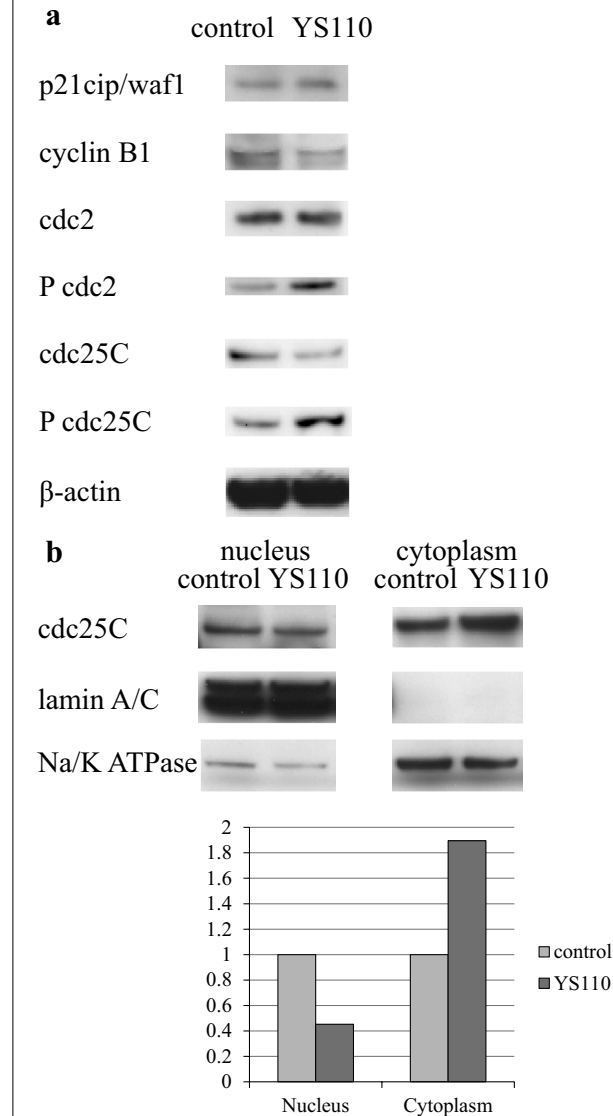


Fig. 3 YS110 alters expressions and phosphorylation of cell cycle regulators. **a** At 24 h after treatment with 2 μ g/mL of YS110, p21 protein expression increased while cyclinB1 protein expression decreased. Inhibitory phosphorylation of cdc2 Tyr15 and cdc25C Ser216 were elevated while there was no significant change in whole cdc2 and cdc25C protein. β -actin was used as an internal control. **b** Alteration in subcellular distribution of whole cdc25C by YS110 treatment is shown. At 24 h after treatment with 2 μ g/mL of YS110, nuclear cdc25C protein decreased while cytoplasmic cdc25C protein increased. LaminA/C was used as a nuclear marker and Na-K ATPase was used as a cytoplasmic marker. The bar graph demonstrates the densitometric analysis of a Western blot of whole cdc25C. Results are normalized by the densitometry of control cells. All experiments were performed in triplicate and a representative experiment is shown

(Fig. 6C-d), and both YS110 and PMX (Fig. 6C-e). The number of Ki-67 positive nuclei was decreased after combined treatment of YS110 and PMX and the necrotic area is indicated by an asterisk (Fig. 6C-e).

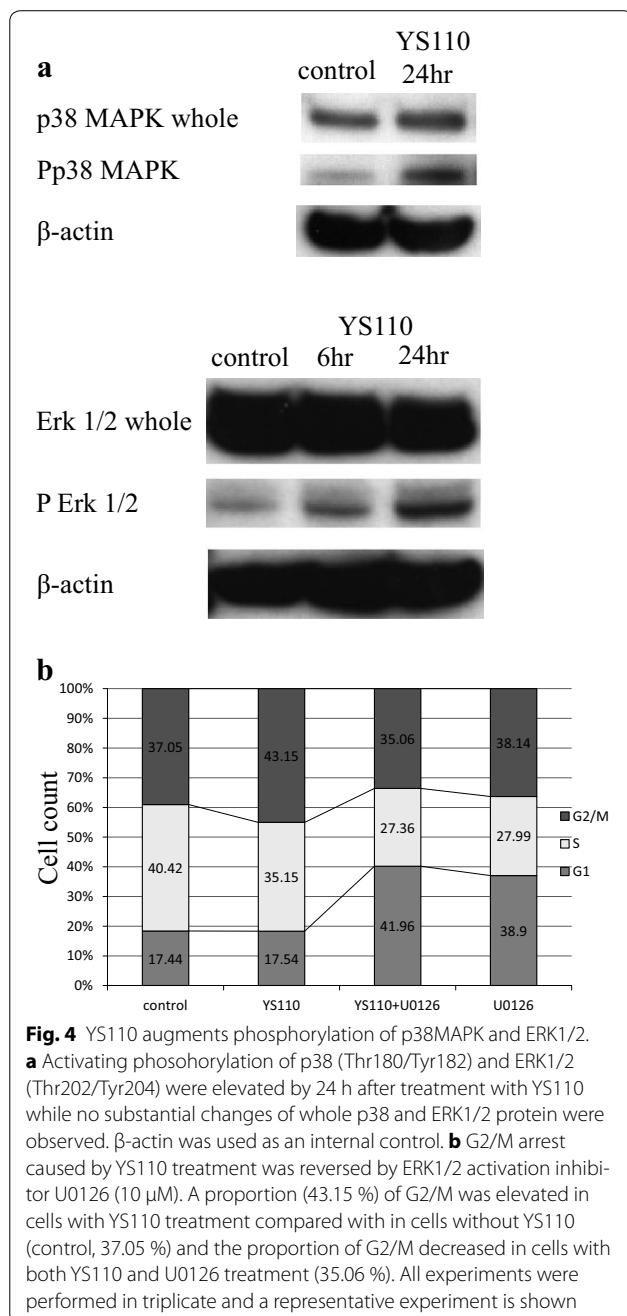


Fig. 4 YS110 augments phosphorylation of p38MAPK and ERK1/2. **a** Activating phosphorylation of p38 (Thr180/Tyr182) and ERK1/2 (Thr202/Tyr204) were elevated by 24 h after treatment with YS110 while no substantial changes of whole p38 and ERK1/2 protein were observed. β -actin was used as an internal control. **b** G2/M arrest caused by YS110 treatment was reversed by ERK1/2 activation inhibitor U0126 (10 μ M). A proportion (43.15 %) of G2/M was elevated in cells with YS110 treatment compared with in cells without YS110 (control, 37.05 %) and the proportion of G2/M decreased in cells with both YS110 and U0126 treatment (35.06 %). All experiments were performed in triplicate and a representative experiment is shown

Discussion

Novel molecular targeted therapies are in high demand since the aggressive trimodality approach against MM has been proved to be limited. We developed a humanized monoclonal antibody against CD26, designated as YS110, a molecular targeted therapy against MM [11]. We expected YS110 to cause ADCC to eliminate CD26 positive MM cells. In addition to the ADCC effect, YS110 demonstrated direct anti-proliferative effects in vitro

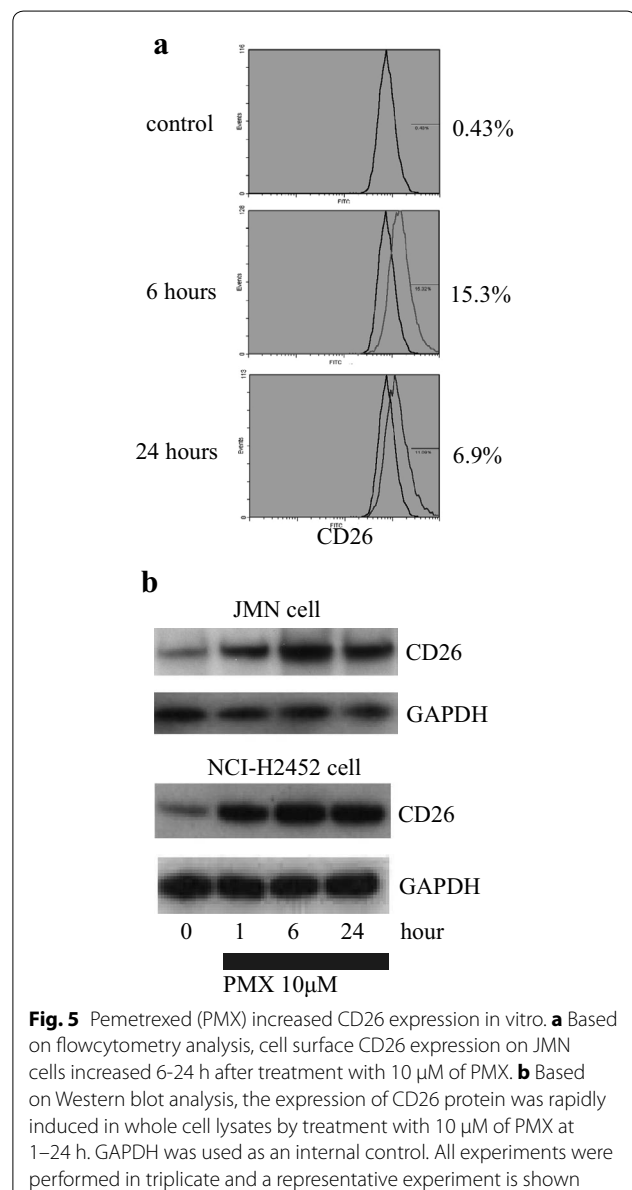


Fig. 5 Pemetrexed (PMX) increased CD26 expression in vitro. **a** Based on flowcytometry analysis, cell surface CD26 expression on JMN cells increased 6–24 h after treatment with 10 μ M of PMX. **b** Based on Western blot analysis, the expression of CD26 protein was rapidly induced in whole cell lysates by treatment with 10 μ M of PMX at 1–24 h. GAPDH was used as an internal control. All experiments were performed in triplicate and a representative experiment is shown

against CD26-positive MM cell lines. We proposed that investigation into the molecular mechanisms of the direct anti-proliferative effect against MM cells would be beneficial for both understanding anti-tumor effect of YS110, as well as uncover the underlying mechanism its proliferation and progression. Although the direct anti-proliferative effect of YS110 is limited to a repression rate of approximately 20 % in vitro, the molecular mechanism was associated with the proliferative signal transduction system and cell cycle. Cell cycle analysis revealed that YS110 caused significant delay of the G2/M transition. To our knowledge, only one anti-cancer MoAb, anti-IGF-IR antibody A12 against the androgen-independent prostate

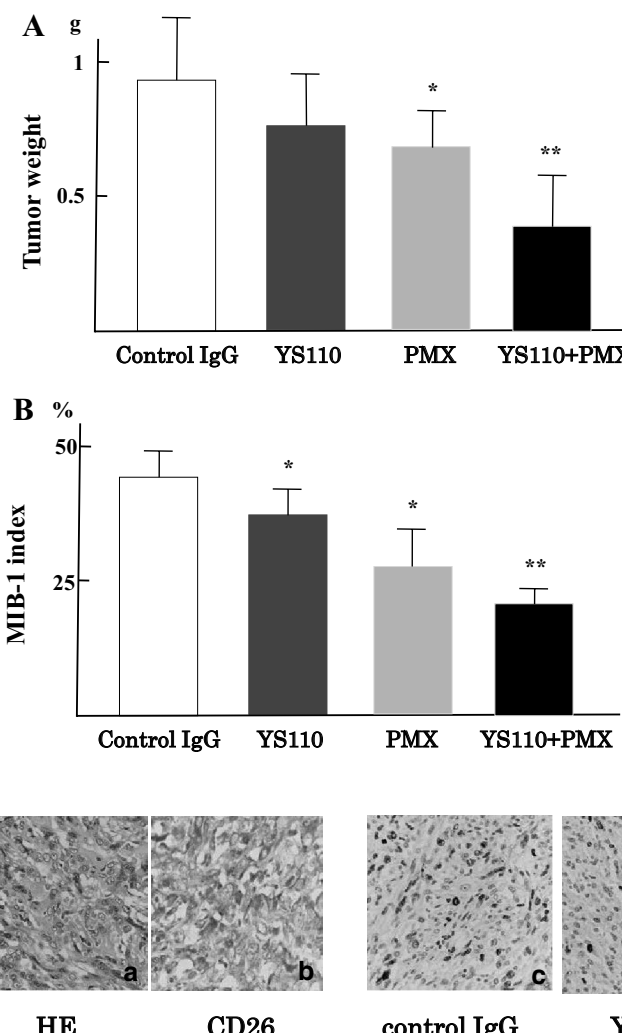


Fig. 6 Effective inhibition of mesothelioma cell growth in vivo. **A** Combination effects of YS110 and PMX were examined using xenograft models with JMN cells transplantation subcutaneously. The weight of tumors treated with YS110 was insignificantly reduced but PMX treatment induced a significantly reduced tumor weight (* $p < 0.05$). A combination of YS110 and PMX treatment reduced tumor weight compared with the weight of tumors with YS110 single treatment and PMX single treatment synergistically (** $p < 0.05$). **B** Combination effects of tumor growth in vivo were examined using a measurement of MIB-1 index histologically. MIB-1 index was significantly reduced with YS110 or PMX single treatment compared with control IgG treatment (* $p < 0.05$). The MIB-1 index after combinatory treatment with YS110 and PMX was significantly reduced compared with YS110 or PMX single treatment (** $p < 0.05$). **C** Sarcomatous mesothelioma is shown in HE staining (a) and stained with anti-CD26 polyclonal antibody (R&D) (b) MIB-1 index was measured by immunohistochemistry using the anti-Ki-67 monoclonal antibody (DAKO, clone MIB-1). Staining of Ki-67 antigens in nucleus is seen in tumors treated with control IgG (c), YS110 (d), and both YS110 and PMX (e). The number of Ki-67 positive nucleus was reduced after combinatory treatment of YS110 and PMX and the necrotic area is indicated by an asterisk (e)

cancer cell line LaCaP 35 V, has been reported to result in G2/M delay although its molecular mechanism is not yet understood [15]. Therefore, we are the first to report results on the molecular mechanisms underlying G2/M delay from a cancer targeted-antibody. In order to elucidate the mechanism of G2/M delay mediated by YS110, we analyzed the quantities and phosphorylation status of G2/M regulators using Western blot analysis. At 24 h after treatment with YS110, inhibitory phosphorylation

of cdc2 and its upstream regulator cdc25C were elevated. Phosphorylation of Cdc25C on Ser216 is sequestered into the cytoplasm and therefore restrained from contact with nuclear cdc2. Increased levels of cytoplasmic whole cdc25 protein and decreased levels of nuclear whole cdc25C protein at 24 h occurred after YS110 treatment, confirming sequestration. Western blot analysis also revealed an increased amount of cell cycle inhibitor p21 and decreased amount of cyclinB1 promotes

G2/M progression at 24 h after YS110 treatment. These alterations may be compatible with the retarded G2/M transition.

To determine the upstream regulator of the altered cdc25C phosphorylation state caused by YS110, we investigated several molecules known to regulate cdc25C. 24 h after YS110 treatment, activated phosphorylation levels of p38 MAPK (Thr180/Thy182) and ERK 1/2 (Thr202/Tyr204) were elevated. Inhibitor assays indicated that YS110 treatment activated the ERK signal pathway, but not the p38MAPK pathway, which induced G2/M delay.

MAPK activation results in many different biological responses, including proliferation, differentiation, and cell death. Although ERK1/2 activation is associated with cell survival and proliferation, a number of studies have shown that activation of ERK1/2 can mediate cell cycle arrest and cell death depending on the stimuli and cell types involved [17]. A number of anti-cancer reagents and an anti-cancer antibodies have been reported to induce G2/M cell cycle arrest and/or apoptosis mediated by ERK1/2 activation [18, 19]. These reagents, like YS110, cause G2/M cell cycle delay by inhibiting phosphorylation of cdc2 and cdc25C and by activating phosphorylation of ERK1/2. The G2/M delay caused by these drugs is antagonized by MEK inhibitors. Among monoclonal antibodies that have been investigated for their anti-cancer characteristics, the anti-CD40 antibody has been reported to cause apoptosis of diffuse large B-cell lymphoma cell lines with ERK1/2 activation through CD40 signaling [20]. In these reported cases, as well as our findings of YS110-CD26 interaction, the mechanisms underlying G2/M delay or apoptosis through ERK1/2 activation is still unknown. As for G1/S cell cycle regulation, a report has indicated that HER2 signaling related to trastuzumab treatment had effects on CDC25A protein stability [21]. The involvement of cell cycle regulators on the effect of anti-tumor antibodies should be further investigated.

Previously, we reported that YS110 induces intranuclear transportation of CD26. When bound to YS110, CD26 is translocated to the nucleus via caveolin-dependent endocytosis. This translocation suppresses transcription of the POLR2A gene, which encodes a large subunit of RNA polymerase, in MM cell lines [22, 23]. The relationship between POLR2A suppression and G2/M cell cycle delay also requires further investigation.

The NCI-H2452 cell line is derived from the epithelioid type of MM and its growth rate is lower than the sarcomatoid type of MM, the JMN cell line [24]. Profiles of cell cycling for synchronization assay in S-phase by thymidine block are available for NCI-H2452 cells but not for JMN cells. NCI-H2452 cells have no tumorigenicity in immunodeficient mice but JMN cells form subcutaneous

tumors or diffuse and spread into the thorax [11, 22, and 23]; therefore, after YS110 treatment, we examined the in vitro cell cycle using NCI-H2452 cells and in the in vivo xenograft model using JMN cells.

Pemetrexed (PMX) induced augmented CD26 expression in both NCI-H2452 cells and JMN cells rapidly (Fig. 5b); this induction of cell surface CD26 on MM cells may be useful for anti-CD26 MoAb therapy against MM. The combination of YS110 and PMX therapy against xenografted MM tumors was applied using JMN cell transplanted immunodeficient mice. As a result, anti-tumor effects were significantly shown in xenografted tumors with YS110 and PMX combined treatment compared to tumors with single treatment of YS110 or PMX, which was accompanied by a significantly reduced MIB-1 index. The combined treatment with YS110 and PMX showed a tendency to retard both G1/S and G2/M transition; however, significant differences of G1/S or G2/M proportion were not seen between YS110 plus PMX treatment and YS110 or PMX single treatment (data not shown).

There have been many anti-cancer monoclonal antibodies (MoAbs) developed and their anti-cancer mechanisms are highly variable. Investigations into each molecular mechanism of an anti-cancer MoAb are significant because it is valuable for the optimization of antibody therapies against cancer and contributes to elucidating the mechanisms of oncogenesis and cancer proliferation. This is the first report of a novel anti-proliferative mechanism of a humanized anti-CD26 monoclonal antibody YS110 causing G2/M cell cycle delay through ERK1/2 phosphorylation and identifying PMX as a CD26 inducer.

Conclusions

Humanized anti-CD26 monoclonal antibody YS110 suppressed proliferation of CD26 positive MM cell lines through a novel mechanism causing G2/M cell cycle delay through ERK1/2 phosphorylation. Anti-tumor agent PMX was identified as a CD26 inducer.

Methods

Reagents and antibodies

The humanized anti-CD26 antibody YS110 was constructed from the anti-CD26 mouse monoclonal antibody 14D10 coding sequence as previously described [11] and normal human IgG1 (Southern Biotech, Birmingham, AL) was used as a control. Rabbit monoclonal antibody to cyclinB1, p21cip/waf1, cdc2, phospho-cdc2 (Tyr15), cdc25c, phospho-cdc25c (Ser216), Erk1/2, phospho-Erk1/2(Thr202/Tyr204), p38MAPK, and phospho-p38MAPK (Thr180/Tyr182) were from Cell Signaling Technology Inc. (Danvers, MA) and the mouse monoclonal antibody against β -actin or Glyceraldehyde

3-phosphate dehydrogenase (GAPDH) was from DAKO (Glostrup, Denmark). The goat anti-CD26 polyclonal antibody and MEK 1/2 inhibitor U0126 was from Cell Signaling Technology Inc. (Danvers, MA).

Cell culture

NCI-H2452, NCI-H28 and JMN, CD26-positive cell lines established from malignant mesothelioma, were kind gifts from Dr. Chikao Morimoto (Departement of Therapy Development and Innovation for Immune Disorders and Cancers, Juntendo University). Both cell lines were grown in RPMI medium (Sigma-Aldrich, Tokyo, Japan) supplemented with 10 % heat-inactivated fetal bovine serum (FBS), ABPC (100 unit/mL), Streptomycin (100 µg/mL), and 5 % CO₂ at 37 °C.

Cell proliferation assay

The effect of YS110 on the proliferation of NCI-H2452 cells was measured using a colorimetric cell proliferation kit WST-1 (Roche Diagnostics, Tokyo, Japan) based on the colorimetric detection of a formazan salt. In brief, 5 × 10³ NCI-H2452 cells were seeded in RPMI1640 medium supplemented with 10 % heat inactivated FBS on 96-well plate with or without 2 µg/mL YS110. After 48 h of incubation at 37 °C in 5 % CO₂, a reading at 450 nm was carried out according to the manufacturer's instructions. Background absorbance of each sample at 630 nm was subtracted from the readings at 450 nm. The experiment was performed in triplicate and a representative experiment is shown.

Cell cycle assay and flowcytometry

For the cell cycle study, NCI-H2452 and NCI-H28 cells were synchronized in the S-phase by a repeated thymidine block. In brief, 5 × 10⁵ cells seeded in RPMI1640 medium supplemented with 10 % heat inactivated fetal bovine serum on 10 cm culture dishes were treated with 0.56 mM thymidine for 18 h, released for 10 h by three washes, and then treated again with 0.56 mM thymidine for 15 h. Synchronized cells were then returned to thymidine free medium with or without 2 µg/mL YS110 and incubated for 24 h. Cell cycle profiles were performed by flowcytometry using a procedure for propidium iodide staining of nuclei. Acquisition was performed using an EPICS XL/XL-MCL version 3.0 (Beckman Coulter, Brea, CA, USA) and data were analyzed using Flowjo software (TreeStar, Ashland, OR, USA). The experiment was performed in triplicate and a representative experiment is shown.

Western blotting

For total cell lysate preparation, NCI-H2452 cells or JMN cells cultured with or without 2 µg/mL YS110 for 24 h

were lysed at 4 °C by lysis buffer with phosphatase inhibitors (50 mM Tris-HCl, 150 mM NaCl, 1 % NP-40, 0.25 % deoxycholate, 500 µM NaVO₃, 50 mM NaF). For the preparation of nuclear and cytoplasmic extracts, NCI-H2452 cells were processed using NE-PER Nuclear and Cytoplasmic Extraction Reagents (Thermo scientific, Waltham, LA) according to the manufacturer's instruction. For Western blot analyses, 30 µg of each cell lysate was separated on an SDS-polyacrylamide gel and transferred to a PVDF membrane Hybond-P (GE Healthcare, Little Chalfont, UK). The membranes were blocked in blocking buffer [5 % dry milk and 0.2 % Tween 20 in Tris buffered saline (TBS)] for 2 h at room temperature, and incubated with the primary antibodies in antibody dilution buffer (5 % bovine serum albumin, 0.2 % Tween 20 in TBS) overnight at 4 °C. Dilutions of primary antibodies were 1:200, except anti p21cip/waf1 antibody, which was diluted at 1:100. After three washes, the blots were incubated with secondary antibodies (goat anti-rabbit polyclonal antibody and rabbit anti-mouse polyclonal antibody) diluted 1:1000 with dilution buffer for 1 h at room temperature and developed using the ECL Western Blotting Detection Reagents (GE Healthcare, Little Chalfont, UK). Quantification of relative band densities was performed using standard densitometry scanning techniques using Image-Quant 350 and ImageQuant TL software (GE Healthcare, Little Chalfont, UK). All the experiments performed in triplicate and a representative experiment is shown.

Xenograft model using human mesothelioma cell lines

NOD/Shi-scid, IL-2 receptor gamma null (NOG) mice were obtained from the Central Institute for Experimental Animals. JMN cells (1 × 10⁶) were implanted subcutaneously in the back flank of NOG mice. Mice were injected intratumorally with control human IgG₁ (n = 3) or YS110 (n = 3) at doses of 5 mg/kg body weight. JMN cells expressing CD26 were inoculated into the thoracic cavities of NOG mice. Thereafter, mice were intraperitoneally injected with control human IgG₁ (n = 3) or YS110 (5 µg per injection; n = 3), and/or pemetrexed (PMX, purchased from Eli Lilly; 100 mg/kg body weight) commencing on the day of cancer cell injection. Each antibody was administered three times per week. Mice were then monitored for the development and progression of tumors. Tumor weight was measured by scale. All experiments were approved by the Animal Care and Use Committee of Keio University and were performed in accordance with the institute guidelines.

Histology and immunohistochemistry

Tumor tissues were fixed in 10 % neutral buffered formalin, embedded in paraffin, and sectioned at a thickness of 5 µm. Sections were paraffin depleted and rehydrated in a

graded series of ethanol solutions. For histology, sections were stained with hematoxylin and eosin. For immunohistochemistry, sections were washed with PBS, subjected to antigen retrieval by heating at 100 °C in 0.01 M sodium citrate (pH 6.0) for 10 min, then treated with 3 % H₂O₂, before incubation with the following primary antibodies: goat anti-CD26 pAb (AF1180, R&D Systems, Minneapolis, MN) (1:100) and mouse anti-Ki-67 mAb (MIB-1, DAKO Japan) (1:100). Immune complexes were detected by using an ImmPRESS REAGENT KIT (Vector Laboratories, Burlingame, CA) with 3, 3'-diaminobenzidine, and sections were counterstained with hematoxylin

Statistical analyses

Statistical analyses were assessed using SPSS version 17.0 (SPSS Inc., Chicago, IL). The *p* value, from which statistical significance was assumed, was set to *p* < 0.05.

Abbreviations

MM: malignant mesothelioma; PMX: pemetrexed; NOG mouse: NOD/Shi-scid, IL-2 receptor gamma null mouse.

Authors' contributions

MH and TY designed and performed the research; HN and CM provided reagents and cells and examined protein expressions; HM, MS and TY analyzed the data; MH and TY wrote the manuscript. All authors read and approved the final manuscript.

Author details

¹ Department of Pathology, Keio University School of Medicine, 35 Shinanomachi, Tokyo, Shinjuku-ku 160-8582, Japan. ² Department of Pediatrics, Keio University School of Medicine, 35 Shinanomachi, Tokyo, Shinjuku-ku 160-8582, Japan. ³ Laboratory of Nuclear Transport Dynamics, National Institute of Biomedical Innovation, 7-6-8 Saito-Asagi, Ibaraki City, Osaka Prefecture 567-0085, Japan. ⁴ Department of Therapy Development and Innovation for Immune Disorders and Cancers, Juntendo University, 2-1-2 Hongo, Tokyo, Bunkyo-ku 113-8421, Japan. ⁵ Department of Pathology, Saitama Medical University, 38 Morohongo, Saitama, Moroyama-machi 350-0495, Japan.

Acknowledgements

We thank H. Suzuki for technical assistance and A. Sato and K. Tsutsumi for animal care and support of tumorigenicity assay.

Competing interests

YS110 was provided by Y's therapeutics. TY and CM are possessing non-listed stock of Y's therapeutics. MH and HN are paid by the consignment study cost of Y's therapeutics. TY and CM are advisers for Kissei Pharmaceutical Co., Ltd, which carried out the Phase I clinical trial for YS110 against CD26 positive cancers. HM, KY, and MS have no competing interests.

Ethical approval

All animal experiments were approved by the Animal Care and Use Committee of Keio University and were performed in accordance with the institute guidelines.

Funding

This study was supported by the Program for Promotion of Fundamental Studies in Health Sciences of the National Institute of Biomedical Innovation (07-17 to TY and CM), a Grant-in-Aid for Scientific Research (B) (23390086 and 16H04714 to TY and 22790355 to MH) and Global COE Program "Education and Research Center for Stem Cell Medicine" (to KY) from the Ministry of Education, Culture, Sports, Science and Technology of Japan, and a Grant-in-Aid for Drug Design Biomarker Research (H24-B10-003 to TY and CM) from the Ministry of Health, Labor and Welfare and a Grant-in-Aid for Industrial Accident

Clinical Research (H27-150401-01 to TY and CM) from the Ministry of Health, Labor and Welfare.

Received: 23 December 2015 Accepted: 24 April 2016

Published online: 30 April 2016

References

1. Sugarbaker DJ. Multimodality management of malignant pleural mesothelioma: introduction. *Semin Thorac Cardiovasc Surg*. 2009;21:95–6.
2. Krug LM, Pass HI, Rusch VW, Kindler HL, Sugarbaker DJ, Rosenzweig KE, Flores R, Friedberg JS, Pisters K, Monberg M, Obasaju CK, Vogelzang NJ. Multicenter phase II trial of neoadjuvant pemetrexed plus cisplatin followed by extrapleural pneumonectomy and radiation for malignant pleural mesothelioma. *J Clin Oncol*. 2009;27:3007–13.
3. Vogelzang NJ, Rusthoven JJ, Symanowski J, Denham C, Kaukel E, Ruffie P, Gatzemeier U, Boyer M, Emri S, Manegold C, Niyikiza C, Paoletti P. Phase III study of pemetrexed in combination with cisplatin versus cisplatin alone in patients with malignant pleural mesothelioma. *J Clin Oncol*. 2003;21:2636–44.
4. Van Schil PE, Baas P, Gaafar R, Maat AP, Van de Pol M, Hasan B, Klomp HM, Abdelrahman AM, Welch J, van Meerbeeck JP. Trimodality therapy for malignant pleural mesothelioma: results from an EORTC phase II multicentre trial. *Eur Respir J*. 2010;36:1362–9.
5. Greillier L, Marco S, Barlesi F. Targeted therapies in malignant pleural mesothelioma: a review of clinical studies. *Anticancer Drugs*. 2011;22:199–205.
6. Ohnuma K, Uchiyama M, Yamochi T, Nishibashi K, Hosono O, Takahashi N, Kina S, Tanaka H, Lin X, Dang NH, Morimoto C. Caveolin-1 triggers T-cell activation via CD26 in association with CARMA1. *J Biol Chem*. 2007;282:10117–31.
7. Bauvois B. Transmembrane proteases in cell growth and invasion: new contributors to angiogenesis? *Oncogene*. 2004;23:317–29.
8. Aoe K, Amatya VJ, Fujimoto N, Ohnuma K, Hosono O, Hiraki A, Fujii M, Yamada T, Dang NH, Takeshima Y, Inai K, Kishimoto T, Morimoto C. CD26 overexpression is associated with prolonged survival and enhanced chemosensitivity in malignant pleural mesothelioma. *Clin Cancer Res*. 2012;18:1447–56.
9. Amatya VJ, Takeshima Y, Kushitani K, Yamada T, Morimoto C, Inai K. Overexpression of CD26/DPPIV in mesothelioma tissue and mesothelioma cell lines. *Oncol Rep*. 2011;26:1369–75.
10. Antczak C, De Meester I, Bauvois B. Ectopeptidases in pathophysiology. *Bio Essays*. 2001;23:251–60.
11. Inamoto T, Yamada T, Ohnuma K, Kina S, Takahashi N, Yamochi T, Inamoto S, Katsuoka Y, Hosono O, Tanaka H, Dang NH, Morimoto C. Humanized anti-CD26 monoclonal antibody as a treatment for malignant mesothelioma tumors. *Clin Cancer Res*. 2007;13:4191–200.
12. Le X-F, Pruefer F, Bast RC. HER2-targeting antibodies modulate the cyclin-dependent kinase inhibitor p27kip1 via multiple signaling pathways. *Cell Cycle*. 2005;4:87–95.
13. Vincenzi B, Schiavon G, Silletta M, Santini D, Tonini G. The biological properties of cetuximab. *Crit Rev Oncol Hematol*. 2008;68:93–106.
14. Weiner GJ. Rituximab: mechanism of action. *Semin Hematol*. 2010;47:115–23.
15. Wu JD, Odman A, Higgins LM, Haugk K, Vessella R, Ludwig DL, Plymate SR. In vivo effects of the human type I insulin-like growth factor receptor antibody A12 on androgen-dependent and androgen-independent xenograft human prostate tumors. *Clin Cancer Res*. 2005;11:3065–74.
16. Takizawa CG, Morgan DO. Control of mitosis by changes in the subcellular location of cyclin-B1-Cdk1 and Cdc25C. *Curr Opin Cell Biol*. 2000;12:658–65.
17. Mebratu Y, Tesfaigzgi Y. How ERK1/2 activation controls cell proliferation and cell death: is subcellular localization the answer? *Cell Cycle*. 2009;8:1168–75.
18. Zhang Z, Miao L, Lv C, Sun H, Wei S, Wang B, Huang C, Jiao B. Wentilactone B induces G2/M phase arrest and apoptosis via the Ras/Raf/MAPK signaling pathway in human hepatoma SMMC-7721 cells. *Cell Death Dis*. 2013;4:e657.

19. Chuang M-J, Wu S-T, Tang S-H, Lai X-M, Lai H-C, Hsu K-H, Sun K-H, Sun G-H, Chang S-Y, Yu D-S, Hsiao P-W, Huang S-M, Cha T-L. The HDAC inhibitor LBH589 induces ERK-dependent prometaphase arrest in prostate cancer via HDAC6 inactivation and down-regulation. *PLoS One*. 2013;8:e73401.
20. Hollmann CA, Owens T, Nalbantoglu J, Hudson TJ, Sladek R. Constitutive activation of extracellular signal-regulated kinase predisposes diffuse large B-cell lymphoma cell lines to CD40-mediated cell death. *Cancer Res*. 2006;66:3550–7.
21. Brunetto E, Ferrara AM, Rampoldi F, Talarico A, Cin ED, Grassini G, Spagnuolo L, Sassi I, Ferro A, Cuorvo LV, Barbareschi M, Piccinin S, Maestro R, Pecciarini L, Doglioni C, Cangi MG. CDC25A protein stability represents a previously unrecognized target of HER2 signaling in human breast cancer: implication for a potential clinical relevance in trastuzumab treatment. *Neoplasia*. 2013;15:579–90.
22. Yamada K, Hayashi M, Du W, Ohnuma K, Sakamoto M, Morimoto C, Yamada T. Localization of CD26/DPPIV in nucleus and its nuclear translocation enhanced by anti-CD26 monoclonal antibody with anti-tumor effect. *Cancer Cell Int*. 2009;9:17.
23. Yamada K, Hayashi M, Madokoro H, Nishida H, Du W, Ohnuma K, Sakamoto M, Morimoto C, Yamada T. Nuclear localization of CD26 induced by a humanized monoclonal antibody inhibits tumor cell growth by modulating of POLR2A transcription. *PLoS ONE*. 2013;8:e62304.
24. Penno MB, Askin FB, Ma H, Carbone M, Vargas MP, Pass HI. High CD44 expression on human mesotheliomas mediates association with hyaluronan. *Cancer J Sci Am*. 1995;1:196–203.

Submit your next manuscript to BioMed Central and we will help you at every step:

- We accept pre-submission inquiries
- Our selector tool helps you to find the most relevant journal
- We provide round the clock customer support
- Convenient online submission
- Thorough peer review
- Inclusion in PubMed and all major indexing services
- Maximum visibility for your research

Submit your manuscript at
www.biomedcentral.com/submit



RESEARCH ARTICLE

Identification of Nedd9 as a TGF- β -Smad2/3 Target Gene Involved in RANKL-Induced Osteoclastogenesis by Comprehensive Analysis



CrossMark
click for updates

OPEN ACCESS

Citation: Omata Y, Nakamura S, Koyama T, Yasui T, Hirose J, Izawa N, et al. (2016) Identification of Nedd9 as a TGF- β -Smad2/3 Target Gene Involved in RANKL-Induced Osteoclastogenesis by Comprehensive Analysis. PLoS ONE 11(6): e0157992. doi:10.1371/journal.pone.0157992

Editor: Dominique Heymann, Faculté de médecine de Nantes, FRANCE

Received: November 23, 2015

Accepted: June 8, 2016

Published: June 23, 2016

Copyright: © 2016 Omata et al. This is an open access article distributed under the terms of the Creative Commons Attribution License, which permits unrestricted use, distribution, and reproduction in any medium, provided the original author and source are credited.

Data Availability Statement: All relevant data are within the paper.

Funding: This work was supported by a Grant-in-aid for Scientific Research from the Japanese Ministry of Education, Culture, Sports, Science and Technology (#26253075). The URL is as follows: <https://www.jsps.go.jp/j-grantsinai/index.html>. The funders had no role in study design, data collection and analysis, decision to publish, or preparation of the manuscript.

Competing Interests: The authors have declared that no competing interests exist.

Yasunori Omata^{1*}, Shinya Nakamura^{1*}, Takuma Koyama^{1*}, Tetsuro Yasui¹, Jun Hirose¹, Naohiro Izawa¹, Takumi Matsumoto¹, Yuuki Imai², Sachiko Seo³, Mineo Kurokawa³, Shuichi Tsutsumi⁴, Yuho Kadono¹, Chikao Morimoto⁵, Hiroyuki Aburatani⁴, Takeshi Miyamoto^{1,6}, Sakae Tanaka^{1*}

1 Department of Orthopaedic Surgery, Faculty of Medicine, The University of Tokyo, Bunkyo-ku, Tokyo, Japan, **2** Division of Integrative Pathophysiology, Proteo-Science Center, Graduate School of Medicine, Ehime University, Ehime 791-0295, Japan, **3** Department of Hematology and Oncology, Graduate School of Medicine, University of Tokyo, Tokyo, Japan, **4** Genome Science Division, Research Center for Advanced Science and Technology (RCAST), The University of Tokyo, Tokyo, Japan, **5** Department of Therapy Development and Innovation for Immune Disorders and Cancers, Juntendo University, Tokyo, Japan, **6** Department of Orthopedic Surgery, Keio University, Tokyo, Japan

* TANAKAS-ORT@h.u-tokyo.ac.jp

Abstract

TGF- β is a multifunctional cytokine that is involved in cell proliferation, differentiation and function. We previously reported an essential role of the TGF- β -Smad2/3 pathways in RANKL-induced osteoclastogenesis. Using chromatin immunoprecipitation followed by sequencing, we comprehensively identified Smad2/3 target genes in bone marrow macrophages. These genes were enriched in the gene population upregulated by TGF- β and downregulated by RANKL. Recent studies have revealed that histone modifications, such as trimethylation of histone H3 lysine 4 (H3K4me3) and lysine 27 (H3K27me3), critically regulate key developmental steps. We identified Nedd9 as a Smad2/3 target gene whose histone modification pattern was converted from H3K4me3(+)/H3K4me27(+) to H3K4me3(+)/H3K4me27(-) by TGF- β . Nedd9 expression was increased by TGF- β and suppressed by RANKL. Overexpression of Nedd9 partially rescued an inhibitory effect of a TGF- β inhibitor, while gene silencing of Nedd9 suppressed RANKL-induced osteoclastogenesis. RANKL-induced osteoclastogenesis were reduced and stimulatory effects of TGF- β on RANKL-induced osteoclastogenesis were partially abrogated in cells from Nedd9-deficient mice although knockout mice did not show abnormal skeletal phenotypes. These results suggest that Nedd9 is a Smad2/3 target gene implicated in RANKL-induced osteoclastogenesis.

Introduction

Skeletal homeostasis is strictly controlled by osteoclasts, which mediate bone resorption, and osteoblasts, which regulate bone formation. Osteoclasts are multinucleated cells derived from monocyte-macrophage lineage hematopoietic progenitor cells and specifically differentiated for bone resorption [1]. The differentiation of osteoclasts is regulated by two cytokines: receptor activator of nuclear factor kappa B ligand (RANKL) and macrophage colony-stimulating factor (M-CSF). In addition to these two essential cytokines, we recently reported a critical role for TGF- β in osteoclastogenesis [2] [3]. TGF- β is abundantly stored in bone matrix and has profound biological functions such as angiogenesis, cellular differentiation, apoptosis and bone homeostasis [4] [5]. The binding of TGF- β to its type II receptors recruits and phosphorylates type I receptors, which in turn activate downstream signaling including Smad and non-Smad pathways [6]. Phosphorylated Smad2/3 forms a complex with Smad4, and the molecular complex translocates into the nucleus and regulates specific gene expression [7] [8] [9].

We previously reported that TGF- β is required for osteoclast differentiation in response to RANKL and M-CSF by regulating the interaction of Smad2/3 with TRAF (tumor necrosis factor receptor-associated factor) 6, an adaptor molecule associated with RANK [2]. In addition, we identified Smad2/3-binding sites in open chromatin regions during osteoclastogenesis and found that Smad2/3 binding is necessary for the nuclear translocation of c-Fos, an essential transcription factor for osteoclastogenesis [3]. Moreover, it was reported that combined treatment of TGF- β and TNF- α promotes maximal osteoclast formation compared to treatment with other cytokine combinations in the presence of RANKL based on a multiparameter cytokine assay [10]. However, direct target genes that regulate osteoclast differentiation downstream of TGF- β -Smad2/3 pathways still remain elusive.

Multiple epigenetic modifications, such as DNA methylation and, histone acetylation and methylation, are involved in organization of chromatin structures at various levels and regulation of gene expression. The methylated sites in H3 or H4 are mainly located in the histone tail (H3K4, H3K9, H3K36 and H4K20) and the center of the nucleosome (H3K79) [11]. Among the five histones, which are designated as H1, H2A, H2B, H3 and H4 [12], Stahl et al. reported that the methylation of histone H3 at lysine 4 is highly conserved and correlated with transcriptionally active nuclei in *Tetrahymena* [13]. Bernstein et al. revealed that histone modifications such as trimethylation of histone H3 lysine 4 (H3K4me3) and lysine 27 (H3K27me3) play a critical role in gene expression, and in embryonic stem cells, key developmental genes tend to change histone modification patterns from the H3K4me3/H3K27me3 bivalent pattern to the H3K4me3 monovalent pattern [14]. Similar modifications of histone methylation have been observed in many other types of cells, and we previously reported that RANKL induced bivalent to monovalent changes in the *nuclear factor of activated T-cells cytoplasmic 1 (NFATc1)* gene during osteoclastogenesis [15]. Through chromatin immunoprecipitation with sequencing (ChIP-seq) analysis using anti-Smad2/3, anti-H3K4me3 and anti-H3K27me3 antibodies [16], here we investigated Smad2/3-regulating genes that are critically involved in the differentiation of osteoclasts and identified Nedd9 as a putative regulator of osteoclastogenesis downstream of TGF- β -Smad2/3 pathways.

Results

Identification of genes regulated by the TGF- β -Smad2/3 axis

To identify genes regulated by the TGF- β -Smad2/3 axis, we performed ChIP-seq analysis using anti-Smad2/3 antibody in M-CSF-dependent bone marrow macrophages (BMMs) treated with 2 ng/ml TGF- β for 1.5 h. Total read number was 15,108,905, and 10,837,516 reads (71.7%)

were mapped to the mouse genome. A total of 2,786 Smad2/3-binding regions (SBRs) were identified (peak signal ratio ≥ 8). Genes with peak positions of SBRs between 10 kb upstream from transcription start sites (TSSs) and first intron were defined as Smad2/3 target genes, and 903 genes were selected as Smad2/3 target genes.

As shown in Fig 1A, we confirmed that Smad2/3 bound to the promoter regions of known TGF- β -regulating genes such as *Cdkn1a*, *Smad7* and *Serpine1*. We selected Smad2/3-binding regions in 8 of these genes (*Serpine1*, *Cdkn1a*, *Smad7*, *Smad6*, *Ski*, *Tmepai*, *Nedd9* and *Pdgfb*) and confirmed a TGF- β -dependent increase in Smad2/3 binding by ChIP-realtime PCR (Fig 1B). SBRs were widely distributed from distant upstream regions to intronic regions, with prominent enrichment close to the TSSs of RefSeq genes (Fig 1C).

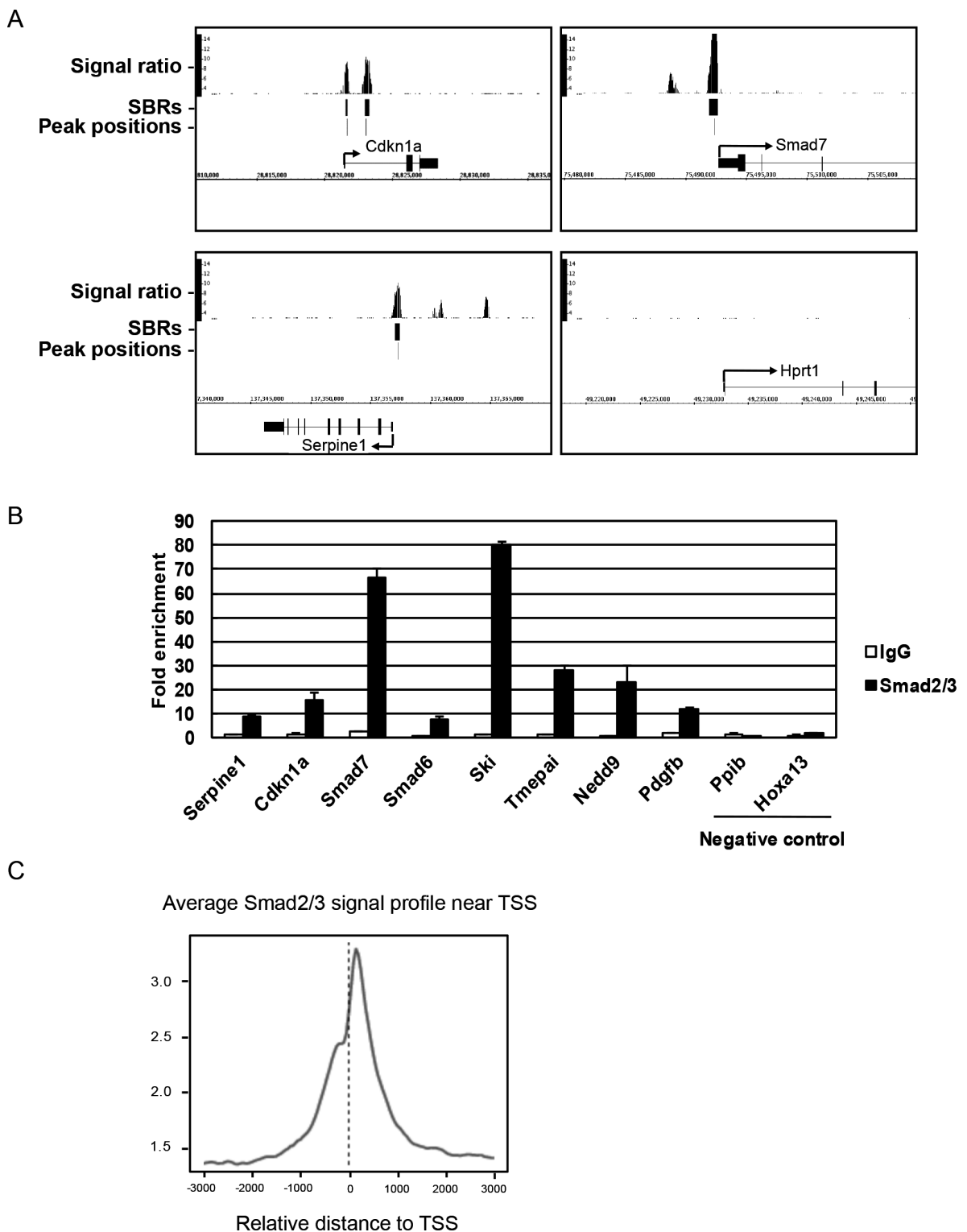
Histone modification by TGF- β

To analyze TGF- β -induced histone modification, BMMs treated with 1 ng/ml TGF- β [designated as TGF- β (+) BMMs] or 5 μ M SB431542 [TGF- β (-) BMMs] were subjected to ChIP-seq analysis using anti-H3K4me3 or anti-H3K27me3 antibody. SB431542 is a potent and specific kinase inhibitor of TGF- β type I receptor that strongly suppresses RANKL-induced osteoclastogenesis [2]. Genes with H3K4me3 peaks within +/- 1kb from the TSSs were defined as K4(+) genes (peak signal ratio ≥ 8), and genes with H3K27me3 peaks within +/- 1kb from the TSSs were defined as K27(+) genes (peak signal ratio ≥ 5). A total of 9,962 and 9,505 K4(+) genes and 2,600 and 2,827 K27(+) genes were identified in TGF- β (-) and TGF- β (+) BMMs, respectively. Smad2/3 target genes were significantly enriched in genes with K4(+)K27(+) marks in TGF- β (-) BMMs and K4(+)K27(-) marks in TGF- β (+) (7.8 fold enrichment; $P < 10^{-5}$ by chi square test) (Fig 2A). The average signal intensity of H3K4me3 around TSS was higher in TGF- β (+) BMMs than in TGF- β (-) BMMs while that of H3K27me3 was lower (Fig 2B). Indeed, mRNA expression of Smad target genes with K4(+)K27(+) marks in TGF- β (-) BMMs and K4(+)K27(-) marks in TGF- β (+) BMM were up-regulated after TGF- β stimulation (Fig 2C).

TGF- β positively and RANKL negatively regulates Smad2/3 target genes

Using 14,177 probes (8,839 genes) with expression values of more than 70 by MOE430 Gene-Chips at least one time point, we found that Smad2/3 target genes were significantly enriched in the genes whose expression was more than 2-fold upregulated, but not in those whose expression was less than 0.5-fold downregulated, by TGF- β (Fig 3, upper and lower panels; $P < 10^{-5}$ by chi square test). Enrichment scores calculated by Gene Set Enrichment Analysis (GSEA) [17] exhibited statistically significant enrichment ($P < 10^{-6}$) (Fig 3, lower panel).

We then analyzed the change of the expression of Smad2/3 target genes by RANKL stimulation. We used 16,631 probes (10,004 genes) with expression values of more than 70 at least one time point for further analysis. Interestingly, Smad2/3 target genes were significantly enriched in the genes whose expression was less than 0.5-fold downregulated, but not in those whose expression was more than 2-fold upregulated, after 24, 48 and 72 h of RANKL stimulation (Fig 4, upper and lower panels; $P < 10^{-5}$ by chi square test). In addition, genes whose histone modification was changed from K4(+)K27(+) to K4(+)K27(-) patterns by TGF- β treatment were enriched in downregulated genes by RANKL (Fig 4, upper panel). The statistical significance of the enrichment was analyzed by calculating GSEA enrichment scores ($P < 10^{-6}$) (Fig 4, lower panel).



of each SBR are shown by black bars. (B) Eight positive regions and two negative regions for Smad2/3 binding were selected from ChIP-seq data and validated by realtime PCR. ChIP using mouse IgG was used as control. Values are presented as n-fold enrichment over Hprt1. (C) Average Smad2/3 signal profile around transcriptional start site (TSS) in ChIP-seq analysis. Smad2/3 binding was enriched around TSS.

doi:10.1371/journal.pone.0157992.g001

Identification of Nedd9 as a possible Smad2/3 target in BMMs

We identified 14 Smad2/3 target genes in which histone modification patterns changed from K4(+)K27(+) to K4(+)K27(−) by TGF- β treatment (Fig 5A). Nedd9, also called Cas-L or HEF-1 (human enhancer of filamentation 1), is a member of the CAS (crk-associated substrate) family proteins [18] [19] [20]. Nedd9 is a scaffold protein localized in focal adhesion that is involved in the development and progression of cancer cells [21] [22] [23]. As shown in Fig 3A, Smad2/3 binding was enriched around the TSS of *Nedd9* gene. Histone modification status changed from K4(+)K27(+) to K4(+)K27(−) patterns by TGF- β stimulation in BMMs and then returned to K4(+)K27(+) patterns in response to RANKL stimulation. In fact, *Nedd9* gene expression was upregulated by TGF- β in BMMs and downregulated by RANKL stimulation (Fig 5B).

We then analyzed a potential function for Nedd9 in osteoclastogenesis. Retroviral overexpression of *Nedd9* significantly increased the expression of *Cathepsin K*, a marker gene of osteoclasts (Fig 6A). In addition, *Nedd9* overexpression partially rescued the inhibitory effect of SB431542 on RANKL-induced osteoclastogenesis ($P < 0.05$; Fig 6B–6D). Conversely, *Nedd9* knockdown by retrovirus carrying *shNedd9* markedly suppressed RANKL-induced osteoclastogenesis (Fig 7A–7C). All of these findings strongly suggest a critical function for Nedd9 in RANKL-induced osteoclastogenesis.

Finally, we assessed the function of Nedd9 in osteoclastogenesis using *Nedd9*−/− mice. BMMs from *Nedd9*−/− mice exhibited reduced osteoclastogenesis similar to *shNedd9*-treated cells (Fig 8A and 8B). Stimulatory effects of TGF- β on RANKL-induced osteoclastogenesis observed in wild-type BMMs was reduced in *Nedd9*-deficient BMMs (Fig 8B). Expression of *Cathepsin K*, as determined by Western blotting, was downregulated in *Nedd9*-deficient osteoclasts as compared to wild-type osteoclasts (Fig 8C). However, no significant difference in the skeletal phenotypes, as assessed by soft X ray in the lower extremities, micro CT in lumbar vertebral bodies, and dual energy X ray absorptiometry was observed between *Nedd9*-knockout and wild-type mice (Fig 9A–9C).

Discussion

We previously reported that TGF- β is indispensable for RANKL and M-CSF-induced osteoclastogenesis. However, the effector genes acting downstream of TGF- β -Smad2/3 pathways remain elusive. In the present study, we comprehensively analyzed Smad2/3-binding regions and identified Smad2/3 target genes in BMMs by ChIP-seq analysis. Smad2/3 target genes were enriched in TGF- β upregulated genes as expected. Interestingly, these genes were enriched in the gene population whose expression was downregulated by RANKL treatment, indicating the possibility that the role of TGF- β is to prepare an appropriate condition for BMMs to differentiate into mature osteoclasts upon RANKL stimulation.

Histone modifications play important roles in cell differentiation. H3K4me3 is enriched in the active and poised promoter regions [24, 25], while H3K27me3 is involved in polycomb-mediated gene repression [26]. Recent studies have revealed that key developmental genes tend to change histone modification patterns from the H3K4me3/H3K27me3 bivalent pattern to the H3K4me3 monovalent pattern in various types of cells. In an attempt to narrow down the candidates of Smad2/3 target genes involving in osteoclast differentiation, we identified *Nedd9* as a Smad2/3 target gene whose histone modification pattern changed from K4(+)K27(+) to

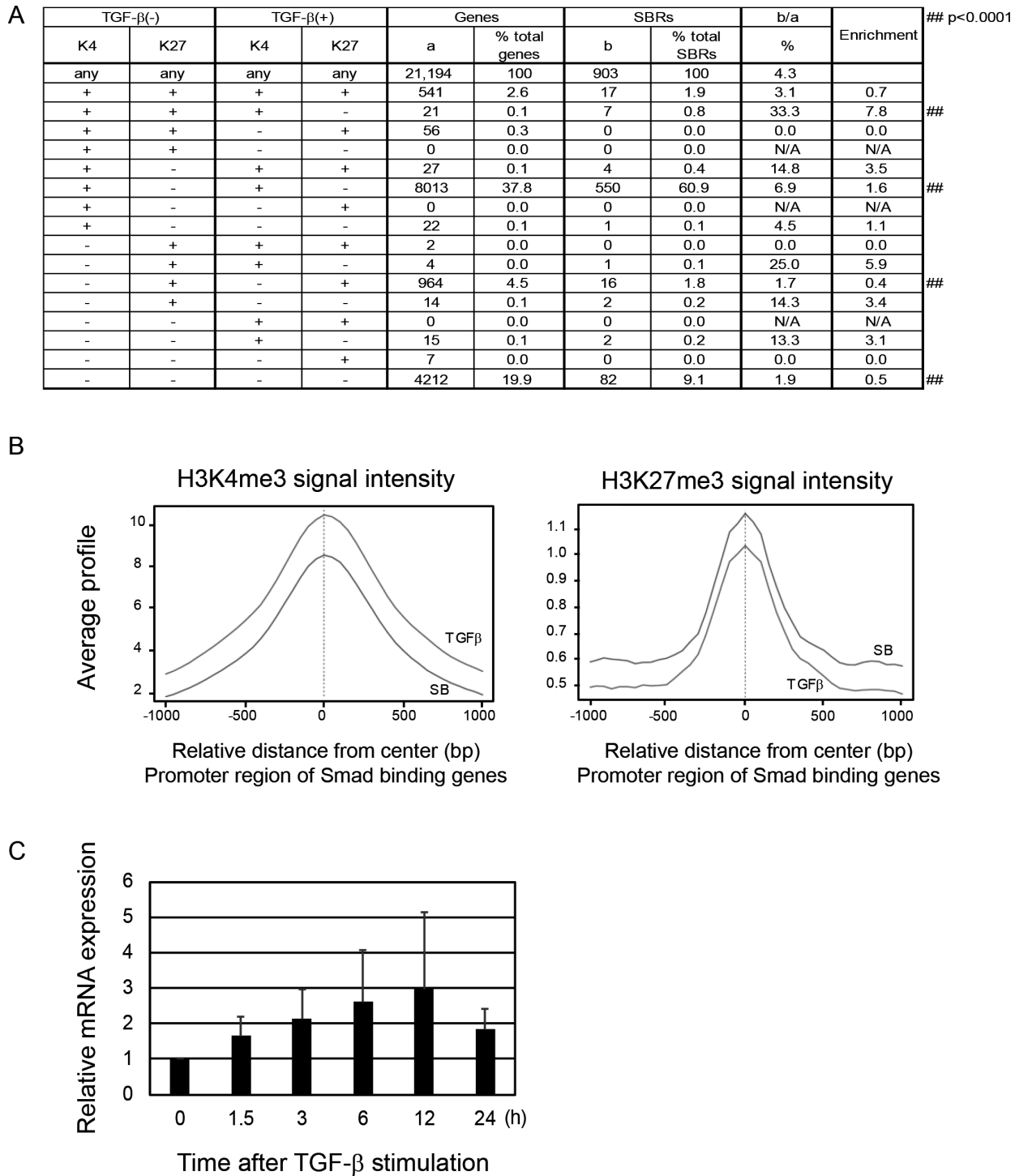
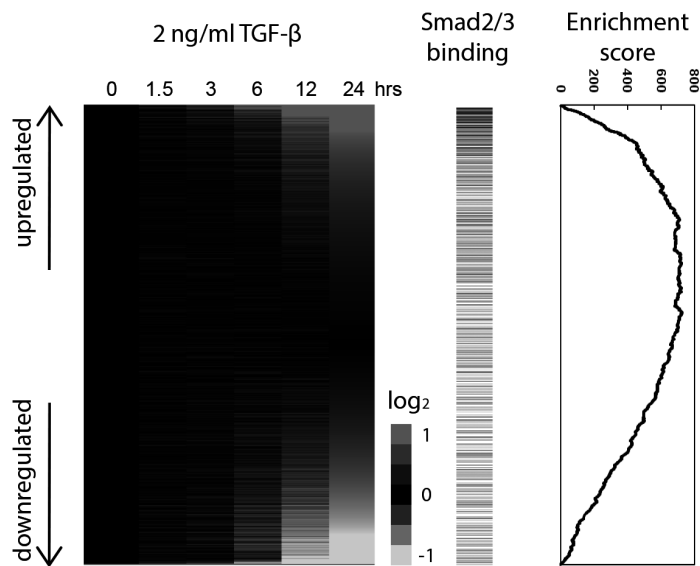


Fig 2. (A) Genes with H3K4me3 peaks within \pm 1 kb from TSS were defined as K4(+) genes, and genes with H3K27me3 peaks within \pm 1 kb from TSS were defined as K27(+) genes. Genes with each combination of K4 and K27 status were identified and enrichment of Smad2/3 target genes was calculated. Highest enrichment was observed in genes with K4(+)K27(+) marks in TGF- β (-) BMMs and K4(+)K27(-) marks in TGF- β (+) BMM. (B) The intensity of histone marks around TSS of Smad2/3 target genes. The signal intensity of H3K4me3 in BMMs treated with TGF- β was higher than those treated with SB431542, while the signal intensity of H3K4me27 was lower in TGF- β (+) BMMs than that in TGF- β (-) BMMs. (C) mRNA expression of Smad target genes with K4(+)K27(+) marks in TGF- β (-) BMMs and K4(+)K27(-) marks in TGF- β (+) BMM.

doi:10.1371/journal.pone.0157992.g002



$*p < 10^{-5}$

		All genes		Smad2/3 target genes		#b/#a
		Genes (#a)	% total genes	Genes (#b)	% total genes	
Total		8839	100.0	592	100.0	6.7
≥ 2 -fold increase	1.5 hrs	80	0.9	34	5.7	42.5*
	6 hrs	279	3.2	64	10.8	22.9*
	24 hrs	616	7.0	83	14.0	13.5*
≤ 0.5 -fold decrease	1.5 hrs	47	0.5	4	0.7	8.5
	6 hrs	206	2.3	13	2.2	6.3
	24 hrs	684	7.7	29	4.9	4.2

Fig 3. Identification of downstream effectors of TGF-β in osteoclastogenesis. Upper: The expression scores after TGF-β stimulation of BMMs relative to time 0 are illustrated by a heat map with red or green color representing increased or decreased gene expression, respectively. The probes were sorted by the ratio at 24 h (ranked gene list). Horizontal bars indicate Smad2/3 target genes. GSEA enrichment scores are graphically shown in the right panel [17]. Smad2/3 target genes were significantly enriched in genes upregulated by TGF-β. Lower: The expression scores after RANKL stimulation of BMMs relative to time 0 are illustrated by a heat map. Genes whose expression was upregulated more than 2-fold or downregulated less than 0.5-fold relative to RANKL treatment were counted. Enrichment of Smad2/3 target genes in up- or downregulated genes was evaluated by chi-square test ($P < 10^{-5}$).

doi:10.1371/journal.pone.0157992.g003

K4(+)K27(−) patterns in response to TGF-β. Nedd9, also known as CasL and HEF1, was originally identified as a 105 kDa protein that is tyrosine phosphorylated by the ligation of β1 integrins in peripheral T cells [18]. Nedd9 is induced by TGF-β and directly interacts with Smads in various types of cells [27] [28]. We found that Smad2/3 binds to the promoter region of *Nedd9* gene and TGF-β upregulates *Nedd9* expression in BMMs. Overexpression of *Nedd9* promoted and knockdown or knockout of *Nedd9* suppressed osteoclastogenesis, indicating a role of Nedd9 downstream of RANKL-RANK pathways. Previous studies reported that Nedd9 is

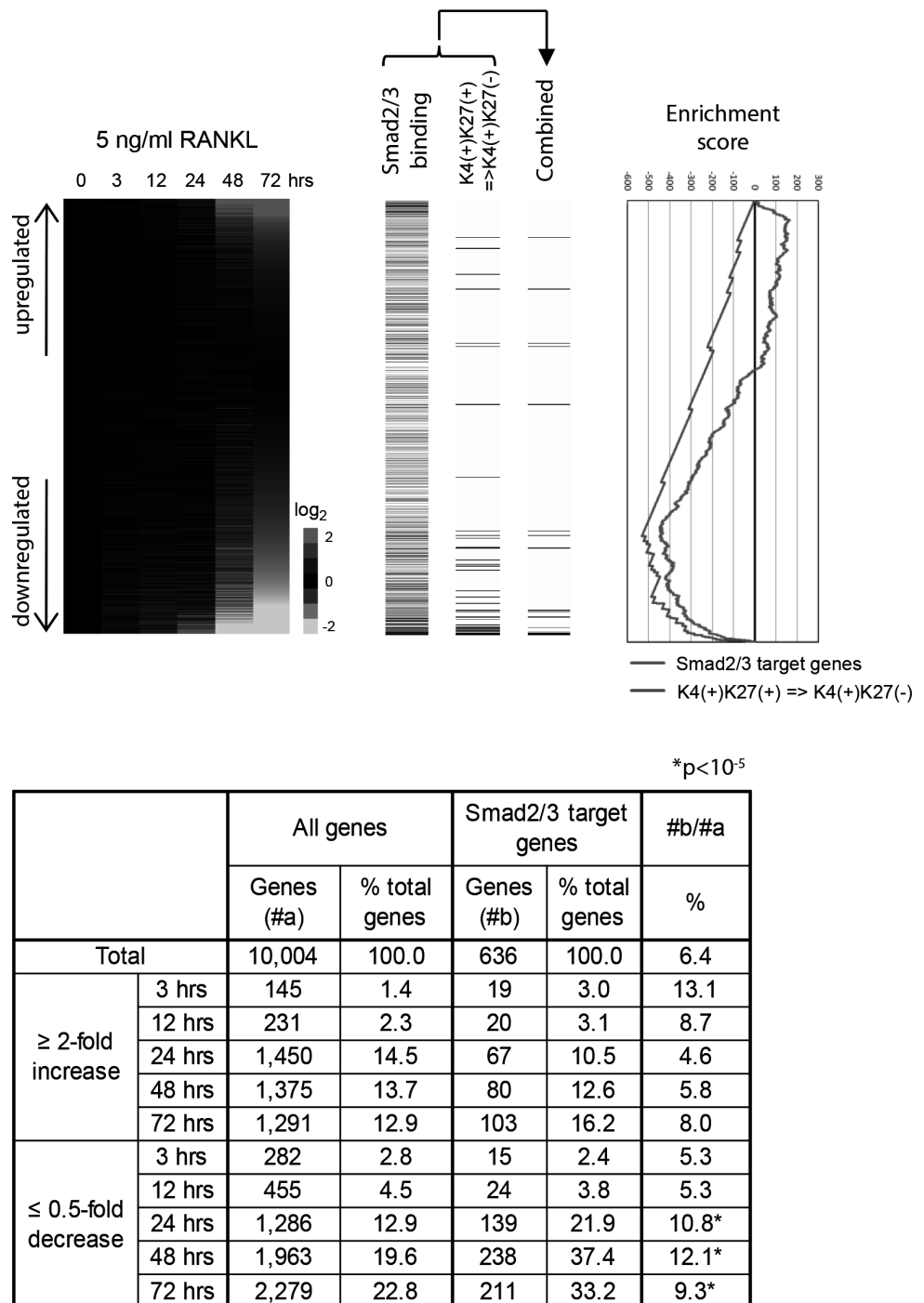
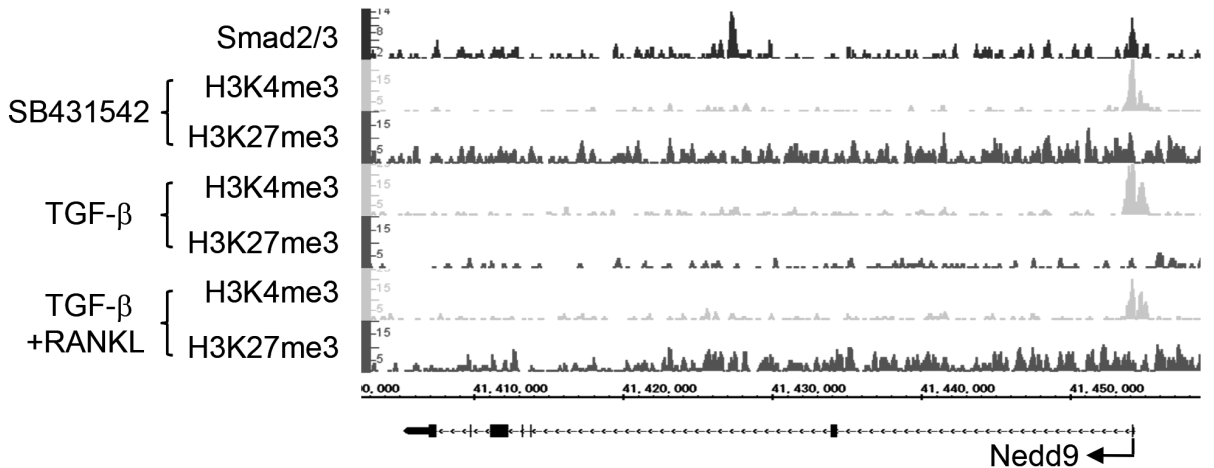


Fig 4. Upper: TGF- β (+) BMMs were treated with 5 nM GST-RANKL for 0, 3, 12, 24, 48, and 72 h. Relative expression levels of Smad2/3 target genes as compared with those in time 0 are illustrated by a heat map. The probes were sorted by the value at 72 h after RANKL treatment. Horizontal bars indicate Smad2/3 target genes and genes with K4(+)K27(+) marks in TGF- β (-) BMMs and K4(+)K27(-) marks in TGF- β (+) BMMs. GSEA enrichment scores are graphically shown in the right panel. Lower: Enrichment of Smad2/3 target genes in the gene population whose relative expression levels were upregulated more than 2-fold or downregulated less than 0.5-fold by RANKL. Smad2/3 target genes were significantly enriched in downregulated genes by RANKL.

doi:10.1371/journal.pone.0157992.g004

A



B

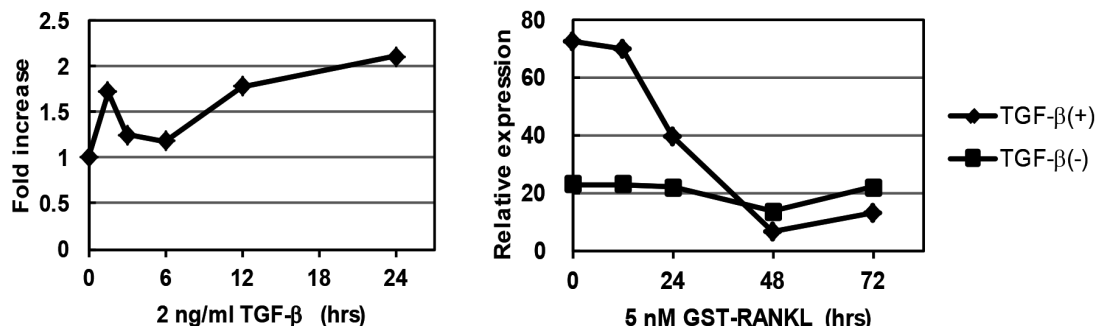


Fig 5. Epigenetic regulation of Nedd9 gene during osteoclastogenesis. (A) Smad2/3 binding and histone modification changes of Nedd9 gene during osteoclastogenesis. Histone modification patterns in BMMs changed from K4(+)K27(+) to K4(+)K27(-) patterns by TGF- β and returned to K4(+)K27(+) patterns after RANKL treatment. (B) Nedd9 mRNA expression after TGF- β or RANKL stimulation. The expression increased by TGF- β stimulation and was reduced after RANKL treatment. The expression remained at low levels in the presence of SB431542.

doi:10.1371/journal.pone.0157992.g005

involved in tumor differentiation, migration and metastasis [29], and therefore, it is also possible that Nedd9 supports osteoclast motility as well.

A previous study reported the association between Nedd9 and Smad6 or Smad7 [30], and our ChIP-seq analysis showed that Smad2/3 bound to the promoter region of *Smad6* and *Smad7*. Although we did not address the association between inhibitory Smads and Nedd9 in BMMs, it is possible that Nedd9 regulates TGF- β signaling in a negative feedback manner by interacting with inhibitory Smads.

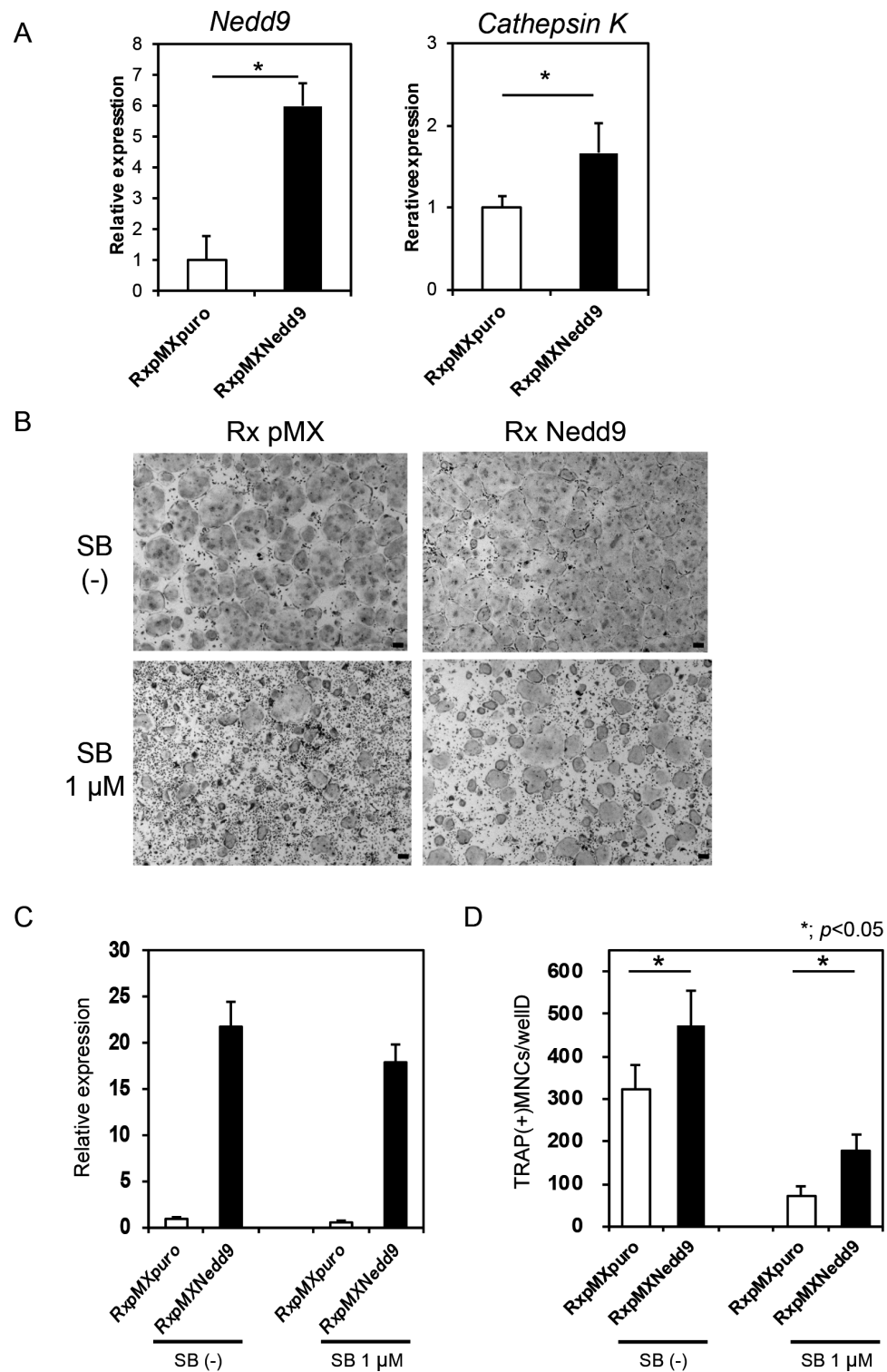


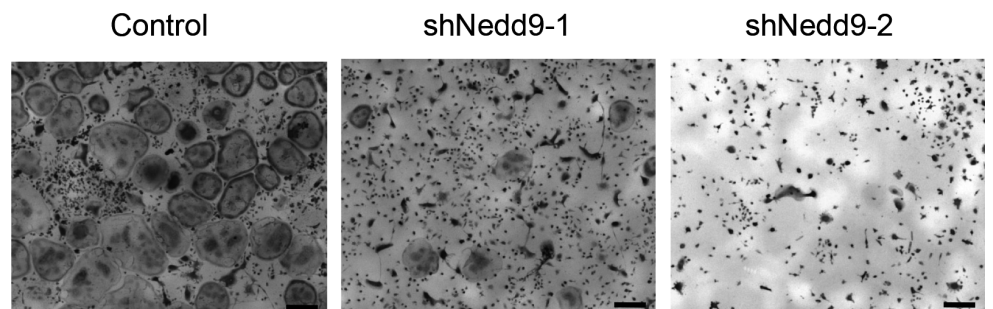
Fig 6. Nedd9 is critical for osteoclast differentiation. (A) Realtime PCR analysis of effects of retroviral overexpression of *Nedd9* gene on RANKL-induced osteoclastogenesis, as indicated by expression of *Nedd9* and *Cathepsin K* mRNAs. (B) Effects of SB431542 (SB) treatment on osteoclastogenesis, as evaluated by TRAP staining, in *Nedd9*-overexpressing cells treated with RANKL. Overexpression of *Nedd9* increased

RANKL-induced osteoclastogenesis. SB431542 suppressed osteoclastogenesis, which was partly recovered by *Nedd9* overexpression. Cultures were stained by TRAP. Bars = 100 μ m. (C) The expression of *Nedd9* gene as determined by realtime PCR. (D) The number of TRAP positive osteoclasts was significantly increased by *Nedd9* overexpression, and the suppression of osteoclastogenesis by SB431542 was partly suppressed by *Nedd9* overexpression. * $P < 0.05$.

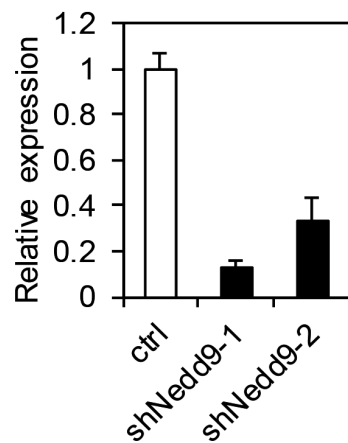
doi:10.1371/journal.pone.0157992.g006

The role of *Nedd9* in skeletal homeostasis *in vivo* is not clear. Seo et al. generated *Nedd9*-deficient mice and reported that lymphocyte trafficking was altered [22]. In addition, Katayose et al. recently reported that *Nedd9*-/- mice exhibited decreased onset of collagen-induced arthritis compared with wild-type mice and that joint destruction was reduced in the knockout mice [31]. We found that RANKL-induced osteoclastogenesis was impaired in BMMs from *Nedd9*-/- mice, and the stimulatory effect of TGF- β on RANKL-induced osteoclastogenesis was partially abrogated. However, we were unable to find the abnormal bone phenotypes in

A



B



C

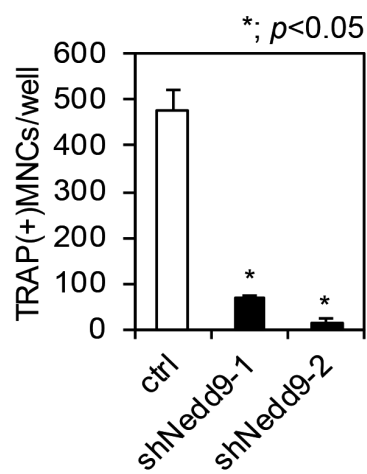
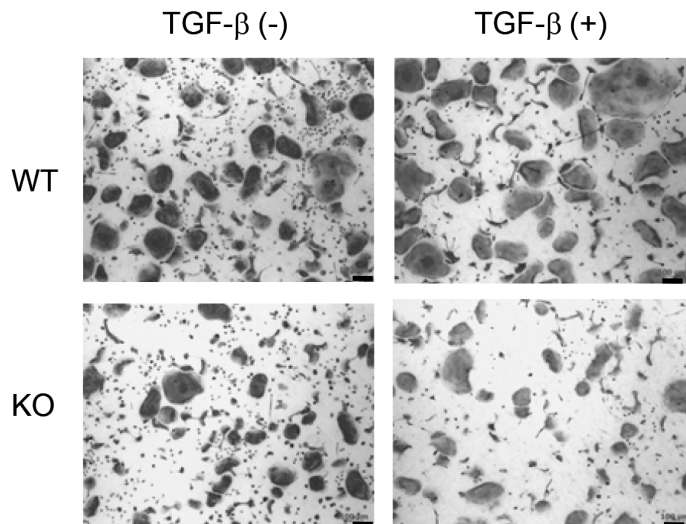


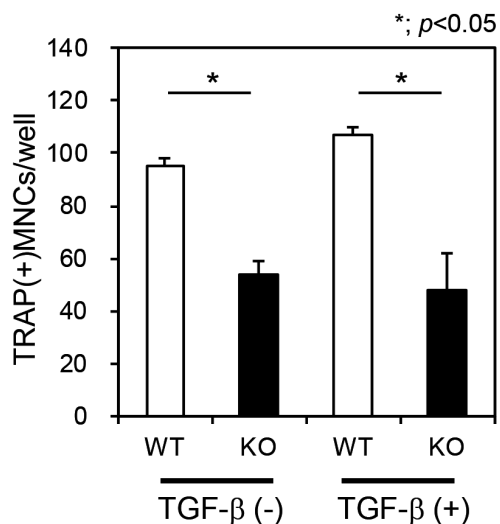
Fig 7. (A) Effects of knockdown of *Nedd9* gene by shRNA on osteoclastogenesis. BMMs infected with retrovirus vector carrying *shNedd9* were treated with 5 nM RANKL for 3 days and stained with TRAP. (B) Expression of *Nedd9* gene by realtime PCR. (C) The number of TRAP positive osteoclasts was significantly reduced by retroviral introduction of *shNedd9*. Bars = 100 μ m. * $P < 0.05$.

doi:10.1371/journal.pone.0157992.g007

A



B



C

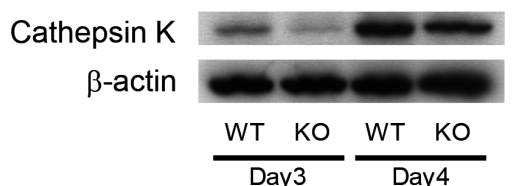
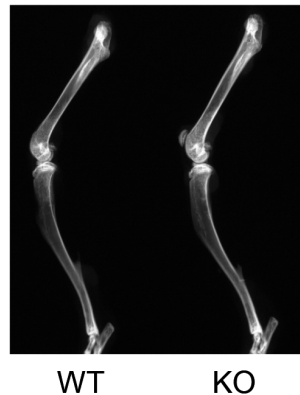


Fig 8. Impaired osteoclastogenesis in Nedd9-/- BMMs. (A) BMMs were isolated from *Nedd9* knockout (KO) and wild-type (WT) mice and cultured in the presence of RANKL with or without TGF-β. Osteoclastogenesis was evaluated by TRAP staining (A), the number of multi-nuclear osteoclasts (B) and the expression of Cathepsin K protein (C).

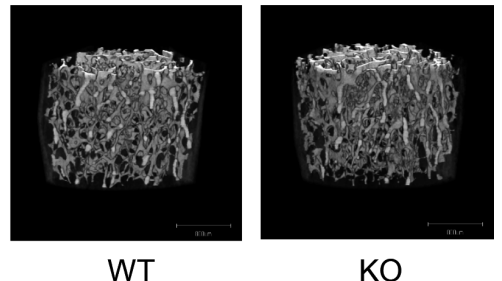
doi:10.1371/journal.pone.0157992.g008

Nedd9-/- mice. This may be due to the effect of Nedd9 on other types of cells such as osteoblasts or osteocytes, or the effect of Nedd9 deficiency is only observed in mice under pathological conditions such as ovariectomy and arthritis, or those treated by TGF-β. Further studies are required to fully understand the role of Nedd9 in the skeletal milieu.

A



B



C

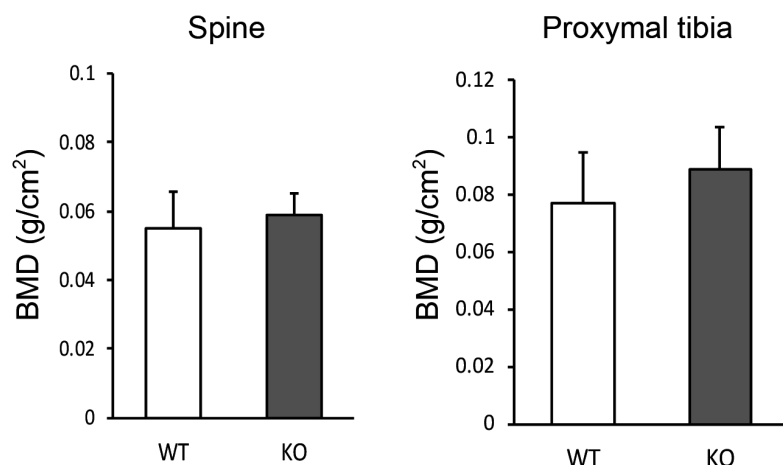


Fig 9. (A) Bone phenotypes of 12-week-old male *Nedd9*-/- and wild-type mice were evaluated using soft-X ray of the lower extremities. (B) micro CT in lumbar vertebral bodies (C) DEXA in lumbar vertebral bodies and proximal tibia.

doi:10.1371/journal.pone.0157992.g009

Materials and Methods

Reagents

Recombinant human M-CSF was purchased from R&D Systems (Minneapolis, MN, USA), and TGF- β and SB431542 were from Sigma-Aldrich (St Louis, MO, USA). GST-RANKL was purchased from Oriental Yeast Co., Ltd (Shiga, Japan). Alpha-minimum essential medium (α -MEM) and fetal bovine serum (FBS) were purchased from Life Technologies (Carlsbad, CA, USA). Smad2/3 antibody was purchased from BD Biosciences (Monoclonal antibody, Mouse, 610843, San Jose, CA, USA), anti-trimethyl-histone H3 lysine 4 was from Activemotif (Polyclonal antibody, Rabbit, 39159, Carlsbad, CA, USA), anti-trimethyl-histone H3 lysine 27 was

from Millipore (Polyclonal antibody, Rabbit, 07–449, Billerica, MA, USA), anti- β -actin was from Sigma-Aldrich (Polyclonal antibody, Rabbit, A2066, St Louis, MO, USA).

Animals

Nedd9–/– mice with C57BL/6J (B6) genetic background were generated as previously reported [22]. In short, the exon 2 encoding the N-terminal SH3 domain in the Cas-L protein was replaced with EGFP and a neomycin resistance gene. All animal procedures were approved by the Animal Care and Use Committee of the University of Tokyo.

Cell Culture

Murine bone marrow cells were collected from the femur and tibia of male ddY mice at 4–5 weeks of age. To prepare BMMs, cells were cultured in α -MEM/10% FBS with 100 ng/ml M-CSF for 5 days. BMMs were further cultured in the presence of 10 ng/ml M-CSF and 100 ng/ml RANKL for 4 days to generate osteoclasts. To examine the effect of the TGF- β -Smad pathway on osteoclastogenesis, 1 ng/ml TGF- β or 10 μ M SB431542 was added with RANKL. Cells were stained with tartrate-resistant acid phosphatase (TRAP), and TRAP-positive cells containing more than three nuclei were counted as osteoclasts.

Real-time PCR analysis

Total RNA was extracted with ISOGEN (Wako Pure Chemical Industries, Ltd.), and a 1- μ g aliquot was reverse transcribed using a QuantiTect Reverse Transcription kit (QIAGEN) to produce singlestranded cDNA. PCR was performed on an ABI Prism 7000 Sequence Detection System (Applied Biosystems) using QuantiTect SYBR Green

PCR Master Mix (QIAGEN) according to the manufacturer's instructions. All reactions were performed in triplicate. After data collection, the mRNA copy number of a specific gene was calculated with a standard curve generated with serially diluted plasmids containing PCR amplicon sequences and then normalized to rodent total RNA with mouse β -actin serving as an internal control. Primer sequences were as follows: *Nedd9* forward, 5'-CCACCCCTCCTACCAGAATCA-3'; *Nedd9* reverse, 5'-ATACCCCTTGAGTGCTGTGG-3'; *Cathepsin K*-forward, 5'-ACGGAGGCATTGACTCTGAAGATG-3'; *Cathepsin K*-reverse, 5'-GGAAGCACCAACGAGAGGAGAAAT-3'.

Expression constructs and gene transduction

For retrovirus construction, the full-length cDNAs were amplified by PCR using KODplus (Takara Bio Inc.), subcloned into Zero Blunt TOPO II vectors (Invitrogen), and inserted into pMX-puro vectors. A total of 2×10^6 BOSC23 packaging cells were transfected with 6 μ g of vector using FuGENE 6 (Roche). After 24 h, the medium was replaced with fresh α -MEM/10% FBS, and cells were incubated for an additional 24 h. The supernatant was then collected as retroviral stock after centrifugation at 2,400 rpm for 3 min. A total of 5×10^6 BMMs were incubated with 8 ml of retroviral stock for 5 h in the presence of 6 μ g/ml polybrene and 30 ng/ml recombinant mouse M-CSF. After 5 h of retroviral infection, the medium was changed to α -MEM/10% FBS and 100 ng/ml M-CSF, and cells were cultured for an additional 24 h. BMMs were recovered with trypsin, and puromycin-resistant cells were selected by incubation with α -MEM/10% FBS containing 2 μ g/ml puromycin for 2 d and used for further experiments.

RNA interference (RNAi)

RNAi expression vectors were constructed with piGENEmU6 vector (iGENE Therapeutics; Tokyo, Japan) as described [32] [33], and the U6 promoter and inserts were cloned into pMx vectors. Retroviruses carrying specific genes were prepared by transfecting BOSC packaging cells with retrovirus vectors and collecting the supernatant after 2 days. For retroviral infection, after the first 2 days of culture, BMMs were incubated with retrovirus in the presence of 30 ng/ml M-CSF and 4 ng/ml polybrene (Sigma-Aldrich; St Louis, MO, USA) for 6 h and cultured overnight in the presence of 10 ng/ml M-CSF. To select the transduced BMMs, cells were detached with Trypsin/EDTA (Sigma-Aldrich; St Louis, MO, USA) and cultured with 10 ng/ml M-CSF and 2 µg/ml puromycin (Sigma-Aldrich) for 2 days. Primer sequences were as follows: shNedd9_1 (sense) 5'-gtttGCATTAGATCTTGGTCGACAggtgtgtccTGTGGCC AAAGGTCTGATGCtttt-3', shNedd9_1 (antisense) 5'-atgcaaaaaGCATCAGACCTTGGCC AACAgacagcacacTGTGACCAAAAGATCTAATGC-3', shNedd9_2(sense) 5'-gtttGCAGTG CTAGGAGTGACATGTgtgtgtccACATGTTACTCCTGGTACTGCtttt-3', shNedd9_2 (antisense) 5'-atgcaaaaaGCAGTACCAAGGAGTAACATGTggacagcacACATGTCACTCCT AGCACTGC-3'.

ChIP and ChIP-seq

Cells were cultured in 15-cm plates to approximately 80% confluence. Cells were fixed with 1% formaldehyde at room temperature and then neutralized with glycine. After cells were collected and re-suspended, samples were sonicated. Samples were incubated with protein A/G beads that had been pre-incubated with 4–10 µg of antibody. Immunoprecipitates were washed and reverse-crosslinked, and DNA was purified with a PCR purification kit (Qiagen, Germantown, MD, USA). DNA libraries were prepared for sequencing using the standard Illumina protocol. Purified DNA was applied for cluster generation and sequencing on the cBot Cluster Generation system and Genome Analyzer IIx system (Illumina; San Diego, CA, USA) following the manufacturer's instructions. Obtained sequences were mapped to the reference mouse genome. ChIP primer sequences were as follows: Nedd9 forward: 5'-AGAAGGCAGAGGCAGCATA A-3', Nedd9 reverse: 5'-CCTGTGGCATCATCTCTAAGG-3', Pdgfb forward: 5'-TTTCAAGG CGATGAGGTAC-3', Pdgfb reverse: 5'-GGAGAGTGCCCCAGACCT-3', Smad6 forward: 5'-CATGCAGGGTGTCTCTAGCA-3', Smad6 reverse: 5'-GGCTACATGGATCACGATGG-3', Tmepai forward: 5'-AAACCTACTGCGACGACAGG-3', Tmepai reverse: 5'-ATGAGAGG CACTTGCAACC-3', Ski forward: 5'-TGGAGAGGCTCTGCTCTAGG-3', Ski reverse: 5'- CCTGCAGCTGGTTGTCAA-3', Cdkn1a forward: 5'-TCTGT GTACGTGCCTGTGTG-3', Cdkn1a reverse: 5'-TAAATTCCCGCCTATGTTGG-3', Serpine1 forward: 5'-AGCCCAATA GAGAACTTCAAGTCC-3', Serpine1 reverse: 5'-CAGTACACCTAAACCCAGCC-3', Smad7 forward: 5'-TGCAGAACACAATCGCTT-3', Smad7 reverse: 5'-CTCTGCTCGG CTGGTTCC-3', Ppib forward: 5'-ATGTGGTACGGAAGGGAGGAGA-3', Ppib reverse: 5'- AGCTGCTTAGAGGGATGAGG-3', Hoxa13 forward: 5'-TGGCATTTAGGGACCTC-3', Hoxa13 reverse: 5'-CACATCCTGGGAGGGTCTA-3'.

Microarray expression array analysis

Total RNA was extracted with TRIzol and subjected to GeneChip (Affymetrix; Santa Clara, CA, USA) expression analysis according to the technical manual. Briefly, biotin-labeled cRNA synthesized from total RNA was hybridized to a GeneChip Mouse Genome MOE430 2.0 oligonucleotide array (Affymetrix; Santa Clara, CA, USA). The arrays were stained with streptavidin-phycoerythrin and image data was collected with an Affymetrix scanner. Microarray Suite software 5.0 was used to calculate the average difference (AD) for each gene probe set, shown

as the gene expression intensity value. The AD values were normalized for each array so that the average of all AD values was 100. One array datum was obtained for each sample. Obtained data were verified by qPCRs for various transcripts, and we had no conflicting results between the array data and qPCR data. Affymetrix probe IDs were converted to gene symbols.

Statistical analyses

The results are expressed as mean \pm SD. Statistical analyses were performed using a two-tailed unpaired Student's *t* test for continuous variables and chi-square tests for categorical variables. A p value of less than 0.05 was considered to be statistically significant.

Acknowledgments

We thank Dr. M. Miyagishi (National Institute of Advanced Industrial Science and Technology) for providing advice for designing and cloning strategies for shRNA constructs. We also thank H. Kawahara, R. Yamaguchi and J. Sugita (Department of Orthopaedic Surgery, The University of Tokyo) for providing expert technical assistance.

Author Contributions

Conceived and designed the experiments: TY CM T. Miyamoto HA S. Tanaka. Performed the experiments: YO SN TK TY JH NI T. Matsumoto. Analyzed the data: YO TY NI YI S. Tsutsumi YK T. Miyamoto HA S. Tanaka. Contributed reagents/materials/analysis tools: SS MK S. Tsutsumi CM HA. Wrote the paper: YO TY T. Miyamoto S. Tanaka.

References

1. Tanaka S. Signaling axis in osteoclast biology and therapeutic targeting in the RANKL/RANK/OPG system. *Am J Nephrol*. 2007; 27(5):466–78. doi: [10.1159/000106484](https://doi.org/10.1159/000106484) PMID: [17652963](https://pubmed.ncbi.nlm.nih.gov/17652963/).
2. Yasui T, Kadono Y, Nakamura M, Oshima Y, Matsumoto T, Masuda H, et al. Regulation of RANKL-induced osteoclastogenesis by TGF-beta through molecular interaction between Smad3 and Traf6. *J Bone Miner Res*. 2011; 26(7):1447–56. doi: [10.1002/jbm.357](https://doi.org/10.1002/jbm.357) PMID: [21305609](https://pubmed.ncbi.nlm.nih.gov/21305609/).
3. Omata Y, Yasui T, Hirose J, Izawa N, Imai Y, Matsumoto T, et al. Genomewide comprehensive analysis reveals critical cooperation between Smad and c-Fos in RANKL-induced osteoclastogenesis. *J Bone Miner Res*. 2015; 30(5):869–77. doi: [10.1002/jbm.2418](https://doi.org/10.1002/jbm.2418) PMID: [25431176](https://pubmed.ncbi.nlm.nih.gov/25431176/).
4. Janssens K, ten Dijke P, Janssens S, Van Hul W. Transforming growth factor-beta1 to the bone. *Endocr Rev*. 2005; 26(6):743–74. doi: [10.1210/er.2004-0001](https://doi.org/10.1210/er.2004-0001) PMID: [15901668](https://pubmed.ncbi.nlm.nih.gov/15901668/).
5. Tang SY, Alliston T. Regulation of postnatal bone homeostasis by TGFbeta. *Bonekey Rep*. 2013; 2:255. doi: [10.1038/bonekey.2012.255](https://doi.org/10.1038/bonekey.2012.255) PMID: [24404376](https://pubmed.ncbi.nlm.nih.gov/24404376/); PubMed Central PMCID: [PMC3722719](https://pubmed.ncbi.nlm.nih.gov/PMC3722719/).
6. Ikushima H, Miyazono K. TGF-beta signal transduction spreading to a wider field: a broad variety of mechanisms for context-dependent effects of TGF-beta. *Cell Tissue Res*. 2012; 347(1):37–49. doi: [10.1007/s00441-011-1179-5](https://doi.org/10.1007/s00441-011-1179-5) PMID: [21618142](https://pubmed.ncbi.nlm.nih.gov/21618142/).
7. Massague J, Attisano L, Wrana JL. The TGF-beta family and its composite receptors. *Trends Cell Biol*. 1994; 4(5):172–8. PMID: [14731645](https://pubmed.ncbi.nlm.nih.gov/14731645/).
8. Li MO, Flavell RA. TGF-beta: a master of all T cell trades. *Cell*. 2008; 134(3):392–404. doi: [10.1016/j.cell.2008.07.025](https://doi.org/10.1016/j.cell.2008.07.025) PMID: [18692464](https://pubmed.ncbi.nlm.nih.gov/18692464/); PubMed Central PMCID: [PMC3677783](https://pubmed.ncbi.nlm.nih.gov/PMC3677783/).
9. Graff JM, Bansal A, Melton DA. Xenopus Mad proteins transduce distinct subsets of signals for the TGF beta superfamily. *Cell*. 1996; 85(4):479–87. PMID: [8653784](https://pubmed.ncbi.nlm.nih.gov/8653784/).
10. Huang W, Drissi MH, O'Keefe RJ, Schwarz EM. A rapid multiparameter approach to study factors that regulate osteoclastogenesis: demonstration of the combinatorial dominant effects of TNF-alpha and TGF-ss in RANKL-mediated osteoclastogenesis. *Calcif Tissue Int*. 2003; 73(6):584–93. doi: [10.1007/s00223-003-0059-8](https://doi.org/10.1007/s00223-003-0059-8) PMID: [14517717](https://pubmed.ncbi.nlm.nih.gov/14517717/).
11. Margueron R, Trojer P, Reinberg D. The key to development: interpreting the histone code? *Curr Opin Genet Dev*. 2005; 15(2):163–76. doi: [10.1016/j.gde.2005.01.005](https://doi.org/10.1016/j.gde.2005.01.005) PMID: [15797199](https://pubmed.ncbi.nlm.nih.gov/15797199/).

12. Zhang Y, Reinberg D. Transcription regulation by histone methylation: interplay between different covalent modifications of the core histone tails. *Genes Dev.* 2001; 15(18):2343–60. doi: [10.1101/gad.927301](https://doi.org/10.1101/gad.927301) PMID: [11562345](https://pubmed.ncbi.nlm.nih.gov/11562345/).
13. Strahl BD, Ohba R, Cook RG, Allis CD. Methylation of histone H3 at lysine 4 is highly conserved and correlates with transcriptionally active nuclei in Tetrahymena. *Proc Natl Acad Sci U S A.* 1999; 96(26):14967–72. PMID: [10611321](https://pubmed.ncbi.nlm.nih.gov/10611321/); PubMed Central PMCID: [PMCPMC24756](https://pmid.ncbi.nlm.nih.gov/10611321/).
14. Bernstein BE, Mikkelsen TS, Xie X, Kamal M, Huebert DJ, Cuff J, et al. A bivalent chromatin structure marks key developmental genes in embryonic stem cells. *Cell.* 2006; 125(2):315–26. doi: [10.1016/j.cell.2006.02.041](https://doi.org/10.1016/j.cell.2006.02.041) PMID: [16630819](https://pubmed.ncbi.nlm.nih.gov/16630819/).
15. Yasui T, Hirose J, Tsutsumi S, Nakamura K, Aburatani H, Tanaka S. Epigenetic regulation of osteoclast differentiation: possible involvement of Jmjd3 in the histone demethylation of Nfatc1. *Journal of bone and mineral research: the official journal of the American Society for Bone and Mineral Research.* 2011; 26(11):2665–71. doi: [10.1002/jbmr.464](https://doi.org/10.1002/jbmr.464) PMID: [21735477](https://pubmed.ncbi.nlm.nih.gov/21735477/).
16. Giresi PG, Lieb JD. Isolation of active regulatory elements from eukaryotic chromatin using FAIRE (Formaldehyde Assisted Isolation of Regulatory Elements). *Methods.* 2009; 48(3):233–9. doi: [10.1016/j.ymeth.2009.03.003](https://doi.org/10.1016/j.ymeth.2009.03.003) PMID: [19303047](https://pubmed.ncbi.nlm.nih.gov/19303047/); PubMed Central PMCID: [PMCPMC2710428](https://pmid.ncbi.nlm.nih.gov/19303047/).
17. Subramanian A, Tamayo P, Mootha VK, Mukherjee S, Ebert BL, Gillette MA, et al. Gene set enrichment analysis: a knowledge-based approach for interpreting genome-wide expression profiles. *Proc Natl Acad Sci U S A.* 2005; 102(43):15545–50. doi: [10.1073/pnas.0506580102](https://doi.org/10.1073/pnas.0506580102) PMID: [16199517](https://pubmed.ncbi.nlm.nih.gov/16199517/); PubMed Central PMCID: [PMCPMC1239896](https://pmid.ncbi.nlm.nih.gov/16199517/).
18. Minegishi M, Tachibana K, Sato T, Iwata S, Nojima Y, Morimoto C. Structure and function of Cas-L, a 105-kD Crk-associated substrate-related protein that is involved in beta 1 integrin-mediated signaling in lymphocytes. *The Journal of experimental medicine.* 1996; 184(4):1365–75. PMID: [8879209](https://pubmed.ncbi.nlm.nih.gov/8879209/); PubMed Central PMCID: [PMC2192828](https://pmid.ncbi.nlm.nih.gov/8879209/).
19. Tikhmyanova N, Little JL, Golemis EA. CAS proteins in normal and pathological cell growth control. *Cell Mol Life Sci.* 2010; 67(7):1025–48. doi: [10.1007/s00018-009-0213-1](https://doi.org/10.1007/s00018-009-0213-1) PMID: [19937461](https://pubmed.ncbi.nlm.nih.gov/19937461/); PubMed Central PMCID: [PMCPMC2836406](https://pmid.ncbi.nlm.nih.gov/19937461/).
20. Tornillo G, Defilippi P, Cabodi S. Cas proteins: dodgy scaffolding in breast cancer. *Breast Cancer Res.* 2014; 16(5):443. PMID: [25606587](https://pubmed.ncbi.nlm.nih.gov/25606587/); PubMed Central PMCID: [PMCPMC4384296](https://pmid.ncbi.nlm.nih.gov/25606587/).
21. Law SF, Zhang YZ, Klein-Szanto AJ, Golemis EA. Cell cycle-regulated processing of HEF1 to multiple protein forms differentially targeted to multiple subcellular compartments. *Mol Cell Biol.* 1998; 18(6):3540–51. PMID: [9584194](https://pubmed.ncbi.nlm.nih.gov/9584194/); PubMed Central PMCID: [PMCPMC108935](https://pmid.ncbi.nlm.nih.gov/9584194/).
22. Seo S, Asai T, Saito T, Suzuki T, Morishita Y, Nakamoto T, et al. Crk-associated substrate lymphocyte type is required for lymphocyte trafficking and marginal zone B cell maintenance. *J Immunol.* 2005; 175(6):3492–501. PMID: [16148091](https://pubmed.ncbi.nlm.nih.gov/16148091/).
23. Shagisultanova E, Gaponova AV, Gabbasov R, Nicolas E, Golemis EA. Preclinical and clinical studies of the NEDD9 scaffold protein in cancer and other diseases. *Gene.* 2015; 567(1):1–11. doi: [10.1016/j.gene.2015.04.086](https://doi.org/10.1016/j.gene.2015.04.086) PMID: [25967390](https://pubmed.ncbi.nlm.nih.gov/25967390/); PubMed Central PMCID: [PMCPMC4458429](https://pmid.ncbi.nlm.nih.gov/25967390/).
24. Barski A, Cuddapah S, Cui K, Roh TY, Schones DE, Wang Z, et al. High-resolution profiling of histone methylations in the human genome. *Cell.* 2007; 129(4):823–37. doi: [10.1016/j.cell.2007.05.009](https://doi.org/10.1016/j.cell.2007.05.009) PMID: [17512414](https://pubmed.ncbi.nlm.nih.gov/17512414/).
25. Guenther MG, Levine SS, Boyer LA, Jaenisch R, Young RA. A chromatin landmark and transcription initiation at most promoters in human cells. *Cell.* 2007; 130(1):77–88. doi: [10.1016/j.cell.2007.05.042](https://doi.org/10.1016/j.cell.2007.05.042) PMID: [17632057](https://pubmed.ncbi.nlm.nih.gov/17632057/); PubMed Central PMCID: [PMC3200295](https://pmid.ncbi.nlm.nih.gov/17632057/).
26. Schwartz YB, Pirrotta V. Polycomb silencing mechanisms and the management of genomic programmes. *Nature reviews Genetics.* 2007; 8(1):9–22. doi: [10.1038/nrg1981](https://doi.org/10.1038/nrg1981) PMID: [17173055](https://pubmed.ncbi.nlm.nih.gov/17173055/).
27. Liu X, Elia AE, Law SF, Golemis EA, Farley J, Wang T. A novel ability of Smad3 to regulate proteasomal degradation of a Cas family member HEF1. *EMBO J.* 2000; 19(24):6759–69. doi: [10.1093/emboj/19.24.6759](https://doi.org/10.1093/emboj/19.24.6759) PMID: [11118211](https://pubmed.ncbi.nlm.nih.gov/11118211/); PubMed Central PMCID: [PMCPMC305889](https://pmid.ncbi.nlm.nih.gov/11118211/).
28. Zheng M, McKeown-Longo PJ. Regulation of HEF1 expression and phosphorylation by TGF-beta 1 and cell adhesion. *J Biol Chem.* 2002; 277(42):39599–608. doi: [10.1074/jbc.M202263200](https://doi.org/10.1074/jbc.M202263200) PMID: [12189134](https://pubmed.ncbi.nlm.nih.gov/12189134/).
29. Morimoto K, Tanaka T, Nitta Y, Ohnishi K, Kawashima H, Nakatani T. NEDD9 crucially regulates TGF-beta-triggered epithelial-mesenchymal transition and cell invasion in prostate cancer cells: involvement in cancer aggressiveness. *Prostate.* 2014; 74(8):901–10. doi: [10.1002/pros.22809](https://doi.org/10.1002/pros.22809) PMID: [24728978](https://pubmed.ncbi.nlm.nih.gov/24728978/).
30. Inamoto S, Iwata S, Inamoto T, Nomura S, Sasaki T, Urasaki Y, et al. Crk-associated substrate lymphocyte type regulates transforming growth factor-beta signaling by inhibiting Smad6 and Smad7. *Oncogene.* 2007; 26(6):893–904. doi: [10.1038/sj.onc.1209848](https://doi.org/10.1038/sj.onc.1209848) PMID: [16909115](https://pubmed.ncbi.nlm.nih.gov/16909115/).

31. Katayose T, Iwata S, Oyaizu N, Hosono O, Yamada T, Dang NH, et al. The role of Cas-L/NEDD9 as a regulator of collagen-induced arthritis in a murine model. *Biochemical and biophysical research communications*. 2015; 460(4):1069–75. doi: [10.1016/j.bbrc.2015.03.156](https://doi.org/10.1016/j.bbrc.2015.03.156) PMID: 25847598.
32. Miyagishi M, Taira K. Strategies for generation of an siRNA expression library directed against the human genome. *Oligonucleotides*. 2003; 13(5):325–33. doi: [10.1089/154545703322617005](https://doi.org/10.1089/154545703322617005) PMID: 15000823.
33. Miyagishi M, Taira K. RNAi expression vectors in mammalian cells. *Methods Mol Biol*. 2004; 252:483–91. doi: [10.1385/1-59259-746-7:483](https://doi.org/10.1385/1-59259-746-7:483) PMID: 15017073.

RESEARCH ARTICLE

Open Access



Establishment of anti-mesothelioma monoclonal antibodies

Natsuko Mizutani^{1,2}, Masaaki Abe², Shuji Matsuoka^{2*}, Kazunori Kajino², Midori Wakiya^{2,3}, Naomi Ohtsuki², Ryo Hatano⁴, Chikao Morimoto⁴ and Okio Hino²

Abstract

Background: Mesotheliomas are aggressive, therapy-resistant tumors that are predicted to increase in incidence at least until 2020. The prognosis of patients with mesothelioma is generally poor because they are typically diagnosed at a late stage and their tumors are resistant to current conventional therapies. For these reasons, improved diagnosis and therapy are urgently required. To address these issues, the aim of our research was to develop novel mesothelioma-specific monoclonal antibodies (mAbs) as diagnostic and therapeutic agents.

Methods: To develop anti-mesothelioma mAbs useful for diagnosis and therapy, we repeatedly immunized a BALB/c mouse with viable mesothelioma cells, alternating between those from three mesothelioma cell lines. We hybridized the spleen cells from this immunized mouse with P3U1 myeloma cells. We then screened supernatants harvested from the hybridoma clones by assessing whether they bound to a mesothelioma cell line not used for immunization and altered its morphology. We designed this developmental strategy to reduce the risk of obtaining clonotypic mAbs against a single mesothelioma cell line.

Results: Our newly generated mouse anti-human mAbs immunostained clinical samples of mesotheliomas. One of the newly generated mAbs did not react with any other tumor cell line tested. Two other mAbs significantly inhibited the proliferation of mesothelioma cells.

Conclusion: These newly generated anti-mesothelioma mAbs are potentially useful as diagnostic and therapeutic agents for mesothelioma. Moreover, our novel strategy for establishing antitumor mAbs may facilitate the development of new diagnostic and therapeutic techniques for mesotheliomas and other malignancies.

Keywords: Monoclonal antibody, Mesothelioma, Diagnosis, Therapy, Method

Background

Mesothelioma is an aggressive tumor that develops from mesothelial cells, which line the pleural, peritoneal, and pericardial cavities. The development of mesothelioma is usually associated with chronic exposure to asbestos fibers [1, 2]. The worldwide incidence of mesothelioma is increasing and is expected to peak in approximately 2020 because of the long latent period between exposure to asbestos fibers and the appearance of disease [3]. Asbestos continues to be mined in Russia, China, Brazil, Kazakhstan and other countries [4]. Asbestos is still

imported and used in brake pads, gaskets, etc., even in the US [4]. Diagnosis based on chest X-ray and computed tomography (CT) findings must be confirmed by cytologic serous effusion examination or biopsy [5–7].

Immunohistochemistry has significantly enhanced the accuracy of cytology, although reaching a diagnosis remains frequently difficult [8–10]. Although many diagnostic procedures are available, no single test unambiguously distinguishes mesothelioma from other carcinomas or even benign from malignant cells. The correct combination of antibodies used to detect positive or negative markers should be employed and a comprehensive assessment of the staining results must be conducted [11].

*Correspondence: matsuoka@juntendo.ac.jp

² Departments of Pathology and Oncology, Juntendo University School of Medicine, 2-1-1, Hongo, Bunkyo-ku, Tokyo 113-8421, Japan
Full list of author information is available at the end of the article

Mesothelioma is categorized histologically as epithelioid, sarcomatoid, biphasic, and desmoplastic, among others [9]. The histological subtypes help predict prognosis and the choice of treatment. Therefore, it is important to analyze pathological tissue using an appropriate combination of antibodies for diagnosis and classification. Nevertheless, many cases are difficult to diagnosis [12–16].

Although an anti-CD26 mAb is a promising candidate, no effective molecular target for therapy exists [17, 18]. Therefore, the development of novel anti-mesothelioma mAbs may facilitate diagnosis and serve as therapeutic agents. Subsequent to the development of mAbs by Köhler, Milstein, and Jerne in 1975 [19], excessively large number of mAbs were generated as diagnostic [20, 21] or therapeutic reagents [22].

Diagnostic or therapeutic mAbs are now typically generated by immunizing mice with synthetic peptides or target antigens that are purified to some extent [23, 24]. Except for nude or SCID mice, mice reject inoculated live malignant human tumor cells. During the first or second challenge, tumor cells may be primarily killed by NK and CD8 cytotoxic T cells or ingested by macrophages. However, during the course of repeated immunizations, mouse B cells are generated that produce antibodies against the tumor cells. These antibodies probably make a major contribution to the rejection of the tumor cells. This hypothesis served as the rationale for our experiments that were aimed at establishing anti-mesothelioma mAbs. We report here the generation of anti-human mesothelioma mAbs for diagnosis and treatment. This was accomplished by immunizing a mouse with live mesothelioma cell lines. The hybridomas were selected for their ability to produce antibodies that bound to mesothelioma cell lines not used for immunization. Some of these newly established mAbs reacted specifically with mesothelioma cells or inhibited their proliferation.

Methods

Mice

Female BALB/c mice (6–8 weeks of age) were purchased from Charles River Japan (Yokohama, Japan) and housed in a specific pathogen-free facility in micro-isolator cages. Animal experiments were conducted following protocols approved by the Animal Care Committee of Juntendo University of Medicine.

Cells

The human mesothelioma cell lines ACC-MESO-1 and ACC-MESO-4 were purchased from the RIKEN Cell Bank (Ibaraki, Japan), JMN was a kind gift from Dr. Brenda Gerwin and others (NCI-H226, MSTO-211H, NCI-H28 and NCI-H2452) were purchased from the

American Type Culture Collection (ATCC) (Manassas, VA). The lung cancer cell lines (A549, PC9, Lu24, and WA-hT), and the HuH-7 (hepatocellular carcinoma), MKN1 (gastric cancer), OVK18 (ovarian cancer), VMRC-RCW (renal cell carcinoma) cell lines were purchased from the RIKEN Cell Bank. The MCF7 (breast cancer), KP3 (pancreatic cancer), and HCT 116 (colon cancer) cell lines were purchased from ATCC. All cells were cultured and maintained in RPMI-1640 medium (GIBCO, Grand Island, NY) supplemented with 10 % heat-inactivated fetal calf serum.

Antibodies

The mouse anti-HLA class I (HLA class-A, B, C) mAb (clone: W6/32) was purchased from Harlan Laboratories Inc. (IN). Alexa Flour® 488-conjugated goat anti-mouse IgG was purchased from Invitrogen (CA). Mouse IgG was purchased from Abcam (Cambridge UK). The mAbs for WT-1 (clone: 6F-H2), Calretinin (clone: DAK-Calret 1), Podoplanin (clone: D2-40), Cytokeratin 5/6 (clone: D5/16 B4), EMA (clone: E29), Carcinoembryonic Antigen (CEA) (clone: II-7), TTF-1 (clone: 8G7G3/1), and Epithelial-Related Antigen (clone: Moc-31) were purchased from DAKO. The mAb against Mesothelin (clone: 22A31) and anti-GLUT-1 polyclonal Ab were purchased from IBL (Japan). Anti-CD26 mAbs (clone 1F7, 5F8) were established in our laboratory [25].

Anti-CD25 mAb (clone: BC96) and mouse Ig G1 isotype control (MOPC-21) were purchased from TONBO biosciences (CA).

Generation of mAbs against mesothelioma cells

An eight-week-old female BALB/c mouse was immunized alternately using intraperitoneal injections of $2-5 \times 10^6$ living cells derived from the mesothelioma cell lines ACC-MESO4, MSTO-211H, and NCI-H226 every 2 weeks for 3 months. Three days after the last immunization, spleen cells were fused with P3U1-non-producing myeloma cells using polyethylene glycol 4000 (Merck, Darmstadt, Germany) and cultured in RPMI-1640 supplemented with 10 % fetal calf serum (FCS, Japan Bioserum, Fukuyama, Japan), 5 % BriClone (NICB, Dublin, Ireland), and HAT (Invitrogen, Tokyo, Japan) in the wells of 96-well flat-bottom plates (Costar, Corning Incorporated, Corning, NY). Hybridoma supernatants were screened for reactivity with the mesothelioma NCI-H2452 cells, which were not used for immunization. Light microscopy revealed morphological changes and an aggregation of target cells induced by incubation with supernatants of hybridoma clones after 72 h. The reactivity of hybridoma supernatants for the other mesothelioma cell lines was also determined. Four hybridomas, JMAM1–4, were selected and cloned using limiting

dilution. The isotype of these mAbs was IgG1, and they cross-reacted widely with mesothelioma cell lines.

Flow cytometric (FACS) analysis

The expression of the molecular target(s) of the newly established mouse anti-human mesothelioma mAbs was determined using a BD LSRForessa™ cell analyzer (BD Bioscience, CA, USA). Briefly, the human mesothelioma cell lines and the cell lines derived from other tumors were incubated with the supernatants of hybridomas and then with Alexa Flour® 488-conjugated rat anti-mouse IgG (BD Bioscience) on ice.

Inhibition test

NCI-H226 cells were first incubated with already known existing Abs and further incubated with Alexa Flour® 488-labeled JMAM mAbs.

Immunocytochemistry

Samples of pleural effusions submitted to the Department of Pathology, Juntendo University, were used for immunohistochemistry and other histological staining procedures. Three representative cases of cytologically diagnosed mesothelioma were used for immunohistochemistry, and all cases were stained with positive and negative antibody panels of diagnostic antibodies to confirm the diagnosis of mesothelioma. Cell smears were fixed in 95 % ethanol for Papanicolaou and immunostaining, or air-dried for May-Grunwald-Giemsa staining. Cell sediments were fixed with ethanol and embedded in paraffin for immunostaining. Sections were deparaffinized using three changes of xylene and rehydrated with a graded series of ethanol concentrations. Endogenous peroxidase was inactivated with 0.3 % H₂O₂ in phosphate-buffered saline for 10 min. Samples were incubated with the novel anti-mesothelioma mAbs JMAM1–4 at 4 °C overnight in a humidified chamber, followed by the addition of EnVision™ + DualLink (DAKO) and 3,3'-diaminobenzidine (Dojindo Laboratories) as the chromogen. Cell smears and cell-block sections were counterstained to reveal nuclei using Mayer's hematoxylin. For all cases, we stained cell block sections using antibodies against EMA, Podoplanin, GLUT-1, Calretinin, WT-1, Cytokeratin 5/6, Mesothelin, CEA, TTF-1, and epithelial-related antigen to confirm the diagnosis of mesothelioma (Table 1).

In vitro proliferative assay of mesothelial cells incubated with mAbs

MSTO-211H cells (1 × 10⁴ cells/well) were incubated with 10 % FCS-RPMI supplemented with 0.005–0.4 µg/ml of JMAM1–4 mAbs for 48 h at 37 °C in an atmosphere containing 5 % CO₂. The culture was pulsed with 0.5 µCi

of tritiated thymidine, [³H]-TdR, for the final 24 h. The incorporation of [³H]-TdR was determined using scintillation counting. Data are expressed as the mean ± standard deviation (SD) of triplicate samples and represent three separate experiments.

Wound-healing assay

Mesothelioma NCI-H226 cells were seeded in 6-well plates (Corning) and grown to 90 % confluence in RPMI plus 10 % FCS. The cell monolayer was wounded with the tip of an Eppendorf P200 pipette. After wounding, the wells were washed with media to remove dead cells and debris. The wells were treated with either 3 µg/ml of anti-mesothelioma mAbs (JMAM1–4) or a control IgG (3 µg/ml) and cultured further. The wound closure was observed after 24 h.

Cell invasion assay

For the cell invasion test, a Corning Matrigel Invasion Chamber (8-µm pore size, coated with Matrigel; Discovery Labware Inc., Bedford, MA, USA) was placed into the wells of 24-well culture plates; RPMI-1640 medium with 10 % serum and JMAM1–4 mAbs (each 10 µM) were added into the lower chamber; then, 2 × 10⁴ NCI-H226 cells in serum-free RPMI-1640 medium was added to the upper chamber and cultured at 37 °C. After 15 h of incubation, the cells on the upper surface of the filter membrane that had not migrated were gently scraped away with a cotton swab. The invading cells on the lower surface of the filter membrane were fixed with methanol, stained with Diff-Quick™ (Sysmex), and counted as described above. All tests were performed in triplicate.

Statistical analysis

The data were analyzed using Student's *t* test. The results are expressed as the mean ± SD and P values of <0.05 were considered significant. Statistical analyses were performed using SPSS 14.0 software (IBM, NY).

Results

Morphological changes of mesothelioma cell lines induced by the newly generated mAbs

We found that the newly generated four mAbs reproducibly induced morphological changes in a mesothelioma cell line that was not used for immunization. Light microscopy revealed that the morphology of the NCI-H2452 cells changed from spindle-shaped to round, and the numbers of these cells decreased after incubation with JMAM1–4 mAbs for 72 h compared with control mouse IgG (Fig. 1a, upper column). These morphological changes indicated that the mAbs bound the mesothelial cell lines. These findings were also reproduced using MSTO-211H cells that were used for immunization

Table 1 Antibodies used in this study and immunocytochemical reactivity

Antibody	Clone	Source	Dilution	Specimen	Case 1	Case 2	Case 3
JMAM1		Our laboratory	Undiluted cell supernatant	Cell smear	+	+	+
JMAM2		Our laboratory	Undiluted cell supernatant	Cell smear	+	+	+
JMAM3		Our laboratory	Undiluted cell supernatant	Cell smear	+	+	+
JMAM4		Our laboratory	Undiluted cell supernatant	Cell smear	+	+	+
WT-1	6F-H2	DAKO	1:200	Cell block	+	±	+
Carletnin	Dak-Calret 1	DAKO	1:100	Cell block	+	+	+
Mesothelin	22A31	IBL	1:1000	Cell block	+	+	+
Podoplanin	D2-40	DAKO	1:200	Cell block	+	+	+
CK5/6	D5/16B4	DAKO	1:50	Cell block	+	+	+
EMA	E29	DAKO	1:100	Cell block	+	+	+
GLUT-1	5B12.3	IBL	1:1000	Cell block	+	+	+
CEA	II-7	DAKO	1:50	Cell block	—	—	—
TTF-1	8G7G3/1	DAKO	1:100	Cell block	—	—	—
Epithelial-related antigen	Moc-31	DAKO	1:100	Cell block	—	—	—

(Fig. 1a, lower column). Furthermore, these mAbs aggregated MSTO-211H cells. Taken together, these findings indicate that the newly established mAbs reacted with the mesothelial cell lines.

Analysis of the binding of mAbs to the mesothelial cell lines

The reactivity of the mAbs against the mesothelial cell lines was determined using FACS analysis. JMAM1, JMAM2 and JMAM3 mAbs stained the epithelial (ACC-MESO-4, JMN) and sarcomatous (MSTO-211H, H2452, H28 and MESO-1) cell lines. In contrast, JMAM4 stained the epithelial cell lines but not the sarcomatous cell lines (Fig. 1b).

Competitive inhibition of JMAM mAbs with established mAbs

To determine whether the newly established JMAM mAbs bind to the same epitope of the already existing Abs, we performed an inhibition test by flow cytometry.

NCI-H226 cells were incubated with JMAM mAbs followed by staining with existing Abs already known to bind to mesothelioma [anti-calretinin, anti-podoplanin (D2-40), anti-GLUT-1, anti-CD25 (BC96), anti-CD26 (1F7, 5F8), anti-C-ERC/mesothelin (22A31)]. (Fig. 2).

Anti-calretinin was able to partially inhibit the staining of the NCI-H226 mesothelioma cell line with JMAM2 mAb. This result indicates that the JMAM2 determinant is strongly related to calretinin; however, the other JMAM mAbs have no relationship with already existing Abs, they may bind to mesothelioma cells.

Analysis of the binding of mAbs to other tumor cell lines

Using FACS analysis, we next determined whether the mAbs bound to lung cancer cell lines. Binding of JMAM1 to epithelial-type lung cancer cell lines (A549 and PC9) was not detectable. In contrast, it bound to the small-cell lung cancer cell lines WA-hT and Lu24. The extent of binding of JMAM2 and JMAM3 mAbs to lung cancer cell lines varied. The JMAM4 mAb did not bind to any of the lung cancer cell lines (Fig. 3a).

To determine the cross-reactivity of these novel anti-mesothelioma mAbs to cell lines derived from tumors other than those of the lung, we used FACS analysis to determine their ability to react with MCF7 (breast cancer), HuH-7 (liver cancer), KP3 (pancreatic cancer), MKN-1 (gastric cancer), HCT 116 (colon cancer), OVK18 (ovarian cancer), and VMRC-RCW (renal cell carcinoma) cell lines. The JMAM1 mAb only cross reacted with the VMRC-RCW cell line. JMAM4 mAbs did not react detectably with any of these carcinoma cell lines. The JMAM2 mAb slightly or significantly stained all carcinoma cell lines tested. The JMAM3 mAb did not stain the liver or pancreatic cancer cell lines; however, it lightly stained a gastric cancer cell line and strongly stained breast and colon cancer cell lines (Fig. 3b). Taken together, these data indicate that the JMAM1 mAb distinguished mesothelioma and small-cell lung cancer cells from epithelial lung cancer cells as well as any other cancer cells derived from these tissues except for renal cell carcinoma. These data also suggest that JMAM4 mAb may distinguish epithelial mesotheliomas from all other cancers.

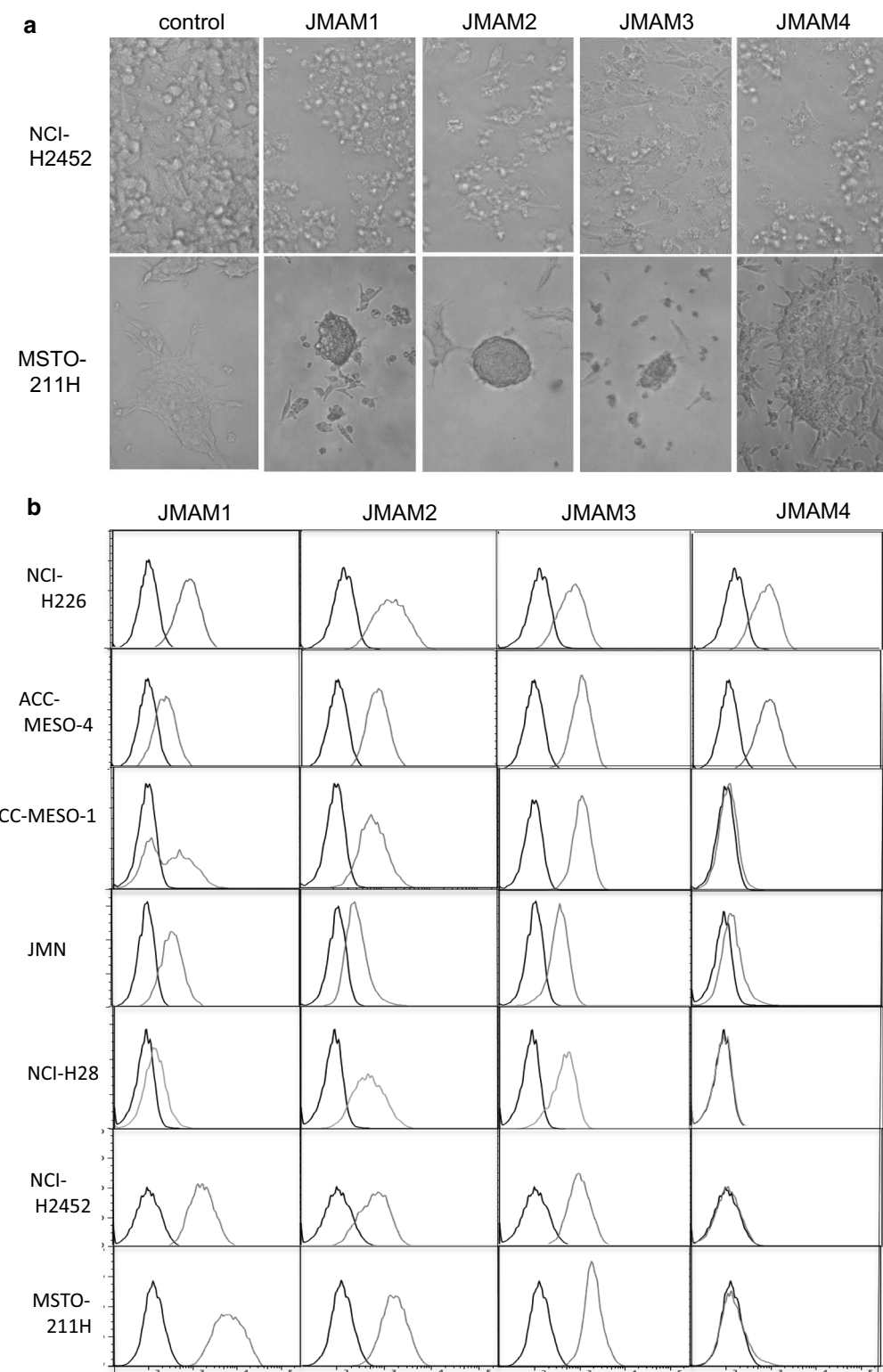


Fig. 1 Reactivity of JMAM mAbs with mesothelioma cell lines. **a** Morphological changes by JMAM mAbs. NCI-H2452 cells were incubated with hybridoma supernatants for 72 h and observed using visible light microscopy. RPMI-1640 medium with 10 % FCS served as the control (upper column). These findings were also reproduced using MSTO-211H cells (lower column). **b** Flow cytometry analysis of JMAM mAb reactivity. Mesothelioma cell lines were incubated with the hybridoma supernatant (green histogram) or control mouse IgG (black histogram), subsequently stained with Alexa Fluor®-488 labeled anti-mouse IgG Ab and analyzed using flow cytometry

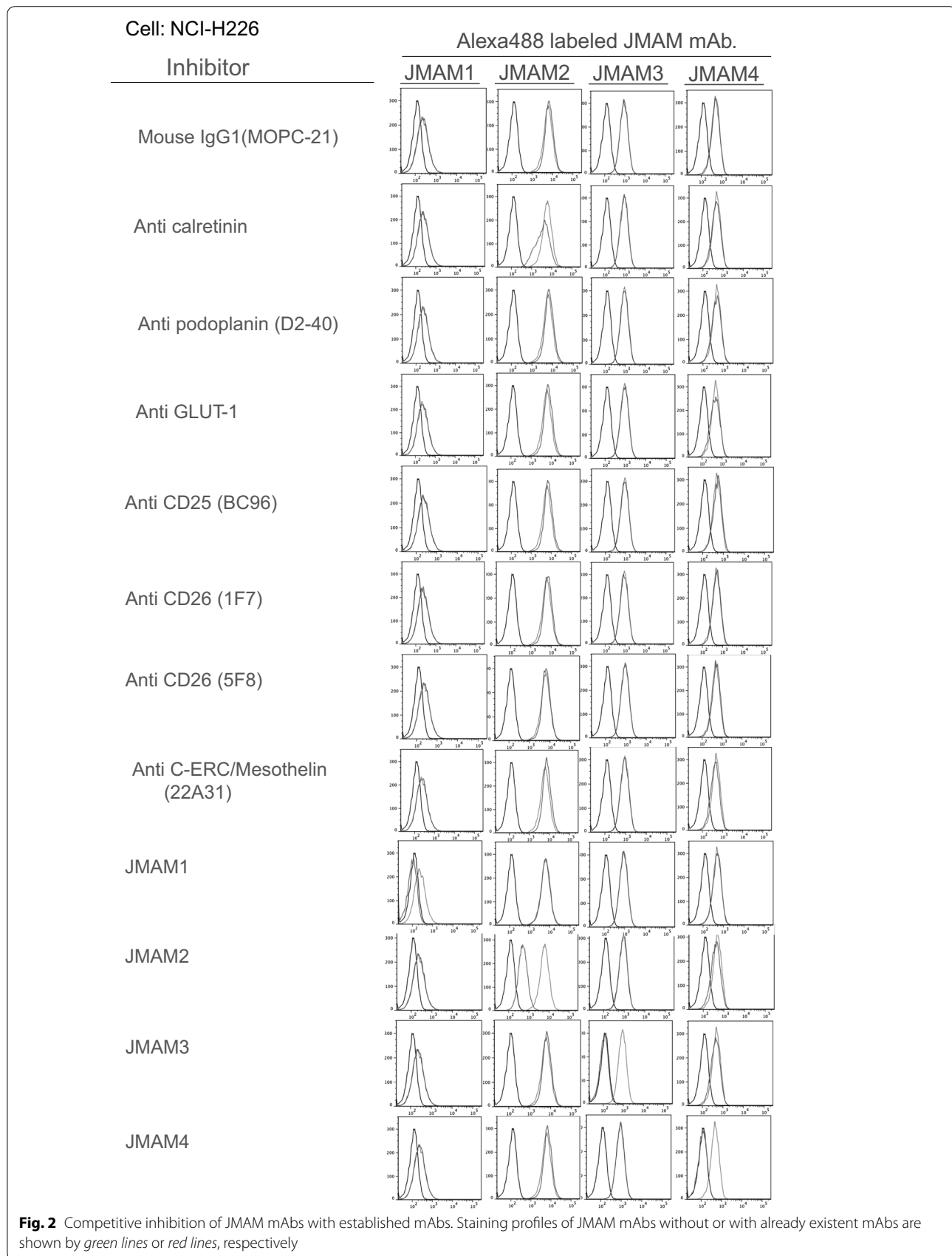


Fig. 2 Competitive inhibition of JMAM mAbs with established mAbs. Staining profiles of JMAM mAbs without or with already existent mAbs are shown by green lines or red lines, respectively

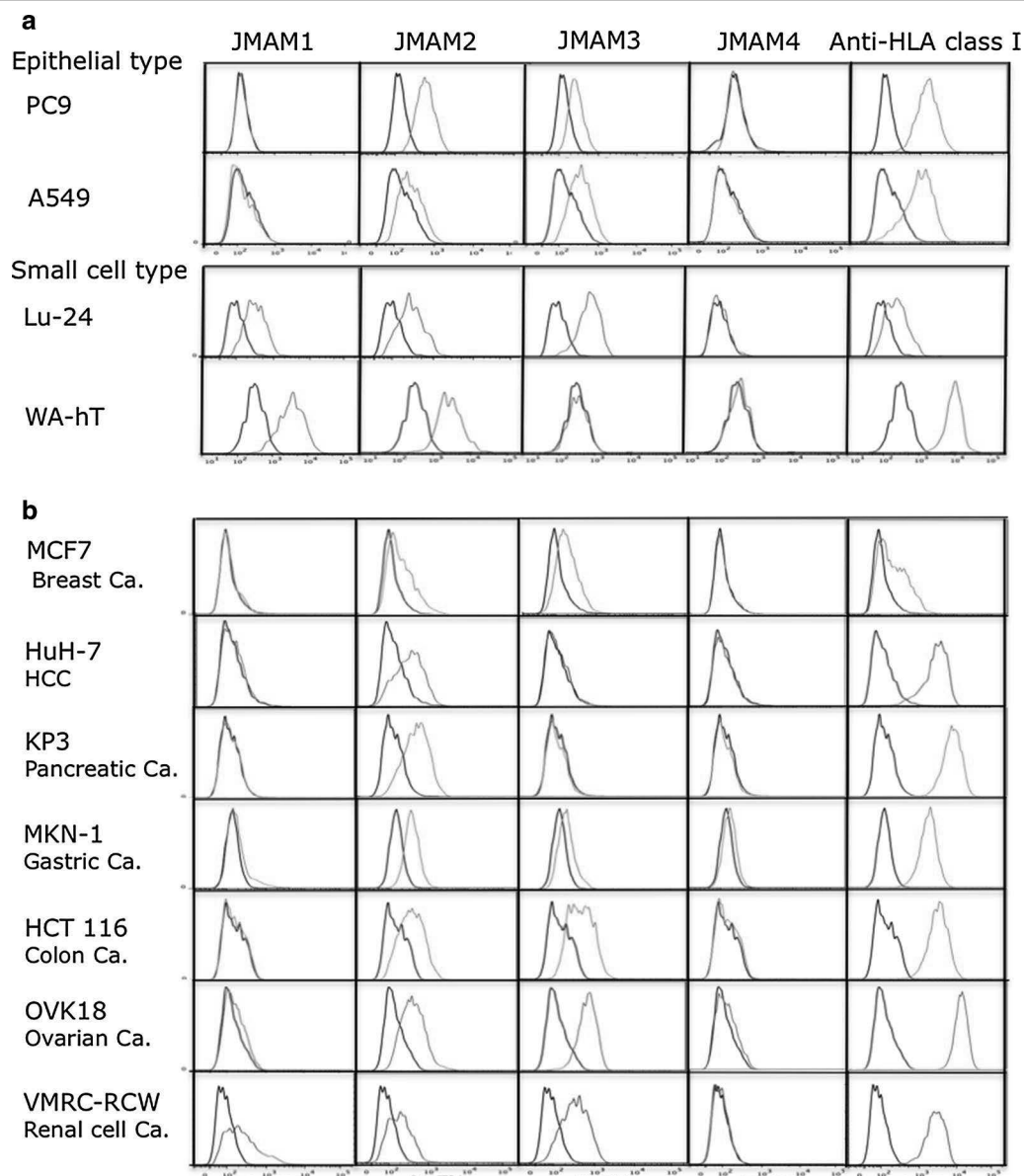


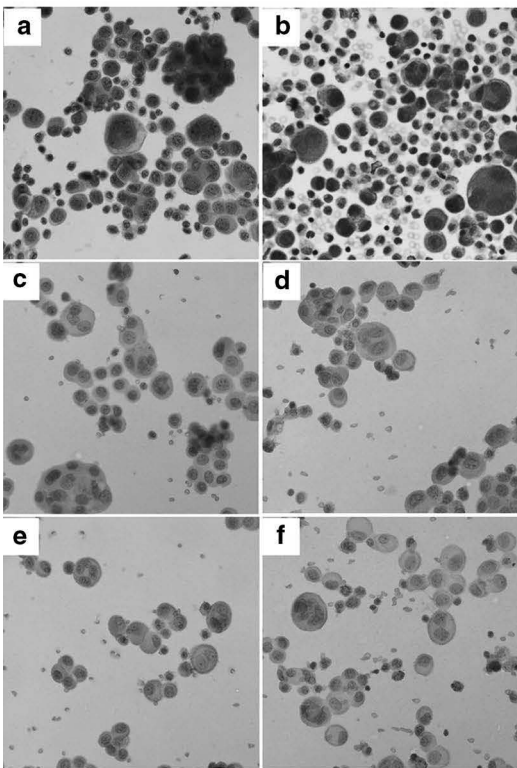
Fig. 3 Reactivity of JMAM mAbs with other cell lines. Epithelial-type and small-cell-type lung cancer (a) and other cancer cell lines (b) were incubated with hybridoma supernatants (green histogram) or control mouse IgG (black histogram), subsequently stained with Alexa Flour® 488-labeled anti-mouse IgG Ab and analyzed using flow cytometry

Analysis of mesotheliomas by mAbs

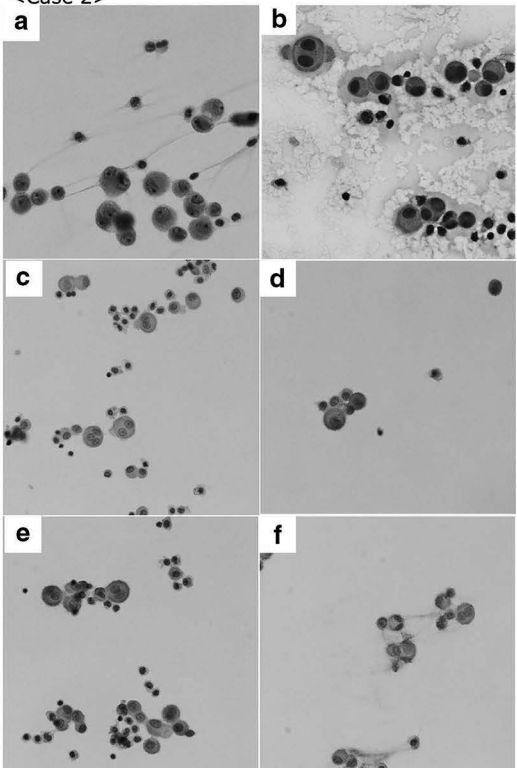
To determine whether these newly generated mAbs were suitable for immunohistochemical staining of formalin-fixed tissue sections, we used them to analyze surgically resected mesothelioma tissue specimens. Unfortunately, we did not detect staining of formalin-fixed paraffin-embedded tissue specimens (data not shown). The antigens recognized by the mAbs might have been masked or antigenically inactivated by formalin fixation.

Body fluid retention is one of the symptoms of many patients with malignant mesothelioma who are often diagnosed with mesothelioma by body fluid cytological examination. Therefore, we investigated whether the mAbs reacted with cytological samples using body fluid specimens that were fixed with ethanol. We analyzed specimens from three patients with malignant mesothelioma and those from patients suspected to have malignant mesothelioma (Fig. 4). All materials were prepared from pleural effusions.

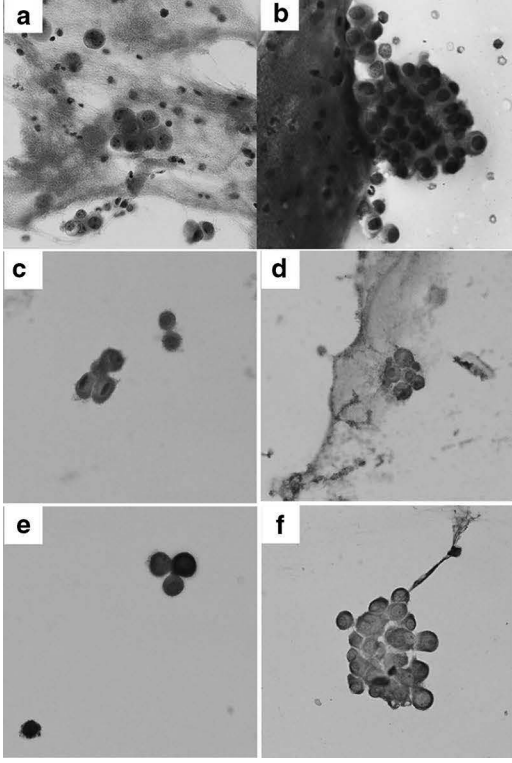
<Case 1>



<Case 2>



<Case 3>



(See figure on previous page.)

Fig. 4 Immunocytochemistry of clinical cases. **a** Papanicolaou; **b** Giemsa; **c** JMAM1; **d** JMAM2; **e** JMAM3; **f** JMAM4. Original magnification 400×. The malignant mesothelioma smear specimens, prepared from pleural effusions. Case 1 JMAM1, JMAM2, JMAM3, and JMAM4 mAbs stained membranes. JMAM2 mAb stained membranes and the cytoplasm. Case 2 All mAbs stained membranes. Case 3 JMAM1 and JMAM4 mAbs stained membranes; JMAM2 and JMAM3 mAbs stained membranes and cytoplasm

Case 1 Many cell clusters were present, including tight and loose clusters with flattened cellular borders. Individual cells showed wide variation in shape and size, ranging from small to very large. The JMAM1–4 mAbs stained membranes, whereas the JMAM2 mAb stained the cytoplasm and the membrane.

Case 2 The few malignant cells present were judged Class III by Papanicolaou classification. All mAbs stained membranes clearly.

Case 3 Present were small to large clusters with knobby borders and a single-cell population. These cells had low nuclear: cytoplasmic ratios, but occasionally showed macronucleoli. The staining of membranes by mAbs JMAM1–4 was distinct. Antibodies against Podoplanin, Mesothelin, EMA, and GLUT-1 stained cell-block specimens, which confirmed these atypical cells as derived from mesothelioma (Table 1). Because JMAM1–4 mAbs stained the membranes of all mesothelioma specimens

tested, they may be useful for the cytological testing of pleural effusions of patients with mesothelioma.

Histopathology and cytology of lung and mesothelial cells

Reactive normal pleura and lung immunoreactive features are shown in Fig. 5. Reactive pleural effusion mesothelial cells stained with JMAM mAbs (a); however, normal pleural mesothelium and lung tissue did not stain with JMAM mAbs (b, c).

Analysis of the effects of mAbs on the proliferation of mesothelioma cells

We next tested whether the mAbs inhibited the proliferation of the MSTO-211H mesothelioma cell line (Fig. 6). The JMAM1 and JMAM3 mAbs inhibited the proliferation of MSTO-211H cells as a function of their dose. Thus, proliferation was reduced by at least 50 and 40 % by 0.4 µg/ml of JMAM1 or JMAM3 mAbs, respectively.

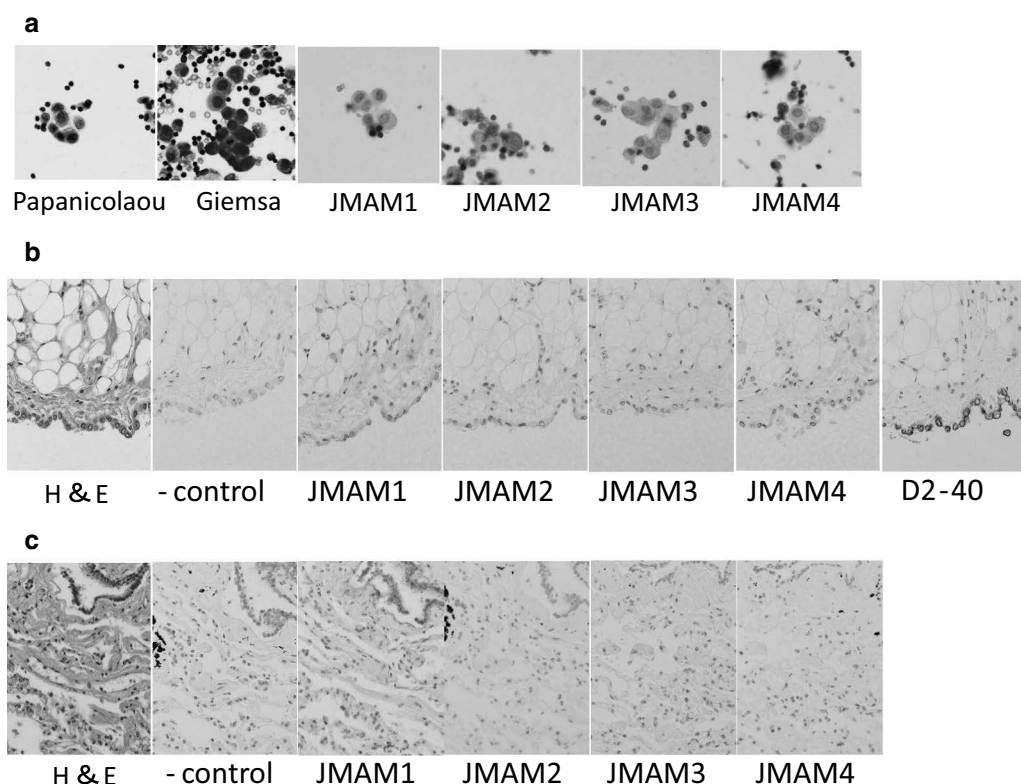
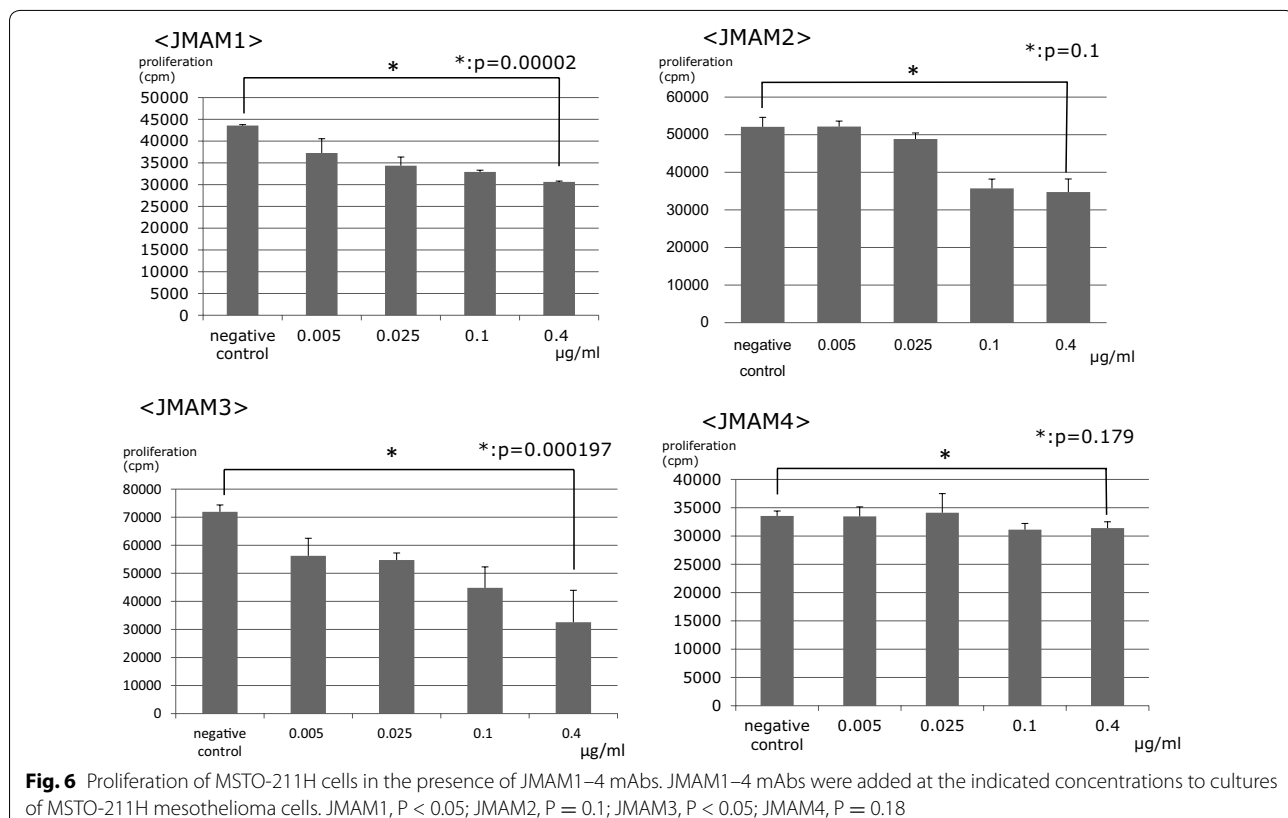


Fig. 5 Histopathology and cytological findings of reactive mesothelial cells, normal pleura and lung, with immunoreactive features. **a** Pleural effusion (reactive mesothelial cells, 1000×). **b** Normal pleura (400×). **c** Normal lung (400×)



The JMAM2 mAb inhibited cell proliferation to some extent. The JMAM4 mAb did not inhibit the proliferation of MSTO-211H cells. These results indicate that JMAM1 and JMAM2 mAbs may be useful for treating patients with mesothelioma, at least those with the epithelioid phenotype.

Analysis of the effect of JMAM mAbs on migration of mesothelioma cells

Cell motility is an essential process of tumor metastasis and progression. Therefore, we investigated whether the mAbs would affect the migration of mesothelioma cells using a wound-healing assay. The anti-mesothelioma mAbs JMAM1, JMAM2, and JMAM3 significantly inhibited the ability of NCI-H226 cells to migrate to and close an experimentally induced wound (Fig. 7). These results show that the anti-mesothelioma mAbs inhibited the motility of mesothelioma cells and suggest that the JMAM1–4 mAbs may possess a remarkable ability to inhibit the progression of mesotheliomas.

Analysis of the effect of JMAM mAbs on invasion of mesothelioma cells

We assessed the cell invasion ability of mesothelioma NCI-H226 cells. Significant inhibition of invasion was observed by JMAM mAbs compared with control mouse

IgG1 Ab (Fig. 8). JMAM1 mAb significantly decreased the trans membrane migration of NCI-H226 cells compared with cells treated with the mouse IgG1 isotype control.

Discussion

Differentiating between a mesothelioma and a papillary adenocarcinoma is sometimes very difficult [25]. Clinicians recommend that the definitive diagnosis of mesothelioma may be achieved using immunohistochemical analysis of cytological or histological specimens with currently available antibodies [8]. Many mAbs are developed for the diagnosis of and therapy for mesothelioma. Previously, we focused on CD26 as a novel therapeutic target for mesothelioma and have developed a humanized anti-CD26 mAb (clone: YS110), which is currently being evaluated in a phase I clinical trial for patients with malignant mesothelioma [26]. We also developed anti-human CD26 mAbs (clone: 1F7, 5F8) that clearly and reliably detect the denatured CD26 molecule in formalin-fixed paraffin-embedded tissue [27]. Although many antibodies are available to aid diagnosis, no single antibody can unambiguously distinguish mesotheliomas from other carcinomas. Anti-CD26 mAb reacts with epithelial and sarcomatoid mesotheliomas. However, anti-CD26 mAb also reacts with several other tumor cells and lymphocytes.

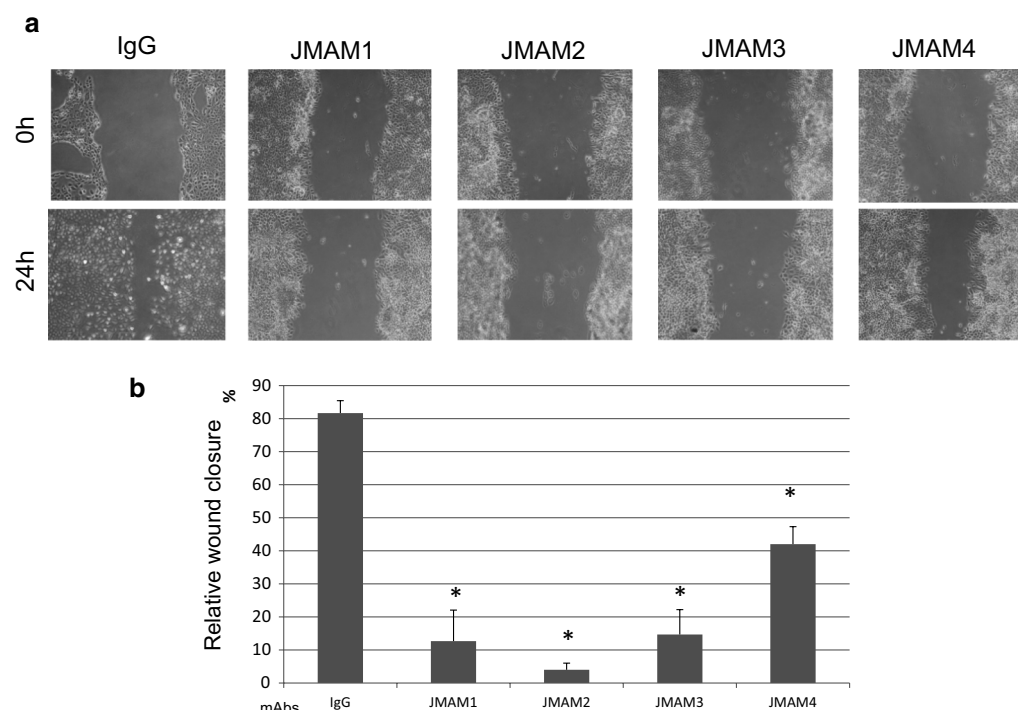


Fig. 7 Wound-healing assays. **a** Representative images of wound closure assays after NCI-H226 cells were incubated with anti-mesothelioma antibodies or control mouse IgG. **b** The extent of wound closure was calculated by analyzing the scratched area covered by the cells after 24 h using ImageJ software. The data were normalized to the control values. The data are represented as the mean \pm SD of three independent experiments. * $P < 0.05$; treated versus IgG control

Anti-mesothelin mAbs react with epithelial but not sarcomatoid mesotheliomas [13]. In contrast, JMAM1, JMAM2, and JMAM3 mAbs react with both subtypes. Anti-mesothelin mAbs react with renal cell carcinomas and pancreatic and ovarian cancers [28–30], unlike the JMAM4 mAbs that did not react with lung, ovarian, or renal cell carcinomas or any of the other cancer cell lines tested. JMAM1 mAb did not cross-react with other carcinoma cell lines except for small-cell-type lung cancer cell lines and renal cell carcinoma cell lines. Taken together, our newly generated mAbs are more specific for mesothelioma than other diagnostic mAbs and may be helpful in the differential diagnosis of mesothelioma. Novel anti-mesothelioma mAbs may either serve as tools to diagnose mesotheliomas as stand-alone reagents or together with other diagnostic mAbs.

It is now commonly accepted that therapeutic mAbs dramatically improve the treatment of cancer patients. However, after repeated therapy, not all patients respond to therapeutic mAbs [31] because clones appear during the course of treatment those do not express the target. Therefore, additional therapeutic options are required to treat these patients. Common therapeutic mAbs against cell surface molecules exert their effects largely through immunological mechanisms, including

complement-dependent cytotoxicity (CDC) and antibody-dependent cellular cytotoxicity (ADCC). ADCC and CDC may not be effective for treating patients with cancer because the patients may be immunocompromised due to radiation, chemotherapy, and the malignancy itself. However, in addition to indirectly inducing Fc-dependent cell death, several mAbs possess a direct antitumor effect that induces cell arrest or programmed cell death [32, 33].

Therefore, in this study, we investigated reactivity with mesothelioma cells as well as the direct antitumor effect of the newly generated anti-mesothelioma mAbs. We found that JMAM1 and JMAM3 mAbs inhibited the proliferation of the MSTO-211H mesothelial cell line, and JMAM1–4 mAbs inhibited wound closure by NCI-H226 cells to varying degrees. JMAM1–4 also inhibited invasion of NCI-H226 cells to various degrees. Unfortunately, we did not identify the target molecules of JMAM1–4 mAbs. Nevertheless, the promising anti-mesothelioma activities of these antibodies warrant continued studies in vitro and in vivo that will include efforts to identify their targets. Our strategy for generating diagnostic and therapeutic mAbs specific for tumor cells differs from those of conventional methods that employ immunization with peptides or DNA. Specifically, we

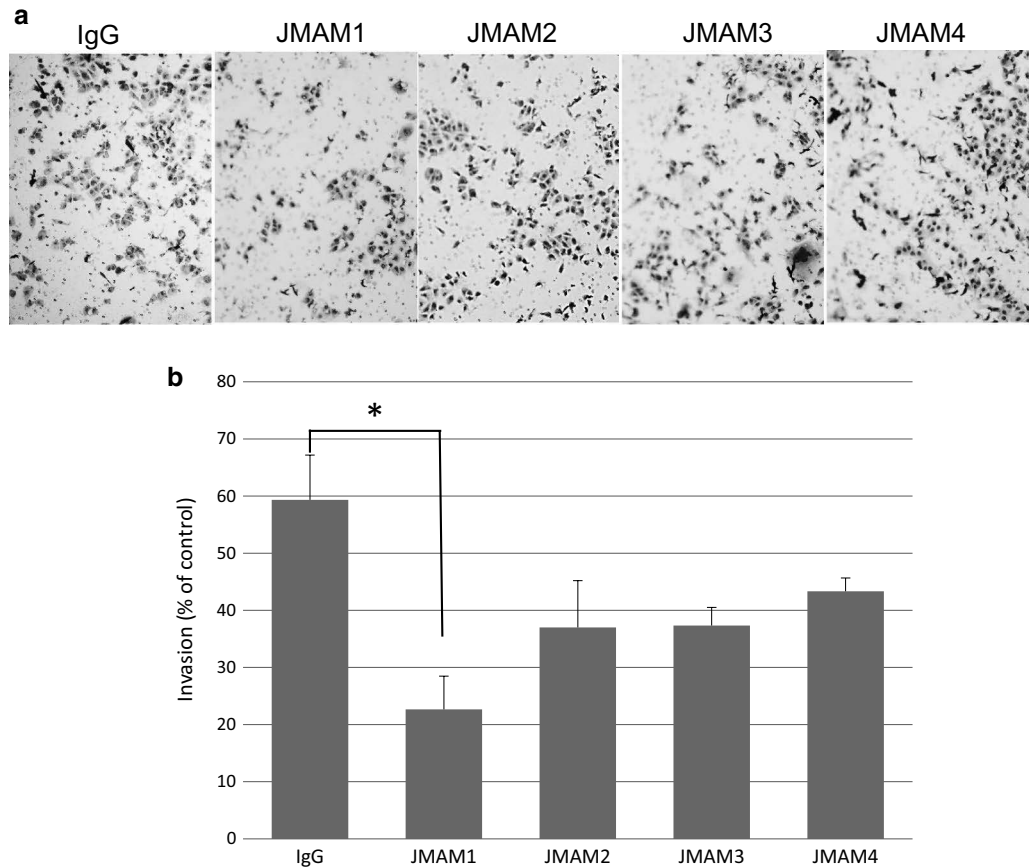


Fig. 8 Analysis of the effect of JMAM mAbs on invasion of mesothelioma cells. Cells (NCI-H226) were seeded into the *upper chamber* and the *lower chamber* was filled with medium as described in the “Methods” section. Photos were captured by a light microscope at $\times 200$ (a). The migration of cells was measured by counting the migrating cells on the lower surface of the membrane in 3 fields (b). JMAM1, *P < 0.05; JMAM2, P = 0.12; JMAM3, P = 0.08; JMAM4, P = 0.18. Each mAb treated versus IgG control

immunized a mouse with three different mesothelioma cell lines and screened the antibodies using a different mesothelioma cell line to potentially obtain novel mAbs that react with unknown targets on the surface of mesothelioma cells.

Conclusion

Newly established anti-mesothelioma mAbs, JMAM1–4, are potentially useful as diagnostic and therapeutic agents for mesothelioma. Moreover, our novel strategy for establishing anti-tumor mAbs may facilitate the development of new diagnostic and therapeutic techniques for other malignancies as well as mesothelioma.

Authors' contributions

NM, SM, RO and MA designed and performed experiments and wrote the paper. MW, KK and NO performed experiments. CM and OH supervised part of the experiments. All authors read and approved the final manuscript.

Author details

¹ Department of Pathology, Kyorin University School of Medicine, 6-20-2, Shinkawa, Mitaka-shi, Tokyo 181-8611, Japan. ² Departments of Pathology

and Oncology, Juntendo University School of Medicine, 2-1-1, Hongo, Bunkyo-ku, Tokyo 113-8421, Japan. ³ Department of Pathology, Tokyo Medical University Hachioji Medical Center, 1163 Tatemachi, Hachioji-shi, Tokyo 193-0998, Japan. ⁴ Therapy Development and Innovation for Immune Disorders and Cancers, Juntendo University School of Medicine, 2-1-1, Hongo, Bunkyo-ku, Tokyo 113-8421, Japan.

Acknowledgements

We thank Dr. T Kamei for constructive discussions, the staff of the Animal Care Committee for animal care, and the staff of the Pathology Department for their assistance in collecting body fluid samples and for consultations.

Competing interests

The authors declare that they have no competing interests.

Ethics

This study has been performed according to the principles of Helsinki and was approved by the Ethics Committee at Juntendo University School of Medicine.

Funding

S. Matsuoka received a Grant from the Japan Society for the Promotion of Science (Web: <https://kaken.nii.ac.jp/d/p/15K06880.en.html>, Grant Number: 15K06880).

The funders had no role in the study design, data collection and analysis, decision to publish, or preparation of the manuscript.

Received: 20 August 2015 Accepted: 16 June 2016

Published online: 24 June 2016

References

1. Kazan-Allen L. Asbestos and mesothelioma: worldwide trends. *Lung Cancer*. 2005;49(Suppl 1):S3–8.
2. Robinson BW, Musk AW, Lake RA. Malignant mesothelioma. *Lancet*. 2005;35:397–408.
3. Carbone M, Ly BH, Dodson RF, Pagano I, Morris PT, Dogan UA, Gazdar AF, Pass HI, Yang H. Malignant mesothelioma: facts, myths and hypotheses. *J Cell Physiol*. 2012;227:44–58.
4. US Department of the Interior, US Geological Survey. Mineral commodity summaries 2015. 2015. p. 22–23.
5. Nguyen G, Akin MM, Villanueva RR, Slatnik J. Cytopathology of malignant mesothelioma of the pleura in fine-needle aspiration biopsy. *Diagn Cytopathol*. 1999;21:253–9.
6. Whitaker D. The cytology of malignant mesothelioma. *Cytopathology*. 2000;11:139–51.
7. Fassina A, Fedeli U, Corradin M, Da FM, Fabbri L. Accuracy and reproducibility of pleural effusion cytology. *Leg Med*. 2008;10:20–5.
8. Pu RT, Pang Y, Michael CW. Utility of WT-1, p63, MOC31, mesothelin, and cytokeratin (CK903 and CK5/6) immunostains in differentiating adenocarcinoma, squamous cell carcinoma, and malignant mesothelioma in effusions. *Diagn Cytopathol*. 2008;36:20–5.
9. Chung A, Inai K, Samet J. Tumor of the pleura. In: Travis WD, Muller BE, Hermelink HK, Harris CG, editors. *Pathology and genetics. Tumours of the lung, pleura, thymus and heart*. Lyon: IARC Press; 2004. p. 128–42.
10. Robinson BW, Lake RA. Advances in malignant mesothelioma. *N Engl J Med*. 2005;353:1591–603.
11. Inai K. Pathology of mesothelioma. *Environ Health Prev Med*. 2008;13:60–4.
12. Ordóñez NG. Immunohistochemical diagnosis of epithelioid mesotheliomas: a critical review of old markers, new markers. *Hum Pathol*. 2002;33:953–67.
13. Ordóñez NG. Value of mesothelin immunostaining in the diagnosis of mesothelioma. *Mod Pathol*. 2003;16:192–7.
14. Betta P, Magnani C, Bensi T, Trincheri FN, Orecchia S. Immunohistochemistry and molecular diagnostics of pleural malignant mesothelioma. *Arch Pathol Lab Med*. 2012;136:253–61.
15. Takeshima Y, Inai K, Amatha V, Gembra K, Aoe K, Fujimoto N, Kato K, Kishimoto T. Accuracy of pathological diagnosis of mesothelioma cases in Japan: clinicopathological analysis of 382 cases. *Lung Cancer*. 2009;66:191–7.
16. Kao CS, Vardy J, Chatfield M, Corte P, Pavlakis N, Clarke C, Zandwijk NV, Clarke S. Validation of prognostic factors in malignant pleural mesothelioma. *Clin Lung Cancer*. 2013;14:70–7.
17. Inamoto T, Yamada T, Ohnuma K, Kina S, Takahashi N, Yamochi T, Inamoto S, Katsuoka Y, Hosono O, Tanaka H, Dang NH, Morimoto C. Humanized Anti-CD26 monoclonal antibody as a treatment for malignant mesothelioma tumors. *Clin Cancer Res*. 2007;13:4191–200.
18. Yamada K, Hayashi M, Du W, Ohnuma K, Sakamoto M, Morimoto C. Yamada T. *cc. Cancer Cell International*. 2009;9:17.
19. Köhler G, Milstein C. Continuous cultures of fused cells secreting antibody of predefined specificity. *Nature*. 1975;256:495–7.
20. Koprowski H, Steplewski Z, Mitchell K, Herlyn M, Herlyn D, Fuhrer P. Colorectal carcinoma antigens detected by hybridoma antibodies. *Somatic Cell Genet*. 1979;5:957–72.
21. Bast CR, Feeney M, Lazarus H, Nadler LM, Colvin BR, Knapp CR. Reactivity of a monoclonal antibody with human ovarian carcinoma. *J Clin Invest*. 1981;68:1331–7.
22. Maloney DG, Grillo-López AJ, White CA, Bodkin D, Schilder RJ, Neidhart JA, Janakiraman N, Foon KA, Liles TM, Dallaire BK, Wey K, Royston I, Davis T, Levy R. IDEC-C2B8 (Rituximab) anti-CD20 monoclonal antibody therapy in patients with relapsed low-grade non-Hodgkin's lymphoma. *Blood*. 1997;90(6):2188–95.
23. Ishikawa K, Segawa T, Hagiwara Y, Maeda M, Abe M, Hino O. Establishment of novel monoclonal antibody to human ERC/mesothelin useful for study and diagnosis of ERC/mesothelin-expressing cancers. *Pathol Int*. 2009;59:161–6.
24. Lewis GD, Figari I, Fendly B, Wong WL, Carter P, Gorman C, Shepard HM. Differential responses of human tumor cell lines to anti-p185/HER2 monoclonal antibodies. *Cancer Immunol Immunother*. 1993;37:255–63.
25. Kwee WS, Veldhuizen RW, Alons CA, Morawetz F, Boon ME. Quantitative and qualitative differences between benign and malignant mesothelial cells in pleural fluid. *Acta Cytol*. 1982;26:401–6.
26. Aoe K, Amatya VJ, Fujimoto N, Ohnuma K, Hosono O, Hiraki A, Fujii M, Yamada T, Dang NH, Takeshima Y, Inai K, Kishimoto T, Morimoto C. CD26 overexpression is associated with prolonged survival and enhanced chemosensitivity in malignant pleural mesothelioma. *Clin Cancer Res*. 2012;18:1447–56.
27. Hatano R, Yamada T, Matsuoka S, Iwata S, Yamazaki H, Komiya E, Okamoto T, Dang NM, Ohnuma K, Morimoto C. Establishment of monoclonal anti-human CD26 antibodies suitable for immunostaining of formalin-fixed tissue. *Diagn Pathol*. 2014. doi:10.1186/1746-1596-9-30.
28. Robinson BW, Creaney J, Lake R, Nowark A, Musk AW, de Klerk N, Winzell P, Hellstrom KE, Hellstrom I. Mesothelin-family proteins and diagnosis of mesothelioma. *Lancet*. 2003;362:1612–6.
29. Hellstrom I, Raycraft J, Kanan S, Sardesai NY, Verch T, Yang Y, Hellstrom KH. Mesothelin variant 1 is released from tumor cells as a diagnostic marker. *Cancer Epidemiol Biomark Prev*. 2006;15:1014–20.
30. Scholler N, Fu N, Yang Y, Ye Z, Goodman GE, Hellstrom KE, Hellstrom I. Soluble member(s) of the mesothelin/megakaryocyte potentiating factor family are detectable in sera from patients with ovarian carcinoma. *Proc Natl Acad Sci USA*. 1999;6:11531–6.
31. O'Brien SM, Kantarjian H, Thomas DA, Giles FJ, Freireich EJ, Cortes J, Lemer S, Keating MJ. Rituximab dose-escalation trial in chronic lymphocytic leukemia. *J Clin Oncol*. 2001;19:2165–70.
32. Matsuoka S, Asano Y, Sano K, Kishimoto H, Yamashita I, Yorifuji H, Utsuyama M, Hirokawa K, Tada T. A novel type of cell death of lymphocytes induced by a monoclonal antibody without participation of lymphocytes. *J Exp Med*. 1995;181:2007–15.
33. Yuniel FM, Alejandro LR. Lonely killers. *mAbs*. 2008;3:528–34.

Submit your next manuscript to BioMed Central and we will help you at every step:

- We accept pre-submission inquiries
- Our selector tool helps you to find the most relevant journal
- We provide round the clock customer support
- Convenient online submission
- Thorough peer review
- Inclusion in PubMed and all major indexing services
- Maximum visibility for your research

Submit your manuscript at
www.biomedcentral.com/submit





Contents lists available at ScienceDirect

Data in Brief

journal homepage: www.elsevier.com/locate/dib

Data Article

Data on CUX1 isoforms in idiopathic pulmonary fibrosis lung and systemic sclerosis skin tissue sections



Tetsurou Ikeda^{a,b,c,*1}, Maria Fragiadaki^b, Xu Shi-wen^a,
 Markella Ponticos^a, Korsa Khan^a, Christopher Denton^a,
 Patricia Garcia^a, George Bou-Gharios^b, Akio Yamakawa^c,
 Chikao Morimoto^c, David Abraham^a

^a Royal Free and University College Medical School, London, UK

^b Imperial College School of Medicine, London, UK

^c University of Tokyo, Institute of Medical Science, Tokyo, Japan

ARTICLE INFO

Article history:

Received 5 July 2016

Received in revised form

4 August 2016

Accepted 8 August 2016

Available online 10 August 2016

ABSTRACT

This data article contains complementary figures related to the research article entitled, "Transforming growth factor- β -induced CUX1 isoforms are associated with fibrosis in systemic sclerosis lung fibroblasts" (Ikeda et al. (2016) [2], <http://dx.doi.org/10.1016/j.bbrep.2016.06.022>), which presents that TGF- β increased CUX1 binding in the proximal promoter and enhancer of the *COL1A2* and regulated *COL1*. Further, in the scleroderma (SSc) lung and diffuse alveolar damage lung sections, CUX1 localized within the α -smooth muscle actin (α -SMA) positive cells (Fragiadaki et al., 2011) [1], "High doses of TGF-beta potently suppress type I collagen via the transcription factor CUX1" (Ikeda et al., 2016) [2]. Here we show that CUX1 isoforms are localized within α -smooth muscle actin-positive cells in SSc skin and idiopathic pulmonary fibrosis (IPF) lung tissue sections. In particular, at the granular and prickle cell layers in the SSc skin sections, CUX1 and α -SMA are co-localized. In addition, at the fibrotic loci in the IPF lung tissue sections, CUX1 localized within the α -smooth muscle actin (α -SMA) positive cells.

DOI of original article: <http://dx.doi.org/10.1016/j.bbrep.2016.06.022>

* Corresponding author at: University of Tokyo, Institute of Medical Science, Tokyo, Japan.

E-mail address: ikedatetsurou@kochi-u.ac.jp (T. Ikeda).

¹ Present address: Kochi Medical School, Kochi, Japan.

<http://dx.doi.org/10.1016/j.dib.2016.08.014>

2352-3409/© 2016 The Authors. Published by Elsevier Inc. This is an open access article under the CC BY license (<http://creativecommons.org/licenses/by/4.0/>).

Specifications Table

Subject area	<i>Biology</i>
More specific subject area	<i>Fibrosis</i>
Type of data	<i>Image</i>
How data was acquired	<i>Confocal microscopy (Zeiss Axioscope light microscope, Carl Zeiss)</i>
Data format	<i>Analysed</i>
Experimental factors	For immunohistochemistry, sections were pretreated with methanol, followed by antigen retrieval in heated 10-mM citrate buffer (pH 6).
Experimental features	The primary antibodies were CUX1 antibody (0.2 mg/ml) and the monoclonal anti- α -SMA clone, 1a Cy3-conjugated antibody (0.7 mg/ml). Sections were sequentially incubated with a 1/200 dilution of an Alexa 488 secondary antibody.
Data source location	<i>London, United Kingdom</i>
Data accessibility	<i>Data presented in this article</i>

Value of the data

- The data provides the evidence that CUX1 isoforms localise within α -smooth muscle actin-positive cells in SSc skin tissue sections, especially in the granular and prickle cell layers.
 - The data provides the evidence that CUX1 isoforms localise within α -smooth muscle actin-positive cells at the fibrotic loci in idiopathic pulmonary fibrosis (IPF) lung tissue sections.
 - The data could further help research on the function of CUX1 isoforms in fibrosis-related diseases.
-

1. Data

Immunohistochemistry revealed the presence of α -SMA-positive fibrotic loci, which are characteristic in the lungs of patients with IPF and in the skin of patients with SSc. In the IPF tissue sections, CUX1 localised at alveolar cells and fibrotic loci. In addition, CUX1 localised within α -SMA-positive cells but was not observed in the normal lung section (Fig. 1). In the SSc skin tissue sections, CUX1 co-localised with α -SMA at the granular cell layer, prickle cell layer and fibrotic loci in the epidermis. In addition, CUX1 localised within α -SMA-positive cells. These were not observed at the epidermis in the normal skin sections (Fig. 2).

2. Experimental design, materials and methods

For formalin-fixed, paraffin-embedded specimens, the tissues were fixed and hydrated as described previously [1,2]. For immunohistochemistry, the sections were pretreated with methanol (VWR, Lutterworth, UK), followed by antigen retrieval in heated 10-mM citrate buffer (pH 6). The primary antibodies were CUX1 antibody (0.2 mg/ml) and the monoclonal anti- α -SMA clone, 1a Cy3-conjugated antibody (0.7 mg/ml). The sections were sequentially incubated with a 1/200 dilution of

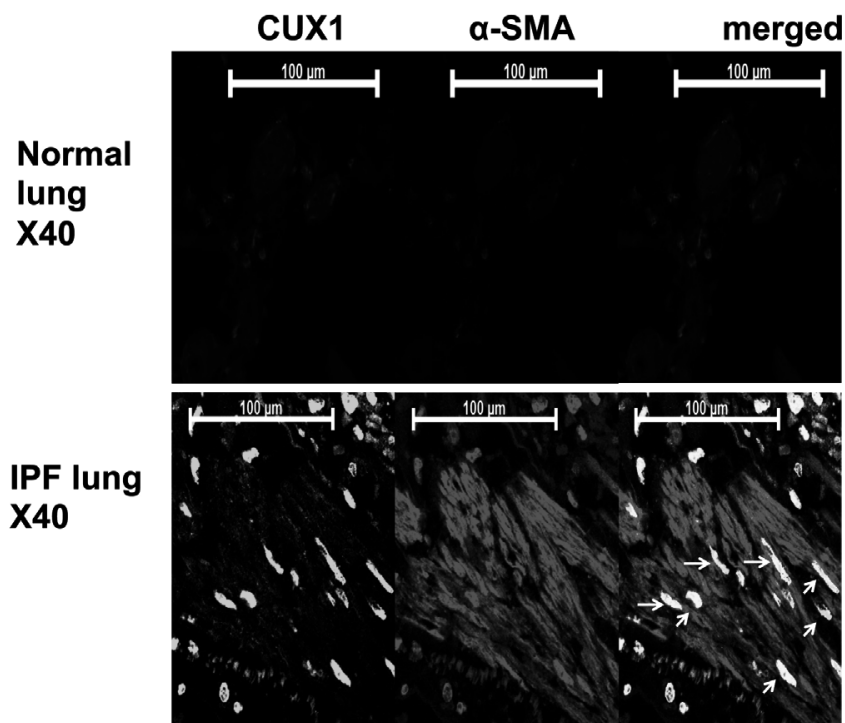


Fig. 1. Idiopathic pulmonary fibrosis (IPF) lung tissue sections stained with antibodies against CUX1 and α -smooth muscle actin (SMA). The figure shows fibrotic loci that were stained by CUX1 and α -SMA antibodies. Alveolar cells around the loci were positive for CUX1 and α -SMA. CUX1 localised within α -SMA-positive cells. Normal lung sections were used as negative control for CUX1 and α -SMA.

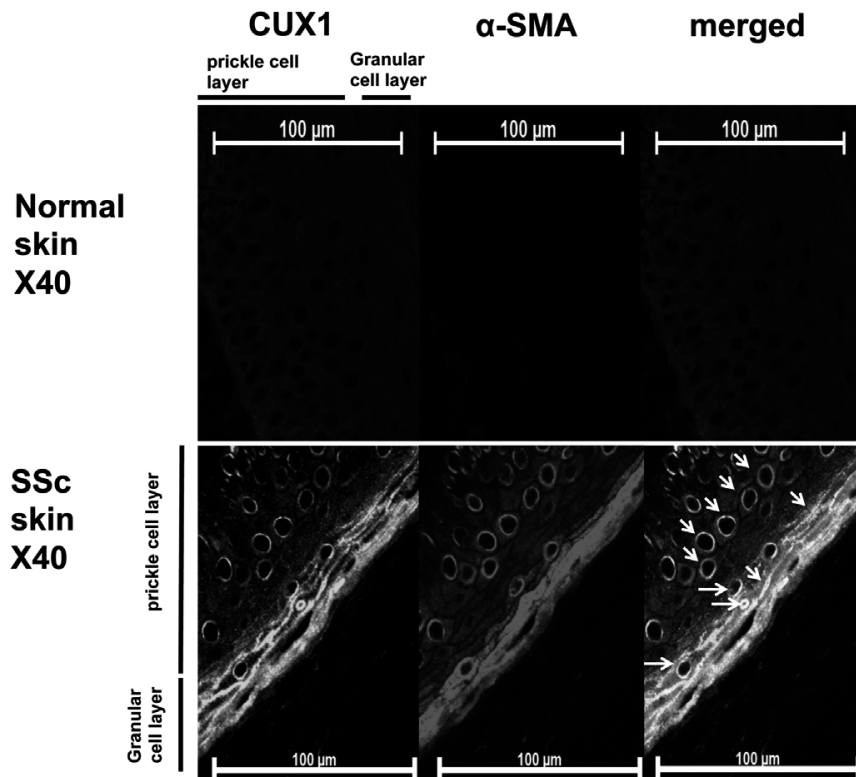


Fig. 2. Systemic sclerosis (SSc) skin tissue sections stained with antibodies against CUX1 and α -smooth muscle actin (SMA). The figure shows epidermis that were stained by CUX1 and α -SMA antibodies. The granular and prickle cells in the epidermis were positive for CUX1 and α -SMA. CUX1 localised within α -SMA-positive cells. Normal skin sections were used as negative control for CUX1 and α -SMA.

an Alexa 488 secondary antibody. The slides were viewed and photographed using a Zeiss Axioscope light microscope with Axiovision software.

Acknowledgments

This work was partly supported by a Grant from the Japanese Society for the Promotion of Science (Grant no. 17109011). Furthermore, this work was supported by the Global COE Program 'Center of Education and Research for the Advanced Genome-Based Medicine-For personalized medicine and the control of worldwide infectious disease,' MEXT Japan. The authors would like to thank Enago for the English language review.

Transparency document. Supplementary material

Transparency data associated with this article can be found in the online version at <http://dx.doi.org/10.1016/j.dib.2016.08.014>.

References

- [1] M. Fragiadaki, T. Ikeda, A. Witherden, R.M. Mason, D. Abraham, G. Bou-Gharios, High doses of TGF-beta potently suppress type I collagen via the transcription factor CUX1, *Mol. Biol. Cell* 22 (2011) 1836–1844.
- [2] T. Ikeda, M. Fragiadaki, X. Shi-wen, M. Ponticos, K. Khan, C. Denton, P. Garcia, G. Bou-Gharios, A. Yamakawa, C. Morimoto, D. Abraham, Transforming growth factor- β -induced CUX1 isoforms are associated with fibrosis in systemic sclerosis lung fibroblasts, *Biochem. Biophys. Rep.* 7 (2016) 246–252.



Transforming growth factor- β -induced CUX1 isoforms are associated with fibrosis in systemic sclerosis lung fibroblasts



Tetsurou Ikeda ^{a,b,c,1,*}, Maria Fragiadaki ^b, Xu Shi-wen ^a, Markella Ponticos ^a, Korsa Khan ^a, Christopher Denton ^a, Patricia Garcia ^a, George Bou-Gharios ^b, Akio Yamakawa ^c, Chikao Morimoto ^c, David Abraham ^a

^a Royal Free and University College Medical School, London, UK

^b Imperial College School of Medicine, London, UK

^c University of Tokyo, Institute of Medical Science, Tokyo, Japan

ARTICLE INFO

Article history:

Received 8 April 2016

Received in revised form

23 June 2016

Accepted 24 June 2016

Available online 2 July 2016

Keywords:

Transforming growth factor- β

CUX1 isoforms

Fibrosis

Cathepsin L inhibitor

ABSTRACT

In the enhancer region of the human type I collagen alpha 2 (*COL1A2*) gene, we identified cis-elements for the transcription factor CUX1. However, the role of CUX1 in fibrosis remains unclear. Here we investigated the role of CUX1 in the regulation of COL1 expression and delineated the mechanisms underlying the regulation of *COL1A2* expression by CUX1 in systemic sclerosis (SSc) lung fibroblasts. The binding of CUX1 to the *COL1A2* enhancer region was assessed using electrophoretic mobility shift assays after treatment with transforming growth factor (TGF)- β . Subsequently, the protein expression levels of CUX1 isoforms were determined using Western blotting. Finally, the expression levels of COL1 and fibrosis-related cytokines, including CTGF, ET-1, Wnt1 and β -catenin were determined. The binding of CUX1 isoforms to the *COL1A2* enhancer region increased after TGF- β treatment. TGF- β also increased the protein levels of the CUX1 isoforms p200, p150, p110, p75, p30 and p28. Moreover, SSc lung fibroblasts showed higher levels of CUX1 isoforms than normal lung fibroblasts, and treatment of SSc lung fibroblasts with a cathepsin L inhibitor (IW-CHO) decreased COL1 protein expression and reduced cell size, as measured using immunocytochemistry. In SSc and diffuse alveolar damage lung tissue sections, CUX1 localised within α -smooth muscle actin-positive cells. Our results suggested that CUX1 isoforms play vital roles in connective tissue deposition during wound repair and fibrosis.

© 2016 The Authors. Published by Elsevier B.V. This is an open access article under the CC BY-NC-ND license (<http://creativecommons.org/licenses/by-nc-nd/4.0/>).

1. Introduction

Scleroderma, or systemic sclerosis (SSc), is a connective tissue disease characterised by excessive type I collagen (COL1) deposition in many organs including the lungs, kidneys and skin [1]. Approximately 40% patients with diffuse SSc experience pulmonary fibrosis, a major cause of mortality [1]. Although the aetiology of this disease is poorly understood, tissue scarring occurs after injury following the release of several mediators including TGF- β , PDGF, CTGF, Wnt1 and ET-1 [2–6]. These factors stimulate fibroblasts to differentiate into myofibroblasts, which are characterised

by the expression of α -SMA and excessive production of extracellular matrix molecules such as COL1 [7,8]. Overexpression of these cytokines results in chronic fibroblast stimulation (fibrosis). Moreover, genetically modified mice with altered TGF- β signalling have been reported to exhibit fibrogenic pathology similar to that observed in patients with SSc, indicating a key role of this cytokine in the pathogenesis of fibrosis [9–11]. Elucidation of pivotal mediators or key signalling pathways that are overactive in fibrosis is crucial for designing better therapeutic strategies for SSc and related disorders.

TGF- β is a potent pro-fibrotic cytokine that promotes myofibroblast differentiation, migration, extracellular matrix synthesis and apoptosis resistance [12–14]. TGF- β induces the expression of the gene encoding human collagen type I alpha 2 (*COL1A2*) via a Smad-dependent pathway that acts on a TGF- β responsive element (TbRE) in the human *COL1A2* proximal promoter [15,16]. COL1 expression *in vivo* is exclusively controlled by an enhancer sequence that contains several DNase I hypersensitive sites (HSSs). These encompass pivotal regulatory sites conferring tissue-, temporal-, cell- and growth factor-specific expression of COL1 [15,16].

Abbreviations: TGF- β , transforming growth factor- β ; CTGF, connective tissue growth factor; ET-1, endothelin-1; Wnt1, wingless-type MMTV integration site family member 1; PDGF, platelet-derived growth factor; α -SMA, α -smooth muscle actin

* Correspondence to: Clinical Immunology, Institute of Medical Science, University of Tokyo, Tokyo, 4-6-1, Shirokanedai, Minato-ku, Japan.

E-mail address: ikedatetsurou@kochi-u.ac.jp (T. Ikeda).

¹ Present, Kochi Medical School, Kochi, Japan.

The results of our recent study illustrated that TGF- β activates *COL1A2* via a non-canonical Smad-independent pathway, which requires enhancer/promoter cooperation. Moreover, we identified a novel TbRE in the human *COL1A2* enhancer region and found that it is necessary for *COL1A2* activation [16]. Further, we reported that high doses of TGF- β increased CUX1 binding in the proximal promoter and suppressed COL1 expression [17].

In this study, we identified CUX1 binding sites near this TbRE of the *COL1A2* enhancer region using *in silico* analyses. These sites exist at identity island 4 (IS4) near HS4 in the enhancer region [18]. In addition, this study demonstrated that CUX1 responds to TGF- β stimulation and is a potential activator of COL1. Based on these findings, we characterised the role of human CUX1 in the regulation of COL1 expression and subsequent release of pro-fibrotic cytokines. We demonstrated that some isoforms of human CUX1 are strongly induced after TGF- β stimulation, which results in the up-regulation of CTGF, Wnt1, ET-1, β -catenin and COL1 *in vitro*. In addition, we investigated the expression pattern of human CUX1 isoforms in lung fibroblasts derived from normal cells and patients with SSc. In lung fibroblasts derived from patients with SSc, protein levels of the CUX1 isoforms p200, p150, p110, p75, p30 and p28 were increased compared with those in normal cells. Using electrophoretic mobility shift assays (EMSA) with nuclear extracts from these cells, we demonstrated that CUX1 binding to the *COL1A2* enhancer region was increased. Cleavage sites for cathepsin L have been found between CR1 and CR2 and those for caspases have been identified between CR3 and HR of CUX1 [19]. Therefore, we confirmed whether cathepsin L inhibitor (IW-CHO) can regulate COL1. IW-CHO inhibited COL1 in both normal and SSc lung fibroblasts. Taken together, our data strongly suggest that CUX1 isoforms up-regulate COL1 and regulate key pro-fibrotic activities of TGF- β . Our results could provide novel insights into CUX1-mediated regulation of *COL1A2* in human lung fibroblasts. These results are an important contribution to the understanding of processes involved in SSc-associated fibrosis.

2. Materials and methods

2.1. Cell culture

Cells were maintained in DMEM supplemented with 10% FBS, 100 U/ml penicillin and 100 mg/ml streptomycin and cultured in a humidified atmosphere of 5% CO₂. We isolated lung fibroblasts from patients with SSc as previously described [20]. The cells were cultured under standard conditions in DMEM containing 10% FBS. Pulmonary fibroblasts were obtained from patients who fulfilled the criteria of the American College of Rheumatology for the diagnosis of SSc with lung involvement. Informed consent and ethical approval were obtained. None of the patients was receiving immunosuppressive medication or corticosteroids at the time of biopsy.

2.2. Western blotting

Nuclear extracts and cytosolic fractions were prepared as previously described [16]. The cells were washed with phosphate-buffered saline (PBS) and treated with Laemmli sample buffer. To analyse collagen, the medium was removed and adjusted to 20% (v/v) ammonium sulphate, followed by incubation at 4 °C overnight. The samples were centrifuged, and the pellet was re-suspended in Laemmli sample buffer with β -mercaptoethanol for SDS-PAGE, followed by Western blotting. The following antibodies were used: lamin A/C (sc20681, Santa Cruz), COL1 (rabbit anti-mouse collagen 1, ref 20151, Novotec), ET-1 (T4049, Peninsula), CUX1 (M-222, sc-13024, Santa Cruz), CTGF (L-20, sc14939, Santa Cruz), GAPDH (ab8245-100, Abcam), β -catenin (ab6302-100,

Abcam) and Wnt1 (anti-human WNT1 S#500-p250, PeproTech, Inc.).

N-(1-naphthalenylsulfonyl)-Ile-Trp-aldehyde (IW-CHO, 0.2 μ M, Alexis Biochemicals) was used as IW-CHO. TGF- β (R&D Systems) was used at 4 ng/ml. The cells were serum-starved for 12 h and incubated with or without TGF- β at 4 ng/ml for a further 24 h.

2.3. Plasmid transfection

Cells were seeded in six-well plates before transfection and 24 h later were transfected using FuGENE 6 (Roche, Basel, Switzerland), according to the manufacturer's instructions; this method was used to transfet sh-CUX1 vector as described previously [17].

2.4. EMSAs

Nuclear extracts were prepared from fibroblasts obtained from patients with SSc using a previously described method [16]. Briefly, double-stranded oligonucleotides were synthesised, end-labelled with ³²P-gamma-ATP using T4 kinase and used in binding reactions with nuclear extracts from the cells. Competition was performed with unlabelled oligonucleotides (1.75 pmol/ μ l). Oligonucleotides for the CUX1-19.51 kb probe (5'-attggcagtggattacttagta-3') were used. We employed the standard conditions recommended by the kit manufacturer (Promega) and separated the reaction on a 4% polyacrylamide gel at 4 °C and 160 V. Consensus oligonucleotides for CUX1 (CDP, sc2593, Santa Cruz) and SP1 (sc-2502, Santa Cruz) were used.

2.5. Immunocytochemistry

The cells were washed in ice-cold PBS twice and fixed with 3% paraformaldehyde in PBS for 15 min at room temperature. The cells were blocked with 3% BSA for 30 min at 25 °C, followed by incubation with CUX1 antibody (0.2 mg/ml) and monoclonal anti- α -SMA clone 1a Cy3-conjugated antibody (0.7 mg/ml) (Sigma-Aldrich) overnight at 4 °C. Subsequently, the cells were washed with ice-cold PBS twice, incubated with an Alexa 488 secondary antibody overnight at 4 °C, washed with ice-cold PBS twice and incubated with DAPI (Roche) for 30 min at room temperature. Slides were viewed and photographed using a Zeiss Axioscope light microscope (Carl Zeiss, Göttingen, Germany) with Axiovision software.

2.6. Immunohistochemistry

For formalin-fixed paraffin-embedded specimens, tissues were fixed and hydrated as previously described [10]. For immunohistochemistry, sections were pre-treated with methanol (VWR, Lutterworth, UK), followed by antigen retrieval in heated 10 mM citrate buffer (pH 6). The primary antibodies were CUX1 antibody (0.2 mg/ml) and monoclonal anti- α -SMA clone 1a Cy3-conjugated antibody (0.7 mg/ml). Sections were sequentially incubated with a 1/200 dilution of an Alexa 488 secondary antibody. Slides were viewed and photographed using a Zeiss Axioscope light microscope with Axiovision software.

2.7. Data analysis

Data are expressed as the mean \pm S.E. of at least three independent experiments. Statistical analysis was performed using Student's *t*-test. Values of *P* < 0.05 were considered significant.

3. Results

3.1. CUX1 binds to the enhancer region of human COL1A2

The CUX1 cis-element CCAAT (Fig. 1A) was identified at IS4 near enhancer-containing DNase I HS4 using *in silico* analyses. Cut repeats and homeodomains bind to this cis-element (Fig. 1A) [21]. To determine whether CUX1 interacts with the enhancer region of human *COL1A2*, we performed EMSAs using transcription factor-binding consensus oligonucleotides, CUX1 antibody and sh-CUX1. In these experiments, we not only verified the binding of CUX1 at CUX1 (–19.51 kb) probe sites but also demonstrated the binding of several other transcription factors, including JunD (data not shown). Nuclear extracts from normal lung fibroblasts incubated with or without TGF- β were used, and CUX1 consensus oligonucleotides, CUX1 antibody and sh-CUX1 decreased the intensity of CUX1 bands (Fig. 1B). Furthermore, the binding of CUX1 at CUX1 (–19.51 kb) probe sites increased post-TGF- β treatment in both normal and SSc lung fibroblasts (Fig. 2A).

3.2. TGF- β up-regulates the expression of CUX1 isoforms

CUX1, also known as CCAAT displacement protein (CDP), CUTL1, CUT or Cux, belongs to a family of homeobox transcription factors that are involved in the regulation of cell growth and differentiation [22]. It is evolutionarily conserved and comprises four DNA binding domains, three of which are known as Cut repeats and one is known as the Cut homeodomain [21]. CUX1 mainly acts as a transcriptional repressor, but it can also act as an activator [23–25]. Transgenic mice with CUX1 overexpression have been

reported to exhibit multi-organ hyperplasia and organomegaly [26]. Moreover, the CUX1 isoforms p200 and p110 can regulate motility and invasiveness through a TGF- β -dependent mechanism [27,28]. However, the role of CUX1 isoforms in the development of fibrosis remains unclear. We performed Western blotting to determine whether the expression levels of CUX1 isoforms were induced by TGF- β . We found that the expression levels of CUX1 isoforms significantly increased in both normal and SSc lung fibroblasts post-TGF- β treatment (Fig. 2B, C). TGF- β treatment resulted in the induction of p200 and p150 in normal lung fibroblasts. Moreover, TGF- β treatment resulted in the induction of p200, p150, p110, p75, p30 and p28 in SSc lung fibroblasts. These results suggested that TGF- β stimulate the expression of CUX1 isoforms. We also verified whether the expression levels of profibrotic proteins were up-regulated. ET-1, COL1, Wnt1, CTGF and β -catenin levels increased post-TGF- β treatment in normal and SSc lung fibroblasts (Fig. 2D).

3.3. Effects of cathepsin L inhibition on lung fibroblasts derived from patients with SSc

Several studies have illustrated that CUX1 is cleaved into p150, P110, p75 and other subunits by nuclear cathepsin L. To confirm the effects of cathepsin L inhibition on SSc lung fibroblasts, we measured the expression levels of COL1 in both normal and SSc lung fibroblasts. IW-CHO (0.2 μ M) was used because its IC₅₀ is 1.9 nM. IW-CHO decreased the expression levels of COL1 in normal and SSc lung fibroblasts (Fig. 2E). To further confirm the effects of cathepsin L on SSc lung fibroblasts, we used immunocytochemistry to study CUX1 localization in these

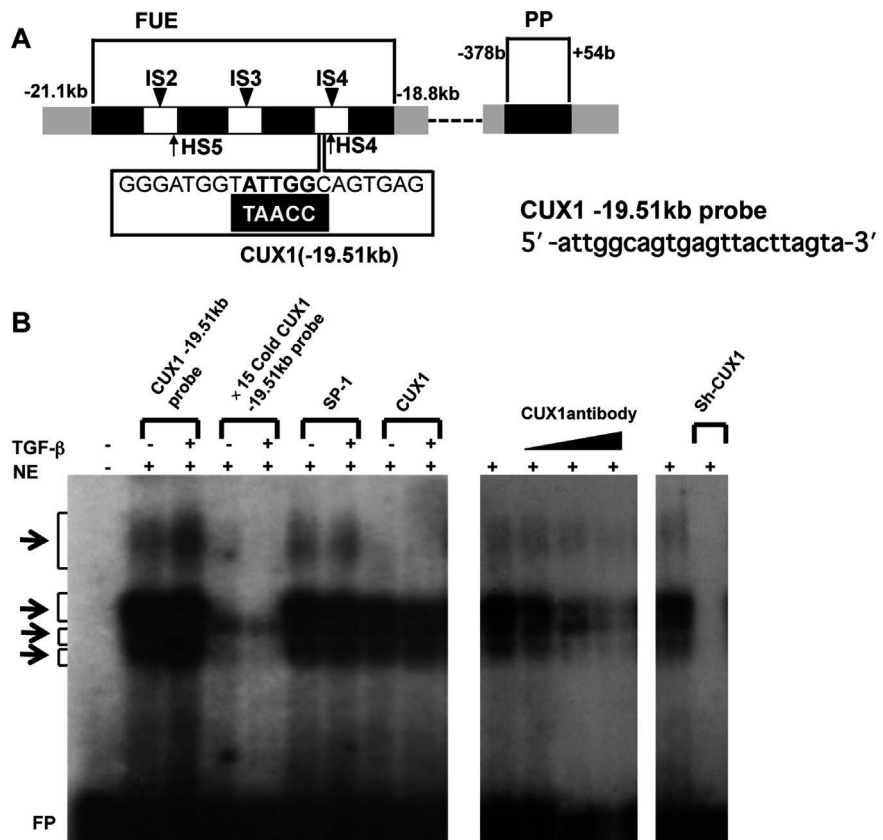


Fig. 1. Electrophoretic mobility shift assays (EMSAs) revealed that CUX1 binds to the human type I collagen alpha 2 gene (*COL1A2*) enhancer. A. Schematic diagrams of the far upstream enhancer region (FUE) with arrows indicating known DNase hypersensitive sites; the white box indicates the known identity islands of human *COL1A2*. CUX1 cis-elements are indicated by bold letters. B. EMSA using the CUX1 (–19.51 kb) probe. NE, nuclear extract from normal lung fibroblasts. The right-hand graph of Fig. 1B shows several bands detected using P^{32} -labelled oligos in Lanes 2 and 3. Bands were confirmed using a cold competitor. Unlabelled competing oligo probes are shown in Lanes 4 and 5. Consensus oligo for CUX1, Lanes 8–9. Consensus oligo for SP1, Lanes 6–7. Antibody for CUX1, Lanes 11–13. Sh-CUX1, Lanes 15. FP, free probe.

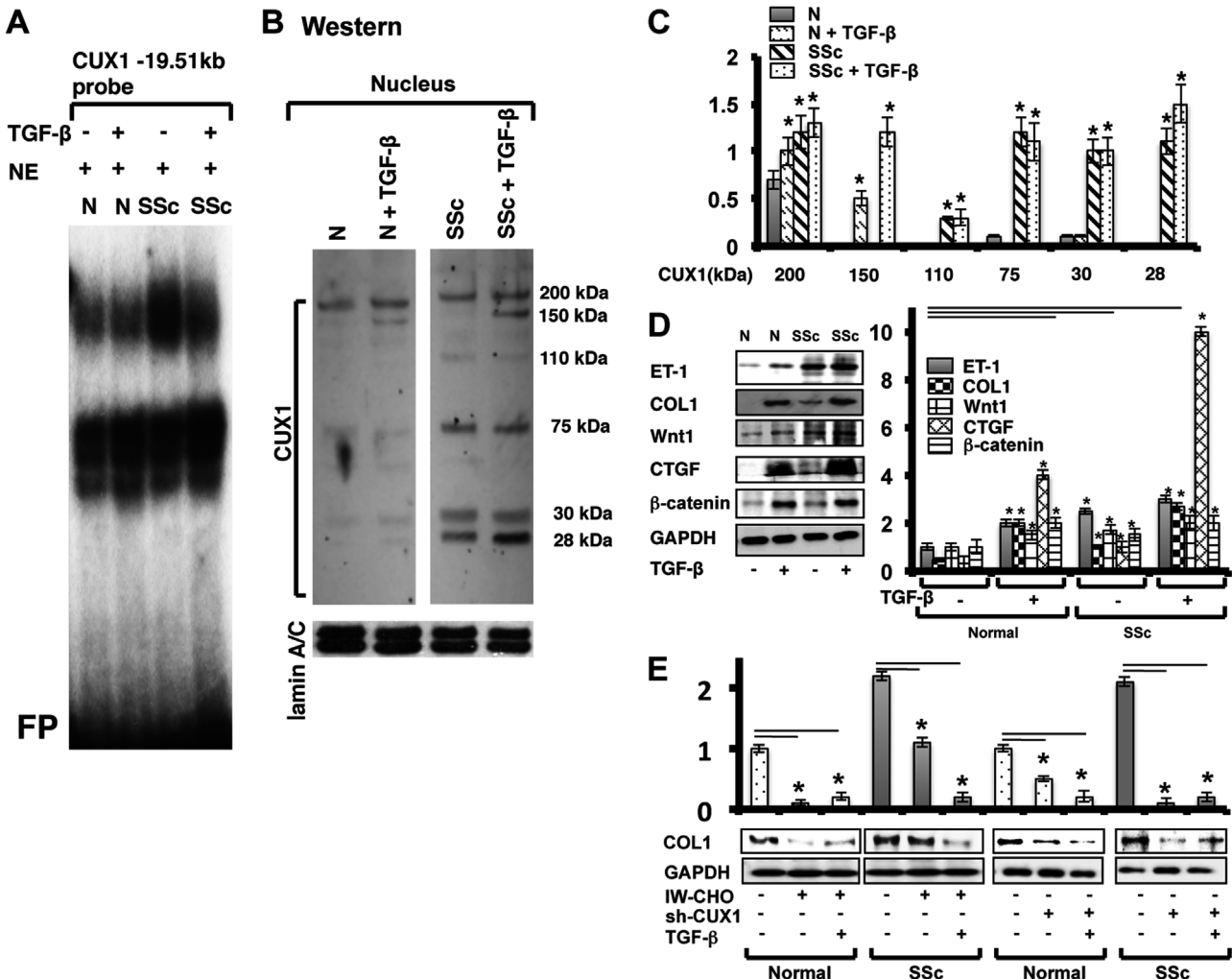


Fig. 2. CUX1 isoforms in normal human and systemic sclerosis (SSc) lung fibroblasts. **A.** Electrophoretic mobility shift assay using normal lung fibroblast (N) nuclear extract (NE) (Lanes 1–2) and SSc lung fibroblast NE (Lanes 3–4) treated with transforming growth factor (TGF- β) (Lanes 2 and 4) or untreated (Lanes 1 and 3) for the CUX1 (-19.51 kb) probe. FP, free probe. **B.** Effects of TGF- β on the expression of CUX1 isoforms as assessed using Western Blotting. TGF- β (4 ng/ml) was added to the fibroblasts after 12 h of serum starvation. Then, the cells were cultured for 24 h. **C.** Graphs represent the results of Fig. 2B. **D.** Effects of TGF- β on the expression of collagen type I and fibrosis-related proteins. Several fibrosis-related cytokines and proteins were detected using the cytosolic fraction as well as the medium and NEs from both normal and SSc lung fibroblasts with or without TGF- β treatment. **E.** Effects of a cathepsin L inhibitor (IW-CHO, 0.2 μ M) and sh-CUX1 on the expression of type I collagen (COL1) in normal and SSc lung fibroblasts. Values represent mean \pm S.E.M., $n=3$. *, significantly different from control, $P < 0.05$ by Student's *t*-test. GAPDH and lamin A/C were used as internal controls.

fibroblasts. As shown in Fig. 3, immunofluorescence analysis indicated that SSc lung fibroblasts were CUX1- and α -SMA-positive, with positivity increasing post-TGF- β treatment. CUX1 localised to the nucleus and cytosol. In addition, SSc lung fibroblasts were larger than normal lung fibroblasts (data not shown). IW-CHO decreased the CUX1 localization in the nucleus and reduced the large size of SSc lung fibroblasts with or without TGF- β treatment (Fig. 3).

3.4. Immunohistochemical analyses of SSc and diffuse alveolar damage (DAD) lung tissue sections stained with antibodies against CUX1 and α -SMA

Immunocytochemistry revealed the presence of α -SMA-positive fibrotic loci (Fig. 4), which is characteristic of patients with SSc and DAD. CUX1 localised at alveolar cells and fibrotic loci. In addition, CUX1 localised within α -SMA-positive cells (Fig. 4, merged).

4. Discussion

This study demonstrated the binding of CUX1 to the IS4 domain of the COL1A2 enhancer region in both normal and SSc lung fibroblasts. Further, our results demonstrated that TGF- β -induced CUX1 isoforms function as transcriptional activators that increase the expression of COL1 proteins. Previous studies implicated CUX1 in both the activation and suppression of several genes [23–25]. Our previous study found that CUX1 bound to the proximal promoter of COL1A2 after treatment with high doses of TGF- β [22]. In this study, we provide evidence that CUX1 also plays a major role in COL1A2 activation both *in vitro* and *ex vivo* via the IS4 domain of the COL1A2 enhancer.

Our data clearly demonstrated that TGF- β induces the expression of CUX1 isoforms, some of which were also up-regulated in SSc lung fibroblasts. In association with this change, the binding of CUX1 to the enhancer region of human COL1A2 increased in response to TGF- β treatment in normal and SSc lung fibroblasts. These results suggested that TGF- β up-regulates CUX1 protein expression, resulting in an increased binding of CUX1 to the human COL1A2 enhancer and COL1 up-regulation.

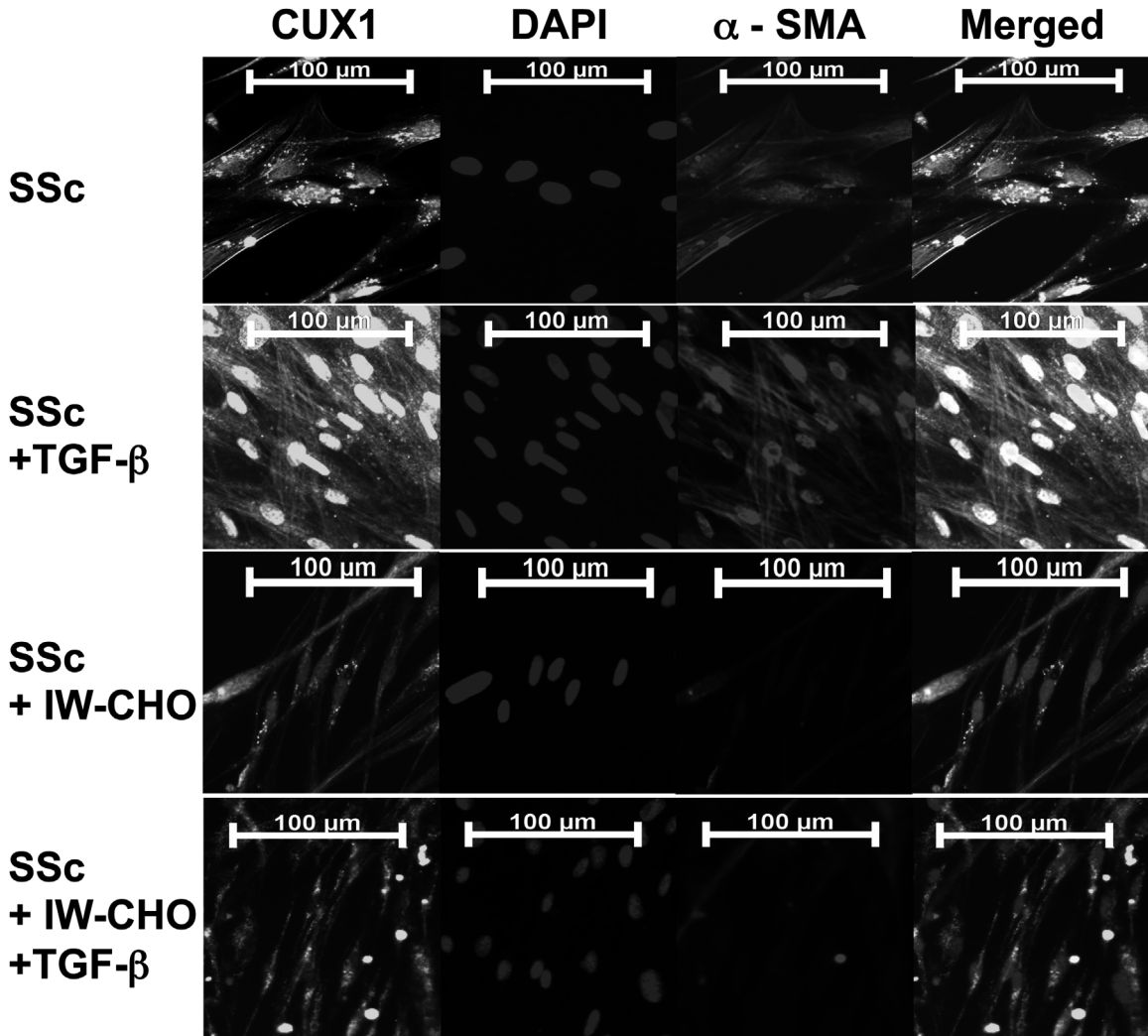


Fig. 3. Effects of IW-CHO on systemic sclerosis (SSc) lung fibroblasts. Immunofluorescence analysis performed using SSc lung fibroblasts treated with or without TGF- β . Cells were stained using CUX1 antibody, DAPI and α -SMA antibody. IW-CHO treatment decreased the CUX localization in the nucleus and reduced the size of lung fibroblasts in patients with SSc. In addition, in the presence of TGF- β , IW-CHO treatment reduced the size of lung fibroblasts in patients.

Another important finding of this study was that TGF- β induces the expression of the CUX1 isoforms p200, p150, p110, p75, p30 and p28 in SSc lung fibroblasts. Cleavage sites have been found for cathepsin L between CR1 and CR2 and for caspase between CR3 and HR of CUX1 [19]. Previous studies have revealed the induction of HA-tagged CUX-1 p200 and p110 in certain cell lines [19,29]. The CUX-1 antibody M-222 simultaneously recognises several CUX1 isoforms in normal and SSc lung fibroblasts following TGF- β treatment. As the molecular weight patterns observed in our study are similar to those previously reported, we believe that all bands observed in this study were specific for CUX1 isoforms.

Our data provide further evidence that CUX1 isoforms may play crucial roles in *COL1A2* regulation. First, the levels of all CUX1 isoforms increased in SSc lung fibroblasts compared with the levels in normal lung fibroblasts. Moreover, compared with the findings in normal lung fibroblasts, data from EMSA revealed significantly increased binding of CUX1 at CUX1 (-19.51 kb) probe sites of human *COL1A2* in SSc lung fibroblasts. Several reports studies have illustrated that CUX1 isoforms have different DNA binding affinities and functions [19,23–25,30]. Second, *COL1* expression decreased by cathepsin L inhibition in normal and SSc lung fibroblasts, highlighting the importance of CUX1 isoforms in fibrosis. Third, CUX1 localised at the nucleus and cytosol (Fig. 3). CUX1 and α -SMA co-localised in the cytosol in SSc lung fibroblasts.

IW-CHO decreased the CUX localization in the nucleus and repressed the large size of SSc lung fibroblasts with or without TGF- β treatment (Fig. 3). In addition, in SSc and DAD lung sections, CUX1 localised around fibrotic loci and alveolar cells. Some of these cells were stained by both CUX1 and α -SMA (Fig. 4). Furthermore, in the SSc skin and idiopathic pulmonary fibrosis (IPF) sections, CUX1 localised within and around α -SMA positive cells (See Figs. 1 and 2, reference [31]). These results indicated that CUX1 isoforms are necessary for fibrosis.

In future, investigations on the mutagenesis of CUX1 cleavage sites are required to determine which CUX1 isoforms are crucial. In addition, we need to verify the effects of CUX1 isoforms on the promoter region of α -SMA and pro-fibrotic cytokines. We speculate that some specific features of CUX1 isoforms are important for the activation of human *COL1A2* via the IS4 domain, which is located in the *COL1A2* enhancer.

In summary, our study demonstrated that the up-regulation of CUX1 isoforms is associated with fibrosis *in vitro* in SSc lung fibroblasts as well as in tissue sections from patients with SSc and DAD. Hence, these data indicate that the expression of CUX1 isoforms is possibly important for fibrosis and could be relevant to the pathogenesis of SSc.

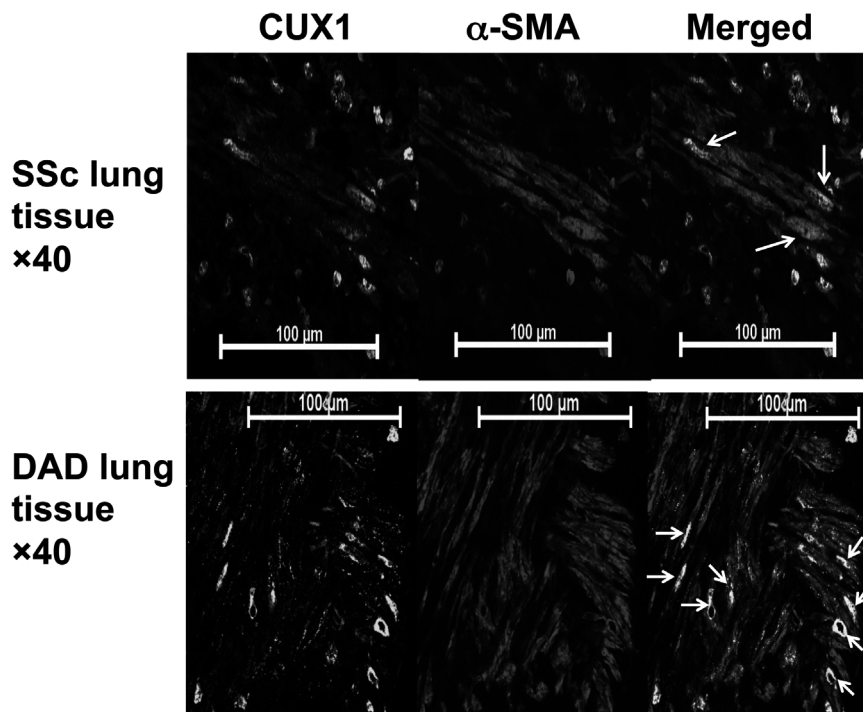


Fig. 4. Systemic sclerosis (SSc) and diffuse alveolar damage (DAD) lung tissue sections stained with antibodies against CUX1 and α -smooth muscle actin (SMA). The figure shows fibrotic loci that were stained by CUX1 and α -SMA antibodies. Alveolar cells around the loci were positive for CUX1 and α -SMA. CUX1 localised within α -SMA-positive cells.

Acknowledgements

This work was supported partly by a grant from the Japan Society for the Promotion of Science (Grant No. 17109011). Further, this work was supported by the Global COE Program 'Center of Education and Research for the Advanced Genome-Based Medicine-For personalized medicine and the control of worldwide infectious disease', MEXT Japan. The authors would like to thank Enago for the English language review.

Appendix A. Transparency document

Transparency document associated with this article can be found in the online version at <http://dx.doi.org/10.1016/j.bbrep.2016.06.022>.

References

- [1] C.P. Denton, C.M. Black, D.J. Abraham, Mechanisms and consequences of fibrosis in systemic sclerosis, *Nat. Clin. Pract. Rheumatol.* 2 (2006) 134–144.
- [2] X. Shi-Wen, A. Leask, D. Abraham, Regulation and function of connective tissue growth factor/Ccn2 in tissue repair, scarring and fibrosis, *Cytokine Growth Factor Rev.* 19 (2008) 133–144.
- [3] S.W. Xu, S.L. Howat, E.A. Renzoni, A. Holmes, J.D. Pearson, M.R. Dashwood, G. Bou-Gharios, C.P. Denton, R.M. du Bois, C.M. Black, A. Leask, D.J. Abraham, Endothelin-1 induces expression of matrix-associated genes in lung fibroblasts through MEK/ERK, *J. Biol. Chem.* 279 (2004) 23098–23103.
- [4] C. Fonseca, G.E. Lindahl, M. Ponticos, P. Sestini, E.A. Renzoni, A.M. Holmes, P. Spagnolo, P. Pantelidis, P. Leoni, N. McHugh, C.J. Stock, X. Shi-Wen, C. P. Denton, C.M. Black, K.I. Welsh, R.M. du Bois, D.J. Abraham, A polymorphism in the CTGF promoter region associated with systemic sclerosis, *N. Engl. J. Med.* 357 (2007) 1210–1220.
- [5] M.L. Whitfield, D.R. Finlay, J.I. Murray, O.G. Troyanskaya, J.T. Chi, A. Pergamenshikov, T.H. McCalmon, P.O. Brown, D. Botstein, M.K. Connolly, Systemic and cell type-specific gene expression patterns in scleroderma skin, *Proc. Natl. Acad. Sci. USA* 100 (2003) 12319–12324.
- [6] J. Yang-Snyder, J.R. Miller, J.D. Brown, C.J. Lai, R.T. Moon, A frizzled homolog functions in a vertebrate Wnt signaling pathway, *Curr. Biol.* 6 (1996) 1302–1306.
- [7] A. Desmouliere, Factors influencing myofibroblast differentiation during wound healing and fibrosis, *Cell Biol. Int.* 19 (1995) 471–476.
- [8] N.K. Harrison, A.C. Argent, R.J. McAnulty, C.M. Black, B. Corrin, G.J. Laurent, Collagen synthesis and degradation by systemic sclerosis lung fibroblasts. Responses to transforming growth factor-beta, *Chest* 99 (1991) 71S–72S.
- [9] C.P. Denton, B. Zheng, L.A. Evans, X. Shi-wen, V.H. Ong, I. Fisher, K. Lazaridis, D. J. Abraham, C.M. Black, B. de Crombrugghe, Fibroblast-specific expression of a kinase-deficient type II transforming growth factor beta (TGF β) receptor leads to paradoxical activation of TGF β signaling pathways with fibrosis in transgenic mice, *J. Biol. Chem.* 278 (2003) 25109–25119.
- [10] R.K. Hoyles, K. Khan, X. Shiwen, S.L. Howat, G.E. Lindahl, P. Leon, R.M. du Bois, A.U. Wells, C.M. Black, D.J. Abraham, C.P. Denton, Fibroblast-specific perturbation of transforming growth factor beta signaling provides insight into potential pathogenic mechanisms of scleroderma-associated lung fibrosis: exaggerated response to alveolar epithelial injury in a novel mouse model, *Arthritis Rheum.* 58 (2008) 1175–1188.
- [11] S. Sonnyalal, C.P. Denton, B. Zheng, D.R. Keene, R. He, H.P. Adams, C.S. Vanpelt, Y. J. Geng, J.M. Deng, R.R. Behringer, B. de Crombrugghe, Postnatal induction of transforming growth factor beta signaling in fibroblasts of mice recapitulates clinical, histologic, and biochemical features of scleroderma, *Arthritis Rheum.* 56 (2007) 334–344.
- [12] W.A. Border, N.A. Noble, Transforming growth factor beta in tissue fibrosis, *N. Engl. J. Med.* 331 (1994) 1286–1292.
- [13] J.C. Horowitz, D.S. Rogers, V. Sharma, R. Vittal, E.S. White, Z. Cui, V. J. Thannickal, Combinatorial activation of FAK and AKT by transforming growth factor-beta1 confers an anoikis-resistant phenotype to myofibroblasts, *Cell Signal.* 19 (2007) 761–771.
- [14] V.J. Thannickal, D.Y. Lee, E.S. White, Z. Cui, J.M. Larios, R. Chacon, J.C. Horowitz, R.M. Day, P.E. Thomas, Myofibroblast differentiation by transforming growth factor-beta1 is dependent on cell adhesion and integrin signaling via focal adhesion kinase, *J. Biol. Chem.* 278 (2003) 12384–12389.
- [15] T.T. Antoniv, S. Tanaka, B. Sudan, S. De Val, K. Liu, L. Wang, D.J. Wells, G. Bou-Gharios, F. Ramirez, Identification of a repressor in the first intron of the human alpha2(I) collagen gene (COL1A2), *J. Biol. Chem.* 280 (2005) 35417–35423.
- [16] M. Ponticos, C. Harvey, T. Ikeda, D. Abraham, G. Bou-Gharios, JunB mediates enhancer/promoter activity of COL1A2 following TGF-beta induction, *Nucleic Acids Res.* 37 (2009) 5378–5389.
- [17] M. Fragiadaki, T. Ikeda, A. Withherden, R.M. Mason, D. Abraham, G. Bou-Gharios, High doses of TGF-beta potently suppress type I collagen via the transcription factor CUX1, *Mol. Biol. Cell* 22 (2011) 1836–1844.
- [18] T.T. Antoniv, S. De Val, D. Wells, C.P. Denton, C. Rabe, B. de Crombrugghe, F. Ramirez, G. Bou-Gharios, Characterization of an evolutionarily conserved far-upstream enhancer in the human alpha 2(I) collagen (COL1A2) gene, *J. Biol. Chem.* 276 (2001) 21754–21764.
- [19] L. Sansregret, A. Nepveu, The multiple roles of CUX1: insights from mouse models and cell-based assays, *Gene* 412 (2008) 84–94.

- [20] X. Shi-Wen, C.P. Denton, A. McWhirter, G. Bou-Gharios, D.J. Abraham, R.M. du Bois, C.M. Black, Scleroderma lung fibroblasts exhibit elevated and dysregulated type I collagen biosynthesis, *Arthritis Rheum.* 40 (1997) 1237–1244.
- [21] R. Harada, G. Berube, O.J. Tamplin, C. Denis-Larose, A. Nepveu, DNA-binding specificity of the cut repeats from the human cut-like protein, *Mol. Cell Biol.* 15 (1995) 129–140.
- [22] A. Nepveu, Role of the multifunctional CDP/Cut/Cux homeodomain transcription factor in regulating differentiation, cell growth and development, *Gene* 270 (2001) 1–15.
- [23] B. Goulet, P. Watson, M. Poirier, L. Leduy, G. Berube, S. Meterissian, P. Jolicoeur, A. Nepveu, Characterization of a tissue-specific CDP/Cux isoform, p75, activated in breast tumor cells, *Cancer Res.* 62 (2002) 6625–6633.
- [24] N.S. Moon, P. Premdas, M. Truscott, L. Leduy, G. Berube, A. Nepveu, S phase-specific proteolytic cleavage is required to activate stable DNA binding by the CDP/Cut homeodomain protein, *Mol. Cell Biol.* 21 (2001) 6332–6345.
- [25] M. Truscott, L. Raynal, P. Premdas, B. Goulet, L. Leduy, G. Berube, A. Nepveu, CDP/Cux stimulates transcription from the DNA polymerase alpha gene promoter, *Mol. Cell Biol.* 23 (2003) 3013–3028.
- [26] A.W. Ledford, J.G. Brantley, G. Kemeny, T.L. Foreman, S.E. Quaggin, P. Igarashi, S.M. Oberhaus, M. Rodova, J.P. Calvet, G.B. Vanden Heuvel, Deregulated expression of the homeobox gene Cux-1 in transgenic mice results in down-regulation of p27(kip1) expression during nephrogenesis, glomerular abnormalities, and multiorgan hyperplasia, *Dev. Biol.* 245 (2002) 157–171.
- [27] P. Michl, J. Downward, CUTL1: a key mediator of TGFbeta-induced tumor invasion, *Cell Cycle* 5 (2006) 132–134.
- [28] P. Michl, A.R. Ramjaun, O.E. Pardo, P.H. Warne, M. Wagner, R. Poulsom, C. D'Arrigo, K. Ryder, A. Menke, T. Gress, J. Downward, CUTL1 is a target of TGF (beta) signaling that enhances cancer cell motility and invasiveness, *Cancer Cell* 7 (2005) 521–532.
- [29] S. Ceru, S. Konjar, K. Maher, U. Repnik, I. Krizaj, M. Bencina, M. Renko, A. Nepveu, E. Zerovnik, B. Turk, N. Kopitar-Jerala, Stefin B interacts with histones and cathepsin L in the nucleus, *J. Biol. Chem.* 285 (2010) 10078–10086.
- [30] M. Truscott, L. Raynal, Y. Wang, G. Berube, L. Leduy, A. Nepveu, The N-terminal region of the CCAAT displacement protein (CDP)/Cux transcription factor functions as an autoinhibitory domain that modulates DNA binding, *J. Biol. Chem.* 279 (2004) 49787–49794.
- [31] T. Ikeda, M. Fragiadaki, X. Shi-Wen, M. Ponticos, K. Khan, C. Denton, P. Garcia, G. Bou-Gharios, A. Yamakawa, C. Morimoto, and D. Abraham, Data on the CUX1 isoforms in the Idiopathic Pulmonary Fibrosis (IPF) tissue section and Systemic Sclerosis (SSc) skin tissue section, Data In Brief. (submitted).

Role of IL-26⁺CD26⁺CD4 T Cells in Pulmonary Chronic Graft-Versus-Host Disease and Treatment with Caveolin-1-Ig Fc Conjugate

Kei Ohnuma,^{a,*} Ryo Hatano,^a Takumi Itoh,^a Noriaki Iwao,^b Nam H. Dang,^c Chikao Morimoto^a

^aDepartment of Therapy Development and Innovation for Immune Disorders and Cancers, Graduate School of Medicine, Juntendo University, 2-1-1, Hongo, Bunkyo-ku, Tokyo 113-8421, Japan; ^bDepartment of Hematology, Juntendo University Shizuoka Hospital, Nagaoka 1129, Izunokuni-city, Shizuoka 410-2295, Japan; ^cDivision of Hematology/Oncology, University of Florida, 1600 SW Archer Road- Box 100278, Room MSB M410A, Gainesville, FL 32610, U.S.A.

*Address all correspondence to: Dr. K. Ohnuma, Department of Therapy Development and Innovation for Immune Disorders and Cancers, Graduate School of Medicine, Juntendo University, 2-1-1, Hongo, Bunkyo-ku, Tokyo 113-8421, Japan; Tel.: +81-3-3868-2310; Fax: +81-3-3868-2310; E-mail: kohnuma@juntendo.ac.jp.

ABSTRACT: Obliterative bronchiolitis is the primary noninfectious pulmonary complication after allogeneic hematopoietic cell transplantation and the only pathognomonic manifestation of pulmonary chronic graft-versus-host disease (cGVHD). In our recent study, we identified a novel effect of IL-26, which is absent in rodents, on transplant related-obliterative bronchiolitis. Sublethally irradiated NOD/Shi-*scid*IL2ry^{null} mice transplanted with human umbilical cord blood gradually exhibited obliterative bronchiolitis with increased collagen deposition and predominant infiltration with human IL-26⁺CD26⁺CD4 T cells. Moreover, we showed that IL-26 increased collagen synthesis in fibroblasts *in vitro* and that collagen contents were increased in a murine GVHD model using *IL26* transgenic mice. *In vitro* analysis demonstrated a significant increase in IL-26 production by CD4 T cells following CD26 costimulation, while immunoglobulin Fc domain fused with the N-terminal of caveolin-1, the ligand for CD26, (Cav-Ig) effectively inhibited production of IL-26. Administration of Cav-Ig before or after onset of GVHD impeded the development of clinical and histologic features of GVHD without interrupting engraftment of donor-derived human cells, with preservation of the graft-versus-leukemia effect. We concluded that cGVHD of the lungs is caused in part by IL-26⁺CD26⁺CD4 T cells, and that treatment with Cav-Ig could be beneficial for cGVHD prevention and therapy.

KEY WORDS: CD26/dipeptidyl peptidase IV; caveolin-1; chronic graft-versus-host disease; obliterative bronchiolitis; IL-26.

ABBREVIATIONS: **A20-luc:** luciferase-transfected A20 cell; **ADA:** adenosine deaminase; **aGVHD:** acute graft-versus-host disease; **alloHSCT:** allogeneic hematopoietic stem cell transplantation; **APC:** antigen presenting cell; **ATG:** antihuman T-lymphocyte immune globulin; **Cav-Ig:** soluble Fc fusion proteins containing the N-terminal domain of caveolin-1; **CB:** cord blood; **cGVHD:** chronic graft-versus-host disease; **DPPIV:** dipeptidyl peptidase IV; **GVHD:** graft-versus-host disease; **GVL:** graft-versus-leukemia; **HSC:** hematopoietic stem cell; **HuCB:** human umbilical cord blood; **IBD:** inflammatory bowel diseases; **IFN:** interferon; **IL:** interleukin; **mAb:** monoclonal antibody; **NHLF:** normal human lung fibroblast; **NOG:** NOD/Shi-*scid*IL2ry^{null}; **OB:** obliterative bronchiolitis; **PBL:** peripheral blood lymphocyte; **RA:** rheumatoid arthritis; **Tg:** transgenic; **TNF:** tumor necrosis factor.

I. I. INTRODUCTION

Graft-versus-host disease (GVHD) is a severe complication and major cause of morbidity and mortality following allogeneic hematopoietic stem cell transplantation (alloHSCT).¹ On the basis of differences in clinical manifestations and histopathol-

ogy, GVHD can be divided into acute and chronic forms.¹ Acute GVHD (aGVHD) and chronic GVHD (cGVHD) are traditionally diagnosed primarily by time of onset, with cGVHD occurring after day 100 of transplantation.² However, cGVHD has distinct clinicopathologic features and is often diagnosed based on these features regardless of time of onset,

being characterized by cutaneous fibrosis, involvement of exocrine glands, hepatic disease, and obliterative bronchiolitis (OB).^{3,4} OB, characterized by airway blockade, peribronchiolar and perivascular lympho-fibroproliferation and obliteration of bronchioles, is a late-stage complication of cGVHD.⁵ Patients diagnosed with OB have a 5-year survival rate of only 10 to 40%, compared to more than 80% in patients without OB.^{6,7} Therefore, the establishment of a humanized murine model of cGVHD manifesting OB is urgently needed to develop novel therapeutic strategies for use in the clinical setting. Furthermore, while multiple strategies to control cGVHD involving T-cell depletion from the graft or global immunosuppression have been developed, cGVHD is still a common clinical outcome in many alloHSCT patients.^{4,8} In addition, immunosuppression potentially abrogates the graft-versus-leukemia (GVL) effect, associated with increased relapses following alloHSCT.⁹ Novel therapeutic approaches are thus needed to prevent cGVHD without eliminating the GVL effect.

GVHD is initiated when donor-derived T cells are primed by professional antigen presenting cells (APCs) to undergo clonal expansion and maturation.¹ Costimulatory pathways are required to induce T-cell proliferation, cytokine secretion, and effector function following antigen-mediated T-cell receptor activation,¹⁰ and the important role of costimulatory pathways in transplant biology has been established.¹ CD26 is associated with T-cell signal transduction processes as a costimulatory molecule and is a marker of T-cell activation.¹¹⁻¹⁴ We previously showed that CD26-mediated costimulation in human CD4 T cells exerts an effect on production of T_H1-type proinflammatory cytokines such as interferon (IFN)- γ .¹⁵ Moreover, CD26^{high}CD4 T cells respond maximally to recall antigens with a high competence for trafficking to inflammatory tissues and for antibody synthesis of B cells.^{12,14,15} We also showed that CD26-caveolin-1 interaction leads to activation of both CD4 T cells and APCs.¹⁶⁻¹⁸ More recently, we performed *in vitro* experiments to demonstrate that blockade of CD26-mediated T-cell costimulation by soluble Fc

fusion proteins containing the N-terminal domain of caveolin-1 (Cav-Ig) diminished primary and secondary proliferative responses not only to recall antigen but also to unrelated allogeneic APC.¹⁹ Other investigators recently reported that CD26^{high} T cells contain T_H17 cells and that CD26^{high} T_H17 cells are enriched in inflamed tissues including rheumatoid arthritis (RA) and inflammatory bowel diseases (IBD).²⁰ These accumulating data strongly suggest that CD26-mediated costimulation plays an important role in memory response to recall antigens and that blockade of CD26 costimulation may be an effective therapeutic strategy for immune disorders including GVHD and autoimmune diseases.

In this review, we summarize our recent work to establish a pulmonary cGVHD murine model induced by transplantation of human umbilical cord blood (HuCB), which exhibited obliterative bronchiolitis (OB) as well as sclerodermatous skin GVHD after HSCT, and to describe a novel effect of IL-26 produced by donor-derived human CD4 T cells on fibroproliferation of OB. We also showed that IL-26 of HuCB CD4 T cells was produced via CD26 costimulation by its ligand caveolin-1. Furthermore, abrogation of CD26 costimulation by Cav-Ig before or during the early onset of GVHD impeded the development of pulmonary cGVHD. These results provide proof of principle that human IL-26⁺CD26⁺CD4 T cells are involved in the pathophysiology of pulmonary cGVHD.

II. CURRENT ISSUES IN CHRONIC GVHD

A. Diagnosis

In the past, cGVHD included any clinical manifestations of GVHD that occurred beyond 100 days after hematopoietic cell transplantation.²¹ According to the NIH consensus criteria published in 2005, the broad category of cGVHD includes classic cGVHD, presenting with manifestations that can be ascribed only to cGVHD. Moreover, cGVHD also includes the so-called overlap syndrome, which has diagnostic or distinctive cGVHD

TABLE 1: Signs and Symptoms of Chronic GVHD

Organ	Diagnostic (sufficient for diagnosis)	Distinctive (insufficient alone for diagnosis)	Common (in both acute and chronic GVHD)
Skin	Poikiloderma, Lichen planus-like, Sclerosis or Morphea	Depigmentation	Erythema, Maculopapular rash, Pruritus
Nails		Dystrophy, Logitudinal ridging or brittle, Onycholysis, Nail loss*	
Scalp and body hair		Alopecia, Scaling	
Mouth	Lichen planus-like, Hyperkeratic plaques	Xerostomia, Mucocele, Ulcer*, Psuedomembrane*	Gingivitis, Erythema, Mucositis, Pain
Eyes		Keratoconjunctivitis**, Sicca syndrome	
Genitalia	Lichen planus-like, Vaginal scarring or stenosis	Erosion*, Fissures*, Ulcers*	
GI tract	Esophageal web, Stricture or stenosis*		Anorexia, Nausea, Vomiting, Diarrhea
Liver			Mixed hepatitis
Lung	OB by biopsy	OB by PFTs and radiology**	BOOP
Muscle, fascia, joints	Fascitis,	Myositis or polymyositis**	
	Joint contractures		Thrombocytopenia,
Hematopoietic and immune			Lymphopenia, Eosinophilia, Hypo or hypergammaglobulinemia, Autoantibody (ITP and AIHA)
Other			Effusions***

Begell Author Proofs

Myositis or polymyositis**

* In all cases, infection, malignancy and adverse effects of drugs must be excluded.

**Diagnosis of chronic GVHD requires biopsy or radiology confirmation (or Schirmer test for eyes).

***Pericardial, pleural effusions or ascites.

AIHA, autoimmune hemolytic anemia; BOOP, bronchiolitis obliterans with organizing pneumonia; GI, gastrointestinal; GVHD, graft-versus-host disease; ITP, idiopathic thrombocytopenic purpura; OB, obliterative bronchiolitis; PFTs, pulmonary function tests.

manifestations together with features typical of aGVHD.²¹ Table 1 shows a summary of the signs and symptoms of cGVHD determined by the NIH consensus criteria.^{3,21} However, several issues regarding the diagnosis of cGVHD have been raised recently: (1) The presentation of cGVHD

can be very polymorphic, ranging from discrete lichenoid features in the mouth alone, to a multisystemic appearance resembling an aggressive lupus or scleroderma-like disease. (2) Although the NIH panel recommended that distinctive but not diagnostic features may require biopsy

to confirm the diagnosis, this may not be easily available without risk for some diseases, including fasciitis or myositis. (3) The NIH criteria for lung involvement include only OB and organizing pneumonia (formally called bronchiolitis obliterans with organizing pneumonia), and the NIH scoring system includes both clinical signs and results of pulmonary function tests. Although the diagnosis of cGVHD is often based on clinical signs and symptoms, pathologic examination is warranted and clearly either helps confirm the diagnosis of cGVHD rather than aGVHD by using validated histologic changes specific for cGVHD (including skin, bronchioles, and salivary glands) or helps narrow down a differential diagnosis between cGVHD and carcinoma for mouth ulcerations.²²

B. Pathophysiology and Clinical Translation

In recent years, significant advances in our understanding of human cGVHD have been made. It is now evident that the clinical manifestations of cGVHD are the result of a highly complex immune pathologic process involving both donor T and B cells as well as other cells.^{4,23,24} Donor T cells clearly play an important role in the immune pathology of chronic GVHD; *in vivo* T-cell depletion is the only prophylactic measure that effectively decreases the incidence of cGVHD.^{25,26} The immune response occurring in chronic lichenoid GVHD showed a mixed T_H1/T_H17 signature with upregulated T_H1/T_H17 cytokine/chemokine transcripts and elevated numbers of IFN- γ and interleukin (IL)-17-producing CD8 $^{+}$ T cells.²⁷ Moreover, patients with active cGVHD have a lower frequency of CD4 $^{+}$ regulatory T cells (T_{reg}) than patients without cGVHD.²⁸ Regarding B cells, it has been recognized since the early description of the disease that patients with cGVHD frequently have circulating antibodies that are reactive with recipient cells.²⁹ However, whether these antibodies are pathogenic or simply reflect a disturbed B-cell homeostasis is still unknown, although T-follicular helper cells (Tfh)s may provide a link between the interacting T- and

B-cell networks in cGVHD.³⁰ Only antihuman T-lymphocyte immune globulin (ATG) has been shown to lower the incidence of chronic GVHD after stem-cell transplantation from an unrelated donor and from an HLA-identical sibling.^{31,32} ATG consists of antibodies exhibiting a direct effect on T cells through opsonization and lysis after complement activation. Because antigens such as CD19 or CD138 are also targeted by ATG, antitumor effects have been observed in B-cell cancers and to a lesser extent in myeloid cancers.³³ Taking into account the effect of donor T and B cells on the development of chronic GVHD,²³ the effect of ATG on APCs such as B cells and dendritic cells (DCs) and the induction of T_{reg} may have contributed to the significant reduction in chronic GVHD.^{34,35}

C. Preclinical Models in cGVHD

Although many preclinical models mimicking human cGVHD including OB have been established,³⁶ control of OB after alloHSCT has not yet been achieved thoroughly.³⁷ The clinical application of murine data is limited because multiple yet limited schema have arisen to identify alloimmune reactions in cross-species comparisons. For instance, one extensively utilized model of cGVHD clearly exhibited immune-complex glomerulonephritis, which is rarely seen in human cGVHD.³⁸ Moreover, transfer of autoantibodies from mice with GVHD to normal mice failed to cause autoimmune pathology.²⁹ These limitations are due to preparative regimens, composition of donor graft, and genetic backgrounds of donor and recipient animals.³⁶ In addition, recent work has demonstrated multiple differences in immunological functions between humans and mice.^{39,40} On the other hand, because *in vivo* T-cell depletion is the only prophylactic measure that effectively decreases the incidence of cGVHD,^{4,41} donor T cells clearly play an important role in the immune pathology of cGVHD. In view of these findings, the development of novel therapeutic strategies for use in the clinical setting and the establishment of a humanized murine model of cGVHD are urgently needed.

III. HUMANIZED MURINE MODEL OF CHRONIC GVHD

A. Donor Source of the Newly Established cGVHD Model

We previously analyzed a humanized murine aGVHD model involving mice transplanted with human adult peripheral blood lymphocytes (PBL). We showed that liver and skin were predominantly involved as target organs in this model of aGVHD, which was clearly impeded by the administration of anti-CD26 monoclonal antibody (mAb).⁴² Our data suggest that CD26⁺ T cells play an effector role in this aGVHD model. However, because the mice studied in our previous work succumbed to aGVHD around 4 weeks after transplantation of human adult PBL, this early-onset model of aGVHD does not permit the assessment of longer-term consequences of interventional therapies such as the development of OB, a form of cGVHD of the lung. Similarly, contaminated PBLs caused aggressive xenogenic reaction in mice transplanted with human bone marrow cells, while depletion of T cells in human bone marrow cells led to graft failure in a humanized murine model.⁴⁵ Therefore, an alternative source for human hematopoietic stem cells (HSC) is required for the establishment of a humanized murine model of cGVHD.

In contrast to adult PBL, the HuCB lymphocytes have been reported to be immature, predominantly consisting of CD45RA⁺ naïve cells.^{43,44} We previously showed that, while all HuCB CD4 T cells constitutively expressed CD26, CD26-mediated costimulation was considerably attenuated in HuCB CD4 T cells, compared to the robust activation via CD26 costimulation of adult PBL.⁴³ These findings provide further insights into the cellular mechanisms of the immature immune response of HuCB. Furthermore, humanized mice transplanted with human HSC isolated from HuCB exhibited human hematopoiesis reconstitution as well as B-cell engraftment with a similar antibody repertoire, as observed in human B cells.^{45,46} Based on these findings, we hypothesized that HuCB naïve CD4 T cells gradually acquire

a xenogeneic response via attenuated stimulatory signaling with indolent inflammation in the target organs, leading eventually to chronic inflammatory changes. We therefore sought to develop a humanized murine pulmonary cGVHD model utilizing HuCB donor cells and to overcome the limitations seen in the humanized murine aGVHD model, such as vigorous activation of all engrafted T cells and extensive loss of B-cell maturation and activation.⁴⁵

B. Pathologic Findings of Humanized cGVHD Murine Model

As described above, the establishment of a humanized murine model of pulmonary cGVHD is needed to better understand and treat this serious and often fatal complication of alloHSCT. To determine whether pulmonary cGVHD is induced by human immune cells in a murine model, we first attempted to establish a humanized murine model utilizing NOD/Shi-scidIL2rg^{null} (NOG) mice as recipients and HuCB as donor cells. To establish a control that did not develop GVHD following hematopoietic reconstitution, we used T-cell-depleted CD34⁺ cells isolated from HuCB.⁴⁷⁻⁴⁹ As shown in Figure 1A-i and ii, T-cell-depleted CD34⁺ transplanted mice (CD34⁺ transplant) survived for 5 months without any signs or symptoms of GVHD. Meanwhile, whole-CB-transplanted mice exhibited clinical signs/symptoms of GVHD as early as 4 weeks post transplant (Fig. 1A-ii) and demonstrated a significantly decreased survival rate (Fig. 1A-i). Human cells were engrafted similarly in both groups, as shown in Fig. 1A-iii. Previous work with other humanized murine models showed that reconstituted human CD45⁺ cells were overcome by CD3⁺ T cells after transplant due to reduced B-cell development,⁴⁵ which may impair the integrity of host immunity. In contrast, we confirmed that NOG mice transplanted with human HuCB maintained a stable number of T and B cells (Fig. 1B), consistent with previously reported results.^{46,48-50} Therefore, the human immune system appeared to be effectively reconstituted in the present murine model involving whole CB as well as CD34⁺ transplant.

We next conducted histological studies of GVHD

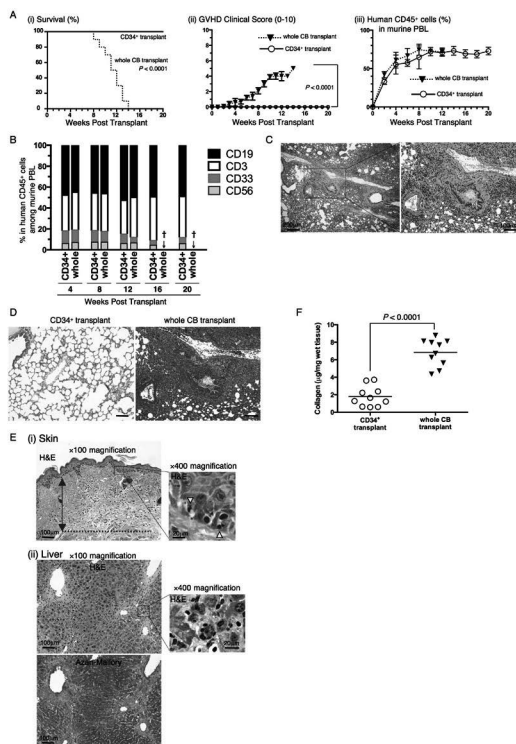


FIG. 1: Obliterative bronchiolitis in sublethally irradiated NOG mice transplanted with human umbilical cord blood cells (HuCB). NOG mice were irradiated at a sublethal dose (200cGy), the next day, they were transplanted with 1×10^5 T-cell-depleted CD34⁺ cells purified from HuCB (CD34⁺ transplant) or with 1×10^7 mononuclear cells isolated from HuCB (whole CB transplant). (A) (i) Survival curve. P value was calculated using the log-rank test. (ii) Clinical GVHD score (mean \pm SEM). P value was calculated using the log-rank test. (iii) Engraftment of human leukocytes in recipient mice. Peripheral blood of recipient mice was harvested at the indicated time points, and the population of human CD45⁺ cells was analyzed using flow cytometry. Data are shown as mean \pm SEM of human CD45⁺ cells among total peripheral blood leukocytes (PBLs). (B) Sustained composition of human leukocyte populations in recipient PBLs. PBLs harvested from each group were stained for human CD3, CD19, CD33, or CD56 among human CD45⁺ cells. Data are presented as mean percentages of human CD45⁺ cells. Cross indicates death of all mice in whole-CB-transplant group. (C) H&E staining of the lung of whole-CB-transplant (8 weeks post transplantation). The left panel shows lower magnification (40X) and the right panel shows higher magnification (100X). (D) Collagen deposition was evaluated in the lung tissues of CD34⁺ or whole-CB-transplant (8 weeks post transplantation) with an Azan-Mallory staining. The histology shown in whole-CB-transplant is a sequential section of panel C. Dark blue areas indicating collagen deposition are clearly observed in whole-CB-transplant mice, compared to those in CD34⁺ transplant mice. Original magnification is 100X. Scale bars indicate 100 μ m. (E) (i) Skin, H&E staining of the skin tissue of whole-CB-transplant mice (8 weeks post transplantation). The skin specimen shows homogenization (sclerosis) of most of the reticular dermis (blue two-way arrow) with fat loss and follicular drop-out (dotted line indicates the border between the hypodermis and muscle layer). In the stratum basale, vacuolar degeneration is presented with apoptotic bodies (yellow arrow heads). (ii) Liver, H&E and Azan-Mallory staining of the liver tissue of whole-CB-transplant mice (8 weeks post transplantation). Low-power magnification shows portal fibrosis and high-power magnification shows cholestasis. (F) Collagen contents in the lung were quantified by Sircol collagen assay. The mean number (\pm SEM) of total collagen contents (μ g) per wet lung tissue weight (mg) was determined. Increased collagen contents were clearly observed in whole-CB-transplant mice, compared to those in CD34⁺ transplant mice. Each dot indicates individual value and horizontal bars indicate mean value (reprinted with permission from The American Association of Immunologists, Inc., Copyright 2015).⁵¹

target organs. The lung of whole-CB-transplant mice showed perivascular and subepithelial inflammation and fibrotic narrowing of the bronchiole (Fig. 1C and right panel of Fig. 1D), while CD34⁺ transplant control group displayed normal appearance of GVHD target organs such as the lung (left panel of Fig. 1D). For the diagnosis of pulmonary cGVHD, it is necessary to show concomitant active GVHD findings in other organs, including skin and liver.²¹ Skin of whole-CB-transplant mice manifested fat loss, follicular drop-out and sclerosis of the reticular dermis in the presence of apoptosis of the basilar keratinocytes, whereas the liver exhibited portal fibrosis and cholestasis (Fig. 1E). These findings indicate that whole-CB-transplant mice develop pulmonary cGVHD as well as concomitant active GVHD in skin and liver. Because OB can be characterized as a fibroproliferative disease,³⁷ we also performed Mallory staining and lung collagen assays to quantify collagen contents as a measurement of the extent of disease. The lung of whole-CB-transplant mice displayed a significant increase in peribronchiolar and perivascular collagen deposition and in total lung collagen content, compared to CD34⁺ transplant mice (Figs. 1D and 1F). Taken together, our data demonstrate that the lung of whole-CB-transplant mice exhibits OB as manifestation of pulmonary GVHD.

C. Pathophysiology of Pulmonary cGVHD in Our Model

To determine the potential cellular mechanisms involved in the pathogenesis of pulmonary GVHD, we next analyzed the composition of donor-derived human lymphocytes in the GVHD lung. In contrast to data demonstrating that recipient PBL contained donor-derived human CD19⁺, CD33⁺, or CD56⁺ as well as CD3⁺ cells (Fig. 1B), donor-derived human CD3⁺ cells were the predominant cell type observed in the lung of whole-CB-transplant mice, comprising more than 99% of the lymphocyte population (Fig. 2A). Moreover, the human CD4 T-cell subset was the predominant population observed in the lung of whole-CB-transplant mice, not CD8 T cells

(Fig. 2B). These findings were also confirmed by immunohistochemistry studies of the lung specimens (Fig. 2C). These data suggest that the development of OB found in whole-CB-transplant mice involves donor-derived human CD3 lymphocytes, particularly CD4 T cells.

We next analyzed the expression profile of mRNAs of various inflammatory cytokines in human CD4 T cells isolated from the lung of whole-CB-transplant mice. We found that *IFNG*, *IL17A*, *IL21*, and *IL26* significantly increased over the course of GVHD development following whole CB transplantation, while *IL2*, *TNF* (TNF- α), *IL4*, *IL6* and *IL10* decreased.⁵¹ In addition, substantial increases were seen in the levels of *IFNG* and *IL26*, with *IL17A* and *IL21* remaining at a low level.⁵¹ It has been reported that IFN- γ and IL-26 are produced by T_H1 cells,⁵² while IFN- γ , IL-17A and IL-26 are produced by T_H17 cells.⁵³ Because both T_H1 and T_H17 cells strongly express CD26,^{15,20} we next analyzed the expression level of CD26/DPP4, demonstrating that *DPP4* mRNA expression in human CD4 T cells infiltrating in the lung of mice with OB significantly increased.⁵¹ These findings on expression levels of mRNA were also confirmed by examining protein levels in sera of recipient mice utilizing ELISA.⁵¹

To determine whether these cytokines were produced by the infiltrating human CD26⁺CD4 T cells, we next conducted flow cytometric analysis of lymphocytes isolated from the lung of whole CB or CD34⁺ transplant control mice. As shown in Fig. 2D, levels of human IFN- γ ⁺, and IL-26⁺CD26⁺CD4 T cells were significantly increased in whole-CB-transplant mice compared to CD34⁺ transplant control mice, while levels of IL-17A⁺CD26⁺CD4 T cells were similarly very low in both groups. These findings were also confirmed by immunohistochemistry studies of the lung specimens (Fig. 2E). To determine whether CD26⁺CD4 T cells produced IL-26, IFN- γ and/or IL17A, multicolor-staining flow cytometric studies were conducted. As shown in Fig. 2F-i, CD26⁺CD4 T cells in the lung of whole-CB-transplant mice predominantly produced IL-26 rather than IFN- γ . In addition, while CD26⁺IFN- γ ⁺CD4 cells exclusively expressed IL-26, CD26⁺IL-26⁺CD4 cells were pre-

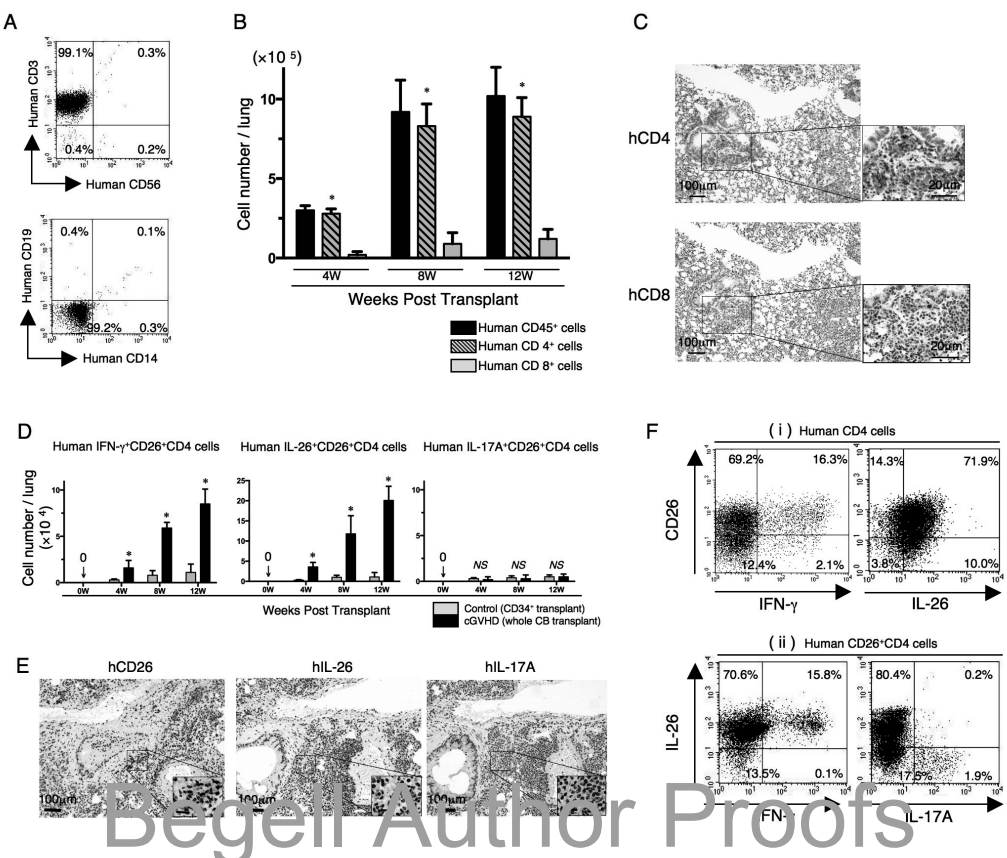


FIG. 2: Predominant infiltration of donor-derived CD4+ T cells in obliterative bronchiolitis of chronic GVHD. NOG mice were preconditioned and transplanted by the same method as in Fig. 1. (A) Representative 2-D dot plots of human lymphocyte composition in the lung of whole-CB-transplant mice (8 weeks post transplantation). Single-suspension cells isolated from the lung of whole-CB-transplant mice (8 weeks post transplantation) were sorted by human CD45⁺ cells and then analyzed using flow cytometry. The upper panel shows representative human CD3 and/or CD56 staining, and the lower panel, representative human CD19 and/or CD14 staining. Numbers indicate relative percentages per quadrant. (B) Absolute cell numbers (mean \pm SEM) of human CD45⁺, CD4⁺, or CD8⁺ cells per lung of whole-CB-transplant mice were quantified by flow cytometry. CD4⁺ T cells were predominantly observed in the lung of whole-CB-transplant mice. * $P<0.0001$ versus CD8⁺ cells. (C) Anti-human CD4 or CD8 immunohistochemistry of sequential sections of lung tissue of whole-CB-transplant mice (8 weeks post transplantation). Predominant infiltration of CD4⁺ cells was observed, with similar results to those obtained by flow cytometry as shown in panel F. Original magnification is 100X or 400X (inset in each panel). (D) Absolute cell numbers of human IFN- γ CD26⁺CD4, IL-26⁺CD26⁺CD4, or IL-17A⁺CD26⁺CD4 cells in the lung of CD34⁺ transplant or whole-CB-transplant mice were quantified by flow cytometry. * $P<0.0001$ versus corresponding CD34⁺ transplant group; NS, not significant. (E) Anti-human CD26, IL-26 or IL-17A immunohistochemical staining of sequential sections of the lung from whole-CB-transplant mice (8 weeks post transplantation). The lung of whole-CB-transplant mice was clearly infiltrated with human CD26 or IL-26 (brown stained cells) but not with IL-17A positive cells. Original magnification is 100X or 400X (inset in each panel). Scale bars in the inset indicate 20 μ m. (F) Representative 2-D dot plots of human CD26 and IFN- γ or IL-26 cells by gating for human CD4⁺ cells (panel i) and of human IFN- γ or IL-17A among IL-26⁺ cells by gating for human CD26⁺CD4⁺ cells (panel ii). Single-suspension cells isolated from the lung of whole-CB-transplant mice (8 weeks post transplantation) were sorted by human CD45⁺ cells then analyzed using flow cytometry. Numbers indicate relative percentages per quadrant [(B) – (F) reprinted with permission from The American Association of Immunologists, Inc., Copyright 2015].⁵¹

dominantly IFN- γ -negative cells, and IL-17A $^+$ cells were exclusively IL-26 negative (Fig. 2F-ii). These data suggest that CD26 $^+$ CD4 T cells in the lung of mice with OB express IL-26 as well as IFN- γ but do not belong to the T_H17 cell population.

IV. ROLE OF IL-26 IN CHRONIC GVHD

A. IL-26 in Immune System: an Overview

Originally discovered in *Herpesvirus saimiri*-transformed T cells,⁵⁴ IL-26 is now classified as belonging to the IL-10 family of cytokines.⁵³ Human IL-26 is a 171-amino acid protein that belongs to the IL-10 family of cytokines, a family that includes IL-10, IL-19, IL-20, IL-22, and IL-24.⁵⁵ The IL-26 protein is encoded by the *IL26* gene located on chromosome 12q15 between genes for interferon IFN- γ and IL-22^{52,56,57} and is conserved in several vertebrate species but not found in mice and rats.⁵² IL-26 is a secreted protein produced by T, NK cells, or synoviocytes,^{58,59} and binding of IL-26 to a distinct cell surface receptor consisting of IL-20RA and IL-10RB results in functional activation via STAT3 phosphorylation (Fig. 3).⁵⁶ Although IL-26 shares approximately 25% of its amino acid homology with IL-10 (and utilizes one of the IL-10 receptor subunits as a cell surface receptor),^{56,60} a growing body of evidence indicates that the functional effects of IL-26 differ substantially from those of IL-10. Functional studies are compatible with IL-26 driving or sustaining inflammation rather than suppressing it. In addition, IL-26 gene expression or protein production has been analyzed in patients with systemic sclerosis, RA, inflammatory bowel diseases (IBD), and hepatitis C virus (HCV) infection.^{59,61-64} IL-26 is evidently involved in chronic inflammatory disorders including autoimmune diseases (Fig. 4), but its role in acute inflammatory disorders and onset of chronic inflammatory disorders has yet to be established.

Because expression of IL-20RA, the key subunit of IL-26 receptor that mediates IL-26 signaling, is restricted to skin, intestine, and lungs, IL-26 is thought to promote defense mechanisms at mucosal

surfaces by bridging immune cells and epithelia. IL-26 exhibits priming effects on various immune cells to boost antiviral and antimicrobial responses. IL-26 induces TNF-related apoptosis-inducing ligand (TRAIL) on human NK cells that kill HCV-infected hepatocytes.⁶⁴ Moreover, IL-26 derived from CD68 $^+$ alveolar macrophages and T_H17 cells propel antimicrobial responses by priming the recruitment of neutrophils toward bacteria and assembled effector immune cells in the lungs and by triggering the production of plasmacytoid DC-derived IFN- α .^{65,66} Furthermore, it was reported that human T_H17-cell-derived IL-26 mediates protective immunity by direct microbicidal action due to its functional similarity to naturally occurring antimicrobial peptides. IL-26 inhibited the growth of gram-negative or -positive bacteria, including *Pseudomonas aeruginosa*, *Escherichia coli*, *Klebsiella pneumonia*, and *Staphylococcus aureus*, by direct bactericidal action.⁶⁶ Therefore, even when the limitations of current knowledge are taken into account, IL-26 emerges as an important player in host defense and inflammation, with the potential to represent a therapeutic target in infections and chronic inflammatory disorders (Fig. 4).

B. IL-26 Contributes to Collagen Deposition in the cGVHD Lung

Because significant collagen deposition was observed in peribronchial blood vessels in the lung of aGVHD (Fig. 1C),^{5,67} we sought to determine whether collagen production was induced by IFN- γ $^+$ and/or IL-26 $^+$ CD26 $^+$ CD4 T-cell infiltration in cGVHD lung. Although IFN- γ is a key regulator of cellular immunity, development of cGVHD lung has been reported to be independent of IFN- γ .⁶⁸ On the other hand, the effect of IL-26 on cGVHD pathophysiology has not yet been determined. We therefore focused on IL-26 as a potential effector cytokine for lung cGVHD. While the human IL-26 gene *IL26* is located adjacent to *IFNG* on chromosome 12q15, and the IL-26 gene is absent in rodents,^{52,69} we cannot formally exclude the possibility that human IL-26 activates murine cells. We therefore conducted *in vitro* assays to determine the effect of human IL-26 on murine

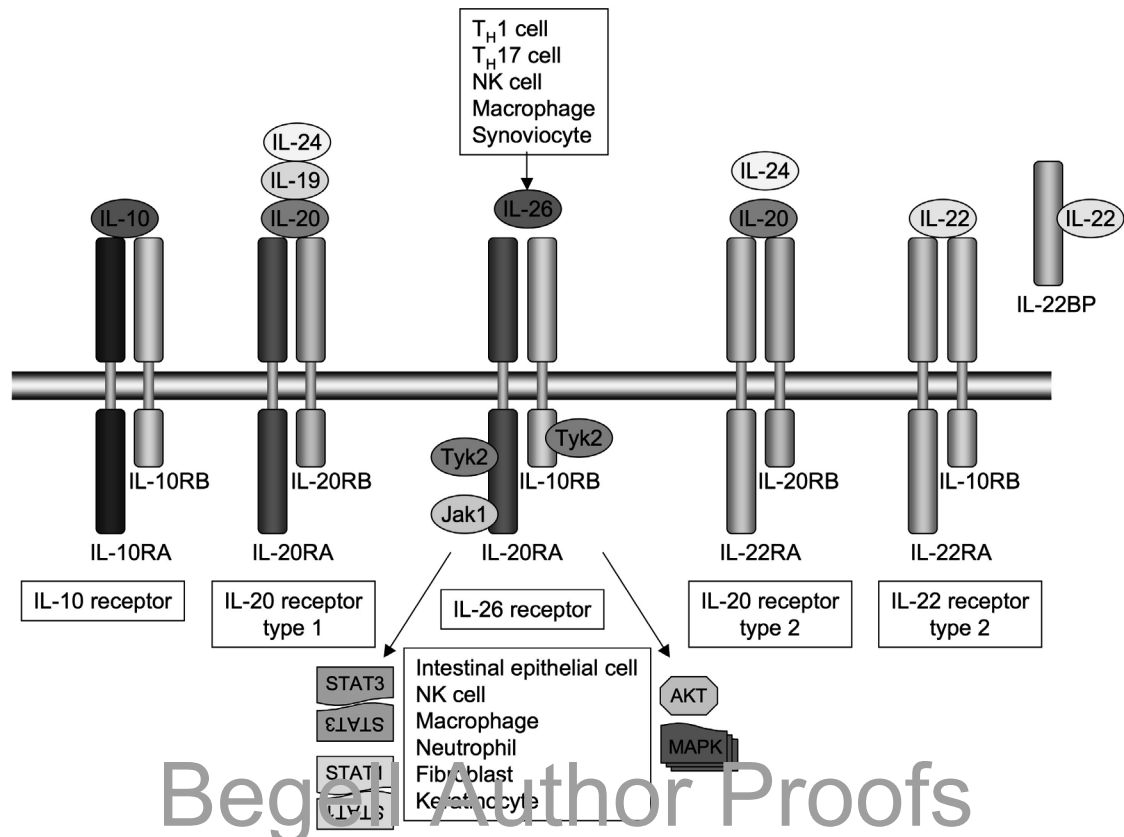


FIG. 3: Receptors and downstream signaling of IL-26 and other IL-10 family cytokines.

cells. We first showed that both IL-20RA and IL-10RB, a functional receptor complex for IL-26, were expressed in the murine fibroblast cell-line NIH3T3 as well as normal human lung fibroblast (NHLF).⁵¹ We next showed that exogenous recombinant human IL-26 induced phosphorylation of STAT3 in both NHLF and NIH3T3.⁵¹ These data indicate that human IL-26 is active not only in NHLF but also in murine fibroblasts. To examine a functional effect of IL-26 on murine fibroblast, we next conducted *in vitro* assays for collagen synthesis. We showed that an increase in collagen production in NIH3T3 as well as in NHLF was observed in a dose-dependent manner following the addition of exogenous IL-26 and that collagen production was inhibited by neutralizing anti-IL-20RA polyclonal antibody (pAb).⁵¹ These results strongly suggest that human IL-26 activates

both human and murine fibroblasts via IL-20RA, leading to increased collagen production.

To further extend the above *in vitro* results to an *in vivo* system, we analyzed the lung of murine alloreactive GVHD using human *IL26* transgenic (Tg) mice. For this purpose, we used mice carrying human *IFNG* and *IL26* transgene (190-*IFNG* Tg mice) or mice carrying human *IFNG* transgene with deleting *IL26* transcription (ΔCNS-77 Tg mice). 190-*IFNG* Tg mice exhibited production of IL-26 by CD4 T cells under T_H1- or T_H17-polarizing conditions, while expression of IL-26 was completely abrogated in ΔCNS-77 Tg mice.⁵² In addition, production of IFN- γ by T or NK cells was equivalent in both 190-*IFNG* Tg and ΔCNS-77 Tg mice.⁵⁷ As shown in Fig. 5A, lung histology of recipient NOG mice deriving from parental C57BL/6 (B6 WT) mice

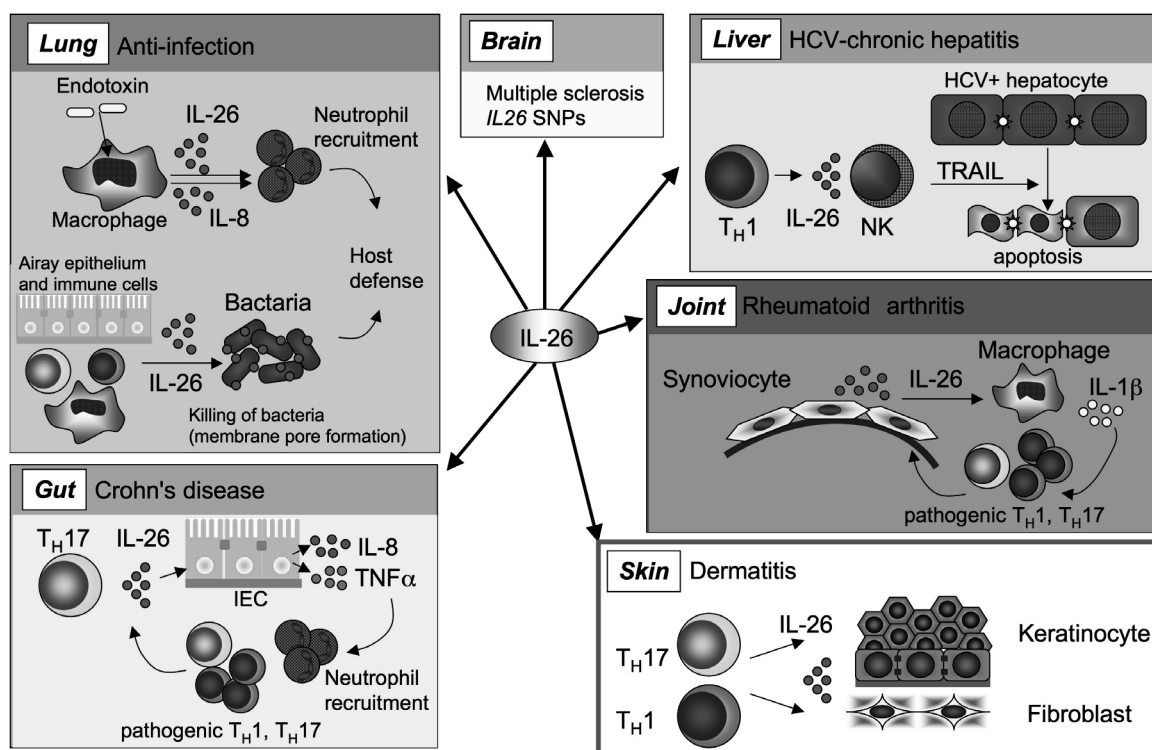


FIG. 4: Multifaceted actions of IL-26 in host defense and autoimmune responses. Upon activation, various immune cells including T_H1, T_H17, NK cells and macrophages secrete IL-26. IL-26 exerts antibacterial and antiviral actions through direct killing of bacteria by forming membrane pores, and by priming immune cells such as neutrophils, NK cells and plasmacytoid dendritic cells. Other cytokines might act in synergy with IL-26 to enhance these host defense actions. IL-26 response requires tight regulation as increased expression of IL-26 has been reported in several autoimmune and inflammatory diseases.

or Δ CNS-77 Tg mice showed peribronchial infiltration and cuffing denoting GVHD (panels a or g), while collagen deposit was not detected by Mallory staining (panels b or h), and IL-26⁺ cells were not detected (panels c or i). On the other hand, histology of recipient NOG mice deriving from 190-*IFNG* Tg mice showed peribronchial infiltration and cuffing denoting GVHD (panel d of Fig. 5A) with collagen deposition and IL-26⁺ cell infiltration (panels e and f of Fig. 5A). Significant increase in collagen deposition in the lungs of recipient NOG mice deriving from 190-*IFNG* Tg mice was quantified by collagen assays and shown in Fig. 5B. These results suggest that human IL-26, but not human IFN- γ , plays a critical role in pulmonary fibrosis associated with lung cGVHD.

V. ROLE OF CD26 IN CHRONIC GVHD

A. Molecular Mechanisms of T-Cell Response via CD26

In 1979, a large-molecular-weight complex composed of adenosine deaminase (ADA) activity was found to be an ADA-binding protein (ADBP), also known as adenosine deaminase complexing protein-2 (ADCP2).⁷⁰ In 1992, this ADBP (or ADCP2) was determined to be identical to CD26, a T-cell activation molecule and a 110-kD glycoprotein that is present also on epithelial cells of various tissues including the liver, kidney, and intestine.⁷¹⁻⁷³ The human CD26 cDNA contains a 3,465 base-pair (bp) open reading frame that encodes a 766-amino-acid protein. The

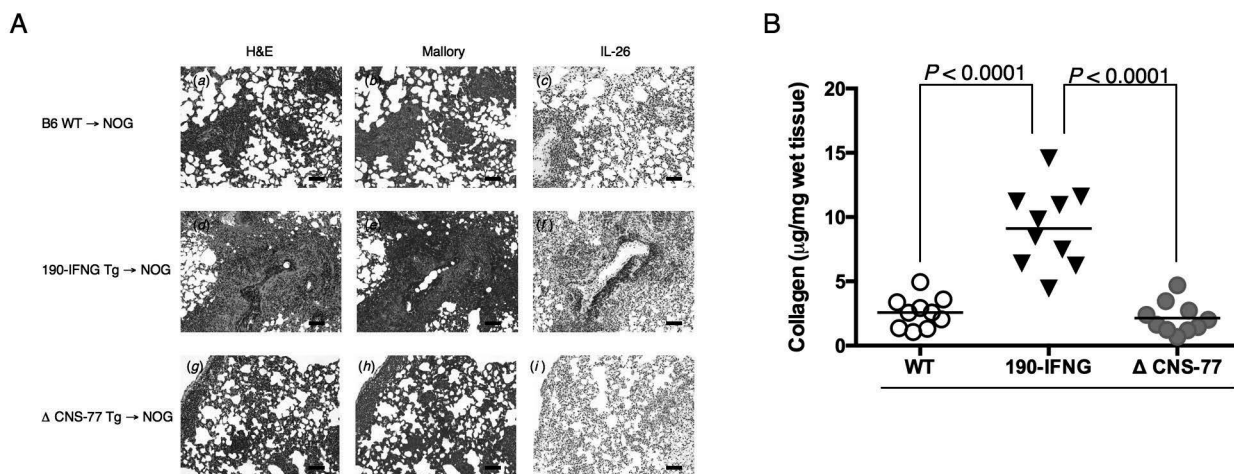


FIG. 5: Collagen deposition in cGVHD lung is induced in NOG mice receiving bone marrow (BM) cells and splenocytes of *IL26* transgenic (Tg) mice. (A) H&E, Azan-Mallory staining and anti-IL-26 immunohistochemistry of sequential sections of lung from NOG mice at 4 weeks after transplantation of BM and splenocytes isolated from parental B6 (WT) (*panels a-c*), 190-IFNG BAC Tg (*panels d-f*) or ΔCNS-77 Tg (*panels g-i*) mice. Lungs of recipients of 190-IFNG BAC Tg mice showed areas of collagen deposition and IL-26⁺ cell infiltration, while recipients of WT or ΔCNS-77 Tg mice showed BO and septal infiltration without collagen deposition or IL-26⁺ cells. Original magnification is 100X. Scale bars indicate 100μm. (B) Collagen contents in the lung were quantified by Sircol collagen assay. Each lung specimen was prepared from mice as shown in panel A. The mean number (\pm SEM) of total collagen contents (μ g) per wet lung tissue weight (mg) was determined. Increased collagen contents were clearly observed in recipients of 190-IFNG Tg mice, compared to those in recipients of B6 WT or ΔCNS-77 Tg mice. Each dot indicates individual value and horizontal bars indicate mean value (reprinted with permission from The American Association of Immunologists, Inc., copyright 2015).⁵¹

human CD26 amino acid sequence has 85% amino acid identity with the mouse and rat CD26.^{72,73} The 5'-flanking region does not contain a TATA box or CAAT box commonly found in housekeeping genes.^{74,75} CD26 does contain a 300-bp G-C-rich region with potential binding sites for NF-κB, AP2, or Sp1.⁷⁶ CD26 expression is activated by IFNs and retinoic acid in chronic lymphocytic leukemia via Stat1 α and the GAS (IFN- γ activation site) response element (TTCnnnGAA located at bp -35 to -27) in the CD26 promoter.⁷⁷

Human CD26 is composed of 766 amino acids (Fig. 6), including a short cytoplasmic domain of 6 amino acids, a transmembrane region of 22 amino acids, and an extracellular domain with dipeptidyl peptidase activity that selectively removes the N-terminal dipeptide from peptides with proline or

alanine at the penultimate position.⁷⁸ Analysis of single amino acid point mutations in the β-propeller motif identified Glu205 and Glu206 to be essential for DPPIV enzyme activity, and the central tunnel and α/β-hydrolase domains both participate in DPPIV inhibitor binding.⁷⁹⁻⁸¹ CD26/DPPIV was initially considered to cleave peptides only after a proline or alanine residue, but its substrates are now known to include hydroxyproline, serine, glycine, valine, threonine, and leucine.^{80,82,83} CD26 binds to caveolin-1 on APC, and residues 201 to 211 of CD26 along with the serine catalytic site at residue 630, which constitute a pocket structure of CD26/DPPIV, contribute to its binding to the caveolin-1 scaffolding domain.¹⁸ This region in CD26 contains a caveolin-binding domain ($\Phi X \Phi \text{XXXX} \Phi XX \Phi$; Φ and X depict aromatic residue and any amino

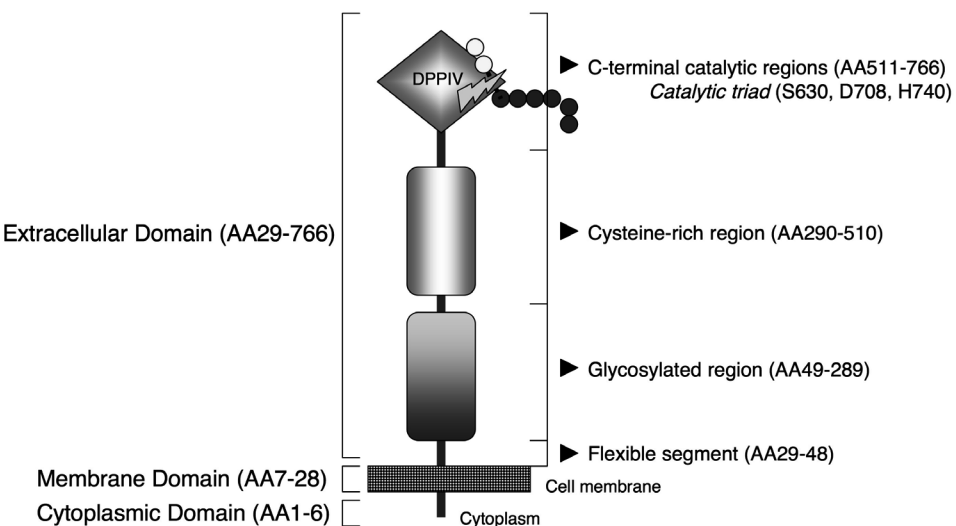


FIG. 6: Schematic diagrams of the amino acids of human CD26. Human CD26 cDNA is composed of 2,301 base pairs, translated to a 766-amino-acid protein. DPPIV catalyzes the hydrolysis of N-terminal dipeptides from polypeptides with proline or alanine in the penultimate position. See text for further details.

acid, respectively) specifically WVYEEFVFSAY in CD26. These observations strongly support the hypothesis that DPPIV enzyme activity is necessary for CD26-mediated T-cell costimulatory activation, as demonstrated in our previous work using CD26-targeted mAbs.^{15,84} Single-amino-acid point-mutation analysis showed that His750 residue is responsible for dimerization,⁸⁵ which is required for T-cell costimulation signaling.¹⁶

In human peripheral blood, CD26 is found on CD4⁺ T memory cells and CD8⁺ effector/memory T cells.^{12,86,87} It has been reported that 0–5% of freshly isolated CD20⁺ B cells do express the CD26 antigen.⁸⁸ Following stimulation with phorbol 12-myristate 13-acetate (PMA) or *Streptococcus aureus* protein, the fraction of CD26-positive cells increased to 51%.^{12,89} Meanwhile, CD26 is not expressed or is found only at low levels on monocytes of healthy adults.^{90,91} Only a small fraction of peripheral NK cells was found to express CD26.⁹²

CD26 is a costimulatory molecule for T-cell signal transduction. Whereas CD26 expression is enhanced following activation of resting T cells, CD4⁺CD26^{high} T cells respond maximally to recall

antigens such as tetanus toxoid.¹² In addition, CD4⁺ T cells with *in vitro* transendothelial migratory capacity appear to express high CD26.⁹³ Moreover, CD26^{high}CD8⁺ T cells in humans belong to early effector memory T cells, and CD26^{high}CD8⁺ T cells exhibit increased expression of granzyme B, TNF- α , IFN- γ and Fas ligand, and exert a cytotoxic effect with CD26-mediated costimulation.⁸⁷

The cytoplasmic tail of CD26 is responsible for T-cell costimulation induced by anti-CD3 plus caveolin-1.¹⁶ We found that CARMA1 binds to the cytoplasmic tail of dimeric CD26 and that a PDZ domain in CARMA1 is necessary for binding to CD26. Following its phosphorylation, CARMA1 functions as a signaling intermediate downstream of protein kinase θ (PKC θ) and upstream of I κ B kinase (IKK) in the T-cell receptor (TCR) signaling transduction pathway, which leads eventually to NF- κ B activation. Dimeric CD26, but not monomeric CD26, binds to CARMA1.¹⁶ The enzymatic pocket structure of the DPPIV catalytic site is necessary for binding of CD26 to caveolin-1, which leads to the upregulation of CD86 expression on APC (Fig. 7).¹⁷ Dimerization of CD26 is therefore not only

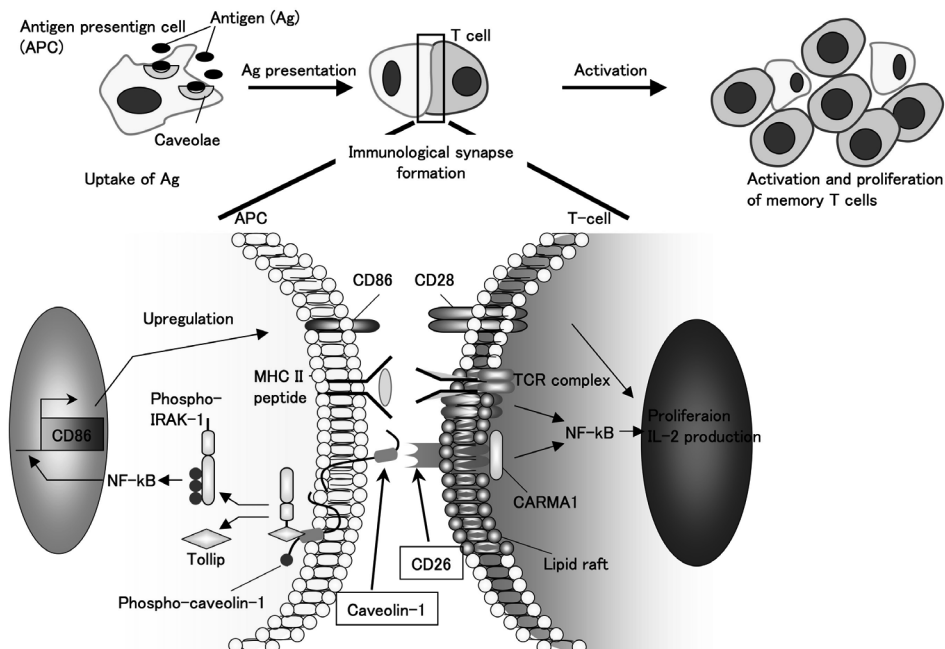


FIG. 7: Molecular mechanisms of CD26-caveolin-1 interaction in memory antigen response. Antigen-presenting cells (APC) take up recall antigens such as tetanus toxoid via caveolae. Following antigen uptake, a portion of caveolin-1 is exposed on the outer cell surface and aggregates in the APC-T-cell contact area in lipid rafts, presumably by homo-oligomerization. Aggregated caveolin-1 then binds to its specific ligand CD26, resulting in caveolin-1 phosphorylation. Phospho-caveolin-1 transduces a signal to the APC leading to dissociation of IRAK-1 and Tollip, followed by activation of NF-κB and finally resulting in CD86 upregulation and T-cell costimulation. On the T-cell side, binding by specific MHC-peptide complexes leads to TCR signal transduction. Additionally, caveolin-1 on the APC ligates CD26 dimers on the T-cell surface resulting in the recruitment of lipid rafts in the plasma membrane and the recruitment of CARMA1 to the cytosolic portion of CD26. Ultimately, these steps lead to the activation of NF-κB, and T-cell proliferation and IL-2 production.

necessary for binding to caveolin-1 but also serves as a scaffolding structure for the cytoplasmic signaling molecule CARMA1. Overall, CD26 ligation by caveolin-1 on APC recruits CD26-interacting CARMA1 to lipid rafts, resulting in the formation of a CARMA1-Bcl10-MALT1-IKK complex, and this membrane-associated Bcl10 complex then activates IKK through ubiquitination of NF-κB essential modulator (NEMO).¹⁴

B. IL-26 Production via CD26-Mediated T-Cell Costimulation

IL-26 is co-expressed with IFN-γ by T_H1 cells,⁵³ and CD26/DPPIV is preferentially expressed on T_H1

cells activated via CD26-mediated costimulation.¹⁵ In addition, CD26⁺CD4 T cells in the cGVHD lung predominantly produced IL-26 rather than IFN-γ (Fig. 2F). Thus, we hypothesize that human CD4 T cells produce IL-26 following CD26 costimulation. To test this hypothesis, we conducted *in vitro* costimulation experiments using HuCB CD4 T cells and analyzed expression of various inflammatory cytokines. We showed that levels of *IL26* and *DPP4* were significantly increased following CD26 costimulation compared with those in CD28 costimulation, while expression levels of *IL26* and *DPP4* were enhanced by CD28 or CD26 costimulation.⁵¹ On the other hand, expression levels of *IL2*, *IFNG*, and *IL17A* were not increased following either CD26 costimulation

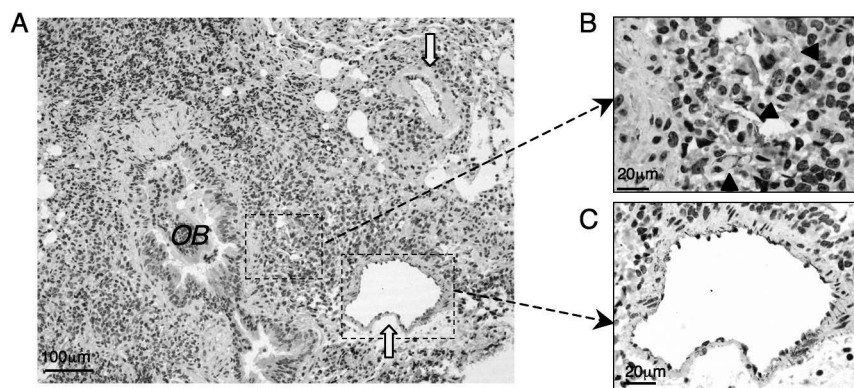


FIG. 8: Expression of caveolin-1 in the cGVHD lung of HuCB-NOG mice. Anti-caveolin-1 immunohistochemistry of the lung of whole-CB-transplant mice (8 weeks post transplantation). Caveolin-1 was detected on the epithelial cell surface (yellow arrows in *panel A*) and macrophage-like large cells (arrow heads in *panel B*) around inflammatory vessels (*panel C*) in obliterative bronchiolitis lesion (*OB* in *panel A*). Original magnification, 100X (*A*) and 400X (*B*, *C*).

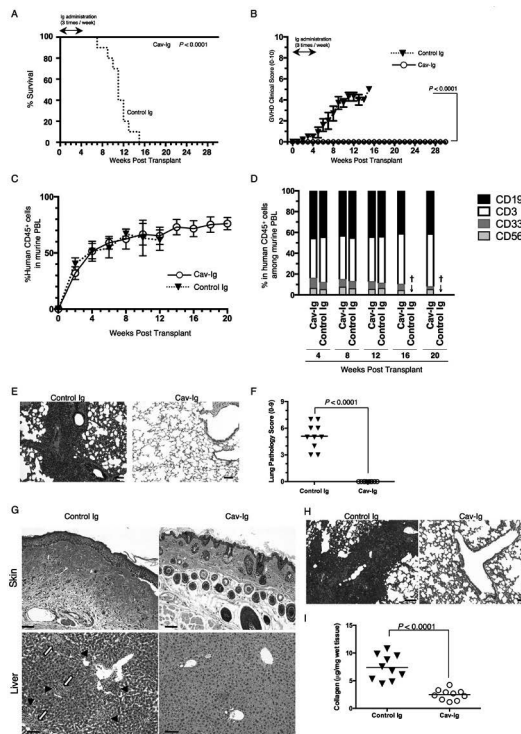
or CD28 costimulation, due to the immaturity of HuCB T cells, as was previously reported.^{43,94} We next conducted costimulation experiments evaluating dose and time kinetics using the CD26 costimulatory ligand Cav-Ig as well as anti-CD26 or anti-CD28 mAbs. We showed that production of IL-26 increased following CD26 costimulation with Cav-Ig or anti-CD26 mAb in dose- and time-dependent manners, while a slight increase in IL-26 level was observed following CD28 costimulation only at higher doses of mAb and longer stimulation periods.⁵¹ Blocking experiments were then performed for further confirmation, showing that IL-26 production induced by Cav-Ig or anti-CD26 mAb was clearly inhibited by treatment with soluble Cav-Ig in a dose-dependent manner, while no change was observed with CD28 costimulation. These findings strongly suggest that production of IL-26 by HuCB CD4 T cells is regulated via CD26-mediated costimulation. Moreover, because the functional sequences of the N-terminal of caveolin-1 are highly conserved between human and mouse,⁹⁵ allowing for the capability to bind human CD26 as a costimulatory ligand, it is conceivable that donor HuCB T cells transferred into mice were activated via CD26 costimulation triggered by murine caveolin-1. In fact, using pAb recognizing the

N-terminal of both human and murine caveolin-1, expression of caveolin-1 was detected in endothelial cells and macrophage-like cells of OB-like lesions in cGVHD lung (Fig. 8). Taken together, CD26-mediated IL-26 production triggered by caveolin-1 is identified as a possible therapeutic target in cGVHD using HuCB NOG mice.

VI. TARGETING CD26 IN CHRONIC GVHD

A. Prophylaxis of Lung cGVHD by Cav-Ig Administration

Given the role of CD26 costimulation in IL-26 production and IL-26 regulation of collagen production, we therefore sought to determine whether disruption of CD26 costimulation by a blocking reagent, Cav-Ig, prolonged survival of the recipient mice associated with a reduction in the incidence of OB. Recipients treated with Cav-Ig survived for 7 months without any clinical findings of GVHD (Figs. 9A and B). Meanwhile, the survival rate of recipient mice treated with control Ig was significantly reduced (Fig. 9A), with clinical signs/symptoms of GVHD (Fig. 9B). Human cells were engrafted similarly in both groups



Begell Author Proofs

FIG. 9: Administration of Cav-Ig prevents obliterative bronchiolitis by reducing the level of IL-26⁺CD26⁺CD4 cells and collagen deposition. Sublethally irradiated NOG mice were transplanted with 1×10^7 mononuclear cells isolated from HuCB. Cav-Ig or control Ig (each 100 μ g/dose) was administered intraperitoneally thrice a week, beginning at day +1 after transplantation until day +28. (A) Overall survival and (B) clinical GVHD score (mean \pm SEM). (C) Engraftment of human leukocytes in recipient mice. Peripheral blood of recipient mice was harvested at the indicated time points, and human CD45⁺ cell population was analyzed using flow cytometry. Data are shown as mean \pm SEM of human CD45⁺ cells among total PBL. (D) Sustained composition of human leukocyte populations in recipient PBL. PBL harvested from each group were stained for human CD3, CD19, CD33 or CD56 among human CD45⁺ cells. Data are presented as mean percentages of human CD45⁺ cells. Cross indicates death of all mice in control Ig group. (E) H&E staining of the lung of recipients administered with control Ig or Cav-Ig group (6 weeks post transplantation). Original magnification is 100X. Scale bars indicate 100 μ m. (F) Pathologic damage in the lung of recipients administered with Cav-Ig or control Ig was examined at 6 weeks post transplantation, using a semi-quantitative scoring system. Each dot indicates individual value and horizontal bars indicate mean value. (G) H&E staining of the skin and liver tissues for the control Ig group or Cav-Ig group evaluated at 6 weeks post transplantation. The skin specimen of the control Ig group showed sclerotic changes including acanthosis, loss of rete ridge, fat loss, follicular drop-out, and homogenized collagen deposition, in contrast to the normal appearance of the skin of the Cav-Ig group. The liver specimen of the control Ig group showed portal inflammation (arrow heads) and portal collagen deposition (yellow arrows), which were not observed in the Cav-Ig group. Original magnification is 100X. Scale bars indicate 100 μ m. (H) Collagen deposition was determined in the lung tissues of recipients of Cav-Ig or control Ig group (6 weeks post transplantation) with an Azan-Mallory staining. Original magnification is 100X. Scale bars indicate 100 μ m. (I) Collagen contents in the lung of recipients of Cav-Ig or control Ig group (6 weeks post transplantation) were quantified by Sircol Collagen Assay. The mean number (\pm SEM) of total collagen contents (μ g) per wet lung tissue weight (mg) was determined. Decreased collagen contents were clearly observed in recipients of Cav-Ig group. Each dot indicates individual value and horizontal bars indicate mean value (reprinted with permission from The American Association of Immunologists, Inc., copyright 2015).⁵¹

as shown in Figs. 9C and D. Histologic findings of the lung showed the development of OB in control Ig while appearing normal in Cav-Ig-recipient mice, with none having positive pathology scores (Figs. 9E and F). These effects of Cav-Ig were also observed in other GVHD-target organs such as the skin and liver (Fig. 9G). Moreover, collagen contents in the lung were reduced in Cav-Ig-administered recipients (Figs. 9H and I). Taken together, these results support the notion that Cav-Ig administration prevents the development of pulmonary GVHD in whole-CB-transplant mice by decreasing the number of IL-26⁺CD26⁺CD4 T cells.

B. Therapeutic Administration of Cav-Ig after Onset of GVHD

Because pulmonary GVHD progresses in an indolent manner over weeks and months, patients are often affected by the clinical findings prior to being diagnosed with cGVHD.²⁴ We therefore sought to determine whether blockade of caveolin-1/CD26 interaction effectively suppresses OB development following the appearance of clinical signs/symptoms. For this purpose, treatment began on day 29 following the appearance of an increase in GVHD scores, indicating the early stages of cGVHD development. Recipients treated with Cav-Ig survived for 7 months with remission of GVHD symptoms (Figs. 10A and B). Meanwhile, the survival rate of recipients treated with control Ig was significantly decreased (Fig. 10A), with progression of clinical signs/symptoms of GVHD (Fig. 10B). Human cells were engrafted similarly in both groups (Figs. 10C and D). In contrast to progressive OB of control Ig treated-recipients, peribronchial inflammation shown at post transplantation week 5 was attenuated at post transplantation week 10 in Cav-Ig-treated recipients (Fig. 10E). On the other hand, the pathologic scores of control Ig-treated recipients were significantly increased at 10 weeks compared to those at week 5 (Fig. 10F). Meanwhile, the pathologic scores of Cav-Ig treated recipients were significantly reduced at week 10 compared to those at week 5 (Fig. 10F), and these scores were clearly less than those of control Ig-treated recipients (Fig. 10F). These effects of Cav-Ig administration were also observed in the skin and liver (Figs. 10G, H, I and J). Moreover, levels of human IFN- γ ⁺ and IL-26⁺CD26⁺CD4 T cells in the lung of control Ig-treated recipients were significantly increased at 10 weeks compared to those at week 5 (* of Fig. 10K). On the other hand, levels of human IFN- γ ⁺ and IL-26⁺CD26⁺CD4 T cells in the lung of Cav-Ig-treated recipients were significantly reduced at week 10 compared to those at week 5 (** of Fig. 10K), and these levels were clearly less than those of control Ig treated-recipients (** of Fig. 10K). Furthermore, total collagen contents in the lung were significantly lower in Cav-Ig-treated recipients than control Ig-treated recipients (Fig. 10L). Taken together, these data suggest that Cav-Ig administration not only prevents the development of cGVHD but also represents a novel therapeutic approach for the early stages of cGVHD by regulating levels of IL-26⁺CD26⁺CD4 T cells.

C. Treatment with Cav-Ig Preserves GVL Capacity

Because GVHD and GVL effect are highly linked immune reactions,⁹⁶ we evaluated the potential influence of Cav-Ig treatment on GVL effect. For this purpose, cohorts of Cav-Ig-treated or control Ig-treated whole-CB-transplant mice were irradiated at sublethal doses and then injected intravenously with luciferase-transfected A20 (A20-luc) cells 1 day prior to whole CB transplantation to allow for dissemination of tumor cells. In day 1 following transplantation, treatment with Cav-Ig or control Ig three times per week began and continued to day 28. Mice inoculated with A20 cells alone all died of tumor progression within 6 weeks (Figs. 11A and B). Recipients treated with control Ig exhibited clinical evidence of GVHD such as weight loss and ruffled fur and died of GVHD without tumor progression in 13 weeks (Figs. 11A and B). In contrast, recipient mice treated with Cav-Ig displayed significantly prolonged survival (Fig. 11A) without involvement of A20-luc cells (Fig. 11B). To better characterize the potency of the GVL effect, we

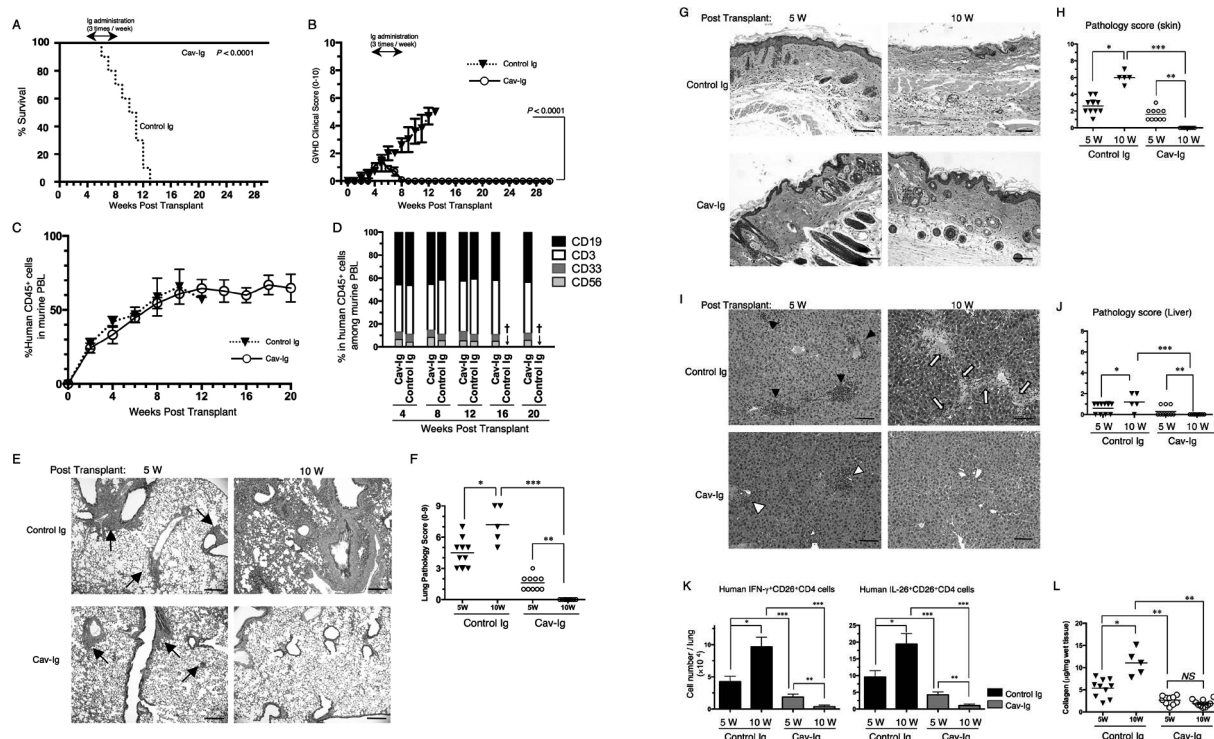


FIG. 10: Administration of Cav-Ig during early GVHD development impedes lethal GVHD by reducing the level of IL-26⁺CD26⁺CD4 cells and collagen deposition in the lung. Splenically irradiated NUG mice were transplanted with 1×10^7 mononuclear cells isolated from HuCB. Cav-Ig or control Ig (each 100 μ g/dose) was administered intraperitoneally three times per week, beginning at day 29 after transplantation and continued until day 56. (A) Overall survival and (B) clinical GVHD score (mean \pm SEM). (C) Peripheral blood of recipients was harvested at the indicated time points, and populations of human CD45⁺ cells were analyzed using flow cytometry. Data are shown as mean \pm SEM of human CD45⁺ cells among total PBL. (D) Sustained composition of human leukocyte populations in recipient PBL. PBL harvested from each group were stained for human CD3, CD19, CD33, or CD56 among human CD45⁺ cells. Data are presented as mean percentages of human CD45⁺ cells. Cross indicates death of all mice in control Ig group. (E) H&E staining of the lung tissues of control Ig group and Cav-Ig group at 5 weeks or 10 weeks post transplantation. Arrows indicate perivascular and peribronchial inflammation of the small airway. Original magnification is 100X. Scale bars indicate 100 μ m. (F) Pathologic damage in the lung of recipients administered with Cav-Ig or control Ig was examined at 5 and 10 weeks post transplantation using a semiquantitative scoring system. Each dot indicates individual value and horizontal bars indicate mean value. (G) H&E staining of the skin tissues of control Ig group or Cav-Ig group at 5 weeks or 10 weeks post transplantation. Normal skin histology was observed in recipient mice with Cav-Ig administration, in contrast to sclerodermatous changes developed in recipient mice with control Ig administration. Original magnification is 100X. Scale bars indicate 100 μ m. (H) Pathologic damage in the skin of recipients administered with Cav-Ig or control Ig was examined at 5 and 10 weeks post transplantation using a semiquantitative scoring system. Recipients of control Ig developed progression of GVHD pathology (*, $P < 0.0001$). In contrast, recipients of Cav-Ig showed significant reduction in GVHD pathology at 10 weeks rather than at 5 weeks post transplantation (**, $P < 0.0001$), and also as compared to recipients of control Ig group at 10 weeks (***, $P < 0.0001$). Each dot indicates individual value and horizontal bars indicate mean value. (I) H&E staining of the liver tissues of control Ig group or Cav-Ig group at 5 weeks or 10 weeks post transplantation. In recipient mice with Cav-Ig administration, portal inflammation was observed at 5 weeks post transplantation (white arrow heads), with restoration to normal appearance at 10 weeks post transplantation. In contrast, portal inflammation was observed in recipient mice with control Ig administration at 5 post transplantation (black arrow heads) and portal

fibrosis, at 10 weeks post transplantation (yellow arrows). Original magnification is 100X. Scale bars indicate 100 μ m. (J) Pathologic damage in the livers of recipients administered with Cav-Ig or control Ig was examined at 5 and 10 weeks post transplantation using a semiquantitative scoring system. Recipients of control Ig developed progression of GVHD pathology (*, $P<0.05$). In contrast, recipients of Cav-Ig showed significant reduction in GVHD pathology at 10 weeks rather than at 5 weeks post transplantation (**, $P<0.0001$), and also as compared to recipients of control Ig group at 10 weeks (***, $P<0.0001$). Each dot indicates individual value and horizontal bars indicate mean value. (K) Absolute cell number of human IFN- γ ⁺ or IL-26⁺CD26⁺CD4 cells in the lung of recipients of Cav-Ig or control Ig group. *, **, or *** indicates $P<0.0001$. (L) Collagen contents in the lung of recipients of Cav-Ig or control Ig group (5 and 10 weeks post transplantation) were quantified by Sircol collagen assay. The mean number (\pm SEM) of total collagen contents (μ g) per wet lung tissue weight (mg) was determined. Each dot indicates individual value and horizontal bars indicate mean value. * or ** indicates $P<0.0001$; NS, not significant [(A) – (F) reprinted with permission from The American Association of Immunologists, Inc., copyright 2015].⁵¹

repeated these studies with injection of A20-luc cells on day 28 after whole CB transplantation to allow for the acquisition of immunosuppression by Cav-Ig treatment. Mice inoculated with A20 cells alone all died of tumor progression within 2 weeks after tumor inoculation (Figs. 11C and D). Recipient mice treated with control Ig demonstrated clinical evidence of GVHD such as weight loss and ruffled fur and died of GVHD without tumor progression within 13 weeks after transplantation (Figs. 11C and D). In contrast, recipients treated with Cav-Ig exhibited significantly prolonged survival (Fig. 11C) without involvement of A20-luc cells (Fig. 11D). Collectively, these results demonstrate that Cav-Ig treatment of whole-CB-transplant mice was effective in reducing the symptoms of cGVHD without a concomitant loss of the GVL effect.

VII. PERSPECTIVES

While the human CD26 amino acid sequence has 85% amino acid identity with the mouse CD26,⁷² the mouse CD26 has different biologic properties from the human CD26, including the fact that the mouse CD26 is not a T-cell activation marker and does not bind to ADA.^{72,97} Therefore, humanized murine models need to be developed to explore the role of CD26-mediated costimulation in cGVHD. With relevance as a costimulatory ligand for human CD26, human caveolin-1 has 95% amino acid identity with the mouse caveolin-1,⁹⁵ and the binding regions

of the mouse caveolin-1 for human CD26 are well conserved. Costimulatory activation of human T cells in NOG mice therefore can occur via CD26–caveolin-1 interaction. Moreover, the N-terminal domain is present in the outer cell surface during the antigen presenting process,¹⁸ and caveolin-1 forms homodimer or homo-oligomer via its N-terminal domain.⁹⁵ These collective data suggest that the administered Cav-Ig binds to the N-terminal of caveolin-1 on the cell surface of APCs as well as to CD26 in T cells, leading to suppression of cGVHD in HuCB-NOG mice via blockade of CD26–caveolin-1 interaction.

In addition to the priming of donor-derived T cells by APCs, production of effector cytokines in the target organs plays an important role in cGVHD development.¹ In the present study, we found that donor-derived CD4 T cells predominantly infiltrated the OB lesions of HuCB-NOG mice and that IL-26 as well as IFN- γ levels were enhanced significantly in the infiltrating human CD26⁺CD4 T cells. Although there has been little information available regarding the biological functions of IL-26 using animal models due to the absence of the IL-26 gene in mouse,^{52,69} we demonstrated the role of IL-26 in lung fibrosis using a humanized murine cGVHD model. Moreover, our murine allogeneic transplantation model utilizing 190-*IFNG* Tg and Δ CNS-77 Tg mice demonstrated that human IL-26, not IFN- γ , induced pulmonary fibrosis. In both 190-*IFNG* Tg and Δ CNS-77 Tg mice, production of IFN- γ by T or NK cells is equivalent in both tissue culture studies and analysis of basal levels in various tissues including spleen, lymph

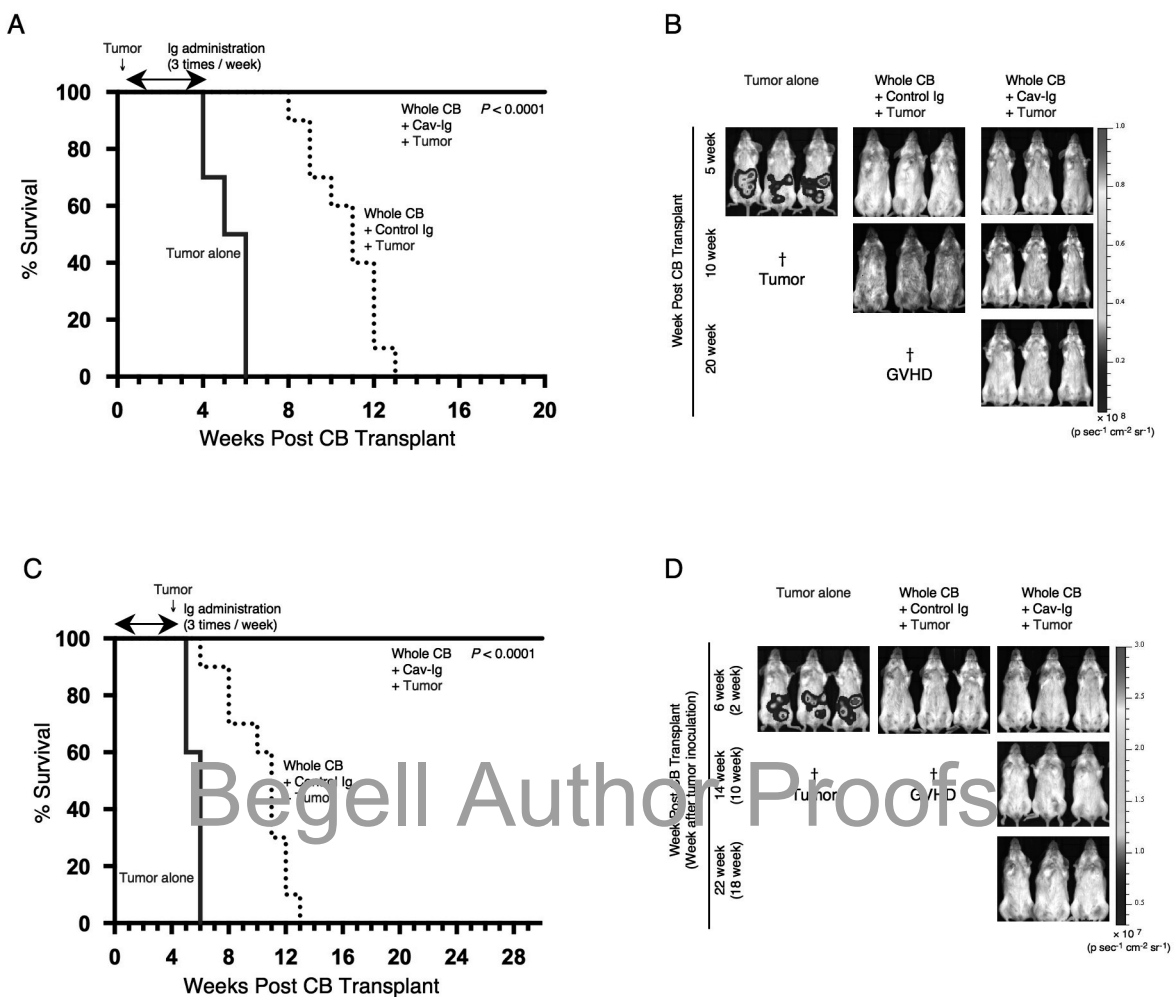


FIG. 11: Cav-Ig preserves GVL effect. (A) NOG mice were irradiated at a sublethal dose (200 cGy) and the next day were inoculated with 1×10^4 A20-luc cells via tail vein. The mice were then transplanted the following day with 1×10^7 mononuclear cells isolated from HuCB. Cav-Ig or control Ig (each 100 μ g/dose) was administered intraperitoneally thrice a week, beginning at day 1 after transplantation and continued until day +28. Overall survival is depicted. $P < 0.0001$ versus recipients of control Ig by log-rank test. (B) *In vivo* bioluminescence imaging (BLI) was performed at the indicated time points after treatment as described in panel A. Representative mice are shown. Cross indicates death of all mice in the group of tumor alone or control Ig groups. Ruffled fur consistent with skin GVHD is shown in recipients of control Ig group at 10 weeks post transplant (middle panel). (C) Sublethally irradiated NOG mice were transplanted with mononuclear cells isolated from HuCB. Cav-Ig or control Ig was administered intraperitoneally three times per week, beginning at day 1 after transplantation and continued until day +28. 1×10^5 A20-luc cells were inoculated via tail vein on day +28 post transplantation. Overall survival is depicted. $P < 0.0001$ versus recipients of control Ig by log-rank test. (D) *In vivo* BLI was performed at the indicated time points after treatment as described in panel C. Representative mice are shown. Cross indicates death of all mice in the group of tumor alone or control Ig groups. Slightly ruffled fur consistent with skin GVHD is shown in recipients of control Ig group at 6 weeks post transplant (middle panel).

node, and colon.⁵⁷ On the other hand, expression of IL-26 is observed in T_H1- or T_H17-polarizing CD4 cells of 190-*IFNG* Tg mice, whereas it is completely abrogated in ΔCNS-77 Tg mice.⁵² Although human and murine IFN- γ share 40% amino acid identity, IFN- γ exhibits species specificity with respect to receptor binding and biological activity.^{98,99} Taken together with the previous report that development of cGVHD lung is independent of IFN- γ ,⁶⁸ the elevated human IFN- γ in HuCB-NOG did not likely function as an inflammatory cytokine but rather as a T_H1 and/or T_H17 cell marker of CD26⁺CD4 T cells.^{15,20,100} Regarding its specific receptor, IL-26 primarily binds to IL-20RA, followed by recruitment of IL-10RB.⁵⁶ Although IL-10RB is broadly expressed on most cell types and tissues, IL-20RA is not expressed in lymphoid organs but is expressed in the lung and skin.¹⁰¹ It is thus conceivable that IL-26-related chronic inflammatory changes in HuCB-NOG mice occur in the lung and skin of cGVHD or autoimmune diseases, including systemic sclerosis.

Recent work with a murine model showed that donor-derived B-cell activation and maturation with the aid of TfH were necessary for cGVHD and that bronchiolitis obliterans syndrome was reversed by the abrogation of IL-21 signaling.³⁰ However, in our present model with OB, a substantial B-cell population was detected in the recipient PBL. In fact, no direct evidence for a causal relationship for autoantibodies or alloantibodies in the pathogenesis of organ manifestation of cGVHD has been observed in humans.²⁹ Furthermore, cGVHD of the visceral organs seemed to respond poorly to B-cell depletion therapy such as rituximab.^{29,37} It is speculated that this observed discrepancy is due to differences in the B-cell maturation process between mice and human.⁴⁰ Despite these limitations of murine or humanized murine models, targeting CD4 T cells to control cGVHD is a reasonable therapeutic approach because T cell help plays a pivotal role in B-cell maturation and activation in cGVHD.¹⁰² A related issue concerns the process of B-cell development in humanized mice. Given the fact that HuCB contains ample HSCs as well as naïve lymphocytes, the use of HuCB as donor cells led to sustained recovery of

lymphocytes in the recipient PBL, as had also been reported by other investigators.^{46,48,49,103} In addition, it has been demonstrated that specific antibodies in human B cells generated in the humanized mice transplanted with HSC isolated from HuCB were effectively synthesized.^{45,46,48,50} Despite the limitations of cross-species comparisons, our study provides insights into the pathogenesis of clinical pulmonary cGVHD induced by human lymphocytes.

Because we previously showed an effect of anti-CD26 mAb on an aGVHD model using adult PBL,⁴² we performed preliminary testing of anti-CD26 mAb effect on recipient mice of whole-CB-transplant, and found a high incidence of graft failure. Our speculation regarding the reason for this failure is this: We previously reported that HuCB CD4 T cells broadly express CD26,⁴³ and other investigators observed that CD34⁺CD38^{low/−} or CD34⁺CD38⁺ hematopoietic stem/progenitor cells in HuCB preferentially express CD26.¹⁰⁴ These findings suggest that treatment with anti-CD26 mAb in a HuCB transplant model may reduce the levels of hematopoietic stem/progenitor and/or CD4 T cells in the graft of HuCB, resulting in increased graft failure.

Importantly, there may be potential adverse events such as off-target effects associated with the proposed use of Cav-Ig therapy. Although caveolin-1 exists in the inner surface of most cell types,⁹⁵ its N-terminus is detected on endothelial cells as well as APCs following cellular activation.¹⁰⁵ Therefore, it is possible that Cav-Ig binds to cell surface caveolin-1, thereby affecting endothelial cell functions. Other issues relate to the GVL effects. Our data demonstrated that Cav-Ig clearly impeded GVHD in our model with preservation of GVL effects. We speculate that CD26-dependent xenogeneic priming of CD4 T cells is inhibited by Cav-Ig,^{19,42} while CD28-dependent GVL effects are exerted after engraftment.¹⁰⁶

Based on our study, it is conceivable that IL-26 may be another potential therapeutic target in the management of clinical cGVHD. We have already developed several clones of anti-IL-26 mAb that have been screened for inhibitory effects on various cells expressing IL-26 receptor. IL-26 has been reported to

Begell Author Proofs

exhibit antibacterial and antiviral effects as part of a host defense mechanism.⁶⁶ We are currently actively investigating whether anti-IL-26 therapy exacerbates bacterial infections in the presence of GVHD following HSCT, and definitive data regarding the effects of IL-26-targeted therapy will be presented in the near future.

In conclusion, our present work demonstrates that caveolin-1 blockade controls cGVHD by suppressing the immune functions of donor-derived T cells and decreasing IL-26 production. Moreover, IL-26⁺CD26⁺CD4 T-cell infiltration appears to play a significant role in cGVHD of the lung and skin. While complete suppression of cGVHD with current interventional strategies represents a difficult challenge at the present time, our data demonstrate that control of cGVHD clinical findings can be achieved in a murine experimental system by regulating IL-26⁺CD26⁺CD4 T cells with Cav-Ig. Our work also suggests that Cav-Ig treatment may be a novel therapeutic approach for chronic inflammatory diseases, including RA and IBD, in which IL-26 plays an important role.

ACKNOWLEDGMENTS

This work was supported by JSPS KAKENHI (grant nos. 15H04879 and 15K15324 to K.O.); JSPS KAKENHI (grant no 16H05345 to C.M.); JSPS KAKENHI (grant no. 16K09878 to N.I.); JSPS Research Fellowships for Young Scientists (R.H.); a grant from the Ministry of Health, Labour, and Welfare, Japan (grant no. 150401-01 to C.M.); and a Grant-in-Aid from the Foundation of Strategic Research Projects in Private Universities from the Ministry of Education, Culture, Sports, Science, and Technology, Japan (grant no. S1311011 to K.O. and C.M.).

REFERENCES

- Blazar BR, Murphy WJ, Abedi M. Advances in graft-versus-host disease biology and therapy. *Nat Rev Immunol*. 2012;12:443–58.
- Deeg HJ, Lin D, Leisenring W, Boeckh M, Anasetti C, Appelbaum FR, Chauncey TR, Doney K, Flowers M, Martin P, Nash R, Schoch G, Sullivan KM, Witherspoon RP, Storb R. Cyclosporine or cyclosporine plus methylprednisolone for prophylaxis of graft-versus-host disease: a prospective, randomized trial. *Blood*. 1997;89:3880–7.
- Filipovich AH. Diagnosis and manifestations of chronic graft-versus-host disease. *Best Pract Res Clin Haematol*. 2008;21:251–7.
- Socie G, Ritz J. Current issues in chronic graft-versus-host disease. *Blood*. 2014;124:374–84.
- Chien JW, Duncan S, Williams KM, Pavletic SZ. Bronchiolitis obliterans syndrome after allogeneic hematopoietic stem cell transplantation—an increasingly recognized manifestation of chronic graft-versus-host disease. *Biol Blood Marrow Transplant*. 2010;16:S106–14.
- Dudek AZ, Mahaseth H, DeFor TE, Weisdorf DJ. Bronchiolitis obliterans in chronic graft-versus-host disease: analysis of risk factors and treatment outcomes. *Biol Blood Marrow Transplant*. 2003;9:657–66.
- Nakasone H, Kanda J, Yano S, Atsuta Y, Ago H, Fukuda T, Kakihana K, Adachi T, Yujiri T, Taniguchi S, Taguchi J, Morishima Y, Nagamura T, Sakamaki H, Mori T, Murata M: GVHD Working Group of the Japan Society for Hematopoietic Cell Transplantation. A case–control study of bronchiolitis obliterans syndrome following allogeneic hematopoietic stem cell transplantation. *Transplant Intl*. 2013;26:631–9.
- Zeiser R, Blazar BR. Preclinical models of acute and chronic graft-versus-host disease: how predictive are they for a successful clinical translation? *Blood*. 2016;127:3117–26.
- Champlin R, Khouri I, Giralt S. Graft versus malignancy with allogeneic blood stem cell transplantation: a potential primary treatment modality. *Pediatr Transplant*. 1999;3 Suppl 1:52–8.
- Rudd CE. T-cell signaling and immunopathologies. *Semin Immunopathol*. 2010;32:91–4.
- Fox DA, Hussey RE, Fitzgerald KA, Acuto O, Poole C, Palley L, Daley JF, Schlossman SF, Reinherz EL. Ta1, a novel 105 KD human T cell activation antigen defined by a monoclonal antibody. *J Immunol*. 1984;133:1250–6.
- Morimoto C, Torimoto Y, Levinson G, Rudd CE, Schriber M, Dang NH, Letvin NL, Schlossman SF. 1F7, a novel cell surface molecule, involved in helper function of CD4 cells. *J Immunol*. 1989;143:3430–9.
- Dang NH, Torimoto Y, Deusch K, Schlossman SF, Morimoto C. Comitogenic effect of solid-phase immobilized anti-1F7 on human CD4 T cell activation via CD3 and CD2 pathways. *J Immunol*. 1990;144:4092–100.
- Ohnuma K, Dang NH, Morimoto C. Revisiting an old acquaintance: CD26 and its molecular mechanisms in T cell function. *Trends Immunol*. 2008;29:295–301.
- Morimoto C, Schlossman SF. The structure and function of CD26 in the T-cell immune response. *Immunol Rev*. 1998;161:55–70.
- Ohnuma K, Uchiyama M, Yamochi T, Nishibashi K, Hosono O, Takahashi N, Kina S, Tanaka H, Lin X, Dang NH, Morimoto C. Caveolin-1 triggers T-cell activation

- via CD26 in association with CARMA1. *J Biol Chem.* 2007;282:10117–31.
- 17. Ohnuma K, Yamochi T, Uchiyama M, Nishibashi K, Iwata S, Hosono O, Kawasaki H, Tanaka H, Dang NH, Morimoto C. CD26 mediates dissociation of Tollip and IRAK-1 from caveolin-1 and induces upregulation of CD86 on antigen-presenting cells. *Mol Cell Biol.* 2005;25:7743–57.
 - 18. Ohnuma K, Yamochi T, Uchiyama M, Ishibashi K, Yoshikawa N, Shimizu N, Iwata S, Tanaka H, Dang NH, Morimoto C. CD26 up-regulates expression of CD86 on antigen-presenting cells by means of caveolin-1. *Proc Natl Acad Sci U S A.* 2004;101:14186–191.
 - 19. Ohnuma K, Uchiyama M, Hatano R, Takasawa W, Endo Y, Dang NH, Morimoto C. Blockade of CD26-mediated T cell costimulation with soluble caveolin-1-Ig fusion protein induces anergy in CD4⁺ T cells. *Biochem Biophys Res Commun.* 2009;386:327–32.
 - 20. Bengsch B, Seigel B, Flecken T, Wolanski J, Blum HE, Thimme R. Human Th17 cells express high levels of enzymatically active dipeptidylpeptidase IV (CD26). *J Immunol.* 2012;188:5438–47.
 - 21. Filipovich AH, Weisdorf D, Pavletic S, Socie G, Wingard JR, Lee SJ, Martin P, Chien J, Przepiorka D, Couriel D, Cowen EW, Dinndorf P, Farrell A, Hartzman R, Henslee-Downey J, Jacobsohn D, McDonald G, Mittleman B, Rizzo JD, Robinson M, Schubert M, Schultz K, Shulman H, Turner M, Vogelsang G, Flowers ME. National Institutes of Health consensus development project on criteria for clinical trials in chronic graft-versus-host disease. I. Diagnosis and staging working group report. *Biol Blood Marrow Transplant.* 2005;11:945–56.
 - 22. Shulman HM, Cardona DM, Greenson JK, Hingorani S, Horn T, Huber E, Kreft A, Longerich T, Morton T, Myerson D, Prieto VG, Rosenberg A, Treister N, Washington K, Ziemer M, Pavletic SZ, Lee SJ, Flowers ME, Schultz KR, Jagasia M, Martin PJ, Vogelsang GB, Kleiner DE. NIH Consensus Development Project on Criteria for Clinical Trials in Chronic Graft-versus-Host Disease: II. The 2014 Pathology Working Group Report. *Biol Blood Marrow Transplant.* 2015;21:589–603.
 - 23. Shlomchik WD. Graft-versus-host disease. *Nat Rev Immunol.* 2007;7:340–52.
 - 24. Soiffer R. Immune modulation and chronic graft-versus-host disease. *Bone Marrow Transplant.* 2008;42 Suppl 1:S66–9.
 - 25. Champlin RE. T-cell depletion for bone marrow transplantation: effects on graft rejection, graft-versus-host disease, graft-versus-leukemia, and survival. *Cancer Treat Res.* 1990;50:99–111.
 - 26. Ho VT, Soiffer RJ. The history and future of T-cell depletion as graft-versus-host disease prophylaxis for allogeneic hematopoietic stem cell transplantation. *Blood.* 2001;98:3192–204.
 - 27. Broady R. Cutaneous GVHD is associated with the expansion of tissue-localized Th1 and not Th17 cells. *Blood.* 2010;116:5748–751.
 - 28. Matsuoka K, Kim HT, McDonough S, Bascug G, Warshauer B, Koreth J, Cutler C, Ho VT, Alyea EP, Antin JH, Soiffer RJ, Ritz J. Altered regulatory T cell homeostasis in patients with CD4⁺ lymphopenia following allogeneic hematopoietic stem cell transplantation. *J Clin Invest.* 2010;120:1479–93.
 - 29. Shimabukuro-Vornhagen A, Hallek MJ, Storb RF, von Bergwelt-Baildon MS. The role of B cells in the pathogenesis of graft-versus-host disease. *Blood.* 2009;114:4919–27.
 - 30. Flynn R, Du J, Veenstra RG, Reichenbach DK, Panoskaltsis-Mortari A, Taylor PA, Freeman GJ, Serody JS, Murphy WJ, Munn DH, Sarantopoulos S, Luznik L, Maillard I, Koreth J, Cutler C, Soiffer RJ, Antin JH, Ritz J, Dubovsky JA, Byrd JC, Macdonald KP, Hill GR, Blazar BR. Increased T follicular helper cells and germinal center B cells are required for chronic GVHD and bronchiolitis obliterans. *Blood.* 2014;123:3988–998.
 - 31. Finke J, Bethge WA, Schmoor C, Ottinger HD, Stelljes M, Zander AR, Volin L, Ruutu T, Heim DA, Schwerdtfeger R, Kolbe K, Mayer J, Maertens JA, Linkesch W, Holler E, Koza V, Bornhauser M, Einsele H, Kolb HJ, Bertz H, Egger M, Grishina O, Socie G. Standard graft-versus-host disease prophylaxis with or without anti-T-cell globulin in haematopoietic cell transplantation from matched unrelated donors: a randomised, open-label, multicentre phase 3 trial. *Lancet Oncol.* 2009;10:855–64.
 - 32. Kröger N, Solano C, Wolschke C, Bandini G, Patriarca F, Pini M, Nagler A, Selleri C, Risitano A, Messina G, Bülge W, Pérez de OJ, Dua te R, Carella AM, Cimminiello M, Guidi S, Stefanofinke J, Mordini N, Ferra C, Sierra J, Russo D, Petrini M, Milone G, Benedetti F, Heinzelmann M, Pastore D, Jurado M, Terruzzi E, Narni F, Vöp A, Ayuk F, Ruutu T, Bonifazi F. Antilymphocyte globulin for prevention of chronic graft-versus-host disease. *N Engl J Med.* 2016;374:43–53.
 - 33. Ayuk FA, Fang L, Fehse B, Zander AR, Kröger N. Antithymocyte globulin induces complement-dependent cell lysis and caspase-dependent apoptosis in myeloma cells. *Exp Hematol.* 2005;33:1531–6.
 - 34. Fang L, Fehse B, Engel M, Zander A, Kröger N. Antithymocyte globulin induces *ex vivo* and *in vivo* depletion of myeloid and plasmacytoid dendritic cells. *Transplantation.* 2005;79:369–71.
 - 35. Shimony O, Nagler A, Gellman YN, Refaeli E, Rosenblum N, Eshkar-Sebban L, Yerushalmi R, Shimoni A, Lytton SD, Stanevsky A, Or R, Naor D. Anti-T lymphocyte globulin (ATG) induces generation of regulatory T cells, at least part of them express activated CD44. *J Clin Immunol.* 2011;32:173–88.
 - 36. Chu YW, Gress RE. Murine models of chronic graft-versus-host disease: insights and unresolved issues. *Biol Blood Marrow Transplant.* 2008;14:365–78.
 - 37. Barker AF, Bergeron A, Rom WN, Hertz MI. Obliterative bronchiolitis. *N Engl J Med.* 2014;370:1820–8.
 - 38. Reddy P, Johnson K, Uberti JP, Reynolds C, Silver S, Ayash L, Braun TM, Ratanatharathorn V. Nephrotic syndrome

- associated with chronic graft-versus-host disease after allogeneic hematopoietic stem cell transplantation. *Bone Marrow Transplant.* 2006;38:351–7.
39. Seok J, Warren HS, Cuenca AG, Mindrinos MN, Baker HV, Xu W, Richards DR, McDonald-Smith GP, Gao H, Hennessy L, Finnerty CC, Lopez CM, Honari S, Moore EE, Minei JP, Cuschieri J, Bankey PE, Johnson JL, Sperry J, Nathens AB, Billiar TR, West MA, Jeschke MG, Klein MB, Gamelli RL, Gibran NS, Brownstein BH, Miller-Graziano C, Calvano SE, Mason PH, Cobb JP, Rahme LG, Lowry SF, Maier RV, Moldawer LL, Herndon DN, Davis RW, Xiao W, Tompkins RG. Genomic responses in mouse models poorly mimic human inflammatory diseases. *Proc Natl Acad Sci U S A.* 2013;110:3507–12.
 40. Benitez A, Weldon AJ, Tatosyan L, Velkuru V, Lee S, Milford TA, Francis OL, Hsu S, Nazeri K, Casiano CM, Schneider R, Gonzalez J, Su RJ, Baez I, Colburn K, Moldovan I, Payne KJ. Differences in mouse and human nonmemory B cell pools. *J Immunol.* 2014;192:4610–19.
 41. Antin JH, Bierer BE, Smith BR, Ferrara J, Guinan EC, Sieff C, Golan DE, Macklis RM, Tarbell NJ, Lynch E, Reichert TA, Blythman H, Bouloux C, Rappeport JM, Burakoff SJ, Weinstein HJ. Selective depletion of bone marrow T lymphocytes with anti-CD5 monoclonal antibodies: effective prophylaxis for graft-versus-host disease in patients with hematologic malignancies. *Blood.* 1991;78:2139–49.
 42. Hatano R, Ohnuma K, Yamamoto J, Dang NH, Yamada T, Morimoto C. Prevention of chronic graft-versus-host disease by humanized anti-CD16 monoclonal antibody. *Br J Haematol.* 2013;162:263–77.
 43. Kobayashi S, Ohnuma K, Uchiyama M, Iino K, Iwata S, Dang NH, Morimoto C. Association of CD26 with CD45RA outside lipid rafts attenuates cord blood T-cell activation. *Blood.* 2004;103:1002–10.
 44. Sato K, Nagayama H, Takahashi TA. Aberrant CD3- and CD28-mediated signaling events in cord blood T cells are associated with dysfunctional regulation of Fas ligand-mediated cytotoxicity. *J Immunol.* 1999;162:4464–71.
 45. Shultz LD, Brehm MA, Garcia-Martinez JV, Greiner DL. Humanized mice for immune system investigation: progress, promise and challenges. *Nat Rev Immunol.* 2012;12:786–98.
 46. Tezuka K, Xun R, Tei M, Ueno T, Tanaka M, Takenouchi N, Fujisawa J. An animal model of adult T-cell leukemia: humanized mice with HTLV-1-specific immunity. *Blood.* 2014;123:346–55.
 47. Ito M, Hiramatsu H, Kobayashi K, Suzue K, Kawahata M, Hioki K, Ueyama Y, Koyanagi Y, Sugamura K, Tsuji K, Heike T, Nakahata T. NOD/SCID/ γ_c^{null} mouse: an excellent recipient mouse model for engraftment of human cells. *Blood.* 2002;100:3175–82.
 48. Matsumura T, Kametani Y, Ando K, Hirano Y, Katano I, Ito R, Shiina M, Tsukamoto H, Saito Y, Tokuda Y, Kato S, Ito M, Motoyoshi K, Habu S. Functional CD5⁺ B cells develop predominantly in the spleen of NOD/SCID/ γ_c^{null} (NOG) mice transplanted either with human umbilical cord blood, bone marrow, or mobilized peripheral blood CD34⁺ cells. *Exp Hematol.* 2003;31:789–97.
 49. Yahata T, Ando K, Nakamura Y, Ueyama Y, Shimamura K, Tamaoki N, Kato S, Hotta T. Functional human T lymphocyte development from cord blood CD34⁺ cells in nonobese diabetic/Shi-*scid*, IL-2 receptor γ null mice. *J Immunol.* 2002;169:204–9.
 50. Ito R, Takahashi T, Katano I, Ito M. Current advances in humanized mouse models. *Cell Mol Immunol.* 2012;9:208–14.
 51. Ohnuma K, Hatano R, Aune TM, Otsuka H, Iwata S, Dang NH, Yamada T, Morimoto C. Regulation of pulmonary graft-versus-host disease by IL-26⁺CD26⁺CD4 T lymphocytes. *J Immunol.* 2015;194:3697–712.
 52. Collins PL, Henderson MA, Aune TM. Lineage-specific adjacent *IFNG* and *IL26* genes share a common distal enhancer element. *Genes Immun.* 2012;13:481–8.
 53. Donnelly RP, Sheikh F, Dickensheets H, Savan R, Young HA, Walter MR. Interleukin-26: an IL-10-related cytokine produced by Th17 cells. *Cytokine Growth Factor Rev.* 2010;21:393–401.
 54. Knappe A, Hor S, Wittmann S, Fickenscher H. Induction of a novel cellular homolog of interleukin-10, AK155, by transformation of T lymphocytes with herpesvirus saimiri. *J Virol.* 2000;74:3881–7.
 55. Kotenko SV. The family of IL-10-related cytokines and their receptors: related, but to what extent? *Cytokine Growth Factor Rev.* 2002;13:223–40.
 56. Hor S, Pirzer H, Dumoutier L, Bauer F, Wittmann S, Sticht H, Renaud JC, de Waal Malefyt R, Fickenscher H. The T-cell lymphokine interleukin-26 targets epithelial cells through the interleukin-20 receptor 1 and interleukin-10 receptor 2 chains. *J Biol Chem.* 2004;279:33343–51.
 57. Collins PL, Chang S, Henderson M, Souto M, Davis GM, McLoed AG, Townsend MJ, Glimcher LH, Mortlock DP, Aune TM. Distal regions of the human *IFNG* locus direct cell type-specific expression. *J Immunol.* 2010;185:1492–501.
 58. Wilson NJ, Boniface K, Chan JR, McKenzie BS, Blumenschein WM, Mattson JD, Basham B, Smith K, Chen T, Morel F, Lecron JC, Kastelein RA, Cua DJ, McClanahan TK, Bowman EP, de Waal Malefyt R. Development, cytokine profile and function of human interleukin 17-producing helper T cells. *Nat Immunol.* 2007;8:950–7.
 59. Corvaisier M, Delneste Y, Jeanvoine H, Preisser L, Blanchard S, Garo E, Hoppe E, Barre B, Audran M, Bouvard B, Saint-Andre JP, Jeannin P. IL-26 is overexpressed in rheumatoid arthritis and induces proinflammatory cytokine production and Th17 cell generation. *PLoS Biol.* 2012;10:e1001395.
 60. Sheikh F, Baurin VV, Lewis-Antes A, Shah NK, Smirnov SV, Anantha S, Dickensheets H, Dumoutier L, Renaud JC, Zdanov A, Donnelly RP, Kotenko SV. Cutting edge: IL-26 signals through a novel receptor complex composed of IL-20 receptor 1 and IL-10 receptor 2. *J Immunol.* 2004;172:2006–10.
 61. Goris A, Marrosu MG, Vandebroeck K. Novel

- polymorphisms in the IL-10 related AK155 gene (chromosome 12q15). *Genes Immun.* 2001;2:284–6.
62. Vandebroeck K, Cunningham S, Goris A, Alloza I, Heggarty S, Graham C, Bell A, Rooney M. Polymorphisms in the interferon- γ /interleukin-26 gene region contribute to sex bias in susceptibility to rheumatoid arthritis. *Arthritis Rheum.* 2003;48:2773–8.
 63. Silverberg MS, Cho JH, Rioux JD, McGovern DP, Wu J, Annese V, Achkar JP, Goyette P, Scott R, Xu W, Barmada MM, Klei L, Daly MJ, Abraham C, Bayless TM, Bossa F, Griffiths AM, Ippoliti AF, Lahaie RG, Latiano A, Pare P, Proctor DD, Regueiro MD, Steinhart AH, Targan SR, Schumm LP, Kistner EO, Lee AT, Gregersen PK, Rotter JI, Brant SR, Taylor KD, Roeder K, Duerr RH. Ulcerative colitis-risk loci on chromosomes 1p36 and 12q15 found by genome-wide association study. *Nat Genet.* 2009;41:216–20.
 64. Miot C, Beaumont E, Duluc D, Le Guillou-Guillemette H, Preisser L, Garo E, Blanchard S, Hubert Fouchard I, Creminon C, Lamourette P, Fremaux I, Cales P, Lunel-Fabiani F, Boursier J, Braum O, Fickenscher H, Roingeard P, Delneste Y, Jeannin P. IL-26 is overexpressed in chronically HCV-infected patients and enhances TRAIL-mediated cytotoxicity and interferon production by human NK cells. *Gut.* 2014;64:1466–75.
 65. Che KF, Tengvall S, Levanen B, Silverpil E, Smith ME, Awad M, Vikstrom M, Palmberg L, Ovurford I, Skold M, Linden A. Interleukin-26 in murine epithelial cells of human lungs. Effects on neutrophil mobilization. *Am J Respir Crit Care Med.* 2014;190:1022–31.
 66. Meller S, Di Domizio J, Voo KS, Friedrich HC, Chamilos G, Ganguly D, Conrad C, Gregorio J, Le Roy D, Roger T, Ladbury JE, Homey B, Watowich S, Modlin RL, Kontoyiannis DP, Liu YJ, Arold ST, Gilliet M. T_H17 cells promote microbial killing and innate immune sensing of DNA via interleukin 26. *Nat Immunol.* 2015;16:970–9.
 67. Shulman HM, Kleiner D, Lee SJ, Morton T, Pavletic SZ, Farmer E, Moresi JM, Greenson J, Janin A, Martin PJ, McDonald G, Flowers ME, Turner M, Atkinson J, Lefkowitch J, Washington MK, Prieto VG, Kim SK, Argenyi Z, Diwan AH, Rashid A, Hiatt K, Couriel D, Schultz K, Hymes S, Vogelsang GB. Histopathologic diagnosis of chronic graft-versus-host disease: National Institutes of Health Consensus Development Project on Criteria for Clinical Trials in Chronic Graft-versus-Host Disease: II. Pathology Working Group Report. *Biol Blood Marrow Transplant.* 2006;12:31–47.
 68. Yi T, Chen Y, Wang L, Du G, Huang D, Zhao D, Johnston H, Young J, Todorov I, Umetsu DT, Chen L, Iwakura Y, Kandeel F, Forman S, Zeng D. Reciprocal differentiation and tissue-specific pathogenesis of Th1, Th2, and Th17 cells in graft-versus-host disease. *Blood.* 2009;114:3101–12.
 69. Fickenscher H, Pirzer H. Interleukin-26. *Int Immunopharmacol.* 2004;4:609–13.
 70. Daddona PE, Kelley WN. Human adenosine deaminase. Stoichiometry of the adenosine deaminase-binding protein complex. *Biochim Biophys Acta.* 1979;580:302–11.
 71. Hopsu-Havu VK, Glenner GG. A new dipeptide naphthylamidase hydrolyzing glycyl-prolyl- β -naphthylamide. *Histochemie.* 1966;7:197–201.
 72. Marguet D, Bernard AM, Vivier I, Darmoul D, Naquet P, Pierres M. cDNA cloning for mouse thymocyte-activating molecule. A multifunctional ecto-dipeptidyl peptidase IV (CD26) included in a subgroup of serine proteases. *J Biol Chem.* 1992;267:2200–8.
 73. Tanaka T, Camerini D, Seed B, Torimoto Y, Dang NH, Kameoka J, Dahlberg HN, Schlossman SF, Morimoto C. Cloning and functional expression of the T cell activation antigen CD26. *J Immunol.* 1992;149:481–6.
 74. Abbott CA, Baker E, Sutherland GR, McCaughan GW. Genomic organization, exact localization, and tissue expression of the human CD26 (dipeptidyl peptidase IV) gene. *Immunogenetics.* 1994;40:331–8.
 75. Bohm SK, Gum JR, Erickson RH, Hicks JW, Kim YS. Human dipeptidyl peptidase IV gene promoter: tissue-specific regulation from a TATA-less GC-rich sequence characteristic of a housekeeping gene promoter. *Biochem J.* 1995;311 (Pt 3):835–43.
 76. Erickson RH, Lai RS, Lotterman CD, Kim YS. Identification of upstream stimulatory factor as an activator of the human dipeptidyl peptidase IV gene in Caco-2 cells. *Gene.* 2000;258:77–84.
 77. Bauvois L, Djafarri-Vergny MC, Rouillard D, Dumont J, Wietzerbin J. Regulation of CD26/DPPIV gene expression by interferons and retinoic acid in tumor B cells. *Oncogene.* 2000;19:265–72.
 78. Heins J, Welker P, Schonlein C, Born I, Hartrodt B, Neubert K, Tsuru D, Barth A. Mechanism of proline-specific proteinases: (I) Substrate specificity of dipeptidyl peptidase IV from pig kidney and proline-specific endopeptidase from *Flavobacterium meningosepticum*. *Biochim Biophys Acta.* 1988;954:161–9.
 79. David F, Bernard AM, Pierres M, Marguet D. Identification of serine 624, aspartic acid 702, and histidine 734 as the catalytic triad residues of mouse dipeptidyl-peptidase IV (CD26). A member of a novel family of nonclassical serine hydrolases. *J Biol Chem.* 1993;268:17247–52.
 80. Abbott CA, Yu DM, Woollatt E, Sutherland GR, McCaughan GW, Gorrell MD. Cloning, expression and chromosomal localization of a novel human dipeptidyl peptidase (DPP) IV homolog, DPP8. *Eur J Biochem.* 2000;267:6140–50.
 81. Rasmussen HB, Branner S, Wiberg FC, Wagtmann N. Crystal structure of human dipeptidyl peptidase IV/CD26 in complex with a substrate analog. *Nat Struct Biol.* 2003;10:19–25.
 82. Yaron A, Naider F. Proline-dependent structural and biological properties of peptides and proteins. *Crit Rev Biochem Mol Biol.* 1993;28:31–81.
 83. Bjelke JR, Kanstrup AB, Rasmussen HB. Selectivity among dipeptidyl peptidases of the S9b family. *Cell Mol Biol.*

- 2006;52:3–7.
84. Tanaka T, Kameoka J, Yaron A, Schlossman SF, Morimoto C. The costimulatory activity of the CD26 antigen requires dipeptidyl peptidase IV enzymatic activity. *Proc Natl Acad Sci U S A*. 1993;90:4586–90.
 85. Chien CH, Huang LH, Chou CY, Chen YS, Han YS, Chang GG, Liang PH, Chen X. One site mutation disrupts dimer formation in human DPP-IV proteins. *J Biol Chem*. 2004;279:52338–45.
 86. Dang NH, Torimoto Y, Sugita K, Daley JF, Schow P, Prado C, Schlossman SF, Morimoto C. Cell surface modulation of CD26 by anti-1F7 monoclonal antibody. Analysis of surface expression and human T cell activation. *J Immunol*. 1990;145:3963–71.
 87. Hatano R, Ohnuma K, Yamamoto J, Dang NH, Morimoto C. CD26-mediated co-stimulation in human CD8⁺ T cells provokes effector function via pro-inflammatory cytokine production. *Immunology*. 2013;138:165–72.
 88. Buhling F, Junker U, Reinhold D, Neubert K, Jager L, Ansorge S. Functional role of CD26 on human B lymphocytes. *Immunol Lett*. 1995;45:47–51.
 89. Fujimaki W, Takahashi N, Ohnuma K, Nagatsu M, Kurosawa H, Yoshida S, Dang NH, Uchiyama T, Morimoto C. Comparative study of regulatory T cell function of human CD25CD4 T cells from thymocytes, cord blood, and adult peripheral blood. *Clin Dev Immunol*. 2008;2008:305859.
 90. Stohlawetz P, Hahn P, Koller M, Hauer J, Fesch H, Smolens J, Pietschmann P. Immunophenotypic characteristics of monocytes in elderly subjects. *Scand J Immunol*. 1998;48:324–6.
 91. Ohnuma K, Munakata Y, Ishii T, Iwata S, Kobayashi S, Hosono O, Kawasaki H, Dang NH, Morimoto C. Soluble CD26/dipeptidyl peptidase IV induces T cell proliferation through CD86 up-regulation on APCs. *J Immunol*. 2001;167:6745–55.
 92. Buhling F, Kunz D, Reinhold D, Ulmer AJ, Ernst M, Flad HD, Ansorge S. Expression and functional role of dipeptidyl peptidase IV (CD26) on human natural killer cells. *Nat Immunol*. 1994;13:270–9.
 93. Masuyama J, Berman JS, Cruikshank WW, Morimoto C, Center DM. Evidence for recent as well as long term activation of T cells migrating through endothelial cell monolayers *in vitro*. *J Immunol*. 1992;148:1367–74.
 94. Kloosterboer FM, van Luxemburg-Heijss SA, Willemze R, Falkenburg JH. Similar potential to become activated and proliferate but differential kinetics and profiles of cytokine production of umbilical cord blood T cells and adult blood naive and memory T cells. *Hum Immunol*. 2006;67:874–83.
 95. Engelman JA, Zhang X, Galbiati F, Volonte D, Sotgia F, Pestell RG, Minetti C, Scherer PE, Okamoto T, Lisanti MP. Molecular genetics of the caveolin gene family: implications for human cancers, diabetes, Alzheimer disease, and muscular dystrophy. *Am J Hum Genet*. 1998;63:1578–87.
 96. Wu CJ, Ritz J. Revealing tumor immunity after hematopoietic stem cell transplantation. *Clin Cancer Res*. 2009;15:4515–17.
 97. Yan S, Marguet D, Dobers J, Reutter W, Fan H. Deficiency of CD26 results in a change of cytokine and immunoglobulin secretion after stimulation by pokeweed mitogen. *Eur J Immunol*. 2003;33:1519–27.
 98. Fidler IJ, Fogler WE, Kleinerman ES, Saiki I. Abrogation of species specificity for activation of tumoricidal properties in macrophages by recombinant mouse or human interferon-gamma encapsulated in liposomes. *J Immunol*. 1985;135:4289–96.
 99. Gibbs VC, Williams SR, Gray PW, Schreiber RD, Pennica D, Rice G, Goeddel DV. The extracellular domain of the human interferon gamma receptor interacts with a species-specific signal transducer. *Mol Cell Biol*. 1991;11:5860–6.
 100. Zielinski CE, Mele F, Aschenbrenner D, Jarrossay D, Ronchi F, Gattorno M, Monticelli S, Lanzavecchia A, Sallusto F. Pathogen-induced human T_H17 cells produce IFN- γ or IL-10 and are regulated by IL-1 β . *Nature*. 2012;484:514–18.
 101. Wolk K, Kunz S, Asadullah K, Sabat R. Cutting edge: immune cells as sources and targets of the IL-10 family members? *J Immunol*. 2002;168:5397–402.
 102. Zhang C, Todorov I, Zhang Z, Liu Y, Kandeel F, Forman S, Strober S, Zeng D. Donor CD4⁺ T and B cells in transplants induce chronic graft-versus-host disease with autoimmune manifestations. *Blood*. 2006;107:2993–3001.
 103. Ishikawa F, Yasukawa M, Lyons B, Yoshida S, Miyamoto T, Yoshimura G, Watanabe T, Akashi K, Shultz LD, Harada M. Development of functional human blood and immune systems in NOD/SCID/IL2 receptor γ chain^{null} mice. *Blood*. 2005;106:1565–73.
 104. Campbell TB, Hangoc G, Liu Y, Pollok K, Broxmeyer HE. Inhibition of CD26 in human cord blood CD34⁺ cells enhances their engraftment of nonobese diabetic/severe combined immunodeficiency mice. *Stem Cells Dev*. 2007;16:347–54.
 105. Ohnuma K, Inoue H, Uchiyama M, Yamochi T, Hosono O, Dang NH, Morimoto C. T-cell activation via CD26 and caveolin-1 in rheumatoid synovium. *Mod. Rheumatol*. 2006;16:3–13.
 106. Blazar BR, Taylor PA, Boyer MW, Panoskaltsis-Mortari A, Allison JP, Vallera DA. CD28/B7 interactions are required for sustaining the graft-versus-leukemia effect of delayed post-bone marrow transplantation splenocyte infusion in murine recipients of myeloid or lymphoid leukemia cells. *J Immunol*. 1997;159:3460–73.

Q1: Please provide running title

Effects of obesity and diabetes on alpha and beta cell mass in surgically resected human pancreas

Jun Inaishi¹, Yoshifumi Saisho¹, Seiji Sato¹, Kinsei Kou¹, Rie Murakami¹, Yuusuke Watanabe¹, Minoru Kitago², Yuko Kitagawa², Taketo Yamada^{3,4}, and Hiroshi Itoh¹

¹ Department of Internal Medicine, Keio University School of Medicine, Tokyo, Japan; ² Department of Surgery, Keio University School of Medicine, Tokyo, Japan; ³ Department of Pathology, Keio University School of Medicine, Tokyo, Japan; ⁴ Department of Pathology, Saitama Medical University, Saitama, Japan Original article

Context: The ethnic difference in beta cell regenerative capacity in response to obesity may be attributable to different phenotypes of type 2 diabetes among ethnicities.

Objective: This study aimed to clarify the effects of diabetes and obesity on beta (BCM) and alpha cell mass (ACM) in the Japanese population.

Design, Setting and Participants: We obtained the pancreases of 99 individuals who underwent pancreatic surgery and whose resected pancreas sample contained adequate normal pancreas for histological analysis. Questionnaires on family history of diabetes and history of obesity were conducted in 59 patients. Pancreatic sections were stained for insulin or glucagon, and fractional beta and alpha cell area were measured. Islet size and density as well as beta cell turnover were also quantified.

Results: In patients with diabetes, BCM was decreased by 46% compared with age- and BMI-matched non-diabetic patients ($1.48 \pm 1.08\%$ vs. $0.80 \pm 0.54\%$, $P < 0.001$), while there was no difference in ACM between the groups. There was no effect of obesity or history of obesity on BCM and ACM irrespective of the presence or absence of diabetes. There was a negative correlation between BCM, but not ACM, and HbA1c before and after pancreatic surgery. In addition, reduced BCM was observed in patients with pancreatic cancer compared with those with other pancreatic tumors.

Conclusions: These findings suggest that the increase in BCM in the face of insulin resistance is extremely limited in Japanese, and BCM rather than ACM has a major role in regulating blood glucose level in humans.

Both type 1 (T1DM) and type 2 diabetes (T2DM) are characterized by a deficit of beta cell mass (BCM) (1). Preservation or recovery of BCM is therefore an important therapeutic strategy for both T1DM and T2DM. On the other hand, the paradoxical increase in glucagon secretion in subjects with diabetes suggests an increase in alpha cell mass (ACM), which was shown in rodent studies to occur through the mechanism of dedifferentiation of beta cells to

alpha cells (2). However, since it is not yet possible to measure BCM as well as ACM *in vivo* in humans, the physiological and pathological changes in BCM and ACM in the face of obesity and diabetes in humans remain to be established.

As plasma insulin level is increased approximately 2 to 3-fold with obesity to compensate insulin resistance (3), it is widely believed that BCM increases with obesity. In

ISSN Print 0021-972X ISSN Online 1945-7197

Printed in USA

Copyright © 2016 by the Endocrine Society

Received February 13, 2016. Accepted April 7, 2016.

Abbreviations: ACA; alpha cell area, ACM; alpha cell mass, BCA; beta cell area, BCM; beta cell mass, CPR; C-peptide immunoreactivity, GA; glycated albumin, GAD; glutamic acid decarboxylase, IPMN; intraductal papillary mucinous neoplasm, PC; pancreatic cancer, PARP; poly(ADP-ribose) polymerase-1, ssDNA; single-stranded DNA, T2DM; type 2 diabetes

adult humans, we and others have shown that BCM increases by approximately 20 to 50% in obese nondiabetic individuals in the Caucasian population (4, 5). However, a meta-analysis of the insulin secretion-sensitivity relationship among different ethnic groups has shown higher insulin sensitivity and lower insulin secretion in Asians compared with Caucasians and African Americans (6), suggesting ethnic differences in insulin secretory ability.

We have recently reported that no significant increase in BCM was observed in obese nondiabetic adults and those treated with corticosteroids in the Japanese population (7, 8). These findings suggest that beta cell regenerative capacity, as well as beta cell functional capacity, may differ between Japanese and Caucasians. These studies were however based on autopsy pancreas where it was not possible to completely exclude the effects of confounding factors, such as underlying diseases leading to death, nutritional change and intensive medical treatment prior to death, and postmortem changes on pancreas morphology.

Therefore, in this study, to overcome these limitations and complement autopsy studies, we sought to address the following questions by using surgically resected pancreas samples in the Japanese population where we were able to obtain detailed medical information and history of obesity: 1) Is there any interaction between the effects of diabetes and obesity on BCM and ACM? 2) Is there any correlation between history of obesity and BCM and ACM? 3) Is there any correlation between BCM or ACM, and pre- and postoperative glycemic control?

Materials and Methods

Patients

The study was approved by the Ethics Committee of Keio University School of Medicine. A total of 99 Japanese individuals (61 men and 38 women) who underwent pancreatic surgery and whose resected pancreas sample contained adequate normal pancreas for histological analysis were included in the study (Table 1 and Supplemental Figure 1). Written informed consent was obtained from each patient, while it was waived for patients who had discontinued hospital visits at the time of study enrollment (N = 40).

Of these, 41 patients had been diagnosed with type 2 diabetes before the diagnosis of pancreatic tumors, and eight patients were diagnosed with pancreatic cancer (PC) and diabetes at the same time. There was no case of type 1 diabetes or case in which glutamic acid decarboxylase (GAD) antibody was positive.

Measurements and questionnaire

Information on each patient including HbA1c, glycated albumin (GA), plasma glucose and serum C-peptide immunoreactivity (CPR) levels were obtained from the medical records. HbA1c was measured by HPLC and expressed as NGSP and IFCC values. GA and CPR were measured by an enzymatic method and chemiluminescent enzyme immunoassay (EIA), respectively. Beta cell function was assessed by serum CPR to plasma glucose ratio (CPR index) calculated as CPR (nmol/l)/plasma glucose (mmol/l), as previously reported (9).

In addition, a questionnaire on family history of diabetes and history of obesity was conducted in 59 patients. The questionnaire consisted of the following categories: 1) history of obesity in childhood and adolescence, 2) body weight at age 20 years and every decade thereafter, 3) maximum body weight in life, and 4)

Table 1. Characteristics of subjects.

	Patients without diabetes (NDM)			Patients with diabetes (DM)			
N (male/female)	Total 50 (26/24)	Lean 40 (17/23)	Obese 10 (9/1)	Total 49 (35/14)	Lean 40 (28/12)	Obese 9 (7/2)	99 (61/38)
Age (years)	64 ± 14	64 ± 14	63 ± 13	67 ± 9	67 ± 8	67 ± 13	65 ± 12
BMI (kg/m ²)	22.5 ± 2.7	21.5 ± 1.9	26.4 ± 1.2*	21.9 ± 3.5	20.7 ± 2.4	27.6 ± 1.6*	22.2 ± 3.1
HbA1c (%) ¹⁾	5.6 ± 0.5	5.7 ± 0.5	5.6 ± 0.6	7.8 ± 1.6#	7.8 ± 1.8#	7.5 ± 0.9#	6.7 ± 1.6
HbA1c (mmol/mol) ¹⁾	38 ± 6	38 ± 6	37 ± 6	61 ± 18#	62 ± 19#	58 ± 10#	50 ± 18
GA (%) ²⁾	14.8 ± 1.8	14.8 ± 1.8	N/A	21.2 ± 4.4#	21.6 ± 4.9#	20.1 ± 2.7#	20.1 ± 4.7
PG (mmol/liter) ³⁾	6.24 ± 1.20	6.21 ± 1.21	6.37 ± 1.23	8.33 ± 2.52#	8.44 ± 2.71#	7.83 ± 1.41#	7.27 ± 2.22
CPR (nmol/liter) ^{3,4)}	0.57 (0.37–0.96)	0.56 (0.36–0.69)	1.03 ⁶⁾	0.51 (0.34–0.71)	0.54 (0.31–0.71)	0.50 (0.39–0.80)	0.56 (0.36–0.73)
CPR index ([nmol/liter]/[mmol/liter]) ⁴⁾	0.101 (0.060–0.155)	0.085 (0.058–0.115)	0.174 ⁶⁾	0.063 (0.045–0.086)	0.056 (0.044–0.085)	0.066 (0.055–0.102)	0.065 (0.047–0.103)
Duration of DM (years)	-	-	-	8 ± 9	7 ± 9	9 ± 6	-
Medication for diabetes, n (%)							
Diet only	-	-	-	14 (28)	13 (33)	1 (11)	-
OHA	-	-	-	20 (41)	13 (33)	7 (78)	-
Insulin ± OHA	-	-	-	15 (31)	14 (35)	1 (11)	-
Clinical diagnosis, n (%)							
Neuroendocrine tumor	13 (26)	10 (25)	3 (30)	7 (14)	7 (18)	0 (0)	20 (20)
Pancreatic cancer	28 (56)	24 (60)	4 (40)	34 (70)	28 (70)	6 (67)	62 (63)
IPMN	9 (18)	6 (15)	3 (30)	7 (14)	5 (12)	2 (22)	16 (17)
Others ⁵⁾	0 (0)	0 (0)	0 (0)	1 (2)	0 (0)	1 (11)	1 (1)
Operative procedure, n (%)							
Distal pancreatectomy	40 (80)	31 (78)	9 (90)	33 (68)	29 (73)	4 (44)	73 (74)
Pancreatoduodenectomy	6 (12)	6 (15)	0 (0)	12 (24)	7 (17)	5 (56)	18 (18)
Total pancreatectomy	4 (8)	3 (7)	1 (10)	4 (8)	4 (10)	0 (0)	8 (8)

Data with normal distribution are expressed as mean ± SD, and non-normally distributed data are expressed as median (interquartile range). * P < 0.05 vs. Lean. # P < 0.05 vs. NDM. 1) HbA1c was obtained in 93 subjects. 2) GA was obtained in 35 subjects. 3) Timing of blood sampling (i.e. fasting or postprandial) was not determined. 4) CPR and CPR index were obtained in 56 subjects. 5) Disseminated sarcoma originating from small intestine. 6) n = 2. CPR index was calculated as CPR (nmol/liter)/PG (mmol/liter). N/A; not available. OHA; oral hypoglycemic agent. IPMN; intraductal papillary mucinous neoplasm.

first-degree family history of diabetes. Duration of obesity was calculated from the responses to the questionnaire.

The cases were classified into four groups according to the presence or absence of diabetes and obesity. Obesity was defined as $\text{BMI} \geq 25 \text{ kg/m}^2$ (10).

Pancreatic tissue processing

The surgically resected pancreas was immediately fixed in formaldehyde and embedded in paraffin for subsequent analysis. In eight cases that underwent total pancreatectomy, pancreas samples were obtained from the head in three cases and the body or tail in five cases. Five-micrometer sections were cut from the tumor-free region and stained for light microscopy as follows: 1) with hematoxylin-eosin, 2) for insulin (peroxidase staining) with hematoxylin, 3) for glucagon with hematoxylin, 4) for insulin and Ki67 for assessment of beta cell replication, and 5) for insulin and single-stranded DNA (ssDNA) or cleaved poly(ADP-ribose) polymerase-1 (PARP) for assessment of beta cell apoptosis, as previously described (7, 8).

Morphometric analysis

To quantify fractional beta cell area (BCA), the entire pancreatic section was imaged at the original magnification $\times 200$ ($\times 20$ objective) using a Mirax Scan and Mirax Viewer (Carl Zeiss MicroImaging GmbH, Goettingen, Germany). The ratio of BCA to total pancreas area was digitally measured using Image Pro Plus software (Media Cybernetics, Silver Springs, MD), as previously reported (7, 8). Likewise, the ratio of alpha cell area to total pancreas area (ACA) was also digitally measured, and the ratio of ACA to BCA was determined in each case. All measurements were conducted by a single investigator (J.I.), and the intraobserver coefficient of variance was 7%. All measurements were conducted twice, and the mean of the two measurements was used. At the time of measurement, the investigator was blinded to both the glycemic and obesity status for each specimen.

To conduct further morphometric analysis, size and density of islets, density of scattered beta cells and insulin-positive duct cells were quantified in randomly selected areas of the pancreas that contained approximately 100 islets in each case (106 ± 6 islets, total 10 491 islets) using a Mirax Viewer (7, 8). Scattered beta cells were defined as a cluster of three or fewer beta cells in acinar tissue. In addition, beta cell replication and apoptosis were quantified and expressed as percentage of islets.

Statistical analysis

Data are presented as mean \pm SD or, if non-normally distributed, median (interquartile range) in the text and tables. Mann-Whitney U test was used to assess difference between two groups, and Spearman correlation coefficient was used to assess the correlation between two parameters. ANCOVA and multivariate regression were used to adjust for covariates. Statistical analyses were performed using SPSS 22 software (IBM, Armonk, NY). A P value of < 0.05 was considered statistically significant.

Results

Change in islet morphology in patients with diabetes

Representative photomicrographs of the pancreas of patients with and without diabetes are shown in Figure 1.

In patients with diabetes (DM group), BCA was decreased by 46% compared with age- and BMI-matched nondiabetic patients (NDM group) ($1.48 \pm 1.08\%$ vs. $0.80 \pm 0.54\%$, $P < .001$, Supplemental Figure 2). There was no difference in ACA between the two groups ($0.49 \pm 0.44\%$ vs. $0.35 \pm 0.31\%$, $P = .09$). ACA to BCA ratio in the DM group was thus increased compared with that in the NDM group (0.35 ± 0.18 vs. 0.46 ± 0.30 , $P = .045$).

Mean islet size (5297 ± 2115 vs. $4486 \pm 1990 \mu\text{m}^2$, $P = .03$) and islet density (4.52 ± 3.05 vs. $3.09 \pm 2.04 / \text{mm}^2$, $P = .003$) were both decreased in the DM group compared with the NDM group. On the other hand, there was no difference in the density of scattered beta cells, density of insulin-positive duct cells and beta cell replication between the two groups. Beta cell apoptosis (ie, ss-DNA and/or cleaved PARP-positive beta cells) was not found in either group (Supplemental Figure 2).

Reduced BCA in the DM group was also observed when patients diagnosed with PC and diabetes at the same time ($N = 8$) were excluded from the analysis ($0.81 \pm 0.55\%$, $P < .001$ vs. NDM). Furthermore, a similar reduction in

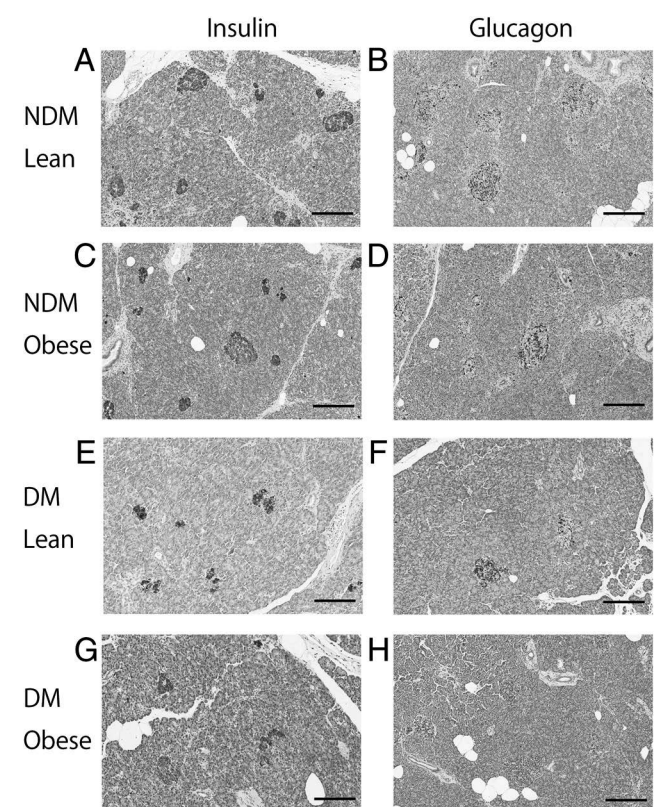


Figure 1. Representative photomicrographs of pancreas immunostained for insulin (brown) (A, C, E, G) or glucagon (brown) (B, D, F, H) and with hematoxylin ($\times 20$ objective). Examples of lean (65-year-old woman, BMI 21.5, HbA1c 5.7% (38 mmol/mol)) (A and B) and obese (63-year-old man, BMI 26.0, HbA1c 5.6% (37 mmol/mol)) (C and D) subjects without diabetes, and lean (63-year-old woman, BMI 19.6, HbA1c 8.2% (66 mmol/mol)) (E and F) and obese (70-year-old man, BMI 29.0, HbA1c 7.7% (60 mmol/mol)) (G and H) subjects with diabetes. Scale bar, 200 μm .

BCA was observed in patients with diabetes duration > 3 years and those with diabetes duration ≤ 3 years ($P = .65$, Supplemental Figure 3A). There was no difference in BCA among patients treated with different medications (Supplemental Figure 3D).

There was no difference in either BCA or ACA according to the pancreas regions from where the samples had been obtained (ie, pancreas head vs. body or tail, Supplemental Figure 4D-I). However, BCA of subjects with PC was significantly lower than that of those with other tumors, irrespective of the presence or absence of diabetes (Supplemental Figure 4A).

Effects of obesity on islet morphology

Patients with or without diabetes were further classified according to presence or absence of obesity (Table 1). In the NDM group, there was no difference in BCA ($1.42 \pm 1.09\%$ vs. $1.71 \pm 1.07\%$, $P = .21$), ACA ($0.48 \pm 0.46\%$ vs. $0.55 \pm 0.37\%$, $P = .33$) and ACA to BCA ratio (0.33 ± 0.16 vs. 0.41 ± 0.26 , $P = .56$) between lean and obese subjects (Figure 2). Similarly, no differences in BCA, ACA and ACA to BCA ratio between lean and obese subjects were observed in the DM group. Accordingly, BCA was similarly decreased with diabetes in the lean and obese groups ($P = .001$ and $P = .04$, respectively). There were no correlations between BMI and BCA, ACA or ACA/

BCA ratio in either the NDM or DM group (Figure 2D-I). No increase in BCA in obese subjects was also confirmed by the ANCOVA model including age, sex, diabetes and PC (adjusted mean (95% confidence interval (CI)) 1.20% (1.01–1.40) vs. 1.20% (0.77–1.62) in lean vs. obese, respectively).

In the DM group, but not the NDM group, mean islet size in obese subjects was increased compared with that in lean subjects (6220 ± 2219 vs. $4096 \pm 1736 \mu\text{m}^2$, $P = .01$, Supplemental Figure 5A), and was positively correlated with BMI ($R = 0.43$, $P = .002$, Supplemental Figure 5H). In both the NDM and DM groups, there was no difference in islet density and beta cell turnover between the lean and obese groups (Supplemental Figure 5B-F).

Effect of history of obesity and family history of diabetes on islet morphology

To examine the effect of history of obesity on islet morphology, cases that answered the questionnaire on history of obesity ($N = 59$) were divided into three groups according to the duration of obesity (lean (ie, no history of obesity), ≤ 10 years and > 10 years, Supplemental Table 1). Among the three groups, no difference in BCA and ACA was found in either the NDM or DM group (Figure 3). Neither BCA nor ACA was correlated with maximum BMI in life (Figure 3E-H). In the DM group, there was a

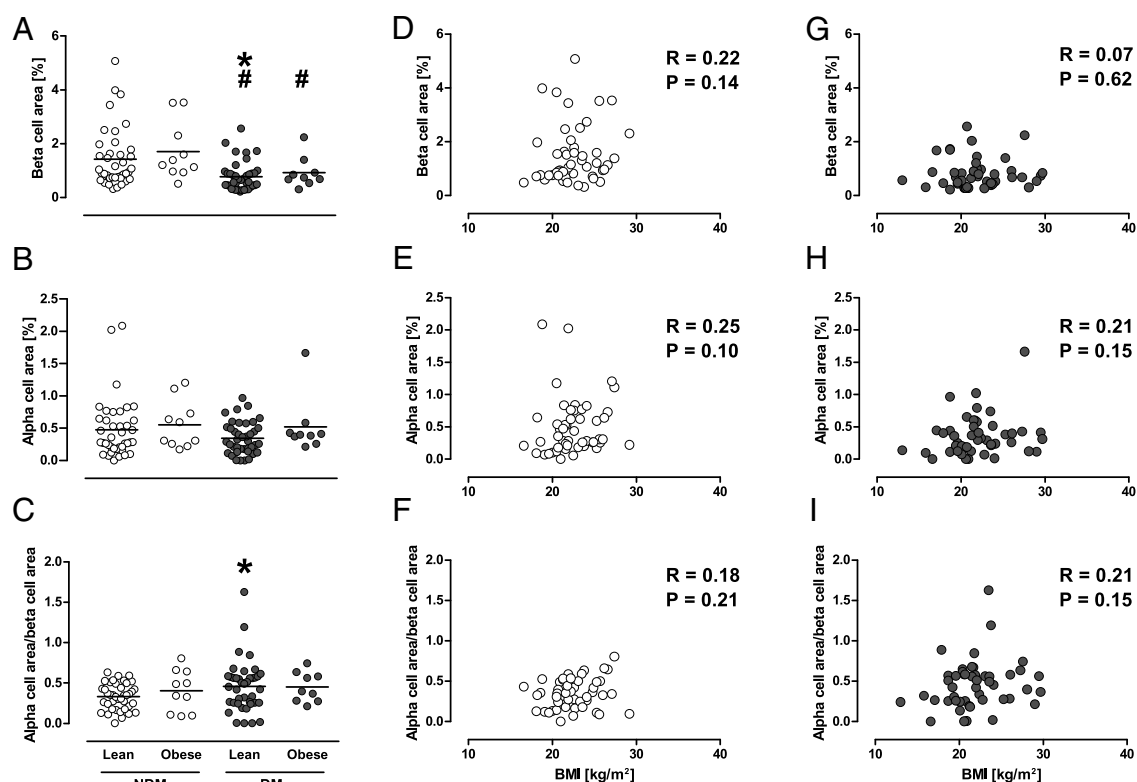


Figure 2. A, B and C: Effects of obesity on beta cell area (BCA), alpha cell area (ACA) and ACA to BCA ratio in cases with and without diabetes. Gray and white circles show cases with and without diabetes, respectively. Bars indicate mean. * $P < .05$ vs. lean cases without diabetes. # $P < .05$ vs. obese cases without diabetes. D-I: Correlations between BMI and BCA, ACA or ACA to BCA ratio in cases with and without diabetes.

positive correlation between mean islet size and maximum BMI ($R = 0.48, P = .003$).

Among the 59 patients, three subjects in the NDM group (12%) and 11 subjects in the DM group (33%) had a first-degree family history of diabetes. Although there was no significant difference in BCA and ACA between patients with and without a family history of diabetes, in the DM group islet density was significantly decreased and mean islet size was increased with borderline significance in patients with a family history compared with those without (Figure 4).

Association between beta cell mass and pre- and postsurgery glycemic markers

BCA was negatively correlated with HbA1c and GA before surgery ($R = -0.42, P < .001$ and $R = -0.49, P = .003$, respectively, Figure 5A and B), while ACA was not ($R = -0.15, P = .15$ and $R = 0.20, P = .25$, respectively). The relationship between BCA and HbA1c remained significant after adjustment for age, sex, BMI and presence of PC ($\beta = -0.21, P = .04$). BCA was correlated with CPR index before surgery ($R = 0.37, P = .005$, Supplemental Figure 6C).

A negative correlation between BCA and HbA1c or GA was also observed at 3 and 6 months after surgery (Figure 5C-D and Supplemental Figure 6A-B). In contrast, ACA was not correlated with postoperative HbA1c or GA at any time point (data not shown). The same results were observed when only cases with distal pancreatectomy were included in the analysis (data not shown).

Discussion

In this study, we report that 1) BCA in individuals with diabetes was decreased by ~45% compared with that in those without diabetes, while there was no difference in ACA, 2) there was little effect of obesity or history of obesity on BCA and ACA irrespective of the presence or absence of diabetes, and 3) BCA, but not ACA, was significantly correlated with preoperative and postoperative glycemic control. The findings of this study extend the current knowledge on the pathophysiological changes in BCM and ACM in humans, as discussed below.

First, the reduction in BCA by ~45% in Japanese patients with T2DM was consistent with our prior report using autopsy pancreas (8). Although it is often difficult to distinguish T2DM and PC-associated diabetes in patients with PC, we confirmed the same results in patients with diabetes duration > 3 years, in whom T2DM was likely to have preceded the development of pancreatic tumors (11). A recent study suggested that beta cell loss in patients with

T2DM is overestimated due to the presence of degranulated beta cells (12); however, the comparable reduction in islet size and density in this study supports the idea that the number of beta cells is indeed reduced in those with T2DM, as reported by prior observations (5, 8, 13–15).

Reduced insulin secretion and a paradoxical increase in glucagon secretion is a hallmark of T2DM (16); however, the change in ACM in patients with diabetes is controversial. ACM has been reported to increase in patients with T2DM (14), but this was not found in other studies (8, 17, 18). A recent rodent study has suggested beta cell to alpha cell transdifferentiation as a mechanism of increased ACM in diabetes (2). In the present study, we observed no significant increase in ACA in patients with T2DM, although the relative proportion of ACA to BCA was significantly increased compared with that in nondiabetic patients. Thus, the present study indicates that the relative increase in ACM compared to BCM in patients with T2DM is mainly driven by reduced BCM, but not an increase in ACM. The reduced islet size and density observed in patients with diabetes also reflect reduced total endocrine cells in patients with diabetes.

The second objective of this study was to clarify the effects of obesity on BCM and ACM in patients with and without diabetes. We have previously reported no increase in BCM in Japanese obese nondiabetic individuals compared with lean controls by using autopsy samples (7). In contrast, in the Caucasian population, autopsy studies have shown that BCM is increased by ~20 to 50% in obese nondiabetic individuals (4, 5). A recent study in the Caucasian population using surgically resected pancreas has also shown a significant increase in BCA in nondiabetic individuals with insulin resistance (19). These inconsistent findings suggest the possibility that the adaptive change in BCM in response to obesity differs among ethnicities.

In this study, using surgically resected pancreas, we confirmed no increase in BCA in Japanese obese individuals with or without diabetes, in line with recent Japanese studies (20, 21). Since it has been reported that beta cell replication rapidly decreases postmortem (22, 23), beta cell turnover might be underestimated in autopsy pancreas. Here, we found that beta cell replication and surrogate markers of beta cell neogenesis in the surgically resected pancreas were also not changed in obese individuals. Furthermore, we here showed that there was no effect of either duration of obesity or maximum BMI in life on BCA in these subjects. Similarly to BCA, ACA was also not changed in obese individuals irrespective of the presence or absence of diabetes. Although studies have shown that beta cell function adjusted for insulin sensitivity is comparable between Japanese and Caucasians (24, 25), con-

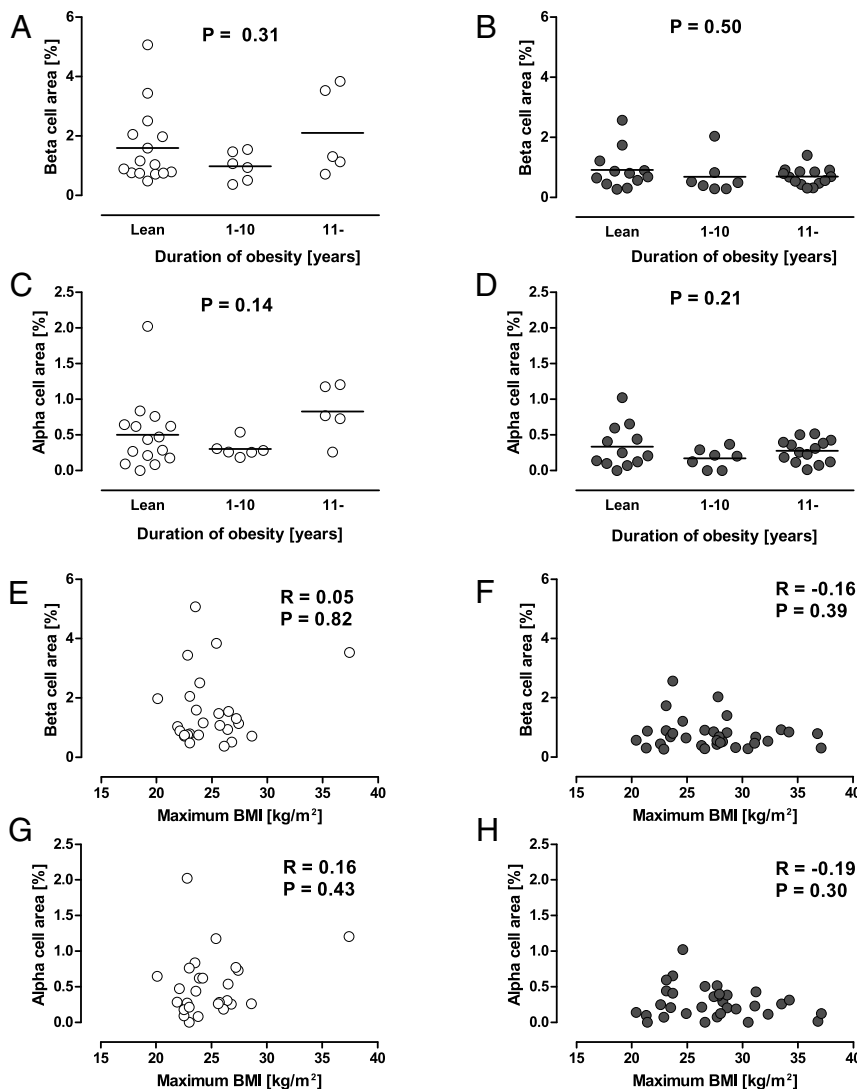


Figure 3. A-D: Effects of history of obesity on beta cell area (BCA) and alpha cell area (ACA). Cases that answered the questionnaire (N = 59) were divided into three groups according to the duration of obesity (ie, no history of obesity), ≤ 10 years and > 10 years). Bars indicate mean. E-H: Correlations between maximum BMI in life and BCA or ACA in cases with and without diabetes. Gray and white circles show cases with and without diabetes, respectively.

sidering the similar incidence of T2DM despite less degree of obesity in Japanese compared with Caucasians (26), our results suggest that the ethnic difference in BCM could be attributable to lower maximum insulin secretory ability in Asians compared with Caucasians. Further studies are needed to determine genetic and environmental factors regulating BCM in humans and clarify the underlying mechanisms of the ethnic difference in beta cell change in response to obesity.

While mean islet size was reduced in patients with T2DM compared with nondiabetic subjects, there was a positive correlation between mean islet size and BMI in patients with T2DM. Considering the lack of significant change in BCA or ACA with obesity, the increase in islet size possibly resulted from an increase in other endocrine cells, amyloid deposits or other components. It has been

reported that islet amyloid deposition is positively correlated with BMI in patients with T2DM (27). It would be of interest to clarify the underlying mechanism of islet remodeling with obesity in patients with T2DM, which may cause further beta cell loss in these patients.

It is also of note that we assessed the effect of a first-degree family history of diabetes on BCM. As a result, in patients with diabetes, reduced islet density with greater islet size was observed in patients with a family history of diabetes. We have previously reported that islet number rather than islet size is a major determinant of BCM, and islet density was negatively correlated with plasma glucose level in nondiabetic humans (28). Reduced islet density with greater islet size has also been reported in nondiabetic subjects with the TCF7L2 polymorphism who are susceptible to T2DM (29). Together with these prior studies, the present study suggests that a genetic factor is associated with T2DM susceptibility through reduced islet number.

Finally, we investigated the clinical significance of BCM, ie, the relationship between BCA and plasma glucose level, and found a negative correlation between BCA and HbA1c, consistent with our and prior reports (8, 14, 30, 31). We also

confirmed the association between BCA and plasma glucose level using another glycemic index, GA. Intriguingly, the relationships between BCA and glycemic markers remained significant even 6 months after surgery in patients with pancreatectomy or distal pancreatectomy where a half of the pancreas had been resected, indicating that BCA predicts glycemic control before and after surgery. The present study and others have also observed a significant correlation between BCA and endogenous insulin secretion assessed by CPR or CPR index (21, 31), which have been shown to predict future glycemic control (32). These findings underpin the importance of BCM rather than ACM in regulation of glucose metabolism in humans.

Another unexpected and novel finding of this study was

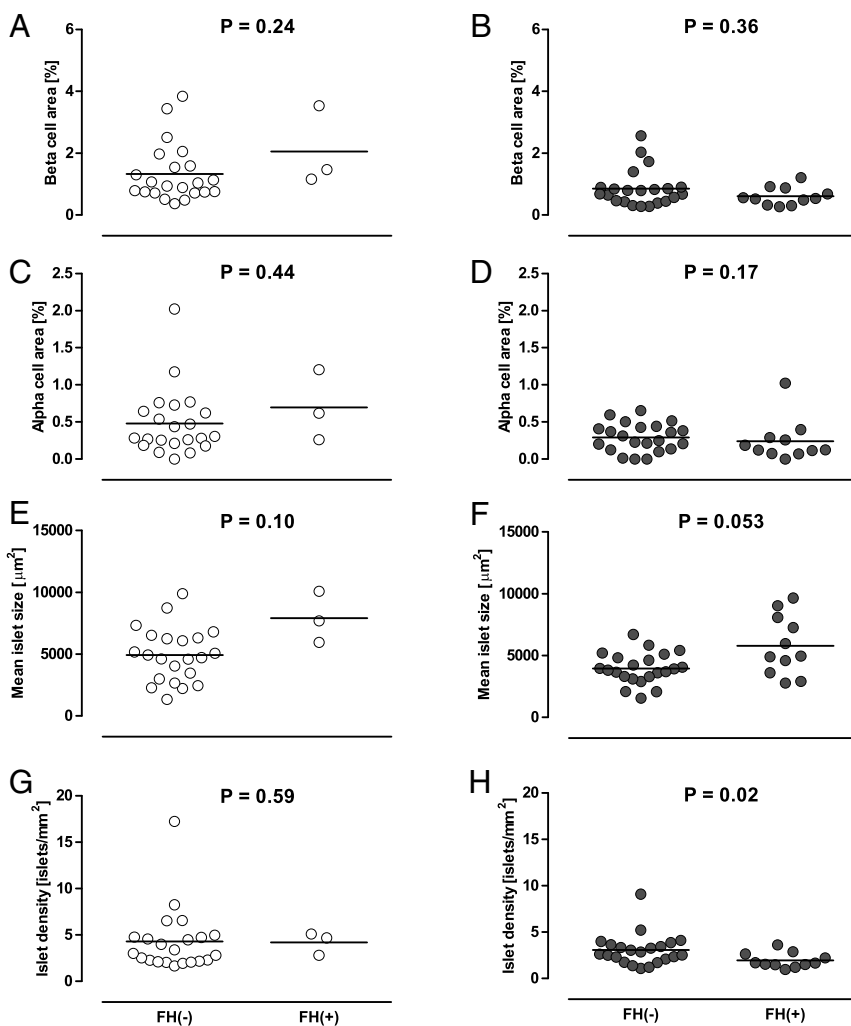


Figure 4. Effects of first-degree family history of diabetes (FH) on beta cell area (BCA) (A and B), alpha cell area (ACA) (C and D) and islet morphology (E-H). Gray and white circles show cases with and without diabetes, respectively. Bars indicate mean.

the reduced BCA in patients with PC compared with those with other pancreatic tumors. It is known that PC is associated with new-onset or worsening of diabetes (33). However, the mechanisms by which PC causes deterioration of glucose metabolism remain largely unknown. It has been reported that beta cell function is impaired in patients with PC (34). One study reported reduced BCA in patients with PC and diabetes (35), while others did not (21, 31). These inconsistent results might have been due to the small sample size in these studies. In this study, reduced BCA in patients with PC was observed irrespective of the presence or absence of diabetes, suggesting that the reduction in BCM is independent of the effect of diabetes. The reduced BCA in the tumor-free region supports the concept that PC may affect endocrine cells indirectly through humoral factors such as adrenomedullin (36). Further study will be needed to clarify the underlying mechanisms by which PC induces glucose intolerance through a reduction in endocrine cells.

The strengths of the present study include 1) the relatively large sample size with well-matched controls, 2) detailed medical information before and after surgery and 3) detailed information on history of obesity and family history of diabetes obtained by questionnaire. The major limitation of this study was that the cases had pancreatic diseases which might have affected pancreatic morphology. However, we confirmed the same results in cases with and without PC, and the findings of this study were consistent with our prior report using autopsy pancreas in which cases with pancreatic disease were excluded (7, 8, 28). Second, the pancreas samples were obtained from different portions of the pancreas according to the operative procedures. However, it has been reported that the proportion of endocrine cells is constant throughout the pancreas with the exception of the ventral portion of the pancreatic head (37), and we confirmed that there was no difference in either BCA or ACA between samples from the head and those from the body or tail. Another limitation of the study was that we evaluated BCA as a surrogate for BCM. Thus, the different pancreas mass in each case might have affected

our findings, although it was difficult to determine pancreas mass because of the presence of pancreatic tumors. Nonetheless, estimates of BCM based on reference data (38) did not change our conclusion (data not shown), and an increase in BCA in obese subjects has been observed in both autopsy and surgically resected pancreas in the Caucasian population (4, 19), supporting our conclusion that the change in BCA in response to obesity is limited in Japanese. Finally, although we evaluated the history of obesity, none of the cases had a history of childhood obesity. Since postnatal beta cell replication is more frequently observed in the first 5 years of life (39, 40), we were not able to exclude the possibility that childhood obesity may promote BCM expansion in the Japanese population.

In conclusion, there was no increase in BCM in Japanese obese individuals who underwent pancreatic surgery, and BCM was not related to BMI, history of obesity or maximum BMI. These findings suggest that the increase in

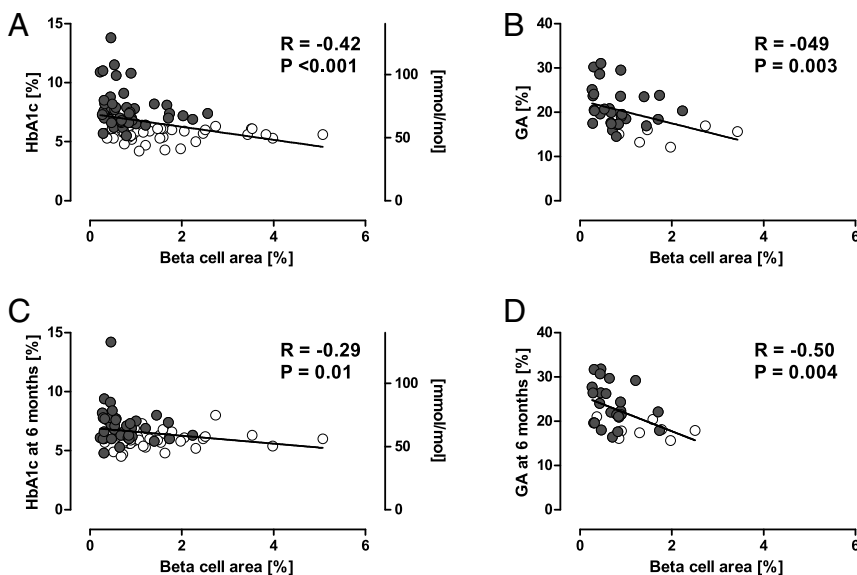


Figure 5. A and B: Correlations between BCA and preoperative HbA1c (N = 93) or glycated albumin (GA) (N = 35). C and D: Correlations between BCA and HbA1c (N = 77) or GA (N = 32) at 6 months after surgery. Gray and white circles show cases with and without diabetes, respectively. C and D: Cases that underwent total pancreatectomy were excluded.

BCM in the face of insulin resistance is extremely limited in Japanese. BCM was reduced by ~45% in patients with T2DM, and BCM, but not ACM, was associated with preoperative and postoperative glycemic control. These findings support the concept that BCM rather than ACM has a major role in regulating blood glucose level in humans.

Acknowledgments

We thank Yuko Madokoro, Department of Pathology, Keio University School of Medicine, for technical assistance and Dr. Wendy Gray, self-employed, for editing the manuscript.

Address all correspondence and requests for reprints to: Yoshifumi Saisho, MD, PhD, Department of Internal Medicine, Keio University School of Medicine, 35 Shinanomachi, Shinjuku-ku, Tokyo 160-8582, Japan, TEL: +81-3-3353-1211 (x62383), FAX: +81-3-3359-2745, E-mail: ysaisho@keio.jp.

This work was supported by Funding: Japan Diabetes Foundation, the Keio Gijuku Academic Development Funds, and a Grant-in-Aid for Scientific Research (15K09399) from the Ministry of Education, Culture, Sports, Science and Technology (MEXT) (Y.S.).

Disclosure statement: The authors have no conflict of interest. Y.S. is the guarantor of this work and, as such, had full access to all the data in the study and takes responsibility for the integrity of the data and the accuracy of the data analysis.

Author contributions: J.I. and Y.S. researched data and wrote the manuscript. S.S., K.K., R.M. and Y.W. contributed to discussion and reviewed/edited the manuscript. M.K. and Y.K. researched data and reviewed/edited the manuscript. T.Y. researched data, contributed to discussion and reviewed/edited the

manuscript. H.I. contributed to discussion and reviewed/edited the manuscript.

References

1. Saisho Y. Beta cell dysfunction: Its critical role in prevention and management of type 2 diabetes. *World J Diabetes*. 2015; 6:109–124.
2. Talchai C, Xuan S, Lin HV, Sussel L, Accili D. Pancreatic beta cell dedifferentiation as a mechanism of diabetic beta cell failure. *Cell*. 2012;150:1223–1234.
3. Polonsky KS, Given BD, Van Cauter E. Twenty-four-hour profiles and pulsatile patterns of insulin secretion in normal and obese subjects. *J Clin Invest*. 1988; 81:442–448.
4. Saisho Y, Butler AE, Manesso E, Elashoff D, Rizza RA, Butler PC. β -cell mass and turnover in humans: Effects of obesity and aging. *Diabetes Care*. 2013;36:111–117.
5. Rahier J, Guiot Y, Goebel RM, Sempoux C, Henquin JC. Pancreatic beta-cell mass in European subjects with type 2 diabetes. *Diabetes Obes Metab* 10 Suppl. 2008;4:32–42.
6. Kodama K, Tojar D, Yamada S, Toda K, Patel CJ, Butte AJ. Ethnic differences in the relationship between insulin sensitivity and insulin response: A systematic review and meta-analysis. *Diabetes Care*. 2013;36:1789–1796.
7. Kou K, Saisho Y, Satoh S, Yamada T, Itoh H. Change in beta-cell mass in Japanese nondiabetic obese individuals. *J Clin Endocrinol Metab*. 2013;98:3724–3730.
8. Sato S, Saisho Y, Inaishi J, Kou K, Murakami R, Yamada T, Itoh H. Effects of glucocorticoid treatment on beta- and alpha-cell mass in Japanese adults with and without diabetes. *Diabetes*. 2015;64: 2915–2927.
9. Saisho Y, Kou K, Tanaka K, Abe T, Kurosawa H, Shimada A, Meguro S, Kawai T, Itoh H. Postprandial serum C-peptide to plasma glucose ratio as a predictor of subsequent insulin treatment in patients with type 2 diabetes. *Endocr J*. 2011;58:315–322.
10. Kanazawa M, Yoshiike N, Osaka T, Numba Y, Zimmet P, Inoue S. Criteria and classification of obesity in Japan and Asia-Oceania. *Asia Pac J Clin Nutr* 11 Suppl. 2002;8:S732–S737.
11. Chari ST, Leibson CL, Rabe KG, Timmons LJ, Ransom J, de Andrade M, Petersen GM. Pancreatic cancer-associated diabetes mellitus: prevalence and temporal association with diagnosis of cancer. *Gastroenterology*. 2008;134:95–101.
12. Marselli L, Suleiman M, Masini M, Campani D, Bugliani M, Syed F, Martino L, Focosi D, Scatena F, Olimpico F, Filipponi F, Masiello P, Boggi U, Marchetti P. Are we overestimating the loss of beta cells in type 2 diabetes? *Diabetologia*. 2014;57:362–365.
13. Butler AE, Janson J, Bonner-Weir S, Ritzel R, Rizza RA, Butler PC. Beta-cell deficit and increased beta-cell apoptosis in humans with type 2 diabetes. *Diabetes*. 2003;52:102–110.
14. Mizukami H, Takahashi K, Inaba W, Tsuboi K, Osonoi S, Yoshida T, Yagihashi S. Involvement of oxidative stress-induced DNA damage, endoplasmic reticulum stress, and autophagy deficits in the decline of beta-cell mass in Japanese type 2 diabetic patients. *Diabetes Care*. 2014;37:1966–1974.
15. Butler AE, Dhawan S, Hoang J, Cory M, Zeng K, Fritsch H, Meier JJ, Rizza RA, Butler PC. Beta-cell deficit in obese type 2 diabetes, a minor role of beta-cell dedifferentiation and degranulation. *J Clin Endocrinol Metab*. 2016;101:523–532.

16. Muller WA, Faloona GR, Aguilar-Parada E, Unger RH. Abnormal alpha-cell function in diabetes. Response to carbohydrate and protein ingestion. *N Engl J Med.* 1970;283:109–115.
17. Henquin JC, Rahier J. Pancreatic alpha cell mass in European subjects with type 2 diabetes. *Diabetologia.* 2011;54:1720–1725.
18. Kilmann G, Zhao B, Jo J, Periwal V, Witkowski P, Misawa R, Hara M. Altered islet composition and disproportionate loss of large islets in patients with type 2 diabetes. *PLoS One.* 2011;6:e27445.
19. Mezza T, Muscoguri G, Sorice GP, Clemente G, Hu J, Pontecorvi A, Holst JJ, Giaccari A, Kulkarni RN. Insulin resistance alters islet morphology in nondiabetic humans. *Diabetes.* 2014;63:994–1007.
20. Mizukami H, Takahashi K, Inaba W, Osonoi S, Kamata K, Tsuboi K, Yagihashi S. Age-associated changes of islet endocrine cells and the effects of body mass index in Japanese. *J Diabetes Invest.* 2014; 5:38–47.
21. Fujita Y, Kozawa J, Iwahashi H, Yoneda S, Uno S, Yoshikawa A, Okita K, Eguchi H, Nagano H, Imagawa A, Shimomura I. Increment of serum C-peptide measured by glucagon test closely correlates with human relative beta-cell area. *Endocr J.* 2015;62:329–337.
22. Sullivan BA, Hollister-Lock J, Bonner-Weir S, Weir GC. Reduced Ki67 staining in the postmortem state calls into question past conclusions about the lack of turnover of adult human beta-cells. *Diabetes.* 2015;64:1698–1702.
23. Caballero F, Siniakowicz K, Hollister-Lock J, Duran L, Katsuta H, Yamada T, Lei J, Deng S, Westermark GT, Markmann J, Bonner-Weir S, Weir GC. Birth and death of human beta-cells in pancreases from cadaver donors, autopsies, surgical specimens, and islets transplanted into mice. *Cell Transplant.* 2014;23:139–151.
24. Jensen CC, Cnop M, Hull RL, Fujimoto WY, Kahn SE. Beta-cell function is a major contributor to oral glucose tolerance in high-risk relatives of four ethnic groups in the U.S. *Diabetes.* 2002;51:2170–2178.
25. Moller JB, Pedersen M, Tanaka H, Ohsugi M, Overgaard RV, Lyngé J, Almind K, Vasconcelos NM, Poulsen P, Keller C, Ueki K, Ingwersen SH, Pedersen BK, Kadokawa T. Body composition is the main determinant for the difference in type 2 diabetes pathophysiology between Japanese and Caucasians. *Diabetes Care.* 2014;37: 796–804.
26. Hsia DS, Larrivee S, Cefalu WT, Johnson WD. Impact of lowering BMI cut points as recommended in the revised American Diabetes Association's Standards of Medical Care in Diabetes—2015 on diabetes screening in Asian Americans. *Diabetes Care.* 2015;38: 2166–2168.
27. Kamata K, Mizukami H, Inaba W, Tsuboi K, Tateishi Y, Yoshida T, Yagihashi S. Islet amyloid with macrophage migration correlates with augmented β -cell deficits in type 2 diabetic patients. *Amyloid.* 2014;21:191–201.
28. Kou K, Saisho Y, Sato S, Yamada T, Itoh H. Islet number rather than islet size is a major determinant of beta- and alpha-cell mass in humans. *J Clin Endocrinol Metab.* 2014;99:1733–1740.
29. Le Bacquer O, Kerr-Conte J, Gargani S, Delalleau N, Huyvaert M, Gmyr V, Froguel P, Neve B, Pattou F. TCF7L2 rs7903146 impairs islet function and morphology in non-diabetic individuals. *Diabetologia.* 2012;55:2677–2681.
30. Ritzel RA, Butler AE, Rizza RA, Veldhuis JD, Butler PC. Relationship between beta-cell mass and fasting blood glucose concentration in humans. *Diabetes Care.* 2006;29:717–718.
31. Meier JJ, Menge BA, Breuer TG, Muller CA, Tannapfel A, Uhl W, Schmidt WE, Schrader H. Functional assessment of pancreatic beta-cell area in humans. *Diabetes.* 2009;58:1595–1603.
32. Saisho Y, Kou K, Tanaka K, Abe T, Shimada A, Kawai T, Itoh H. Association between beta cell function and future glycemic control in patients with type 2 diabetes. *Endocr J.* 2013;60:517–523.
33. Pannala R, Basu A, Petersen GM, Chari ST. New-onset diabetes: a potential clue to the early diagnosis of pancreatic cancer. *The Lancet. Oncology.* 2009;10:88–95.
34. Chari ST, Zapiach M, Yadav D, Rizza RA. Beta-cell function and insulin resistance evaluated by HOMA in pancreatic cancer subjects with varying degrees of glucose intolerance. *Pancreatology.* 2005; 5:229–233.
35. Katsumichi I, Pour PM. Diabetes mellitus in pancreatic cancer: is it a causal relationship? *Am J Surg.* 2007;194:S71–75.
36. Aggarwal G, Ramachandran V, Javeed N, Arumugam T, Dutta S, Klee GG, Klee EW, Smyrk TC, Bamlet W, Han JJ, Rumie Vittar NB, de Andrade M, Mukhopadhyay D, Petersen GM, Fernandez-Zapico ME, Logsdon CD, Chari ST. Adrenomedullin is up-regulated in patients with pancreatic cancer and causes insulin resistance in beta cells and mice. *Gastroenterology.* 2012;143:1510–1517 e1511.
37. Sakuraba H, Mizukami H, Yagihashi N, Wada R, Hanyu C, Yagihashi S. Reduced beta-cell mass and expression of oxidative stress-related DNA damage in the islet of Japanese Type II diabetic patients. *Diabetologia.* 2002;45:85–96.
38. Saisho Y, Butler AE, Meier JJ, Monchamp T, Allen-Auerbach M, Rizza RA, Butler PC. Pancreas volumes in humans from birth to age one hundred taking into account sex, obesity, and presence of type-2 diabetes. *Clin Anat.* 2007;20:933–942.
39. Meier JJ, Butler AE, Saisho Y, Monchamp T, Galasso R, Bhushan A, Rizza RA, Butler PC. Beta-cell replication is the primary mechanism subserving the postnatal expansion of beta-cell mass in humans. *Diabetes.* 2008;57:1584–1594.
40. Gregg BE, Moore PC, Demozay D, Hall BA, Li M, Husain A, Wright AJ, Atkinson MA, Rhodes CJ. Formation of a human beta-cell population within pancreatic islets is set early in life. *J Clin Endocrinol Metab.* 2012;97:3197–3206.

CASE REPORT

Open Access



CrossMark

Anisakiasis mimics cancer recurrence: two cases of extragastrointestinal anisakiasis suspected to be recurrence of gynecological cancer on PET-CT and molecular biological investigation

Yuya Nogami¹, Yoko Fujii-Nishimura², Kouji Banno^{1*}, Atsushi Suzuki¹, Nobuyuki Susumu¹, Taizo Hibi³, Koji Murakami⁴, Taketo Yamada^{5,7}, Hiromu Sugiyama⁶, Yasuyuki Morishima⁶ and Daisuke Aoki¹

Abstract

Background: We report two cases of anisakiasis lesions that were initially suspected to be recurrence of gynecological cancer by positron emission tomography-computed tomography (PET-CT). Both cases were extragastrointestinal anisakiasis that is very rare.

Case presentation: The first case was a patient with endometrial cancer. At 19 months after surgery, a new low density area of 2 cm in diameter in liver segment 4 was found on follow-up CT. In PET-CT, the lesion had abnormal ¹⁸fluoro-deoxyglucose (FDG) uptake with elevation in the delayed phase, with no other site showing FDG uptake. Partial liver resection was performed. A pathological examination revealed no evidence of malignancy, but showed necrotic granuloma with severe eosinophil infiltration and an irregular material with a lumen structure in the center. Parasitosis was suspected and consultation with the National Institute of Infectious Diseases (NIID) showed the larvae to be *Anisakis simplex* sensu stricto by genetic examination.

The second case was a patient with low-grade endometrial stromal sarcoma (LG-ESS). At 8 months after surgery, swelling of the mediastinal lymph nodes was detected on CT and peripheral T-cell lymphoma was diagnosed by biopsy. A new peritoneal lesion with abnormal FDG uptake was detected on pre-treatment PET-CT and this lesion was increased in size on post-treatment PET-CT. Tumorectomy was performed based on suspected dissemination of LG-ESS recurrence. The findings in a pathological examination were similar to the first case and we again consulted the NIID. The larvae was identified as *Anisakis pegreffii*, which is a rare pathogen in humans.

Having experienced these rare cases, we investigated the mechanisms of FDG uptake in parasitosis lesions by immunohistochemical staining using antibodies to glucose transporter type 1 (GLUT-1) and hexokinase type 2 (HK-2). While infiltrated eosinophils were negative, macrophages demonstrated positive for both antibodies. Therefore, mechanisms behind FDG uptake may involve macrophages, which is common among various granulomas. This is the first report to investigate parasitosis in such a way.

Conclusion: These cases suggest that anisakiasis is a potential differential diagnosis for a lesion with FDG uptake in PET-CT, and that it is difficult to distinguish this disease from a recurrent tumor using PET-CT alone.

Keywords: Extragastrointestinal anisakiasis, *Anisakis*, PET-CT, Gynecological cancer, Genetic examination, PCR, Glucose transporter type 1, Hexokinase type 2

* Correspondence: kbanno@z7.keio.jp

¹Department of Obstetrics and Gynecology, Keio University School of Medicine, Shinanomachi 35 Shinjuku-ku, Tokyo 160-8582, Japan
Full list of author information is available at the end of the article

Background

Positron emission tomography (PET)-computed tomography (CT) is increasingly commonly used for various cancers, especially for detection of a metastasis or recurrent lesion. For gynecological cancers, PET-CT is used for examination of possible malignancy of lesions detected by CT or MRI in postoperative follow-up [1]. A lesion with abnormal uptake indicates possible recurrence, and PET-CT is believed to have better accuracy for determining malignancy compared to CT or MRI [2–4]. Surgery is rarely performed for postoperative recurrence, but an exact diagnosis is difficult without a pathological examination. Thus, a lesion that mimics tumor recurrence can lead to unnecessary surgery, chemotherapy, and radiotherapy.

Anisakiasis is relatively common in East Asia due to consumption of raw fish. Anisakiasis often presents with acute abdominal symptoms caused by an allergic reaction in the gastric mucosa. Anisakiasis usually infect gastric or intestinal walls, and the feature of the images including PET-CT have been reported [5, 6]. Extraintestinal anisakiasis is less common, but such cases have been reported [7–9]. After penetrating the bowel wall, *Anisakis* produce a granuloma as their bodies collapse with time. Incidental detection of this lesion is difficult to distinguish from recurrence in patients with a history of malignancy. This may result in unnecessary resection, and in some cases the collapsing worm body may make the final diagnosis difficult, even after resection.

We experienced two cases of extraintestinal anisakiasis in which a recurrent gynecological tumor was initially suspected on imaging. PET-CT showed that the lesions had abnormal uptake in both cases. Even PET-CT could not distinguish between anisakiasis and a tumor metastasis, and diagnosis in the second case was further complicated by collapse of the worm body. A polymerase chain reaction (PCR) using a specific primer for an *Anisakis*-specific region confirmed anisakiasis in both cases.

Besides, we investigated the mechanism of FDG uptake to granuloma of parasitosis. These cases are rare but reported already, however, the mechanisms are still unknown. We investigated it by immunostaining using anti-bodies to glucose transporter type 1 (GLUT-1) and hexokinase type 2 (HK-2), which are recognized as the key factors of FDG uptake in PET.

We describe these two cases with a literature review and molecular biological investigation. We suggest that anisakiasis should be a differential diagnosis for a solitary lesion detected on PET-CT, and we show the utility of PCR for diagnosis of anisakiasis.

Case presentation

Case 1

The patient was a 44-year-old woman who had been diagnosed with endometrial cancer. She underwent semi-

radical hysterectomy, bilateral salpingo-oophorectomy, pelvic and paraaortic lymph node dissection, and partial omentectomy. A pathological examination revealed that the tumor was grade 2 endometrioid adenocarcinoma with more than 50 % myometrial invasion, and clinical stage Ic (FIGO 1988). Given the intermediate risk of recurrence based on the pathological result, she received adjuvant chemotherapy of 6 cycles of a cyclophosphamide-adriamycin-cisplatin (CAP) regimen.

Follow-up CT performed 19 months after surgery detected a new low density area of 15 mm in diameter in segment 4 of the liver (Fig. 1). Serum tumor markers including CA125 and CA19-9 were not elevated, and were similar to the levels before initial therapy. Data from blood tests are shown in Table 1. MRI showed a liver tumor with a high intensity signal in diffusion-weighted imaging (DWI). In a dynamic study using gadolinium ethoxybenzyl diethylenetriaminepentaacetic acid (Gd-EOB-DTPA), early staining in the arterial phase was unclear and the lesion gave a low intensity signal in the hepatobiliary phase (Fig. 2). These findings were compatible with a metastatic tumor.

PET-CT was performed to confirm the presence of a malignant liver tumor and to search for other metastases. The liver lesion had no specific ¹⁸fluoro-deoxyglucose (FDG) uptake compared with normal liver tissue in the early phase, and this was elevated in the delayed phase (standardized uptake value (SUV) max: 2.52 in the early phase, 3.61 in the delayed phase) (Fig. 3). No other metastasis was detected. Recurrence of endometrial cancer was suspected and partial resection of the liver was planned for the solitary metastasis.

The resected liver sample included a white nodule of 17 mm in diameter with a regular border macroscopically (Fig. 4). Microscopic examination showed clear eosinophil infiltration and granuloma with an

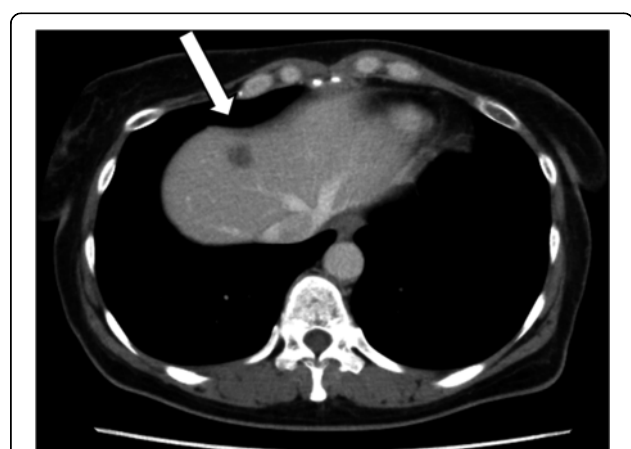


Fig. 1 Axial slice on enhanced CT in the equilibrium phase. A low density area was detected in segment 4 of the liver (arrow)

Table 1 Data from blood test of case 1. Eosinophilia was not shown and no tumor marker was elevated

TB	0.8	mg/dl	(0.4–1.2)	WBC	6000	/μl	(3600–8900)	AFP	1	ng/ml	(<20)
AST	17	U/L	(5–37)	Neutro	55.2	%	(37–72)	PIVKA-II	12	mAU/ml	(<40)
ALT	15	U/L	(6–43)	Lymph	37.6	%	(25–48)	CA19-9	<1	U/ml	(<35)
ALP	245	U/L	(110–348)	Mono	3.7	%	(2–12)	CA125	16	U/ml	(<37)
γGTP	13	U/L	(0–75)	Eosino	3.7	%	(1–9)				
BUN	11.6	mg/dl	(9–21)	Baso	2.2	%	(0–2)				
Cr	0.62	mg/dl	(0.5–0.8)	Hb	13.9	g/dl	(11.2–15.2)				
				HCT	42	%	(35.6–45.4)				
				Plt	2.43	10 ⁶ /μl	(1.53 – 3.46)				

TB total bilirubin, AST aspartate aminotransferase, ALT alanine aminotransferase, ALP alkaline phosphatase, γGTP γ glutamyl transpeptidase, BUN blood urea nitrogen, Cr creatinine, WBC white blood cell, Neutro neutrophil, Lymph lymphocyte, Mono monocyte, Eosino eosinophil, Baso basophil, Hb hemoglobin, HCT haematocrit, Plt platelet, AFP alpha-fetoprotein, PIVKA-II protein induced by vitamin K absence or antagonist-II

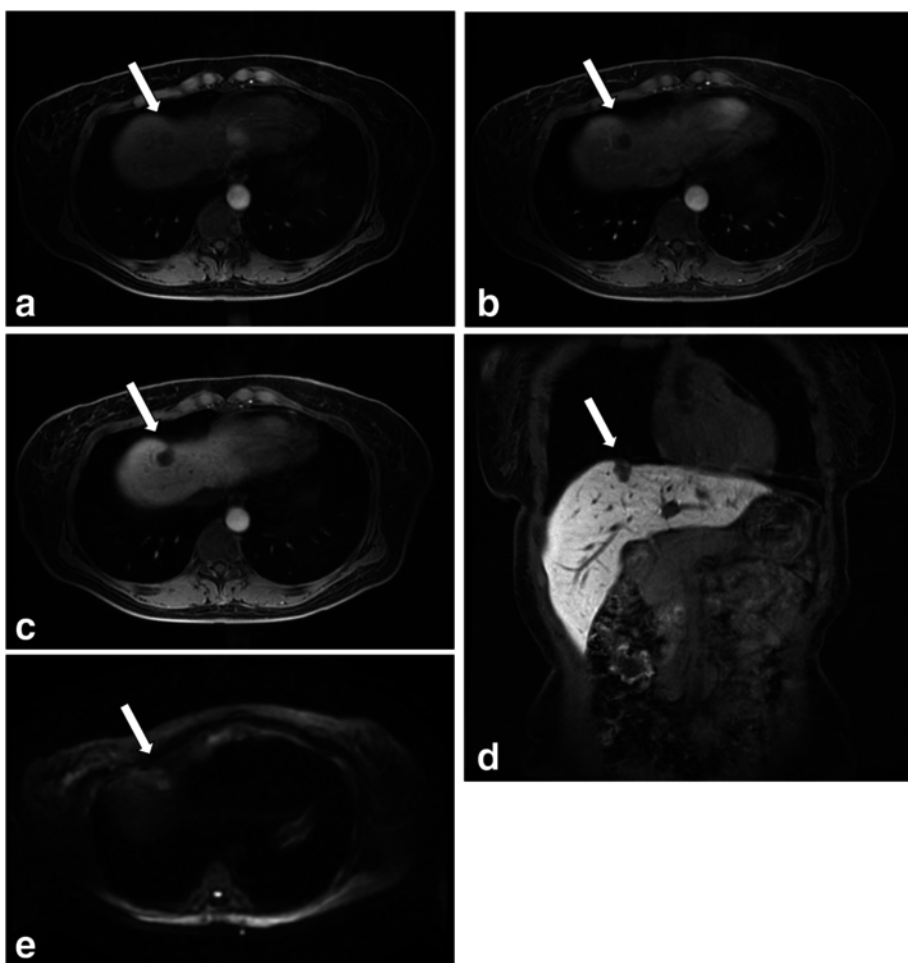


Fig. 2 Axial slices of liver acquisition with volume acceleration flex on dynamic MRI in pre-contrast phase (a), arterial phase (b) and the hepatobiliary phase (c). Coronal slice on enhanced MRI in the hepatobiliary phase (d). The lesion (arrows) gave a low intensity signal in all phases and a high intensity signal in DWI (e)

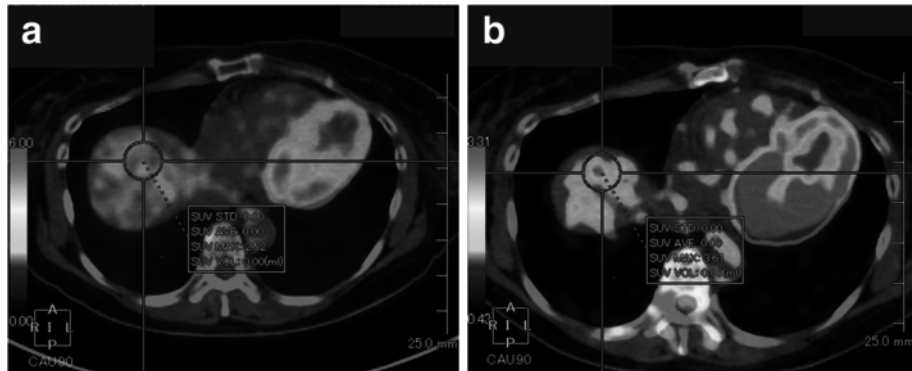


Fig. 3 Axial slice on PET-CT showing the liver lesion in the early (a) and delayed phase (b). FDG uptake was undetectable among physiological uptake of the liver in the early phase; however, uptake elevated (SUVmax: 2.52 to 3.61) and was detectable in the delayed phase

exogenous material in the center. There were no findings consistent with malignancy. The exogenous material had a lumen structure which was suspected to be due to larva migrans. The slide was sent to the National Institute of Infectious Diseases (NIID) to identify the larvae. A detailed microscopic examination revealed that the larvae had Y-shape lateral cords and renette cells, which are specific to *Anisakis* (Fig. 5).

A PCR method using a specific primer pair was performed for identification of the *Anisakis* species. The methods of DNA amplification and sequencing are described under a separate heading. This search revealed that the larvae were *Anisakis simplex* sensu stricto (Fig. 6).

These findings showed that the liver lesion was not due to recurrence of endometrial cancer. The patient has had no recurrence for 4 years.

Case 2

The patient was a 33-year-old woman who had been diagnosed with low-grade endometrial stromal sarcoma (LG-ESS). She underwent extended total hysterectomy and bilateral salpingo-oophorectomy. Pathological examination revealed clinical stage IB (FIGO 2008). High-dose medroxyprogesterone acetate (400 mg/day) was administered as adjuvant therapy.

Follow-up CT 8 months after surgery indicated swelling of mediastinal lymph nodes. Biopsy of these nodes performed by a respiratory surgeon revealed peripheral T-cell lymphoma (PTCL), rather than recurrence of LG-ESS. She was referred to the department of hematology. PET-CT performed for pretreatment staging showed abnormal FDG uptake in a nodule of 10 mm in diameter in the peritoneum just below the lower median abdominal wall, in addition to uptakes in mediastinal lymph nodes. The nodule was located clearly extragastrointestinally. The patient was treated with 3 cycles of a cyclophosphamide-adriamycin-vincristine-prednisolone (CHOP) regimen. Post-treatment PET-CT showed that the nodule in the peritoneum increased in size to 16 mm with abnormal FDG uptake (SUVmax: 4.02 in the early phase, 4.21 in the delayed phase) (Fig. 7), despite a marked effect of the therapy on other lesions. Data from blood tests before chemotherapy are shown in Table 2.

The PET-CT findings for the nodule were not compatible with PTCL; therefore, exploratory laparotomy was performed to examine possible dissemination of LG-ESS. The nodule was on the omentum and partial omentectomy was performed (Fig. 8). No other macroscopic lesion in the abdomen was found. Pathological examination revealed that the nodule had an abscess with clear eosinophil infiltration. An exogenous material that appeared to be a larva was found in the center of the abscess. The larva body had collapsed, but the specific Y-shape lateral cord was recognizable (Fig. 9). Based on the experience of the first case, we sent the slide to the NIID. The PCR method revealed that the worm was *Anisakis pegreffii* (Fig. 6), which is

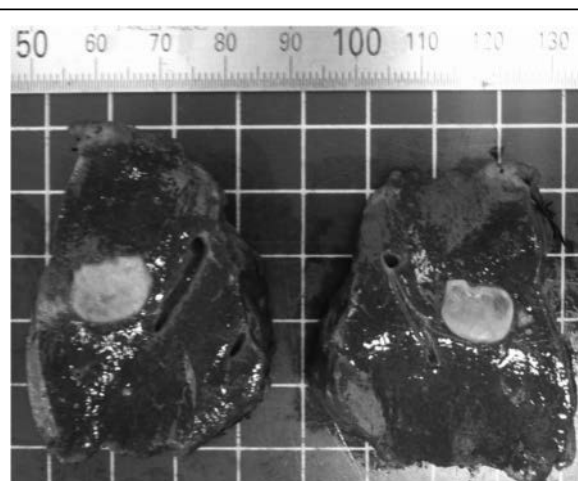


Fig. 4 Macroscopic findings in the resected liver, showing a white node with a regular border of about 2 cm in diameter

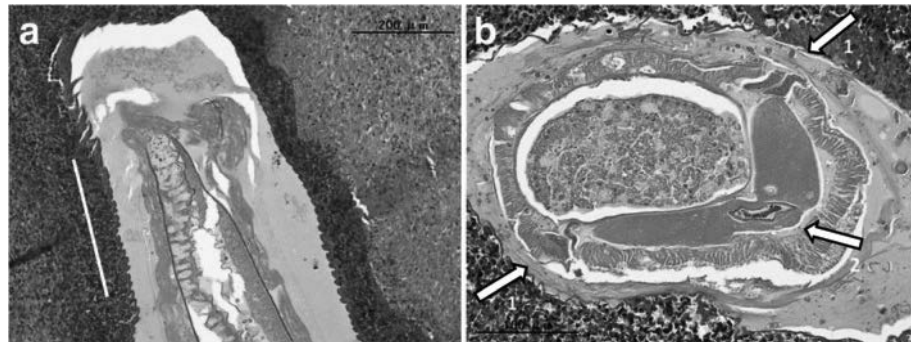


Fig. 5 **a** Sagittal slice of the larva, showing a wave-shaped (cross-striated) border (white line). **b** Axial slice of the larva, showing a Y-shaped lateral cord (arrows 1) and a retene cell (arrow 2). These findings are characteristics of *Anisakis*

rare as an infectious pathogen in human. These findings showed that the patient did not have recurrent LG-ESS. The patient has had no recurrence of LG-ESS for 2 years and that of PTCL for a year.

Imaging parameters of CT, MRI, and PET-CT

CT: The device is an Acquilion ONE (Toshiba Medical Systems, Otawara, Japan) by using a tube voltage of 120 kVp and tube current varied between 96 mA and 160 mA. Slice thickness is 5 mm for abdominal scanning as a post-operative follow up in a cancer patient.

MRI: The device is a Discovery MR750 3.0 T (GEHealthcare, Waukesha, Wisconsin, USA) using 32-channel torso coil as a receiver. Liver acquisition with volume acceleration flex (LAVA-Flex) is practiced with EOB dynamic MRI in our institute. The acquisition sequence is LAVA Flex with parameters as follows: Time of repetition (TR)/time of

echo (TE) = 3.9/1.7 msec, flip angle = 12°, slice thickness/gap = 3.6/1.8 mm, matrices = 256 × 256, acquisition time = 19 s. Gd-EOB-DTPA: Primovist® (Bayer Healthcare AG, Berlin, Germany)-enhanced images in the hepatobiliary phase are taken at 15 min after contrast injection.

PET-CT: Biograph mCT (Siemens Medical Solutions, Knoxville, TN, USA). In our institute, patients routinely receive DPS for differentiation. Patients were administered 3.7 MBq/kg of FDG and received routine PET-CT DPS at 1 and 2 h after administration. Data were analyzed on an AZE workstation (AZE Ltd, Tokyo, Japan).

Molecular investigation

Identification of anisakid nematodes (DNA amplification and sequencing)

The worm body was scratched from the deparaffinized slide under stereoscopic microscopy and placed in a

The primers used for polymerase chain reaction amplification

• 1st round for entire ITS region

NC5 (forward; 5'-GTAGGTGAACTCGCGAAGGATCATT-3')
NC2 (reverse; 5'-TTAGTTCTTTCTCCGCT-3')

• 2nd round for specific region in ITS (made originally by NIID)

AniT1F1 (forward; 5'-GTTGAACAACGGTGACCAATTGGC-3')
AniT1R1 (reverse; 5'-GAGTGATCCACCGCCAAGATTGTAC-3')

The sequences of amplified products of case1 and 2

C1 (As)	GTCTACGCCGTATCTAGCTTCTGCCTGGACCGTCAGTTGCGATGAAAGATGCGGAGAAAG	60
C2 (Ap)	GTCTACGCCGTATCTAGCTTCTGCCTGGACCGTCAGTTGCGATGAAAGATGCGGAGAAAG	60
.....
C1 (As)	TTCTTTGTTTGGCTGCTAATCATCATTGATGAGCAGTAGCTTAAGGCAGAGTTGAGCA	120
C2 (Ap)	TTCTTTGTTTGGCTGCTAATCATCATTGATGAGCAGCTTAAGGCAGAGTTGAGCA	120
.....
C1 (As)	GACTTAATGAGCCACGCTAGGTGGCCGCCAAACCCAAAACACAACCGGTCTATTTGACA	180
C2 (Ap)	GACTTAATGAGCCACGCTAGGTGGCCGCCAAACCCAAAACACAACCGGTCTATTTGACA	180
.....
C1 (As)	TTGTTATTCATTGTATGTGTTGAAAAT	208
C2 (Ap)	TTGTTATTCATTGTATGTGTTGAAAAT	208
.....

Fig. 6 Primers used for genetic identification of *Anisakis* and sequences obtained

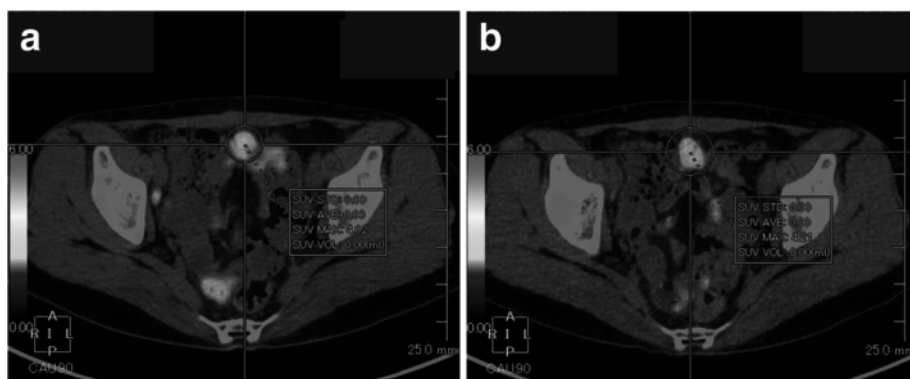


Fig. 7 Axial slice on PET-CT after CHOP therapy in the early (a) and delayed phase (b). The lesion had increased in size compared with pre-treatment and showed FDG uptake (SUVmax: 4.02 to 4.21)

plastic tube. DNA was extracted using proteinase K (Qiagen) and SDS (Sigma-Aldrich) [10]. The entire internal transcribed spacer (ITS) region (ITS1, 5.8S rDNA and ITS2) was amplified by PCR using the primers NC5 and NC2 in the first round. Then nested PCR was performed in the second round to amplify a specific region in the ITS1 using the following primers that were originally constructed: AniT1F1: 5'-GTTGAACAAACGGTGA CCAATTGGC-3', and AniT1R1: 5'. PCR was conducted by the method indicated in reference [10]. An amplification product of 208 bp was obtained. Sequence similarities were determined by a BLAST search of the DNA Data Bank of Japan (DDBJ) (<http://www.ddbj.nig.ac.jp/index-e.html>). Sequence alignment and comparison was facilitated by the GENETYX-WIN program (ver. 7.0, Software Development Co, Tokyo, Japan).

Investigation for the mechanism of FDG uptake (immunochemical staining using anti-bodies to GLUT-1 and HK-2)

Once FDG is uptaken to cells through the GLUT-1 and phosphorylated by HK-2, FDG is unable to pass out of cells unless dephosphorylated by glucose-6-phosphatase

(G6P). Because malignant cells have a high ratio of HK-2/G6P, they present an elevation of FDG uptake in delayed phase in dual-phase scanning (DPS) of PET-CT. Since both cases indicated the elevation, recurrence was a stronger consideration among other differential diagnoses.

Cases of parasitosis suspected as malignancy in PET have been previously reported but are very rare [11–13]. There are no reports investigating the mechanisms of FDG uptake in parasitosis granuloma. We researched them to develop ways to differentiate them by investigating overexpression of GLUT-1 and HK-2.

GLUT-1 expression was evaluated immunohistochemically using rabbit polyclonal anti-Glucose Transporter GLUT1 antibody (ab652, Abcam, Cambridge, UK) at a dilution of 1:500. HK-2 expression was evaluated with rabbit polyclonal anti-Hexokinase Type II (AB3279, Chemicon International, Temecula, USA) diluted at 1:500. Immunohistochemical staining was performed using the Leica Bond-Max automatic immunostainer and the Bond Polymer Refine Detection kit (Leica).

In both cases, only macrophages were positive for both antibodies; GLUT-1 and HK-2. The eosinophils, which

Table 2 Data from blood test of case 2. Eosinophilia was not shown and sIL2R was elevated due to lymphoma

TB	0.5	mg/dl	(0.4–1.2)	WBC	5400	/μl	(3600–8900)	sIL2R	381	U/ml	(<20)
AST	13	U/L	(5–37)	Neutro	53.3	%	(37–72)	CA125	11	U/ml	(<37)
ALT	7	U/L	(6–43)	Lymph	34.9	%	(25–48)				
ALP	237	U/L	(110–348)	Mono	5.8	%	(2–12)				
LDH	184	U/L	(0–75)	Eosino	5.4	%	(1–9)				
BUN	10.4	mg/dl	(9–21)	Baso	0.6	%	(0–2)				
Cr	0.6	mg/dl	(0.5–0.8)	Hb	13	g/dl	(11.2–15.2)				
				HCT	39.1	%	(35.6–45.4)				
				Plt	2.5	10 ⁶ /μl	(1.53–3.46)				

TB total bilirubin, AST aspartate aminotransferase, ALT alanine aminotransferase, ALP alkaline phosphatase, LDH lactate dehydrogenase, BUN blood urea nitrogen, Cr creatinine, WBC white blood cell, Neutro neutrophil, Lymph lymphocyte, Mono monocyte, Eosino eosinophil, Baso basophil, Hb hemoglobin, HCT haematocrit, Plt platelet, sIL-2R soluble interleukin-2 receptor



Fig. 8 Intra-abdominal findings in exploratory laparotomy. The lesion was located on the omentum with adhesion to the parietal peritoneum

were infiltrated around worm bodies, were negative for them (Figs. 10, 11). These results suggest that eosinophil infiltration may not boost FDG uptake or have any specific roles. Instead, the reason for FDG uptake to parasitosis granuloma may be the macrophages, which is commonly seen in granulomas.

Discussion

Extragastrointestinal anisakiasis accounts for 0.45 % of cases of anisakiasis in Japan [14]. The condition is caused by an *Anisakis* worm penetrating the bowel wall and forming an intra-abdominal colony. Cases in the omentum have been described in Japan and Italy [7, 15]. Occurrence as a solitary liver lesion is particularly rare, with the only examples found in eight cases reported in Japan [16, 17]. Most cases of

extragastrointestinal anisakiasis are asymptomatic and detected incidentally.

In the present two cases, malignant metastatic tumor was indicated as first choice of differential diagnosis by two imaging modalities. Dynamic MRI using contrast agent is often performed as the detailed examination for hepatic tumor, as in case 1. Low signal in hepatobiliary phase without early enhancement is compatible with metastatic tumor. However, because Gd-EOB-DTPA contrasting is dependent on expression of OATP1B1/3 [18], and parasitic granuloma does not necessarily show expression of OATP1B1/3, Gd-EOB-DTPA may not be useful for differentiating between metastatic tumor and parasitic granuloma. Using Gd-EOB-DTPA contrast benefits in clarifying the tumor location. The diagnostic efficacy of PET-CT for extragastrointestinal anisakiasis has not been examined because of the rarity of the disease. Our cases indicated that lesions of extragastrointestinal anisakiasis present with abnormal FDG uptake and were difficult to distinguish from a malignant tumor. *Anisakis* cannot live in the human body and die immediately, and thus FDG uptake was not directly associated with the worm body, but with inflammatory cells around the body. Dual-phase scanning is a well-known method for distinguishing between inflammation and malignancy [19–22], based on the observation that malignant lesions have elevated FDG uptake in the delayed phase compared with the early phase. However, the lesions in both of our cases showed elevation in delayed phases, especially in case 1. Without previous CT or MRI, the tumor might not have been detected using only the early phase scan. There has been a report of an anisakiasis case without FDG uptake [16] and the uptake decreased with time in our second case, suggesting that FDG uptake in anisakiasis lesions may decrease with time. This may help to distinguish it from malignancy, but it remains difficult to observe without therapy for cases in which malignancy is suspected.

Anisakiasis occurs due to eating of infected raw fish, such as mackerel, and horse mackerel. Consumption of raw fish is common in Asia, including Japan, and Northern Europe [23], and there is a recent trend to expansion of this behavior in the United States [24]. Food and drug administration in the United States and European Food Safety Authority in Europe recommend the frozen stock required for raw fish to prevent parasitosis. Increased use of imaging modalities such as MRI and PET-CT is likely to lead to more incidental findings of asymptomatic lesions [25], and this may lead to an increase in cases similar to those in this report. This is a concern because differential diagnosis from a malignant tumor is difficult for these lesions. The difficulty was provided by time lag. There is a time lag between infection and detection of a lesion, since generating a granuloma or an abscess in anisakiasis takes 2 months to 2 years [26].



Fig. 9 The nodule had an abscess with clear eosinophil infiltration. The larva body had collapsed, but the specific Y-shaped lateral cord was recognizable (arrow)

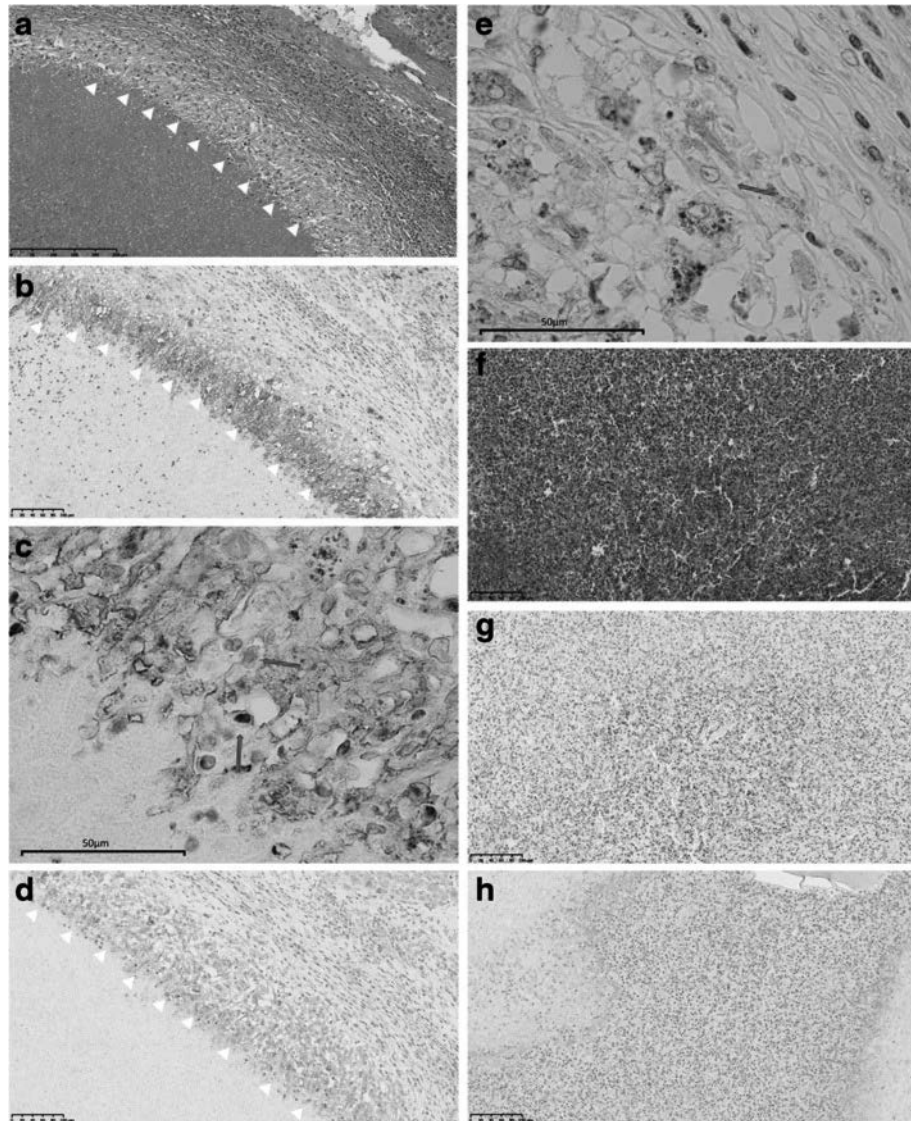


Fig. 10 In case 1, macrophages around abscess (a HE, arrows) were positive for GLUT-1 on the cell membrane (b, c, arrows) and HK-2 in the cytoplasm (d, e, arrows). Extensive eosinophil infiltrate (f HE, throughout the whole figure) were negative for GLUT-1 (g) and HK-2 (h)

The prior imaging to the detection of the tumor was 10 months in case 1, and 2 months in case 2. It is suspected that the patients were infected and granuloma formation occurred during this interval. The hematological or serological acute reaction of infection and the patient's memory of symptoms or food consumption can be lost due to this time lag. In this situation, a test for eosinophilia, a specific antibody test and history taking, which are important in diagnosis of parasitosis, are less useful. In fact, eosinophilia was not seen in either of our cases and a specific antibody for *Anisakis* was negative in the first case. And we retook the patients' history retrospectively after surgery, neither of the patients remembered a characteristic dietary history. The difficulty of diagnosing is not only because of the

vagueness of memory, but is also related to the existence of asymptomatic cases. Our two cases were also asymptomatic cases and there were no imaging findings on contrast CT. Generally, *Anisakis* larvae bite the intestinal wall, which causes acute severe abdominal pain. The pain is caused mainly by allergic reaction, rather than mechanical stimulus. Even in extragastrointestinal anisakiasis, which larvae penetrate the wall of the gastrointestinal tract, many cases are detected incidentally. There seems to be many asymptomatic cases.

The risk of recurrence of a primary malignancy should also be considered. In our first case, the risk of recurrence of endometrial cancer was intermediate, at about 10 % at 20 months after initial therapy [27]. In the

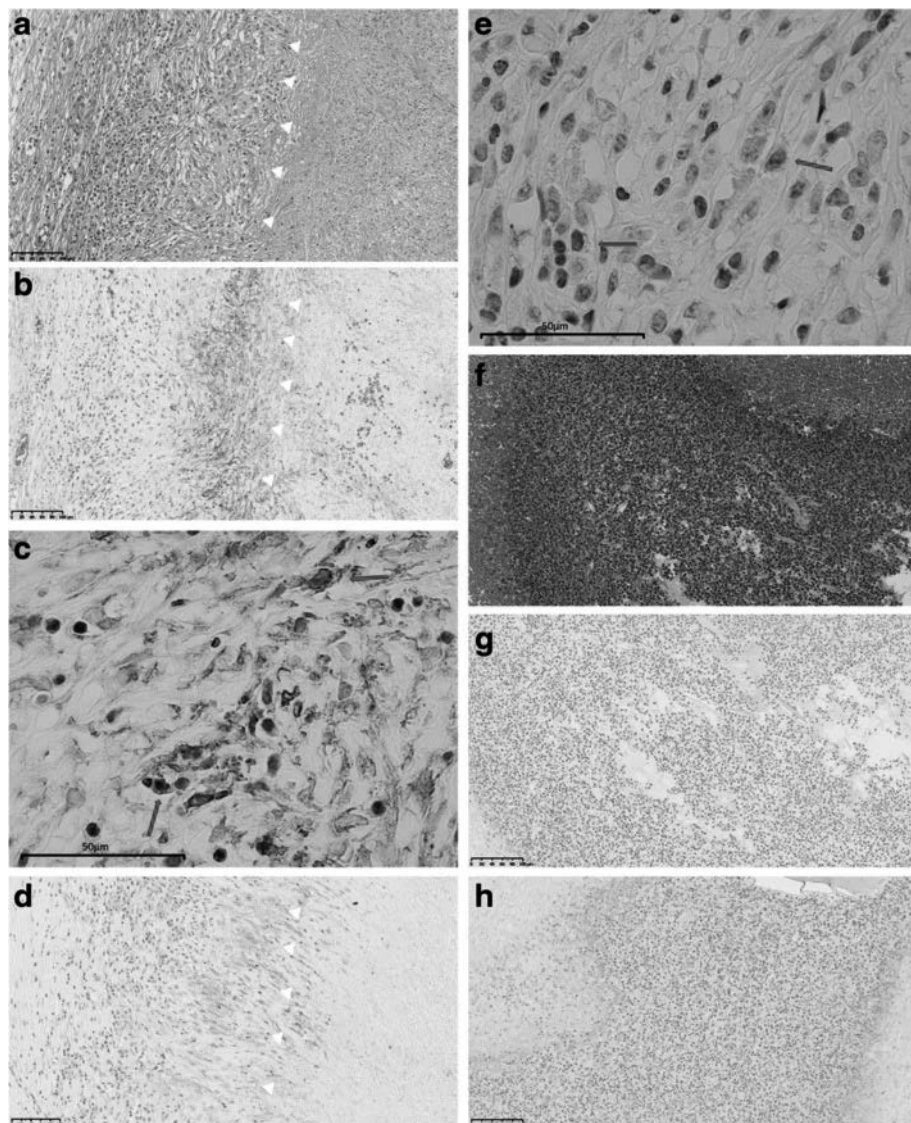


Fig. 11 In case 2, macrophages around abscess (a HE, arrows) were positive for GLUT-1 on the cell membrane (b, c, arrows) and HK-2 in the cytoplasm (d, e, arrows). Extensive eosinophil infiltrate (f HE, throughout the whole figure) were negative for GLUT-1 (g) and HK-2 (h)

second case, the patient had stage I LG-ESS. The recurrence risk for this cancer is over 30 %, even in stage I, although the period of progression-free LG-ESS is generally longer than 8 months [28]. Therefore, both cases had a relatively low risk of recurrence, but this information was difficult to include in the diagnosis with certainty. In addition to the complexity of FDG uptake in PET-CT, the lesion location may also increase the difficulty of diagnosis. If a lesion is detected in the intestinal wall or intramesentery, in which anisakiasis is relatively common, recurrence of gynecological cancer is less likely. However, a lesion in the peritoneum or liver is less likely to be due to extragastrointestinal anisakiasis, and this is also a common site of tumor recurrence.

Cases of extragastrointestinal anisakiasis in the uterus [29, 30] and ovary [31] have also been reported, indicating that differential diagnosis of such lesions is also required.

Generally, inflammatory lesions such as pneumonia and abscess, which need to be differentiated with malignancy, include macrophages and neutrophils. These cells increase the glucose uptake, but the changes seen in the delayed phase in DPS differs with cancer cells because of the difference of HK-2/G6P ratio. The two cases we report had eosinophilic granuloma. We speculated that the elevation of SUV in the delayed phase may be caused by eosinophils, and investigated their feature by immunochemical staining using anti-GLUT-1 and anti-HK-2

antibodies. However, against our expectation, eosinophils showed negative expression of GLUT-1 and HK-2, and only macrophages were strained. Although we have not investigated the expression of G6P, the expression HK-2 in macrophages may cause the elevation of uptake in inflammatory lesion in the delayed phase. Thus, DPS is not necessarily superior to other modalities in distinguishing malignancy and inflammation. New imaging modalities such as PET-CT allow an “abnormality” to be detected incidentally. It is important to determine whether a lesion found on PET-CT is truly abnormal, and this limitation of new technologies should be recognized.

In our cases, a genetic test was used to define the pathogen. The *Anisakis* worm collapses in the human body and this may cause difficulty with diagnosis, as in our second case. The PCR methods described here are useful in these cases. In addition, improved definition of species among *Anisakis* larvae might bring new insights. No studies have been reported about the frequency of species in extragastrointestinal anisakiasis. However, Umehara A. et al. reported that 99 % of all human anisakiasis are due to *Anisakis simplex* sensu stricto [32]. *Anisakis pegreffii* is relatively common among fish that are landed [33]. This discrepancy is explained by the difference of the larvae's ability to penetrate to the fish muscle, thus causing ingested by human [34–36]. In both cases included in the present study, it is thought that the larvae penetrated the gastrointestinal wall. Thus, the case of extragastrointestinal anisakiasis of *Anisakis pegreffii* is very rare and interesting. Accumulation of cases are required to clarify the epidemiology of extragastrointestinal anisakiasis and identify routes of infection.

Conclusion

We experienced two cases of anisakiasis that were initially suspected to be recurrence of gynecological cancer on PET-CT. These cases suggest that anisakiasis should be a differential diagnosis for a lesion presenting with FDG uptake on PET-CT. Our results also indicate that it is difficult to distinguish anisakiasis from a recurrent tumor using PET-CT and there is no specific mechanism of FDG uptake in parasitosis granuloma. These findings are important because current dietary habits and use of imaging modalities suggest that similar cases will increase worldwide.

Consent for publication

Written informed consent was obtained from the patients for publication of this case series and any accompanying images.

Availability of data and materials

The dataset supporting the conclusions of this article is included within the article.

Abbreviations

CT: computed tomography; PET: positron emission tomography; FDG: ¹⁸fluoro-deoxyglucose; NIID: the National Institute of Infectious Diseases; LG-ESS: low-grade endometrial stromal sarcoma; PCR: polymerase chain reaction; GLUT-1: glucose transporter type 1; HK-2: hexokinase type 2; CAP: cyclophosphamide-adriamycin-cisplatin; FIGO: International federation of gynecology and obstetrics; Gd-EOB-DTPA: gadolinium ethoxybenzyl diethylenetriaminepentaacetic acid; DW: diffusion-weighted imaging; SUV: standardized uptake value; PTCL: peripheral T-cell lymphoma; CHOP: cyclophosphamide-adriamycin-vincristine- prednisolone; ITS: internal transcribed spacer; DDBJ: DNA Data Bank of Japan; G6P: glucose-6-phosphatase; DPS: dual-phase scanning.

Competing interests

The authors declare that they have no competing interests.

Authors' contributions

YN is first author and has performed the entire management of this work which has various parts. Majority of this manuscript has been written by the first author. YFN is second author, and she and TY diagnosed anisakiasis by pathological examination. YFN also performed immunochemical staining and interpreted the result. KB is the corresponding author and was involved in establishing the study concept and conferred with YN and DA about additional investigations like immunochemical staining. AS, NS and TH were the doctors in charge for cases and they decided medical options in patient's clinical course and performed surgery. They also submitted tissues to NIID for genetic diagnosis after conference with YFN and TY. KM made diagnoses by PET-CT and reviewed the image retrospectively and calculated SUV and the elevation in delayed phase of DPS. HS and YM performed genetic examination using PCR method to identify the type of larvae. Especially, they prepared shorter primer only for these cases. YFN and HS reviewed the part of manuscript referring experimental methods. All authors read and approved the final manuscript.

Funding

This report received no funding.

Author details

¹Department of Obstetrics and Gynecology, Keio University School of Medicine, Shinanomachi 35 Shinjuku-ku, Tokyo 160-8582, Japan.

²Department of Pathology, Keio University School of Medicine, Shinanomachi 35 Shinjuku-ku, Tokyo 160-8582, Japan. ³Department of Surgery, Keio University School of Medicine, Shinanomachi 35 Shinjuku-ku, Tokyo 160-8582, Japan. ⁴Department of Radiology, Keio University School of Medicine, Shinanomachi 35 Shinjuku-ku, Tokyo 160-8582, Japan. ⁵Division of Diagnostic Pathology, Keio University School of Medicine, Shinanomachi 35 Shinjuku-ku, Tokyo 160-8582, Japan. ⁶Department of Parasitology, National Institute of Infectious Diseases, Toyama 1-23-1 Shinjuku-ku, Tokyo 162-8640, Japan. ⁷Department of Pathology, Saitama Medical University, Moroyama-machi 38, Iruma-gun, Saitama 350-0495, Japan.

Received: 17 November 2015 Accepted: 21 April 2016

Published online: 26 April 2016

References

1. Nogami Y, Iida M, Banno K, Kisu I, Adachi M, Nakamura K, et al. Application of FDG-PET in cervical cancer and endometrial cancer: utility and future prospects. *Anticancer Res.* 2014;34:585–92.
2. Chu Y, Zheng A, Wang F, Lin W, Yang X, Han L, et al. Diagnostic value of ¹⁸F-FDG-PET or PET-CT in recurrent cervical cancer: a systematic review and meta-analysis. *Nucl Med Commun.* 2014;35:144–50.
3. Gu P, Pan LL, Wu SQ, Sun L, Huang G. CA 125, PET alone, PET-CT, CT and MRI in diagnosing recurrent ovarian carcinoma: a systematic review and meta-analysis. *Eur J Radiol.* 2009;71:164–74.
4. Antunovic L, Cimitan M, Borsatti E, Baresic T, Sorio R, Giorda G, et al. Revisiting the clinical value of ¹⁸F-FDG PET/CT in detection of recurrent epithelial ovarian carcinomas: correlation with histology, serum CA-125 assay, and conventional radiological modalities. *Clin Nucl Med.* 2012;37:e184–8.
5. Abe K, Yoshikai T, Baba S, Isoda T, Honda H. PET/CT findings in acute gastric anisakiasis. *Clin Nucl Med.* 2014;39:e340–2.

6. Shibata E, Ueda T, Akaike G, Saida Y. CT findings of gastric and intestinal anisakiasis. *Abdom Imaging*. 2014;39:257–61.
7. Kagei N, Orikasa H, Hori E, Sannomiya A, Yasumura Y. A case of hepatic anisakiasis with a literal survey for extra-gastrointestinal anisakiasis. *Jpn J Parasitol*. 1995;44:346–51.
8. Cancrin G, Magro G, Giannone G. [1st case of extra-gastrointestinal anisakiasis in a human diagnosed in Italy]. *Parasitologia*. 1997;39:13–7. In Italy.
9. Takekawa Y, Kimura M, Sakakibara M, Yoshii R, Yamashita Y, Kubo A, et al. Two cases of parasitic granuloma found incidentally in surgical specimens. *Jpn J Clin Pathol*. 2004;52:28–31 (In Japanese).
10. Sugiyama H, Singh TS, Rangsitruji A. Paragonimus. In: Liu D, editor. *Molecular Detection of Human Parasitic Pathogens*. Boca Raton: CRC press; 2013. p. 421–33.
11. Yoo Ie R, Park HJ, Hyun J, Chung YA, Sohn HS, Chung SK, et al. Two cases of pulmonary paragonimiasis on FDG-PET CT imaging. *Ann Nucl Med*. 2006;20:311–5.
12. Chen CJ, Chou SC, Chen HJ, Chen HY. Solitary necrotic nodule with larval infestation in the liver on F-18 FDG PET/CT. *Clin Nucl Med*. 2010;35:724–5.
13. Cheng W, Li F, Zhuang H, Zhong D, Wu C, Zhu Z. Hepatic paragonimiasis revealed by FDG PET/CT. *Clin Nucl Med*. 2010;35:726–8.
14. Ishikura H, Kikuchi H, Sato N, Ohtani S, Yagi K, Ishikura H, et al. [Changing larva migrans caused by anisakidae larvae]. *Clin Parasitol*. 1992;3:70–3. In Japanese.
15. Pampiglione S, Rivasi F, Criscuolo M, De Benedittis A, Gentile A, Russo S, et al. Human anisakiasis in Italy: a report of eleven new cases. *Pathol Res Pract*. 2002;198:429–34.
16. Ishida M, Sano S, Terada T, Mitsui T, Sudoh Y, Yamaguchi A. A case of hepatic anisakiasis. *J Jpn Surg Assoc*. 2013;74:2557–61. in Japanese.
17. Morita M, Soyama A, Takatuki M, Kuroki T, Abe K, Hayashi T, et al. A case of hepatic mass induced by extra-gastrointestinal anisakiasis. *J Jpn Surg Assoc*. 2013;74:483–7 (in Japanese).
18. Leonhardt M, Keiser M, Oswald S, Kuhn J, Jia J, Grube M, et al. Hepatic uptake of the magnetic resonance imaging contrast agent Gd-EOB-DTPA: role of human organic anion transporters. *Drug Metab Dispos*. 2010;38:1024–8.
19. Zhuang H, Pourdehnad M, Lambright ES, Yamamoto AJ, Lanuti M, Li P, et al. Dual time point 18 F-FDG PET imaging for differentiating malignant from inflammatory processes. *J Nucl Med*. 2001;42:1412–7.
20. Shen G, Hu S, Deng H, Jia Z. Diagnostic value of dual time-point 18 F-FDG PET/CT versus single time-point imaging for detection of mediastinal nodal metastasis in non-small cell lung cancer patients: a meta-analysis. *Acta Radiol*. 2014;56:681–7.
21. Mochizuki Y, Omura K, Nakamura S, Harada H, Shibuya H, Kurabayashi T. Preoperative predictive model of cervical lymph node metastasis combining fluorine-18 fluorodeoxyglucose positron-emission tomography/computerized tomography findings and clinical factors in patients with oral or oropharyngeal squamous cell carcinoma. *Oral Surg Oral Med Oral Pathol Oral Radiol*. 2012;113:274–82.
22. Nogami Y, Banno K, Irie H, Iida M, Masugi Y, Murakami K, et al. Efficacy of 18-FDG PET-CT Dual-phase Scanning for Detection of Lymph Node Metastasis in Gynecological Cancer. *Anticancer Res*. 2015;35:2247–53.
23. EFSA Panel on Biological Hazards. Scientific Opinion on assessment of epidemiological data in relation to the health risks resulting from the presence of parasites in wild caught fish from fishing grounds in the Baltic Sea. *EFSA Journal*. 2011;9:2320.
24. Fein SB, Lando AM, Levy AS, Teisl MF, Noblet C. Trends in U.S. consumers' safe handling and consumption of food and their risk perceptions, 1988 through 2010. *J Food Prot*. 2011;74:1513–23.
25. Organisation for Economic Co-operation and Development, OECD Health Statistics 2014. 2014. <http://www.oecd.org/health/>. Accessed 20 May 2015.
26. Kojima K, Koyanagi T, Shiraki K. Pathological analysis of anisakiasis. *Jpn J Clin Med*. 1966;24:134–43 (in Japanese).
27. Susumu N, Sagae S, Udagawa Y, Niwa K, Kuramoto H, Satoh S, et al. Randomized phase III trial of pelvic radiotherapy versus cisplatin-based combined chemotherapy in patients with intermediate- and high-risk endometrial cancer: a Japanese Gynecologic Oncology Group study. *Gynecol Oncol*. 2008;108:226–33.
28. Li AJ, Giuntoli 2nd RL, Drake R, Byun SY, Rojas F, Barbuto D, et al. Ovarian preservation in stage I low-grade endometrial stromal sarcomas. *Obstet Gynecol*. 2005;106:1304–8.
29. Takao Y, Fukuma T, Shigeki M, Shyono Y, Tokunaga K, Uchiyama A. [An Anisakis larva observed in the utero-cervix]. *Clin Parasitol*. 1993;4:200–2. in Japanese.
30. Shiozaki Y, Kudo M, Adachi T, Takizawa K, Iguchi T, Takeda Y. A case of anisakiasis by the histological examination after the operation of uterus. *Clin Parasitol*. 1993;4:205–6 (in Japanese).
31. Mori H, Hirata M, Kase Y, Takagi Y, Sekine I, Aoki Y, et al. A case of ovarian anisakiasis. *Sankatofujinka*. 1982;49:1361–3 (in Japanese).
32. Umehara A, Kawakami Y, Araki J, Uchida A. Molecular identification of the etiological agent of the human anisakiasis in Japan. *Parasitol Int*. 2007;56:211–5.
33. Umehara A, Kawakami Y, Ooi HK, Uchida A, Ohmae H, Sugiyama H. Molecular identification of Anisakis type I larvae isolated from hairtail fish off the coasts of Taiwan and Japan. *Int J Food Microbiol*. 2010;143:161–5.
34. Suzuki J, Murata R, Hosaka M, Araki J. Risk factors for human Anisakis infection and association between the geographic origins of *Scomber japonicus* and anisakid nematodes. *Int J Food Microbiol*. 2010;137:88–93.
35. Arizono N, Yamada M, Tegoshi T, Yoshikawa M. Anisakis simplex sensu stricto and Anisakis pegreffii: biological characteristics and pathogenetic potential in human anisakiasis. *Foodborne Pathog Dis*. 2012;9:517–21.
36. del Carmen RM, Valero A, Navarro-Moll MC, Martin-Sanchez J. Experimental comparison of pathogenic potential of two sibling species Anisakis simplex s.s. and Anisakis pegreffii in Wistar rat. *Trop Med Int Health*. 2013;18:979–84.

Submit your next manuscript to BioMed Central and we will help you at every step:

- We accept pre-submission inquiries
- Our selector tool helps you to find the most relevant journal
- We provide round the clock customer support
- Convenient online submission
- Thorough peer review
- Inclusion in PubMed and all major indexing services
- Maximum visibility for your research

Submit your manuscript at
www.biomedcentral.com/submit



ANTICANCER RESEARCH

International Journal of Cancer Research and Treatment

ISSN: 0250-7005

Computed Tomographic Features of Malignant Peritoneal Mesothelioma

KATSUYA KATO^{1§}, KENICHI GEMBA², NOBUKAZU FUJIMOTO², KEISUKE AOE⁴,
YUKIO TAKESHIMA⁵, KOUKI INAI⁵ and TAKUMI KISHIMOTO³

¹*Department of Radiology, Okayama University Hospital, Shikatacho, Okayama, Japan;*
Departments of ²Respiratory Medicine and ³Internal Medicine,
Okayama Rosai Hospital, Chikkomidorimachi, Okayama, Japan;

⁴*Department of Medical Oncology, National Hospital Organization Yamaguchi-Ube Medical Center,*
Higashikiwa, Ube, Japan;

⁵*Department of Pathology, Graduate School of Biomedical Sciences,*
Hiroshima University, Minamiku, Hiroshima, Japan

Reprinted from
ANTICANCER RESEARCH 36: 1067-1072 (2016)

ANTICANCER RESEARCH

International Journal of Cancer Research and Treatment



ISSN (print): 0250-7005

ISSN (online): 1791-7530

Editorial Board

P. A. ABRAHAMSSON, Malmö, Sweden

B. B. AGGARWAL, Houston, TX, USA

T. AKIMOTO, Kashiwa, Chiba, Japan

P. Z. ANASTASIADIS, Jacksonville, FL, USA

A. ARGIRIS, San Antonio, TX, USA

J. P. ARMAND, Toulouse, France

V. I. AVRAMIS, Los Angeles, CA, USA

R. C. BAST, Houston, TX, USA

D.-T. BAU, Taichung, Taiwan, ROC

G. BAUER, Freiburg, Germany

E. E. BAULIEU, Le Kremlin-Bicetre, France

E. J. BENZ, Jr., Boston, MA, USA

J. BERGH, Stockholm, Sweden

F. T. BOSMAN, Lausanne, Switzerland

G. BROICH, Monza, Italy

Ø. S. BRULAND, Oslo, Norway

J. M. BUATTI, Iowa City, IA, USA

M. M. BURGER, Basel, Switzerland

M. CARBONE, Honolulu, HI, USA

C. CARLBERG, Kuopio, Finland

J. CARLSSON, Uppsala, Sweden

A. F. CHAMBERS, London, ON, Canada

P. CHANDRA, Frankfurt am Main, Germany

L. CHENG, Indianapolis, IN, USA

J.-G. CHUNG, Taichung, Taiwan, ROC

E. DE CLERCQ, Leuven, Belgium

W. DEN OTTER, Amsterdam, The Netherlands

E. P. DIAMANDIS, Toronto, ON, Canada

G. TH. DIAMANDOPOULOS, Boston, MA, USA

D. W. FELSHER, Stanford, CA, USA

J. A. FERNANDEZ-POL, Chesterfield, MO, USA

I. J. FIDLER, Houston, TX, USA

A. P. FIELDS, Jacksonville, FL, USA

B. FUCHS, Zurich, Switzerland

D. FUCHS, Innsbruck, Austria

G. GABBIANI, Geneva, Switzerland

R. GANAPATHI, Charlotte, NC, USA

A. F. GAZDAR, Dallas, TX, USA

J. H. GESCHWIND, Baltimore, MD, USA

A. GIORDANO, Philadelphia, PA, USA

G. GITSCHE, Freiburg, Germany

R. H. GOLDFARB, Guilford, CT, USA

L. HELSON, Quakertown, PA, USA

R. M. HOFFMAN, San Diego, CA, USA

S. C. JHANWAR, New York, NY, USA

J. V. JOHANNESSEN, Oslo, Norway

B. KAINA, Mainz, Germany

P. -L. KELLOKUMPU-LEHTINEN, Tampere, Finland

D. G. KIEBACK, Marl, Germany

R. Klapdor, Hamburg, Germany

S. D. KOTTARIDIS, Athens, Greece

G. R. F. KRUEGER, Köln, Germany

Pat M. KUMAR, Manchester, UK

Shant KUMAR, Manchester, UK

O. D. LAERUM, Bergen, Norway

F. J. LEJEUNE, Lausanne, Switzerland

L. F. LIU, Piscataway, NJ, USA

D. M. LOPEZ, Miami, FL, USA

E. LUNDGREN, Umeå, Sweden

Y. MAEHARA, Fukuoka, Japan

J. MAHER, London, UK

J. MARESCAUX, Strasbourg, France

J. MARK, Skövde, Sweden

S. S. MARTIN, Baltimore, MD, USA

S. MITRA, Houston, TX, USA

S. MIYAMOTO, Fukuoka, Japan

M. MUELLER, Villingen-Schwenningen, Germany

F. M. MUGGIA, New York, NY, USA

M. NAMIKI, Kanazawa, Ishikawa, Japan

R. NARAYANAN, Boca Raton, FL, USA

K. NILSSON, Uppsala, Sweden

S. PATHAK, Houston, TX, USA

J. L. PERSSON, Malmö, Sweden

G. J. PILKINGTON, Portsmouth, UK

C. D. PLATSOUCAS, Norfolk, VA, USA

A. POLLIACK, Jerusalem, Israel

M. RIGAUD, Limoges, France

U. RINGBORG, Stockholm, Sweden

M. ROSELLI, Rome, Italy

A. SCHAUER, Göttingen, Germany

M. SCHNEIDER, Wuppertal, Germany

A. SETH, Toronto, ON, Canada

G. V. SHERBET, Newcastle-upon-Tyne, UK

G.-I. SOMA, Kagawa, Japan

G. S. STEIN, Burlington, VT, USA

T. STIGBRAND, Umeå, Sweden

T. M. THEOPHANIDES, Athens, Greece

P. M. UELAND, Bergen, Norway

H. VAN VLIERBERGHE, Ghent, Belgium

R. G. VILE, Rochester, MN, USA

M. WELLER, Zurich, Switzerland

B. WESTERMARK, Uppsala, Sweden

Y. YEN, Duarte, CA, USA

M.R.I. YOUNG, Charleston, SC, USA

B. ZUMOFF, New York, NY, USA

J. G. DELINASIOS, Athens, Greece

Managing Editor

G. J. DELINASIOS, Athens, Greece

Assistant Managing Editor and

Executive Publisher

E. ILIADIS, Athens, Greece

Production Editor

Editorial Office: International Institute of Anticancer Research, 1st km Kapandritou-Kalamou Rd., Kapandriti, P.O. Box 22, Attiki 19014, Greece. Tel / Fax: +30-22950-53389.

U.S. Branch: Anticancer Research USA, Inc., 111 Bay Avenue, Highlands, NJ 07732, USA.

E-mails: Editorial Office: journals@iiar-anticancer.org

Managing Editor: editor@iiar-anticancer.org

ANTICANCER RESEARCH supports: (a) the establishment and the activities of the INTERNATIONAL INSTITUTE OF ANTICANCER RESEARCH (IIAR; Kapandriti, Attiki, Greece); and (b) the organization of the International Conferences of Anticancer Research. The IIAR is a member of UICC. For more information about ANTICANCER RESEARCH, IIAR and the Conferences, please visit the IIAR website: www.iiar-anticancer.org

Publication Data: ANTICANCER RESEARCH (AR) is published monthly from January 2009. Each annual volume comprises 12 issues. Annual Author and Subject Indices are included in the last issue of each volume. ANTICANCER RESEARCH Vol. 24 (2004) and onwards appears online with Stanford University HighWire Press from April 2009.

Copyright: On publication of a manuscript in AR, which is a copyrighted publication, the legal ownership of all published parts of the paper passes from the Author(s) to the Journal.

Annual Subscription Rates 2016 per volume: Institutional subscription US\$ 1,890.00 (online) or US\$ 2,277.00 (print & online). Personal subscription US\$ 897.00 (online) or US\$ 1,277.00 (print & online). Prices include rapid delivery and insurance. The complete previous volumes of Anticancer Research (Vol. 1-35, 1981-2015) are available at 50% discount on the above rates.

Subscription Orders: Orders can be placed at agencies, bookstores, or directly with the Publisher. (e-mail: subscriptions@iiar-anticancer.org)

Advertising: All correspondence and rate requests should be addressed to the Editorial Office.

Book Reviews: Recently published books and journals should be sent to the Editorial Office. Reviews will be published within 2-4 months.

Articles in ANTICANCER RESEARCH are regularly indexed in all bibliographic services, including Current Contents (Life Sciences), Science Citation Index, Index Medicus, Biological Abstracts, PubMed, Chemical Abstracts, Excerpta Medica, University of Sheffield Biomedical Information Service, Current Clinical Cancer, AIDS Abstracts, Elsevier Bibliographic Database, EMBASE, Compendex, GEOBASE, EMBiology, Elsevier BIOBASE, FLUIDEX, World Textiles, Scopus, Progress in Palliative Care, Cambridge Scientific Abstracts, Cancergram (International Cancer Research Data Bank), MEDLINE, Reference Update - RIS Inc., PASCAL-CNRS, Inpharma-Reactions (Datastar, BRS), CABS, Immunology Abstracts, Telegen Abstracts, Genetics Abstracts, Nutrition Research Newsletter, Dairy Science Abstracts, Current Titles in Dentistry, Inpharma Weekly, BioBase, MedBase, CAB Abstracts/Global Health Databases, Investigational Drugs Database, VINITI Abstracts Journal, Leeds Medical Information, PubsHub, Sociedad Iberoamericana de Información Científica (SIIC) Data Bases.

Authorization to photocopy items for internal or personal use, or the internal or personal clients, is granted by ANTICANCER RESEARCH, provided that the base fee of \$2.00 per copy, plus 0.40 per page is paid directly to the Copyright Clearance Center, 27 Congress Street, Salem, MA 01970, USA. For those organizations that have been granted a photocopy license by CCC, a separate system of payment has been arranged. The fee code for users of the Transactional Reporting Service is 0250-7005/2016 \$2.00 +0.40.

The Editors and Publishers of ANTICANCER RESEARCH accept no responsibility for the opinions expressed by the contributors or for the content of advertisements appearing therein.

Copyright© 2016, International Institute of Anticancer Research (Dr. John G. Delinasios), All rights reserved.

D.T.P. BY IIAR

PRINTED BY ENTYPO, ATHENS, GREECE. PRINTED ON ACID-FREE PAPER

Computed Tomographic Features of Malignant Peritoneal Mesothelioma

KATSUYA KATO^{1§}, KENICHI GEMBA², NOBUKAZU FUJIMOTO², KEISUKE AOE⁴,
YUKIO TAKESHIMA⁵, KOUKI INAI⁵ and TAKUMI KISHIMOTO³

¹Department of Radiology, Okayama University Hospital, Shikatacho, Okayama, Japan;

Departments of ²Respiratory Medicine and ³Internal Medicine,

Okayama Rosai Hospital, Chikkomidorimachi, Okayama, Japan;

⁴Department of Medical Oncology, National Hospital Organization Yamaguchi-Ube Medical Center, Higashikiwa, Ube, Japan;

⁵Department of Pathology, Graduate School of Biomedical Sciences, Hiroshima University, Minamiku, Hiroshima, Japan

Abstract. *Aim:* The objective of this study was to determine the computed tomographic (CT) features of malignant peritoneal mesothelioma (MPM). *Patients and Methods:* We analyzed CT features of MPM cases and compared them to those of other malignant conditions (non-MPM). *Results:* Multiple nodular lesions occurred more frequently in the MPM group compared to non-MPM cases ($p=0.013$). Thickening of the mesentery was detected more frequently in MPM cases than in non-MPM cases (56% vs. 18%, $p=0.029$). Pleural plaques were detected in 13 cases (45%) in the MPM group but were not detected in the non-MPM group. The MPM-CT index score, determined in each case as the sum of the findings which are potentially characteristic of MPM, was significantly higher in MPM than in non-MPM cases ($p=0.001$). *Conclusion:* MPM presented characteristic CT findings, and the MPM-CT index may be useful for differential diagnosis of MPM.

Malignant mesothelioma (MM) is an aggressive tumor that develops from mesothelial cells of the pleura, peritoneum, pericardium, or testicular *tunica vaginalis*. It is generally associated with a history of asbestos exposure (1) and has a very poor prognosis (2). Once rare, the incidence of MM has increased worldwide as a result of past wide-spread exposure

to asbestos. Malignant peritoneal mesothelioma (MPM) represents the second most common site of MM, accounting for 10-20% of MM (3, 4).

A diagnosis of MPM should be based on the histology of an adequate specimen of the peritoneum or cytological analyses of ascites, but this is often difficult. Paracentesis with fluid cytology has a variable sensitivity of 32-76%, with the major limitation being difficulty in distinguishing benign from malignant lesions (4, 5). In particular, the differential diagnosis between MPM and peritoneal carcinomatosis is a critical issue. Radiological analysis is essential for this differential diagnosis; computed tomographic (CT) imaging is the most common initial imaging modality and can reveal moderate to extensive ascites with peritoneal, visceral, or omental involvement. Magnetic resonance imaging may more accurately quantify the extent of disease; however, its routine use is not yet supported (6). The role of positron-emission tomography is not well defined in detection of this disease (7).

In the current study, we retrospectively examined the CT features for patients with MPM.

Patients and Methods

Study approval. All procedures performed in the current study were in accordance with the Helsinki declaration. This study was performed in accordance with the Ethical Guidelines for Epidemiological Research of the Japanese Ministry of Education, Culture, Sports, Science and Technology, and Ministry of Health, Labour and Welfare and was approved by the Japan Labour Health and Welfare Organization and the Institutional Review Boards of Okayama Rosai Hospital. Patient confidentiality was strictly maintained. As described below, informed consent was provided by the closest living relatives of each patient.

Patients. This study was a part of our previous nationwide survey of MM. Methods of the retrospective survey have been described

[§]Present address: Department of Diagnostic Radiology 2, Kawasaki Medical School, Nakasange, Kitaku, Okayama, Japan.

Correspondence to: Nobukazu Fujimoto, MD, Ph.D., Department of Respiratory Medicine, Okayama Rosai Hospital, 1-10-25 Chikkomidorimachi, Okayama 7028055, Japan. Tel: 81-86-2620131, Fax: 81-86-2623391, e-mail: nobufujimot@gmail.com

Key Words: Asbestos, peritoneum, mesothelioma, CT image.

previously (1, 8). In brief, we requested and received authorization to view the death records from the Vital Statistics database in Japan. We then extracted all cases of death due to MM between 2003 and 2005. There were 2,742 deaths due to MM (Figure 1). We contacted the closest living relatives of each patient to obtain consent for our study by postal mail. As a result, informed consent was obtained by postal mail for 1,153 cases. Based on authorization from relatives, we contacted the patients' medical institutions to obtain medical information, including medical records, X-ray and CT images by postal mail. These data were obtained in 743 cases. Among them, we found 105 cases in which the clinical diagnosis of MPM had been made. Pathological specimens were provided in 53 out of the 105 cases. We reviewed the pathological specimen of these cases according to World Health Organization criteria (9), and analyzed the radiological features of the cases.

CT analysis of MPM. The items examined on the CT images were as follows: (i) degree of accumulation of ascites, (ii) location of the lesion, (iii) maximum dimensions of the nodular lesion, (iv) number of tumor masses, (v) extent of peritoneal thickening, (vi) extent of thickening of the mesentery, (vii) stellate pattern findings in the mesentery, and (viii) pleural plaques. These items were examined according to the criteria listed in Table I.

Statistical analysis. Comparisons between independent groups were performed using the Chi-square test and non-parametric analysis was performed with the Mann-Whitney *U*-test. Average values were compared by *t*-test. Areas under the receiver operating characteristic (ROC) curves (AUCs) were calculated using standard techniques. Statistical calculations were performed with SPSS statistical package, version 11.0 (SPSS Inc., Chicago, IL, USA).

Results

Pathological review of the cases. As shown in Figure 2, pathological diagnosis of MPM was confirmed in 34 cases. Among the 34 cases, there were 27 (79.0%) cases of epithelioid, four (12.0%) cases of biphasic, and three (9%) cases of sarcomatous sub-types. There were 16 cases ultimately diagnosed as other conditions (non-MPM), including six cases of serous papillary adenocarcinoma, four cases of adenocarcinoma, two cases each of carcinosarcoma and unclassified sarcoma, and one case each of peritoneal metastasis of renal cell carcinoma and rhabdomyosarcoma. Differentiation between the epithelioid sub-type of mesothelioma and poorly differentiated adenocarcinoma was impossible in one case. In another case, a confirmed pathological diagnosis could not be made as to whether it was an epithelioid sub-type of mesothelioma, another malignant condition, or reactive mesothelium. In addition, there was one case in which a malignant condition was highly suspected from CT images, but only reactive mesothelium was demonstrated in the pathological specimen. These three cases were finally categorized as "diagnosis could not be made," and they were excluded from further analyses. The MPM group included 30 (88.2%) males and 4 (11.8%) females and the non-MPM group included two (12.5%) males and 14 (87.5%) females.

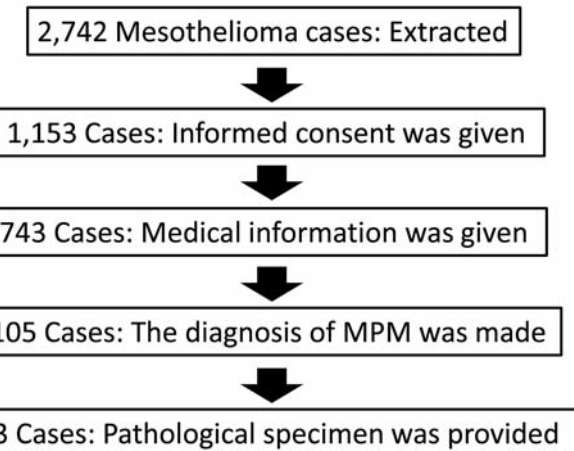


Figure 1. The schema of the case collection of this study.

Radiological analyses. Among the 50 cases, abdominal and pelvic CT scans were available in 32 MPM cases and 11 non-MPM cases (three cases of serous papillary adenocarcinoma, two cases each of adenocarcinoma, carcinosarcoma and unclassified sarcoma, and one case each of peritoneal metastasis of renal cell carcinoma and rhabdomyosarcoma). Chest CT images were available in 40 cases (29 MPM and 11 non-MPM). CT findings of the MPM and non-MPM groups are shown in Table I.

There were 19/32 (59%) cases of moderate to massive accumulation of ascites in the MPM group, and 3/11 (27%) cases in the non-MPM group. Although the proportion was higher in the MPM compared to non-MPM group, the difference did not reach statistical significance ($p=0.066$). We analyzed the location of MPM. For this purpose, the existence or non-existence of MPM in the parahepatic space, great omentum, paracolic gutter, mesentery proper, rectovesical pouch, and perisplenic space was determined. There was no difference concerning the location of the disease between the MPM and non-MPM groups.

We next categorized the maximum dimension of the nodular lesion as <1 cm, 1-3 cm, >3-5 cm, or >5 cm based on the abdominal CT images (Figure 3A). As shown in Table I, the proportion of cases with a maximum dimension of <1 cm was higher in the MPM group than in the non-MPM group, but this difference was not statistically significant (47% vs. 18%, $p=0.097$).

In the MPM group, there were multiple nodular lesions in 30 cases (94%), which was significantly more frequent in MPM than in non-MPM cases ($p=0.013$).

Thickening of the peritoneum was categorized as none, mild, irregular, or massive (defined as ≥ 1 cm, Figure 3B). As shown in Table I, MPM cases had a higher proportion of irregular or massive thickening compared to non-MPM cases, although this

Table I. Computed tomographic findings of malignant peritoneal mesothelioma (MPM) and finding of cases ultimately diagnosed as other conditions (non-MPM).

Characteristic	Findings	Proportion of cases with the finding (%)		<i>p</i> -Value
		MPM	Non-MPM	
Ascites accumulation	None	2 (6.3)	2 (18.2)	0.066
	Small	11 (34.4)	6 (54.5)	
	Moderate	12 (37.5)	2 (18.2)	
	Massive	7 (21.9)	1 (9.1)	
Maximum dimension of nodular lesion	<1 cm	15 (46.9)	2 (18.2)	0.097
	1-3 cm	6 (18.8)	2 (18.2)	
	>3-5 cm	2 (6.3)	3 (27.3)	
	>5 cm	9 (28.1)	4 (36.4)	
Location of MPM	Yes	18 (56.3)	5 (45.5)	0.536
	No	14 (43.8)	6 (54.5)	
	Yes	29 (90.6)	8 (72.7)	0.139
	No	3 (9.4)	3 (27.3)	
	Yes	18 (56.3)	5 (45.5)	0.536
	No	14 (43.8)	6 (54.5)	
	Yes	25 (78.1)	8 (72.7)	0.715
	No	7 (21.9)	3 (27.3)	
	Yes	18 (56.3)	9 (81.8)	0.13
	No	14 (43.8)	2 (18.2)	
Perisplenic space	Yes	14 (43.8)	3 (27.3)	0.668
	No	18 (56.3)	8 (72.7)	
	Solitary	2 (6.3)	4 (36.4)	
	Multiple	30 (93.8)	7 (63.6)	
Thickening of the peritoneum	None	3 (9.4)	3 (27.3)	0.013
	Slight thickening	15 (46.9)	6 (54.5)	
	Irregular thickening	6 (18.8)	2 (18.2)	
	Massive thickening	8 (25.0)	0 (0.0)	
Thickening of the mesentery	None	14 (43.8)	9 (81.8)	0.066
	Slight thickening	12 (37.5)	2 (18.2)	
	Irregular thickening	4 (12.5)	0 (0.0)	
	massive thickening	2 (6.3)	0 (0.0)	
Stellate pattern findings	Yes	11(34.4)	3 (27.3)	0.029
	No	21(65.6)	8 (72.7)	
Pleural plaques	Yes	13 (44.8)	0 (0.0)	0.665
	No	16 (55.2)	11(100.0)	

difference was not statistically significant (44% vs. 18%, *p*=0.066).

Thickening of the mesentery was categorized as none, mild, irregular thickening, or massive thickening (defined as ≥ 3 mm, Figure 3C). Thickening of the mesentery was detected more frequently in MPM cases than in non-MPM cases (56% vs. 18%, *p*=0.029).

We examined stellate pattern findings as an indicator of mesenteric vascular enlargement (Figure 3D). Stellate patterns were detected in 11 cases (34%) in the MPM group and in three cases (27%) in the non-MPM group. This difference was not statistically significant (*p*=0.665).

Finally, pleural plaques were examined in chest CT images, which were available for 29 out of the 32 MPM

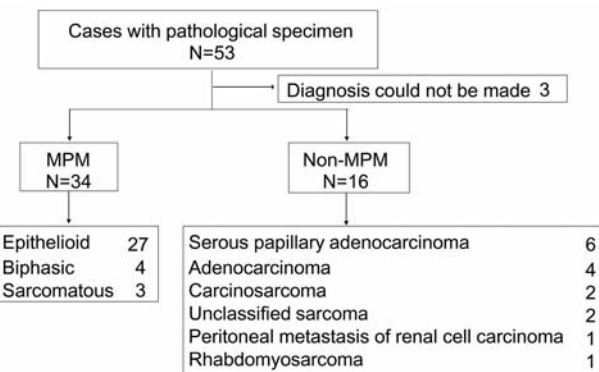


Figure 2. The breakdown of the confirmed pathological diagnosis of enrolled patients.

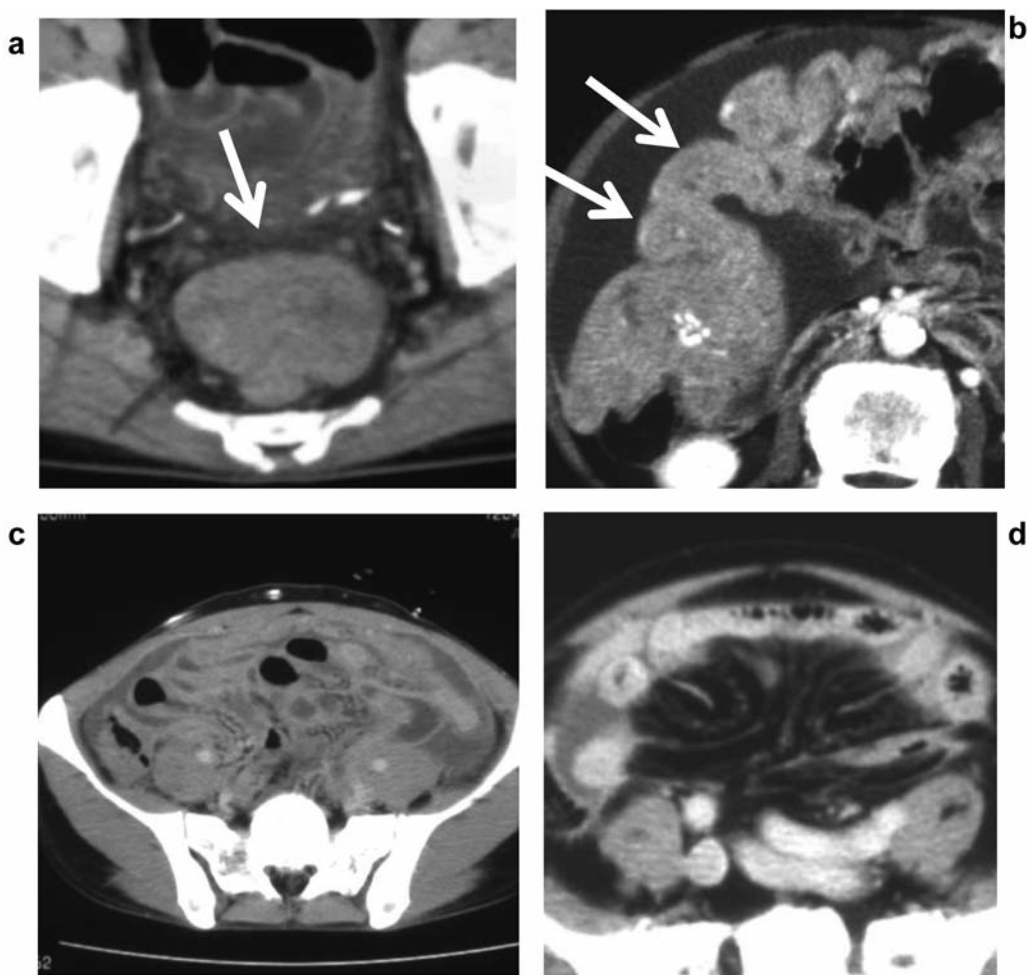


Figure 3. Examples of computed tomographic images of malignant peritoneal mesothelioma with maximum dimension of the nodular lesion >5 cm (A), massive thickening of the peritoneum (B), massive thickening of the mesentery (C), and stellate structure findings (D).

cases and 11 of the non-MPM cases. Pleural plaques were detected in 13 cases (45%) in the MPM group. None were detected among the non-MPM cases.

Proposal of an MPM-CT index. Among the findings analyzed above, we selected six findings that were detected more frequently in MPM than in non-MPM with a *p*-value of <0.100 : degree of accumulation of ascites, maximum dimension of the nodular lesion, number of tumor masses, extent of peritoneal thickening, extent of thickening of the mesentery, and pleural plaques. In each case, CT findings were scored as 1 in the case of (i) moderate to massive accumulation of ascites, (ii) maximum dimension of nodular lesion <1 cm, (iii) multiple nodular lesions, (iv) irregular to massive thickening of the peritoneum, and (v) mild to massive thickening of the mesentery. The MPM-CT index was determined in each case as the sum of these six findings. As shown in Figure 4A, the index was significantly higher

in MPM than in non-MPM cases ($p=0.001$). To evaluate the utility of the index for differentiation between MPM and non-MPM cases, we performed an ROC analysis. The AUC value for the differential diagnosis between the two groups was 0.821 (95% confidence interval=0.694-0.945) (Figure 4B). Based on a cutoff value of 3, sensitivity was 53% and specificity was 100%.

Discussion

MPM is poorly described and the knowledge of its natural history is very limited. In previous reports, at least 70% of cases of MPM were associated with chronic exposure to asbestos (10, 11); however, it is not clear how inhaled asbestos induces peritoneal neoplasms.

It is often difficult to make a pathological distinction between MPM and peritoneal metastatic adenocarcinoma (12, 13), although some immunohistochemical markers, such

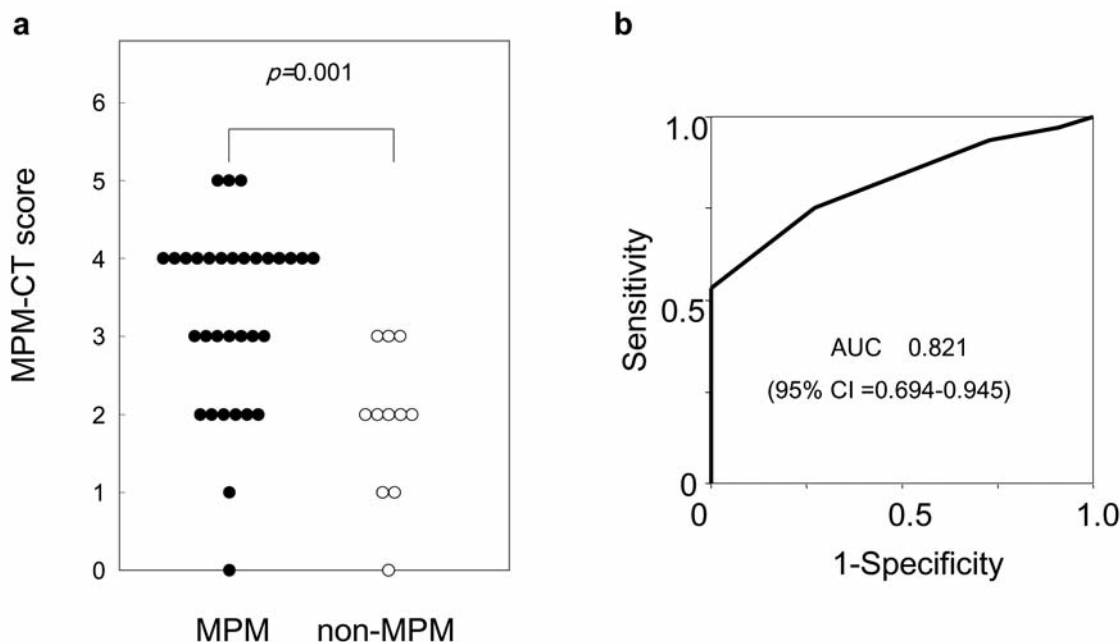


Figure 4. A: Comparison of malignant peritoneal mesothelioma (MPM)–computed tomography (CT) index between MPM and non-MPM groups. B: Receiver operating characteristic curves to evaluate the usefulness of the MPM-CT index for the differentiation between MPM and non-MPM.

as calretinin, thrombomodulin, and cytokeratin 5/6, could facilitate this (14, 15). In the current study, we reviewed the pathological specimens of 53 cases that had been diagnosed as MPM, and confirmed a diagnosis of MPM in only 34 cases (64.2%). The difficulty involved in making a clinical and pathological differential diagnosis often results in a diagnostic delay. Factors contributing to the diagnostic delay include the rarity of this entity, the long latent period from the exposure to asbestos, and the non-specific clinical features of the disease. Biochemistry and tumor markers are of limited assistance in this regard.

In the current study, we analyzed CT features of MPM. For this purpose, we extracted all cases of death due to MM between 2003 and 2005 based on death records from the Vital Statistics in Japan. A strength of our study is that it contained many cases of MPM. To the best of our knowledge, this is the largest study of radiological analysis of MPM. We tried to analyze 105 cases in which the clinical diagnosis of MPM had been made, and after the pathological review of the provided specimens, we determined there were 34 MPM cases. We had to accept the low collection rate of the study based on the postal mail method. However, there is no selection bias throughout the process of data collection.

There is a wide spectrum of imaging findings in MPM, the most common of which include a thickening of the mesentery and peritoneum. Findings on CT images are highly variable; therefore differentiating MPM from other intra-abdominal

malignancies is difficult (12, 16-18). Based on the results of the current study, we proposed the use of an MPM-CT index that comprises accumulation of ascites, maximum dimension of the nodular lesion, number of tumor masses, extent of peritoneal thickening, extent of mesenteric thickening, and pleural plaques. We found marked differences in these findings between the MPM and non-MPM groups. With a cut-off score of 3, diagnostic sensitivity was 53% and specificity of 100%, while ROC analysis revealed an AUC value of 0.821. These results indicate the clinical utility of this MPM-CT index for the differential diagnosis of MPM. In fact, the sensitivity is around 50%; however, the high specificity would contribute to the differentiation.

A limitation of the current study is that this was a retrospective analysis. A validation study to confirm the utility of the index is warranted, with a new patient cohort that includes pathologically confirmed MPM cases and other peritoneal malignant conditions.

Conclusion

MPM is a rare tumor that is difficult to diagnose and treat. An accurate diagnosis of MPM is essential in order to determine the prognosis, and occupation-related compensation claims following asbestos exposure. MPM demonstrates characteristic radiological findings, and the MPM-CT index may be useful for the differential diagnosis of MPM.

Conflicts of Interest

None.

Acknowledgements

This study was supported by the Research and Development and the Dissemination of Projects Related to the Nine Fields of Occupational Injuries and Illnesses of the Japan Labour Health and Welfare Organization. This work is also supported by grants-in-aid from the Ministry of Health, Labor and Welfare, Japan. These study sponsors had no involvement in in study design, writing of the manuscript, the collection of data, and decision to submit the manuscript for publication.

References

- 1 Gemba K, Fujimoto N, Kato K, Aoe K, Takeshima Y, Inai K and Kishimoto T: National survey of malignant mesothelioma and asbestos exposure in Japan. *Cancer Sci* 103: 483-490, 2012.
- 2 Gemba K, Fujimoto N, Aoe K, Kato K, Takeshima Y, Inai K and Kishimoto T: Treatment and survival analyses of malignant mesothelioma in Japan. *Acta Oncol* 52: 803-808, 2013.
- 3 Blackham AU and Levine EA: Cytoreductive surgery with hyperthermic intraperitoneal chemotherapy for malignant peritoneal mesothelioma. *European J Clin Med Oncol* 4: 25-32, 2012.
- 4 Kindler HL: Peritoneal mesothelioma: the site of origin matters. *Am Soc Clin Oncol Educ Book* 2013, 182-188, 2013.
- 5 Turner KM, Varghese S and Alexander HR Jr.: Surgery for peritoneal mesothelioma. *Curr Treat Options Oncol* 12: 189-200, 2011.
- 6 Low RN, Sebrechts CP, Barone RM and Muller W: Diffusion-weighted MRI of peritoneal tumors: comparison with conventional MRI and surgical and histopathologic findings – a feasibility study. *AJR* 193: 461-470, 2009.
- 7 Cao Q, Lu M, Heath J, Hausner PF, Alexander HR, Dilsizian V and Chen W: 18F-FDG PET/CT in a recurrent diffuse malignant peritoneal mesothelioma. *Clin Nucl Med* 37: 492-494, 2012.
- 8 Takeshima Y, Inai K, Amatya VJ, Gemba K, Aoe K, Fujimoto N, Kato K and Kishimoto T: Accuracy of pathological diagnosis of mesothelioma cases in Japan: clinicopathological analysis of 382 cases. *Lung Cancer* 66: 191-197, 2009.
- 9 Churg A, Cagle PT and Roggli VL: Tumors of the serosal membrane. AFIP atlas of tumor pathology. Series 4. 48-49, 2006.
- 10 D'Albuquerque LA, Padilla JM, Rodrigues AL, Souza MV, Quireze Junior C, Meniconi MT, Copstein JL, dos Santos Junior ED, de Melo CR, Santo GC and de Oliveira e Silva A: Diffuse primary malignant mesothelioma in abdominal cavity. *Arq Gastroenterol* 34: 163-168, 1997.
- 11 Cocco P and Dosemeci M: Peritoneal cancer and occupational exposure to asbestos: results from the application of a job-exposure matrix. *Am J Ind Med* 35: 9-14, 1999.
- 12 Clark JR and Ross WB: An unusual case of ascites: pitfalls in diagnosis of malignant peritoneal mesothelioma. *Aust NZ J Surg* 70: 384-388, 2000.
- 13 Mohamed F and Sugarbaker PH: Peritoneal mesothelioma. *Curr Treat Options Oncol* 3: 375-386, 2002.
- 14 Ordonez NG: Role of immunohistochemistry in distinguishing epithelial peritoneal mesotheliomas from peritoneal and ovarian serous carcinomas. *Am J Surg Pathol* 22: 1203-1214, 1998.
- 15 Attanoos RL, Webb R, Dojcicov SD and Gibbs AR: Value of mesothelial and epithelial antibodies in distinguishing diffuse peritoneal mesothelioma in females from serous papillary carcinoma of the ovary and peritoneum. *Histopathology* 40: 237-244, 2002.
- 16 Ros PR, Yuschock TJ, Buck JL, Shekitka KM and Kaude JV: Peritoneal mesothelioma. Radiologic appearances correlated with histology. *Acta Radiol* 32: 355-358, 1991.
- 17 Smith TR: Malignant peritoneal mesothelioma: marked variability of CT findings. *Abdom Imaging* 19: 27-29, 1994.
- 18 Gupta S, Gupta RK, Gujral RB, Agarwal D, Saxena R and Tandon P: Peritoneal mesothelioma simulating pseudomyxoma peritonei on CT and sonography. *Gastrointest Radiol* 17: 129-131, 1992.

Received November 21, 2015

Revised January 24, 2016

Accepted February 2, 2016

Instructions for Authors 2016

General Policy. ANTICANCER RESEARCH (AR) will accept original high quality works and reviews on all aspects of experimental and clinical cancer research. The Editorial Policy suggests that priority will be given to papers advancing the understanding of cancer causation, and to papers applying the results of basic research to cancer diagnosis, prognosis, and therapy. AR will also accept the following for publication: (a) Abstracts and Proceedings of scientific meetings on cancer, following consideration and approval by the Editorial Board; (b) Announcements of meetings related to cancer research; (c) Short reviews (of approximately 120 words) and announcements of newly received books and journals related to cancer, and (d) Announcements of awards and prizes.

The principal aim of AR is to provide prompt publication (print and online) for original works of high quality, generally within 1-2 months from final acceptance. Manuscripts will be accepted on the understanding that they report original unpublished works in the field of cancer research that are not under consideration for publication by another journal, and that they will not be published again in the same form. All authors should sign a submission letter confirming the approval of their article contents. All material submitted to AR will be subject to review, when appropriate, by two members of the Editorial Board and by one suitable outside referee. The Editors reserve the right to improve manuscripts on grammar and style.

The Editors and Publishers of AR accept no responsibility for the contents and opinions expressed by the contributors. Authors should warrantee due diligence in the creation and issuance of their work.

NIH Open Access Policy. The journal acknowledges that authors of NIH funded research retain the right to provide a copy of the final manuscript to the NIH four months after publication in ANTICANCER RESEARCH, for public archiving in PubMed Central.

Copyright. Once a manuscript has been published in ANTICANCER RESEARCH, which is a copyrighted publication, the legal ownership of all published parts of the paper has been transferred from the Author(s) to the journal. Material published in the journal may not be reproduced or published elsewhere without the written consent of the Managing Editor or Publisher.

Format. Two types of papers may be submitted: (i) Full papers containing completed original work, and (ii) review articles concerning fields of recognisable progress. Papers should contain all essential data in order to make the presentation clear. Reasonable economy should be exercised with respect to the number of tables and illustrations used. Papers should be written in clear, concise English. Spelling should follow that given in the "Shorter Oxford English Dictionary".

Manuscripts. Submitted manuscripts should not exceed fourteen (14) pages (approximately 250 words per double - spaced typed page), including abstract, text, tables, figures, and references (corresponding to 4 printed pages). Papers exceeding four printed pages will be subject to excess page charges. All manuscripts should be divided into the following sections:

(a) *First page* including the title of the presented work [not exceeding fifteen (15) words], full names and full postal addresses of all Authors, name of the Author to whom proofs are to be sent, key words, an abbreviated running title, an indication "review", "clinical", "epidemiological", or "experimental" study, and the date of submission. (Note: The order of the Authors is not necessarily indicative of their contribution to the work. Authors may note their individual contribution(s) in the appropriate section(s) of the presented work); (b) *Abstract* not exceeding 150 words, organized according to the following headings: Background/Aim - Materials and Methods/Patients and Methods - Results - Conclusion; (c) *Introduction*; (d) *Materials and Methods/Patients and Methods*; (e) *Results*; (f) *Discussion*; (g) *Acknowledgements*; (h) *References*. All pages must be numbered consecutively. Footnotes should be avoided. Review articles may follow a different style according to the subject matter and the Author's opinion. Review articles should not exceed 35 pages (approximately 250 words per double-spaced typed page) including all tables, figures, and references.

Figures. All figures should appear at the end of the submitted document file. Once a manuscript is accepted all figures and graphs should be submitted separately in either jpg, tiff or pdf format and at a minimum resolution of 300 dpi. Graphs must be submitted as pictures made from drawings and must not require any artwork, typesetting, or size modifications. Symbols, numbering and lettering should be clearly legible. The number and top of each figure must be indicated. Pages that include color figures are subject to color charges.

Tables. All tables should appear at the end of the submitted document file. Once a manuscript is accepted, each table should be submitted separately, typed double-spaced. Tables should be numbered with Roman numerals and should include a short title.

References. Authors must assume responsibility for the accuracy of the references used. Citations for the reference sections of submitted works should follow the standard form of "Index Medicus" and must be numbered consecutively. In the text, references should be cited by number. Examples: 1 Sumner AT: The nature of chromosome bands and their significance for cancer research. Anticancer Res 1: 205-216, 1981. 2 McGuire WL and Chamnes GC: Studies on the oestrogen receptor in breast cancer. In: Receptors for Reproductive Hormones (O' Malley BW, Chamnes GC (eds.). New York, Plenum Publ Corp., pp 113-136, 1973.

Nomenclature and Abbreviations. Nomenclature should follow that given in "Chemical Abstracts", "Index Medicus", "Merck Index", "IUPAC –IUB", "Bergery's Manual of Determinative Bacteriology", The CBE Manual for Authors, Editors and Publishers (6th edition, 1994), and MIAME Standard for Microarray Data. Human gene symbols may be obtained from the HUGO Gene Nomenclature Committee (HGNC) (<http://www.gene.ucl.ac.uk/>). Approved mouse nomenclature may be obtained from <http://www.informatics.jax.org/>. Standard abbreviations are preferable. If a new abbreviation is used, it must be defined on first usage.

Clinical Trials. Authors of manuscripts describing clinical trials should provide the appropriate clinical trial number in the correct format in the text.

For International Standard Randomised Controlled Trials (ISRCTN) Registry (a not-for-profit organization whose registry is administered by Current Controlled Trials Ltd.) the unique number must be provided in this format: ISRCTNXXXXXXX (where XXXXXXX represents the unique number, always prefixed by "ISRCTN"). Please note that there is no space between the prefix "ISRCTN" and the number. Example: ISRCTN47956475.

For Clinicaltrials.gov registered trials, the unique number must be provided in this format: NCTXXXXXXX (where XXXXXXX represents the unique number, always prefixed by 'NCT'). Please note that there is no space between the prefix 'NCT' and the number. Example: NCT00001789.

Ethical Policies and Standards. ANTICANCER RESEARCH agrees with and follows the "Uniform Requirements for Manuscripts Submitted to Biomedical Journals" established by the International Committee of Medical Journal Editors in 1978 and updated in October 2001 (www.icmje.org). Microarray data analysis should comply with the "Minimum Information About Microarray Experiments (MIAME) standard". Specific guidelines are provided at the "Microarray Gene Expression Data Society" (MGED) website. Presentation of genome sequences should follow the guidelines of the NHGRI Policy on Release of Human Genomic Sequence Data. Research involving human beings must adhere to the principles of the Declaration of Helsinki and Title 45, U.S. Code of Federal Regulations, Part 46, Protection of Human Subjects, effective December 13, 2001. Research involving animals must adhere to the Guiding Principles in the Care and Use of Animals approved by the Council of the American Physiological Society. The use of animals in biomedical research should be under the careful supervision of a person adequately trained in this field and the animals must be treated humanely at all times. Research involving the use of human foetuses, foetal tissue, embryos and embryonic cells should adhere to the U.S. Public Law 103-41, effective December 13, 2001.

Submission of Manuscripts. Please follow the Instructions for Authors regarding the format of your manuscript and references.

Manuscripts must be submitted only through our online submission system at: <http://www.iar-submissions.com/login.html>

In case a submission is incomplete, the corresponding Author will be notified accordingly.

Questions regarding difficulties in using the online submission system should be addressed to: email: journals@iar-anticancer.org

Galley Proofs. Unless otherwise indicated, galley proofs will be sent to the corresponding Author of the submission. Corrections of galley proofs should be limited to typographical errors. Reprints, PDF files, and/or Open Access may be ordered after the acceptance of the paper. Authors of online open access articles published in 2015 are entitled to a complimentary online subscription to Anticancer Research 2015. Requests should be addressed to the Editorial Office. Galley proofs should be returned corrected to the Editorial Office by email within two days.

Copyright© 2016 - International Institute of Anticancer Research (J.G. Delinasios). All rights reserved (including those of translation into other languages). No part of this journal may be reproduced, stored in a retrieval system, or transmitted in any form or by any means, electronic, mechanical, photocopying, microfilming, recording or otherwise, without written permission from the Publisher.

Specific information and additional instructions for Authors

1. Anticancer Research (AR) closely follows the new developments in all fields of experimental and clinical cancer research by (a) inviting reviews on topics of immediate importance and substantial progress in the last three years, and (b) providing the highest priority for rapid publication to manuscripts presenting original results judged to be of exceptional value. Theoretical papers will only be considered and accepted if they bear a significant impact or formulate existing knowledge for the benefit of research progress.
2. Anticancer Research will consider the publication of conference proceedings and/or abstracts provided that the material submitted fulfils the quality requirements and instructions of the journal, following the regular review process by two suitable referees. (For further information please [click here](#))
3. An acknowledgement of receipt, including the article number, title and date of receipt is sent to the corresponding author of each manuscript upon receipt. If this receipt is not received within 20 days from submission, the author should call or write to the Editorial Office to ensure that the manuscript (or the receipt) was not lost in the mail or during electronic submission.

4. Each manuscript submitted to AR is sent for review in confidence to two suitable referees with the request to return the manuscript with their comments to the Editorial Office within 12 days from receipt. If reviewers need a longer time or wish to send the manuscript to another expert, the manuscript may be returned to the Editorial Office with a delay. All manuscripts submitted to AR, are treated in confidence, without access to any person other than the Managing Editor, the journal's secretary, the reviewers and the printers.
 5. All accepted manuscripts are peer-reviewed and carefully corrected in style and language, if necessary, to make presentation clear. (There is no fee for this service). Every effort is made (a) to maintain the personal style of the author's writing and (b) to avoid change of meaning. Authors will be requested to examine carefully manuscripts which have undergone language correction at the pre-proof or proof stage.
 6. Authors should pay attention to the following points when writing an article for AR:
 - The Instructions to Authors must be followed in every detail.
 - The presentation of the experimental methods should be clear and complete in every detail facilitating reproducibility by other scientists.
 - The presentation of results should be simple and straightforward in style. Results and discussion should not be combined into one section, unless the paper is short.
 - Results given in figures should not be repeated in tables.
 - Figures (graphs or photographs) should be prepared at a width of 8 or 17 cm with legible numbers and lettering.
 - Photographs should be clear with high contrast, presenting the actual observation described in the legend and in the text. Each legend should provide a complete description, being self-explanatory, including technique of preparation, information about the specimen and magnification.
 - Statistical analysis should be elaborated wherever it is necessary. Simplification of presentation by giving only numerical or % values should be avoided.
 - Fidelity of the techniques and reproducibility of the results, should be points of particular importance in the discussion section. Authors are advised to check the correctness of their methods and results carefully before writing an article. Probable or dubious explanations should be avoided.
 - Authors should not cite results submitted for publication in the reference section. Such results may be described briefly in the text with a note in parenthesis (submitted for publication by... authors, year).
 - The References section should provide as complete a coverage of the literature as possible including all the relevant works published up to the time of submission.
 - By following these instructions, Authors will facilitate a more rapid review and processing of their manuscripts and will provide the readers with concise and useful papers.
 7. Following review and acceptance, a manuscript is examined in language and style, and galley proofs are rapidly prepared. Second proofs are not sent unless required.
 8. Authors should correct their galley proofs very carefully and preferably twice. An additional correction by a colleague always proves to be useful. Particular attention should be paid to chemical formulas, mathematical equations, symbols, medical nomenclature etc. Any system of correction marks can be used in a clear manner, preferably with a red pen. Additions or clarifications are allowed provided that they improve the presentation but do not bring new results (no fee).
 9. Articles submitted to AR may be rejected without review if:
 - they do not fall within the journal's policy.
 - they do not follow the instructions to authors.
 - language is unclear.
 - results are not sufficient to support a final conclusion.
 - results are not objectively based on valid experiments.
 - they repeat results already published by the same or other authors before the submission to AR.
 - plagiarism is detected by plagiarism screening services.

(Rejection rate (2015): 64%).
 10. Authors who wish to prepare a review should contact the Managing Editor of the journal in order to get confirmation of interest in the particular topic of the review. The expression of interest by the Managing Editor does not necessarily imply acceptance of the review by the journal.
 11. Authors may inquire information about the status of their manuscript(s) by calling the Editorial Office at +30-22950-53389, Monday to Friday 9.00-16.00 (Athens time), or by sending an e-mail to journals@iilar-anticancer.org
 12. Authors who wish to edit a special issue on a particular topic should contact the Managing Editor.
 13. Authors, Editors and Publishers of books are welcome to submit their books for immediate review in AR. There is no fee for this service.
- (This text is a combination of advice and suggestions contributed by Editors, Authors, Readers and the Managing Editor of AR).
- Copyright © 2016 IIAR (J.G. Delinasios)

Fatal pleural mesothelioma in Japan (2003–2008): evaluation of computed tomography findings

**Katsuya Kato, Kenichi Gemba,
Nobukazu Fujimoto, Keisuke Aoe,
Yukio Takeshima, Kouki Inai & Takumi
Kishimoto**

Japanese Journal of Radiology
(formerly: Radiation Medicine)

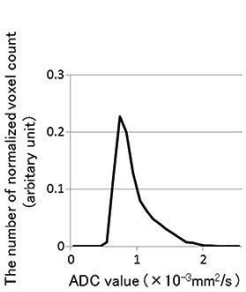
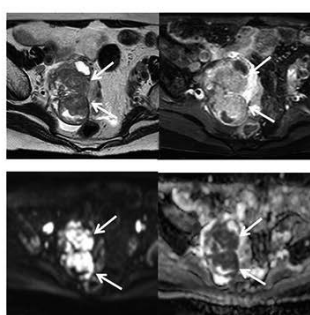
ISSN 1867-1071

Jpn J Radiol
DOI 10.1007/s11604-016-0539-1

Jpn J Radiol (2017) 36(2):161–166
© 2016 The Japanese Society of Radiology
Published online: 31 January 2017

**ONLINE
FIRST**

**JAPANESE JOURNAL OF
RADIOLOGY**



Springer

JRS
JAPANESE RADIOLOGICAL SOCIETY

Your article is protected by copyright and all rights are held exclusively by Japan Radiological Society. This e-offprint is for personal use only and shall not be self-archived in electronic repositories. If you wish to self-archive your article, please use the accepted manuscript version for posting on your own website. You may further deposit the accepted manuscript version in any repository, provided it is only made publicly available 12 months after official publication or later and provided acknowledgement is given to the original source of publication and a link is inserted to the published article on Springer's website. The link must be accompanied by the following text: "The final publication is available at link.springer.com".

Fatal pleural mesothelioma in Japan (2003–2008): evaluation of computed tomography findings

Katsuya Kato^{1,6} · Kenichi Gemba^{2,7} · Nobukazu Fujimoto² · Keisuke Aoe³ · Yukio Takeshima⁴ · Kouki Inai^{4,8} · Takumi Kishimoto⁵

Received: 4 February 2016 / Accepted: 14 March 2016
© Japan Radiological Society 2016

Abstract

Purpose The purpose of this study was to clarify the characteristic findings of mesothelioma at the time of diagnosis, and determine precautions and guidelines for diagnosing mesothelioma early in imaging studies.

Materials and methods Overall, 327 patients with pleural mesothelioma were selected from 6030 patients who died of mesothelioma between 2003 and 2008 in Japan. Their imaging findings were examined retrospectively.

Results Plaques were found in 35 % of computed tomography (CT) scans. Asbestosis, diffuse pleural thickening, and rounded atelectasis were found in only seven (2 %),

five (2 %), and two cases (1 %), respectively. Pleural thickening findings on CT scans were classified into four stages: no irregularity, mild irregularity, high irregularity, and mass formation. Overall, 18 % of cases did not show a clear irregularity. Localized thickening was observed in the mediastinal (77 %) and basal (76 %) pleura and in the interlobar fissure (49 %). Eight percent of cases did not have any thickening in these three areas.

Conclusions Upon examination of the CT scans at diagnosis, 18 % of mesothelioma cases did not show a clear irregularity. When diagnosing pleural effusion of unknown etiology, it is necessary to consider the possibility of mesothelioma even when no plaque and pleural irregularity are observed.

✉ Katsuya Kato
kato-rad@med.kawasaki-m.ac.jp

¹ Department of Radiology, Okayama University Hospital, 2-1-1 Shikatacho, Okayama 7008558, Japan

² Department of Medical Oncology, Okayama Rosai Hospital, 1-10-25 Chikkomidorimachi, Okayama 7028055, Japan

³ Department of Medical Oncology, National Hospital Organization Yamaguchi-Ube Medical Center, 685 Higashikiwa, Ube 7550241, Japan

⁴ Department of Pathology, Hiroshima University Graduate School of Medicine, 1-2-3 Kasumi, Hiroshima 7340037, Japan

⁵ Department of Internal Medicine, Okayama Rosai Hospital, 1-10-25 Chikkomidorimachi, Okayama 7028055, Japan

⁶ Present Address: Department of Diagnostic Radiology 2, Kawasaki Medical School, 2-1-80 Nakasange, Kita-ku, Okayama 7008505, Japan

⁷ Present Address: Department of Respiratory Medicine, Chugoku Chuo Hospital, 148-13 Miyukicho Oaza Kamiwanari, Fukuyama 7200001, Japan

⁸ Present Address: Pathologic Diagnostic Center, Inc., 11-28 Hacchobori, Naka-ku, Hiroshima 7300013, Japan

Keywords Mesothelioma · Computed tomography · Japan

Introduction

Mesothelioma is a rare, asbestos-related disease [1, 2] with a poor prognosis [3]. Asbestos was used extensively in Japan for construction and industrial products owing to its useful characteristics; however, since the discovery of its carcinogenic potential, alternative products have been introduced and the manufacture and use of asbestos is now prohibited. It takes 30–40 years of incubation to develop mesothelioma or lung cancer originating from asbestos [4–7], and the number of patients with mesothelioma has been increasing over recent years; this has become a problem in many countries. The United States prohibited asbestos usage earlier compared to other countries, and the number of patients developing asbestos-related problems reached a peak there in 2004, with the number now decreasing. In Europe, the peak is expected to be around 2015–2020, and in Japan, where the

prohibition occurred later, the peak will be around 2025, which implies that the number of patients will keep increasing until this time [6]. In accordance with Japanese law, crocidolite and amosite usage was stopped in 1995; chrysotile usage was stopped in 2004. The country's recent discontinuation is evidence of the delay in asbestos regulations in our country, and the damage caused by these delays is apparent. A newspaper article published in June 2005 reported that five residents who lived near the now-closed asbestos cement pipe plant in Amagasaki, Japan, developed pleural mesothelioma [8]. Since this report, asbestos-related problems have raised significant social concern. We performed a nationwide retrospective survey to evaluate all cases of mesothelioma in Japan. As a result, we analyzed more than 6000 cases of mesothelioma that were registered in the Vital Statistics yearly survey performed by the Japanese Ministry of Health, Labour, and Welfare between 2003 and 2008. To the best of our knowledge, this is the largest study of Japanese cases of mesothelioma. Our study used images, mainly computed tomography (CT) and plain radiography, from deceased patients with pleural mesothelioma that were acquired with family and institutional permissions. In a review of the literature, we found no other reports examining the number of cases with mesothelioma and their images. The clinical features of the cases with mesothelioma in this study have already been reported [9]. The purpose of the current study was to clarify the characteristics of the imaging findings obtained at the time of the diagnosis of pleural mesothelioma, and determine precautions and guidelines for diagnosing mesothelioma early in imaging studies.

Subjects and methods

Study approval

This study was conducted according to the Ethical Guidelines for Epidemiological Research by the Japanese Ministry of Education, Culture, Sports, Science and Technology, and the Ministry of Health, Labor, and Welfare. The study was approved by the relevant institutional ethical review boards.

Patient selection and imaging studies

The methods of this retrospective survey have been previously described [9]. In brief, we requested and received authorization to view the death records in the Vital Statistics register in Japan, and we extracted all cases of death due to malignant mesothelioma between 2003 and 2008; in total, 6030 deaths were found to be due to mesothelioma. We contacted the closest living relatives of each patient to obtain consent for

our study by postal mail. As a result, informed consent was obtained by mail from the relatives of 2069 patients (34.3%). Subsequently, we contacted the patients' respective medical institutions to obtain the following information by mail: medical records, radiographs, and/or CT images. Different institutions had different types of CT images. We accepted both digital and film CT scans for review to examine as many cases as possible. We also reviewed the medical records and radiological images to confirm the clinical and pathological diagnoses of malignant mesothelioma.

Image interpretation

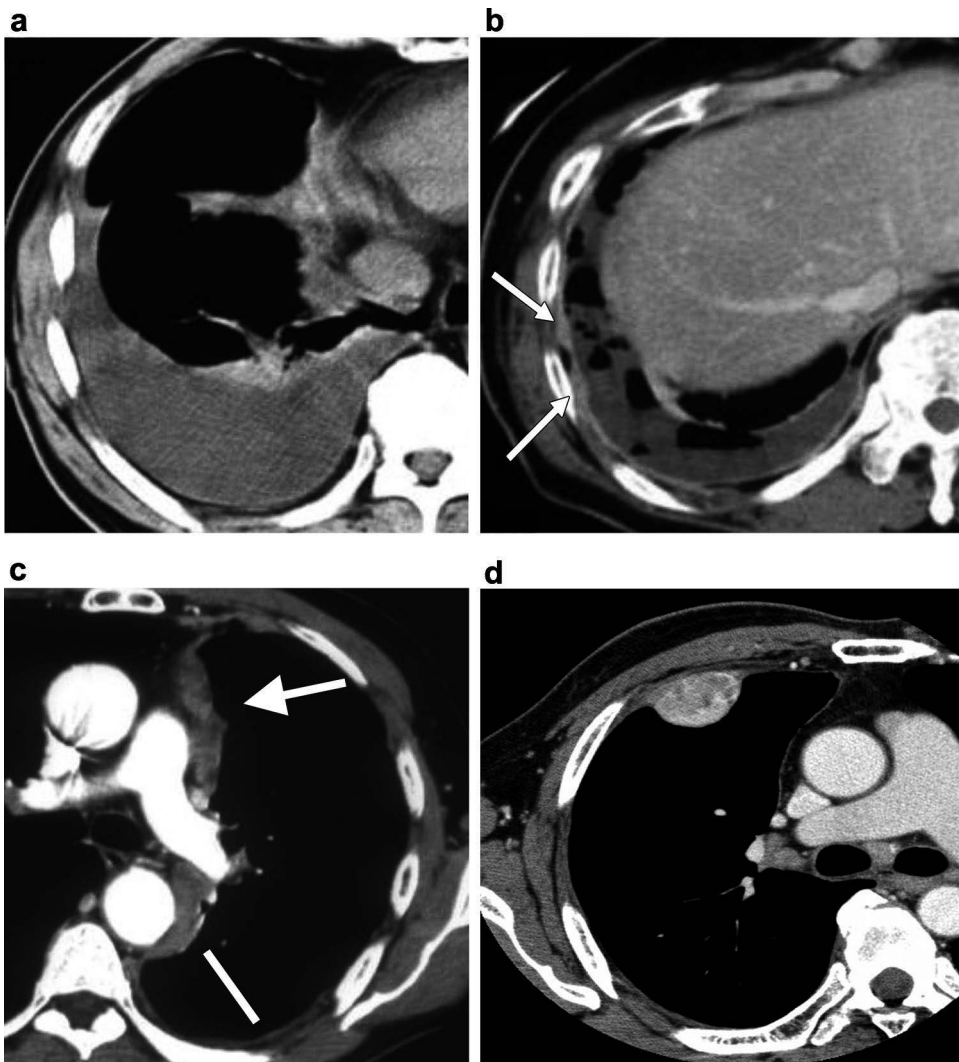
All patients underwent CT and plain radiography at the time of diagnosis of pleural mesothelioma. CT images were obtained using various CT scanners and a range of scan protocols at each institution. CT scans with a 5-mm thickness were the most common, but other slice thicknesses were found, ranging from 1 to 10 mm. Plain radiographs and CT images were retrospectively reviewed with consensus by three co-researchers: one chest radiologist and two pulmonologists. The chest radiologist (K.K.) had 24 years of experience and the two respiratory physicians (T.K. and K.G.) had 28 and 20 years of experience, respectively. Additionally, all three co-researchers had worked in a hospital that specialized in occupational respiratory disease for more than 10 years, and they were members of the official pneumoconiosis examination committee for laborers in the Okayama prefecture.

Evaluating items

First, pleural plaque and its calcification were evaluated on CT images. Pleural plaques were also assessed on plain chest radiographs of the same cases. Additionally, the images were checked for pleural effusion, lung asbestosis, diffuse pleural thickening, and rounded atelectasis.

Next, the pleural findings from the CT images were classified into four stages: no irregularity, mild irregularity, high irregularity, and mass formation. The four stages are shown in Fig. 1. No irregularity indicated that there was no pleural thickening found or that the thickening was ≤ 3 mm with no irregular surface. Mild irregularity indicated a regular surface with a thickening > 3 mm but ≤ 5 mm; this stage also included cases of slight asperity with no clear nodular irregularity. Clinically, this was non-specific thickening due to either a benign or a malignant lesion. Mild irregular findings on CT may indicate benign pleural lesions such as pleurisy. High irregularity indicated a thickening > 5 mm. Clear nodular thickening was required for this classification, and clinically, a malignancy was strongly suspected. Mass formation indicated that the irregularity was even more severe and that

Fig. 1 **a** No irregularity: pleural effusion but no irregularity of the pleura. **b** Mild irregularity: a slight irregularity of the pleura; however, the irregularity does not indicate a severe irregularity, such as a malignancy. **c** High irregularity: severe irregular thickening of the pleura; a malignant lesion is suspected. **d** Mass formation: severe irregular thickening of the pleura, with clear mass formation; this finding suggests a malignant lesion



a partial mass with a diameter of >1 cm was clearly formed. We did not include massive irregularity in mass formation; we included only the CT findings that identified a clearly formed mass. We examined the entire pleura very carefully, because the grading of pleural irregularity changes even with a localized pleural thickening. Both multiple and isolated masses were defined as a mass formation; clinically, this indicated a malignant lesion.

When we considered the tumor (T) part of the tumor node metastasis classification of malignant tumors staging system, used by the International Mesothelioma Interest Group, for pleural mesothelioma, it was difficult to distinguish between T1 and T2 by using CT alone; therefore, T1 and T2 were considered a single group. Thus, our examination was based on three groups: T1–2, T3, and T4.

Following the staging classification, localization of the pleural lesions was examined; we evaluated for signs of mediastinal pleural lesions, which are characteristic of mesothelioma [10]. The interlobar pleura, where pleural

lesions are more easily identified, and the basal lung, which frequently has lesions, were also examined for the presence of abnormalities (Fig. 2).

Statistical analysis

Statistical analysis was performed using the chi-squared test to analyze the correlation of each CT finding with the pathological diagnoses that were divided into the epithelial type and non-epithelial type. We considered $p < 0.05$ significant. Statistical calculations were performed using the SPSS statistical package, version 22.0 (IBM Corp., Armonk, NY, USA).

Results

Data from 1111 patients were obtained. We confirmed the clinical diagnosis of mesothelioma in 929 patients,

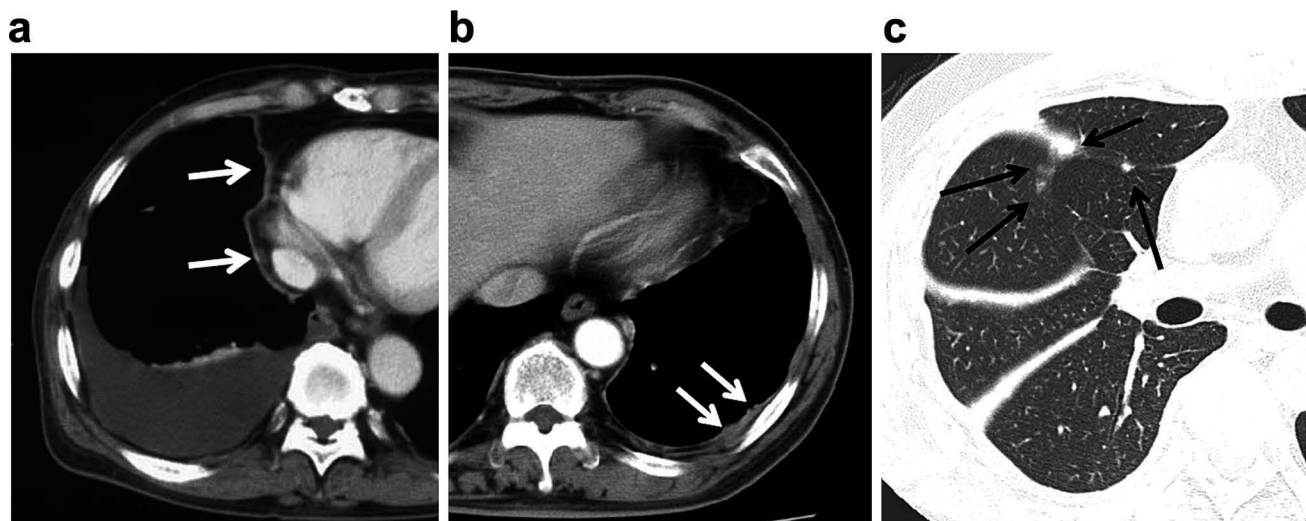


Fig. 2 **a** Mediastinal pleural irregularity: a thickened pleura with a slight irregularity in a broad area of the mediastinal pleura. The thickness is not severe in this classification, but if broad thickening is found in this area, a high potential for mesothelioma can be suspected. **b** Pleura irregularity in the base of the lungs: Tuberous irregular pleural thickening at the base of the left lung. A malignant pleural lesion can be suspected. **c** Irregular interlobar pleura: Tuberous

thickening begins in the right interlobar pleura. The interlobar pleural layer is surrounded by lung parenchyma; therefore, the pleura can be easily evaluated on the images. High-resolution computed tomography (CT) can provide clearer images, but evaluation of the interlobar pleural irregularities is also possible using average CT scans, if carefully examined

including 753 men (81.1 %) and 176 women (18.9 %). The median age at diagnosis was 67.0 years (range, 16–94 years). The origin of mesothelioma was the pleura in 794 patients (85.5 %), peritoneum in 123 (13.2 %), pericardium in seven (0.8 %), and testicular tunica vaginalis in five (0.5 %). Of those 794 patients, 327 (273 men, 54 women; mean age, 68 years) had chest CT images obtained at the time of diagnosis; we examined those images (Fig. 3).

The histological subtypes of mesothelioma were determined in 327 cases based on the World Health Organization's criteria [11]: 176 (54 %) with epithelioid mesothelioma, 75 (23 %) with sarcomatoid mesothelioma, 59 (18 %) with biphasic mesothelioma, and 17 (5 %) with other types.

Pleural plaque was found on chest CT images of 114/327 patients (35 %), and 56 of those (49 %) had calcification. Plain chest radiographs showed that only 36 (11 %) of 327 patients had plaque.

Pleural effusion was found in 304 patients (93 %), but lung asbestosis, diffuse pleural thickening, and rounded atelectasis were only found in seven (2 %), five (2 %), and two patients (1 %), respectively.

Table 1 shows the classification of pleural findings into the four stages. Table 1 compares these four stages with the T classification system. Among the 327 cases of pleural mesothelioma, seven were classified with no irregularity (2 %); 53 with a mild irregularity that included a possible benign lesion (16 %); 140 with a high irregularity that included seemingly malignant lesions (43 %); and 127 with a mass formation that indicated a malignant lesion. Thus,

82 % of cases showed severe pleural irregularities on CT images that were indicative of a potential malignancy, and 18 % of cases did not have irregularities that were indicative of malignant lesions. All the cases with no irregularity were classified as T1–2; 49 cases (92 %) with a mild irregularity were also classified as T1–2. Cases with a high irregularity progressed slowly. However, cases with a high irregularity and mass formation had a high malignant potential; 78 % of cases with a high irregularity and 84 % of cases with a mass formation were classified as T3–4.

Lesion localization was as follows: the mediastinal pleura in 251 patients (77 %), base of the lungs in 250 (76 %), and interlobular pleura in 159 (49 %) (Table 2). Only 27 cases (8 %) had no lesions in the mediastinal and interlobular pleurae.

Statistically, there was no significant correlation between the CT findings and pathological subtypes (Table 2).

Discussion

Eighty percent of patients with pleural malignant mesothelioma are men [6, 12]. In the present study, 273 patients (83 %) were men. The high percentage of men in our study is similar to the finding of a previous report [6]. The age range of our study was extremely wide, ranging from 16–94 years at diagnosis. This wide age range indicates that cases of mesothelioma caused by environmental

Fig. 3 Procedures used to select computed tomography images of the cases with pleural mesothelioma

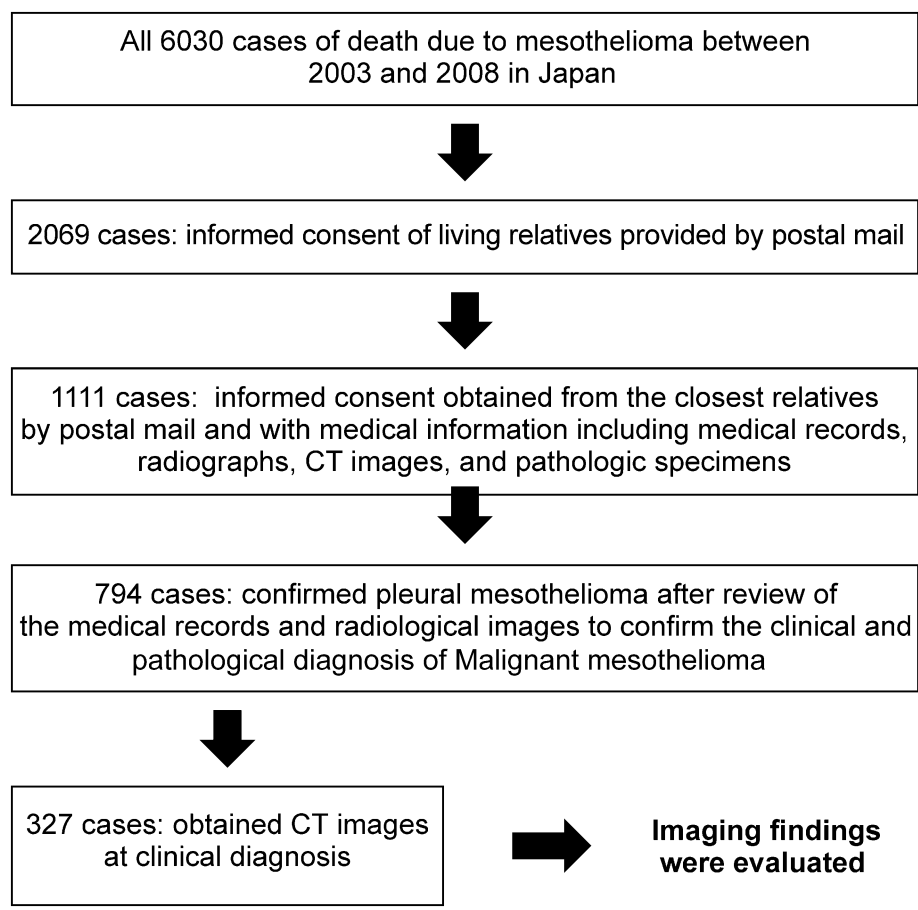


Table 1 CT images at the time of the diagnosis of pleural mesothelioma and pleural findings from CT images at the time of the diagnosis of pleural mesothelioma compared to the T classification system in 327 cases

Pleural findings	No irregularity	Mild irregularity	High irregularity	Mass formation
No. of cases	7	53	140	127
Percentage	2	16	43	39
T1–2	7	49	31	20
T3	0	4	89	58
T4	0	0	20	49

CT computed tomography, no. number

exposure were included in this study. The average latency period (i.e., the time interval between the first asbestos exposure and death) for mesothelioma development is 30–40 years [13]. Bianchi et al. [7] reported that the latency period ranges from 14–75 years (mean 48.8 years, median 51.0 years). This suggests that if the onset is diagnosed at 16 years old, the patient must have been exposed to the attributing environmental conditions since birth. This could be the case, for example, if the patient was born in a neighborhood with an asbestos factory. Due to this environmental exposure, juvenile mesothelioma would occur; these cases were also included in our study.

The image findings, mainly CT results, of 327 patients with pleural mesothelioma were selected from 6030

patients who died of mesothelioma between 2003 and 2008. Although there are a number of previous studies that have described the findings of pleural mesothelioma on CT scans [10, 13–16], no reports have evaluated the CT scans of as many as 327 patients by using uniform criteria. Therefore, the results of our study are of interest, as we present the first broad report on the results of mesothelioma on CT scans obtained at the time of the initial diagnosis.

Pleural plaque was observed in 35 % of the CT scans but in only 11 % of plain chest radiographs. Previous studies that used CT have shown pleural plaque in 12.1–78 % of cases [10, 14–16]. Additionally, only one-third of cases that had plaque on CT scans also had plaque on radiographs; this result is similar to that of a previous study [17]. Only

Table 2 Results of the statistical evaluation of the difference in CT findings between the epithelial type and non-epithelial type of mesothelioma

	Epithelial	Non-epithelial	<i>p</i> value (χ^2 -test)
CT findings			
Asbestosis	+	3	4
	–	176	144
Plaque	+	119	94
	–	60	54
Rounded atelectasis	+	1	1
	–	178	147
Diffuse pleural thickening	+	1	4
	–	178	144
Pleural effusion	+	167	137
	–	12	11
CT stages			
No irregularity		5	2
Mild irregularity–mass formation		174	146
No irregularity–mild irregularity		36	24
High irregularity–mass formation		143	124
No irregularity–high irregularity		75	52
Mass formation		104	96

CT computed tomography, + positive, – negative

2 % of cases had pulmonary fibrosis equivalent to asbestosis in the current study. Asbestosis results from high-dose asbestos exposure. This examination was a national investigation that included patients who did not work with asbestos and those who worked in asbestos-related industries. Plaque was observed in only 35 % of cases. Therefore, we believe that the ratio of persons with a high concentration of asbestos exposure among the target cases was low.

Regarding pleural irregularities, 18 % of cases had either no irregularity (no clear malignancy on the image) or a mild irregularity (these cases were mainly T1–2). Although previous reports have described the pleural effusion occurrence rate [5, 18], to our knowledge, no reports to date have described the difficulties in diagnosing malignancy based on CT images among the more than 300 known cases. To make a successful early diagnosis, it is necessary to be aware that there could be cases with no irregularities among T1–2 cases. It is necessary to pay extra attention to the possibility of a mild pleural irregularity. According to the International Mesothelioma Interest Group staging system, the median overall survival (OS) rates for patients with stages I and II (T1–2 and N0), stage III, and stage IV tumors were 11.2 months (9.4–13.0 months), 7.9 months

(7.1–8.7 months), and 3.9 months (3.0–4.6 months) (95 % confidence interval), respectively. The OS was significantly shorter for stage III patients than for stages I and II patients ($p < 0.001$); the OS was significantly shorter for stage IV patients than for stage III patients ($p < 0.001$) [8].

Regarding lesion localization, the mediastinal pleura was the most common site (77 % of cases). Abnormal findings were also observed in the basal lung and interlobular pleurae. Overall, lesions in these three sites encompassed 82 % of all cases. Mediastinal pleural lesions can be considered to have a relatively high specificity as malignant pleural lesions, and the basal lung and interlobular pleura are surrounded by lung parenchyma, which makes the evaluation of microlesions easier. Therefore, focusing on these three locations on CT images during diagnosis could improve the sensitivity and potential for diagnosing mesothelioma earlier.

There was no significant correlation between each CT finding and the pathological subtypes. Although the epithelial type of mesothelioma is associated with a better prognosis than the sarcomatous and biphasic subtypes [19], less irregularity subtype groups are not significantly correlated with the epithelial subtype of mesothelioma.

There are a number of limitations in our study. First, our study was retrospective, and the cases were collected from many institutions. Therefore, a variety of imaging devices and methods for both CT and plain radiography were used. However, because we evaluated CT images obtained with various scanners, our image evaluation process was simple; the principal objective was to identify irregular findings that the mesothelioma expert believed to be malignant. In Japan, there is a wide range of CT imaging techniques, but in most cases, an evaluable image was obtained. However, an advantage of this multi-center study was the large number of cases we were able to collect and examine. Secondly, the ability to diagnose mesothelioma differed among the hospitals. As the timing of the mesothelioma diagnosis varied according to the diagnostic ability of each institution, this may have introduced bias into our study; the progression of the mesothelioma lesion could be associated with a delay in diagnosis. Therefore, we speculate that the number of cases with mesothelioma with less severe irregularity findings would increase if each institution had made the diagnosis at an appropriate time. Additionally, in our study, we did not evaluate interobserver variation, thus this was a limitation too. However, all observers were adequately experienced with asbestos-related diseases, and thus good evaluation for radiologic images was performed.

In conclusion, 18 % of cases with mesothelioma in our study did not display a clear irregularity on CT images, and these cases were classified as low T-stage at the time of diagnosis. Therefore, when diagnosing pleural effusion of unknown etiology, the possibility of pleural mesothelioma

must be considered even in cases with no identifiable plaque. When the findings do not indicate a malignant lesion, we can still suspect potential mesothelioma when slight changes are observed in the mediastinal or interlobar pleura. Images of early-stage mesothelioma need to be interpreted accurately.

Acknowledgements This research was funded primarily by grants from the research foundation of the Ministry of Health, Labor, and Welfare of Japan (200500129A, 200635021A, 200733015A, 200733015B, 200836010A, 200938007A, and 201032004B) and by the Industrial Disease Clinical Research Grants from the Ministry of Health, Labor, and Welfare of Japan (1403101). This study is one of the research and development and dissemination projects related to the 13 fields of occupational injuries and illnesses of the Japan Health, Labor, and Welfare Organization. The sponsors had no involvement in the study design, collection, and analysis and interpretation of the data; writing of the manuscript; or decision to submit the manuscript for publication. We thank the living relatives of the patients with mesothelioma who provided consent; medical institutions that provided the medical information on the patients with mesothelioma; and Mrs. Rie Sugimoto, Mrs. Keiko Fujimura, Miss Naomi Ogura, and Miss Shiori Sato for collecting data.

Compliance with ethical standards

Conflict of interest The authors declare that they have no conflicts of interest.

Funding This research was funded primarily by grants from the research foundation of the Ministry of Health, Labor, and Welfare of Japan (200500129A, 200635021A, 200733015A, 200733015B, 200836010A, 200938007A, and 201032004B) and by Industrial Disease Clinical Research Grants from the Ministry of Health, Labor, and Welfare of Japan (1403101).

Ethical statement This study was conducted according to the Ethical Guidelines for Epidemiological Research by the Japanese Ministry of Education, Culture, Sports, Science and Technology, and the Ministry of Health, Labor, and Welfare. This study was approved by the Japan Health, Labor, and Welfare Organization and the institutional review boards of each institution. Patient confidentiality was strictly maintained. Informed consent was obtained from the closest living relatives of each patient.

References

- Wagner JC, Sleggs CA, Marchand P. Diffuse pleural mesothelioma and asbestos exposure in the North Western Cape Province. *Br J Ind Med*. 1960;17:260–71.
- Prazakova S, Thomas PS, Sandrini A, Yates DH. Asbestos and the lung in the 21st century: an update. *Clin Respir J*. 2014;8:1–10.
- Muers MF, Stephens RJ, Fisher P, Darlison L, Higgs CM, Lowry E, et al. Active symptom control with or without chemotherapy in the treatment of patients with malignant pleural mesothelioma (MS01): a multicentre randomised trial. *Lancet*. 2008;371:1685–94.
- Rusch VW. A proposed new international TNM staging system for malignant pleural mesothelioma from the International Mesothelioma Interest Group. *Lung Cancer*. 1996;14:1–12.
- Metintas M, Ucgun I, Elbek O, Erginol S, Metintas S, Kolsuz M, et al. Computed tomography features in malignant pleural mesothelioma and other commonly seen pleural diseases. *Eur J Radiol*. 2002;41:1–9.
- Robinson BW, Lake RA. Advances in malignant mesothelioma. *New Engl J Med*. 2005;353:1591–603.
- Bianchi C, Brollo A, Ramani L, Bianchi T, Giarelli L. Asbestos exposure in malignant mesothelioma of the pleura: a survey of 557 cases. *Ind Health*. 2001;39:161–7.
- Oshima H. 51 death asbestos-related illness in ten years. *Mainichi Newspapers*. 2005;1.
- Gemba K, Fujimoto N, Aoe K, Kato K, Takeshima Y, Inai K, et al. Treatment and survival analyses of malignant mesothelioma in Japan. *Acta Oncol*. 2013;52:803–8.
- Leung AN, Muller NL, Miller RR. CT in differential diagnosis of diffuse pleural disease. *AJR Am J Roentgenol*. 1990;154:487–92.
- Churg A, Cagle PT, Roggli VL. Separation of benign and malignant mesothelial proliferations. In: AFIP Atlas of tumor pathology. Series 4. Tumors of the serosal membrane. Silver Springs: ARP Press; 2006. p. 83–101.
- Roe OD, Stella GM. Malignant pleural mesothelioma: history, controversy and future of a manmade epidemic. *Eur Respir Rev*. 2015;24:115–31.
- Erzen C, Eryilmaz M, Kalyoncu F, Bilir N, Sahin A, Baris YI. CT findings in malignant pleural mesothelioma related to nonoccupational exposure to asbestos and fibrous zeolite (erionite). *J Comput Assist Tomogr*. 1991;15:256–60.
- Kawashima A, Libshitz HI. Malignant pleural mesothelioma: CT manifestations in 50 cases. *AJR Am J Roentgenol*. 1990;155:965–9.
- Senyigit A, Bayram H, Babayigit C, Topcu F, Nazaroglu H, Bilici A, et al. Malignant pleural mesothelioma caused by environmental exposure to asbestos in the Southeast of Turkey: CT findings in 117 patients. *Respiration*. 2000;67:615–22.
- Seely JM, Nguyen ET, Churg AM, Müller NL. Malignant pleural mesothelioma: computed tomography and correlation with histology. *Eur J Radiol*. 2009;70:485–91.
- Staples CA. Computed tomography in the evaluation of benign asbestos-related disorders. *Radiol Clin North Am*. 1992;30:1191–207.
- Okten F, Koksal D, Onal M, Ozcan A, Simsek C, Erturk H. Computed tomography findings in 66 patients with malignant pleural mesothelioma due to environmental exposure to asbestos. *Clin Imaging*. 2006;30:177–80.
- Meyerhoff RR, Yang CF, Speicher PJ, Gulack BC, Hartwig MG, D'Amico TA, et al. Impact of mesothelioma histologic subtype on outcomes in the surveillance, epidemiology, and end results database. *J Surg Res*. 2015;196:23–32.

Angiosarcoma of the thoracic wall responded well to nanoparticle albumin-bound paclitaxel: A case report

Naofumi Hara¹, Nobukazu Fujimoto^{2,*}, Yosuke Miyamoto¹, Tomoko Yamagishi¹, Michiko Asano¹, Yasuko Fuchimoto¹, Sae Wada¹, Shinji Ozaki¹, Hideyuki Nishi³, Takumi Kishimoto⁴

¹ Department of Respiratory Medicine, Okayama Rosai Hospital, Okayama, Japan;

² Department of Medical Oncology, Okayama Rosai Hospital, Okayama, Japan;

³ Department of Surgery, Okayama Rosai Hospital, Okayama, Japan;

⁴ Department of Internal Medicine, Okayama Rosai Hospital, Okayama, Japan.

Summary

An 81-year-old woman visited a local clinic due to chest pain and a skin induration on the right precordia. She had a history of right breast cancer, and she had undergone a mastectomy and radiation therapy 10 years prior. Computed tomography (CT) imaging of the chest demonstrated a lobular mass that involved the right anterior thoracic wall and partially extruded from the thoracic cavity into the subcutaneous tissue. The tumor was surgically excised, and pathological analyses yielded a diagnosis of angiosarcoma. Five months after the operation, CT imaging showed multiple masses on the right pleura, indicating a local relapse and pleural dissemination of the angiosarcoma. Systemic chemotherapy composed of nanoparticle albumin-bound paclitaxel (nab-PTX) (80 mg/m²) was delivered weekly. After 4 courses of chemotherapy, the tumors regressed remarkably. Nab-PTX may be an effective treatment option for recurrent or metastatic angiosarcoma.

Keywords: Angiosarcoma, paclitaxel, chemotherapy

1. Introduction

Angiosarcoma is an extremely rare malignant vessel tumor that comprises 1% of all soft tissue sarcomas (1). It develops in subcutaneous tissue at many sites in the body, and a previous medical history of trauma, breast cancer, and/or radiotherapy are considered risk factors for the disease. Localized tumors are treated with surgical removal. However, for recurrent and unresectable conditions, there is limited evidence to support chemotherapy regimens. Here, we describe a patient with angiosarcoma that developed in the thoracic wall, which responded well to systemic chemotherapy composed of nanoparticle albumin-bound paclitaxel (nab-PTX).

2. Case report

An 81-year-old woman was referred to our hospital for an examination due to right chest pain. She had a history of right breast cancer and had undergone a mastectomy and adjuvant radiotherapy 10 years prior. Upon examination, a skin induration with tenderness was found on the right precordia. Computed tomography (CT) imaging of the chest demonstrated right pleural effusion and a lobular mass that involved the right anterior thoracic wall; this mass had partially extruded from the thoracic cavity into the subcutaneous tissue (Figure 1A). On enhanced CT images, the mass showed a contrast effect in the early stages of the arterial phase. The tumor was surgically excised. Pathological analyses of the tumor showed disarrayed growth of hyperchromatic and vasoformative mesenchymal tumor cells with abnormal mitosis (Figure 2A). Immunohistochemical analyses revealed that the cells were positive for CD31 (Figure 2B) and CD34 (Figure 2C), but negative for epithelial markers, S-100 (Figure 2D) and D2-40 (Figure 2E). Based on these findings, the diagnosis was confirmed as angiosarcoma. Five months after the operation, CT images showed

Released online in J-STAGE as advance publication February 15, 2016.

*Address correspondence to:

Dr. Nobukazu Fujimoto, Department of Medical Oncology, Okayama Rosai Hospital, 1-10-25 Chikkomidorimachi, Okayama 702-8055, Japan.
E-mail: nobufujimot@gmail.com

multiple masses on the right pleura, indicating a local relapse and pleural dissemination of the angiosarcoma (Figure 1B). Systemic chemotherapy composed of nab-PTX (80 mg/m²) was delivered weekly. After 4 courses of chemotherapy, the masses in the pleura regressed remarkably (Figure 1C). The only adverse event was alopecia, no myelosuppression or neurotoxicity was observed. After a total of 14 courses of chemotherapy, multiple tumors reappeared, and the patient died at

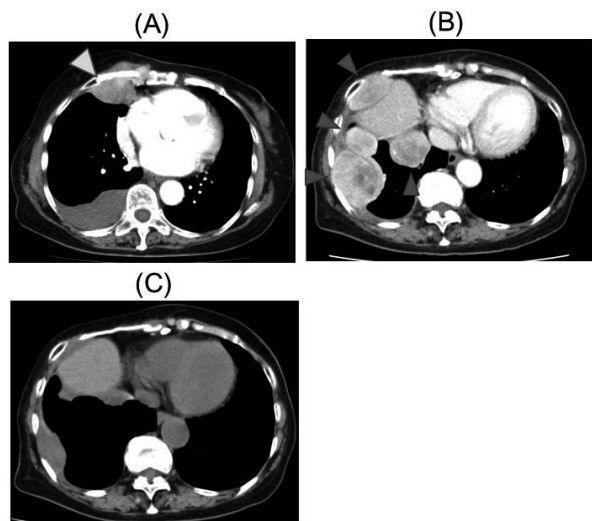


Figure 1. Computed tomography images of the chest. (A) Right pleural effusion and a lobular mass (white arrowhead) were observed at the initial examination. (B) Multiple masses on the right pleura (red arrowheads) appeared 5 months after the operation. (C) Regressed masses on the pleura after 4 courses of chemotherapy.

18 months after the initial diagnosis. Autopsy was not allowed.

3. Discussion

Angiosarcoma is an uncommon malignant vessel tumor. Angiosarcoma can develop in the subcutaneous tissue in almost all parts of the body, but the most common sites are the head and neck, followed by the breast and liver (2). Angiosarcoma of the pleura is extremely rare (3). A history of breast cancer and radiation therapy are known risk factors for this disease (4,5), and both these factors were present in the current case study. There is limited evidence to support chemotherapy regimens for unresectable and recurrent angiosarcomas; however, a few reports have suggested that anthracyclines, ifosfamide, and taxanes are potential treatment options. A retrospective study showed that, when paclitaxel was used to treat unresectable angiosarcomas, progression-free survival was achieved for 6.8 months for scalp angiosarcoma and 2.8 months for sites below the clavicle (6). Nab-PTX is a novel, soluble, polyoxyethylated, castor oil-free, biologically interactive form of paclitaxel, which allows shorter infusion times and requires no premedication for hypersensitive reactions. Nab-PTX has been approved for breast cancer (7), non-small cell lung cancer (8), and gastric cancer (9) in Japan. Moreover, in the future, it will be used in more patients as an alternative to PTX. In the current case, nab-PTX was delivered to an aged patient with recurrent angiosarcoma that had disseminated in the pleura. This

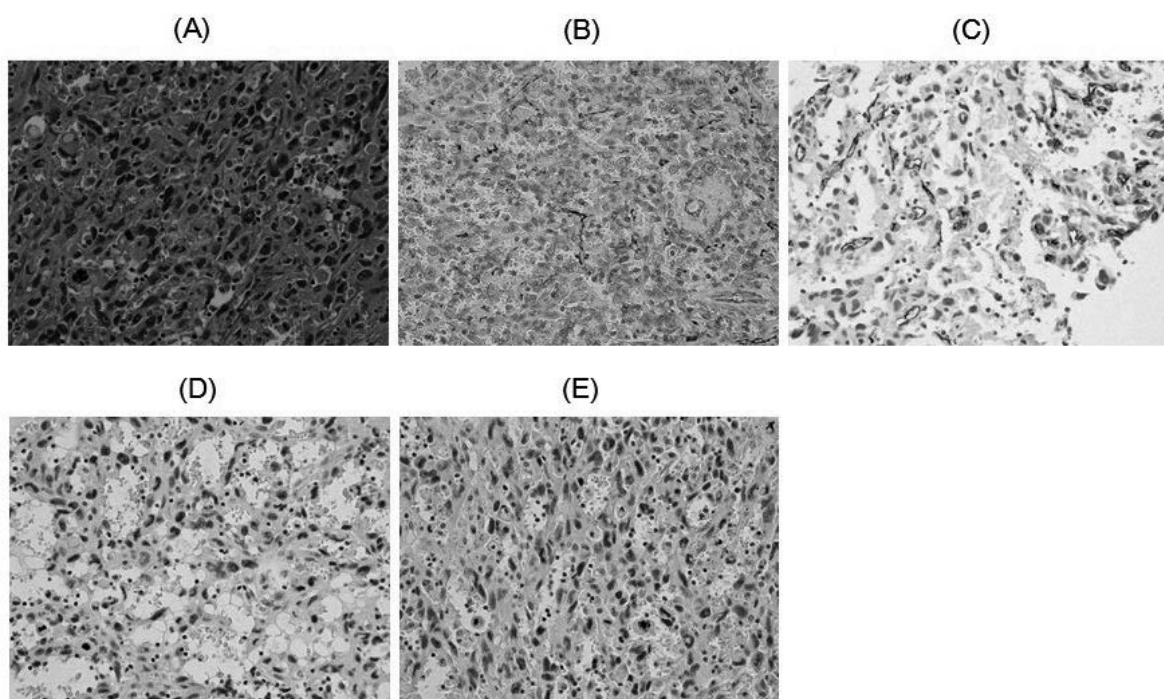


Figure 2. Pathological analyses. (A) Resected tumor specimen showed disarrayed growth of hyperchromatic and vasoformative mesenchymal tumor cells with abnormal mitosis ($\times 40$). Immunohistochemical analyses revealed that the cells were positive for CD31 (B) and CD34 (C), but negative for epithelial markers, S-100 (D) and D2-40 (E) ($\times 40$).

treatment elicited a favorable response and few adverse events, though the tumor acquired resistance eventually. To our knowledge, the current case was the first to show that angiosarcoma significantly responded to nab-PTX. Our results suggested that weekly administration of nab-PTX may be an effective treatment option for recurrent angiosarcoma.

In conclusion, we described a case of angiosarcoma in the pleura, which showed a significant response to nab-PTX.

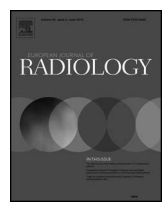
Acknowledgements

Supported by "The research, development, and dissemination of projects related to nine fields of occupational injuries and illnesses" of the Japan Labour Health and Welfare Organization and by grants-in-aid from the Ministry of Health, Labor and Welfare, Japan.

References

1. Wanebo HJ, Koness RJ, MacFarlane JK, Eilber FR, Byers RM, Elias EG, Spiro RH. Head and neck sarcoma: report of the Head and Neck Sarcoma Registry. Society of Head and Neck Surgeons Committee on Research. Head Neck. 1992; 14:1-7.
2. Albores-Saavedra J, Schwartz AM, Henson DE, Kostun L, Hart A, Angeles-Albores D, Chable-Montero F. Cutaneous angiosarcoma. Analysis of 434 cases from the Surveillance, Epidemiology, and End Results Program, 1973-2007. Ann Diagn Pathol. 2011; 15:93-97.
3. Zhang S, Zheng Y, Liu W, Yu X. Primary epithelioid angiosarcoma of the pleura: a case report and review of literature. Int J Clin Exp Pathol. 2015; 8:2153-2158.
4. Karlsson P, Holmberg E, Johansson KA, Kindblom LG, Carstensen J, Wallgren A. Soft tissue sarcoma after treatment for breast cancer. Radiother Oncol. 1996; 38:25-31.
5. Blanchard DK, Reynolds C, Grant CS, Farley DR, Donohue JH. Radiation-induced breast sarcoma. Am J Surg. 2002; 184:356-358.
6. Fury MG, Antonescu CR, Van Zee KJ, Brennan MF, Maki RG. A 14-year retrospective review of angiosarcoma: clinical characteristics, prognostic factors, and treatment outcomes with surgery and chemotherapy. Cancer J. 2005; 11:241-247.
7. Gradishar WJ, Tjulandin S, Davidson N, Shaw H, Desai N, Bhar P, Hawkins M, O'Shaughnessy J. Phase III trial of nanoparticle albumin-bound paclitaxel compared with polyethylated castor oil-based paclitaxel in women with breast cancer. J Clin Oncol. 2005; 23:7794-7803.
8. Rizvi NA, Riely GJ, Azzoli CG, Miller VA, Ng KK, Fiore J, Chia G, Brower M, Heelan R, Hawkins MJ, Kris MG. Phase I/II trial of weekly intravenous 130-nm albumin-bound paclitaxel as initial chemotherapy in patients with stage IV non-small-cell lung cancer. J Clin Oncol. 2008; 26:639-643.
9. Koizumi W, Morita S, Sakata Y. A randomized Phase III trial of weekly or 3-weekly doses of nab-paclitaxel versus weekly doses of Cremophor-based paclitaxel in patients with previously treated advanced gastric cancer (ABSOLUTE Trial). Jpn J Clin Oncol. 2015; 45:303-306.

(Received January 5, 2016; Revised February 8, 2016; Accepted February 9, 2016)



Pleural irregularities and mediastinal pleural involvement in early stages of malignant pleural mesothelioma and benign asbestos pleural effusion



Katsuya Kato^{a,*}, Kenichi Gemb^{b,1}, Nobukazu Fujimoto^b, Keisuke Aoe^c, Yukio Takeshima^d, Kouki Inai^{d,2}, Takumi Kishimoto^e

^a Department of Radiology, Okayama University Hospital, 2-1-1 Shikatacho, Okayama 7008558, Japan

^b Department of Medical Oncology, Okayama Rosai Hospital, 1-10-25 Chikkomidorimachi, Okayama 7028055, Japan

^c Department of Medical Oncology, National Hospital Organization Yamaguchi-Ube Medical Center, 685 Higashikiwa, Ube 7550241, Japan

^d Department of Pathology, Hiroshima University Graduate School of Medicine, 1-2-3 Kasumi, Hiroshima 7340037, Japan

^e Department of Internal Medicine, Okayama Rosai Hospital, 1-10-25 Chikkomidorimachi, Okayama 7028055, Japan

ARTICLE INFO

Article history:

Received 8 March 2016

Received in revised form 23 May 2016

Accepted 19 June 2016

Keywords:

Mesothelioma

Benign asbestos pleural effusion

CT scan

ABSTRACT

Objective: To elucidate differences in the level and localization of pleural irregularities in early malignant pleural mesothelioma (eMPM) and benign asbestos pleural effusion (BAPE) using CT.

Study design: Retrospective assessment of CT findings of consecutive patients with BAPE at a single centre and patients with eMPM reported in Japanese vital statistics.

Methodology: Thirty-six patients with confirmed diagnoses of BAPE and sixty-six patients with confirmed diagnoses of eMPM (mesothelioma stages T1 or T2) were included. Informed consent, CT scans, and clinical and pathologic details were obtained for all patients and were reviewed by one radiologist, two pathologists, and two pulmonologists. Asbestosis, pleural plaque, rounded atelectasis, and diffuse pleural thickening were assessed in all patients.

Results: Prevalence of asbestosis, pleural plaque, rounded atelectasis, and diffuse pleural thickening was significantly higher in the BAPE group. Low-level irregularity was more common in the BAPE group ($p < 0.001$), whereas high-level irregularity, mediastinal localization, and interlobar fissure were more prevalent in the eMPM group ($p < 0.001$). Interlobar pleural irregularity was not observed in any patients in the BAPE group, although 55% of patients in the eMPM group showed interlobar pleural irregularity. Mediastinal pleural involvement was observed in 74% of patients in the eMPM group and had a positive predictive value of 89%.

Conclusion: This study demonstrates that the level and localization of plural irregularities significantly differed between patients with BAPE and eMPM. Large-scale prospective studies are needed to fully establish the diagnostic utility of such differences.

© 2016 Elsevier Ireland Ltd. All rights reserved.

1. Introduction

Malignant pleural mesothelioma (MPM) is a neoplasm of meso-dermal origin and is associated with exposure to asbestos [1]. MPM has a poor prognosis, but detection in early stages can significantly increase patient survival, as distant metastasis occurs at consider-

ably later stages. Unfortunately, however, the diagnosis of MPM is often delayed, either because of nonspecific symptoms or the unreliability of radiological imaging and pleural biopsy techniques [2]. In particular, the variability of pleural findings makes features of anatomical imaging modalities complicated [3], leading to poor differential diagnosis with benign tumours and with other malignant tumours, such as sarcomas and adenocarcinomas [4–6].

Benign asbestos pleural effusion (BAPE) is a complication of chronic exposure to asbestos. It is generally classified as the accumulation of pleural fluid and may be asymptomatic or associated with pain, fever, and dyspnoea. Differentiation of BAPE from early stages of MPM is difficult, due to several overlapping radiological features [7,8]. Considerable work has been conducted to discern

* Corresponding author at: Department of Diagnostic Radiology 2, Kawasaki Medical School, 2-1-80 Nakasange, Kita-ku, Okayama 700-8505, Japan.

E-mail address: kato-rad@med.kawasaki-m.ac.jp (K. Kato).

¹ Present address: Department of Respiratory Medicine, Chugoku Chuo Hospital, Fukuyama, Japan.

² Present address: Pathologic Diagnostic Center, Inc., Hiroshima, Japan.

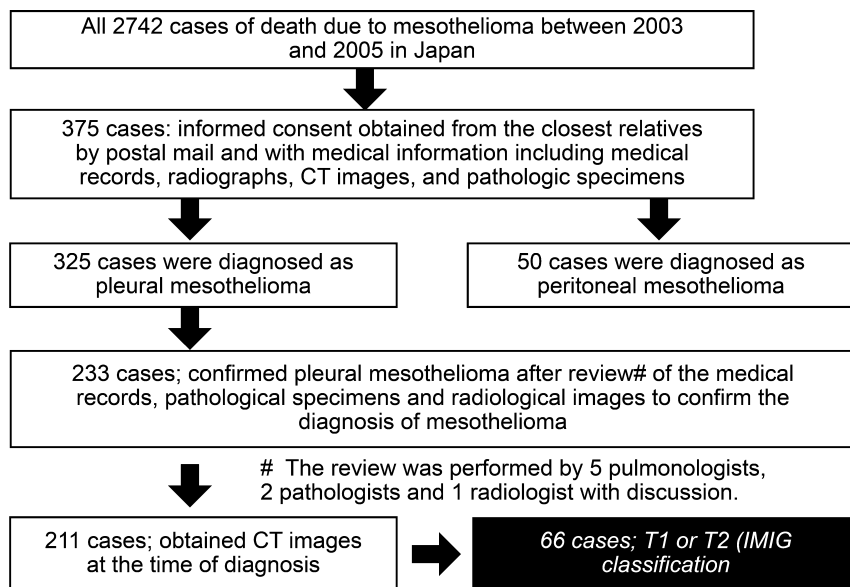


Fig. 1. Flow chart summarizing enrolment of patients in eMPM group.

distinct features of MPM and BAPE, using different diagnostic modalities including X-ray, PET, MRI, and CT [9–11]. However, confirmatory diagnoses of MPM mostly still depend on histopathologic evaluations of biopsy specimens, even though the procedure is associated with complications [12].

In Japan, the production and application of asbestos have been prohibited since 2004. However, since asbestos-related diseases have long latency periods, the number of mesothelioma patients has increased in recent years [13–15]. Evidence suggests that it takes 30–40 years of incubation to develop mesothelioma after exposure to asbestos. It has therefore been postulated that the number of MPM patients in Japan will peak in 2025. The trend is in line with other advanced countries, as in the past, asbestos was used extensively for construction and industrial products [16,17]. We researched the Vital Statistics survey carried out by the Japanese Ministry of Health, Labour, and Welfare and found more than 6000 mesothelioma cases [17]. These statistics, along with the diagnostic issues outlined above, clearly stress an immediate need for efficient strategies for the early diagnosis and management of MPM.

Computed tomography (CT) has been used as a non-invasive tool for diagnosing, staging, and following-up MPM. Asbestos exposure may lead to pleural effusion, pleural thickening, and pleural plaques, which can be effectively diagnosed using CT scans [18]. However, the differences between the CT features of benign and malignant pleural diseases are poorly understood [3,4,19]. The purpose of this study was to evaluate the differences between the CT findings of patients diagnosed with stage I and II MPM and patients diagnosed with BAPE. We also attempted to assess changes in the grade of pleural irregularity, localization of pleural irregularity, and changes in CT scan features during follow-up.

2. Subjects and methods

2.1. BAPE group

Thirty-six patients who were referred to the Okayama Rosai Hospital between Mar 1, 2005 and Apr 30, 2008 and who had a definitive diagnosis of BAPE were included. BAPE was indicated by symptoms including chronic cough, abnormal pulmonary function tests, chest pain, breathlessness, hoarseness of the voice, and CT scan results. All patients had a history of asbestos exposure. Pleural biopsy was performed in all cases. All pathologic specimens were

reviewed by a pathologist, and the histological assessment of malignancy was made on the basis of standard cytological tests. BAPE was defined on the basis of four criteria: (a) history of asbestos exposure, (b) radiologic or thoracentesis confirmation of pleura, (c) absence of another cause for the pleural effusion, and (d) no malignant tumour developing within one year [20–22]. Follow-up was conducted through routine visits. Informed consent was obtained from all patients, and the Institutional Ethical Review Board of Okayama Rosai Hospital approved the study.

The CT scans were obtained using X-vigor in 6 cases and AquilionTM32 (Toshiba Medical Systems, Otawara, Tochigi, Japan) in 30 cases. Patients were screened in the supine position with or without injection of contrast media, depending on the radiologists' judgment; 9 cases were screened without contrast media, while 24 cases used it and 3 cases were screened both with and without contrast media. A slice thickness of 5 mm and mediastinal and lung parenchymal window settings were used. The window width was 1500 HU for parenchymal imaging and 350 HU for soft tissues. Parenchymal and soft tissue images were reconstructed with sharp and smooth filters, respectively. Intravenous iodinated contrast medium was used to determine lymph node enlargement and pleural irregularities. The CT scans and accompanying chest radiographs were reviewed by one radiologist and two pulmonologists (K. K., T. K., and N. F.) who were familiar with asbestos-related disease and who were members of the official pneumoconiosis examination committee for labourers in the Okayama prefecture. The observers were unaware of the pathologic diagnosis; a conclusion was reached by consensus.

2.2. Early MPM (*eMPM*) group

Sixty-six patients were included in the early MPM group. The subjects were selected from mesothelioma death cases in the Japanese Vital Statistics (2003–2005). The detailed method for patient selection and data collection has been described elsewhere [23]. In brief, we extracted all cases of death due to malignant mesothelioma in the Vital Statistics register in Japan (2003–2005). Informed consent was obtained from living relatives, and complete medical records, radiographs, and/or CT images were obtained from the respective medical institutions. We reviewed medical records and radiological images with clinically and pathologically confirmed diagnoses of malignant mesothelioma based on ICD CD46.

Table 1
Characteristics of patients in BAPE and eMPM groups.

Characteristic	Total (n = 102)	BAPE (n = 36)	eMPM (n = 66)	P value
Age, years (Mean \pm SD)	69.3 \pm 9.3	72.0 \pm 7.2	67.8 \pm 10.1	0.0297
Sex (M/F)	92/10	36/0	56/10	0.0133
History of asbestos exposure, years (Mean \pm SD)	24.1 \pm 15.9	28.1 \pm 14.7	16.6 \pm 17.0	0.0009
Latency, years (Mean \pm SD)	31.3 \pm 21.6	46.3 \pm 11.5	24.0 \pm 21.6	0.0001
eMPM histological subtype				
Epithelioid			41 (62.12%)	
Sarcomatoid			8 (12.12%)	
Biphasic			12 (18.18%)	
Unknown			5 (7.58%)	

Table 2
Clinical imaging characteristics in BAPE and eMPM groups.

	BAPE (n = 36)	eMPM (n = 66)	P value
Asbestosis			
PR classification			
PR1	6 (17%)	1 (2%)	<0.05
PR2	4	1	
PR3	1	0	
Pleural plaque			
Calcification (+)	33 (92%)	23 (35%)	<0.001
Rounded atelectasis	25	10	
Diffuse pleural thickesses	16 (44%)	0 (0%)	<0.001
Pleural effusion	9 (25%)	1 (2%)	<0.001
	36 (100%)	64 (97%)	0.291

PR: profusion rate.

Thirty-four cases were screened without contrast media, while 27 cases used contrast media, and 5 cases were screened both with and without contrast media. Patients with incomplete CT findings were excluded. All CT scans were retrospectively reviewed at our institution by one radiologist and two pulmonologists (K. K., T. K., and K. G.) who were familiar with asbestos-related disease and who were members of the official pneumoconiosis examination committee for labourers in the Okayama prefecture. The TNM Classification of Malignant Tumors staging system used by the International Mesothelioma Interest Group (IMIG) for pleural mesothelioma was used to stage MPM [24]. Only patients with stage T1 and T2 tumours were included in the analysis (Fig. 1).

2.3. Pleural findings

The images were analysed to identify pleural plaques and calcification, pleural effusion, lung asbestosis, diffuse pleural thickening, and rounded atelectasis. Pleural plaques were defined as circumscribed, pleural areas of opacity with well-demarcated edges [25]. The pleural findings from the CT images were classified into four stages: "no irregularity", "low-level irregularity", "high-level-irregularity", and "mass formation". These four stages are shown in Supplementary Figs. 1–4. "No irregularity" indicated complete absence of pleural thickening or thickening \leq 3 mm with no irregular surface. "Low-level irregularity" indicated a regular surface with a thickening $>$ 3 mm but \leq 1 cm; this stage also included cases of slight asperity with no clear nodular irregularity $<$ 5 mm. Clinically, this was non-specific thickening due to either a benign or a malignant lesion. Mild irregular findings on CT may indicate benign pleural lesions such as pleurisy. "High-level-irregularity" indicated a regular thickening $>$ 1 cm, an irregular thickening $>$ 5 mm, and clear nodularity $>$ 3 mm but not "mass formation". For an irregular thickening, slight asperity was required for this classification. Clinically "high-level irregularities" have a high index of suspicion for malignancy. "Mass formation" indicated a clearly formed partial mass with a diameter of $>$ 1 cm. We examined the entire pleura very carefully, to ensure careful grading of pleural irregularity changes, even with localized pleural thickening. Both multiple and isolated masses were defined as mass formation; clinically, this indicated

a malignant lesion [17]. Metintas et al. showed that thicknesses $>$ 1 cm were not a meaningful variable in univariate analyses [9]. In this work, we therefore proposed criteria based on much lower pleural thickening (no irregularities \leq 3 mm; low-level irregularities $>$ 3 mm but \leq 5 mm, high-level $>$ 5 mm, and mass formation was noted at $>$ 1 cm). We believe that these criteria can be useful for the diagnosis of the early stages of MPM (I & II) [26]. In the case of the BAPE and eMPM groups, all pleural thickenings were measured on the monitor with electronic callipers in the DICOM medical image viewer at an appropriate digital magnification. In the BAPE group, all measurements were made with the Synapse medical imaging and information management system (Fuji Medical, Tokyo, Japan). In the eMPM group, when digital data were available, measurements were performed in the POP-net system (Image ONE, Tokyo, Japan). When digital images were not available, we measured the numbers of pixels in a 1 cm scale on the scanned film and used the pixels in the pleura to calculate the thickness of the pleura. All cases where diffuse pleural thickening was observed involved contrast CT, and we could differentiate thickened pleura from the collapsed lung.

2.4. Statistical analysis

Statistical analysis was carried out using the SPSS 20 software. Descriptive statistical tests were used for analysis of data. Unpaired *t*-tests and Mann-Whitney tests were used to compare differences. P values less than 0.05 were considered to be statistically significant.

3. Results

Thirty-six patients (all males), with a mean age of 72.0 years, were included in the BAPE group, and sixty-six patients, with a mean age 67.8 years, were included in the eMPM group. In the BAPE group, histopathological results indicated chronic inflammation in the majority of cases; the average history of exposure to asbestos was 28.1 years and the mean latency (the gap between exposure to asbestos and diagnosis) was 46.3 years. In the eMPM group, complete data and informed consent were obtained from

Table 3

Grade of pleural irregularity in BAPE and eMPM groups.

	BAPE (n = 36)	eMPM (n = 66)	P value
No irregularity	8 (22%)	6 (9%)	<0.001 [#]
Low-level irregularity	26 (72%)	36 (54%)	
High-level irregularity	2 (5%)	15 (23%)	<0.001 [*]
Mass formation	0 (0%)	9 (14%)	

“Low-level irregularity” indicated a regular surface with a thickening >3 mm but ≤1 cm, and “High-level-irregularity” indicated a regular thickening >1 cm, or an irregular thickening >5 mm, and clear nodularity >3 mm but not “mass formation”. [#]No- and low-level pleural irregularity together (BAPE vs. eMPM: 94.4% vs. 63.6%; P < 0.001).

^{*}High-level pleural irregularity and mass formation together (BAPE vs. eMPM: 5.5% vs. 36.4%; P < 0.001 (χ^2 test)).

Table 4

Localization of pleural irregularity in BAPE and eMPM groups.

	BAPE (n = 36)	eMPM (n = 66)	P value
Mediastinal	8 (22%)	49 (74%)	<0.001
Basal	32 (91%)	51 (77%)	0.150
Interlobar fissure	0 (0%)	36 (55%)	<0.001

1111 patients, and thoracoscopic biopsy, pleural biopsy, and pleural fluid cytology confirmed the diagnosis of stage I and stage II MPM in 66 patients. The mean age at diagnosis was 67.8 years, and the origin of eMPM was epithelioid in 41 cases, sarcomatoid in 8 cases, biphasic in 12 cases, and unknown in 5 cases. Of the eMPM subjects, 60.6% had an occupational exposure to asbestos, with a mean duration of exposure of 16.6 years and a mean latency of 24.0 years (Table 1).

Asbestosis was found in 6 patients in the BAPE group, and the incidence was higher than that observed in the eMPM group. The prevalence of pleural plaque was notably higher in the BAPE group. Rounded atelectasis and diffuse pleural thickening were also significantly more common in the BAPE group, although there was no significant difference in pleural effusion (Table 2).

The grades of pleural irregularity are presented in Table 3. No irregularity was found in 22% of the BAPE group and 9% of the eMPM group. No mass formation was observed in the BAPE group, but it was found in 14% of patients in the eMPM group. Interestingly, no- or low-level pleural irregularity together were more prevalent in the BAPE group and high-level pleural irregularity and mass formation together were more prevalent in the eMPM group.

Table 4 presents the locations of pleural irregularity. Mediastinal and interlobar fissure were found to be statistically different between the two groups. Interlobar pleural fissure was not observed in any of the patients in the BAPE group, although 55% of patients in the eMPM group had interlobar pleural fissure (P < 0.001). Mediastinal pleural involvement was observed in 74% of patients in the eMPM group and just 22% in the BAPE group (P < 0.001); notably, mediastinal involvement had a sensitivity of 79.5%, specificity of 81%, positive predictive value of 89%, and negative predictive value of 68% for eMPM diagnosis. Basal irregularities were higher in the BAPE group (91% vs. 77%), although the difference did not reach statistical significance.

In addition to differences in pleural irregularity, location, and plaques in the BAPE and eMPM groups, a significant difference was observed in the pleural parameters during follow-up. In patients diagnosed with BAPE, pleural irregularities either regressed or remained unchanged, whereas in patients diagnosed with eMPM, pleural irregularities were found to worsen or remain unchanged during follow-up. Fig. 2 presents a representative case of a patient in the BAPE group who had shown high-level unilateral pleural irregularities at diagnosis. During the 5-year follow-up period, the level of pleural irregularities remained high, with little change in features. Fig. 3(A–D) shows changes in the CT scan features during

follow-up of two patients in the BAPE group. One patient showed bilateral mediastinal pleural thickening at diagnosis, which significantly regressed within two months in both axial and coronal CT scans. In another patient (Fig. 3C,D), unilateral mediastinal pleural thickening and effusion in the right thorax was observed at presentation and significantly regressed before the CT scan recorded 3 months later. Fig. 4 shows a CT scan of a patient in the eMPM group at presentation and follow-up; CT findings did not indicate any regression of pleural irregularities. Fig. 5 shows a CT scan of another patient diagnosed with eMPM at presentation and at follow-up; it was evident that pleural irregularities rapidly worsened within a period of few months.

4. Discussion

Our results indicate that CT imaging features can aid early diagnosis of MPM. One distinct feature was the involvement of mediastinal pleura, which was found to be significantly more prevalent in patients with eMPM than in patients with BAPE. Metintas et al. reviewed the CT findings of patients with MPM and benign pleural disease [9]. They concluded that circumferential lung encasement by multiple nodules and pleural thickening with irregular pleuropulmonary margins were more prevalent in patients with MPM. They also reported mediastinal pleural involvement as an independent factor that could be used for differentiation of MPM from benign pleural diseases; in our work, mediastinal pleural involvement was observed in 74% of patients with eMPM and just 22% of patients with BAPE (P < 0.001), highlighting the mediastinal pleural involvement even in early stages of MPM. Leung et al. investigated differential diagnoses of benign and malignant pleural diseases using CT scans and also reported mediastinal pleural involvement [25]. In our work, asbestosis was found more frequently in the BAPE group, which supports the belief that asbestosis is probably not involved in the initial stages of asbestos-induced lung carcinogenesis, though it might increase the risk of lung cancer [1,19,27].

Ökten et al. reported pleural effusion in 83% of patients with MPM [28]; they cautioned that no CT scan findings were pathognomonic for MPM, although such findings may provide clues for differential diagnosis. In another study, plural effusion was observed in almost 80% of the cases, but an independent association was not established [29]. In our work, we found 97% and 100% pleural effusion in the BAPE and eMPM groups, respectively, without any statistical difference. This observation supports the findings of Ökten et al. and indicates that pleural effusion should be used with caution for the diagnosis of MPM, especially in the early stages. Interestingly, we found that pleural plaques were more prevalent in the BAPE group than in the eMPM group (92% vs. 35%, P < 0.001), undermining the diagnostic utility of pleural plaques for the diagnosis of eMPM. This finding is of particular importance since pleural plaques are reported in some studies to have strong association with mesothelioma [27], even after adjustment for time since first exposure to asbestos and cumulative exposure index. Conversely, out of 13 identified studies on the association of pleural plaques with lung cancer, only three have reported such correlations [19,27,30]. In spite of disagreement among different studies on association of pleural plaques with MPM, the markedly higher prevalence of pleural plaques observed in patients with BAPE in this work provides strong evidence for the poor utility of pleural plaques for the diagnosis of early stages of MPM.

Our results suggest that pleural irregularity grade and location have different features in BAPE and eMPM patients. Patients with BAPE showed a high prevalence of low-level pleural irregularity, whereas MPM patients had high-level pleural irregularity and mass formation. We defined irregularities on the basis of pleural

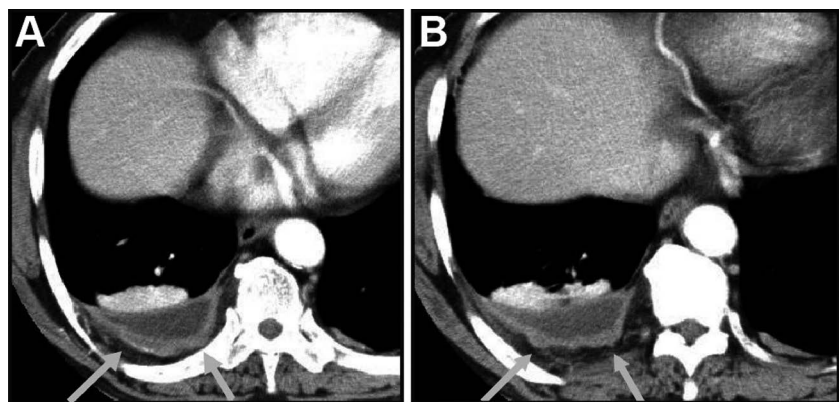


Fig. 2. Changes in the CT scan features of a patient in the BAPE group (male, 70 years) with a 21-year history of asbestos exposure. (A) Axial CT scan at diagnosis, showing high-level irregular pleural thickening (arrows). (B) Axial CT scan after five years of follow-up; a similar level irregular pleural thickening persists.

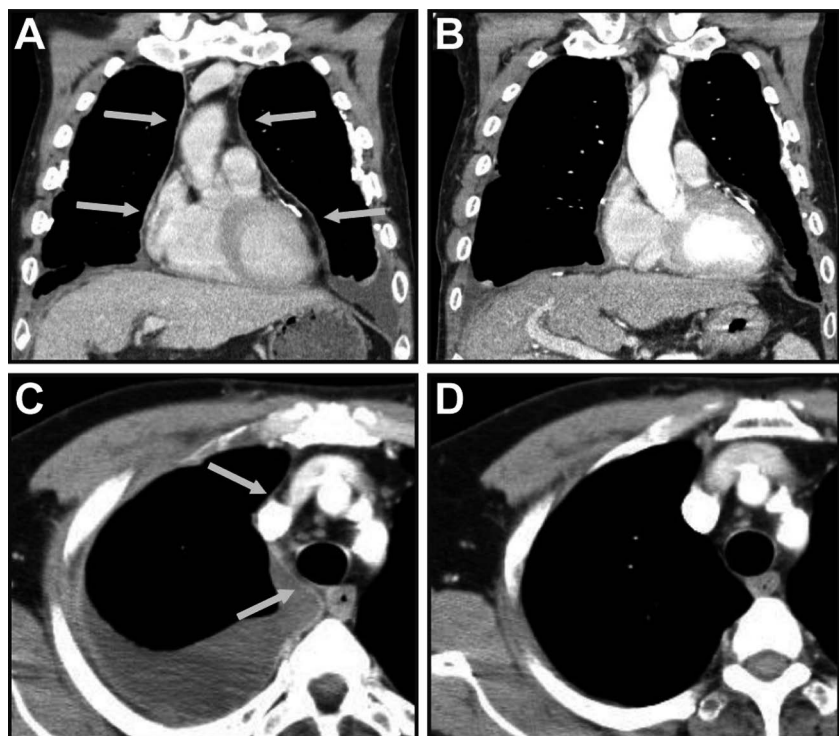


Fig. 3. Changes in the contrast-enhanced CT scan features of a patient in the BAPE group (male, 64 years) with a 39-year history of asbestos exposure. (A) Coronal view of the patient at diagnosis, with visible bilateral mediastinal pleural thickening and left pleural effusion. (B) Coronal view of the same patient after two months, showing regression. (C) Another patient (male, 69 years) with a 42-year history of asbestos exposure. Axial CT scan at diagnosis, showing unilateral mediastinal pleural thickening and effusion in the right thorax (arrows). (D) Axial CT scan after three months of follow-up, showing regression.

thickening. Leung et al. reported that parietal pleural thickening greater than 1 cm was helpful in distinguishing benign cases from malignant ones, although they also used criteria such as circumferential and nodular pleural thickening [28]. MPM is generally locally aggressive, with frequent invasion of the chest wall, mediastinum, and diaphragm, which might complicate CT scan. In the analysis of follow-up CT scans, it was evident that in cases of BAPE, pleural effusion either regressed or remained constant, whereas in cases of eMPM, pleural effusion either advanced or remained constant. Mavi et al. used dual time point 18F-fluorodeoxyglucose positron emission tomography to differentiate between benign and malignant plural diseases [31]. They showed that, in MPM, 18F-FDG uptake increased with time. Conversely, in benign pleural disease, the uptake of 18F-FDG decreased with time. Our results indicated that changes in pleural irregularities during follow-up might be useful for eMPM and BAPE diagnosis, although a more extensive

study is needed to clearly establish the suitability of follow-up CT scans for differential diagnosis.

Our study had certain limitations. First, as the eMPM group used retrospective data collection from multiple centres, there was an inhomogeneity in the CT scan parameters and protocols used. However, the multicentre nature of the eMPM group helped us avoid any regional biases. Furthermore, adding to the strength of this work, obtaining a prospective group with this much sample size is practically difficult considering the rarity of the disease, and all CT scan image analyses were done by a team of independent reviewers who were blinded to the histopathologic results. The other limitation was that the BAPE group was another unique group and was single centre based. There is therefore a possibility that the patients were representative only of a particular region in Japan. Another limitation is that there could be an effect of contrast media in CT scan images; however, being a retrospective and registry-based

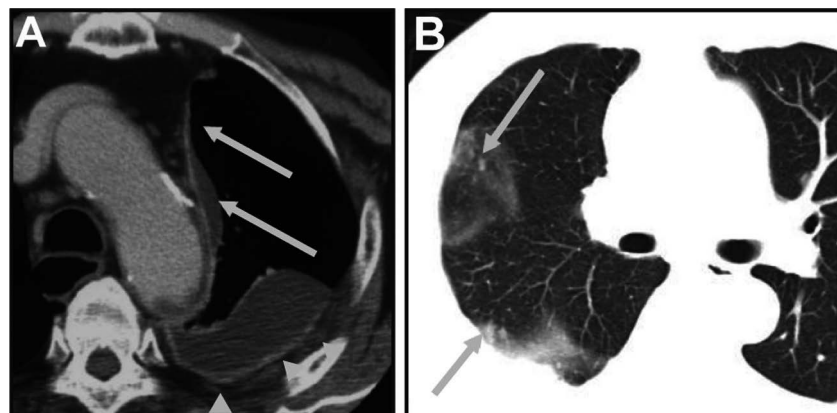


Fig. 4. A representative axial CT scan showing mediastinal pleural thickening and interlobar fissural pleural thickening of patients in eMPM group. (A) Male, 75 years old, with a 33-year history of asbestos exposure, showing unilateral mediastinal pleural thickening. (B) Posterior pleural thickening in the same patient. Mediastinal pleural thickening (arrows) and basal pleural thickening (arrow heads).

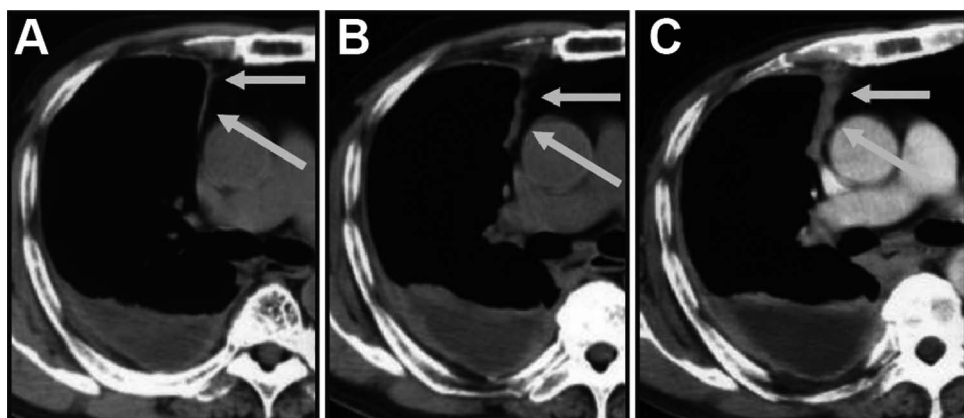


Fig. 5. A representative axial CT scan depicting changes during follow-up in a male, 78 years old, with a 35-year history of asbestos exposure. (A) Unilateral mediastinal and posterior pleural thickening and pleural effusion. (B) Progressed irregular pleural thickening after two months. (C) Progressed irregular pleural thickening after 8 months.

study, we could not investigate the effect of contrast media on pleural irregularities in all cases. Nevertheless, in 8 cases (3 BAPE and 5 eMPM) we could obtain CT scans both with and without contrast media. Our analysis indicated no difference between CT scans with or without contrast media. Despite this, a dedicated independent study with a large sample size is needed to further strengthen the effect of contrast media. Additionally, in this study, to avoid ambiguity, decisions on CT findings were made by relying on the agreement within a team of one radiologist and two pulmonologists. Inter-rater reliability and independent association between parameters should to be taken in future studies.

However, in spite of these limitations, this work clearly underscores the significance of level and localization of pleural irregularities, which could provide important clues for the diagnosis of early stages of MPM. More large-scale, multicentre studies with long-term follow-up are needed to establish a diagnostic standard for eMPM and to fully elucidate pleural irregularities in the early stages of MPM. This study serves as a basis for such studies.

5. Conclusion

This study indicated that the level and location of pleural irregularities could be of potential help in the differential diagnosis between BAPE and eMPM. There was no significant difference between the two groups in term of prevalence of pleural effusion. However, mediastinal pleural involvement was found more frequently in patients with early MPM. Large-scale multicentre

prospective studies with long-term follow-up are needed to fully establish a standard protocol.

Conflict of interest

The authors declare that they have no conflicts of interest to disclose.

Funding

This research was funded primarily by grants from the research foundation of the Ministry of Health, Labour, and Welfare of Japan (200500129A, 200635021A, 200733015A, 200733015B, 200836010A, 200938007A, and 201032004B) and by Industrial disease clinical research grants from the Ministry of Health, Labour, and Welfare of Japan (150401).

Role of funding

The funding source had no role in study design and concept, data acquisition, data analysis and interpretation, and manuscript preparation and submission.

Author contribution

Katsuya Kato: image reading/interpretation (BAPE, eMPM), analysis of imaging results.

Kenichi Gemba; image reading/interpretation (eMPM), statistical analysis, clinical analysis.

Nobukazu Fujimoto: image reading/interpretation (BAPE), gathering cases, clinical analysis.

Keisuke Aoe: gathering and management of cases, clinical analysis.

Yukio Takeshima: pathological investigation.

Kouki Inai: pathological investigation.

Takumi Kishimoto: image reading/interpretation (BAPE, eMPM), gathering and management of cases, research supervision.

All authors have approved the final article.

Appendix A. Supplementary data

Supplementary data associated with this article can be found, in the online version, at <http://dx.doi.org/10.1016/j.ejrad.2016.06.013>.

References

- [1] S. Prazakova, P.S. Thomas, A. Sandrini, D.H. Yates, Asbestos and the lung in the 21st century: an update, *Clin. Resp. J.* 8 (2014) 1–10.
- [2] L.T. Nickell, J.P. Lichtenberger, L. Khorashadi, G.F. Abbott, B.W. Carter, Multimodality imaging for characterization, classification, and staging of malignant pleural mesothelioma, *Radiographics* 34 (2014) 1692–1706.
- [3] M.B. Gotway, Pleural abnormalities and volume loss: imaging considerations, *Clin. Pulm. Med.* 16 (2009) 346–349.
- [4] S.G. Armato III, A.K. Nowak, R.J. Francis, M. Kocherginsky, M.J. Byrne, Observer variability in mesothelioma tumor thickness measurements: defining minimally measurable lesions, *J. Thorac. Oncol.* 9 (2014) 1187–1194.
- [5] K.H. Lee, et al., Mesenchymal tumours of the thorax: CT findings and pathological features, *Clin. Radiol.* 58 (2003) 934–944.
- [6] R. Maeda, N. Isowa, H. Onuma, et al., Minute localized malignant pleural mesothelioma coexisting with multiple adenocarcinomas, *Gen. Thorac. Cardiovasc. Surg.* 58 (2010) 91–94.
- [7] M. Metintas, I. Ucgun, O. Elbek, et al., Computed tomography features in malignant pleural mesothelioma and other commonly seen pleural diseases, *Eur. J. Radiol.* 41 (2002) 1–9.
- [8] C.S. Ng, R.F. Munden, H.I. Libshitz, Malignant pleural mesothelioma: the spectrum of manifestations on CT in 70 cases, *Clin. Radiol.* 54 (1999) 415–421.
- [9] A.M. Khan, K. Tlemcani, N. Shanmugam, A localized pleural based mass with intense uptake on positron emission tomography scan, *Chest* 131 (2007) 294–299.
- [10] J.M. Seely, E.T. Nguyen, A.M. Churg, et al., Malignant pleural mesothelioma: computed tomography and correlation with histology, *Eur. J. Radiol.* 70 (2009) 485–491.
- [11] T. Terada, C. Tabata, R. Tabata, et al., Clinical utility of 18-fluorodeoxyglucose positron emission tomography/computed tomography in malignant pleural mesothelioma, *Exp. Ther. Med.* 4 (2012) 197–200.
- [12] N.A. Maskell, F.V. Gleeson, R.J.O. Davies, Standard pleural biopsy versus CT-guided cutting-needle biopsy for diagnosis of malignant disease in pleural effusions: a randomised controlled trial, *Lancet* 361 (2003) 1326–1330.
- [13] A. Iyoda, T. Yusa, C. Kadoyama, et al., Diffuse malignant pleural mesothelioma: a multi-institutional clinicopathological study, *Surg. Today* 38 (2008) 993–998.
- [14] N. Fujimoto, K. Aoe, K. Gemba, et al., Clinical investigation of malignant mesothelioma in Japan, *J. Cancer Res. Clin. Oncol.* 136 (2010) 1755–1759.
- [15] K. Gemba, N. Fujimoto, K. Aoe, et al., Treatment and survival analyses of malignant mesothelioma in Japan, *Acta Oncol.* 52 (2013) 803–808.
- [16] T. Kishimoto, K. Morinaga, S. Kira, The prevalence of pleural plaques and/or pulmonary changes among construction workers in Okayama, Japan, *Am. J. Ind. Med.* 37 (2000) 291–295.
- [17] C. Bianchi, A. Brollo, L. Ramani, T. Bianchi, L. Giarelli, Asbestos exposure in malignant mesothelioma of the pleura: a survey of 557 cases, *Ind. Health* 39 (2001) 161–167.
- [18] K. Chaisaowong, T. Aach, P. Jäger, et al., Computer-assisted diagnosis for early stage pleural mesothelioma: towards automated detection and quantitative assessment of pleural thickenings from thoracic CT images, *Methods Inf. Med.* 46 (2007) 324–331.
- [19] J. Ameille, P. Brochard, M. Letourneau, C. Paris, J.C. Pairon, Asbestos-related cancer risk in patients with asbestosis or pleural plaques, *Rev. Mal. Respir.* 28 (2011) e11–e17.
- [20] G.R. Epler, T.C. McLoud, E.A. Gaensler, Prevalence and incidence of benign asbestos pleural effusion in a working population, *JAMA* 247 (1982) 617–622.
- [21] T.L. Guidotti, C.A. Brodkin, D. Christiani, et al., Diagnosis and initial management of nonmalignant diseases related to asbestos, *Am. J. Resp. Crit. Care Med.* 170 (2004) 691–715.
- [22] D.W. Henderson, et al., Asbestos, asbestosis, and cancer: the Helsinki criteria for diagnosis and attribution, *Scand. J. Work Environ. Health* 23 (1997) 311–316.
- [23] T. Kishimoto, K. Gemba, N. Fujimoto, et al., Clinical study on mesothelioma in Japan: relevance to occupational asbestos exposure, *Am. J. Ind. Med.* 53 (2010) 1081–1087.
- [24] V.W. Rusch, A proposed new international TNM staging system for malignant pleural mesothelioma: from the international mesothelioma interest group, *Lung Cancer* 14 (1996) 1–12.
- [25] A.N. Leung, N.L. Muller, R.R. Miller, CT in differential diagnosis of diffuse pleural disease, *Am. J. Roentgenol.* 154 (1990) 487–492.
- [26] A. Orki, O. Akin, A.E. Tasci, et al., The role of positron emission tomography/computed tomography in the diagnosis of pleural diseases, *Thorac. Cardiovasc. Surg.* 57 (2009) 217–221.
- [27] J.C. Pairon, F. Laurent, M. Rinaldo, et al., Pleural plaques and the risk of pleural mesothelioma, *J. Natl. Cancer Inst.* 105 (2013) 293–301.
- [28] F. Ökten, D. Köksal, M. Onal, et al., Computed tomography findings in 66 patients with malignant pleural mesothelioma due to environmental exposure to asbestos, *Clin. Imaging* 30 (2006) 177–180.
- [29] O. Tamer Dogan, I. Salk, F. Tas, et al., Thoracic computed tomography findings in malignant mesothelioma, *Iran. J. Radiol.* 9 (2012) 209–211.
- [30] U. Elboga, M. Yilmaz, M. Uyar, et al., The role of FDG PET-CT in differential diagnosis of pleural pathologies, *Rev. Esp. Med. Nucl. Imagen Mol.* 31 (2012) 187–191.
- [31] A. Mavi, S. Basu, T.F. Cermik, et al., Potential of dual time point FDG-PET imaging in differentiating malignant from benign pleural disease, *Mol. Imaging Biol.* 11 (2009) 369–378.

Utility and pitfalls of immunohistochemistry in the differential diagnosis between epithelioid mesothelioma and poorly differentiated lung squamous cell carcinoma

Kei Kushitani,¹ Vishwa J Amatya,¹ Yasuko Okada,² Yuya Katayama,² Amany S Mawas,^{1,3} Yoshihiro Miyata,⁴ Morihito Okada,⁴ Kouki Inai,^{1,5} Takumi Kishimoto⁶ & Yukio Takeshima¹

¹Department of Pathology, Institute of Biomedical and Health Sciences, Hiroshima University, Hiroshima, Japan,

²Faculty of Medicine, Hiroshima University, Hiroshima, Japan, ³Department of Pathology and Clinical Pathology,

Faculty of Veterinary Medicine, South Valley University, Qena, Egypt, ⁴Department of Surgical Oncology, Research Centre for Radiation Casualty Medicine, Research Institute for Radiation Biology and Medicine, Hiroshima University, Hiroshima, Japan, ⁵Pathologic Diagnostic Centre, Inc., Hiroshima, Japan, and ⁶Department of Internal Medicine, Okayama Rosai Hospital, Okayama, Japan

Date of submission 30 June 2016

Accepted for publication 30 August 2016

Published online Article Accepted 2 September 2016

Kushitani K, Amatya V J, Okada Y, Katayama Y, Mawas A S, Miyata Y, Okada M, Inai K, Kishimoto T & Takeshima Y

(2016) *Histopathology*. DOI: 10.1111/his.13073

Utility and pitfalls of immunohistochemistry in the differential diagnosis between epithelioid mesothelioma and poorly differentiated lung squamous cell carcinoma

Aims: The aims of this study were to clarify the usefulness of immunohistochemistry in the differential diagnosis of epithelioid mesothelioma with a solid growth pattern [solid epithelioid mesothelioma (SEM)] and poorly differentiated squamous cell carcinoma (PDSCC), and to confirm the validity of a specific type of antibody panel. Additionally, we aimed to clarify the pitfalls of immunohistochemical analyses.

Methods and results: Formalin-fixed paraffin-embedded specimens from 36 cases of SEM and 38 cases of PDSCC were immunohistochemically examined for calretinin, podoplanin (D2-40), Wilms' tumour gene product (WT1), cytokeratin (CK) 5/6, p40, p63, carcinoembryonic antigen (CEA), epithelial-related antigen (MOC31), claudin-4, thyroid transcription factor-1 (TTF-1), and napsin A. WT1 showed the highest diagnostic accuracy (85.1%) as a mesothelial marker, and CEA, p40 and claudin-4

showed higher diagnostic accuracies (95.9%, 94.6%, and 93.2%, respectively) as carcinoma markers. Calretinin (diagnostic accuracy: 75.7%), D2-40 (diagnostic accuracy: 67.6%), CK5/6 (diagnostic accuracy: 63.5%), TTF-1 (diagnostic accuracy: 55.4%) and napsin A (diagnostic accuracy: 52.7%) could not differentiate between SEM and PDSCC. Among these markers, the combination of calretinin and WT1 showed the highest diagnostic accuracy (86.5%) as a positive marker, and the combination of p40 and CEA showed the highest diagnostic accuracy (97.3%) as a negative marker. The combination of CEA and claudin-4 also showed relatively high diagnostic accuracy (94.6%) as a negative marker.

Conclusions: We recommend the combination of WT1 and calretinin as a positive marker, and the combination of CEA and claudin-4 as a negative marker, for differential diagnoses of SEM and PDSCC.

Keywords: calretinin, carcinoembryonic antigen, claudin-4, immunohistochemistry, mesothelioma, p40, squamous cell carcinoma, WT1 protein

Introduction

Address for correspondence: Yukio Takeshima, MD, PhD, 1-2-3 Kasumi, Minami-ku, Hiroshima 734-8551, Japan. e-mail: ykotake@hiroshima-u.ac.jp

Malignant mesothelioma (MM) is a rare, aggressive malignant neoplasm that most commonly arises from

pleural mesothelial cells. MM is correlated with occupational and environmental asbestos exposure.^{1–5} As the incidence of MM has increased in many countries, pathologists encounter this disease frequently. In Japan, the death toll from MM has been increasing since the 1990s, and it is predicted to peak in the 2030s.⁶

A diffuse pleurotropic growth pattern is characteristic of MM.^{7,8} However, a number of non-mesotheliomatous neoplasms showing diffuse pleurotropic growth patterns (described as 'pseudomesotheliomatous growth') have been reported, and most of these tumours are peripheral lung carcinomas.^{9–13} Although the majority of pseudomesotheliomatous lung carcinomas are adenocarcinomas (ACs), a few pseudomesotheliomatous pulmonary squamous cell carcinoma (SCC) cases have also been reported.¹⁴ Lately, the incidence of peripheral-type pulmonary SCC, but not central SCC, has been increasing.^{15,16} Thus, the chance of encountering 'pseudomesotheliomatous' SCCs might increase. Additionally, MM may occur as a localized mass similar to peripheral lung cancer and other pleural tumours; it is then classified as 'localized MM' according to the new World Health Organization (WHO) classification.⁷ Therefore, the histopathological differential diagnosis of MM and SCC will become crucial in the future.

Malignant mesotheliomas are divided into three major histological subtypes: epithelioid, sarcomatoid, and biphasic. Among these, epithelioid mesothelioma (EM) shows a wide range of histological and cytological patterns, such as papillary, tubular, solid, clear cell, deciduoid, rhabdoid, and pleomorphic.¹⁷ Poorly differentiated SCC (PDSCC) shows a nested, sheet-like or cord-like histological pattern, and lacks obvious keratinization and/or intercellular bridges in some parts of or throughout the tumour.¹⁸ Therefore, the differential diagnosis between EM showing a solid histological pattern [solid EM (SEM)] and PDSCC can be challenging with conventional light

microscopy (haematoxylin and eosin-stained specimen) alone.

The role of immunohistochemistry in distinguishing pleural EM from pulmonary AC has received much attention. Currently, many immunohistochemical markers are available for distinguishing pleural EM from pulmonary AC. Among these, calretinin, cytokeratin (CK) 5/6, podoplanin (D2-40) and Wilms' tumour gene product (WT1) are regarded as the best positive markers for EM, and carcinoembryonic antigen (CEA), MOC31 [epithelial-related antigen (ERA)], Ber-EP4, BG-8, thyroid transcription factor-1 (TTF)-1, and napsin A are regarded as the best positive markers for lung AC.^{19–22}

However, there are only a few reports on the immunohistochemical differential diagnosis of EM and lung SCC. Ordonez *et al.* have reported the immunohistochemical analyses of 30 EMs showing a solid pattern and 30 pulmonary non-keratinizing SCCs, and have recommended the combination of two positive (WT1 and calretinin/mesothelin) and two negative (p63 and ERA) markers for differentiating EM from lung SCC.²³

Here, we examined 11 commercially available immunohistochemical markers in histological specimens of SEM and PDSCC obtained from Japanese cases. We aimed to evaluate the usefulness of immunohistochemistry in differentiating SEM from PDSCC, and to recommend the best antibody panel for use in pathological laboratories, after considering the pitfalls of immunohistochemical analyses.

Materials and methods

PATIENTS AND HISTOLOGICAL SAMPLES

We used formalin-fixed paraffin-embedded (FFPE) specimens from 36 patients with a definite histological diagnosis of SEM who had undergone pleural biopsy, pleurectomy/decortication, extrapleural pneumonectomy or autopsy between 2000 and 2014.

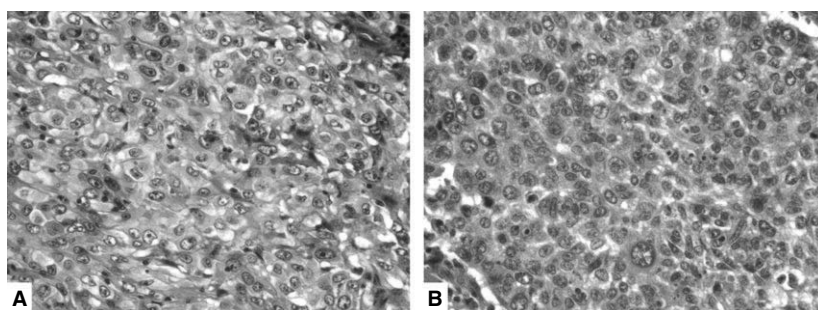


Figure 1. Representative histological images of solid epithelioid mesothelioma and poorly differentiated squamous cell carcinoma. (A) Solid epithelioid mesothelioma. (B) Poorly differentiated squamous cell carcinoma.

SEM was defined as 'EM consisting of mainly solid, sheet-like or cord-like proliferations of cuboidal or polygonal epithelioid cells' (Figure 1A). All SEM cases used in this study were comprehensively diagnosed according to a combination of clinical history (e.g. occupational asbestos exposure), radiographic examination (e.g. diffuse pleurotropic growth pattern, lack of intrapulmonary mass, or the presence of pleural plaques), and histopathological findings. In all cases, we performed immunohistochemical investigation with 15–20 markers, including the 11 markers examined in this study.

Formalin-fixed paraffin-embedded histological samples of the surgical specimens from 38 patients with a histological diagnosis of primary pulmonary PDSCC were obtained by surgical resection (wedge resection, segmentectomy, lobectomy, or pneumonectomy) from 2000 to 2014. PDSCC included keratinizing SCC with minimal squamous differentiation (keratinization and/or intercellular bridge) and non-keratinizing SCC, as defined in the WHO 2015 criteria (Figure 1B).²⁴ The samples were collected from the archives of the Department of Pathology at Hiroshima University. Among 38 PDSCCs that we examined, 34 were of the peripheral type, and four were of the central type. Ten cases showed invasion to the visceral pleura but not right through and exposed on the surface of the pleura, seven cases showed focal invasion to the parietal pleura or chest wall, and 21 cases were intrapulmonary lesions without pleural invasion. There was no case showing diffuse pleurotropic growth.

Each tumour specimen was reviewed by three pathologists (K.K., V.J.A., and Y.T.); all of the cases were rediagnosed on the basis of the currently accepted histological criteria.^{17,18}

This study was performed in accordance with the Ethics Guidelines for Human Genome/Gene Research enacted by the Japanese government for the collection of tissue specimens, and was approved by the institutional ethics review committee (Hiroshima University E-48).

IMMUNOHISTOCHEMICAL PROCEDURES

Immunohistochemical staining of sections from the FFPE tissue samples was performed with Ventana BenchMark GX (Roche Diagnostics, Basel, Switzerland), by use of the Ventana ultraView Universal DAB Detection Kit; the staining procedure is based on the indirect biotin-free system. Protocols involving heat induction-based or protease digestion-based antigen retrieval were performed as recommended by the

Table 1. Primary antibodies used in this study

Marker	Clone	Manufacturer	Dilution	Location of evaluation
Calretinin	SP65	Ventana	Prediluted	Nucleus
Podoplanin	D2-40	Nichirei Bioscience	Prediluted	Membrane
WT1	6F-H2	Ventana	Prediluted	Nucleus
CK5/6	D5/16 B4	Dako	1:25	Membrane and/or cytoplasm
p40	BC28	Biocare Medical	1:100	Nucleus
p63	DAK-p63	Dako	1:25	Nucleus
CEA	COL-1	Nichirei Bioscience	Prediluted	Membrane and/or cytoplasm
ERA	MOC31	Dako	1:25	Membrane
Claudin-4	3E2C1	Life Technologies	1:100	Membrane
TTF-1	SPT24	Nichirei Bioscience	Prediluted	Nucleus
Napsin A	MRQ-60	Ventana	Prediluted	Cytoplasm

CEA, carcinoembryonic antigen; CK, cytokeratin; ERA, epithelial-related antigen; TTF-1, thyroid transcription factor-1; WT1, Wilms' tumour gene product.

manufacturer, with some modifications. Table 1 shows the list of primary antibodies, clones, sources, and antibody dilutions.

Immunoreactivity was scored as either negative (no immunostaining) or positive. Cells showing nuclear staining for calretinin, WT1, p40, p63, and TTF-1, membranous staining for podoplanin, ERA, and claudin-4, cytoplasmic staining for napsin A or membranous and/or cytoplasmic staining for CK5/6 and CEA were regarded as 'positive'. The immunoreactivity grade was semiquantified as follows: 0, 0% positive cells or trace staining; 1+, 1–10% positive cells; 2+, 11–50% positive cells; and 3+, >51% positive cells.

EVALUATION OF UTILITY OF EACH MARKER AND COMBINATIONS OF TWO MARKERS

Sensitivity, specificity, positive predictive values (PPVs), negative predictive values (NPVs) and diagnostic accuracies were calculated for each marker and combination of two markers.

Results

IMMUNOREACTIVITY OF ANTIBODIES FOR SEM AND PDSCC

The detection rates of each antibody in SEM and PDSCC are shown in Table 2. Representative immunohistochemical staining images for SEM and PDSCC are shown in Figures 2 and 3, respectively. The staining pattern for each antibody for the two tumour types is described in the following paragraphs.

CALRETININ

Thirty-three of 36 SEMs (91.7%) and 15 of 38 PDSCCs (39.5%) were positive for calretinin. In SEMs, immunoreactivity was generally strong and diffuse (grade 3+). In contrast, in PDSCCs, the staining grade was distributed from 1+ to 3+ approximately equally.

D 2 - 4 0

Thirty-five of 36 SEMs (97.2%) and 23 of 28 PDSCCs (60.5%) were positive for D2-40. In the majority of SEMs, immunoreactivity was strong and diffuse

(grade 3+), whereas the majority of PDSCCs showed a focal or multifocal positive pattern (grade 1+/2+).

W T 1

Twenty-six of 36 SEMs (72.2%) were positive for WT1, with most of them showing grade 3+, whereas only one PDSCC (2.6%) was focally positive (grade 1+) for WT1.

C K 5 / 6

Twenty-six of 36 (72.2%) of SEMs and 37 of 38 (97.4%) of PDSCCs were positive for CK5/6. For both tumours, the majority of cases showed diffuse and strong immunoreactivity (grade 3+).

P 4 0

Only two SEMs (5.6%) were positive for p40, and staining was observed in an extremely confined area (grade 1+). In contrast, 36 of 38 PDSCCs (94.7%) were positive for p40, and most cases showed diffuse and strong immunoreactivity (grade 3+).

Table 2. Immunohistochemical findings for solid epithelioid mesothelioma (SEM) and poorly differentiated squamous cell carcinoma (PDSCC) for various antibodies

Marker	SEM, n (%)	SEM staining grade				PDSCC, n (%)	PDSCC staining grade			
		0	1+	2+	3+		0	1+	2+	3+
Calretinin	33/36 (91.7)	3	0	2	31	15/38 (39.5)	23	7	4	4
D2-40	35/36 (97.2)	1	3	2	30	23/38 (60.5)	15	5	12	6
WT1	26/36 (72.2)	10	5	3	18	1/38 (2.6)	37	1	0	0
CK5/6	26/36 (72.2)	10	5	6	15	37/38 (97.4)	1	2	6	29
p40	2/36 (5.6)	34	2	0	0	36/38 (94.7)	2	0	4	32
p63	6/36 (16.7)	30	5	0	1	37/38 (97.4)	1	1	2	34
CEA	0/36 (0)	36	0	0	0	35/38 (92.1)	3	14	13	8
ERA	12/36 (33.3)	24	8	3	1	34/38 (89.5)	4	5	11	18
Claudin-4	2/36 (5.6)	34	2	0	0	35/38 (92.1)	3	3	17	15
TTF-1	0/36 (0)	36	0	0	0	5/38 (13.2)	33	5	0	0
Napsin A	0/36 (0)	36	0	0	0	3/38 (7.9)	35	3	0	0

CEA, carcinoembryonic antigen; CK, cytokeratin; ERA, epithelial-related antigen; TTF-1, thyroid transcription factor-1; WT1, Wilms' tumour gene product.

The grade of immunoreactivity was semiquantified as follows: 0, 0% positive cells or trace staining; 1+, 1–10% positive cells; 2+, 11–50% positive cells; 3+, >51% positive cells.

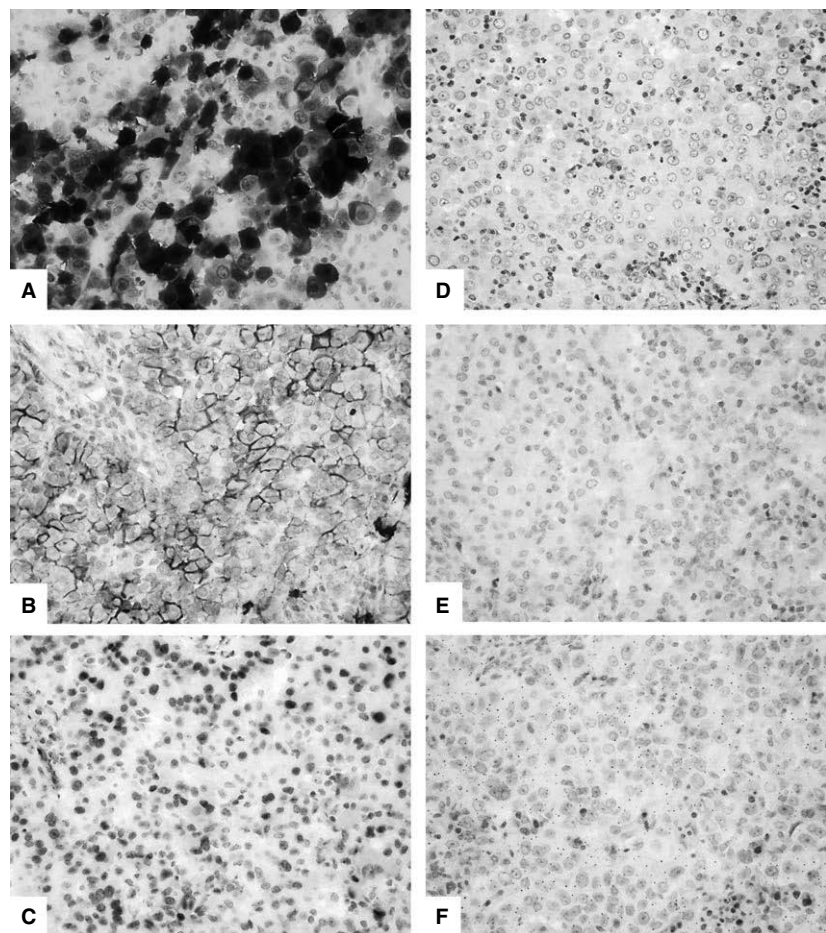


Figure 2. Representative immunohistochemical staining panel for solid epithelioid mesothelioma. The mesothelioma cells showed positivity for calretinin (nuclear) (A), D2-40 (membranous) (B), and Wilms' tumour gene product (nuclear) (C), but were negative for carcinoembryonic antigen (D), p40 (E), and claudin-4 (F).

P 6 3

Six of 36 SEMs (16.7%) were positive for p63, and most of them showed staining in an extremely confined area (grade 1+). However, one SEM showed diffuse and strong immunoreactivity (grade 3+). In contrast, 37 of 38 PDSCCs (97.4%) were positive for p63, and most of them showed diffuse and strong immunoreactivity (grade 3+).

CEA

None of the SEMs were positive CEA. In contrast, 92.1% of PDSCCs were positive for CEA. However, in the majority of the CEA-positive PDSCCs, staining was limited to $\leq 50\%$ of the tumour cells (grades 1+ and 2+).

ERA

Approximately 33.3% of SEMs and 89.5% of PDSCCs were positive for ERA. In the majority of the ERA-

positive SEMs, staining was limited to $\leq 50\%$ of the tumour cells (grades 1+ and 2+). In contrast, approximately half of the ERA-positive PDSCCs showed diffuse and strong immunoreactivity (grade 3+).

CLAUDIN-4

Only two SEMs (5.6%) were positive for claudin-4, and staining was observed in an extremely confined area (grade 1+). In contrast, 35 of 38 PDSCCs (92.1%) were positive for claudin-4, and, in most of them, staining was observed in $\geq 10\%$ of the tumour cells (grade 2+ or 3+).

TTF-1 AND NAPSIN A

None of the SEMs were positive for TTF-1 or napsin A; five PDSCCs that were positive for TTF-1 and three PDSCCs that were positive for napsin A showed focal immunoreactivity (grade 1+).

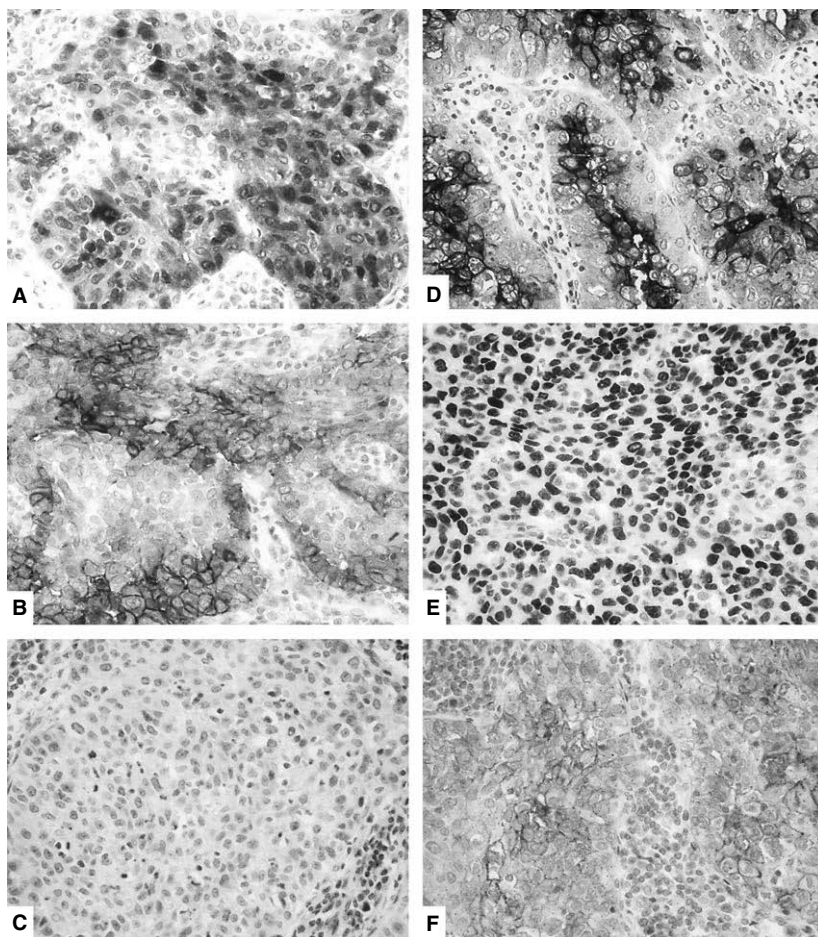


Figure 3. Representative immunohistochemical staining panel for poorly differentiated squamous cell carcinoma. The carcinoma cells were positive for calretinin (nuclear) (A), D2-40 (membranous) (B), carcinoembryonic antigen (cytoplasmic) (D), p40 (nuclear) (E), and claudin-4 (membranous) (F), but negative for Wilms' tumour gene product (C).

SENSITIVITY, SPECIFICITY, PPVs, NPVs AND DIAGNOSTIC ACCURACIES OF EACH ANTIBODY FOR DIFFERENTIAL DIAGNOSIS BETWEEN SEM AND PDSCC

The sensitivity, specificity, PPVs, NPVs and diagnostic accuracies of each marker and combination of two markers for the differential diagnosis between SEM and PDSCC are shown in Tables 3–5.

For SEM, WT1 as a positive marker and p40, p63, CEA and claudin-4 as negative markers showed relatively high diagnostic accuracy (>80%). Among the 11 antibodies evaluated, that for CEA showed the highest sensitivity, NPV and diagnostic accuracy (Table 3).

Among the combinations of two markers, the combination of calretinin and WT1 (both calretinin positivity and WT1 positivity) showed the highest specificity, PPV and diagnostic accuracy as a positive marker (Table 4), and the combination of p40 and CEA (both p40 negativity and CEA negativity)

showed the highest specificity, PPV and diagnostic accuracy as a negative marker (Table 5).

Discussion

Here, we used various commercially available markers to differentiate SEM with a solid growth pattern from PDSCC showing minimal or no keratinization, and attempted to identify the best antibody panel for differentiating SEM and PDSCC, with their pitfalls in interpretation. We found that WT1 had the highest diagnostic accuracy as a positive marker, and that CEA, p40, p63 and claudin-4 showed high diagnostic accuracies as negative markers (>90%).

Wilms' tumour gene product encodes a zinc-finger transcription factor that controls the expression of many growth factors and their receptors.²⁵ Nuclear immunoreactivity for WT1 has been reported in 43–100% of EMs,^{20–22,26} whereas it is negligibly expressed in pulmonary ACs and SCCs.^{20,21,23,27} In

Table 3. Sensitivity, specificity, positive predictive values (PPVs), negative predictive values (NPVs) and diagnostic accuracies of each antibody for the differential diagnosis between solid epithelioid mesothelioma and non-keratinizing squamous cell carcinoma

Immunohistochemical findings	Sensitivity (%)	Specificity (%)	PPV (%)	NPV (%)	Diagnostic accuracy (%)
Calretinin-positive	91.7	60.5	68.8	88.5	75.7
D2-40-positive	97.2	39.5	60.3	93.8	67.6
WT1-positive	72.2	97.4	96.3	78.7	85.1
CK5/6-positive	72.2	2.6	41.3	9.1	36.5
p40-negative	94.4	94.7	94.4	94.7	94.6
p63-negative	83.3	97.4	96.8	86.0	90.5
CEA-negative	100	92.1	92.3	100	95.9
ERA-negative	66.7	89.5	85.7	73.9	78.4
Claudin-4-negative	94.4	92.1	91.9	94.6	93.2
TTF-1-negative	100	13.2	52.2	100	55.4
Napsin A-negative	100	7.9	50.7	100	52.7

CEA, carcinoembryonic antigen; CK, cytokeratin; WT1, TTF-1, thyroid transcription factor-1; Wilms' tumour gene product.

Table 4. Sensitivity, specificity, positive predictive values (PPVs), negative predictive values (NPVs) and diagnostic accuracies of combinations of two positive markers for the differential diagnosis between solid epithelioid mesothelioma and non-keratinizing squamous cell carcinoma

Combination of two markers	Sensitivity (%)	Specificity (%)	PPV	NPV	Diagnostic accuracy
Calretinin-positive and D2-40-positive	88.9	73.7	76.2	87.5	81.1
Calretinin-positive or D2-40-positive	100	26.3	56.3	100	62.2
Calretinin-positive and WT1-positive	72.2	100	100	79.2	86.5
Calretinin-positive or WT1-positive	91.7	57.9	67.3	88	74.3
D2-40-positive and WT1-positive	72.2	97.4	96.3	78.7	85.1
D2-40-positive or WT1-positive	97.2	39.5	60.3	93.8	67.6

WT1, Wilms' tumour gene product.

this study, although the sensitivity of WT1 (72.2%) was the lowest among the positive markers, its high specificity (97.4%) and the fact that it showed the highest diagnostic accuracy (85.1%) among three positive markers (calretinin, D2-40, and WT1) for differentiating SEM from PDSCC led us to consider WT1 as the best positive marker. Previously, Ordonez *et al.* had reported WT1 positivity in 93% (28 of 30 cases) of the EMs studied.²³ In this study, 72.2% of EMs

tested positive for WT1, which is lower than the positivity percentage reported by Ordonez *et al.* Differences in the source of the primary antibody or staining system might explain this discrepancy. The positivity rate for WT1 in SEMs in this study was similar to that observed in our previous studies on EMs with a tubulopapillary pattern,^{20,21} indicating that the WT1 positivity rate is not different between tubulopapillary and solid EMs. Additionally, we

Table 5. Sensitivity, specificity, positive predictive values (PPVs), negative predictive values (NPVs) and diagnostic accuracies of combinations of two negative markers for the differential diagnosis between solid epithelioid mesothelioma and non-keratinizing squamous cell carcinoma

Combination of two markers	Sensitivity (%)	Specificity (%)	PPV (%)	NPV (%)	Diagnostic accuracy (%)
p40-negative and CEA-negative	94.4	100	100	95	97.3
p40-negative or CEA-negative	100	86.8	87.8	100	93.2
p40-negative and claudin-4-negative	91.7	100	100	92.7	95.9
p40-negative or claudin-4-negative	100	86.8	87.8	100	93.2
CEA-negative and claudin-4-negative	94.4	94.7	94.4	94.7	94.6
CEA-negative or claudin-4-negative	100	89.5	90	100	94.6

CEA, carcinoembryonic antigen.

detected positivity in the endothelium of blood vessels in the same sections of SEM, which excludes the possibility of false-negative results.

Calretinin is a 29-kDa, calcium-binding protein involved in calcium signalling, and is strongly expressed in the neurons of the retina and sensory pathways.^{28,29} Immunoreactivity for calretinin has been reported in 55–100% of EM cases.²² In this study, calretinin showed relatively high sensitivity (91.7%) as a positive marker for SEM. However, the specificity (60.5%) and diagnostic accuracy (75.7%) were not sufficiently high, although the distribution of the reactive grade in PDSCC was lower than that in EM. Therefore, the utility of calretinin for differentiation between SEM and PDSCC is limited. However, the combination of calretinin and WT1 antibodies would be helpful for elevating the low sensitivity of WT1 (72.2%) for practical application and detection of mesothelial origin. D2-40 is not useful for differentiating SEM from PDSCC; although D2-40 showed the highest sensitivity (97.2%) as a positive marker for SEM, its specificity (39.5%) and diagnostic accuracy (67.6%) were the lowest among the three positive markers for mesothelioma (calretinin, D2-40, and WT1).

p40 (ΔNp63), a non-transactivating isoform of p63, is a squamous/basal-type biomarker.³⁰ p63 and p40 are expressed in most SCCs, but are rarely expressed in EMs; p40 shows higher sensitivity and specificity than p63.^{30,31} In addition, Bishop *et al.* reported that p63 was expressed in various proportions of ACs and large-cell lymphomas, and p40 showed much higher specificity for SCC.³² In this study, both p40 and p63 showed high sensitivity, specificity, and diagnostic accuracy, but the

sensitivity and diagnostic accuracy of p40 were higher than those of p63, suggesting that p40 is a useful negative marker for distinguishing SEM from PDSCC. However, a small number of EMs showed positivity for p40 and/or p63 (most cases were graded as 1+); this phenomenon must be kept in mind when p40 is used in practical pathological diagnosis.

Claudin-4 is a major component of tight junctions, and is widely expressed in most epithelial and carcinoma cells.^{33–35} Membranous immunoreactivity for claudin-4 has been reported in 88–100% of carcinomas of various origins and in 0–29% of EMs.^{33,34,36,37} Therefore, claudin-4 is considered to be a useful immunohistochemical marker for distinguishing EM from various carcinomas. In this study, claudin-4 showed high sensitivity (94.4%), specificity (92.1%), and diagnostic accuracy (93.2%), implying that claudin-4 is a useful negative marker for distinguishing SEM from PDSCC.

Carcinoembryonic antigen was the first accepted immunohistochemical marker for differentiating EM from lung AC;³⁸ because of its high sensitivity and specificity, it is still considered to be one of the best markers.³⁹ Ordnez reported that CEA is also useful for differentiating EM from lung SCC.²³ In this study, CEA showed the best sensitivity (100%) and diagnostic accuracy (95.9%) among all 11 evaluated markers, suggesting that CEA is the best negative marker for distinguishing SEM from PDSCC.

Ordnez *et al.* and the IMIG2012 update recommend MOC31 (ERA) as a negative marker (positivity rate: EM, 2–10%; SCC, 97–100%).^{17,23} However, on the basis of the results of the present study, we cannot recommend the use of MOC31 as a negative marker

(positivity rate: EM, 33.3; SCC, 89.5). This discrepancy may be attributable to the different clones of antibodies and differences in the antigen detection systems used.

The IMIG2012 guideline recommended consideration of two mesothelial and two carcinoma markers, on the basis of morphology at initial workup,¹⁷ and the new WHO classification recommends calretinin, CK5/6, WT1 and D2-40 as the best mesothelial markers.⁷ However, the choice of markers for differentiating SEM from poorly differentiated non-small cell carcinoma requires attention. Calretinin, D2-40 and CK5/6 are useful mesothelial markers for differentiating EM from AC. However, these markers are not useful for distinguishing SEM from PDSCC, because of their low sensitivity or specificity. Therefore, when two of these three markers are chosen as mesothelial markers, there is some possibility of misdiagnosing PDSCC as SEM. Similarly, although TTF-1 and napsin A are useful carcinoma markers for differentiating EM from pulmonary AC, they are not useful for differentiating EM from SCC. Therefore, the use of TTF-1 and napsin A as carcinoma markers may also lead to misdiagnosis of PDSCC as SEM.

In this study, the combination of calretinin and WT1 showed the highest diagnostic accuracy as a positive marker panel, and the combination of p40 and CEA showed the highest diagnostic accuracy (97.3%) as a negative marker panel. From these results, the combination of calretinin, WT1, p40 and CEA seems to be the best immunohistochemical marker panel for distinguishing SEM from PDSCC. However, when p40 is chosen as one of the carcinoma markers, there is some possibility of misdiagnosing solid AC as SEM, because p40 is rarely expressed in AC.^{30–32} In contrast, claudin-4 is widely expressed in both AC and SCC,^{33–35} and the diagnostic accuracy of the combination of CEA and claudin-4 (94.6%) was comparable to that of p40 and CEA (97.3%). On the basis of these considerations, claudin-4 should be used as a carcinoma marker instead of p40, in the histopathological differential diagnosis of pleural tumours consisting of solid, sheet-like or cord-like proliferations of epithelioid cells, which require differentiation from PDSCC or solid AC.

In conclusion, we conducted immunohistochemical analyses for differentiating SEM from PDSCC, using 11 commercially available antibodies. On the basis of our results, we recommend the use of a combination of WT1 and calretinin as a positive marker, and a combination of CEA and claudin-4 as a negative marker, to overcome the weaknesses of the individual markers to some extent. In the future, there should

be an emphasis on the identification and utilization of new markers, especially mesothelial-specific positive markers.

Conflicts of interest

The authors have no conflicts of interest to declare.

Author contributions

K. Inai, T. Kishimoto and Y. Takeshima designed the research study. K. Kushitani, Y. Miyata, M. Okada and Y. Takeshima contributed to the collection of cases. K. Kushitani, Y. Okada and Y. Katayama performed the research. K. Kushitani wrote the first draft of the manuscript. V. J. Amatya, A. S. Mawas and Y. Takeshima contributed to the final approval of the manuscript.

Acknowledgements

The authors thank the Technical Centre, Hiroshima University, for technical assistance, and thank Editage (www.editage.jp) for English-language editing. This study was funded in part by the Japanese Ministry of Health, Labour and Welfare.

References

1. Gemba K, Fujimoto N, Aoe K *et al*. Treatment and survival analyses of malignant mesothelioma in Japan. *Acta Oncol*. 2013; 52: 803–808.
2. Gemba K, Fujimoto N, Kato K *et al*. National survey of malignant mesothelioma and asbestos exposure in Japan. *Cancer Sci*. 2012; 103: 483–490.
3. Prazakova S, Thomas PS, Sandrini A, Yates DH. Asbestos and the lung in the 21st century: an update. *Clin. Respir. J.* 2014; 8: 1–10.
4. Robinson BW, Musk AW, Lake RA. Malignant mesothelioma. *Lancet* 2005; 366: 397–408.
5. Roggli VL, Sharma A, Butnor KJ, Sporn T, Vollmer RT. Malignant mesothelioma and occupational exposure to asbestos: a clinicopathological correlation of 1445 cases. *Ultrastruct. Pathol.* 2002; 26: 55–65.
6. Murayama T, Takahashi K, Natori Y, Kurumatani N. Estimation of future mortality from pleural malignant mesothelioma in Japan based on an age-cohort model. *Am. J. Ind. Med.* 2006; 49: 1–7.
7. Galateau-Salle F, Churg A, Roggli V *et al*. Tumours of the pleura. In Travis WD, Brambilla E, Burke AP, Marx A, Nicholson AG eds. *World Health Organization classification of tumours of the lung, pleura, thymus and heart*. Lyon: IARC Press, 2015; 153–181.
8. Churg A, Cagle P, Roggli V. *Tumors of the serosal membranes*. Washington, DC: American Registry of Pathology, 2006; 147.

9. Harwood TR, Gracey DR, Yokoo H. Pseudomesotheliomatous carcinoma of the lung. A variant of peripheral lung cancer. *Am. J. Clin. Pathol.* 1976; **65**; 159–167.
10. Koss MN, Fleming M, Przygodzki RM, Sherrod A, Travis W, Hochholzer L. Adenocarcinoma simulating mesothelioma: a clinicopathologic and immunohistochemical study of 29 cases. *Ann. Diagn. Pathol.* 1998; **2**; 93–102.
11. Mayall FG, Gibbs AR. 'Pleural' and pulmonary carcinosarcomas. *J. Pathol.* 1992; **167**; 305–311.
12. Oka K, Otani S, Yoshimura T *et al.* Mucin-negative pseudomesotheliomatous adenocarcinoma of the lung: report of three cases. *Acta Oncol.* 1999; **38**; 1119–1121.
13. Shah IA, Salvatore JR, Kummet T, Gani OS, Wheeler LA. Pseudomesotheliomatous carcinoma involving pleura and peritoneum: a clinicopathologic and immunohistochemical study of three cases. *Ann. Diagn. Pathol.* 1999; **3**; 148–159.
14. Attanoos RL, Gibbs AR. 'Pseudomesotheliomatous' carcinomas of the pleura: a 10-year analysis of cases from the Environmental Lung Disease Research Group, Cardiff. *Histopathology* 2003; **43**; 444–452.
15. Funai K, Yokose T, Ishii G *et al.* Clinicopathologic characteristics of peripheral squamous cell carcinoma of the lung. *Am. J. Surg. Pathol.* 2003; **27**; 978–984.
16. Sakurai H, Asamura H, Watanabe S, Suzuki K, Tsuchiya R. Clinicopathologic features of peripheral squamous cell carcinoma of the lung. *Ann. Thorac. Surg.* 2004; **78**; 222–227.
17. Husain AN, Colby T, Ordonez N *et al.* Guidelines for pathologic diagnosis of malignant mesothelioma: 2012 update of the consensus statement from the International Mesothelioma Interest Group. *Arch. Pathol. Lab. Med.* 2013; **137**; 647–667.
18. Travis WD, Brambilla E, Nicholson AG *et al.* The 2015 World Health Organization classification of lung tumors: impact of genetic, clinical and radiologic advances since the 2004 classification. *J. Thorac. Oncol.* 2015; **10**; 1243–1260.
19. Galateau-Salle F, Churg A, Roggli V, Travis WD; World Health Organization Committee for Tumors of the Pleura. The 2015 World Health Organization classification of tumors of the pleura: advances since the 2004 classification. *J. Thorac. Oncol.* 2016; **11**; 142–154.
20. Kushitani K, Takeshima Y, Amatya VJ, Furukawa O, Sakatani A, Inai K. Immunohistochemical marker panels for distinguishing between epithelioid mesothelioma and lung adenocarcinoma. *Pathol. Int.* 2007; **57**; 190–199.
21. Amatya VJ, Takeshima Y, Kohno H *et al.* Caveolin-1 is a novel immunohistochemical marker to differentiate epithelioid mesothelioma from lung adenocarcinoma. *Histopathology* 2009; **55**; 10–19.
22. Ordonez NG. Application of immunohistochemistry in the diagnosis of epithelioid mesothelioma: a review and update. *Hum. Pathol.* 2013; **44**; 1–19.
23. Ordonez NG. The diagnostic utility of immunohistochemistry in distinguishing between epithelioid mesotheliomas and squamous carcinomas of the lung: a comparative study. *Mod. Pathol.* 2006; **19**; 417–428.
24. Tsao M-S, Brambilla E, Nicholson AG *et al.* Squamous cell carcinoma. In: Travis WD, Brambilla E, Burke AP, Marx A, Nicholson AG eds. *World Health Organization classification of tumours of the lung, pleura, thymus and heart*. Lyon: IARC Press, 2015; 51–55.
25. Hohenstein P, Hastie ND. The many facets of the Wilms' tumour gene, WT1. *Hum. Mol. Genet.* 2006; **15**(Spec. No. 2); R196–R201.
26. Takeshima Y, Amatya VJ, Kushitani K, Inai K. A useful antibody panel for differential diagnosis between peritoneal mesothelioma and ovarian serous carcinoma in Japanese cases. *Am. J. Clin. Pathol.* 2008; **130**; 771–779.
27. Ordonez NG. The immunohistochemical diagnosis of mesothelioma: a comparative study of epithelioid mesothelioma and lung adenocarcinoma. *Am. J. Surg. Pathol.* 2003; **27**; 1031–1051.
28. Rogers JH. Calretinin: a gene for a novel calcium-binding protein expressed principally in neurons. *J. Cell Biol.* 1987; **105**; 1343–1353.
29. Doglioni C, Dei Tos AP, Laurino L *et al.* Calretinin: a novel immunocytochemical marker for mesothelioma. *Am. J. Surg. Pathol.* 1996; **20**; 1037–1046.
30. Pelosi G, Rossi G, Cavazza A *et al.* Deltanp63 (p40) distribution inside lung cancer: a driver biomarker approach to tumor characterization. *Int. J. Surg. Pathol.* 2013; **21**; 229–239.
31. Tatsumori T, Tsuta K, Masai K *et al.* P40 is the best marker for diagnosing pulmonary squamous cell carcinoma: comparison with p63, cytokeratin 5/6, desmocollin-3, and SOX2. *Appl. Immunohistochem. Mol. Morphol.* 2014; **22**; 377–382.
32. Bishop JA, Teruya-Feldstein J, Westra WH, Pelosi G, Travis WD, Rekhtman N. P40 (DeltaNp63) is superior to p63 for the diagnosis of pulmonary squamous cell carcinoma. *Mod. Pathol.* 2012; **25**; 405–415.
33. Facchetti F, Lonardi S, Gentili F *et al.* Claudin 4 identifies a wide spectrum of epithelial neoplasms and represents a very useful marker for carcinoma versus mesothelioma diagnosis in pleural and peritoneal biopsies and effusions. *Virchows Arch.* 2007; **451**; 669–680.
34. Soini Y, Kinnula V, Kahlos K, Paakkonen P. Claudins in differential diagnosis between mesothelioma and metastatic adenocarcinoma of the pleura. *J. Clin. Pathol.* 2006; **59**; 250–254.
35. Lodi C, Szabo E, Holczbauer A *et al.* Claudin-4 differentiates biliary tract cancers from hepatocellular carcinomas. *Mod. Pathol.* 2006; **19**; 460–469.
36. Lonardi S, Manera C, Marucci R, Santoro A, Lorenzi L, Facchetti F. Usefulness of claudin 4 in the cytological diagnosis of serosal effusions. *Diagn. Cytopathol.* 2011; **39**; 313–317.
37. Ordonez NG. Value of claudin-4 immunostaining in the diagnosis of mesothelioma. *Am. J. Clin. Pathol.* 2013; **139**; 611–619.
38. Wang NS, Huang SN, Gold P. Absence of carcinoembryonic antigen-like material in mesothelioma: an immunohistochemical differentiation from other lung cancers. *Cancer* 1979; **44**; 937–943.
39. Ordonez NG. What are the current best immunohistochemical markers for the diagnosis of epithelioid mesothelioma? A review and update *Hum. Pathol.* 2007; **38**; 1–16.

MUC4, a novel immunohistochemical marker identified by gene expression profiling, differentiates pleural sarcomatoid mesothelioma from lung sarcomatoid carcinoma

Vishwa Jeet Amatya¹, Kei Kushitani¹, Amany Sayed Mawas^{1,2}, Yoshihiro Miyata³, Morihiro Okada³, Takumi Kishimoto⁴, Kouki Inai^{1,5} and Yukio Takeshima¹

¹Department of Pathology, Hiroshima University Graduate School of Biomedical and Health Sciences, Hiroshima, Japan; ²Department of Pathology and Clinical Pathology, South Valley University, Qena, Egypt;

³Department of Surgical Oncology, Research Institute for Radiation Biology and Medicine, Hiroshima University, Hiroshima, Japan; ⁴Department of Internal Medicine, Okayama Rosai Hospital, Okayama, Japan and ⁵Pathologic Diagnostic Center, Inc., Hiroshima, Japan

Sarcomatoid mesothelioma, a histological subtype of malignant pleural mesothelioma, is a very aggressive tumor with a poor prognosis. Histological diagnosis of sarcomatoid mesothelioma largely depends on the histomorphological feature of spindled tumor cells with immunohistochemical reactivity to cytokeratins. Diagnosis also requires clinico-radiological and/or macroscopic evidence of an extrapulmonary location to differentiate it from lung sarcomatoid carcinoma. Although there are promising immunohistochemical antibody panels to differentiate mesothelioma from lung carcinoma, a consensus on the immunohistochemical markers that distinguish sarcomatoid mesothelioma from lung sarcomatoid carcinoma has not been reached and requires further study. We performed whole gene expression analysis of formalin-fixed paraffin-embedded tissue from sarcomatoid mesothelioma and lung sarcomatoid carcinoma and observed significant differences in the expression of MUC4 and other genes between sarcomatoid mesothelioma and lung sarcomatoid carcinoma. Immunohistochemistry demonstrated that MUC4 was expressed in the spindled tumor cells of lung sarcomatoid carcinoma (21/29, 72%) but was not expressed in any sarcomatoid mesothelioma (0/31, 0%). To differentiate sarcomatoid mesothelioma from lung sarcomatoid carcinoma, negative MUC4 expression showed 100% sensitivity and 72% specificity and accuracy rate of 87%, which is higher than immunohistochemical markers such as calretinin, D2-40 and Claudin-4. Therefore, we recommend to include MUC4 as a novel and useful negative immunohistochemical marker for differentiating sarcomatoid mesothelioma from lung sarcomatoid carcinoma.

Modern Pathology advance online publication, 27 January 2017; doi:10.1038/modpathol.2016.181

Malignant pleural mesothelioma, a highly aggressive tumor with a poor prognosis, is strongly associated with asbestos exposure; its incidence is increasing in Japan and Western countries and is expected to increase in developing countries.¹ It is histologically classified into three subtypes: epithelioid, biphasic,

and sarcomatoid mesothelioma.² The International Mesothelioma Interest Group (IMIG) has published guidelines for the differential diagnosis of epithelioid mesothelioma from lung adenocarcinoma and squamous cell carcinoma using immunohistochemical antibody panels of mesothelioma markers (calretinin, D2-40, WT1, cytokeratin 5/6), lung adenocarcinoma markers (CEA, TTF-1, Napsin-A, MOC-31, BerEP4, BG8, B72.3) and lung squamous carcinoma markers (p63, p40, MOC-31, Ber-EP4, cytokeratin 5/6).³

However, a consensus on the immunohistochemical markers that differentiate sarcomatoid mesothelioma from lung sarcomatoid carcinoma

Correspondence: Dr Y Takeshima, MD, PhD, Department of Pathology, Hiroshima University Graduate School of Biomedical and Health Sciences, 1-2-3 Kasumi, Minami-ku, Hiroshima 734-8551, Japan.

E-mail: ykotake@hiroshima-u.ac.jp

Received 15 June 2016; revised 3 September 2016; accepted 6 September 2016; published online 26 January 2017

has not been reached and requires further study. The histological diagnosis of sarcomatoid mesothelioma largely depends on the histomorphological feature of spindled tumor cells supported by immunohistochemical cytokeratin reactivity; it also requires clinico-radiological and/or macroscopic evidence of an extrapulmonary location. The immunohistochemical markers for lung adenocarcinoma and squamous carcinoma are not useful for diagnosing lung sarcomatoid carcinoma. To date, D2-40 and calretinin are two commonly used positive mesothelial markers expressed in sarcomatoid mesothelioma.^{4–7} However, without convincing calretinin and D2-40 positivity, it is difficult to differentiate sarcomatoid mesothelioma from sarcomatoid carcinoma. In previous reports, including ours, high D2-40 sensitivity has been reported to differentiate sarcomatoid mesothelioma from lung sarcomatoid carcinoma; however, D2-40 specificity is not perfect.^{6,7} Therefore, the clinico-radiological identification of tumor location at the extrapulmonary site remains essential to differentiate between these two diseases.

In recent decades, gene expression profiling has been used in many cancers to identify the pathways involved in malignant transformation and to identify novel candidate diagnostic and prognostic markers. We have recently reported the application of gene expression analysis to identify novel markers differentiating epithelioid mesothelioma from reactive mesothelial hyperplasia by PCR array.⁸ Although gene expression analysis requires specimens with a high proportion of tumor cells containing good quality RNA, we successfully analyzed the RNA extracted from formalin-fixed paraffin-embedded samples.

The aim of this study was to perform gene expression analysis on spindled tumor cells dissected from formalin-fixed paraffin-embedded tissue of sarcomatoid mesothelioma and lung sarcomatoid carcinoma. Our gene expression microarray data identified several novel genes that are differentially expressed between sarcomatoid mesothelioma and lung sarcomatoid carcinoma, and of these, we validated MUC4 as a novel and useful negative immunohistochemical marker differentiating sarcomatoid mesothelioma from lung sarcomatoid carcinoma.

Materials and methods

Formalin-Fixed Paraffin-Embedded Tissue Samples

Sarcomatoid mesothelioma and lung sarcomatoid carcinoma cases were retrieved from surgical pathology archives of our department during 2005–2014. The clinical details were also reviewed from the patient record files. The location of tumor was confirmed by reviewing clinical information (especially chest computed tomography findings to confirm the tumor localization), gross findings and

reviewing histological sections stained with H&E and Elastica van Gieson. All lung sarcomatoid carcinoma cases in this study were located in the pulmonary parenchyma, which was confirmed by radiological, thoracoscopic and operative findings. None of the lung sarcomatoid carcinoma showed diffuse pleurotropic growth pattern described as 'pseudomesotheliomatous growth'. Sarcomatoid mesothelioma was located in extrapulmonary site showing dominant pleurotrophic growth pattern without obvious tumor mass in lung parenchyma. Pathological diagnosis of each case was confirmed by histological findings and immunohistochemical marker panel recommended by Guidelines for Pathologic Diagnosis of Malignant Mesothelioma-2012 Update of the Consensus Statement from the International Mesothelioma Interest Group³ and current 2015 WHO histological classification of tumors of the lung, pleura, thymus and heart.⁹ Sarcomatoid mesothelioma is characterized by a proliferation of spindle cells arranged in fascicles or having a haphazard distribution involving adjacent adipose tissue, parietal pleura or lung parenchyma.⁹ Lung sarcomatoid carcinoma is a poorly differentiated non-small cell lung carcinoma that contains a component of sarcoma or sarcoma-like (spindle and/or giant cell) differentiation. Lung sarcomatoid carcinoma is a group of five types of carcinomas based on specific histological criteria and described as giant cell carcinoma, pleomorphic carcinoma, carcinosarcoma, spindle cell carcinoma and pulmonary blastoma. Of these, spindle cell carcinoma and pleomorphic carcinoma with predominant spindle cell component requires the differentiation from sarcomatoid mesothelioma. The number of patients who were diagnosed as sarcomatoid mesothelioma and lung sarcomatoid carcinoma after surgical resection and/or autopsy examination in Hiroshima University Hospital during 2005–2014 were 35 and 34 respectively, suggesting similar frequencies of their incidence. Localization of four cases of sarcomatoid mesothelioma and five cases of lung sarcomatoid carcinoma could not be confirmed and thus were excluded from this study. Finally, 31 cases of sarcomatoid mesothelioma and 29 cases of lung sarcomatoid carcinoma were analyzed in the present study. Sarcomatoid mesothelioma included 25 cases of pure sarcomatoid growth (pure sarcomatoid mesothelioma) and 6 cases of biphasic mesothelioma showing predominantly sarcomatoid growth. Lung sarcomatoid carcinoma included 5 cases of spindle cell carcinoma and 24 of pleomorphic carcinoma with predominant spindle cell carcinoma component. Minor foci of squamous cell carcinoma and adenocarcinoma component were present in 5 and 19 cases of pleomorphic carcinoma. Carcinosarcoma, giant cell carcinoma and pulmonary blastema were not included in this study.

The anonymized (unlinkable) tissue samples were provided by the Department of Pathology for gene expression analysis and immunohistochemical

study. This study is in accordance with the Ethics Guidelines for Human Genome/Gene Research enacted by the Japanese Government for the collection of tissue specimens and was approved by the institutional ethics review committee (Hiroshima University E-48).

Gene Expression Analysis

Formalin-fixed paraffin-embedded sections from six cases of sarcomatoid mesothelioma and six cases of lung sarcomatoid carcinoma were used for gene expression analysis. RNA extraction for gene expression analysis was performed from the spindled tumor cells of these cases. Five 10- μ m-thick formalin-fixed paraffin-embedded tissue sections containing >90% spindled tumor tissue were processed for total RNA extraction using the Maxwell 16 LEV RNA FFPE Purification Kit (Promega, Tokyo, Japan) according to the manufacturer's protocol. After deparaffinization and lysis with proteinase K treatment, the samples were treated with a DNase cocktail for 15 min at room temperature, followed by RNA purification using a MAXWELL 16 instrument according to the manufacturer's protocol (Promega).

RNA quality was analyzed with an RNA StdSens Analysis kit using an Experion automated electrophoresis system (Bio-Rad Laboratories, Hercules, CA, USA). RNA quantity was estimated with a Qubit RNA HS Kit using a Qubit Fluorometer 2.0 (Molecular Probes/Life Technologies, Carlsbad, CA, USA). The Almac Xcel Array GeneChip (Affymetrix, Santa Clara, CA, USA) contains probe sets of >97 000 transcripts and was used to analyze gene expression profiles. Total RNA was amplified and labeled with a 3' IVT Labeling Kit (Affymetrix) before hybridization onto the GeneChip. Briefly, 100 ng total RNA was amplified with a SensationPlus FFPE Amplification Kit (Affymetrix) to generate 30 μ g of SenseRNA according to the manufacturer's protocol. Twenty-five micrograms of SenseRNA was labeled with a 3' IVT Labeling Kit (Affymetrix) and hybridized to a Almac Xcel Array GeneChip (Affymetrix) at 45 °C for 16 h using a GeneChip Hybridization Oven 645 (Affymetrix). The hybridized GeneChip was washed, stained using GeneChip Fluidic Station 450 (Affymetrix) and scanned with a GeneChip Scanner 3000 7G (Affymetrix) using the GeneChip Operating Software (Affymetrix). The data were analyzed using the Gene Expression Console Software (Affymetrix), and further statistical analyses were performed using the Subio Software Platform (Subio, Amami-shi, Japan) to calculate plot graphs, fold change of expression and hierarchical clustering.

Validation of Gene Expression Analysis

The same 12 cases of sarcomatoid mesothelioma and lung sarcomatoid carcinoma that were analyzed for gene expression profiling were used to validate the

microarray expression data. The relative mRNA expression of *MUC4*, a highly expressed gene in lung sarcomatoid carcinoma, and *IGF2*, highly expressed in sarcomatoid mesothelioma, was assessed with SYBR Green-based real-time RT-PCR using GAPDH as a control. A total of 100 ng RNA was used for mRNA expression with a one-step SYBR Green RT-PCR Kit (Takara-Bio, Tokyo, Japan) using a MX3000P real-time PCR thermal cycler (Stratagene, Agilent Technologies, Tokyo, Japan). The primer pairs used were *MUC4*-F: CAGGCCACCAACTTCA TCG; *MUC4*-R: ACACGGATTGCGCTGTGAG; *IGF2*-F: GTGGCATCGTTGAGGAGTG; *IGF2*-R: CACGTCC CTCTCGGACTTG; *GAPDH*-F: ACAACTTGGTATC GTGGAAGG; and *GAPDH*-R: GCCATCACGCCA CAGTTTC. Data analysis was performed using the $\Delta\Delta$ CT method for relative quantification. Briefly, threshold cycles (CT) for *GAPDH* (reference) and *MUC4*, *IGF2* (samples) were determined in triplicate. The relative expression (rI) was calculated using the formula: $rI = 2^{-(CT_{\text{sample}} - CT_{\text{normal}})}$.

Immunohistochemistry

Immunohistochemistry was performed using 3- μ m tissue sections from the best representative formalin-fixed paraffin-embedded sarcomatoid mesothelioma and lung sarcomatoid carcinoma tissue blocks. All of the immunohistochemical staining was performed with a Benchmark GX automated immunohistochemical station (Ventana, Roche Diagnostics, Tokyo, Japan) using the ultraView Universal DAB Detection Kit (Ventana, Roche Diagnostic, Tokyo, Japan). The antigen retrieval methods and antibodies used in this study are summarized in Table 1. Immunoreactivity was scored as negative (0, no immunostaining) or positive. Positive immunoreactivity was graded as +1 for up to 10% of tumor cells showing positive immunostaining, +2 for >10–50% of the tumor cells, and +3 for >50% of the tumor cells. Only spindled tumor cells from sarcomatoid mesothelioma and lung sarcomatoid carcinoma were evaluated for the immunoreactivity of various markers. Statistical analyses were performed using Fisher's exact test. Sensitivity, specificity, positive predictive value, negative predictive value and accuracy rate were calculated using a simple 2 \times 2 table.

Results

Differential Gene Expression and Validation in Sarcomatoid Mesothelioma and Lung Sarcomatoid Carcinoma

Out of the 97 000 analyzable transcripts on the Almac Xcel Array GeneChip, 2099 statistically significant mRNA transcripts were differentially expressed between sarcomatoid mesothelioma and lung sarcomatoid carcinoma by a more than a two-fold difference (Figure 1, plot graph). The

Table 1 List of antibodies with their clone, commercial source and reaction conditions

Antibody to	Clone	Provider	Dilution	Antigen retrieval
MUC4	8G7	Santa Cruz Biotechnology	× 25	CC1, 60 min
Calretinin	SP65	Ventana	Prediluted	CC1, 30 min
Podoplanin	D2-40	Nichirei	Prediluted	CC1, 60 min
WT1	6F-H2	Dako	× 25	CC1, 60 min
Pancytokeratin	AE1/AE3	Ventana	Prediluted	Protease 8 min
Cytokeratin	CAM5.2	Ventana	Prediluted	Protease 8 min
p40	BC28	Biocare Medical	× 50	CC1, 60 min
TTF-1	SP141	Ventana	Prediluted	CC1, 60 min
Claudin-4	3E2C1	Life Technologies	× 50	CC1, 60 min

Abbreviation: CC1, cell conditioning buffer 1 (Tris-based buffer, pH 8.5 from Ventana).

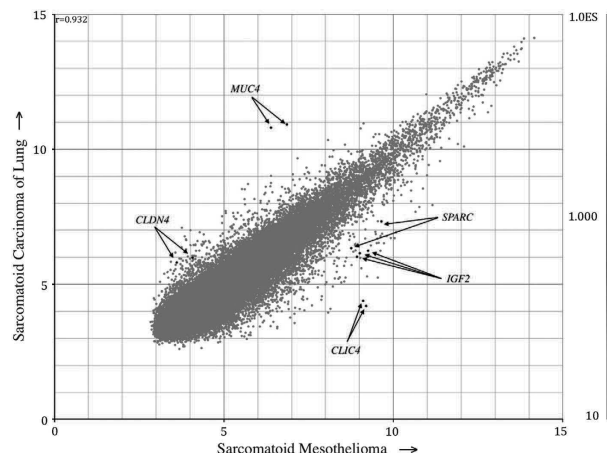


Figure 1 Scatter plot of raw data from the microarray experiments demonstrating MUC4 and CLDN4 with lower expression and IGF2, CLIC4 and SPARC4 with higher expression in sarcomatoid mesothelioma compared with that of lung sarcomatoid carcinoma.

hierarchical clustering of mRNAs with more than a five-fold difference in expression revealed 156 upregulated mRNA transcripts, including *IGF2*, *MEG3*, *CLIC4* and *SPARC*, in sarcomatoid mesothelioma and 46 upregulated mRNA transcripts, including *MUC4* and *Claudin4*, in lung sarcomatoid carcinoma (Figure 2, hierarchical clustering; Supplementary Table S1). The mRNA expression hits were validated by real-time RT-PCR of *MUC4* and *IGF2*. *MUC4* mRNA expression was negligible in all six sarcomatoid mesothelioma, and the expression was observed in five of the six lung sarcomatoid carcinoma samples. *IGF2* mRNA was expressed in all of the sarcomatoid mesothelioma samples, although it was also expressed in three of the six lung sarcomatoid carcinoma samples (detailed data not shown).

Immunohistochemical Profiles of Sarcomatoid Mesothelioma and Lung Sarcomatoid Carcinoma

The percentage of positivity and immunohistochemical score for MUC4, mesothelioma markers

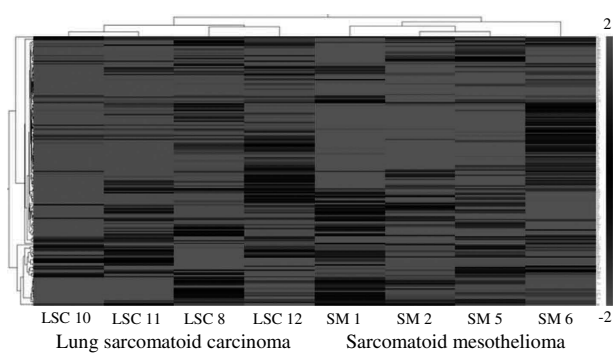


Figure 2 The hierarchical clustering of RNA transcripts with more than five-fold differential expression between sarcomatoid mesothelioma and lung sarcomatoid carcinoma revealed 156 upregulated mRNA transcripts, including *IGF2*, *MEG3*, *CLIC4* and *SPARC*, in sarcomatoid mesothelioma and 46 upregulated mRNA transcripts, including *MUC4* and *Claudin4*, in lung sarcomatoid carcinoma.

(calretinin, D2-40, WT1) and lung carcinoma markers (TTF-1, p40, Claudin-4) along with the cytokeratins AE1/AE3 and CAM5.2 are shown in Table 2.

MUC4 Expression

MUC4 expression was observed in the cytoplasm of tumor cells, and the positivity of spindled tumor cells alone was evaluated. *MUC4* was also observed in the surrounding normal lung tissue, particularly in bronchial tissue, and was considered an internal positive marker. It was expressed in spindled tumor cells of 21 lung sarcomatoid carcinoma (21/29, 72%; Figure 3b) but none in sarcomatoid mesothelioma (0/31, 0%; Figure 4b). In addition to spindled tumor cells of lung sarcomatoid carcinoma, *MUC4* was also expressed in the non-small cell carcinoma component consisting of adenocarcinoma or squamous cell carcinoma in pleomorphic carcinoma. Among lung sarcomatoid carcinoma, 3 cases showed expression in >50% of tumor cells, 9 cases in 10–50% of tumor cells and 9 cases in <10% of tumor cells. Out of the 21 lung sarcomatoid carcinoma cases with *MUC4*

Table 2 Potential immunohistochemical markers for sarcomatoid mesothelioma and lung sarcomatoid carcinoma

Antibody	Sarcomatoid mesothelioma					Lung sarcomatoid carcinoma							
	Positive cases	(%)	Immunohistochemical score ^a			Positive cases	(%)	Immunohistochemical score ^a			P-value ^b	P-value ^c	
			0	1+	2+			0	1+	2+			
MUC4	0/31	0	31	0	0	0	21/29	72	8	9	3	< 0.01	< 0.01
Calretinin	23/31	74	8	7	11	5	13/29	45	16	5	6	< 0.05	< 0.05
D2-40	22/31	71	9	9	12	1	9/29	31	20	9	0	< 0.01	< 0.01
WT1	6/31	19	25	5	1	0	1/29	3	28	1	0	NS	NS
AE1/AE3	29/31	94	2	2	8	19	29/29	100	0	5	22	NS	NS
CAM5.2	28/31	90	3	1	8	19	28/29	97	1	6	5	17	NS
TTF-1	0/31	0	31	0	0	0	15/29	52	14	0	4	11	< 0.01
p40	2/31	7	29	2	0	0	6/29	21	23	0	3	3	NS
Claudin-4	0/31	0	31	0	0	0	13/29	45	16	4	5	4	< 0.01

Abbreviations: NA, not available; NS, not significant; TTF-1, thyroid transcription factor; WT1, Wilms' tumor gene product.

^aCalculated by Fisher's exact test of the positive rate between two groups.

^bCalculated by the Mann-Whitney *U*-test of reactivity scores of the markers between two groups.

^cImmunohistochemical score was semiquantified as follows: 0: 0%; 1+: 1–10%; 2+: 11–50%; 3+: >51% of spindled tumor cells.

expression, p40 expression was observed only in 3 cases, TTF-1 in 12 cases and Claudin-4 in 10 cases. Of the nine lung sarcomatoid carcinoma cases without MUC4 expression, p40 expression was observed in three cases, TTF-1 in three cases and Claudin-4 in three cases.

Calretinin, D2-40 and WT1

Calretinin was expressed in the nucleus and cytoplasm of spindled tumor cells of 23 (74%) sarcomatoid mesothelioma and 13 (45%) lung sarcomatoid carcinoma samples, and D2-40 was expressed in the spindled tumor cells of 21 (71%) sarcomatoid mesothelioma and 9 (31%) lung sarcomatoid carcinoma. The immunohistochemical scoring pattern for calretinin expression was not different between sarcomatoid mesothelioma and lung sarcomatoid carcinoma. However, the immunohistochemical scoring pattern for D2-40 expression showed a higher score in sarcomatoid mesothelioma than in lung sarcomatoid carcinoma. WT1 nuclear expression was present in only 6 (19%) sarcomatoid mesothelioma and 1 (3%) lung sarcomatoid carcinoma, revealing it to be a poor immunohistochemical marker to differentiate sarcomatoid mesothelioma from lung sarcomatoid carcinoma.

TTF-1, p40, Claudin-4

Nuclear expression of TTF-1 and P40 was observed in 15 (52%) and 6 (21%) cases of lung sarcomatoid carcinoma, respectively. TTF-1 expression was not observed in sarcomatoid mesothelioma, but p40 expression was observed in 2 (7%) sarcomatoid mesothelioma cases. TTF-1 and/or p40 immunoreactivity was present in 19 of the 29 (66%) cases of

lung sarcomatoid carcinoma and 2 of the 31 (7%) cases of sarcomatoid mesothelioma. Claudin-4 and/or TTF-1/p40 immunoreactivity was present in 25 of the 29 (86%) of lung sarcomatoid carcinoma and 2 of the 31 (7%) cases of sarcomatoid mesothelioma. However, p40 expression in sarcomatoid mesothelioma was focal and heterogeneous with an immunohistochemical score of 1.

Cytokeratins, AE1/AE3, CAM5.2

Cytokeratin AE1/AE3 and CAM5.2 expression was present in >90% of both lung sarcomatoid carcinoma and sarcomatoid mesothelioma samples. The majority of sarcomatoid mesothelioma and lung sarcomatoid carcinoma cases showed the expression of both cytokeratins, and the remaining two lung sarcomatoid carcinoma cases and one sarcomatoid mesothelioma case expressed at least one of the two cytokeratins.

Sensitivity and Specificity of Each Marker to Differentially Diagnose Sarcomatoid Mesothelioma and Lung Sarcomatoid Carcinoma

The sensitivity, specificity, positive predictive value, negative predictive value and accuracy rate of each marker differentiating sarcomatoid mesothelioma from lung sarcomatoid carcinoma are shown in Table 3. The negative expression of the carcinoma markers TTF-1 and Claudin-4 showed 100% sensitivity, whereas p40 showed 94%; however, their specificity was restricted around or below 50%. The positive expression of calretinin showed 74% sensitivity and 55% specificity, and D2-40 showed 71% sensitivity and 69% specificity. Although WT1 showed the highest specificity of 97%, its sensitivity

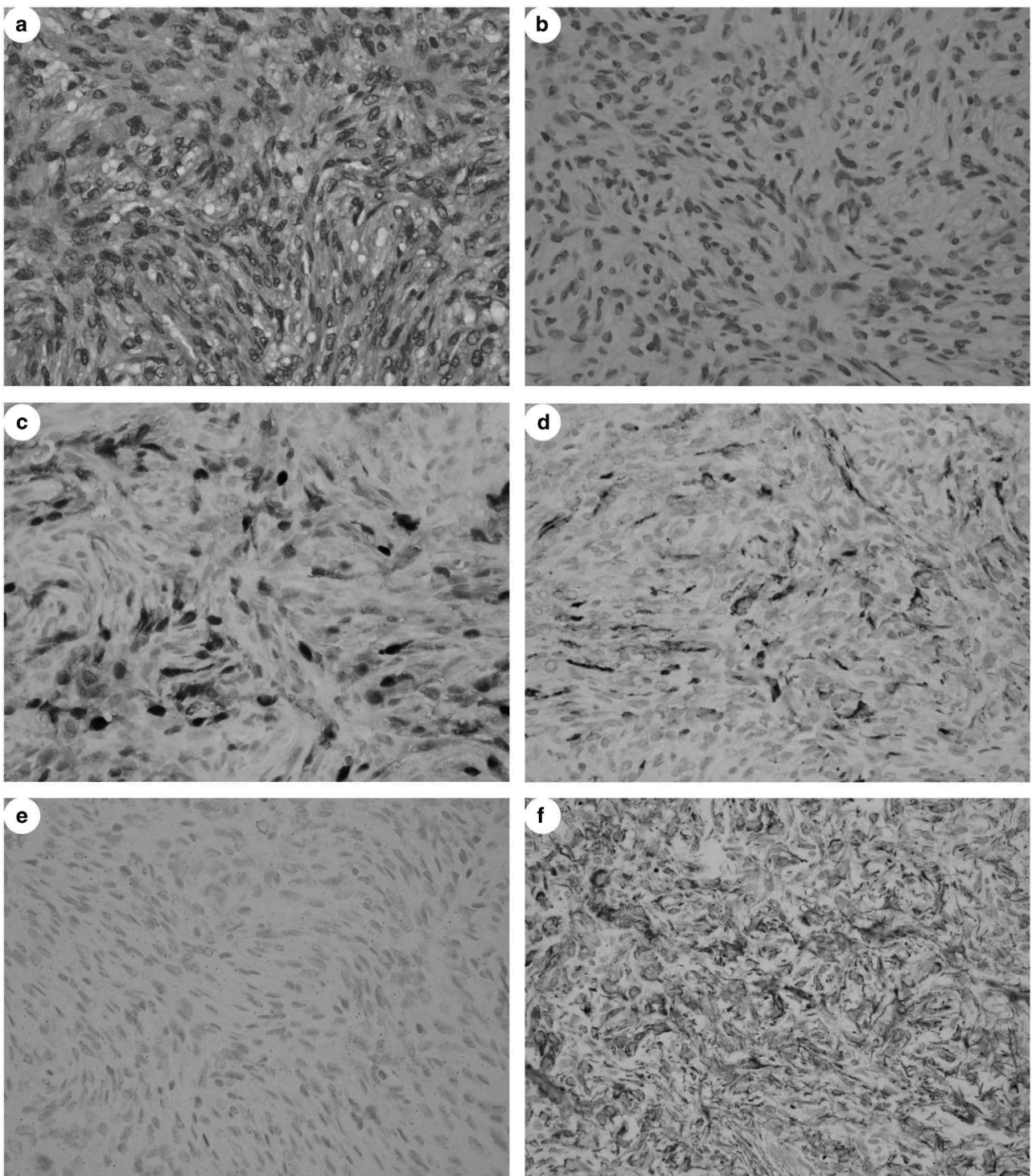


Figure 3 Representative pictures of immunohistochemical expression of MUC4 (b), Calretinin (c), D2-40 (d), Claudin-4 (e) and AE1/AE3 (f) from sarcomatoid mesothelioma (a). None of the sarcomatoid mesotheliomas showed immunohistochemical MUC4 expression.

was < 20%. AE1/AE3 and CAM5.2 showed high 94 and 90% sensitivities and near 0% specificity. In comparison to all of these known immunohistochemical markers, negative expression of MUC4 showed 100% sensitivity and 72% specificity, making the accuracy rate of 87%, the highest among these immunohistochemical markers.

Value of Immunohistochemical Marker Panel to Differentially Diagnosis Sarcomatoid Mesothelioma and Lung Sarcomatoid Carcinoma

MUC4 showed the highest sensitivity and specificity among the immunohistochemical markers for differentiation of sarcomatoid mesothelioma from lung

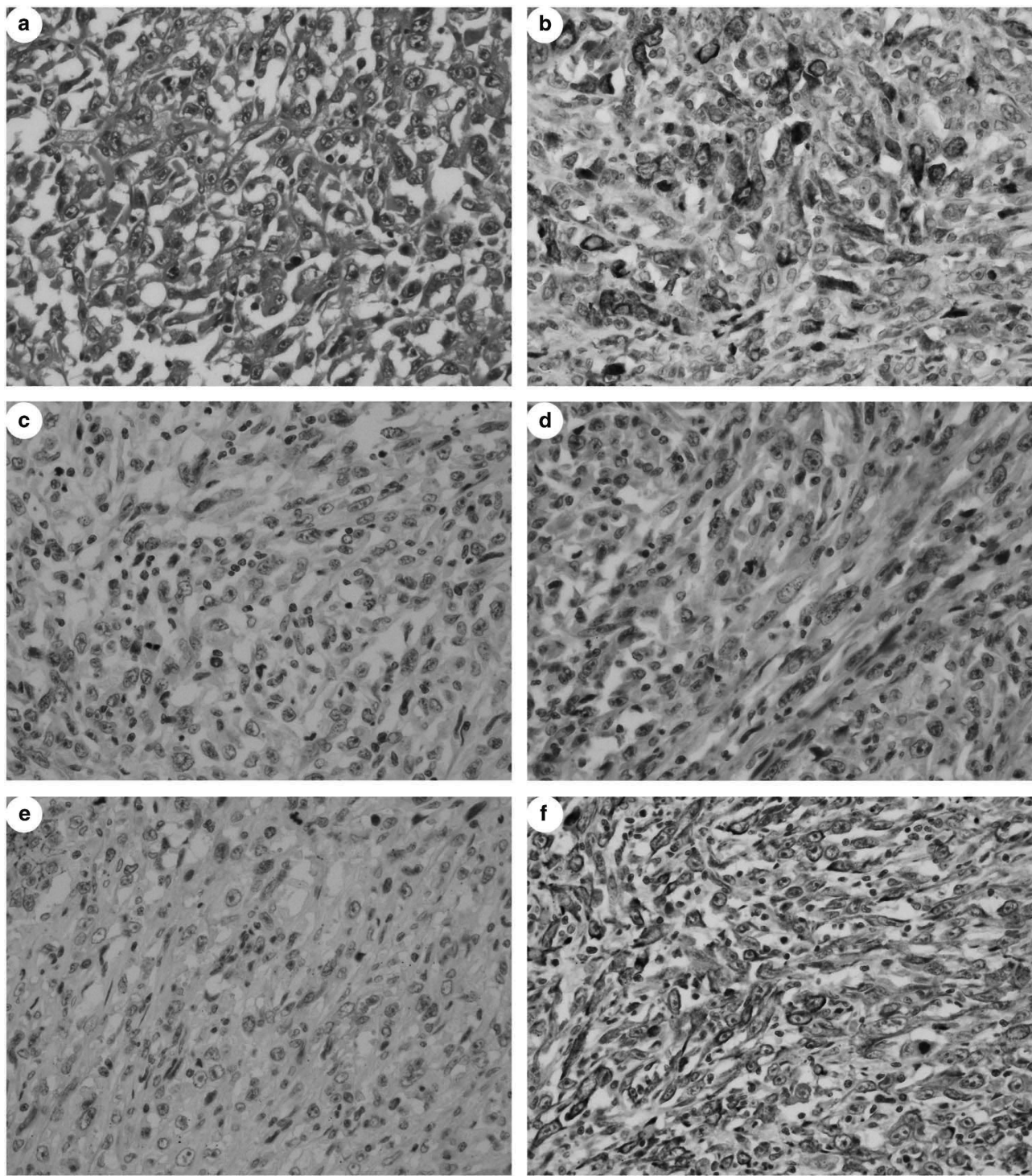


Figure 4 Representative pictures of immunohistochemical MUC4 expression (b), Calretinin (c), D2-40 (d), Claudin-4 (e) and AE1/AE3 (f) of lung sarcomatoid carcinoma (a). Twenty-one of the 29 (72%) lung sarcomatoid carcinomas exhibited cytoplasmic expression of MUC4.

sarcomatoid carcinoma. However, the specificity was 72%. Therefore, a combination of various markers was considered. Various combinations of immunohistochemical markers are shown in Table 4. Among the negative immunohistochemical markers, combination of MUC4, TTF-1 and p40 was

observed in 26 of the 29 lung sarcomatoid carcinoma cases (90% specificity) and 2 of the 31 sarcomatoid mesothelioma cases (93% sensitivity). Combination of MUC4 and Claudin-4 expression was found in 24 of the 29 lung sarcomatoid carcinoma cases (83% specificity) and none of the sarcomatoid

Table 3 Sensitivity, specificity, PPV, NPV and accuracy rate of each antibody to differentially diagnose sarcomatoid mesothelioma from lung sarcomatoid carcinoma

Findings	Sensitivity (%)	Specificity (%)	PPV (%)	NPV (%)	Accuracy rate (%)	P-value
MUC4 (-)	100	72	80	100	87	< 0.01
Calretinin (+)	74	55	64	67	65	< 0.05
D2-40 (+)	71	69	71	69	70	< 0.01
WT1 (+)	19	97	86	53	57	NS
AE1/AE3 (+)	94	0	50	0	48	NS
CAM5.2 (+)	90	3	50	25	48	NS
TTF-1 (-)	100	52	69	100	77	< 0.01
p40 (-)	94	21	56	75	58	NS
Claudin-4 (-)	100	45	66	100	73	< 0.01

Abbreviations: NPV, negative predictive value; NS, not significant; PPV, positive predictive value.

Table 4 Sensitivity, specificity, PPV, NPV and accuracy rate of two or more markers to differentially diagnose sarcomatoid mesothelioma from lung sarcomatoid carcinoma

Immunohistochemical markers	Sensitivity (%)	Specificity (%)	PPV (%)	NPV (%)	Accuracy rate (%)	P-value
p40 (-)/TTF-1 (-)	94	66	74	91	80	< 0.01
Claudin-4 (-)/TTF-1 (-)/p40 (-)	94	90	91	93	92	< 0.01
Claudin-4 (-)/TTF-1 (-)	100	83	86	100	92	< 0.01
MUC4 (-)/TTF-1 (-)/p40 (-)	94	93	94	93	93	< 0.01
MUC4 (-)/Claudin-4 (-)	100	83	86	100	92	< 0.01
MUC4 (-)/TTF-1 (-)/Claudin-4 (-)	100	90	91	100	95	< 0.01
MUC4 (-)/TTF-1 (-)/p40 (-)/Claudin-4 (-)	94	97	97	93	95	< 0.01

Abbreviations: NPV, negative predictive value; PPV, positive predictive value.

mesothelioma cases (100% sensitivity). The combination of MUC4, TTF-1 and Claudin-4 was observed in 26 of the 29 lung sarcomatoid carcinoma cases (90% specificity) and 0 of the 31 sarcomatoid mesothelioma cases (100% sensitivity).

Discussion

Sarcomatoid mesothelioma has the histomorphological feature of spindled tumor cells and resembles many tumors with spindled cells, including true sarcoma or sarcomatoid carcinomas. The immunohistochemical reactivity to cytokeratin remains critical to differentiate it from true sarcomas. However, differentiating sarcomatoid mesothelioma from lung sarcomatoid carcinoma is challenging, as the histomorphological and immunohistochemical characteristics are extremely similar. For this reason, clinical and/or gross evidence of an extrapulmonary location is indispensable for its diagnosis. Although the mesothelioma markers calretinin and D2-40 have been utilized to differentiate sarcomatoid mesothelioma from lung sarcomatoid carcinoma, they are not absolute, as their sensitivity and specificity are not sufficiently high. Although we previously reported the sensitivity of calretinin (78%) and D2-40 (87%), specificity was not high for calretinin (41%) and D2-40 (74%).⁷ Our past and present data on calretinin and D2-40 were similar to reports by Ordóñez *et al*⁴

and Padgett *et al*.⁶ Considering the low specificity of calretinin, D2-40 is considered the single most important immunohistochemical marker for its differentiation. However, in our practical experience, it is still very difficult to interpret the reactivity of D2-40 in these tumors, particularly in cases showing prominent fibro-collagenous proliferation.

TTF-1, a lung adenocarcinoma marker, and p40, a squamous cell carcinoma marker, have emerged as useful markers for non-small cell lung carcinoma^{10,11} and are thus supposed to be expressed in pleomorphic lung carcinoma. TTF-1 might be identified as a novel marker differentiating pleomorphic carcinoma from sarcomatoid mesothelioma because of its low expression in sarcomatoid mesothelioma. However, in this study, despite their specificity of 100 or 94%, the sensitivity of TTF-1 (51%) and p40 (21%) are not good to distinguish sarcomatoid mesothelioma and lung sarcomatoid carcinoma. Though p40 expression is good marker of squamous cell carcinoma, it has been also reported in a few mesothelioma cases.¹² In this study too, we observed p40 expression in two sarcomatoid mesothelioma cases but very focal and heterogeneous, unlike its expression in squamous cell carcinoma. Claudin-4, which is reported to be a very reliable universal carcinoma marker differentiating epithelioid mesothelioma from various carcinomas,^{13,14} showed limited value in lung sarcomatoid carcinoma cases. In this study, only half of lung sarcomatoid

carcinoma expressed Claudin-4, and its punctate expression in the cytoplasm of spindled cells of lung sarcomatoid carcinoma resembled that of the punctate expression in the cytoplasm of sarcomatoid mesothelioma. TTF-1, p40 and Claudin-4 expression can be reliable markers for pleomorphic carcinomas with a prominent carcinoma component, such as adenocarcinoma or squamous cell carcinoma.

In this study, we analyzed all of the genes expressed in sarcomatoid mesothelioma and lung sarcomatoid carcinoma with the aim of identifying novel markers for their differential diagnosis. Although frozen tissue yields better and less degradable RNA for gene expression analysis, we preferred formalin-fixed paraffin-embedded tissue samples because they included the microscopically identifiable spindle cell tumor tissue. For this analysis, we have to amplify the small amount of RNA extracted from the formalin-fixed paraffin-embedded tissue before hybridization to the GeneChip. The Almac Xcel GeneChip from Affymetrix, which we used here, has been reported to produce identical results to the GeneChip using RNA derived from frozen tissue samples. In addition, it contains proprietary Almac-sequenced data and filtered public data for biomarker discovery and the validation of oncogene-related transcripts for a much higher detection rate in degraded samples.

From the differential expression analysis, a more than five-fold expression change in *IGF2*, *CLIC4* and *SPARC* was observed in sarcomatoid mesothelioma, and *IGF2* expression was validated by real-time RT-PCR. We did not uncover significant differential expression of *IGF2* between sarcomatoid mesothelioma and lung sarcomatoid carcinoma (data not shown). The discrepancy between the microarray data and real-time RT-PCR data can be explained because *IGF2* mRNA expression on a microarray chip is the relative expression between both lung sarcomatoid carcinoma and sarcomatoid mesothelioma but in a different quantity. We later investigated the immunohistochemical expression *IGF2*, *CLIC4* and *SPARC* proteins in sarcomatoid mesothelioma and lung sarcomatoid carcinoma. However, there was no significant differential expression of these proteins between lung sarcomatoid carcinoma and sarcomatoid mesothelioma, limiting their applicability as an immunohistochemical positive marker of sarcomatoid mesothelioma.

In contrast, microarray gene expression analysis showed increased expression of *MUC4* in lung sarcomatoid carcinoma compared with that of sarcomatoid mesothelioma, and we found negligible *MUC4* mRNA expression in sarcomatoid mesothelioma at the mRNA level. *MUC4* stands for member of mucin protein of high molecular weight glycoprotein.¹⁵ It is expressed in various normal epithelium of the respiratory tract, particularly in the trachea and bronchi¹⁶ and in the epithelium of the digestive and urogenital tracts.¹⁷ *MUC4* expression has been reported in various human

carcinomas, including pancreatic,¹⁸ breast¹⁹ and lung adenocarcinoma.²⁰ Llinares *et al*²¹ reported the diagnostic value of *MUC4* expression in distinguishing epithelioid mesothelioma and lung adenocarcinoma. They found that *MUC4* was expressed in 0 of the 41 epithelioid mesotheliomas and in 32 of the 35 (91%) lung adenocarcinoma. To our knowledge, this report has not been validated by other laboratories, as the antibody to *MUC4* was not commercially available in the past. We observed *MUC4* expression in lung adenocarcinoma and lung squamous cell carcinoma and observed no expression in epithelioid mesothelioma using a commercially available anti-*MUC4* antibody. The current study is the first report to describe *MUC4* expression in lung sarcomatoid carcinoma and no *MUC4* expression in sarcomatoid mesothelioma. We observed a high specificity (72%) and absolute sensitivity (100%) for negative *MUC4* expression to differentiate sarcomatoid mesothelioma from lung sarcomatoid carcinoma, with an accuracy rate of 87%. These values are far better than any previously identified immunohistochemical markers differentiating sarcomatoid mesothelioma from lung sarcomatoid carcinoma.

The sensitivity of *MUC4* expression as a negative marker was the highest of the immunohistochemical markers in this study. Lung sarcomatoid carcinoma cases showing *MUC4* expression (21 cases) also demonstrated co-expression of TTF-1 in 12 cases, Claudin-4 in 10 cases and p40 in 3 cases. Furthermore, lung sarcomatoid carcinoma cases without *MUC4* expression showed TTF-1 expression in three cases, p40 in three cases and Claudin-4 in three cases. Therefore, *MUC4* expression has better additional value of the immunohistochemical markers for the differential diagnosis of sarcomatoid mesothelioma from lung sarcomatoid carcinoma. The sensitivity of these markers can be improved by combining two or more, and the addition of TTF-1 and Claudin-4 to *MUC4* expression improved the accuracy rate up to 95% for the differential diagnosis of sarcomatoid mesothelioma from lung sarcomatoid carcinoma.

In conclusion, we identified a novel immunohistochemical marker *MUC4* that differentiates sarcomatoid mesothelioma from lung sarcomatoid carcinoma by applying whole gene expression analysis. The combination of *MUC4* with TTF-1/p40 and Claudin-4 improved the sensitivity and specificity for differential diagnosis. Therefore, we propose including *MUC4* as an additional negative marker to the immunohistochemical marker panel to differentiate sarcomatoid mesothelioma from lung sarcomatoid carcinoma.

Acknowledgments

We thank Ms Naomi Fukuwara for her administrative assistance. This work was supported in part by the

Japan Society for the Promotion of Science, Grants-in-Aid Scientific Research No. JP26460452 (YT) from the Ministry of Education, Science, Sports and Culture. Part of this study was performed at the Analysis Center of Life Science, Hiroshima University.

Disclosure/conflict of interest

The authors declare no conflict of interest.

References

- 1 Delgermaa V, Takahashi K, Park EK, *et al*. Global mesothelioma deaths reported to the World Health Organization between 1994 and 2008. *Bull World Health Organ* 2011;89:716–724, 24A–24C.
- 2 Roggli V, Churg A, Chiriac LR, *et al*. Sarcomatoid, desmoplastic, and biphasic mesothelioma. In: Travis WD, Brambilla E, Burke S, *et al*. (eds). WHO Classification of Tumours of the Lung, Pleura, Thymus, and Heart. IARC: Lyon, France, 2015, pp 165–168.
- 3 Husain AN, Colby T, Ordonez N, *et al*. Guidelines for pathologic diagnosis of malignant mesothelioma: 2012 update of the consensus statement from the International Mesothelioma Interest Group. *Arch Pathol Lab Med* 2013;137:647–667.
- 4 Ordonez NG. D2-40 and podoplanin are highly specific and sensitive immunohistochemical markers of epithelioid malignant mesothelioma. *Hum Pathol* 2005;36:372–380.
- 5 Chu AY, Litzky LA, Pasha TL, *et al*. Utility of D2-40, a novel mesothelial marker, in the diagnosis of malignant mesothelioma. *Mod Pathol* 2005;18:105–110.
- 6 Padgett DM, Cathro HP, Wick MR, *et al*. Podoplanin is a better immunohistochemical marker for sarcomatoid mesothelioma than calretinin. *Am J Surg Pathol* 2008;32:123–127.
- 7 Takeshima Y, Amatya VJ, Kushitani K, *et al*. Value of immunohistochemistry in the differential diagnosis of pleural sarcomatoid mesothelioma from lung sarcomatoid carcinoma. *Histopathology* 2009;54:667–676.
- 8 Kushitani K, Amatya VJ, Mawas AS, *et al*. Use of anti-Noxa antibody for differential diagnosis between epithelioid mesothelioma and reactive mesothelial hyperplasia. *Pathobiology* 2016;83:33–40.
- 9 Kerr KM, Pelosi G, Austin JHM, *et al*. Pleomorphic, spindle cell, and giant cell carcinoma. In: Travis WD, Brambilla E, Burke AP, *et al*. (eds). WHO Classification of Tumours of the Lung, Pleura, Thymus and Heart, 4th edn. IARC: Lyon, France, 2015, pp 88–90.
- 10 Travis WD, Noguchi M, Yatabe Y, *et al*. Adenocarcinoma. In: Travis WD, Brambilla E, Burke AP, *et al*. (eds). WHO Classification of Tumours of the Lung, Pleura, Thymus and Heart, 4th edn. IARC: Lyon, France, 2015, pp 26–37.
- 11 Tsao M-S, Brambilla E, Nicholson AG, *et al*. Squamous cell carcinoma. In: Travis WD, Brambilla E, Burke AP, *et al*. (eds). WHO Classification of Tumours of the Lung, Pleura, Thymus and Heart, 4th edn. IARC: Lyon, France, 2015, pp 51–55.
- 12 Tatsumori T, Tsuta K, Masai K, *et al*. p40 is the best marker for diagnosing pulmonary squamous cell carcinoma: comparison with p63, cytokeratin 5/6, desmocollin-3, and sox2. *Appl Immunohistochem Mol Morphol* 2014;22:377–382.
- 13 Ordonez NG. Value of claudin-4 immunostaining in the diagnosis of mesothelioma. *Am J Clin Pathol* 2013;139: 611–619.
- 14 Facchetti F, Lonardi S, Gentili F, *et al*. Claudin 4 identifies a wide spectrum of epithelial neoplasms and represents a very useful marker for carcinoma versus mesothelioma diagnosis in pleural and peritoneal biopsies and effusions. *Virchows Arch* 2007;451: 669–680.
- 15 Chaturvedi P, Singh AP, Batra SK. Structure, evolution, and biology of the MUC4 mucin. *FASEB J* 2008;22: 966–981.
- 16 Copin MC, Devisme L, Buisine MP, *et al*. From normal respiratory mucosa to epidermoid carcinoma: expression of human mucin genes. *Int J Cancer* 2000;86: 162–168.
- 17 Audie JP, Janin A, Porchet N, *et al*. Expression of human mucin genes in respiratory, digestive, and reproductive tracts ascertained by *in situ* hybridization. *J Histochem Cytochem* 1993;41: 1479–1485.
- 18 Moniaux N, Chaturvedi P, Varshney GC, *et al*. Human MUC4 mucin induces ultra-structural changes and tumorigenicity in pancreatic cancer cells. *Br J Cancer* 2007;97:345–357.
- 19 Rakha EA, Boyce RW, Abd El-Rehim D, *et al*. Expression of mucins (MUC1, MUC2, MUC3, MUC4, MUC5AC and MUC6) and their prognostic significance in human breast cancer. *Mod Pathol* 2005;18: 1295–1304.
- 20 Kwon KY, Ro JY, Singhal N, *et al*. MUC4 expression in non-small cell lung carcinomas: relationship to tumor histology and patient survival. *Arch Pathol Lab Med* 2007;131:593–598.
- 21 Llinares K, Escande F, Aubert S, *et al*. Diagnostic value of MUC4 immunostaining in distinguishing epithelial mesothelioma and lung adenocarcinoma. *Mod Pathol* 2004;17:150–157.

Supplementary Information accompanies the paper on Modern Pathology website (<http://www.nature.com/modpathol>)

A phase II study of topotecan and cisplatin with sequential thoracic radiotherapy in elderly patients with small-cell lung cancer: Okayama Lung Cancer Study Group 0102

Toshio Kubo¹ · Keiichi Fujiwara² · Katsuyuki Hotta^{3,4} · Toshiaki Okada^{5,7} · Shoichi Kuyama^{6,7} · Shingo Harita⁷ · Takashi Ninomiya^{3,8} · Haruhito Kamei^{8,9} · Shinobu Hosokawa¹⁰ · Akihiro Bessho¹⁰ · Tadashi Maeda⁹ · Toshiyuki Kozuki¹¹ · Nobukazu Fujimoto¹² · Kiichiro Ninomiya³ · Mitsuhiro Takemoto^{13,14} · Susumu Kanazawa¹⁴ · Nagio Takigawa¹⁵ · Masahiro Tabata¹ · Mitsune Tanimoto¹⁶ · Hiroshi Ueoka^{7,9} · Katsuyuki Kiura³

Received: 16 June 2016 / Accepted: 11 August 2016 / Published online: 20 August 2016
© Springer-Verlag Berlin Heidelberg 2016

Abstract

Purpose The treatment outcome in elderly patients with limited-disease small-cell lung cancer (LD-SCLC) remains poor. We carried out a phase II trial of split topotecan and cisplatin (TP) therapy and sequential thoracic radiotherapy for elderly LD-SCLC patients as a follow-up to our previous phase I trial.

Methods In total, 30 patients aged 76 years or older, with untreated LD-SCLC were enrolled. Four courses of topotecan (1.0 mg/m², days 1–3) and cisplatin (20 mg/m², days 1–3) were administered, followed by thoracic radiotherapy

(1.8 Gy/day, total of 45 Gy). The primary end point was the overall response rate (ORR).

Results The trial was terminated early with 22 patients because of slow accrual. Their median age was 79 years. The median number of courses of chemotherapy administered was three, and the actual completion rate of the entire treatment course was 41 %. The ORR was 68 % with a 95 % confidence interval of 47–89 % (15/22 cases). The median progression-free survival and overall survival were 9.1 and 22.2 months, respectively. The main toxicity was myelosuppression, with grades 3–4 neutropenia (96 %), thrombocytopenia (50 %), and febrile neutropenia (32 %).

Conclusions This regimen produced a favorable survival outcome, despite moderate-to-severe toxicity profiles.

Electronic supplementary material The online version of this article (doi:10.1007/s00280-016-3135-2) contains supplementary material, which is available to authorized users.

✉ Katsuyuki Hotta
khotta@okayama-u.ac.jp

¹ Center for Clinical Oncology, Okayama University Hospital, Okayama, Japan

² Department of Respiratory Medicine, Okayama Medical Center, Okayama, Japan

³ Department of Respiratory Medicine, Okayama University Hospital, Okayama, Japan

⁴ Center for Innovative Clinical Medicine, Okayama University Hospital, 2-5-1 Shikata-cho, Kita-ku, Okayama 700-8558, Japan

⁵ Department of Respiratory Medicine, Fukuyama Medical Center, Fukuyama, Japan

⁶ Department of Respiratory Medicine, Iwakuni Medical Center, Iwakuni, Japan

⁷ Department of Respiratory Medicine, Chugoku Central Hospital, Fukuyama, Japan

⁸ Department of Clinical Oncology, Sumitomo Besshi Hospital, Niihama, Japan

⁹ Department of Medical Oncology, Yamaguchi-Ube Medical Center, Ube, Japan

¹⁰ Department of Respiratory Medicine, Japanese Red Cross Okayama Hospital, Okayama, Japan

¹¹ Department of Thoracic Oncology and Medicine, Shikoku Cancer Center, Matsuyama, Japan

¹² Department of Respiratory Medicine, Okayama Rosai Hospital, Okayama, Japan

¹³ Department of Radiotherapy, Japanese Red Cross Society Himeji Hospital, Himeji, Japan

¹⁴ Department of Radiology, Okayama University Hospital, Okayama, Japan

¹⁵ Department of General Internal Medicine 4, Kawasaki Medical School, Okayama, Japan

¹⁶ Department of Hematology and Oncology, Okayama University Hospital, Okayama, Japan

Further efforts are necessary to define an optimal regimen for elderly patients with limited SCLC.

Keywords Lung cancer · Elderly patient · Chemotherapy · Topotecan

Introduction

The standard treatment for patients with limited-disease small-cell lung cancer (LD-SCLC) is a combination of early concurrent twice-daily thoracic radiotherapy (TRT) and chemotherapy, consisting of etoposide (ETP) and cisplatin (CDDP) [1]. For extensive disease (ED)-SCLC, chemotherapy consisting of CDDP and ETP (PE) [2, 3] or CDDP and irinotecan (CPT-11) (PI) has widely been investigated [4].

However, elderly patients were excluded from these previous trials [4]. PE with early concurrent twice-daily TRT in elderly patients was effective, but highly toxic [5]. A combination of carboplatin and CPT-11 caused a high incidence of diarrhea (grade 2 or greater: 40 % [6]). Also, a combination of carboplatin and VP-16 is now often used for elderly patients [7], but no standard regimen has been established. Thus, there is ongoing need to further develop treatment strategies for the elderly.

Topotecan (TOP) is a promising drug for relapsed SCLC patients. TOP monotherapy produced better survival than best supportive care in a phase III trial [8]. In previously untreated SCLC patients, TOP monotherapy showed a 39 % overall response rate (ORR) [9]. Non-hematological toxicities were mild. In particular, diarrhea, which is the dose-limiting toxicity (DLT) of CPT-11, is reportedly rare [10, 11]. However, its utility in a first-line setting in the elderly remains unclear.

In a prior phase I trial, we demonstrated the safety profile of split TOP and CDDP (TP) therapy; the DLTs were febrile neutropenia (FN), persistent neutropenia, hyponatremia, and hepatic toxicity [12]. In that study, the ORR was 60 % in LD-SCLC patients and 55 % in ED-SCLC patients, with median survival times of 16.0 and 11.0 months, respectively. Based on these findings, we subsequently conducted a phase II trial of split TP therapy, with the primary end point of ORR and secondary end points of 1-year survival rate and toxicity.

Patients and methods

Eligibility

The eligibility criteria are listed in Supplemental Table 1. The baseline pretreatment evaluations included a complete

history, physical examination, laboratory tests, a chest radiograph, computed tomography (CT) scans of the chest and abdomen, bronchoscopy, magnetic resonance imaging of the brain, and a radionuclide bone scan, if medically indicated.

Written informed consent was obtained from each patient before any screening or inclusion procedure. This study was conducted in compliance with the principles of the Declaration of Helsinki. The protocol was approved by the institutional review board of each participating institution.

Treatment schedule

The dose and schedule of the investigational regimen were intended to be the same as in the phase I trial [12]. TOP (1 mg/m², days 1–3), diluted in 100 mL of physiological saline, was administered intravenously for 30 min on days 1–3. After completion of the TOP infusion, CDDP (20 mg/m², days 1–3), diluted in 300 mL of physiological saline, was administered intravenously over 1 h on the same days. The treatment was repeated every 3 weeks until PD or a maximum of four cycles. Each patient was pre-medicated with dexamethasone and 5-HT3 inhibitor.

Initiation of the next cycle of chemotherapy was delayed until recovery of the white blood cell count to $\geq 3000/\text{mm}^3$, the neutrophil count to $\geq 1500/\text{mm}^3$, the platelet count to $\geq 10 \times 10^4/\text{mm}^3$, hemoglobin to $\geq 8.0 \text{ g/dL}$, and serum creatinine to $\leq 1.5 \text{ mg/dL}$. If grade 4 leukopenia, neutropenia, or FN was noted, the use of granulocyte colony-stimulating factor (G-CSF) was permitted.

Patients with LD-SCLC received thoracic irradiation at a total of 45 Gy in 25 fractions after the completion of chemotherapy. Prophylactic cranial irradiation was not planned.

Assessments of toxicity and antitumor activity

All toxicities were graded according to National Cancer Institute Common Terminology Criteria for Adverse Events (ver. 2). The standard Response Evaluation Criteria in Solid Tumors (ver. 1) was used to evaluate responses. A CT scan to assess target and nontarget lesions was designed to be done every 3 weeks during treatment. After the planned treatment, a CT scan was done at least every 6 months.

Statistical considerations

The efficacy of this combination therapy was assessed separately for LD- and ED-SCLC. In the LD group, assuming that an ORR of 90 % in eligible patients would indicate potential utility, whereas a rate of 70 % would be the lower limit of interest, with $\alpha = 0.05$ and $1 - \beta = 0.8$, and the estimated accrual number was 30 patients. An interim

Table 1 Clinical demographics of the 22 patients with LD-SCLC

Age, years (median, range)	79 (76–84)
Gender (male/female)	19 (86 %)/3 (14 %)
Staging (I/II/IIIA/IIIB)	3 (14 %)/3 (14 %)/7 (32 %)/9 (41 %)
ECOG PS (0–1/2)	20 (91 %)/2 (9 %)
Smoking (never/ever)	4 (18 %)/18 (82 %)
Median Charlson score (range)	3 (2–6)

LD-SCLC limited-disease small-cell lung cancer, ECOG Eastern Cooperative Oncology Group, PS performance status

analysis was preplanned, so that the regimen would be rejected if 19 or fewer of the first 23 patients had an objective response with Simon's minimax design. The primary end point would be considered to be met if 22 or more patients had an overall response at the final analysis.

In the ED group, assuming that an ORR of 85 % would indicate potential utility, whereas a rate of 60 % would be the lower limit of interest, with $\alpha = 0.05$ and $1 - \beta = 0.8$, and the estimated accrual number was 25 patients. This regimen would be rejected if three or fewer of the first five patients showed an objective response. The primary end point would be considered to be met if 18 or more patients had an overall response at the final analysis.

Results

Patient characteristics

Enrollment in this study began in December 2004. In the ED group, the trial was terminated at the time of the interim analysis for ED-SCLC (performed in 2007) because only

three of the first five patients had an objective response (Supplemental Table 2). Therefore, further investigations were not evaluated in ED group. For LD-SCLC patients, the trial was also terminated early with 22 of the planned 30 patients because of slow accrual. The demographics of the 22 patients are listed in Table 1. The median age was 79 years (range 76–84), and 86 % of the patients were male (19/3). Most patients were ever smokers (82 %) had a performance status of 0–1 (91 %) and had a median Charlson score of 3 (range 2–6). Treatment delivery is shown in Fig. 1. Ultimately, 9 of 22 (41 %) patients completed the planned treatment.

Efficacy

With an intention to treat analysis, the ORR was 68 % (15/22, 95 % confidence interval [CI] 47–89 %) with no complete response; this did not meet the primary end point. The disease control rate, defined as the percentage of patients with partial responses and stable disease, was 77 % (95 % CI 58–96 %; Table 2).

For the survival analysis, with a median follow-up time for surviving patients of 17.9 months, 19 (86 %) patients experienced disease progression or died. The median progression-free survival (PFS) was 9.1 (95 % CI 4.7–14.9) months (Fig. 2a), and the median overall survival (OS) was 22.2 (95 % CI 9.8–35.4) months (Fig. 2b). The 1-year survival rate was 72 % (95 % CI 49–87 %).

Toxicity

We assessed toxicity in 22 patients. The main grade 3 or 4 toxicities are listed in Table 3. The most common adverse event was neutropenia (96 %, 21/22), followed

Fig. 1 Study flow. TRT thoracic radiotherapy, AE adverse event, MOF multiple organ failure

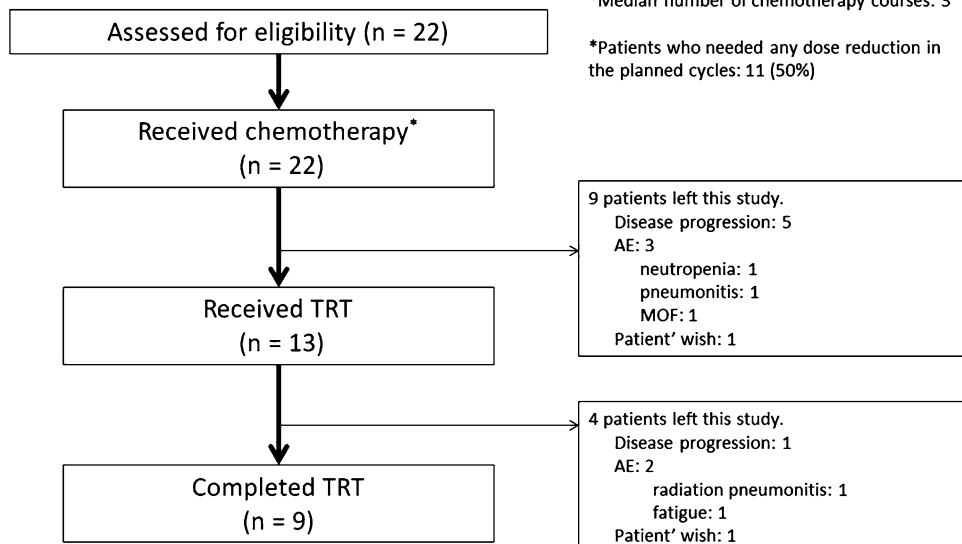
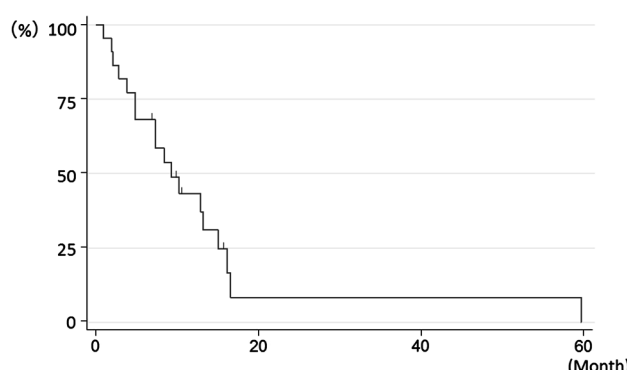
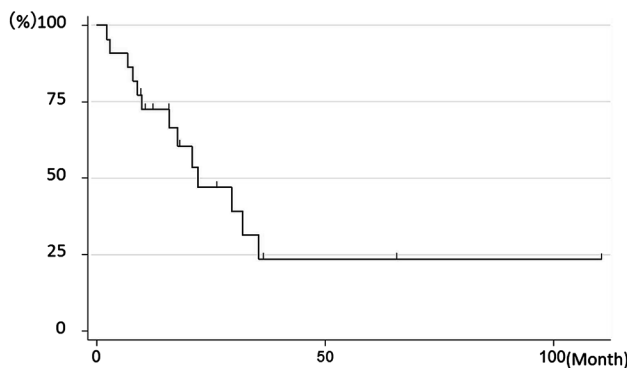


Table 2 Overall response rate ($n = 22$)

	No. of patients	%
Response rate	15	68
Disease control rate	17	77
Partial response	15	68
Complete response	0	0
Stable disease	2	9
Progressive disease	4	18
Not evaluated	1	4.5

Disease control rate was defined as the proportion of partial response, complete response, and stable disease

A**B****Fig. 2** **a** Progression-free survival curve ($n = 22$). **b** Overall survival curve ($n = 22$)

by thrombocytopenia (50 %, 11/22), and anemia (36 %, 8/22). These hematological adverse events were tolerable with an appropriate treatment or dose reduction of the protocol treatment. Other common adverse events were FN (32 %, 7/22), pneumonitis (18 %, 4/22), and nausea (14 %, 3/22). One treatment-related death during cycle 4 was observed, due to multiple organ failure, followed by hepatotoxicity.

Table 3 Adverse events ($n = 22$)

Toxicity	No. of patients			
		Any grades	3	4
<i>Hematological</i>				
Neutropenia	22 (100 %)	5 (23 %)	16 (73 %)	0 (0 %)
Thrombocytopenia	18 (82 %)	7 (32 %)	4 (18 %)	0 (0 %)
Anemia	17 (77 %)	7 (32 %)	1 (4.5 %)	0 (0 %)
<i>Non-hematological</i>				
Febrile neutropenia	7 (32 %)	7 (32 %)	0 (0 %)	0 (0 %)
Creatinine elevation	5 (23 %)	1 (4.5 %)	0 (0 %)	0 (0 %)
AST/ALT increased	10 (45.5 %)	0 (0 %)	0 (0 %)	1 (5 %)
Nausea/vomiting	12 (54 %)	3 (13 %)	0 (0 %)	0 (0 %)
Diarrhea	6 (27 %)	0 (0 %)	0 (0 %)	0 (0 %)
Esophagitis	8 (36 %)	0 (0 %)	0 (0 %)	0 (0 %)
Pneumonitis	11 (50 %)	4 (18 %)	0 (0 %)	0 (0 %)

Subsequent treatments

At the time of the analysis, 17 (77 %) patients showed recurrence, 7 (41 %) developed distant metastases, 8 (47 %) had loco-regional disease, and 2 (12 %) developed both loco-regional disease and distant metastases. Brain metastases were observed in 2 patients (12 %). Of the 17 patients, 13 (76 %) received subsequent treatment (Table 4).

Response and survival stratified by clinical factors

The efficacy stratified by several clinical factors is shown in Supplemental Table 3. No significant difference in ORR or survival time was evident between the groups.

Discussion

We conducted a phase II trial of split TP therapy in elderly SCLC patients. In the ED group, the ORR was 68 %, which did not meet the primary end point. The survival outcome was somewhat favorable with a median PFS time of 9.1 months and median OS of 22.2 months, but moderate-to-severe toxicities were observed with one treatment-related death, leading to a low completion rate of the whole treatment (41 %).

Regarding ORR (the primary end point), it did not satisfy the preplanned criterion. Although this study was terminated early, the registered number of 22 patients was sufficient to determine whether the ORR did meet the end point in the interim analysis. The ORR of 68 % in this

Table 4 Subsequent treatments ($n = 17$)

Chemotherapy	7 (41 %)
CBDCA + ETP	4
CPT-11 + AMR	1
ETP	1
AMR	1
Chemotherapy + TRT	4 (24 %)
AMR followed by TRT	2
CBDCA + ETP followed by TRT	1
ETP + TRT	1
Palliative RT	2 (12 %)
Best supportive care	4 (24 %)

CBDCA carboplatin, *ETP* etoposide, *CPT-11* irinotecan, *AMR* amrubicin, *TRT* thoracic radiotherapy, *RT* radiotherapy

phase II trial was consistent with our phase I trial result—2 of 3 (67 %) patients at the recommended dose responded to treatment [12]. This reproducibility suggests that the current negative result was attributable simply to the pre-defined statistical consideration that was too strict in this phase II trial, and, possibly, to the moderate-to-severe toxicity profile and low completion rate of the planned treatment.

The median survival time of 22.2 months was favorable. It was not inferior to those noted in previous trials (Supplemental Table 4) [6, 7, 13, 14]. This was partly attributable to the high proportion of subsequent treatment after progression. This might mean that TP therapy is a regimen that can easily be transitioned to a subsequent treatment. Another reason might be patient selection; in fact, the median Charlson score was 3, meaning that the patients who participated in this trial were in good general condition.

In terms of safety, the main toxicity was myelosuppression, especially neutropenia (Table 3). Thus, several of the toxicities that occurred with this regimen may be preventable using prophylactic PEGylated G-CSF administration. In fact, it can reduce the proportion of FN by 6–68 % [15, 16], and 6–22 % in elderly patients. In total, the toxicities were more severe than those in previous trials, although there was no severe diarrhea, which is an advantage of TOP versus CPT-11 (Supplemental Table 4). Of note, severe pneumonitis was observed in 4 (18 %) patients, while its severity in TOP and radiotherapy has rarely been reported. The reason for this high proportion is unclear, but it might be due to patient selection. Careful patient follow-up is needed with our regimen, even though there was no treatment-related death due to pneumonitis.

This study has several limitations. The time period of accrual was too long, and factors other than the investigational regimen itself potentially affected the outcome, including the starting situation and any change in

supportive care. Unfortunately, we could not obtain information about the actual number of patients who underwent a positron emission tomography scan. Also, we did not have detailed information as to how large the volume of lung receiving at least 20 Gy (V20) was and how the radiotherapy field was set in each patient, although these might have affected the efficacy, including PFS and OS. Thus, our results should be interpreted cautiously. Furthermore, we did not have any biomarker of this regimen for efficient patient selection, as is often the case with other cytotoxic agents.

In summary, split TP therapy and sequential thoracic radiation therapy did not meet the primary outcome criteria, with moderate-to-severe toxicities. The regimen is not useful and further efforts are necessary to define an optimal regimen for elderly patients with limited SCLC.

Acknowledgments We thank the patients and their families for participating in this trial. We also thank Yasunari Nakata, Masafumi Fujii, Hiroshi Date (Kyoto University Hospital), Masahiro Osawa, Daisuke Morichika, Tomoki Tamura (Okayama University Hospital), Hiromasa Takeda (Tsuyama Central Hospital), Nobuhiro Honda (Kawasaki Hospital), and Toshi Murakami (Japanese Red Cross Society Himeji Hospital), for cooperating in this trial. This study has been conducted with support from the Center for Innovative Clinical Medicine, Okayama University Hospital.

Author contributions TK, KH, and KN had full access to all of the data and take responsibility for the integrity of the data and accuracy of the data analysis. KF, NT, KH, and KK contributed to the study design. TK, KH, and KN contributed to data collection and analysis. All of the authors contributed to the writing of the manuscript and provided final approval of the version to be published.

Compliance with ethical standards

Conflict of interest K.H. has received honoraria from AstraZeneca, Eli Lilly Japan, Daiichi-Sankyo Pharmaceutical, Boehringer-Ingelheim, Nihon Kayaku, Taiho Pharmaceutical, and Chugai Pharmaceutical. KH also has received research funding from Eli Lilly Japan, MSD, and Chugai Pharmaceutical. J.S. has received honoraria from Pfizer, Eli Lilly, Taiho Pharmaceutical, Chugai Pharmaceutical, Boehringer-Ingelheim, AstraZeneca, and Kyowa Kirin. N.T. has received honoraria from Eli Lilly Japan, AstraZeneca, Daiichi-Sankyo Pharmaceutical, Chugai Pharmaceutical, Taiho Pharmaceutical, Pfizer Japan Inc, and Boehringer-Ingelheim in Japan. K.K. has received honoraria from Eli Lilly Japan, Nihon Kayaku, AstraZeneca, Daiichi-Sankyo Pharmaceutical, Chugai Pharmaceutical, Taiho Pharmaceutical, and Sanofi-Aventis. The remaining authors have stated that they have no conflicts of interest.

References

1. Socinski MA, Bogart JA (2008) Limited-stage small-cell lung cancer: the current status of combined-modality therapy. *J Clin Oncol* 25:4137–4145
2. Roth BJ, Johnson DH, Einhorn LH, Schacter LP, Cherng NC, Cohen HJ, Crawford J, Randolph JA, Goodlow JL, Broun GO et al (1992) Randomized study of cyclophosphamide,

- doxorubicin, and vincristine versus etoposide and cisplatin versus alternation of these two regimens in extensive small-cell lung cancer: a phase III trial of the Southeastern Cancer Study Group. *J Clin Oncol* 10:282–291
3. Fukuoka M, Furuse K, Saijo N, Nishiwaki Y, Ikegami H, Tamura T, Shimoyama M, Suemasu K (1991) Randomized trial of cyclophosphamide, doxorubicin, and vincristine versus cisplatin and etoposide versus alternation of these regimens in small-cell lung cancer. *J Natl Cancer Inst* 83:855–861
 4. Noda K, Nishiwaki Y, Kawahara M, Negoro S, Sugiura T, Yokoyama A, Fukuoka M, Mori K, Watanabe K, Tamura T, Yamamoto S, Saijo N (2002) Irinotecan plus cisplatin compared with etoposide plus cisplatin for extensive small-cell lung cancer. *N Engl J Med* 346:85–91
 5. Okamoto K, Okamoto I, Takezawa K, Tachibana I, Fukuoka M, Nishimura Y, Nakagawa K (2010) Cisplatin and etoposide chemotherapy combined with early concurrent twice-daily thoracic radiotherapy for limited-disease small cell lung cancer in elderly patients. *Jpn J Clin Oncol* 40:54–59
 6. Murata Y, Hirose T, Yamaoka T, Shirai T, Okuda K, Sugiyama T, Kusumoto S, Nakashima M, Ohmori T, Adachi M (2011) Phase II trial of the combination of carboplatin and irinotecan in elderly patients with small-cell lung cancer. *Eur J Cancer* 47:1336–1342
 7. Okamoto H, Watanabe K, Nishiwaki Y, Mori K, Kurita Y, Hayashi I, Masutani M, Nakata K, Tsuchiya S, Isobe H, Saijo N (1999) Phase II study of area under the plasma-concentration-versus-time curve-based carboplatin plus standard-dose intravenous etoposide in elderly patients with small-cell lung cancer. *J Clin Oncol* 17:3540–3545
 8. O'Brien ME, Culeanu TE, Tsekov H, Shparyk Y, Cuceviá B, Juhasz G, Thatcher N, Ross GA, Dane GC, Crofts T (2006) Phase III trial comparing supportive care alone with supportive care with oral topotecan in patients with relapsed small-cell lung cancer. *J Clin Oncol* 24:5441–5447
 9. Schiller JH, Kim K, Hutson P, DeVore R, Glick J, Stewart J, Johnson D (1996) Phase II study of topotecan in patients with extensive-stage small-cell carcinoma of the lung: an Eastern Cooperative Oncology Group Trial. *J Clin Oncol* 14:2345–2352
 10. Masuda N, Fukuoka M, Kusunoki Y, Matsui K, Takifumi N, Kudoh S, Negoro S, Nishioka M, Nakagawa K, Takada M (1992) CPT-11: a new derivative of camptothecin for the treatment of refractory or relapsed small-cell lung cancer. *J Clin Oncol* 10:1225–1229
 11. Negoro S, Fukuoka M, Masuda N, Takada M, Kusunoki Y, Matsui K, Takifumi N, Kudoh S, Niitani H, Taguchi T (1991) Phase I study of weekly intravenous infusions of CPT-11, a new derivative of camptothecin, in the treatment of advanced non-small-cell lung cancer. *J Natl Cancer Inst* 83:1164–1168
 12. Fujiwara K, Ueoka H, Kiura K, Tabata M, Takigawa N, Hotta K, Umemura S, Sugimoto K, Shibayama T, Kamei H, Harita S, Okimoto N, Tanimoto M (2006) A phase I study of 3-day topotecan and cisplatin in elderly patients with small-cell lung cancer. *Cancer Chemother Pharmacol* 57:755–760
 13. Inoue A, Ishimoto O, Fukumoto S, Usui K, Suzuki T, Yokouchi H, Maemondo M, Kanbe M, Ogura S, Harada T, Oizumi S, Harada M, Sugawara S, Fukuhara T, Nukiwa T (2009) A phase II study of amrubicin combined with carboplatin for elderly patients with small-cell lung cancer: North Japan Lung Cancer Study Group Trial 0405. *Ann Oncol* 21:800–803
 14. Tada A, Ueoka H, Kiura K, Tabata M, Takemoto M, Yamane H, Hiyama J, Aoe K, Shibayama T, Kamei H, Kawahara S, Harita S, Sato T, Kobayashi M, Eguchi K, Hiraki S, Hiraki Y, Tanimoto M (2002) Combination chemotherapy with carboplatin and etoposide for elderly patients aged 76 years or older with small cell lung cancer. *Gan To Kagaku Ryoho* 29:751–756
 15. Kosaka Y, Rai Y, Masuda N, Takano T, Saeki T, Nakamura S, Shimazaki R, Ito Y, Tokuda Y, Tamura K (2015) Phase III placebo-controlled, double-blind, randomized trial of pegfilgrastim to reduce the risk of febrile neutropenia in breast cancer patients receiving docetaxel/cyclophosphamide chemotherapy. *Support Care Cancer* 23:1137–1143
 16. Balducci L, Al-Halawani H, Charu V, Tam J, Shahin S, Dreiling L, Ersler WB (2007) Elderly cancer patients receiving chemotherapy benefit from first-cycle pegfilgrastim. *Oncologist* 12:1416–1424

臨床リウマチ医のための基礎講座

CD26分子に基づくトランスレーショナルリサーチ

順天堂大学大学院医学研究科

免疫病・がん先端治療学講座

森 本 幾 夫

はじめに

我が国の生命科学分野の基礎研究成果は *Nature* や *Science* 等の主要科学雑誌に掲載されるなど、国際的にも高い評価を受けている。しかし我が国においては臨床研究、特に臨床でのトランスレーショナルリサーチに対する支援体制などが十分に整備されていないため研究成果が、医療、製薬等の臨床現場に届いておらず、国民に成果が還元されないと指摘されている。更に免疫病やがん領域の新薬はほとんど欧米発で占められ、日本発の創薬は非常に数少ない。一個の薬が世に出るまでには約500億円から1000億円の費用がかかるといわれている。従来は製薬会社が創薬の中心的役割を果たしていたが、大学等のアカデミアの基礎研究成果を産学共同体制で効率よく創薬に結びつけていくという気運が欧米諸国、日本ともに高まっている。このような背景で、日本政府は2007年から東京大学、京都大学など旧帝大系を中心として全国7カ所の大学及び神戸先端医療振興財団に「トランスレーショナルリサーチ」(橋渡し研究)施設整備のための研究資金援助をスタートした。

トランスレーショナルリサーチとは

トランスレーショナルリサーチ(橋渡し研究)(以下 TR)という「ことば」は耳慣れないと思われるが最近医学界で頻回に聞く。要は、医学研究における研究室での基礎研究成果を臨床応用し

ていく探索的な研究をいい、早期の臨床試験にまでもっていくことを指す。

医学研究に従事している者は、誰しもがその研究成果を患者の病気の治癒、改善あるいは早期診断のために応用したいと思っている。ベンチ(研究成果)からベッド(臨床応用)ということばはこのことに相当する。TRのことばの定義について早期の臨床試験を行うことなども TR を施行していると表現する場合もあり、その定義が混乱している面もある。

これに関して、Dr. Birmingham が *Nature Medicine* (2002年) にて以下のように定義している¹⁾。つまりアカデミアで医学研究、特に病気の原因究明やヒト検体を用いて研究を行なっている研究者は誰しもが自分はそうだと思っている。しかし彼は「自からの仕事が以下を試みる研究者」の研究を指すと定義する。つまり 1. 患者の病気の診断または予後を改善する。2. 患者の病気の予防を向上させる。3. 患者における新しい治療を着想し実行する。更に上記に加えて通常基礎研究は個人で行う研究であるが TR はむしろチームで行うものとしている。要は、その構成メンバーとして、研究室ベースの研究者、患者の治療を行ったり、イメージングなどの評価を行う放射線や病理診断医、更に看護師、データマネージャー、薬剤師などから成っており、お互いに協力して TR を施行するのである。筆者もこの定義に同意している。

Translational research based on CD26 molecule.

Chikao Morimoto.

Department of Therapy Development and Innovation for Immune disorders and Cancers, Graduate School of Medicine, Juntendo University.

DOI: 10.14961/cra.28.91

CD26分子の構造と機能

CD26は細胞表面分子で, dipeptidyl peptidase IV(DPPIV)酵素を含む110kDaの膜蛋白でT細胞共刺激分子であり, 関節リウマチなどの炎症局所でCD26強陽性T細胞が集積しており, 炎症のエフェクターT細胞といわれている。またコラーゲン, フィブロネクチン, Adenosine deaminase(ADA)の結合蛋白であるなど多彩な機能を有している²⁻⁴⁾。DPPIV酵素阻害薬はすでに糖尿病治療薬として幅広く臨床現場で用いられている(図1)。

CD26陽性T細胞リンパ腫株やヒトT細胞クローンを用いて試験管でCD26抗体で処理するとcyclin dependent kinase inhibitor(CDKI)のp21が誘導され細胞周期が止まることを見出し, T細胞リンパ腫株を移植した免疫不全マウスの系でも, 抗体投与マウスは長期生存した。この結果はCD26抗体がT細胞異常を示す免疫病やT細胞腫瘍の治療に利用できる可能性を示した⁴⁾。そこでCD26抗体の抗原結合部位のアミノ酸及び遺伝子配列解析を施行し, 米国Abmaxis社と共にインシリコ法にて良質なヒト化CD26抗体を開発した(図2)。

CD26と悪性中皮腫

アスベストは石綿とも呼ばれ, 耐久性, 耐熱性に優れ, 幅広い用途に使用されてきた。しかし肺に吸入されると約30-40年の潜伏期間を経て悪性中皮腫などを引き起こす⁵⁾。

日本では高度成長期に建築物などにアスベストが大量に消費されており, その潜伏期間が終わる21世紀に入りアスベストが原因で発生したと思われる悪性中皮腫による死亡者数が増加し, 2030年をピークとして益々増加すると予測されており, 大きな社会問題となっている。さらに悪性中皮腫は有効な化学療法剤に乏しく, 予後はきわめて不良で, 新規かつ有効な治療法開発は急務である。

ヒトT細胞共刺激分子のCD26がなぜ悪性中皮腫に関連しているのかという点であるが, 著者ら

はCD26はコラーゲンの結合蛋白であることを報告している⁶⁾。この研究過程でCD26は免疫系細胞だけでなく悪性中皮腫由来株JMNにも発現することを発見した。悪性中皮腫の患者組織でCD26発現を検討したところ, 正常中皮では全く発現しないのに悪性中皮腫では8割以上が強く発現していることを見出し, ヒト化CD26抗体が新規治療法になり得るのではないかと考えた⁷⁾。膠原病の臨床に携わっている筆者としては, ヒト化CD26抗体をまず膠原病などの免疫病の新規治療法にという考えがよぎった。2005年にヒト化CD26抗体を開発したがこの頃クボタショックといってアスベスト工場の周辺の人々にも悪性中皮腫が多発し, 連日新聞にアスベストと中皮腫の記事が報道されていた。悪性中皮腫は全く有効な治療法が存在しないことに鑑み, 悪性中皮腫の治療に使用できないかと考えた。CD26分子の遺伝子をCD26陰性中皮腫株に発現させたところ, 親株と比して細胞遊走能, 渗潤能とともに亢進が認められCD26そのものが悪性中皮腫の細胞増殖, 渗潤に関与していることも明らかになった⁷⁾。また, 胸腔内でびまん性に中皮腫細胞が浸潤する中皮腫モデルマウスを作製し, このモデルマウスに抗体を投与して本抗体が有効である結果も得て, ヒトCD26抗体は悪性中皮腫の新規治療法として有望な可能性が示唆された。

ヒト化CD26抗体のFirst in Man第1相臨床試験

ヒト化CD26抗体は悪性中皮腫細胞株を用いたin vitroの実験でcyclin dependent kinase inhibitor(CDKI)のp21, p27などを誘導し, S期の細胞を減少させるとともにG2/M期で細胞周期を遅延させることが明らかになった。また本抗体はIgGであり, Antibody dependent cellular cytotoxicity(ADCC)により腫瘍細胞の腫瘍破壊をもたらす⁷⁾。

ヒト化CD26抗体をヒトに投与するためにサルを用いた前臨床反復毒性試験を行い, その安全性を確認している。そこでフランスにおいて化学療法抵抗性の悪性中皮腫及びその他CD26陽性固形癌をターゲットとして第I/II相臨床試験をスタートした。

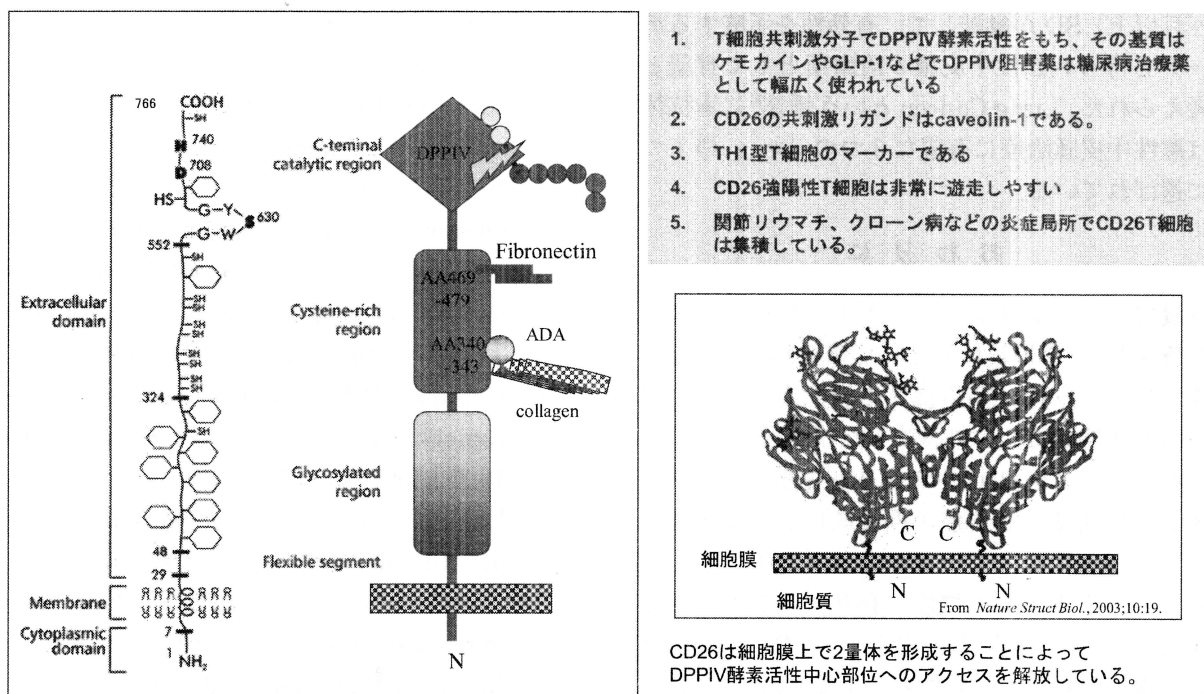


図1 CD26分子の構造と機能

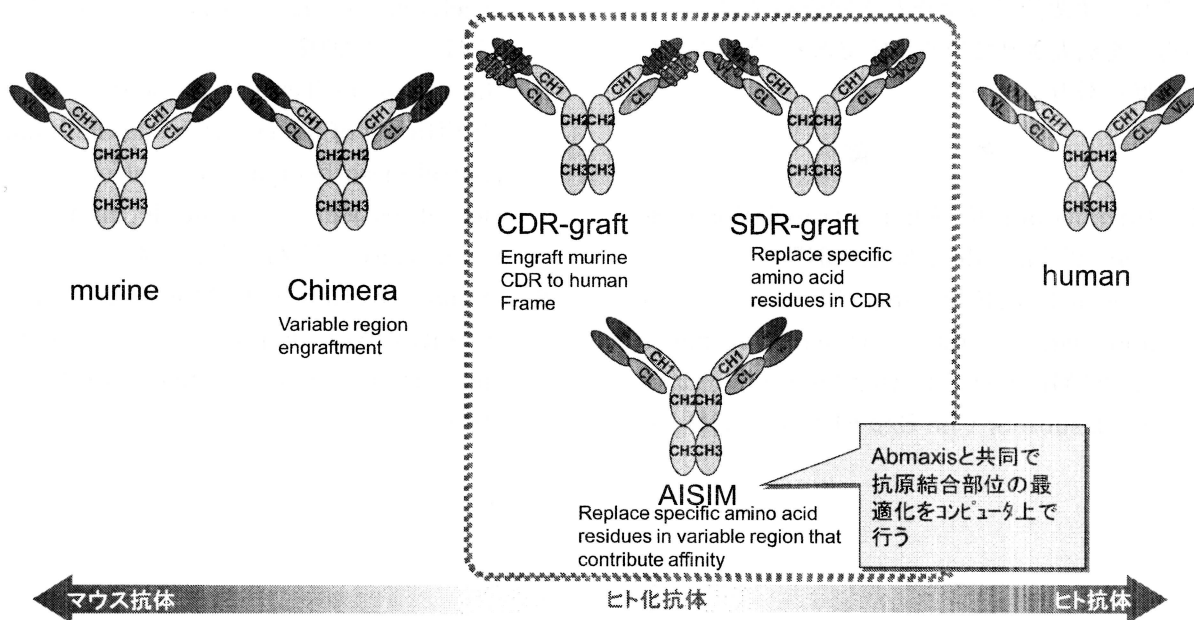


図2 ヒト化抗体作成技術

平成26年9月に第I相臨床試験は終了し、安全性を確認でき、また統計33例中評価ができた症例26症例中13例がStable Disease (SD), 13例が

Progress Disease (PD)という結果を得た。特に治療抵抗性悪性中皮腫では19例中10例がSDとなり、しかもその内6例が3ヶ月以上(5例は6

ヶ月以上) SD が継続して、有効性を示唆するデータも得られ悪性中皮腫の治療薬として有望と考えられた。Lung Cancer という雑誌⁸⁾に本抗体は悪性中皮腫治療に有望な 3 つの Drug の 1 つに選ばれている。

おわりに

本稿ではトランスレーショナルリサーチについて概説して、その具体例として筆者が現在取り組んでいるヒト化 CD26 抗体の悪性中皮腫への新規治療法開発について説明した。

現在 CTLA-4 や PD-1への抗体が免疫チェックポイント阻害薬として癌免疫領域において非常にポピュラーになっているが最近 CD26 分子も免疫チェックポイント機能が存在することが示唆され、この分子は自己免疫制御のみならず癌免疫にも深く係わっていることが示唆されている⁹⁾。

ヒト化 CD26 抗体は 2016 年に本邦においても悪性中皮腫をターゲットに第 I 相臨床試験をスタートする予定で近い将来、悪性中皮腫以外の癌のみならず関節リウマチなど膠原病領域にもその適応を拡大させていく予定であり、今後の更なる発展に努力したい。

文 献

- 1) Birmingham K: What is translational research?. Nat Med. 2002, 8:647.
- 2) Morimoto C, Schlossman SF: Human naive and memory T cells revisited: new markers (CD31 and CD27) that help define CD4+ T cell subsets. Clin Exp Rheum, 11:241-247,

1993.

- 3) Morimoto C, Schlossman SF: The structure and function of CD26 in The T-cell immune response. Immunol Review, 161:55-70, 1998.
- 4) Ohnuma K, Dang NH, Morimoto C: Revising an old acquaintance: CD26 and its molecular mechanisms in T cell function. Trend Immunol, 29:296-301, 2008.
- 5) Robinson BW, Lake RA: Advances in malignant mesothelioma. N Engl J Med, 353:1591-603, 2005.
- 6) Dang NH, Torimoto Y, Schlossman SF, et al: Human CD4 helper T cell activation: functional involvement of two distinct collagen receptors, 1F7, and VLA integrin family. J Exp Med, 172:649-652, 1990.
- 7) Inamoto T, Yamada T, Morimoto C, et al: Humanized Anti-CD26 monoclonal antibody as a treatment for malignant mesothelioma tumors. Clin Cancer Res, 13:4191-200, 2007.
- 8) Raphael J, Le Teuff G, Hollebecque A, et al: Efficacy of phase 1 trials in malignant pleural mesothelioma: description of a series of patients at a single institution. Lung Cancer, 85:251-257, 2014.
- 9) Ohnuma K, Hatano R, Morimoto C: DPP4 in anti-tumor immunity: going beyond the enzyme. Nat Immunol, 16:791-792, 2015.